NUREG/CR-6672, Vols. 1,2
SAND2000-0234

Reexamination of Spent Fuel Shipment Risk Estimates

Volume I: Main Report

Manuscript Completed: February 2000
Date Published: March 2000

Prepared by
J. L. Sprung, D. J. Ammerman, N. L. Breivik, R. J. Dukart, F. L. Kanipe,
J. A. Koski, G. S. Mills, K. S. Neuhauser, H. D. Radloff, R. F. Weiner, H. R. Yoshimura

Sandia National Laboratories
Albuquerque, NM 87185-0718

Prepared for
Spent Fuel Project Office
Office of Nuclear Material Safety and Safeguards
U.S. Nuclear Regulatory Commission
Washington, DC 20555
NRC Job Code J5160

Page intentionally left blank.

ABSTRACT

The risks associated with the transport of spent nuclear fuel by truck and rail are reexamined and compared to results published in NUREG-0170 and the Modal Study. The reexamination considers transport by truck and rail in four generic Type B spent fuel casks. Cask and spent fuel response to collision impacts and fires are evaluated by performing three-dimensional finite element and one-dimensional heat transport calculations. Accident release fractions are developed by critical review of literature data. Accident severity fractions are developed from Modal Study truck and rail accident event trees, modified to reflect the frequency of occurrence of hard and soft rock wayside route surfaces as determined by analysis of geographic data. Incident-free population doses and the population dose risks associated with the accidents that might occur during transport are calculated using the RADTRAN 5 transportation risk code. The calculated incident-free doses are compared to those published in NUREG-0170. The calculated accident dose risks are compared to dose risks calculated using NUREG-0170 and Modal Study accident source terms. The comparisons demonstrate that both of these studies made a number of very conservative assumptions about spent fuel and cask response to accident conditions, which caused their estimates of accident source terms, accident frequencies, and accident consequences to also be very conservative. The results of this study and the previous studies demonstrate that the risks associated with the shipment of spent fuel by truck or rail are very small.

Page intentionally left blank.

CONTENTS

Figures

Tables

Page intentionally left blank.

Acknowledgements

Thanks are owed to a number of people for the contributions they made to the performance of this study or the preparation of this report. The ORIGEN, CONTAIN, and VICTORIA calculations described in Section 7 were performed on short notice by J.D Smith, Nathan Bixler, and Kenneth Murata, respectively. Philip Reardon ressurected the RADTRAN 1 code and supported the analyses described in Section 7 of impact fracturing of spent fuel and also of cesium release fractions. Mona Aragon prepared the conceptual design drawings of the generic casks in Section 4 and almost all of the figures in Section 5.

Thanks are especially owed to the reviewers of this report. They identified many topics that needed to be better explained and even more sentences that required rewriting. Without their efforts, many parts of this report would be close to inscrutable. At Sandia National Laboratories, David Harding reviewed Sections 4 and 5 of the report, Dana Powers reviewed Section 7, and the entire report was reviewed by Robert Luna and Charles Massey. External review of the report was performed by Brian Anderson, Moe Dehgahani, Larry Fisher, Edwin Jones, Mike Shaffer, and Monika Witte of Lawrence Livermore National Laboratories assisted by Theo Theofanous of the University of California at Santa Barbara. The report was also reviewed by a number of technical experts at NRC. The NRC reviews were directed and partly performed by M. Wayne Hodges and Earl Easton.

Lastly, we wish to acknowledge the support, guidance, encouragement, and patience of John Cook, the NRC project manager for this study. Without his help, we would never have finished.

Page intentionally left blank.

ACRONYMS

AAR	American Association of Railroads
ANL	Argonne National Laboratory
BDF	building dose factor
BMCS	Bureau of Motor Carrier Safety
BWR	boiling water reactor
CCDF	Complementary Cumulative Distribution Function
DOE	Department of Energy
DOT	U.S. Department of Transportation
DU	depleted uranium
EIS	Environmental Impact Statement
EQPS	Equivalent Plastic Strain
G	acceleration due to gravity
GES	General Estimates System
GIS	Geographic Information System
GWDt/MTU	gigawatt-days thermal per metric ton of uranium
LCF	latent cancer fatalities
LHS	Latin Hypercube Sampling
LLNL	Lawrence Livermore National Laboratory
LOS	loss of shielding
MPC	multi-purpose cask
NMSS	Nuclear Material Safety and Safeguards
NRC	Nuclear Regulatory Commission
PWR	pressurized water reactor
RAM	radioactive material
SETU	Structural Evaluation Test Unit
SNL	Sandia National Laboratories
TE	total plastic elongation
TIFA	Trucks Involved in Fatal Accidents
UE	uniform plastic elongation
USGS	U.S. Geologic Survey

Page intentionally left blank.

EXECUTIVE SUMMARY

Introduction

In September of 1977, the Nuclear Regulatory Commission (NRC) issued a generic Environmental Impact Statement (EIS), titled "Final Environmental Statement on the Transportation of Radioactive Material by Air and Other Modes," NUREG-0170, that covered the transport of all types of radioactive material by all transport modes (road, rail, air, and water) [E-1]. That EIS provides the regulatory basis for issuance of general licenses for transportation of radioactive material under 10 CFR 71. Based in part on the findings of NUREG-0170, the NRC's Commission concluded that "present regulations are adequate to protect the public against unreasonable risk from the transport of radioactive materials" (46 FR 21629, April 13, 1981) and stated that "regulatory policy concerning transportation of radioactive materials be subject to close and continuing review."

In 1996 the NRC decided to reexamine the risks associated with the shipment of spent power reactor fuel by truck and rail. The reexamination was initiated (1) because many spent fuel shipments are expected to be made during the next few decades, (2) because these shipments will be made to facilities along routes and in casks not specifically examined by NUREG-0170, and (3) because the risks associated with these shipments can be estimated using new data and improved methods of analysis. This report documents the methodology and results of the study that performed this reexamination of the risks of transporting spent fuel from commercial reactor sites to possible interim storage sites and/or permanent geologic repositories.

Overview of NUREG-0170

NUREG-0170 estimated the radiation doses and latent cancer fatalities that might be associated with the transportation of 25 different radioactive materials by plane, truck, train, and ship or barge. The estimates were made using Version 1 of the RADTRAN code (RADTRAN 1) [E-2], that was developed specifically to perform the NUREG-0170 study. One of the 25 radioactive materials examined by NUREG-0170 was spent power reactor fuel.

For spent fuel shipments that occur without accidents (incident-free transport), radiation doses were estimated for two population groups: (1) shipment workers (e.g., the truck or train crew, cask handlers, and persons who inspect the cask, truck, or train) and (2) members of the general public who would be exposed to low levels of radiation, because they lived near the shipment route or came near the cask while traveling on the route. For transportation accidents, release of radioactive material from spent fuel to the environment, the probability of these releases, and the population doses and radiation-induced latent cancer fatalities that such releases might cause were estimated.

The influence of accident severity on accident consequences was examined by dividing all accidents into eight categories according to their severity. Because "little information relating the response of packages to accident environments" [E-3] was available in 1975, release of radioactive materials to the environment as a result of accidents was examined using two release models that were constructed largely by expert judgement. The first model, Model I [E-4],

assumed [E-5] that "zero release occurs up to the regulatory test level and that the packaging fails catastrophically in all environments that exceed that level." Because the Model I cask release behavior was considered to be unrealistic, a second release model (Model II) was formulated. In Model II, for accidents that exceed the regulatory test level, release fractions increased more gradually with accident severity [E-6], becoming equal for catastrophic accidents to the release specified for all severe accidents by Model I.

Because the NUREG-0170 spent fuel accident source terms were not developed by examining the response of spent fuel and spent fuel casks to severe accident conditions, NRC had the response of generic steel-lead-steel truck and rail spent fuel casks to collision and fire accident conditions examined by the performance of finite element impact and thermal heat transport calculations. The results of these calculations were published in 1987 in NUREG/CR-4829, "Shipping Container Response to Severe Highway and Railway Accident Conditions," which is usually called the Modal Study [E-7]. Although that study did not perform any consequence calculations, comparison of the probabilities and magnitudes of the accident source terms developed for that study to those developed for NUREG-0170 allowed the authors of the Modal Study to conclude that the risks per spent fuel shipment for shipments by both truck and rail were "at least 3 times lower that those documented in NUREG-0170" [E-1].

Methodology

The risks associated with the transport of spent nuclear fuel were estimated using Version 5 of the RADTRAN code [E-8, E-9]. Risks were estimated (1) for incident-free transport, (2) for transportation accidents so severe that they result in the release of radioactive materials from the cask to the environment, and (3) for less severe accidents that cause the cask shielding to be degraded but result in no release of radioactive material (Loss of Shielding accidents).

Based on prior sensitivity studies [E-10, E-11, E-12], RADTRAN 5 input parameters were divided into three groups: (1) source term parameters (severity and release fractions); (2) other input parameters that strongly influence RADTRAN estimates of radiation dose, which were collectively called other "more important parameters"; and (3) RADTRAN input parameters that have little impact on estimates of radiation dose, which were collectively called "less important parameters." Central (best) estimate values were selected for each of the "less important" parameters, e.g., breathing rate.

For the source term parameters, review of studies of transportation accidents, in particular the Modal Study [E-7], allowed representative sets of truck and train accidents and their impact and fire environments to be defined. This analysis developed 19 representative truck accidents and 21 representative train accidents. Severity fraction and release fraction values were estimated for each representative accident.

Severity fractions specify the fraction of all possible accidents that are represented by each of the representative accidents. Severity fraction values were estimated by review of the accident event trees, accident speed distributions, and accident fire distributions that were developed for the Modal Study [E-7]. Because only impact onto a very hard surface can result in the release of radioactive materials during a collision accident, new event tree frequencies of occurrence of

route wayside surfaces (e.g., hard rock; concrete, soft rock, and hard soil; soft soil; water) were developed using Department of Agriculture data [E-13] and Geographic Information System (GIS) methods of analysis [E-14].

Release fractions were estimated as the product of (a) the fraction of the rods in the cask that are failed by the severe accident, (b) the fraction of each class of radioactive materials (e.g., noble gases, volatile, particulates) that might escape from a failed spent fuel rod to the cask interior, and (c) the fraction of the amount of each radioactive material released to the cask interior that is expected to escape from the cask to the environment. Rod failure during high speed collision accidents was estimated by scaling rod strains calculated for relatively low speed impacts [E-15] and then comparing the scaled rod strains to a strain failure criterion [E-15]. Heating of the cask by a hot long duration fire to rod burst rupture temperatures was assumed to fail all unfailed rods (those not failed by collision impact). Rod-to-cask release fractions were estimated by review of literature data, especially the experimental results of Lorenz [E-16, E-17, E-18]. Cask-to-environment release fractions were based on MELCOR [E-19] fission product transport calculations [E-20] that estimated the dependence of these release fractions on the cross-sectional area of the cask leak path through which the release to the environment occurs.

Specifications for generic steel-lead-steel truck and rail casks and for a generic steel-DU-steel truck cask and a generic monolithic steel rail cask were developed from literature data [E-21]. The response of these generic casks to severe collisions (e.g., seal leak areas) was examined by performing three-dimensional finite element calculations for impacts onto an unyielding surface at various impact speeds. Unyielding surface impact speeds were converted to equivalent impact speeds onto yielding surfaces (e.g., soft rock) by considering the energy that would be absorbed by the yielding surface, increasing the energy of the unyielding surface calculation by that amount, and converting the new total energy to an initial impact speed. Seal degradation and rod burst rupture temperatures due to heating during fires were estimated from literature data. The durations of engulfing, optically dense fires needed to produce seal leakage and rod burst rupture were estimated by performing one-dimensional heat transport calculations.

For the other "more important" parameters (e.g., route lengths, population densities, accident rates, durations of truck stops, and cask surface dose rates), distributions of parameter values were constructed that reflected the likely real-world range and frequency of occurrence of the value of each parameter. Next, 200 sets of parameter values were constructed by sampling these distributions using a structured Monte Carlo sampling technique called Latin Hypercube Sampling (LHS) [E-12, E-22]. This procedure generated one set of 200 parameter values for spent fuel transportation by truck and a second set for transportation by rail. Each set included parameter values for 200 representative highway or railway routes that spanned the length and breadth of the continental United States but had no specific origins or destinations.

By taking all possible combinations of the single set of central estimate values for the "less important" RADTRAN input parameters, the 200 sets of other "more important" truck parameter values, and the 19 sets of representative truck accident severity and release fraction values, input for 3800 single-pass RADTRAN 5 truck spent fuel transportation calculations was developed for each generic truck cask. Similarly, by taking all possible combinations of the set of "less important" parameter values, the 200 sets of other "more important" rail parameter values, and

the 21 sets of representative rail accident severity and release fraction values, input for 4200 single-pass RADTRAN 5 rail spent fuel transportation calculations was developed. Finally, application of standard statistical methods to the results of these 3800 truck or 4200 rail transportation calculations then allowed the results to be displayed as Complementary Cumulative Distribution Functions (CCDFs) and estimates of the expected (mean) result for radiological consequences (e.g., population dose) to be calculated.

Results

Seven sets of RADTRAN calculations are described in the body of this report. Each set of calculations developed estimates of the radiological consequences and risks that are associated with the shipment of power reactor spent fuel. Two types of consequences and risks were estimated, those that are associated with the occurrence of accidents during the shipment and those associated with shipments that take place without the occurrence of accidents. The calculations examine four generic cask designs, two shipment modes, two sets of routes, and three sets of accident source terms. The four generic cask designs examined are steel-lead-steel truck and rail casks, a steel-DU-steel truck cask, and a monolithic steel rail cask. The two shipment modes are truck and rail. The two sets of routes are (a) 200 representative truck or rail routes selected by LHS sampling of route parameter distributions and (b) for each mode, the four illustrative real routes plus the NUREG-0170 shipment route. The three sets of accident source terms are the NUREG-0170 [E-1] source terms, the Modal Study source terms [E-7], and the new source terms developed by this study.

Calculational sets one and two examine spent fuel transportation by truck and rail using the 200 sets of other "more important" truck or rail input parameter values that were constructed by LHS sampling of the real-world distributions of the values of these parameters. Sets three and four examine transportation by truck and rail over four "illustrative" truck or rail routes and the NUREG-0170 truck or rail route. Comparison of the results of these illustrative route calculations to the results obtained for the calculations that used the 200 representative routes showed that the results obtained for the "illustrative" real routes fall within the range of the results obtained for the representative routes. Set five examined the influence of NUREG-0170 exposure pathway modeling on accident consequence predictions. And sets six and seven compared the accident consequence predictions developed using the accident source terms developed by this study to those developed using the accident source terms developed by the Modal Study [E-7] and NUREG-0170 [E-1].

The full study provides results for transport of PWR and BWR spent fuel by truck or rail in four generic casks. In this Executive Summary, results are presented only for the six RADTRAN 5 calculations that examined transport of PWR spent fuel in steel-lead-steel truck or rail spent fuel casks. These results are typical of those obtained for BWR spent fuel and/or transportation in other generic casks. Each of the six calculations discussed here used the set of "less important" values for all RADTRAN 5 input parameters assigned central estimate values. Each calculation used the other "more important" truck or rail parameter values, that were generated by LHS sampling. Thus, these calculations differed only in the source terms used (i.e., NUREG-0170 source terms, Modal Study source terms, or the source terms developed by this study), and the set of exposure pathways modeled (the calculations that used Modal study source terms or the source

terms developed by this study examined all exposure pathways; the calculations that used NUREG-0170 source terms calculated exposures only for the inhalation pathway because only the inhalation pathway was examined by the NUREG-0170 study).

Table E.1 compares the NUREG-0170 incident-free truck and rail doses to the incident-free doses developed by this study. Because the NUREG-0170 doses were developed for all of the spent fuel shipments expected to occur in 1975 or 1985, doses for single shipments are calculated by dividing the 1975 or 1985 doses by the number of spent fuel shipments that NUREG-0170 estimated would occur during these years. Table E.1 shows that for single shipments the sum of the other incident-free doses (i.e., crew, on-link, off-link, and stop doses) developed by this study for spent fuel transport by truck with two-person crews is about one-fourth of the sum of the corresponding NUREG-0170 truck doses. It also shows that the sum of this study's incident-free doses for transport by rail is about two-thirds of the sum of the corresponding NUREG-0170 rail doses. The similarity of these incident-free results is not surprising, because both studies assume that the surface dose rates of spent fuel transportation casks are somewhat below the regulatory limit and both use along-route population densities and the population densities at rest stops that are not very different. Table E-1 also shows that shipment of the 1994 spent fuel inventory at a constant number of shipments per year over 30 years leads to average yearly population doses for transport by truck and rail that are respectively about half and one-tenth of the NUREG-0170 estimates for 1985.

Table E.1 Comparison of NUREG-0170 Incident-Free Doses (person-rem) to the Incident-Free Doses Developed by this Study[a]

Study	Year	Mode	Number of Shipments	Doses (person-rem)			
				Multiple Shipments		Single Shipment	
				Hand/Stor[b]	Other[c]	Hand/Stor[b]	Other[c]
NUREG-0170	1975	Truck	254	52.06	41.74	0.205	0.164
NUREG-0170	1985	Truck	1530	313.6	251.4	0.205	0.164
This Study		Truck	2489[d]	Not Calc.[e]	110	Not Calc.[e]	0.0441
NUREG-0170	1975	Rail	17	7.227	0.553	0.425	0.0325
NUREG-0170	1985	Rail	652	277.4	20.60	0.425	0.0316
This Study		Rail	100.5[d]	Not Calc.[e]	2.040	Not Calc.[e]	0.0203

a. Modal Study incident-free doses are not presented because the Modal Study did not perform any consequence calculations.
b. Handler + storage doses.
c. Crew + on-link + off-link + stop doses.
d. Average number of shipments per year required to ship the full 1994 spent fuel inventory over 30 years in steel-lead-steel truck and rail casks.
e. NUREG-0170 assumed that intermodal cask transfers and temporary storage of the cask would occur during cask shipments; this study assumed that they would not occur and therefore did not calculate any handling/storage doses.

Figures E.1 and E.2 present the CCDFs generated by these calculations. CCDFs are plots of the chance of obtaining a result equal to or larger than the consequence value that corresponds to the probability. For example, in Figure E.1, the NUREG-0170 Model I CCDF shows that the probability per shipment of an accident that leads to a population dose ≥ 10 person-rem is estimated to be 10^{-4} (0.0001). Figures E.1 and E.2 both present four CCDFs: the NUREG-0170 Model I CCDF, the NUREG-0170 Model II CCDF, the Modal Study CCDF, and the CCDF developed by this study. In each figure, the highest lying CCDF is the NUREG-0170 Model I CCDF, the next highest is the NUREG-0170 Model II CCDF, the next is the Modal Study CCDF, and the lowest lying CCDF is the CCDF developed by this study.

The area under each CCDF represents the expected risk from a single shipment of spent fuel for the calculation that generated the CCDF. Table E.2 presents these expected accident population dose risks. Thus, Table E.2 allows the expected dose risks calculated using the new truck and train accident source terms developed by this study to be compared to those calculated using NUREG-0170 Model I and Model II and Modal Study source terms. Because source term magnitudes directly reflect spent fuel and cask response to accidents, the results presented in this table and in Figures E.1 and E.2 display the effects of the different treatments of spent fuel and spent fuel casks made by each study.

Table E.2 Comparison of Mean Accident Population Dose Risks (person-rem) Calculated Using NUREG-0170 Model I and Model II Source Terms and Modal Study Source Terms to Those Calculated Using the Source Terms Developed by this Study

Study	Truck Accidents	Train Accidents
NUREG-0170 Model I[a]	1.3E-2	1.9E-2
NUREG-0170 Model II[a]	7.7E-4	4.9E-4
Modal Study[b]	1.3E-4	1.9E-3
This Study[b]	8.0E-7	9.4E-6

a. Calculated assuming exposures only by the inhalation pathway.
b. Calculated assuming exposures by all exposure pathways.

Comparison of the results presented in Tables E.1 and E.2 shows that the ratio of this study's estimates of single shipment mean incident-free dose risks to this study's single shipment mean accident dose risks is about are $5x10^4$ for truck and about $2x10^3$ for rail. Thus, single shipment incident-free dose risks, which are quite small, greatly exceed single shipment accident dose risks.

Inspection of Table E.2 shows that the expected accident population dose risks stand in the following order and have the following relative magnitudes when normalized to the NUREG-0170 Model I result:

Truck Accidents: NUREG-0170 Model I (1.0) > NUREG-0170 Model II (0.06) > Modal Study (0.01) > This Study (0.00006)

Rail Accidents: NUREG-0170 Model I (1.0) > Modal Study (0.1) > NUREG-0170 Model II (0.03) > This Study (0.0005)

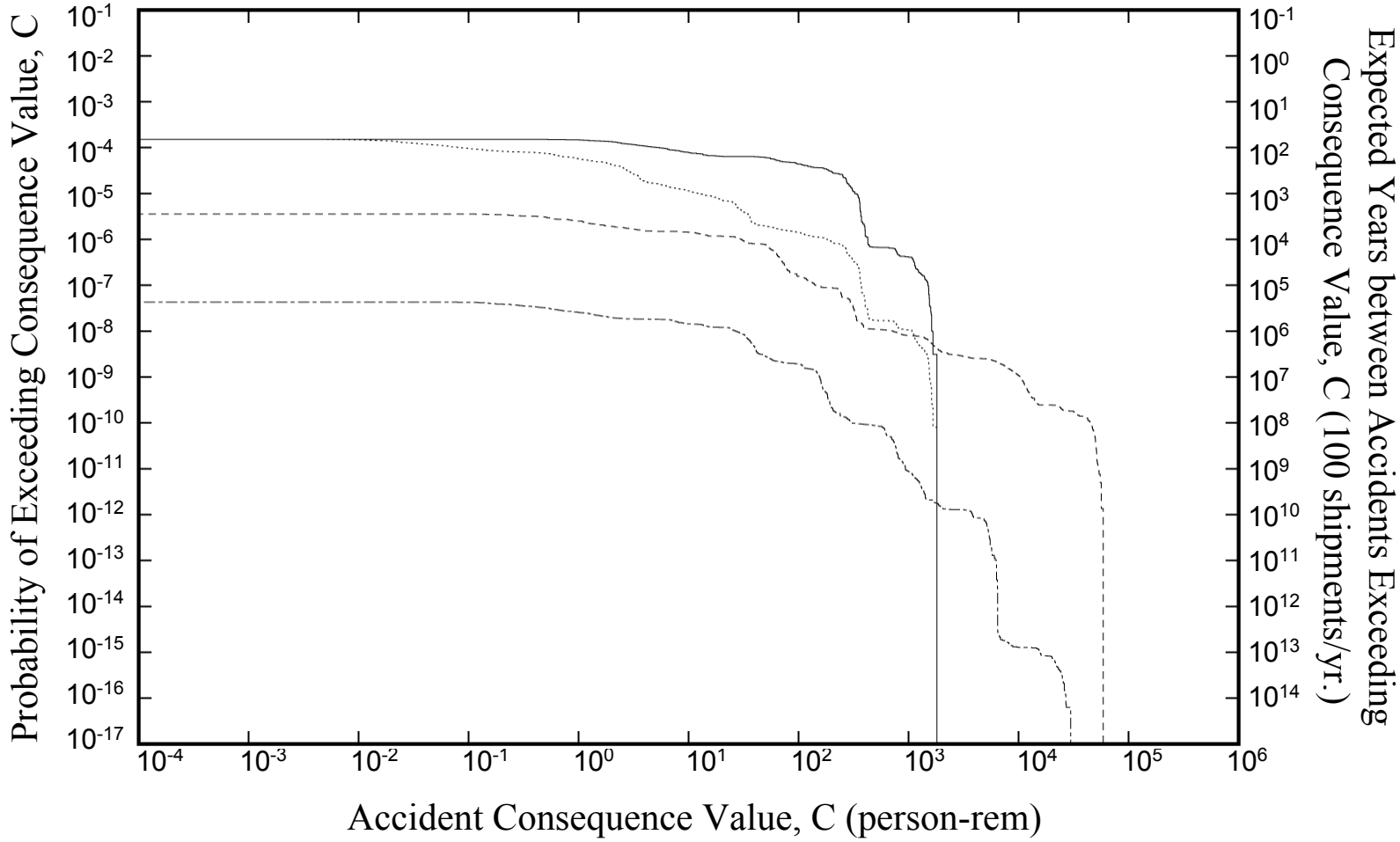

Figure E.1 Mean truck accident population dose risk CCDFs for calculations that compared the source terms developed by NUREG-0170, the Modal Study, and this study. Each RADTRAN 5 calculation assumed transport in a steel-lead-steel truck cask over each of the 200 representative truck routes and each calculation generated results for all of the 19 representative truck accident source terms.

NUREG-0170 accident release inventory, NUREG-0170 Model I release fractions, only inhalation pathways
NUREG-0170 accident release inventory, NUREG-0170 Model II release fractions, only inhalation pathways
PWR inventory, 20 Modal Study source terms, all exposure pathways
PWR inventory, 19 truck accident source terms developed for this study, all exposure pathways

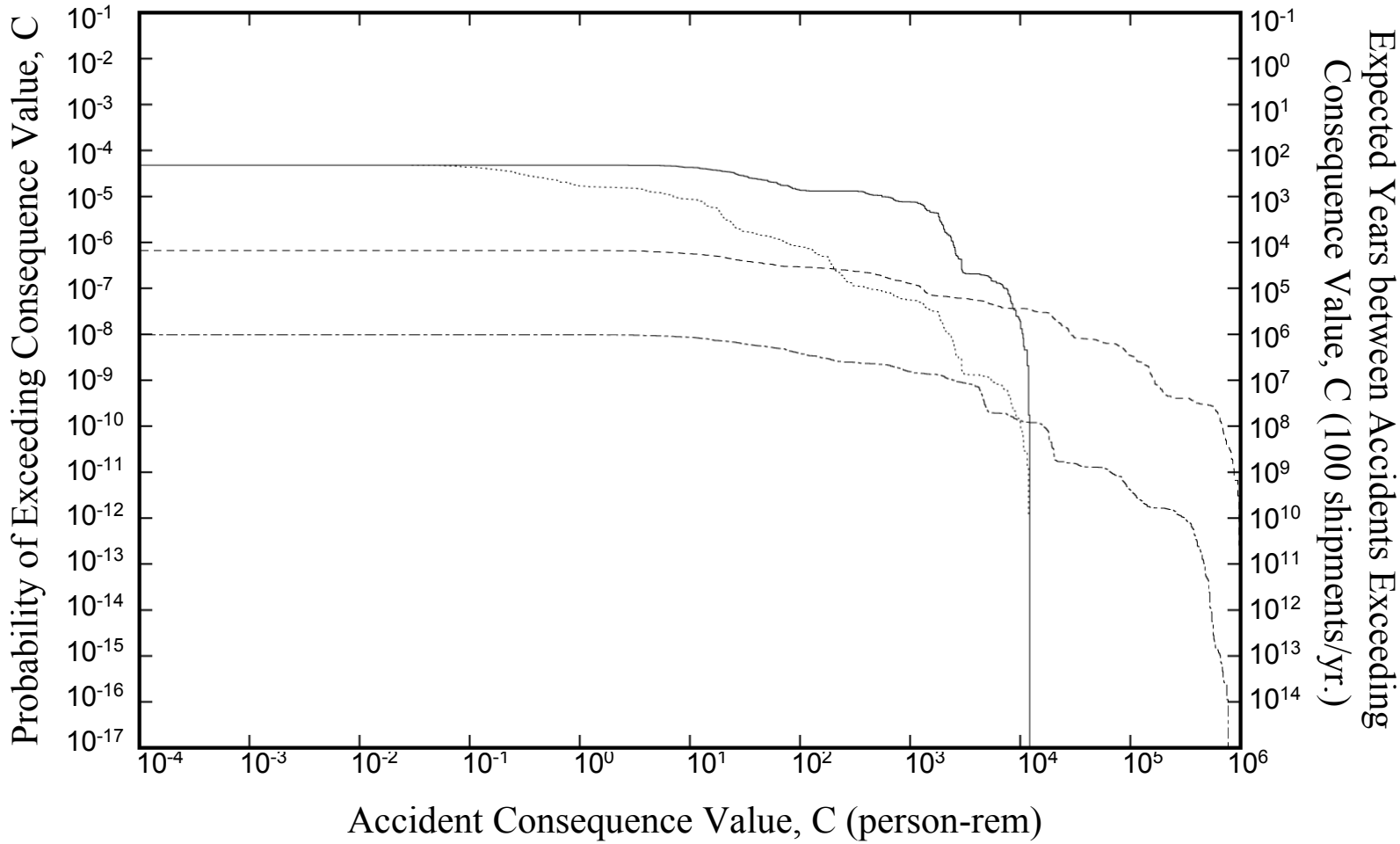

Figure E.2 Mean rail accident population dose risk CCDFs for calculations that compared the source terms developed by NUREG-0170, the Modal Study, and this study. Each RADTRAN 5 calculation assumed transport in a steel-lead-steel rail cask over each of the 200 representative rail routes and each calculation generated results for all of the 21 representative rail accident source terms.

- **NUREG-0170 accident release inventory, NUREG-0170 Model I release fractions, only inhalation pathways**
- **NUREG-0170 accident release inventory, NUREG-0170 Model II release fractions, only inhalation pathways**
- **PWR inventory, 20 Modal Study source terms, all exposure pathways**
- **PWR inventory, 19 truck accident source terms developed for this study, all exposure pathways**

The relative ordering of these accident results is entirely consistent with the assumptions made by each study regarding the probability of radionuclide leakage from the cask during transportation accidents and the magnitude of the source terms generated by accidents of differing severities. Because both Model I and Model II in NUREG-0170 assumed that spent fuel casks might release a portion of their contents when subjected to the loads that characterize minor accidents, the fraction of all truck and train accidents predicted by these models to cause releases is very large and extremely conservative. Similarly, because the NUREG-0170 Model I assumed that all cask leaks led to the release of the entire NUREG-0170 accident inventory (the largest amount of radioactive material expected to be released during a severe accident), the mean accident population doses calculated using the NUREG-0170 Model I for truck and rail accidents are quite large. When, as was done by the Modal Study, cask failure and thus source term probabilities and magnitudes are estimated from the response of the cask shell to mechanical and thermal loads, both source term probabilities and most source term magnitudes decrease. Consequently, relative to the NUREG-0170 Model I result, mean accident population dose risks for rail and truck are decreased respectively by one and two orders of magnitude. When, as was done by this study, cask release and thus source term probabilities and magnitudes are estimated by examining the response of cask closures and spent fuel rods to impact loads and the burst rupture of spent fuel rods due to heating by fires, cask release is found to be even less likely and retention of particles and condensable vapors by deposition onto cask interior surfaces is found to be substantial. Accordingly, source term probabilities and most source term magnitudes, except those for the most severe accidents examined, decrease further. Consequently, relative to the Modal Study result, expected (mean) accident population dose risks for both rail and truck are each further decreased by about two orders of magnitude.

Source term magnitudes for the most severe accidents examined by the Modal Study and this study are larger than the largest source term magnitude postulated in NUREG-0170. They are larger because the product of the cask inventory and the largest accident release fractions developed by this study is larger than the largest source term examined by NUREG-0170. Nevertheless, although the largest source terms developed by the analyses performed by the Modal Study and this study are larger than the largest NUREG-0170 source term, the accident risks posed by these source terms are substantially smaller because these source terms are so very improbable.

Conclusions

The results described in detail in the body of this report lead to the following conclusions:

- The single cask truck shipment expected incident-free population doses developed by this study are about one-quarter of those in NUREG-0170.
- The single cask rail shipment expected incident-free population doses developed by this study are about two-thirds of those in NUREG-0170.
- The use of very conservative cask failure criteria in NUREG-0170 caused its estimates of the fraction of all accidents that release radioactive materials to be much too large and thus very conservative.

- The NUREG-0170 estimate of the largest source term that might be released from a failed spent fuel cask during an unusually severe transportation accident is significantly lower than the largest source terms calculated using Modal Study release fractions or the release fractions developed by this study. However, the risks associated with these source terms are lower than the risk of the largest NUREG-0170 source term because these source terms are so very improbable.
- The source terms developed by the Modal Study and by this study, which reflect the complexities of rod failure and cask response to transportation accident impact and thermal loads, yield estimates of expected (mean) spent fuel transportation accident population doses that are orders of magnitude smaller than those developed by the NUREG-0170 study.

Overall, the results of this study confirm the validity of the NUREG-0170 estimates of spent fuel incident-free population doses. The results also show that the NUREG-0170 estimates of spent fuel accident population dose risks were very conservative, as was believed to be true when NUREG-0170 was published [E-23].

References

[E-1] "Final Environmental Statement on the Transportation of Radioactive Material by Air and Other Modes," NUREG-0170, U.S. Nuclear Regulatory Commission, Washington, DC, December 1977.

[E-2] J. M. Taylor and S. L. Daniel, "RADTRAN: A Computer Code to Analyze Transportation of Radioactive Material," SAND76-0243, Sandia National Laboratories, Albuquerque, NM, April 1977.

[E-3] Ref. [E-1], p. 5-20.

[E-4] Ref. [E-1], p. 5-22.

[E-5] Ref. [E-1], p. 5-21.

[E-6] Ref. [E-1], p. 5-23.

[E-7] L. E. Fischer, et al., "Shipping Container Response to Severe Highway and Railway Accident Conditions," NUREG/CR-4829, Lawrence Livermore National Laboratory, Livermore, CA, February 1987.

[E-8] K. S. Neuhauser and F. L. Kanipe, "RADTRAN 5, Technical Manual," Sandia National Laboratories, Albuquerque, NM (in preparation, draft available on request).

[E-9] K. S. Neuhauser and F. L. Kanipe, "RADTRAN 5, User Guide," Sandia National Laboratories, Albuquerque, NM (draft available on the RADTRAN web site).

[E-10] G. S. Mills, G. S., K. S. Neuhauser, and F. L. Kanipe, "RADTRAN 4 Truck Accident Risk Sensitivity Analysis," Proceedings of Waste Management 95, WM Symposia, Tucson, AZ, 1995.

[E-11] G. S. Mills and K. S. Neuhauser, "Sensitivity Analysis for RADTRAN 4 Input Parameters," 88th Annual Meeting of the Air & Waste Management Association., San Antonio, TX, 1995.

[E-12] G. S. Mills, et al., "Application of Latin Hypercube Sampling to RADTRAN 4 Truck Accident-Risk Sensitivity Analysis," Proceedings of the 11th International Conference on the Packaging and Transportation of Radioactive Materials (PATRAM '95), IAEA, Vol. 4, p. 705, 1995.

[E-13] State Soil Graphics (STATSGO) Data Base, available on the Internet at ftp.ftw.nrcs.usda.gov/pub/statsgo.

[E-14] ARC/INFO Coverages and Arc View Project, K. C. Bayer Digital Map of the U.S., purchased from Geologic Data Systems, Inc., 1600 Emerson St., Denver, CO 80218.

[E-15] T. L. Sanders, et al., "A Method for Determining the Spent-Fuel Contribution to Transport Cask Containment Requirements, Appendix III, Spent Fuel Response to Transport Environments," SAND90-2406, Sandia National Laboratories, Albuquerque, NM, November 1992.

[E-16] R. A. Lorenz, et al., "Fission Product Release from Highly Irradiated LWR Fuel," NUREG/CR-0722, Oak Ridge National Laboratory, Oak Ridge, TN, February 1980.

[E-17] R. A. Lorenz, et al., "Fission Product Release from Simulated LWR Fuel," NUREG/CR-0274, Oak Ridge National Laboratory, Oak Ridge, TN, July 1978.

[E-18] R. A. Lorenz, et al., "Fission Product Source Terms for the LWR Loss-of-Coolant Accident," NUREG/CR-1288, Oak Ridge National Laboratory, Oak Ridge, TN, July 1980.

[E-19] R. M. Summers, et al., "MELCOR 1.8.0: A Computer Code for Nuclear Reactor Severe Accident Source Term and Risk Assessment Analyses," NUREG/CR-5531, SAND90-0364, Sandia National Laboratories, Albuquerque, NM, January 1991.

[E-20] J. L. Sprung, et al., "Data and Methods for the Assessment of the Risks Associated with the Maritime Transport of Radioactive Materials: Results of the SeaRAM Program," SAND97-2222, Sandia National Laboratories, Albuquerque, NM, August 1997.

[E-21] "Shipping and Storage Cask Data for Commercial Spent Nuclear Fuel," JAI Corp., July 1996.

[E-22] G. D. Wyss and K. H. Jorgensen, "A User's Guide to LHS: Sandia's Latin Hypercube Sampling Software," SAND98-0210, Sandia National Laboratories, Albuquerque, NM, 1998.

[E-23] Ref. [E-1], p. ix.

Page intentionally left blank

1. INTRODUCTION

1.1 NUREG-0170

In September of 1977, the Nuclear Regulatory Commission (NRC) issued a generic environmental impact statement (EIS), titled "Final Environmental Statement on the Transportation of Radioactive Material by Air and Other Modes," NUREG-0170, that covered the transport of all types of radioactive material by all transport modes (road, rail, air, and water) [1-1]. That EIS provided the regulatory basis for continued issuance of general licenses for transportation of radioactive material under 10 CFR 71. Based in part on the findings of NUREG-0170, NRC staff concluded (1) that "the average radiation dose to the population at risk from normal transportation is a small fraction of the limits recommended for members of the general public from all sources of radiation other than natural and medical sources and is a small fraction of natural background dose" and (2) that "the radiological risk from accidents in transportation is small, amounting to about one-half percent of the normal transportation risk on an annual basis" [1-2]. In addition, the NRC Commission concluded that "present regulations are adequate to protect the public against unreasonable risk from the transport of radioactive materials" (46 FR 21629, April 13, 1981) and stated that "regulatory policy concerning transportation of radioactive materials be subject to close and continuing review."

1.2 NUREG-0170 Spent Fuel Transportation Risks

NUREG-0170 estimated the radiation doses and latent cancer fatalities that might be associated with the transport of 25 different radioactive materials by plane, truck, train, and ship or barge. The 25 materials were chosen to encompass 90 percent of all shipments in the United States and 90 percent of the activity contained in shipments. The estimates were made using Version 1 of the RADTRAN code (RADTRAN 1) [1-3], which was developed specifically to support the performance of the NUREG-0170 study.

One of the 25 radioactive materials examined by NUREG-0170 was spent nuclear power reactor fuel. For spent fuel shipments that occur without accidents (incident-free transport), radiation doses were estimated for members of the general public who would be exposed to radiation, for example, because they lived near the shipment route, and also for workers (e.g., crew, handlers, inspectors). Release of radioactive materials from spent fuel to the environment as a result of transportation accidents, the probability of these releases, and the latent cancer fatalities that such releases might cause were also estimated.

Spent fuel transport risks were estimated for shipment by truck and by train over a generic highway and a generic rail route [1-4]. Table 1.1 describes attributes of these two generic routes. Radiological consequences (population doses for incident-free transport and expected numbers of latent cancer fatalities for transportation accidents) were estimated for spent fuel shipments expected to occur during 1975 and 1985. Tables 1.2 and 1.3 respectively present the incident-free and accident consequences estimated for these spent fuel shipments.

Table 1.1 NUREG-0170 Spent Fuel Truck and Train Route Data

Parameter	Truck Route	Rail Route
Route Length (km)	2530	1210
Fraction Urban	0.05	0.05
Fraction Suburban	0.05	0.05
Fraction Rural	0.9	0.9
Population Densities (people km^{-2})		
Urban	3861	3861
Suburban	719	719
Rural	6	6
Shipments per year (single cask)		
1975	254	17
1985	1530	652

Table 1.2 NUREG-0170 Annual Incident-Free Spent Fuel Transportation Doses (person-rem)

Incident-Free Shipment Doses	Truck		Train	
	1975	1985	1975	1985
Crew	31.3	188	0.68	2.6
Handlers	50.8	306	6.8	261
Storage	1.26	7.6	0.427	16.4
General Public				
Off-Link[a]	3.8	22.9	0.175	6.69
On-Link[b]	1.88	11.3	0.222	8.53
Stops[c]	4.82	29.0	0.089	3.44
Total Population Dose	93.8	565	7.78	298

a. Residents living by the transport route.
b. Travelers exposed while traveling in cars, buses, or trains.
c. Travelers exposed at rest stops.

Table 1.3 Expected (Mean) Latent Cancer Fatalities Predicted in NUREG-0170 to be Caused by Truck and Train Accidents that Occur during Spent Fuel Transport

Year	Release Model	Truck	Train	Truck + Train
1975	I	0.047	0.021	0.068
1985	I	0.29	0.8	1.09
1975	II	NA	NA	0.0000356
1985	II	NA	NA	0.000422

For calculations of radiological consequences that might be caused by accidents, accidents were divided into eight categories (Categories I through VIII) of increasing severity. Because "little information relating the response of packages to accident environments" [1-5] was available in 1975 for spent fuel and other highly radioactive materials shipped in Type B packages, release of radioactivity as a result of accidents was examined using two release models. The first model, Model I [1-6], assumed [1-7] that "zero release occurs up to the regulatory test level and that the packaging fails catastrophically in all environments that exceed that level." The amounts of each radionuclide that were assumed [1-8] to be released to the environment by this "catastrophic" failure are presented in Table 1.4. Thus, Model I assumed that the radioactive release specified in Table 1.4 would take place whenever a Type B spent fuel package was subjected to mechanical or thermal loads in excess of the mechanical and thermal loads encountered during package certification tests [1-9]. Because the Model I cask release behavior was considered to be unrealistic, a second release model (Model II) was formulated. In Model II, for accidents that exceed the regulatory test level, release fractions increased more gradually with accident severity [1-10], becoming equal for catastrophic accidents to the release specified for all severe accidents by Model I.

Table 1.5 shows that the Model I and Model II release fractions are used for both truck and train accidents. Model I and Model II release fractions are the same for accident categories I, II, V, VI, VII, and VIII and differ only for categories III, and IV. Finally, Table 1.3 shows that accident consequences are substantially decreased if, as is done in Model II, release is assumed to increase with increasing accident severity.

Table 1.4 Inventory (Ci) Assumed in NUREG-0170 to be Released to the Environment from a Type B Spent Fuel Cask as a Result of an Accident

Fission Products	Truck Cask	Rail Cask
Kr-85	1700	10,900
I-131	0.022	0.138
Volatiles as Cs-137	200	1280

1.3 Need for Reevaluation of NUREG-0170 Spent Fuel Transportation Risks

While NUREG-0170 was an important analysis that delineated transportation risks in the context of the information available at that time, its results were developed using rather simple models and limited data. In the interim, there has been significant growth in analytical capabilities and data. While the casks and the specific routes for spent fuel movements have not yet been designated, it is clear that the generic cask and routes used in NUREG-0170 are now less than typical. For example, spent fuel may soon be shipped in the dual-purpose or multi-purpose canisters (MPCs) from commercial reactors to Interim Spent Fuel Storage Installations and/or Centralized Storage Facilities in addition to shipment to a permanent geologic repository. In fact, the Office of Nuclear Material Safety and Safeguards (NMSS) has received several applications for dual-purpose (storage and transport) spent fuel casks, and additional applications

Table 1.5 NUREG-0170 Model I and Model II Severity and Release Fractions for Spent Fuel Transport by Truck and Rail

Accident Category	Severity Fractions[a]		Release Fractions	
	Models I and II		Truck and Rail	
	Truck	Rail	Model I	Model II
I	0.55	0.50	0.0	0.0
II	0.36	0.30	0.0	0.0
III	0.07	0.18	1.0	0.01
IV	0.016	0.018	1.0	0.1
V	0.0028	0.0018	1.0	1.0
VI	0.0011	1.3×10^{-4}	1.0	1.0
VII	8.5×10^{-5}	6.0×10^{-5}	1.0	1.0
VIII	1.5×10^{-5}	1.0×10^{-5}	1.0	1.0

a. Fraction of accidents that fall into this severity range

are expected in the near future. In addition, many improvements have been made to the risk assessment models implemented in the RADTRAN code since the initial version of that code was used to estimate spent fuel transportation risks for NUREG-0170, and a major study of the response of spent fuel casks to severe transportation accidents, "Shipping Container Response to Severe Highway and Railway Accident Conditions," NUREG/CR-4829, often called the Modal Study, has been published [1-11].

Because new data and analytical methods were now available to apply to the analysis of power reactor spent fuel transportation risks, and because spent fuel is likely to be shipped to facilities along routes and in casks not specifically examined by NUREG-0170, the NRC decided the conclusions reached in NUREG-0170 should be reexamined in order to determine if the risks of the spent fuel shipments that are expected to take place during the next few decades are bounded by the risk estimates published in NUREG-0170. Accordingly, this report documents the methodology and results of a reevaluation of the risks of transporting spent fuel from commercial reactor sites to possible interim storage sites and/or permanent geologic repositories.

1.4 Study Objectives

This study had three objectives:

- Estimation of the radiological and non-radiological, routine and accident, transportation risks associated with the anticipated spent fuel shipments and determination of whether those risks are bounded by the estimates and projections of spent fuel shipment risks published in 1977 in NUREG-0170.

- Examination of any outstanding spent fuel transportation issues or environmental concerns not resolved by NUREG-0170 and the Modal Study.

- Documentation of the approach, data, and computational methods used to reestimate spent fuel transportation risks in detail sufficient to allow other transportation experts to fully understand the analyses performed, and preparation of a summary of the results in a form accessible to concerned citizens.

1.5 General Approach

The risks associated with the transport of spent fuel were estimated using Version 5 of the RADTRAN code [1-12, 1-13]. As in NUREG-0170, risks were estimated for incident-free transport and also for transportation accidents severe enough to cause radioactive material to be released from the cask to the environment.

Based on prior sensitivity studies [1-14, 1-15, 1-16], RADTRAN 5 input parameters were divided into three groups:

- Source term parameters (accident severity fractions and their corresponding accident release fractions),

- Other "more important" parameters that strongly influence RADTRAN estimates of radiation dose (for values within their likely range), and

- "Less important" parameters which have little impact on estimates of radiation dose (for values within their likely range).

For each of the "less important parameters," e.g., breathing rate, central (best) estimate values were selected. For each of the more important parameters (e.g., route lengths, population densities, accident rates, durations of truck stops, and cask surface dose rates), distributions of parameter values were constructed that reflected the likely real-world range and frequency of occurrence of the value of each parameter. Next, for both truck and rail analyses, 200 sets of the other "more important" parameter values were constructed by sampling these distributions using a structured Monte Carlo sampling technique called Latin Hypercube Sampling [1-16, 1-17].

For the source term parameters, review of studies of actual transportation accidents, in particular the Modal Study [1-11], allowed representative sets of truck and train accidents and their impact and fire environments to be defined. This analysis developed 19 representative truck accidents and 21 representative train accidents. Severity fraction and release fraction values were estimated for each representative accident.

Severity fraction values were developed by a review of the accident event trees, accident speed distributions, and accident fire distributions that were published in the Modal Study [1-11]. New event tree frequencies of occurrence of route wayside surfaces (e.g., hard rock; concrete, soft rock, and hard soil; soft soil; water) were developed using Department of Agriculture data [1-18] and Geographic Information System (GIS) methods of analysis [1-19].

Release fractions were estimated as the product of (a) the fraction of the rods in the cask that are failed by the severe accident, (b) the fraction of each class of radioactive materials (e.g., particulates) that might escape from a failed spent fuel rod to the cask interior, and (c) the

fraction of the amount of radionuclides released to the cask interior that is expected to escape from the cask to the environment. Rod failure during high speed collision accidents was estimated by scaling rod strains calculated for low speed impacts and then comparing the scaled rod strains to a strain failure criterion [1-20]. Heating of the cask by a fire to rod burst rupture temperatures was assumed to fail all unfailed rods. Rod-to-cask release fractions were estimated by review of literature data, especially the experimental results of Lorenz [1-21, 1-22, 1-23]. Cask-to-environment release fractions were based on MELCOR fission product transport calculations [1-24] that estimated the dependence of these release fractions on the size (cross-sectional area) of the cask failure that allows the release to the environment to occur.

Specifications for two generic truck and two generic rail spent fuel casks were developed from literature data [1-25]. Cask damage (e.g., seal leak areas) during severe collisions was estimated from the results of finite element calculations that modeled impacts onto an unyielding surface at various impact speeds. Unyielding surface impact speeds were converted to equivalent impact speeds onto yielding surfaces (e.g., soft rock) by considering the energy that would be absorbed by the yielding surface, increasing the energy of the unyielding surface calculation by that amount, and converting the new total energy to an initial impact speed. Seal leakage and rod burst rupture temperatures due to heating during fires were estimated from literature data. The durations of engulfing optically dense fires needed to produce large seal leak areas and rod failure by burst rupture were estimated by performing one-dimensional heat transport calculations.

By taking all possible combinations of the single set of central estimate values for the "less important" RADTRAN input parameters, the 200 sets of other "more important" truck parameter values, and the 19 sets of representative truck accident severity and release fraction values, input for 3800 single-pass RADTRAN 5 truck spent fuel transportation calculations was developed for each generic truck cask. Similarly, by taking all possible combinations of the set of "less important" parameter values, the 200 sets of other "more important" rail parameter values, and the 21 sets of representative rail accident severity and release fraction values, input for 4200 single-pass RADTRAN 5 rail spent fuel transportation calculations was developed. Application of standard statistical methods to the results of these 3800 truck or 4200 rail transportation calculations then allowed the results to be displayed as Complementary Cumulative Distribution Functions (CCDFs) and estimates of the expected (mean) result for radiological consequences (e.g., population dose) to be calculated. Finally, the results of these RADTRAN 5 calculations were compared to the results of RADTRAN 5 calculations that used the spent fuel source terms (severity fractions and release fractions) developed by the NUREG-0170 study [1-1] and those developed by the Modal Study [1-11] and differences in predicted risks are discussed.

1.6 References

[1-1] "Final Environmental Statement on the Transportation of Radioactive Material by Air and Other Modes," NUREG-0170, U.S. Nuclear Regulatory Commission, Washington, DC, December 1977.

[1-2] Ref. [1-1], Summary and Conclusions, p. vii.

[1-3] J. M. Taylor and S. L. Daniel, "RADTRAN: A Computer Code to Analyze Transportation of Radioactive Material," SAND76-0243, Sandia National Laboratories, Albuquerque, NM, April 1977.

[1-4] Ref. [1-1], Vol.1, pp. 1-17, 4-16, 4-23, A-13, and E-4.

[1-5] Ref. [1-1], p. 5-20.

[1-6] Ref. [1-1], p. 5-22.

[1-7] Ref. [1-1], p. 5-21.

[1-8] Ref. [1-1], p. A-14.

[1-9] Code of Federal Regulations, Volume 10, Part 71.73 (10 CFR 71.73).

[1-10] Ref. [1-1], p. 5-23.

[1-11] L. E. Fischer, et al., "Shipping Container Response to Severe Highway and Railway Accident Conditions," NUREG/CR-4829, Lawrence Livermore National Laboratory, Livermore, CA, February 1987.

[1-12] K. S. Neuhauser and F. L. Kanipe, "RADTRAN 5, Technical Manual," Sandia National Laboratories, Albuquerque, NM (in preparation, draft available on request).

[1-13] K. S. Neuhauser and F. L. Kanipe, "RADTRAN 5, User Guide," Sandia National Laboratories, Albuquerque, NM (draft available on the RADTRAN web site).

[1-14] G. S. Mills, K. S. Neuhauser, and F. L. Kanipe, "RADTRAN 4 Truck Accident Risk Sensitivity Analysis," Proceedings of Waste Management 95, WM Symposia, Tucson, AZ, 1995a.

[1-15] G. S. Mills and K. S. Neuhauser, "Sensitivity Analysis for RADTRAN 4 Input Parameters," 88th Annual Meeting of the Air & Waste Management Assoc., San Antonio, TX, 1995.

[1-16] G. S. Mills, et al., "Application of Latin Hypercube Sampling to RADTRAN 4 Truck Accident-Risk Sensitivity Analysis," Proceedings of the 11th International Conference on the Packaging and Transportation of Radioactive Materials (PATRAM '95), IAEA, Vol. 4, p. 705, 1995.

[1-17] G. D. Wyss and K. H. Jorgensen, "A User's Guide to LHS: Sandia's Latin Hypercube Sampling Software," SAND98-0210, Sandia National Laboratories, Albuquerque, NM 1998.

[1-18] State Soil Graphics (STATSGO) Data Base, available on the Internet at ftp.ftw.nrcs.usda.gov/pub/statsgo.

[1-19] ARC/INFO Coverages and Arc View Project, K. C. Bayer Digital Map of the U.S., purchased from Geologic Data Systems, Inc., 1600 Emerson St., Denver, CO 80218.

[1-20] T. L. Sanders, et al., "A Method for Determining the Spent-Fuel Contribution to Transport Cask Containment Requirements, Appendix III, Spent Fuel Response to Transport Environments," SAND90-2406, Sandia National Laboratories, Albuquerque, NM, November 1992.

[1-21] R. A. Lorenz, et al., "Fission Product Release from Highly Irradiated LWR Fuel," NUREG/CR-0722, Oak Ridge National Laboratory, Oak Ridge, TN, February 1980.

[1-22] R. A. Lorenz, et al., "Fission Product Release from Simulated LWR Fuel," NUREG/CR-0274, Oak Ridge National Laboratory, Oak Ridge, TN, July 1978.

[1-23] R. A. Lorenz, et al., "Fission Product Source Terms for the LWR Loss-of-Coolant Accident," NUREG/CR-1288, Oak Ridge National Laboratory, Oak Ridge, TN, July 1980.

[1-24] J. L. Sprung, et al., "Data and Methods for the Assessment of the Risks Associated with the Maritime Transport of Radioactive Materials: Results of the SeaRAM Program," SAND97-2222, Sandia National Laboratories, Albuquerque, NM, August 1997.

[1-25] "Shipping and Storage Cask Data for Commercial Spent Nuclear Fuel," JAI Corp., July 1996.

2. METHODOLOGY OVERVIEW AND REPORT ROADMAP

2.1 Introduction

NUREG-0170 [2-1] documents estimates of the radiological consequences and risks associated with the shipment by truck, train, plane, or barge of about 25 different radioactive materials, including power reactor spent fuel. The estimates were calculated using Version 1 of the RADTRAN code [2-2], which was developed for the NRC by Sandia National Laboratories (SNL) specifically to support the conduct of the NUREG-0170 study. When the NRC asked SNL to reexamine the consequences and risks associated with the transport of spent fuel by truck and train, RADTRAN Version 5 [2-3, 2-4], the most recent version of the RADTRAN code, was the computational tool of choice.

The basic methodology employed in the RADTRAN code is widely accepted. Changes to the code are tracked by a software quality assurance plan that is consistent with American National Standards Institute guidelines. Two reviews of RADTRAN Version 4, in which the RADTRAN calculations were benchmarked against hand calculations and other codes, have been published [2-5, 2-6]. Because the models implemented in RADTRAN 5 are almost identical to those implemented in RADTRAN 4, the benchmarking results for RADTRAN 4 also apply to RADTRAN 5.

2.2 RADTRAN

The RADTRAN code calculates the radiological consequences and risks associated with the shipment of a specific radioactive material (RAM) in a specific packaging along a specific route. The code estimates consequences and risks (a) for shipments that proceed without incident, that is, for shipments during which no serious accidents occur, and (b) for accident scenarios that might occur during these shipments that could lead to a loss of package shielding or to the release of radioactive material to the environment. Radiation doses caused by shipments that take place without the occurrence of serious accidents are called "incident free." The doses and risks associated with accident scenarios are referred to as "accident consequences and accident risks, respectively."

For incident-free shipments, RADTRAN calculates the radiological doses that would be received by workers (e.g., drivers, handlers, inspectors, escorts) and by members of the general public (e.g., persons who live near the RAM transport route and travelers who pass near the RAM transport vehicle while it traverses the transport route). For each accident scenario severe enough to cause a release of radioactive material, RADTRAN estimates (a) the doses that might be received by people who reside downwind of the assumed accident location during the passage of the windborne radioactive plume and as a result of deposition of radioactive materials from that plume onto the ground, (b) the probability of the hypothesized accidental release, and (c) the radiological risks that would be caused by the release (i.e., the product of each radiological consequence and the probability of the release that causes those consequences). RADTRAN can also be used to estimate the radiation doses associated with loss of shielding accidents, that is, with accidents that do not result release of radioactive materials from the package but do cause the radiation shielding of the package to be degraded.

2.3 RADTRAN Input

To perform its calculations, RADTRAN requires values for a large number of input parameters. For many of these parameters (e.g., breathing rates, stop times), appropriate values are available in the RADTRAN User's Guide [2-4]. However, the following parameters, all of which strongly influence consequences and risks, have values that vary greatly with route, radioactive material, or packaging characteristics: (a) route lengths; (b) the fractions of those lengths that are urban, suburban, or rural; (c) the population densities and accident rates that characterize those route fractions; (d) the number of people in other vehicles traveling on the route (e) the durations of stops taken while traveling the route; (f) the weather conditions that might prevail at the time of an accident; (g) the surface dose rate of the package; (h) the amount of each radionuclide in the package inventory that might be released to the atmosphere as the result of an accident; (i) the probability of the release; and (j) the time required to conduct an evacuation should a release occur. Because each of these parameters can take on a wide range of values, representative sets of parameter values were developed for each of these parameters. The following sections discuss the more complicated development methods.

2.3.1 Route Parameters

In the summer of 1996, when this study was initiated, power reactor spent fuel was stored at 79 locations. Although DOE was required by law [2-7] to begin accepting this spent fuel in early 1998 and overseeing its shipment to temporary and/or permanent storage sites, these shipments have yet to begin because no temporary or permanent storage sites have yet been built. Because the locations of the temporary and permanent storage sites that must eventually be built are not known, this study could not examine a specific set of routes that were certain to be used whenever spent fuel shipments actually take place.

The study could have examined a few specific highway and rail routes that connect some of the sites where spent fuel is presently stored to a few sites that have been mentioned as possible interim or permanent storage site locations. However, because such a minimal set of hypothetical routes could not be shown to be representative (i.e., could not be shown to include routes with characteristics that span the full range of possible routes), a different approach to route construction was adopted.

First, six hypothetical interim storage site locations were selected. Each location selected had been mentioned at some time as a possible site for interim storage of spent fuel and each site was located in a different geographic region of the continental United States, i.e., in the northeast, north-central, northwest, southeast, south-central, and southwest portions of the country. In addition, three possible permanent repository locations (three of the nine sites that entered the Yucca Mountain down-select process [2-8]) were selected, one each in the southeast, south central, and southwest portions of the country. HIGHWAY [2-9] and INTERLINE [2-10] route calculations were then performed that developed route lengths and urban, suburban, and rural route fractions and population densities for 492 routes for each transport mode. Four hundred seventy four of these routes connect the 79 current spent fuel storage locations to each of the 6 hypothetical interim storage site locations. The remaining 18 routes connect these hypothetical interim site locations to the 3 hypothetical permanent storage site locations. These sets of 492

truck or rail routes were then substantially increased in size by adding the results of 249 HIGHWAY and 249 INTERLINE route calculations that had been developed for a prior spent fuel transportation study [2-8]. Thus, route parameter values were available or were developed for a total of 741 different truck and 741 different rail routes.

Next, for both highway and rail routes, distributions of route lengths as well as length fractions and populations densities for the urban, suburban, and rural portions of these routes were constructed using the pooled route data. Then sets of 200 highway and 200 rail routes were generated by sampling these distributions using structured Monte Carlo sampling (Latin Hypercube Sampling [2-11]) methods. Because this sample of routes was constructed by sampling distributions of route parameters based on the characteristics of 741 real truck or 741 real rail routes located throughout the length and breadth of the continental United States, they are believed to constitute a representative set of hypothetical spent fuel shipment routes, even though none of the routes constructed by sampling these route parameter distributions corresponds exactly to any specific real truck or rail route and none has a specific origin or a specific destination.

Because route segment accident rates are not calculated by HIGHWAY or INTERLINE, accident rate distributions had to be developed separately. Heavy truck accident rates on interstate highways and mainline rail accident rates were compiled by Saricks and Kvitek [2-12] for each of the 48 states in the continental United States. For truck accidents (but not train accidents), separate accident rates were reported for accidents that occurred within and outside of incorporated areas. Inspection of state population data for the unincorporated (i.e., rural) and incorporated (i.e., suburban and urban) regions of each state allowed the truck accident rates to be divided into sets of urban, suburban, and rural accident rates. The sets of suburban and rural truck accident rates developed by this procedure were large enough to support the construction of distributions. Because the set of urban accident rates was small, these rates were averaged and the resulting single average urban heavy truck accident rate was applied to all urban route segments.

Because mainline rail accident rates were not developed separately for incorporated and unincorporated areas, a single mainline rail accident rate distribution was constructed using all of the state rail accident rates reported by Saricks and Kvitek [2-12]. Accident rates selected by sampling the resulting distribution were applied to each of the rail route segments in the representative set of 200 rail routes regardless of the population density of the segment. Because mainline rail route traffic densities are determined principally by regional shipping schedules (local shipments are made by truck), they should be largely independent of local wayside population densities. Thus, the use of rail accident rates that do not vary with route segment population density is believed to be reasonable.

2.3.2 Weather Parameters

Should a spent fuel shipment be involved in an accident (a collision and/or a fire) that releases radioactive materials to the atmosphere, the radiological consequences of the accident would be determined principally by the amount released, the degree of dilution during downwind transport of the radioactive plume produced by the release, and the size of the exposed population. The

degree to which the plume is diluted during downwind transport is determined by the turbulence of the air through which the plume passes, which in turn is determined by the prevailing weather conditions. Because plume dilution is a strong function of atmospheric turbulence, RADTRAN develops accident consequences for six sets of prevailing weather conditions that correspond to the six Pasquill-Gifford atmospheric stability classes [2-13] using national average frequencies of occurrence for each of the classes.

The population exposed to significant levels of radiation is determined principally by the direction in which the wind is blowing at the time of the accident. Because accident locations cannot be predicted and, for most locations, wind speed and direction data (wind roses) would be unavailable, the probability of a specific initial wind direction could not be determined. Therefore, for accident calculations, RADTRAN assumes that all wind directions are equally probable and uses a uniform population density for each route segment selected by sampling the population density distributions developed from the HIGHWAY and INTERLINE results. Although accident consequences would be larger, when the wind is blowing from the accident site toward a small population center then when it is blowing away from that population center, the absence of wind direction data means that this effect could not be modeled. The use of uniform population densities for route segments means that the population densities of small population centers are smeared out, which ensures that the plume always encounters population no matter which way the wind is blowing, even for accidents that occur on lightly populated rural route segments. Thus, the neglect of wind direction, when combined with the use of the uniform segment population densities, is expected to yield a reasonable estimate of mean (expected) accident consequences, even for rural route segments.

2.4 Package Inventories and Surface Dose Rates

Although the surface dose rate of a package can be calculated from the package inventory and package design data, this calculation is not performed by the RADTRAN code. Instead surface dose rate and package inventory are both RADTRAN input parameters. Because they are both input parameters, a package inventory may be specified that will not generate the specified package surface dose rate. This study uses package inventories calculated by the ORIGEN code and a distribution of package surface dose rates. To be consistent with regulations, the distribution of package surface dose rates had its maximum value set equal to the regulatory limit for package surface dose rates. Then, in order to assure that accident source terms were conservative, all accident calculations used PWR or BWR ORIGEN [2-14] inventories calculated for high burnup fuel that had cooled for only three years, even though these inventories, if shipped in the generic casks examined by this study, would produce surface dose rates that would exceed the regulatory limit.

2.5 Accident Source Terms

Representative accident source terms are developed for discrete sets of truck and train accident conditions. The conditions that define the representative accidents are cask impact speed onto an unyielding surface, impact orientation, and fire duration. For each set of representative accident conditions, the quantities of radionuclides available for release are calculated from the number of rods that fail and the fraction of the rod inventory released upon failure. The amounts released to

the interior of the cask are reduced by deposition onto cask internal surfaces. The fraction of the remaining gasborne radionuclides that are transported out of the cask is determined from the fraction of the cask gases that escape from the cask after the cask is pressurized by rod failure and heating of cask gases by accident initiated fires. Deposition times are estimated from cask leak areas which are estimated from the results of finite element cask impact calculations. The probabilities of these representative accident source terms are estimated from the probabilities of the accident scenarios and the probabilities of the accident speeds, cask impact orientations, impact surface hardnesses, occurrence of fires, and fire durations that can be associated with each scenario. These probabilities are called severity fractions because they specify the fraction of all accidents that have characteristics like those that define each representative accident.

2.5.1 Source Term Probabilities

The probability of occurrence of a representative accident source term is the product of the chance that an accident of any severity occurs during shipment of the spent fuel and the fraction of all of the possible accidents that yield source terms similar to that source term. Severity fractions were calculated as follows. First, the accident scenarios depicted on the Modal Study [2-15] truck and train accident event trees were determined by inspection to encompass the full spectrum of possible accidents. Next, each scenario probability on these trees was multiplied by the chance that the accident speed falls within one of four speed ranges and/or the chance that the scenario involves a fire that heats the cask to temperatures in one of three temperature ranges. This was done because the conditional scenario probabilities do not reflect the chance that the accident scenario occurs at some particular speed or leads to a fire of some particular severity.

Because Modal Study event trees specify impact surfaces for all collision scenarios, the product of a Modal Study event tree collision scenario conditional probability and the chance that the accident speed falls within one of four speed ranges yields the severity fraction for that collision scenario and speed range. If the collision can also initiate a fire, the product of the scenario probability and the speed range probability is multiplied by the chance that a fire ensues and then by the chance that the fire falls within one of three severity ranges that specify the chance that the fire is an engulfing, optically dense fire that burns hot enough and long enough to cause or increase the release of radioactive materials from the cask to the environment. For non-collision accidents that initiate fires, the chance that a fire of a particular severity ensues is simply the chance that the fire is a severe fire as defined in the preceding sentence. Finally, because accidents of a given severity can be initiated by several different accident scenarios, the probabilities of all scenario, speed, and fire combinations that lead to accidents having similar severities are summed, which gives an estimate of the severity fraction for that set of accidents.

The chance that the accident speed falls within a given speed range is calculated as the difference of the probabilities of the two speeds that define the speed range. These probabilities are read from the accident speed distributions presented in the Modal Study using the impact speeds onto the yielding surface specified for each scenario that are equivalent to one of the four speeds (30, 60, 90, and 120 mph after crushing of the impact limiter, which is equivalent to impact speeds of 42, 67, 95, and 124 mph for an uncrushed impact limiter) examined by the finite element calculations of cask impacts onto unyielding surfaces. The chance that the fire duration is long enough to heat the cask to the temperature where its elastomer seal develops a substantial leak or

rods not failed by impact are failed by burst rupture is read from the fire duration distributions presented in the Modal Study.

2.5.2 Source Term Magnitudes

The amount of radioactive material that might be released from a failed spent fuel Type B cask as a result of a collision and/or a fire is called the accident source term. The source term can be expressed as the product of four parameters: (1) the inventory of each important radionuclide being transported in the spent fuel cask, (2) the fraction of the fuel rods in the cask failed by the accident, (3) the fraction of the inventory of a single rod that is released from the failed rod to the cask interior, and (4) the fraction of the material that is released from the rods to the cask interior that also is released from the cask interior to the environment. Because cask radionuclide inventories can be precisely calculated by ORIGEN [2-14], development of reasonable estimates of accident source term magnitudes depends on the development of reasonable estimates of rod failure fractions and rod-to-cask and cask-to-environment release fractions for each representative accident examined.

Release of fission products from segments of real and surrogate spent fuel rods has been examined experimentally by Lorenz [2-16, 2-17, 2-18] and Burian [2-19]. A critical review of these experimental results allowed rod-to-cask release fractions to be developed for noble gases, cesium (Cs) compounds, ruthenium (Ru) compounds, and particulates and also for cobalt (Co) in the CRUD [2-20] deposits on fuel rod external surfaces. The values developed reflect blowdown of the rods upon failure, release of Cs and Ru compounds both as vapors and as constituents of particulates, impact fracturing of fuel pellets, formation of particle beds in pellet crack networks and in the pellet-cladding gap, and filtering of particles by these beds during particle transport toward the rod failure location.

Transport of fission products released to the interior of a TN-125 spent fuel cask has been examined by MELCOR [2-21] calculations [2-22]. These calculations show that the efficiency of vapor and particle deposition processes inside of the cask is determined principally by the rate at which the cask depressurizes after pressurization by the failure of spent fuel rods. The calculations also show that depressurization times are determined by the cross-sectional area of the leak path. Because a large leak leads to short depressurization times while a small leak leads to long depressurization times, cask-to-environment release fractions increase as cask leak areas increase. Accordingly, cask-to-environment release fractions can be estimated using the MELCOR results provided the cross-sectional areas of the leaks can be estimated by other methods.

2.6 Response of Representative Casks to Accident Conditions

Cask leak areas will depend on cask design and on accident conditions. Specifications (materials of construction and the dimensions of the cask body, lid, and closure) for four generic Type B spent fuel casks (a steel-lead-steel truck cask, a steel-lead-steel rail cask, a steel-DU-steel truck cask, and a monolithic steel rail cask) were developed by review of the characteristics of existing Type B spent fuel cask designs.

The response of these four generic casks to collision and fire accident conditions was then examined by performing finite element calculations and one-dimensional heat transport calculations. The finite element calculations examined cask response to impacts. The heat transport calculations estimated the heating times in engulfing fires that would lead to seal failure due to thermal degradation and rod failure by burst rupture. In addition, the probability of cask puncture during collision accidents was estimated by review of rail tank car accident data.

2.6.1 Finite Element Impact Calculations

The response to end, center-of-gravity over corner, and side impacts onto an unyielding surface at 30, 60, 90, and 120 mph of each generic cask, with its impact limiter already fully crushed, was modeled using a version of the PRONTO 3D finite element code [2-23] that runs on a parallel processing computer. PRONTO 3D is a three-dimensional, transient solid-dynamics code that models the large deformations produced in highly nonlinear materials when these materials are subjected to extremely high strain rates. Thus, PRONTO 3D can model the material and geometric non-linearities associated with the large deformations of cask structures that would be produced by high-speed cask impacts. In PRONTO 3D, the modeling of contact between distinct structures allows the various components of the cask to properly transmit loads from one structure to a neighboring structure. This is especially important for modeling the behavior of the cask closure (the cask lid, lid well, and lid bolts). Material failure was not included in any of the models, but accurate depictions, for example, of the deformations and loads on bolts, allows the failure of any single bolt to be predicted although sequential failure of bolts cannot be reliably predicted. The PRONTO code has been validated by comparison of analysis and test results for a wide range of problems, comparison to other finite element analysis results and to theoretical solutions for problems of simple geometry[1]. Many of the validation problems have been developed to exercise the code in regimes typical of impact analyses of spent fuel casks. For example, the Structural Evaluation Test Unit Program [2-24] performed by SNL involved comparison of experimental and analytical results for cask impacts of up to 60 mph. Thus, impacts at speeds as great as 120 mph should be realistically modeled.

Regardless of impact speed and orientation, the strains in truck and rail cask bodies predicted by the PRONTO 3D calculations were always too small to suggest failure of the cask body or of any penetrations that enter the cask through its body. Cask seal leakage and leakage areas were estimated by examining radial and circumferential displacements of the cask closure (i.e., separation of the lid from the lid well). The calculations suggest that truck cask seals are not compromised by impacts at any orientation onto an unyielding surface at 30, 60, and 90 mph and may not leak even after impacts at any orientation at speeds as high as 120 mph. Nevertheless, all 120 mph truck cask impacts were arbitrarily assumed to cause seal leaks with 1 mm^2 cross-

1. A Validation and Verification Manual is being prepared, personal communication, M. Blanford, Sandia National Laboratories, 1999.

sectional areas. The results obtained using the finite element models of the two generic rail casks suggest seal leakage may occur for some impact orientations at speeds as low as 60 mph and certainly occurs for some or all impact orientations for impact speeds of 90 and 120 mph.

2.6.2 Impacts onto Yielding Surfaces

For any impact speed and orientation, the damage done to the cask by impact onto an unyielding surface would be greater than the damage done by impact onto a yielding surface (hard and soft rock, hard and soft soils, concrete, water, drainage ditches, and road and rail beds). Because unyielding surfaces rarely occur in the real world, the impact speeds onto real world yielding surfaces, that are equivalent (cause the same cask damage) to each impact speed used for the unyielding surface, finite element calculations (30, 60, 90, and 120 mph) had to be calculated. This was done as follows.

First, for each unyielding surface impact calculation, a cask velocity time-history was calculated from the kinetic energy time-history. Next, the displacement of the center of gravity of the cask and the cask's rigid body acceleration were calculated respectively by numerical integration and differentiation of the velocity time-history. A force time-history was now calculated assuming that the contact force between the cask and the unyielding surface is equal to the rigid-body acceleration times the mass of the cask. Combination of the force time-history and the displacement time-history for any cask impact then produced a force-deflection curve for that unyielding surface impact calculation.

Impact of a cask onto a real yielding surface will produce damage equivalent to that observed for impact onto an unyielding surface only if the peak contact force for cask impact onto the yielding surface equals the peak contact force on the force-deflection curve developed for impact onto an unyielding surface. The energy absorbed by the yielding surface during each impact that developed a peak-contact force of this magnitude was now added to the initial kinetic energy of the unyielding surface impact. The velocity that corresponds to this total kinetic energy is the velocity for impact onto the yielding surface that is equivalent to the unyielding surface impact velocity (i.e., the velocity that would produce the same cask damage as that predicted for the unyielding surface impact at the specified impact velocity and orientation).

2.7 Rod Failure Fractions

The fraction of the fuel rods in each generic cask that are failed by end, corner, and side impacts of the cask at 30, 60, 90, or 120 mph onto an unyielding surface after crushing of the cask impact limiter was estimated from the peak rigid-body accelerations predicted by finite element analysis at each speed and impact orientation. First, the rod cladding strains calculated by Sanders, et al. [2-25] for 100 G side impacts onto an unyielding surface by a spent fuel cask carrying a typical pressurized water reactor or a typical boiling water reactor assembly were scaled to match the peak rigid-body accelerations predicted by the finite element impact analyses for each generic cask at each impact speed and impact orientation. Then, the fraction of rods that fail was estimated by comparing the scaled cladding strains to the 4 percent strain level predicted by Sanders, et al. to lead to cladding failure in typical spent fuel rods. Because rod strains generated by side impacts were used to evaluate all of the finite element results, the fraction of rods

estimated to be failed by end and corner impacts is conservative as rod damage for these impacts is expected to be less than that produced by side impacts with the same cask acceleration.

2.8 Thermal Calculations

Rod failure by burst rupture and times to failure for fire accident scenarios were estimated using the PATRAN/PThermal [2-26] analysis code, which is available commercially [2-27]. PATRAN/PThermal models all of the heat transfer processes (i.e., conduction, convection, and thermal radiation) that determine the heating rates of structures. Thus, the code can be used to perform one-, two-, and three-dimensional simulations of the effects of ambient conditions and fire conditions on the temperatures of spent fuel packages. PATRAN/Pthermal, formerly called Q/TRAN, has been validated by comparison of its results to analytic solutions and to predictions made by other thermal transport codes widely used in the transportation industry [2-28, 2-29].

PATRAN/PThermal results were developed for each of the four generic spent fuel casks examined by the finite element calculations. For these thermal calculations, the cask's neutron shield material compartment was assumed to be empty. The compartment was modeled as empty because, after the shield material in the compartment drains or burns away, as would be expected to happen during a severe fire accident, radiative and convective heat transport to the cask body through the empty compartment will significantly influence the rate of temperature rise of the cask body.

For each generic cask, the PATRAN/PThermal calculations determined the duration of a fully engulfing, optically dense, hydrocarbon fuel fire that would heat the cask to the temperature at which spent fuel rods would fail by burst rupture. The probability of fires of this duration was then used as an input to the calculation of accident severity fractions. During the calculation of release fractions, it was assumed that any fire that raised cask internal temperatures to rod burst rupture temperatures would also cause the failure of all unfailed rods in the cask. To assure that the calculated fire durations were conservative (shorter than the times actually required to reach seal leakage or rod burst rupture temperature), all of these calculations used a heat flux to the inner surface of the shell of the cask that was appropriate for high burnup fuel that had cooled for only three years.

The temperatures that cause seal leakage and the cross-sectional leak areas produced by thermal degradation of cask seals are estimated from literature data as follows. About 70 percent of the mass of elastomeric seal materials, including Viton, was lost during thermogravimetric analysis (TGA) experiments [2-30] during which these seal materials were heated to 500ºC at heating rates like those predicted here for heating of the four generic casks in engulfing optically dense hydrocarbon fires. Thus, heating a spent fuel cask to 500ºC is assumed to cause the cask's elastomeric seals to fail completely due to extensive thermal degradation. If a cask containment is lost due to thermal degradation of its elastomeric seal, the cask depressurization time will be determined by the leak rate of cask gases through the metal-to-metal gap between the cask lid and the lid well. Because bolt softening during cask heating by a hot, long-duration fire is expected to essentially eliminate the compression between the lid and the lid well around the entire circumference of the cask closure, the resulting leak area is assumed to equal the product of the surface roughness of the closure and the closure circumference.

2.9 RADTRAN Calculations

Seven sets of RADTRAN calculations were performed. Most of the calculations were performed with RADTRAN Version 5. A few calculations in the fifth set of calculations were performed with RADTRAN Version 1.

Sets one and two used the 200 representative truck and rail routes that were developed by Latin Hypercube Sampling of the route parameter distributions. The results of these calculations depict the possible range of spent fuel transportation consequences and risks.

Sets three and four developed results for ten specific shipment routes, five truck and five rail routes. Two of the ten routes were the national average spent fuel shipment truck and train routes constructed for the NUREG-0170 study [2-1]. The other eight routes were the truck and train routes that connect reactor sites to hypothetical interim storage locations. This set of calculations was performed in order to show that the results obtained for real routes fall within the envelope of results developed using the 200 representative routes constructed by sampling route parameter distributions.

Set five compared the consequences and risks predicted for spent fuel shipments by RADTRAN Version 1, the version of RADTRAN used during the NUREG-0170 study [2-1], to those predicted for this study using RADTRAN Version 5. These calculations depict the influence of cask inventory, spent fuel release fractions, and exposure pathway models on spent fuel transportation consequences and risks.

Sets six and seven compared the consequences and risks obtained using the cask inventory and release assumptions developed for the NUREG-0170 study [2-1], the Modal Study [2-15], and this study. These calculations illustrate the influence of the chemical and physical phenomena modeled on source term magnitudes and thus on consequences and risks.

2.10 Report Roadmap

The methods briefly outlined in this section are fully described in the following sections of this report. RADTRAN input parameter values are discussed in Section 3. Section 3.1 describes the selection of the RADTRAN parameters for which distributions are developed, Section 3.2 specifies values for the RADTRAN parameters for which central estimate values are used and provides a brief description of the basis for each value, and Section 3.3 describes how the parameter distributions were constructed.

The review of spent fuel transportation cask properties and the development of specifications for the four generic casks examined by this study is described in Section 4. Section 5 presents the results of the finite element unyielding surface impact calculations performed using the finite element model of each generic cask and the extrapolation of these results to yielding surfaces. The thermal analyses of the four generic casks are presented in Section 6.

The development of accident source terms is described in Section 7. Section 7.1 reexamines the truck and train accident scenarios depicted by the accident event trees constructed for the Modal Study [2-30]. Severity fraction and release fraction expressions are developed in Section 7.2.

Sections 7.3 and 7.4 respectively develop values for the parameters in these severity and release fraction expressions. Section 7.5 then presents the source terms (sets of release fractions and the severity fraction to which they correspond) calculated using these parameter values.

The RADTRAN calculations performed for this study and the results (spent fuel transportation incident free and accident consequences and risks) of these calculations are described and discussed in Section 8. Section 8.1 presents the results of the calculations that used the route samples of size 200 that were constructed by Latin Hypercube Sampling of route parameter distributions; Section 8.2 presents the results obtained for the ten specific routes for which calculations were performed; Section 8.3 compares the estimates of consequences and risks obtained using the source terms developed for the NUREG-0170 study, the Modal Study, and this study; and Section 8.4 examines the effects of changing the inventory, release fraction, and pathways modeled during the NUREG-0170 study to those used during this study.

Finally, Section 9 briefly discusses the results of the study and presents the study's conclusions.

2.11 References

[2-1] "Final Environmental Statement on the Transportation of Radioactive Material by Air and Other Modes," NUREG-0170, U.S. Nuclear Regulatory Commission, December 1977.

[2-2] J. M. Taylor and S. L. Daniel, "RADTRAN: A Computer Code to Analyze Transportation of Radioactive Material," SAND76-0243, Sandia National Laboratories, Albuquerque, NM, 1977.

[2-3] K. S. Neuhauser and F. L. Kanipe, "RADTRAN 5, Technical Manual," Sandia National Laboratories, Albuquerque, NM (in preparation, draft available on request).

[2-4] K. S. Neuhauser and F. L. Kanipe, "RADTRAN 5, User Guide," Sandia National Laboratories, Albuquerque, NM (draft available on the RADTRAN web site).

[2-5] J. J. Hancox and H. L. Wilkinson, "A Review of INTERTRAN/RADTRAN and Associated Codes," SRD/RMD 93/37/REP, SRD, UK Atomic Energy Authority, Culcheth, Cheshire, UK, 1993.

[2-6] S. Maheras, "Validation of the Transportation Computer Codes HIGHWAY, INTERLINE, RADTRAN 4, and RISKIND," DOE/ID-10511, Idaho National Engineering Laboratory, Idaho Falls, ID, 1995.

[2-7] Nuclear Waste Policy Act of 1982, and its 1987 amendments.

[2-8] J. W. Cashwell, et al., "Transportation Impacts of the Commercial Radioactive Waste Management Program," SAND85-2715, Sandia National Laboratories, Albuquerque, NM, April 1986.

[2-9] P. E. Johnson, et al., "Highway 3.1 - An Enhanced Highway Routing Model: Program Description, Methodology, and Revised User's Manual," ORNL/TM-12124, Oak Ridge National Laboratory, Oak Ridge, TN, March 1993.

[2-10] P. E. Johnson, et al., "Interline 5.0 – An Expanded Railroad Routing Model: Program Description, Methodology, and Revised User's Manual," ORNL/TM-12090, Oak Ridge National Laboratory, Oak Ridge, TN, March 1993.

[2-11] G. D. Wyss and K. H. Jorgensen, "A User's Guide to LHS: Sandia's Latin Hypercube Sampling Software," SAND98-0210, Sandia National Laboratories, Albuquerque, NM 1998.

[2-12] C. Saricks and T. K. Kvitek, "Longitudinal Review of State-Level Accident Statistics for Carriers of Interstate Freight," ANL/ESD/TM-68, Argonne National Laboratory, Argonne, IL, 1994.

[2-13] F. A. Gifford, "Use of Routine Meteorological Observations for Estimating Atmospheric Dispersion," *Nuclear Safety* **2**, 47 (1961).

[2-14] A. G. Croff, "ORIGEN2 - A Revised and Updated Version of the Oak Ridge Isotope Generation and Depletion Code," ORNL-5621, Oak Ridge National Laboratory, Oak Ridge, TN, July 1980.

[2-15] L. E. Fischer, et al., "Shipping Container Response to Severe Highway and Railway Accident Conditions," NUREG/CR-4829, Lawrence Livermore National Laboratory, Livermore, CA, February 1987.

[2-16] R. A. Lorenz, et al., "Fission Product Release from Highly Irradiated LWR Fuel," NUREG/CR-0722, Oak Ridge National Laboratory, Oak Ridge TN, February 1980.

[2-17] R. A. Lorenz, et al., "Fission Product Release from Simulated LWR Fuel," NUREG/CR-0274, Oak Ridge National Laboratory, Oak Ridge TN, July 1978.

[2-18] R. A. Lorenz, et al., "Fission Product Source Terms for the LWR Loss-of-Coolant Accident," NUREG/CR-1288, Oak Ridge National Laboratory, Oak Ridge TN, July 1980.

[2-19] R. J. Burian, et al., "Response of Spent LWR Fuel to Extreme Environments," Contractor Report, SAND85-7213, Battelle Columbus Laboratories, Columbus, OH, August 1985.

[2-20] R. P. Sandoval, et al., "Estimate of CRUD Contribution to Shipping Cask Containment Requirements," SAND88-1358, Sandia National Laboratories, Albuquerque, NM, January 1991.

[2-21] R. M. Summers, et al., "MELCOR 1.8.0: A Computer Code for Nuclear Reactor Severe Accident Source Term and Risk Assessment Analyses," NUREG/CR-5531, SAND90-0364, Sandia National Laboratories, Albuquerque, NM, January 1991.

[2-22] J. L. Sprung, et al., "Data and Methods for the Assessment of the Risks Associated with the Maritime Transport of Radioactive Materials: Results of the SeaRAM Program," SAND97-2222, Sandia National Laboratories, Albuquerque, NM, August 1997.

[2-23] L. M. Taylor and D. P. Flanagan, "PRONTO 3D: a Three-Dimensional Transient Solid Dynamics Program," SAND87-1912, Sandia National Laboratories, Albuquerque, NM, 1987.

[2-24] J. S. Ludwigsen and D. J. Ammerman, Analytical Determination of Package Response to Severe Impacts, Proceedings of PATRAM '95, Las Vegas, NV, December 1995.

[2-25] T. L. Sanders, et al., "A Method for Determining the Spent-Fuel Contribution to Transport Cask Containment Requirements," SAND90-2406, Sandia National Laboratories, Albuquerque, NM, November 1992

[2-26] PATRAN Thermal User Guide and Model Description Manual (http://www.macsch.com/support/support.html).

[2-27] The MacNeal Schwindler Corp., 2975 Redhill Ave., Costa Mesa, CA, (http://www.macsch.com/cgibin/MSCStore.storefront/1771903604/Catalog/DOC&2AMSC&2FPATRAN).

[2-28] R. E. Glass, "Sample Problem Manual For Benchmarking of Cask Analysis Codes, SAND88-0190," Sandia National Laboratories, Albuquerque, NM, February 1988.

[2-29] R. E. Glass, et al, "Standard Thermal Problem Set for the Evaluation of Heat Transfer Codes Used in the Assessment of Transportation Packages," SAND88-0380, Sandia National Laboratories, Albuquerque, NM, August 1988.

[2-30] P. J. Nigrey, "Prediction of Packaging Seal Life Using Thermoanalytical Techniques," Proceedings of the 12th International Conference on the Packaging and Transportation of Radioactive Materials (PATRAM '98), IAEA, Vol. 4, p. 1730, 1998.

Page intentionally left blank.

3. RADTRAN INPUT

The RADTRAN code [3-1, 3-2] calculates estimates of the risks associated with the transportation of radioactive materials, for example spent nuclear fuel. For a specific material, package, and route, the code develops estimates of a variety of consequences and risks for both incident-free transport and transport subject to accidents.

The RADTRAN code requires a very large quantity of data to describe the incident-free transportation of a radioactive material and also the accident scenarios and the radiological doses that might be received by population groups located along the shipment route. Selecting appropriate values for all the parameters used by the RADTRAN code to estimate transportation consequences and risks is a substantial undertaking. Selection of parameter values is further complicated by the fact that the casks and routes that will be used in the real spent fuel shipping campaigns are presently unknown. Fortunately, there is a large body of existing analyses that provide guidance on ranges of variables and their importance to the result. This knowledge base is significant in performing multiple analyses addressing a variety of conditions contained in this document. Experience allows the analyst to focus on identifying the variables that affect the results directly and getting their reasonable ranges correct while spending much less time (and computing resources) on less important parameters.

3.1 Fixed and Sampled Input Variables

For spent fuel shipments, many RADTRAN input variables can take on a wide range of real-world values (e.g., route lengths, wayside population densities, evacuation times). Fortunately, not all of these variables strongly influence predictions of the consequences and risks associated with the transportation of spent nuclear fuel. Spent fuel transportation risks are strongly influenced by a number of RADTRAN input variables [3-3, 3-4], some of which may take on a wide range of values in the real world. For these variables, construction of distributions and selection of values from these distributions by structured sampling methods offers an efficient way to assure coverage of the full range of each variable and also of the many possible combinations of the values of different variables that might be encountered in the real world.

RADTRAN input variables may be divided into two groups:

- those required for accident analysis, and
- those required for incident-free analysis.

Within each of these groups, RADTRAN input variables can be further divided into:

- variables that strongly affect incident-free or accident consequences or risks (More Important Variables)
- variables that do not strongly affect incident-free or accident consequences or risks (Less Important Variables)

Finally, the “More Important” RADTRAN variables can be divided into Source Term Variables (i.e., accident severity fractions and release fractions) and other “More Important” Variables.

The difference between More Important and Less Important Variables may be conceptually described as follows. Let R be incident-free dose or accident dose-risk, v_i be a RADTRAN input variable, and the fractional change in risk for a fractional change in the variable be

$$\frac{\Delta R}{R} = k_i \frac{\Delta v_i}{v_i}$$

Then, $k_i \approx 1.0$ for More Important Variables and $k_i << 1.0$ for Less Important Variables. Thus, for More Important Variables, a fractional change (e.g., a 10 percent increase) in the value of the variable produces about the same fractional change in risk (e.g., about a 10 percent increase or decrease). Conversely, for Less Important Variables, a fractional change in the value of the variable produces a much smaller fractional change in risk.

Central Estimates are Used for Less Important Variables

Although the values of nearly all RADTRAN input variables could be selected by sampling from distributions, constructing distributions for Less Important Variables is pointless because variation of the values of Less Important Variables influences consequence and risk results only slightly, if at all. Several RADTRAN input variables had been shown previously to have little influence on estimates of accident risk [3-5]. To verify the conclusions of this study specifically for spent fuel, single parameter sensitivity calculations were performed to investigate the effect of these variables on spent fuel transportation risks. Table 3.1 lists these variables, the trial values of each variable used in these sensitivity calculations, and the corresponding changes in total accident risk produced by the change. Table 3-1 shows that none of the five variables examined by these sensitivity calculations strongly affect risk. Therefore, for these variables, and all other variables known to have little effect on risk, central estimate values were used as input to all calculations performed for this study.

Table 3.1 Results of Sensitivity Calculations: Changes in Total Accident Risk Produced by Changes in the Values of Several Input Variables

Variable Name	Variable Definition	Base Case Value	Base Case Result	Sensitivity Case Value(s)	Sensitivity Case Result
BRATE	Breathing rate	3.3E-4	5.5E-06	1.6E-04	3.9E-6
BDF	Respirable aerosol fraction inside buildings	0.05	5.5E-06	5.0E-03 0.5	5.4E-06 6.8E-06
RPD	Ratio of pedestrian and resident population densities	6.0	5.5E-06	3.0 12.0	4.6E-06 7.4E-06
RU	Urban shielding factor	0.018	5.5E-06	0.01 0.18	5.5E-06 5.5E-06
CULVL	Clean-up level	0.20	5.5E-06	0.10 0.02	5.3E-06 4.8E-06

Central Estimates are Used for More Important Variables with Little Variation

Distributions need not be constructed for More Important Variables that have values that are fixed or that only vary over a narrow range. For example, some Important Variables have precisely defined values (e.g., radionuclide half lives) or have values that are fixed by regulations. Thus, central estimate values were also used for all More Important Variables that are invariant or that only vary over narrow ranges.

Central Estimates are Used for all Source Term Variables that can Vary Widely

RADTRAN source term magnitudes are specified by the product of the cask inventory, which can be precisely determined by ORIGEN calculations [3-6], and an accident release fraction. The probability of the release (the source term probability) is specified as the product of a severity fraction, which specifies the fraction of all possible accidents that lead to the given source term, and the probability that any accident occurs, which is calculated as the product of a route length and an accident rate. Because insufficient information exists from which to construct distributions for these important RADTRAN variables, as is described in Section 7, their variation was treated by constructing representative sets of truck and train accident release and severity fractions.

Distributions are Used for Other More Important Variables with Wide Value Ranges

Consequently, distributions were constructed only for other More Important Variables that have real-world values spanning a wide range (e.g., route lengths, accident rates, route wayside population densities, evacuation times). For these other More Important Variables, as is discussed below, distributions were constructed, usually by analysis of historic data for the variable, and then representative sets of values for each variable were selected from these distributions by structured Monte Carlo Sampling using Sandia National Laboratories' Latin Hypercube Sampling (LHS) computer code [3-7].

3.2 RADTRAN 1 and RADTRAN 5 Input Variables

Although the exposure and dose models implemented in RADTRAN 5 are the same as those implemented in RADTRAN 1, models for a variety of other phenomena have either been modified or added. In particular, RADTRAN 5 allows considerably greater flexibility in the way that transportation routes are modeled. The principal differences between these two versions of the RADTRAN code are summarized in Table 3.2.

Tables 3.3 and 3.4 respectively describe the incident-free and accident analysis input variables used in RADTRAN 1 and RADTRAN 5, and present the RADTRAN 1 and RADTRAN 5 names of each variable, the location (array name and position in the array) of the variable in RADTRAN 5, the sensitivity of RADTRAN output to each variable, the RADTRAN 1 and RADTRAN 5 value used for each variable, and clarifying comments or explanations. In Tables 3.3 and 3.4, the term "not in code" in the RADTRAN 1 or RADTRAN 5 variable name column indicates that no model implemented in the indicated version of the code uses this variable, and "Distribution" in

Table 3.2 Comparison of RADTRAN 1 and RADTRAN 5

	RADTRAN 1	RADTRAN 5
Route	Entire route modeled in three segments occurring in fixed proportions related to population density designations	Route may be divided into up to 60 user-defined segments (links)
Right-of-way width	Fixed for freeway, non-freeway, urban	User-defined
Population density	Rural, suburban, urban[a] – fixed densities	User-defined
Population density distribution along the route	Fraction of route that is rural = 0.9, suburban = 0.05, urban = 0.05	Population density can be defined for each link
Distribution of population along the route	Population is distributed in bands ½ mile (800 m.) wide on either side of the route	Band depth is user defined
Lane width	Fixed for rural, suburban, urban	User-defined
Vehicle speed	Fixed for rural, suburban, urban	User-defined for each link
Vehicle density (traffic count)	Fixed for rural, suburban, urban	User-defined for each link
Traffic distribution: rush hour, non-rush	Fixed fractions for rural, suburban, urban	Not needed, because speeds are user-defined
Traffic distribution by road type	Fixed fractions for rural, suburban, urban	Road type is user-defined
Stop time, distance from cargo, number of people	Fixed for rural, suburban, urban	User defined: each stop can be treated separately, like a link
Package shape factor	Not used directly	Used
Dose to close-in receptors	approximately $1/r^2$ dependence	approximately 1/r dependence
Dose to handlers	Treated like stop dose	Activity-specific parameters (distance, etc.) are user defined
Dose to crew	Fixed for various modes	User-defined
LCF/person rem (incident-free transportation)	2.57×10^{-4} LCF/person rem (accepted regulatory value in late 1970s) (disaggregated by target organ)	User-defined; current guidance is: 5×10^{-4} LCF/rem for public; 4×10^{-4} LCF/rem for workers
LCF (transportation accidents)	3.79×10^{-4} LCF/rem (disaggregated by target organ)	User-defined; current guidance is: 5×10^{-4} LCF/rem for public; 4×10^{-4} LCF/rem for workers
Accident frequencies	1974-75 national average data	User defined; 1988 state-by-state data are most recent available values
Accident severity categories	8 categories	Up to 30 categories available; number of categories and frequencies both user-defined
Loss of shielding accidents	Included	Included
Atmospheric dispersion meteorology	Fixed: national average meteorology	User-defined combination of stability classes
Ingestion model	Model similar to WASH-1400 [3-8]	COMIDA2 [3-9]

a. Rural, suburban, and urban areas are called low-density, medium-density, and high-density, respectively, in NUREG-0170.

Table 3.3 Comparison of RADTRAN 1 and RADTRAN 5 Input Variables that Affect Incident-Free Dose

Variable Definition	Variable Name		RADTRAN 5 Input Location	Sensitivity of Dose to Variable	Variable Value		Comments
	RADTRAN 1	RADTRAN 5	Array Name (position)		RADTRAN 1 (NUREG-0170)	RADTRAN 5 (this study)	
Maximum Dose Rate at 1 m from package surface (mrem/hr)	TIPKG	Package Dose Rate (DR)	PACKAGE (2nd)	Proportional	(not used)	Distribution (See Sect. 3.4.3.4)	For NUREG-0170, TIPKG was set to 1.0 which forced the package dose rate factor K to have a value of 1000 mrem-ft^2/hr.
Maximum dose rate at 1 m from vehicle surface (mrem/hr)	(not in code)	Vehicle Dose Rate	VEHICLE (3rd)	Proportional		Distribution (see package dose rate above)	The NUREG-0170 model did not treat the package and vehicle separately; for spent fuel, the package and vehicle dose rates were assumed to be the same.
Fraction of package dose rate that is gamma radiation	(not in code)	Gamma Fraction	PACKAGE (3rd)	Small	(1.0)	1.0	NUREG-0170 model assumed 100% gamma radiation, which is conservative.
Fraction of package dose rate that is neutron radiation	(not in code)	Neutron Fraction	PACKAGE (4th)	Small	(0.0)	0.0	NUREG-0170 model assumed 100% gamma radiation. Neutrons readily attenuated by concrete, humidity, etc.
Fraction of vehicle dose rate that is gamma radiation	(not in code)	Gamma Fraction	VEHICLE (4th)	Small	(1.0)	1.0	NUREG-0170 model assumed 100% gamma radiation, which is conservative.
Fraction of vehicle dose rate that is neutron radiation	(not in code)	Neutron Fraction	VEHICLE (5th)	Small	(0.0)	0.0	NUREG-0170 model assumed 100% gamma radiation. Neutrons readily attenuated by concrete, humidity, etc.
Characteristic package dimension (m)	PKGOE	Package Size	PACKAGE (5th)	Proportional	(not used)	5.2 for truck 4.8 for rail	Package dimension was not used by the NUREG-0170 spent fuel model. It was used offline to estimate the package dose rate factor (see TIPKG above) Values are for casks currently in service.
Characteristic vehicle dimension (m)	(not in code)	Vehicle Size	VEHICLE (6th)	Proportional		5.2 for truck 4.8 for rail	The NUREG-0170 model did not treat the package and vehicle separately.
Flag for exclusive use vs non-exclusive use	(not in code)	Exclusive Use	VEHICLE (modifies 2nd value in array)	N/A	Exclusive Use	Exclusive Use	
Number of shipments	SPY	Number of Shipments	VEHICLE (7th)	Proportional	For 1975, 254 for truck and 17 for rail.	1	NUREG-0170 examined results per year (1975); this study looks at results per shipment.

Table 3.3 Comparison of RADTRAN 1 and RADTRAN 5 Input Variables that Affect Incident-Free Dose (continued)

Variable Definition	Variable Name		RADTRAN 5 Input Location	Sensitivity of Dose to Variable	Variable Value		Comments
	RADTRAN 1	RADTRAN 5	Array Name (position)		RADTRAN 1 (NUREG-0170)	RADTRAN 5 (this study)	
Number of crew persons	1st value in DNORM array	Crew Size	VEHICLE (8th)	Proportional (crew dose only)	Truck: 2	Truck: 2	Because of distance from the cask rail car, both studies assume the train crew receives negligible in transit exposures.
Average distance of crew from nearest package surface (m)	3rd value in DNORM array	Crew Distance	VEHICLE (9th)	Proportional (crew dose only)	Truck: 3.0 m	Truck: 7.4 m	Dose calculated from package surface nearest crew rather than from source location at geometric center of package.
"Crew-view" package dimension (m)	(not in code)	Crew View	VEHICLE (11th)	Proportional		Truck: 2 m	See preceding comment on distance from package to crew.
Crew Modification Factor; accounts for shielding of crew, if any	(not in code)	Crew Modfac	VEHICLE (10th)		(1.0)	1.0	RADTRAN 5 allows cab shielding to be modeled; however, no shielding of crew was assumed in current calculations.
Number of packages per shipment	PKGSHP	Number of Packages	VEHICLE	Proportional	1	1	
Population Density at stop (persons/km^2)	POPZON	Population Density	STOP (3rd)	Proportional (stop dose only)	Rural: 6 Suburban: 719 Urban: 3861	Truck: 3E+04 Rail: Rural, 8; Suburban, 340	For RADTRAN 5, truck value based on empirical data; rail value reflects fact that, even in cities, rail yards are not surrounded by urban population density.
Minimum and Maximum radii of annular area around stopped vehicle	Fixed Value	Minimum Dist. Maximum Dist.	STOP (4th, 5th)	Proportional (stop dose only)	10 ft 2600 ft	Truck: 1, 10 m Rail: 30, 800 m Rail classification yard: 400, 800 m	In NUREG-0170 model, the 10 & 2600 ft values could not be changed. RADTRAN 5 values are for members of public; worker doses are computed separately.
Shielding factor	(not in code)	Shield Factor	STOP (6th)	Proportional (stop dose only)		1.0	Not in NUREG-0170 model; assumed to be 1.0 (i.e., everyone is outdoors). Set to 1.0 in this study for conservatism.
Stop time (hours)	8th, 9th, & 10th values in DNORM array	Stop Time	STOP (7th)	Proportional (stop dose only)	Truck Rail R: 1 24 S: 5 0 U: 2 0	Truck: Distribution (See Sect. 3.4.3.1) Rail: classification yard stops, 60 hr; all other rail stops, 0.033 hr/km.	In NUREG-0170 model, aggregate stop time for rural, suburban, and urban travel was entered. In RADTRAN 5, stop time can be aggregated or entered separately for each stop. Because trucks transporting spent fuel do not make stops to sleep. A correction factor to the results calculated using the truck stop time distribution is developed in Section 8.6.

Table 3.3 Comparison of RADTRAN 1 and RADTRAN 5 Input Variables that Affect Incident-Free Dose (continued)

Variable Definition	Variable Name		RADTRAN 5 Input Location	Sensitivity of Dose to Variable	Variable Value		Comments
	RADTRAN 1	RADTRAN 5	Array Name (position)		RADTRAN 1 (NUREG-0170)	RADTRAN 5 (this study)	
Storage time per shipment (hours)	DTSTOR		(not in code)	Small	Truck: 2 Rail: 4	N/A	RADTRAN 5 calculations assumed stops for storage didn't occur.
Population density of persons exposed during storage (mi^2)	PDSTOR		(not in code)	Small	Truck: 896 Rail: 25	N/A	RADTRAN 5 calculations assumed stops for storage didn't occur.
Minimum and maximum radii of annular area around storage location (ft)	(not in code)		(not in code)	Small	(5 ft, 1000 ft)	N/A	RADTRAN 5 calculations assumed stops for storage didn't occur. Storage exposure distance range was fixed in RADTRAN 1.
Link Length (km)	[FMPS]	Dist.	LINK (3rd)	Proportional	R: 2530 × 0.09 S: 2530 × 0.05 U: 2530 × 0.05	Distribution (See Sect. 3.4.1.2)	1975 Model used fixed route length (FMPS) and fixed fractions of rural, suburban, and urban travel as indicated.
Shipment velocity (mph) for calculation of incident-free results	V	Speed	LINK (4th)	Proportional	Truck: 55 mph Rail: R: 40 mph S: 25 mph U: 16 mph	Truck: 55 mph Rail: R: 40 mph S: 25 mph U: 16 mph	Truck value (55 mph) is used for interstates for all population densities. Applies to incident-free only; accident speeds not a direct RADTRAN input (see Chapter 7).
Persons per Vehicle	26th value in DNORM array	Persons per Veh	LINK (5th)	Proportional (on-link dose only)	2	Distribution (See Sect. 3.4.3.6)	
Link Population Density (persons/km2)	POPZON	Pop Den	LINK (6th)	Proportional (off-link dose only)	R: 6 S: 719 U: 3861	Distribution (See Sect. 3.4.1.4)	Values in NUREG-0170 Model were fixed.
Link Vehicle Density (one-way vehicles/hour)	23rd, 24th & 25th values in DNORM array	Vehicle Density	LINK (7th)	Proportional (on-link dose only)	R: 470 S: 780 U: 2800	Distribution (See Sect. 3.4.3.5)	
Population Zone Index (rural 1, suburban 2, or urban 3)	(not in code)	Pop Zone	LINK (9th)	N/A		1,2, or 3, as appropriate	Designation determines shielding factor used; rural, suburban, and urban population density ranges are the same as in NUREG-0170.
Designates link as Freeway (=1), Other roadway (=2), or Other mode (=3)	(not in code)	RD	LINK (10th)	Small		Truck: 1 Rail: 3	NUREG-0170 model assumed 5% travel on city streets and 10% on non-interstate highways. This study used 0% for both values.

Table 3.3 Comparison of RADTRAN 1 and RADTRAN 5 Input Variables that Affect Incident-Free Dose (continued)

Variable Definition	Variable Name		RADTRAN 5 Input Location	Sensitivity of Dose to Variable	Variable Value		Comments
	RADTRAN 1	RADTRAN 5	Array Name (position)		RADTRAN 1 (NUREG-0170)	RADTRAN 5 (this study)	
Fraction of land under cultivation (rural links only)	(not in code)	Farm Frac	LINK (11th)	Small (ingestion dose only)		No effect	Used to calculate ingestion dose. Not present in NUREG-0170 model; not calculated for present study.
Number of Handlers	Fixed Value	Number of Handlers per Package	HANDLING (3rd)	Proportional (handler dose only)	2	5	NUREG-0170 model only required number of handlings to be entered (7th value in DNORM array); other variables that can now be user-defined were fixed values in NUREG-0170 model. Number of handlers has been updated based on recent empirical data.
Average package-to-handler distance (m)	Fixed Value	Handling Distance	HANDLING (4th)	Proportional (handler dose only)	1	1	Value used in RADTRAN 5 based on empirical data that confirm original NUREG-0170 value.
Handling time per package (hr/package)	Fixed Value	Handling Time	HANDLING (5th)	Proportional (handler dose only)	0.5	0.5	Value used in RADTRAN 5 based on empirical data that confirm original NUREG-0170 value.
Used to calculate total exposed population for multi-year shipment campaigns	(not in code)	CAMPAIGN	MODSTD	None		20 yrs	Not present in NUREG-0170 model.
Distance-dependent rail worker exposure factor	(not in code)	DDRWEF	MODSTD	Proportional (crew/worker dose only)		0.0018 hr/km	Not present in NUREG-0170 model; used to calculate rail worker dose for crew change stops outside of classification yards.
Array of 3 distances for off-link dose calculation	(not in code)	DISTOFF	MODSTD	Inversely Proportional	(Truck: 27, 30, & 800 m)	Truck: 27, 30, & 800 m	Values were fixed in NUREG-0170 model.
Minimum distance to on-link vehicles (m)	Fixed Values	DISTON	MODSTD	Inversely Proportional	Truck: 3 m, Rail: 3 m	Truck: 3 m, Passing car: 4 m, Rail: 3 m	NUREG-0170 model did not treat passing cars.
Number of railcar inspections per trip	(not in code)	FMINCL	MODSTD	Proportional (crew dose only)		2	Used to calculate rail worker dose at classification yards. Not present in NUREG-0170 model.

Table 3.3 Comparison of RADTRAN 1 and RADTRAN 5 Input Variables that Affect Incident-Free Dose (continued)

Variable Definition	Variable Name		RADTRAN 5 Input Location	Sensitivity of Dose to Variable	Variable Value		Comments
	RADTRAN 1	RADTRAN 5	Array Name (position)		RADTRAN 1 (NUREG-0170)	RADTRAN 5 (this study)	
Ratio of pedestrian density to residential density	(not in code)	RPD	MODSTD	Proportional		6	Not present in NUREG-0170 model. Used to calculate dose to unshielded persons in cities.
Rural shielding factor	(not in code)	RR	MODSTD	Small	(1.0)	1.0	Recommended value reflects large fraction of time spent outdoors on farms.
Suburban shielding factor	(not in code)	RS	MODSTD	Small	(1.0)	0.87	Recommended value for wood frame construction. NUREG-0170 model assumed no shielding.
Urban shielding factor	(not in code)	RU	MODSTD	Small	(1.0)	0.018	Recommended value for masonry construction. NUREG-0170 model assumed no shielding.
Threshold dimension for handling by forklift or crane (m)	(not in code)	SMALLPKG	MODSTD	Small	(0.5 and 1.0)	0.5	RADTRAN 5 model has only one threshold – variables for large packages are defined by user.
Latent cancer fatality (LCF) conversion factors (LCF/rem) for general public and workers	ORGLCF	LCFCON	MODSTD	Proportional	2.22E-05 lung, 1.34E-5 thyroid, 1.21E-04 whole body, 6.9E-6 bone, 3.4E-6 LLI	5E-04 general public; 4E-04 workers (dose equivalent to whole-body dose)	NUREG-0170 model used organ-level factors rather than CEDE or dose-equivalent-based factors and did not distinguish public and worker populations. RADTRAN 5 model is based on BEIR V and ICRP 60.
Interdiction threshold for contaminated land ($\mu Ci/m^2$)	(not in code)	INTERDICT	MODSTD	Proportional		8	NUREG-0170 model didn't include clean-up/interdiction thresholds.
Urban building fraction; fraction of land occupied by buildings (aggregate route data) or fraction of population indoors (route-specific data)	(not in code)	UBF	MODSTD	Proportional (urban dose only)		Aggregate analyses, 0.52 Route-specific analyses, 0.9	NUREG-0170 model did not account for fraction of urban area not occupied by buildings (aggregate analyses) or fraction of population in buildings (route-specific analyses).
Fraction urban land occupied by sidewalks (aggregate route data) or fraction of population outdoors (route-specific data)	(not in code)	USWF	MODSTD	Proportional (urban dose only)		0.1	NUREG-0170 model did not account for fraction of urban area occupied by pedestrians on sidewalks (aggregate analyses) or fraction of persons out of doors (route-specific analyses)

Table 3.4 Comparison of RADTRAN 1 and RADTRAN 5 Input Variables that Affect Accident Risk

Variable Definition	Variable Name		RADTRAN 5 Input Location	Sensitivity of Dose to Variable	Variable Value		Comments
	RADTRAN 1	RADTRAN 5	Array Name (position)		RADTRAN 1 (NUREG-0170)	RADTRAN 5 (this study)	
Accident Rate (accidents/vehicle-km)	APM	Accidents per vehicle-km	LINK (8th)	Proportional	Truck: 1.06E-6 Rail: 9.3E-7	Distributions (See Sect. 3.4.2)	In RADTRAN 1, for each Accident Category, APM and γ were entered as a product.
Fraction of all accidents that are of severity j	γ	Severity	SEVERITY	Proportional	8 truck and 8 rail Accident Categories (See Table 1.5)	19 truck and 21 rail Accident Categories (See Table 7.31)	In RADTRAN 1, for each Accident Category, APM and γ were entered as a product.
Fraction of package contents released in accident of severity j	RF	RFRAC	RELEASE	Proportional	8 truck and 8 rail Accident Categories (See Table 1.5)	19 truck and 21 rail Accident Categories (See Table 7.31)	NUREG-0170 values give fraction of inventory of largest release that is released for each Accident Category (see Table 1.4).
Fraction of released material that is aerosols	AER	AERSOL	RELEASE	Proportional	(1.0)	1.0	Not explicitly treated by NUREG-0170 model.
Fraction of aerosols that are respirable	RESP	RESP	RELEASE	Proportional	(1.0)	1.0	Not explicitly treated by NUREG-0170 model.
Frequencies of occurrence for Pasquill stability categories A through F (array of six values)	(not in code)	Pasquill	PARM	Proportional		Distribution (See Sect. 3.4.3.3)	RADTRAN 1 treats only a single set of weather conditions. RADTRAN 5 treats 6 sets of weather conditions.
Breathing rate (m^3/sec)	(not in code)	BRATE	MODSTD	Small	(3.3E-04)	3.3E-04	Treated as part of RADTRAN 1 inhalation dose model.
Evacuation time (days)	(not in code)	EVACUATION	MODSTD	Proportional		Distribution (See Sect. 3.4.3.2)	Because NUREG-0170 model did not treat groundshine, evacuation was not modeled.
Clean-up level (μCi/m^2)	(not in code)	CULVL	MODSTD	Proportional		0.2	Because NUREG-0170 model did not treat groundshine, decontamination was not modeled.
Threshold for interdiction of contaminated land (μCi/m^2)	(not in code)	INTERDICT	MODSTD	Proportional		8	Because NUREG-0170 model did not treat groundshine, interdiction was not modeled.

Table 3.4 Comparison of RADTRAN 1 and RADTRAN 5 Input Variables that Affect Accident Risk (continued)

Variable Definition	Variable Name		RADTRAN 5 Input Location	Sensitivity of Dose to Variable	Variable Value		Comments
	RADTRAN 1	RADTRAN 5	Array Name (position)		RADTRAN 1 (NUREG-0170)	RADTRAN 5 (this study)	
Latent cancer fatality (LCF) conversion factors (LCF/rem) for general public and workers	LCF	LCFCON	MODSTD	Proportional	2.22E-05 lung; 1.21E-04 whole body	5E-04 general public; 4E-04 workers (dose equivalent to whole-body dose)	NUREG-0170 model used organ-level factors rather than CEDE or dose-equivalent-based factors and did not distinguish public and worker populations. RADTRAN 5 model is based on BEIR V and ICRP 60.
Genetic effects (GE) conversion factor (GE/rem)	(not in code)	GECON	MODSTD	Proportional		1.00E-04	No genetic effects were computed in NUREG-0170 model.
Neutron emission factor for LOS accidents.	(not in code)	Neutron Emission	MODSTD	Small	(0.0)	0.0	NUREG-0170 model did not treat neutron emission. This model was not used by this study. LOS exposures were calculated from surface dose rate of an unshielded assembly.
Specifies radii for annular areas of exposure in LOS accidents	RADIST	RADIST	MODSTD	Inversely Proportional	10, 20, 30, 40, 50, 100, 200, 300, 500, and 1000 ft	3.05, 6.1, 9.1, 12.2, 15.2, 30.5, 61, 91.4, 152, 305 m	Change in units only.
1-year dose to thyroid (rem); radio-iodines only	(not in code)	RPCTHYROID	MODSTD	Small		isotope values	Used to estimate early effects.
Time needed to survey contaminated land (days)	(not in code)	SURVEY	MODSTD	Small		10	Post-accident survey and clean-up activities were not treated in NUREG-0170 model.
Time to evacuation following LOS accident (days)		TIMENDE	MODSTD	Small	1.0	R: 0.67 S: 0.67 U: 0.42	In NUREG-0170 model, this variable was defined as exposure time.
Urban building fraction; fraction of land occupied by buildings (aggregate route data) or fraction of population indoors (route-specific data)	(not in code)	UBF	MODSTD	Proportional (urban dose only)		0.52 for aggregate analyses; 0.9 for route-specific analyses;	NUREG-0170 model did not account for fraction of urban area not occupied by buildings (aggregate) or fraction of population in buildings (route-specific).
Urban sidewalk fraction; fraction land occupied by sidewalks (pedestrians) (aggregate route data) or fraction of population out of doors (route-specific data)	(not in code)	USWF	MODSTD	Proportional (urban dose only)		0.1 for all analyses	NUREG-0170 model did not account for fraction of urban area occupied by pedestrians on sidewalks (aggregate) or fraction of persons out of doors (route-specific).

the RADTRAN 5 variable value column indicates that values for this variable were selected from a real-world distribution of the values of this variable. A "fixed value" is one that was held constant throughout this study, either because it was a Less Important Variable or for the other reasons outlined previously in connection with Important Variables. If a variable that is not explicitly modeled has an implicit value or a value that is not accessible through input (i.e., a hard-wired variable), then that value is enclosed in parentheses in the RADTRAN 1 or RADTRAN 5 variable value column. In the variable value columns, R, S, and U respectively mean Rural, Suburban, and Urban. Finally, in the "Sensitivity" column, "Proportional" and "Small" have the meanings given above in the discussion of Important and Less Important Variables.

The rationale for the selection of RADTRAN incident-free and accident input variables for which distributions are constructed and the data used to construct each distribution are each presented in detail in Sections 3.3 and 3.4.

3.3 Variables Selected for Sampling

Less Important Variables are identified in Tables 3.3 and 3.4 by the word "Small" in column five, the column that specifies the sensitivity of radiation dose estimates to changes in the value of the indicated variable. Because these variables have little impact on calculated radiation doses, a central estimate value (the value listed in column seven of these tables) was selected for each of these variables and that value was used in all of the RADTRAN 5 calculations performed for this study.

More Important Variables are identified in Tables 3.3 and 3.4 by the word "Proportional" in column five. Although radiation doses are strongly affected by changes in the value of any More Important Variable, not all More Important Variables have values that take on a wide range of values in the real world. Thus, More Important Variables can be subdivided into two groups, those that have values that are constant or that vary only slightly, and those that take on a wide range of values in the real world.

3.3.1 Incident-Free Variables Selected for LHS Sampling

All variables that have proportional effects on the value of the result (i.e., Important Variables) were initially candidates for probabilistic treatment. Variables were selected for probabilistic treatment (selection of variable value by LHS sampling of the variable's distribution) principally by examination of the importance analysis performed in RADTRAN output, which shows the magnitude of the effect that a specified value change (1 percent) has on the result. As described in detail below, fixed values were assigned to those with a proportional effect but which experience little actual variation or are problem-specific. For example, incident-free dose calculations are highly sensitive to the Package Dimension variable (PKGOE in RADTRAN 1), but the characteristic dimension used in the analyses in this study is invariant for a given cask. Thus, fixed values were assigned to that variable, 5.2 m for the truck cask and 4.8 m for the rail cask (see Section 4). In contrast, an equally important variable (Package Dose Rate at 1 m) was selected for probabilistic treatment (construction of a distribution of parameter values and selection of values by sampling from the distribution), because the variety of fuel ages and

burnups that characterize spent fuel causes the external dose rate of spent fuel casks to vary over a substantial range.

The incident-free variables for which distributions of parameter values were constructed are:

- Package Dose Rate at 1 m (mrem/hour)
- Link Length (km)
- Link Population Density (person/km^2)
- Persons per Vehicle (truck only)
- Link Vehicle Density (one-way vehicles/hour)
- Stop Time (truck only)

The package dose rate variable has been discussed already. Link length is treated by constructing distributions because dose to the general public residing near the road or railroad (off-link dose) is directly proportional to distance traveled and because the distances to possible destinations investigated in this study vary considerably. Link population density also directly influences risk to the general public and varies from link to link. The persons per vehicle variable directly influences dose to general public in vehicles that sharing the road with the spent fuel truck, and sufficient high-quality data regarding vehicle occupancy are now available from the Department of Transportation (DOT) to permit construction of a vehicle-occupancy distribution. Link vehicle density has a similar influence on on-link dose, and distribution data are available. The distributions used to characterize these variables are described below in Sections 3.4.1 and 3.4.3.

3.3.2 Incident-Free Variables Not Selected for LHS Sampling

The remaining variables, some of which can affect consequences or risks proportionally, include those

- that exhibit little or no actual variation,
- that cause only small changes in consequences or risks,
- for which there are not adequate data to determine the variable's distribution,
- that are problem-specific and thus have different values for specific casks (e.g., the characteristic dimension of the cask), and shipping campaigns (e.g., the number of shipments in the campaign), and
- that have no effect on truck or rail transport consequences or risks (e.g., variables used only for other modes, such as number of flight attendants).

Variables with small effects on risk and variables that vary over small ranges will be considered together.

3.3.2.1 Variables with Little or No Variation or with Small Impacts

The following variables fall into this category:

- Number of Crew Persons
- Average Distance of Crew from Package Surface (m)
- Crew Modification Factor
- Number of Railcar Inspections per Trip (FMINCL)
- Distance-Dependent Rail Worker Exposure Factor (DDRWEF)
- Number of Handlers
- Handling time per Package
- Package-to-Handler Distance (m)
- Threshold Dimension for Handling by forklift or crane (SMALLPKG) (m)
- Genetic Effects Conversion Factor (GECON)
- Latent Cancer Fatality Conversion Factor (LCFCON)

Each of these variables is now discussed even though several of them (all of the handling variables, GECON, LCFCON) are not used in any of the risk calculations performed for this study or are used only in sensitivity calculations.

The number of crew persons varies little because it is determined by trucking and rail industry practices. The value of 2 for truck transportation is by far the most common [3-10]. There is little variation in the value of this parameter, and the selected value is representative. No in-transit crew dose is calculated for rail mode because of the large separation distances and large amount of shielding between the crew and the package(s).

The average distance of crew from package surface is a new variable in RADTRAN 5. Previously, the distance from the crew compartment to the geometric center of the package was used and the same point-source model used to calculate off-link and on-link dose was used to calculate crew dose. However, for cylindrical packages such as spent-fuel casks, where the crew view of the package is from the end rather than the side, a modification of the basic point-source model yields less conservative results. For a given cask design, there is still some variability in this value because of variation in trailer length, but it is not large. The distance used is the old value less half the cask length, which relocates the crew-view point source from the geometric center of the package to the center of the side closest to the crew.

The crew modification factor is part of a new model in RADTRAN 5 intended to account for crew shielding (e.g., shielded truck cabs) and is not present in RADTRAN 1. It is a fraction that, when multiplied by the package dose rate, reflects the reduced dose rate to the crew from the presence of shielding, if any. The crew dose is limited by the maximum permissible dose rate in the crew area (2 mrem/hour). The contribution of crew dose to the total result consequently cannot exceed a maximum value, which is determined for a given dose rate by the total time in

transit. Furthermore, the value of this variable has a relatively small effect on overall population dose. It should be noted, however, that the effect of dose rate changes within the subgroup itself is not necessarily small. The affected subgroup (in this case, truck or rail crew) is noted in parentheses under the column titled Sensitivity of Dose to Variable in Table 3.2.

The value of 2 assigned to FMINCL is determined by rail-carrier business practices, which require one inspection at the beginning of a trip and one at the end. The possibility of other inspections en route cannot be ruled out, but the experience base is insufficient to permit statistical treatment of this variable. Thus, the value is set to 2, the total number of inspections that are known to always occur (i.e., 1 at the beginning and 1 at end of each trip).

The DDRWEF applies to rail mode only. It is used to calculate the component of rail-worker dose that depends on distance traveled (e.g., engine changes and shift changes) rather than on time spent in a classification yard. The value of 0.0018 hour/km was determined from industry-supplied data [3-11] and is relatively invariant because of the uniformity of industry practices, union agreements, etc. Furthermore, it is a small component of total rail worker dose because the majority of the worker dose is incurred in classification yards.

The number of handlers was originally fixed at 2 in RADTRAN 1. The number is user-definable in RADTRAN 5, and the recommended value for spent-fuel handling is now 5. This recommendation is based on data from observations of 12 spent-fuel off loadings at the Port of Newport News, Virginia [3-12]. The value includes workers who guide the crane to the proper orientation for casks enclosed in ISO containers both to pick up the cask and to lower it into position on the vehicle. It also includes a spotter and workers who lock and check the tiedowns after the cask is in place. There may be more than 5 individuals involved but no more than 5 in proximity to the cask at any given time. The standardization of handling equipment means there is little variation in this value in normal operations.

Handling time per package was also a fixed value in RADTRAN 1 and was set to 1/2 hour (30 minutes). Empirical data on spent-fuel off-loadings has since confirmed that this is a somewhat conservative estimate [3-12]. As is the case for the other handling-related variables, standardization of handling equipment means there is little variation in this value in normal operations. For spent fuel casks, which are lifted with cranes, the time during which workers are in proximity to a cask is 30 minutes or less. This includes the time required to guide a crane into position; attach the crane to cask trunnions or to an enclosing ISO container; lift the cask; move it over to the transport vehicle (e.g., truck or rail car); lower it into place; fasten the tiedowns; and detach the crane once the tiedowns have been fastened. The time required for the reverse process is the same. It includes additional safety steps (e.g., checking that the tiedowns are properly secured) and also includes the time between cask movements for multiple cask handlings. Time is required, for example, for a truck to drive out of the loading zone and be replaced by a second truck ready to receive a second cask. Time is also required to reposition the crane over the next railcar, ship hold, etc. from which the next cask is to be lifted. If only one cask is being handled, then the latter actions are not necessary, which reduces the total elapsed time and makes the 30-minute value somewhat conservative.

Package-to-handler distance was fixed at 1 m in RADTRAN 1. This value has since been shown to be somewhat conservative but generally correct on the basis of empirical data [3-12] and to have little variation. It is the recommended value for RADTRAN 5.

SMALLPKG has no effect on the results for spent-fuel handling. It merely defines the minimum dimension above which mechanical handling methods must be used [3-13]. That dimension is a function of the capabilities of the package-handling machinery available and is not subject to wide variation.

Values of GECON and LDFCON are based on the most recent radiological data available. The values used must conform with federal guidance [3-14]. The values change with time, however, as more and better data become available. That is clearly seen in the difference between the 1975 and 1999 values.

3.3.2.2 Variables Where Distribution Data is Not Available

Variables for which distributions have not been developed include

- Gamma and Neutron Dose-Rate Fractions
- Rural, Suburban, and Urban Shielding Factors (RR, RS, and RU, respectively)
- Shipment velocity (km/hour)
- Urban building fraction or fraction of persons indoors (UBF)
- Urban sidewalk fraction or fraction of persons out of doors (USWF)
- Array of distances for off-link dose calculation (DISTOFF)
- Minimum distances to on-link vehicles (DISTON)
- Population density at stops (persons/km^2)
- Minimum and maximum radii of annular area around stopped vehicle (m)
- Shielding factor
- Ratio of Pedestrian Density (RPD)

Gamma and neutron dose rates vary considerably with fuel age and burn-up and the mix of fuel ages and burn-ups in any given shipment. For these reasons, especially the currently unpredictable mix of assemblies in any given shipment, no distribution of gamma/neutron ratios has been developed, and the conservative point estimates of 100 percent gamma and 0 percent neutron are used instead. This approach is conservative because neutrons are more rapidly attenuated by air and other hydrogen-rich media (e.g., concrete, shrubbery) through which they might pass during the course of normal transport prior to reaching human receptors.

The rural, suburban, and urban shielding factors were not present in RADTRAN 1 (i.e., no shielding effects were accounted for in RADTRAN 1). The variables are present in RADTRAN 5, but no distribution of weighted-average shielding factor values for urban or other areas has been developed. In lieu of such distributions, point estimates based on typical or representative

construction types in the population zones have been used [3-15]. The value recommended for urban shielding (RU) in RADTRAN 5 is representative of masonry construction. The suburban factor represents frame construction. Although some suburban structures are constructed of brick or other materials, frame construction and its analogs (e.g., mobile homes) are common throughout the country. In the absence of a distribution, the frame-construction assumption also is conservative. The rural factor is set somewhat conservatively to 1.0 (i.e., no shielding) to reflect the large amount of time spent outdoors by many rural residents. No actual data on time spent indoors versus out of doors has been combined with construction-type data to generate a rural shielding factor distribution. These values were developed for RADTRAN II [3-16].

All spent-fuel shipments are highly regulated. Truck shipments have armed escorts for much if not all of their travel time. Although escorts are only required in urban areas, past experience indicates that escorts will accompany spent-fuel shipments for greater distances (e.g., in Virgina, shipments are escorted over the entire route within the state). While speeds in excess of 88 kph (55 mph) are common for ordinary commercial trucking, it is anticipated that spent-fuel shipments would not significantly exceed 55 mph. Current experience with Waste Isolation Pilot Plant (WIPP) shipments confirms this assumption [3-17]. Rail shipments travel at speeds controlled by the rail companies, and speeds for trains carrying hazardous materials are generally lower than those for general freight, although trains generally traverse urban areas at reduced speeds.

In the absence of adequate data from which to construct truck or train speed distributions, the typical interstate truck speed and typical train speeds for hazardous material shipments were used as point estimates. Thus, shipment velocity is set to 88 kph (55 mph) in all population zones for interstate truck transportation. For rail transportation, different values were used for rural, suburban, and urban route segments: 64.37 kph (40 mph) on rural segments; 40.3 kph (25 mph) on suburban segments; and 24.1 kph (16 mph) on urban segments. Because these speeds are believed to be somewhat conservative (lower than may actually occur), they should lead to a small overestimation of incident-free dose. Because these speeds are not used to estimate cask impact speeds during collision accidents, they have no effect on accident risks.

UBF and USWF were not present in RADTRAN 1. They were added in RADTRAN II. At that time, aggregated population-density data was the only type of population information available. The population density assigned to urban links, therefore, was treated as being uniform across the entire bandwidth (area within 800 m on either side of the road or railroad). This would have led to an overestimate of the off-link urban population if used without modification. The UBF and USWF correction factors restricted population to areas occupied by buildings and sidewalks; the values came from the Urban Study [3-18]. In current analyses, however, population densities are derived from GIS-based systems with census-block population data. That is, they represent *actual counts* that should not be reduced by any correction factors. Thus, the UBF and USWF values are now used to simply designate what fraction of the population is indoors and what fraction is out of doors. The sum of the two fractions must now be unity. The data indicating what fraction of the urban population is out of doors at any given time are from the Urban Study, which examined only New York City. The 0.1 estimate (10 percent), which applies only to a weekday during working hours in Manhattan, has been used as a conservative point estimate; the 0.9 indoors value (90 percent) was obtained by subtraction from 1.0. The Manhattan value is

conservative because of the number of workers who are out of doors for significant portions of the workday (e.g., garment-district carriers and messengers).

DISTOFF consists of an array of three distances, the first two of which define a pedestrian zone adjacent to the road or railroad and the last of which establishes the maximum depth or bandwidth for off-link dose calculation. These variables were present in RADTRAN 1 and have not changed since 1975. There undoubtedly is variation in the minimum distance to the road at which people may reside; it may frequently be greater than 30 m and occasionally may be less, but no distribution for this variable is available in the literature. The maximum distance was set at 800 m (0.5 mi) in the 1975 model to conform with the previously published Reactor Safety Study [3-8] although dose rates drop below measurable values at much shorter distances from the road or railroad. All analyses since then have used the same value, and, even though RADTRAN 5 allows the value to be altered, 800 m is used here to provide comparability with earlier studies. The pedestrian zone width was set at 3 m in RADTRAN 1 on the basis of civil-engineering standards for walkway widths, and in the absence of any data to support use of a distribution, the 3 m width also is used here to provide comparability.

DISTON is used in the calculation of on-link dose and is the minimum distance from the package to traffic in nearby lanes. The user enters up to four values for interstate highways, secondary roads, city streets, railroads, and passing vehicles, respectively. The interstate value is based on a 1986 model of a minimal four-lane configuration with an average lane width of 5 m. The secondary and city-street values, which are smaller (3 m), are not used in this study. The railroad value of 3 m is based on the minimum clearance between passing trains on double-rail route segments. The value for passing vehicles (4 m) is the median value for all interstate and secondary-road lane widths. These variables are not equally uncertain. The minimum interstate lane width, for example, is determined by engineering standards that apply to all interstate highways. However, no published data are available that indicate the range of magnitudes of these variables, and the point estimates described above are used here.

Two population densities are used to calculate public dose at ordinary truck stops (rest and refueling stops). The first population density is a derived value that yields approximately nine persons fully unshielded within a 10-m radius in order to conform to the observations of Griego et al. [3-19]. The second density is used to calculate exposures to more distantly located persons. It is set equal to the suburban aggregate value used in the 1975 model since it is not possible to predict exact stop locations in advance. The Griego et al. study [3-19] examined two separate truck stops, one suburban and one rural in nature. Their data include many hours of observation of truck-stop operations. The standard deviation of their data for persons within 10 m is small. The reasons for this uniformity are that

- truck stops provide standardized services (refueling bays, restaurants, etc.),
- service area and refueling bay designs tend to be standardized, and
- truck parking parameters (average row spacing and average distance from the service area) have low variability.

Thus, the mean value of the Griego et al. data [3-19] was used in this analysis for the inner annulus of truck stops. For rail stops, public dose is also estimated using the suburban aggregate population density. This is done because most rail yards are located in regions with suburban population densities, and because a distribution for this variable can not be constructed without knowing the actual locations of rail stops, which of course can only be specified for the real routes used during a real shipping campaign.

The minimum and maximum radii in RADTRAN 1 established an annular area around a stop location in which exposed persons were located. They were arbitrarily fixed at 10 ft (≈ 3 m) and 2600 ft (≈ 800 m). Recent observations of actual truck stops have shown that the minimum is too large [3-19]. The minimum approach distance was in the 1 m range. These observations also led to the partitioning of the surrounding population into two nested annular areas. The innermost annulus has minimum and maximum radii of 1 and 10 m, and all persons within the area are unshielded; the outer annulus has minimum and maximum radii of 10 and 800 m, respectively. Proximity of the shipment to structures and other trucks provides some shielding for this outer population. For calculation of public dose at rail stops in classification yards, the minimum radius coincides with the typical classification-yard boundary (400 m) and the maximum radius remains 800 m. For rail stops outside of classification yards, the minimum radius is 30 m and the maximum radius remains 800 m. The maximum radius is set to 800 m solely to provide calculational consistency between modes and between stop-related and in-transit contributions to dose. In the absence of advance knowledge of stop locations, exact minimum values cannot be used, and no distribution of population densities around possible stops has been developed.

The shielding factor is set to 1.0 (no shielding) on the basis of the data in [3-19] for the inner annular area at truck stops (radii of 1 m and 10 m). References [3-19] and [3-10] are the basis for the selection of 0.2 as a shielding factor for the outer annular area. The shielding factor of 0.1 for rail classification stops was calculated in [3-11]. The shielding factor for rail stops outside of classification yards has been set to a conservative 1.0 because of the lack of empirical information on presence or absence of surrounding structures at intermediate rail stops. No distribution that describes the frequency distribution of shielding factors for public exposure at either truck or rail stops has been developed.

The ratio of pedestrian density allows the user to account for persons out of doors in urban areas and persons who are not residents (shoppers, drivers, etc.). It acts as a direct multiplier for the out-of-doors urban population. The value used in this study is 6 and it is taken from the Urban Study [3-18], which examined only New York City. The value is generally conservative because commercial districts remain robust, unlike many other American cities where much of the business activity has relocated to suburban shopping centers and industrial parks. The ratio of the number of retail businesses to the residential population is 6.95 for New York City, as opposed to values near 1 for most other East Coast cities (e.g., 1.01 for Boston); it also is greater than the same ratio for large West Coast cities such as Los Angeles (ratio = 5.65) [3-20]. No distribution of values for this variable has been developed.

3.3.2.3 Problem-Specific Variables

Problem-Specific Variables include:

- Characteristic Package Dimension (m)
- Number of Shipments
- Number of Packages per Shipment
- DTSTOR (Storage time per shipment; hours)
- PDSTOR (Number of persons exposed during storage)
- RSTOR (Radial distances defining annular area within which persons are located around storage location)
- Crew-view Package Dimension (m)
- Distance of crew from nearest package (m)

As noted in the introduction to this section, the characteristic package dimension is determined by the choice of package for a given analysis. The values used in this study are 5.2 m for the truck cask and 4.8 m for the rail cask (see Section 4).

The number of shipments is a variable found in all releases of RADTRAN. It clearly is problem-specific. All of the RADTRAN calculations performed for this study examined single shipments that transport one spent fuel cask, i.e., the number of shipments was set to one, and the number of shipments required to ship the entire on-site spent-fuel inventory (e.g., all of the spent fuel assemblies that will have to be shipped from the sites where they are presently stored) to a repository or intermediate storage facility is addressed in external calculations (spreadsheet). The number of shipments needed to move the spent fuel inventory from on-site storage locations to temporary or permanent storage facilities is discussed in Section 8.6.

The number of packages per shipment also is found in all releases of RADTRAN. For the analyses performed for this study, it was assumed that each shipment carried only one Type B spent fuel cask. This assumption is clearly correct for transport by truck. For transport by rail, it is generally correct when transport is not by dedicated train (shipment by dedicated train was not examined by this study).

The RADTRAN 1 variables DTSTOR, PDSTOR, and RSTOR are not present as distinct variables in RADTRAN 5 because storage is modeled as a special type of stop in RADTRAN 5. No en route storage is anticipated in the spent-fuel shipments analyzed in this study, so storage variables are set to zero for RADTRAN 1 and no special storage stop is modeled in RADTRAN 5.

The crew-view package dimension, like the basic package dimension variable, is determined by the choice of cask and has no associated uncertainty. The values used in this study are 2 m for the truck cask and 5 m for the rail cask.

3.3.2.4 Variables that Do Not Affect Truck or Rail Spent Fuel Transport

There are several variables that do not contribute to dose or risk calculation for spent-fuel transportation by truck and rail modes. They are

- Number of Flight Attendants (FNOATT)
- Fraction of Land under Cultivation
- Exclusive-Use Flag (computer code "switch")
- Population Zone
- Link Type
- CAMPAIGN

Some variables have no effect on the result in this study, regardless of what values are assigned to them. One of these is the number of flight attendants; it applies only to modes of transportation (air modes) not considered in this study. The term "No Effect" is entered for this variable in the Variable Value column in Table 3.1, and no value is entered for FNOATT in the input file. The fraction of land under cultivation variable has no effect on the result in this study because ingestion dose is not computed.

Several flags and control variables found in RADTRAN 5 also should be mentioned. The first of these is the flag for exclusive-use versus non-exclusive use. It is set to exclusive use in all cases in this study. The population zone designation (rural, suburban, or urban) determines which shielding factor is used and what column the link results are entered into in the output. The designation is problem-specific. The designator was intended to allow use of non-standard shielding factors (e.g., use of an "urban" shielding factor in non-urban links with high proportion of masonry construction. However, such highly route-specific data are not employed in this study and the designator thus depends on the definitions of rural, suburban, and urban population densities. The latter are 0 through 66 person/km^2 for rural; 67 through 1,670 persons/km^2 for suburban; and greater than 1,670 persons/km^2 for urban. These ranges were derived from the demographic model in NUREG-0170, and they have been used to develop population zone data for all releases of RADTRAN. The letters R, S, and U are used to designated rural, suburban, and urban zones in RADTRAN 5. A related variable is the Link Type designator. It is set to 1 for interstate highways, 2 for other highway types, and 3 for rail or other modes. These designations are completely problem-specific, and there is no uncertainty as to what value is entered for each link once the route has been established.

The CAMPAIGN variable has no direct effect on the result. It is used to calculate the total off-link population for multi-year campaigns by taking account of in-migration and out-migration of population. It is based [3-21] on 1990 Census Bureau demographic data.

3.3.3 Accident Variables

This section gives information on RADTRAN variables required for accident-risk analysis (Table 3.4). The format is the same as that used for incident-free variables. Variables were selected for probabilistic treatment on the basis of sensitivity analyses performed to determine the magnitude of change in the result associated with a fixed amount of change in an input value.

3.3.3.1 Accident Variables not Selected for LHS Sampling

The following accident-risk variables have been assigned point-estimate values

- Sidewalk Width in early effects calculation (m)
- Building Dose Factor
- Clean-up Level (CULVL) (microCi/m^2)
- Threshold for Interdiction of Contaminated Land (microCi/m^2)
- Time to Survey Contaminated Land (days)
- Breathing Rate (m^3/sec)
- Neutron Emission Factor for Loss of Shielding (LOS) Accidents
- One-year Dose to Thyroid (rem/rem inhaled)
- Radii of annular areas of exposure in an LOS Accident
- Time for Evacuation following an LOS Accident (hours)

Sidewalk width was a RADTRAN 1 variable and is no longer included as a variable in RADTRAN 5. It was used only in calculation of dose to persons following an LOS accident on a city street. Because travel on city streets during spent-fuel transportation historically has occurred only in the case of overseas shipment into U.S. ports, no travel on city streets is considered in this analysis, the model in which the variable is used in RADTRAN 1 is not invoked and no correlation or adjustment is necessary.

The building dose factor is used to account for filtration of particulates from the air by building heating/cooling systems. It was not included in RADTRAN 1. The recommended value of 0.05 for RADTRAN 5 is taken from [3-11]. This value is an average across a number of residential, office, and industrial building types and represents the best available estimate in the absence of a distribution.

Clean-up level (CULVL) was not a variable in RADTRAN 1. This variable is not treated probabilistically because it is defined by regulation. Although there is currently no final guidance for the value of the regulatory clean-up level, draft guidance issued by the U.S. Environmental Protection Agency, recommends a value of 0.2 microCi/m^2 [3-22]. This value is used in all of the RADTRAN calculations performed for this study. Like the clean-up level, there is currently no final regulatory guidance for the Interdiction Threshold contamination level. The value selected for use is 40 times higher than the value selected for CULVL, because the

decontamination factors achieved cleaning up two cases of weapons-related contamination [3-23] suggest that decontamination of areas of moderate size by factors as large as 40 is achievable.

The actual time required to perform a contamination survey would likely be prolonged, but it is not possible to predict because of regulatory and legal complexities [3-23]. The longer deposited material remains on the ground, however, the more is (a) removed by radioactive decay and (b) spread by forces such as wind and rain. In general, the shorter the elapsed time between an accident occurrence and completion of a survey, the higher the survey results would be. Furthermore, because of the rarity of actual contamination events, there is a paucity of empirical data on which to base an estimate. For these reasons, the time to survey contaminated lands was set at a radiologically conservative but practically unrealistic 10 days. The legal and practical realities associated with post-accident response are discussed in Chanin and Murfin [3-23].

The generally accepted standard for breathing rate is used for calculation of inhalation and resuspension doses. The breathing rate of the International Council on Radiation Protection Reference Man (70-kg adult male at light work) is the recommended value; it is 3.3E-04 m^3/sec [3-24]. While not a quantity prescribed by regulation, this variable was developed by a recognized international body (International Council on Radiation Protection) and is commonly used in radiological consequence calculations. Thus, there is no need to treat this variable probabilistically.

The dose-conversion factor for one-year dose to the thyroid is used to calculate thyroid dose via the inhalation pathway. The factor is applied only to radioisotopes of iodine. Values specific to I-131, I-129, and I-125 have been developed for this variable and they are: 1.26E-06, 5.77E+06, and 9.25E+05 rem/Ci inhaled, respectively. These are radiological quantities and are not subject to probabilistic treatment. Because none of the inventories used in this study contain significant quantities of radioiodines, the value of this parameter is not important.

3.3.3.2 Accident Variables Selected for LHS Sampling

The accident variables selected for probabilistic treatment and the sections that describe the treatments are:

- Accident Rate on a Link (accidents/vehicle-km) – Sections 3.4.2.2 and 3.4.2.3
- Evacuation Time – Section 3.4.3.2
- Atmospheric Stability – Section 3.4.3.3

3.4 Development of Distribution Functions

3.4.1 Route Characteristics

3.4.1.1 Introduction

The present study, which is intended to address the risk of transporting spent nuclear fuel from all commercial power reactors to a repository, posed an unusual difficulty. While the locations of the reactors where spent fuel is presently stored are known, final locations for interim storage sites and for a permanent repository have not yet been selected and formally approved. Therefore, specific spent fuel shipment routes could not be examined and small set of hypothetical routes could be shown to be truly representative of all of the routes that might someday be used. The method chosen to address this difficulty was to develop distributions of shipment parameters and route characteristics using data for a very large number of real routes that connect reactor sites to plausible interim storage site and permanent repository location, and then to construct representative set of route parameter values by sampling these distributions using LHS sampling methods. Provided that the distributions constructed represent the full spectrum of possible routes and that sufficient sets of RADTRAN input variables (generated by sampling the distributions) are analyzed, the mean risks and the risk ranges estimated using these sets of route parameter values should accurately represent actual shipment risks.

The set of primary shipment origins is well known (commercial reactors with spent fuel in holding pools). One possible interim storage site location was identified in the northeast, north-central, northwest, southeast, south-central, and southwest portions of the continental United States. In addition, three possible permanent repository locations, one of which was Yucca Mountain, were also selected. The set of interstate truck routes or mainline rail routes that connect each reactor site to each of the possible interim storage sites and each of these interim storage sites to each of the three possible permanent repository locations were examined by performing HIGHWAY [3-25] or INTERLINE [3-26] route calculations. In the case of truck shipments, the routes were specified in compliance with HM-164 rules for "highway route controlled quantity" shipments (49 CFR 177.825) such as the spent nuclear fuel shipments considered here. For rail shipments, the routes conformed to rail carrier practice. For both types of shipments, any NRC regulations (10 CFR 73.37) that would affect route selection were considered.

After the routing calculations were completed, a data base of the lengths, and rural, suburban, and urban length fractions was constructed using the data for the 492 truck or the 492 rail routes. Sets of parameter values from each data base were ordered and aggregated to create cumulative distributions for each of these route parameters. In Figures 3.1a through 3.1d, these NEW distributions for truck routes are compared to OLD distributions constructed from similar sets of route data tabulated in the Yucca Mountain down-select report [3-27]. Figures 3.2a through 3.2d present a similar comparison of NEW and OLD rail-route parameter distributions. After visual inspection of these distributions indicated that each NEW distribution was very similar to its corresponding OLD distribution, the two data sets were combined thereby generating a larger, statistically more comprehensive data base. The final set of route parameter distributions was then constructed using the pooled data.

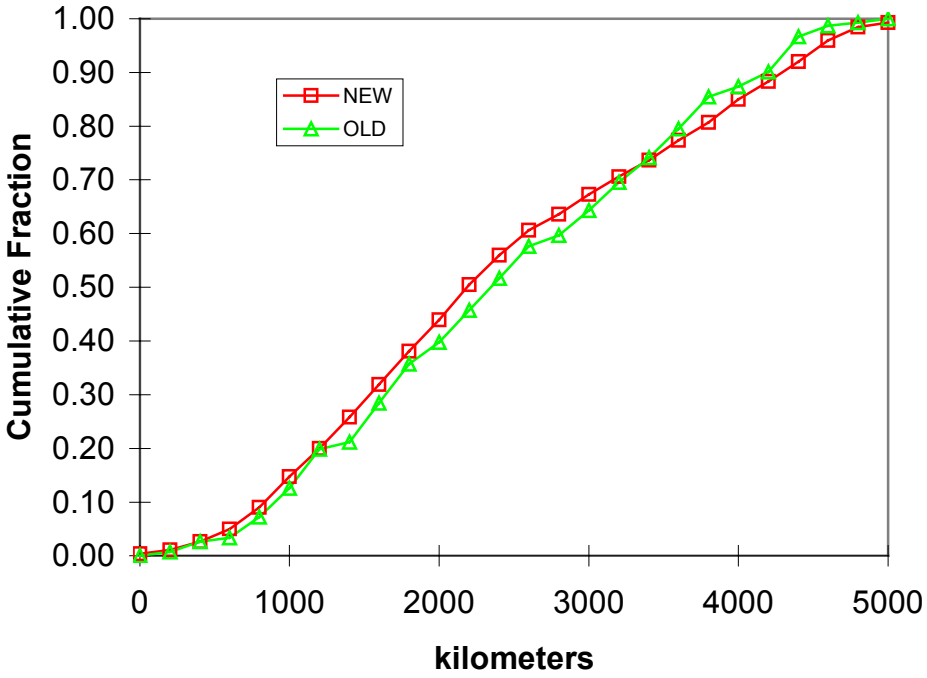

Figure 3.1a Comparison of the cumulative distributions of route *lengths* for truck.

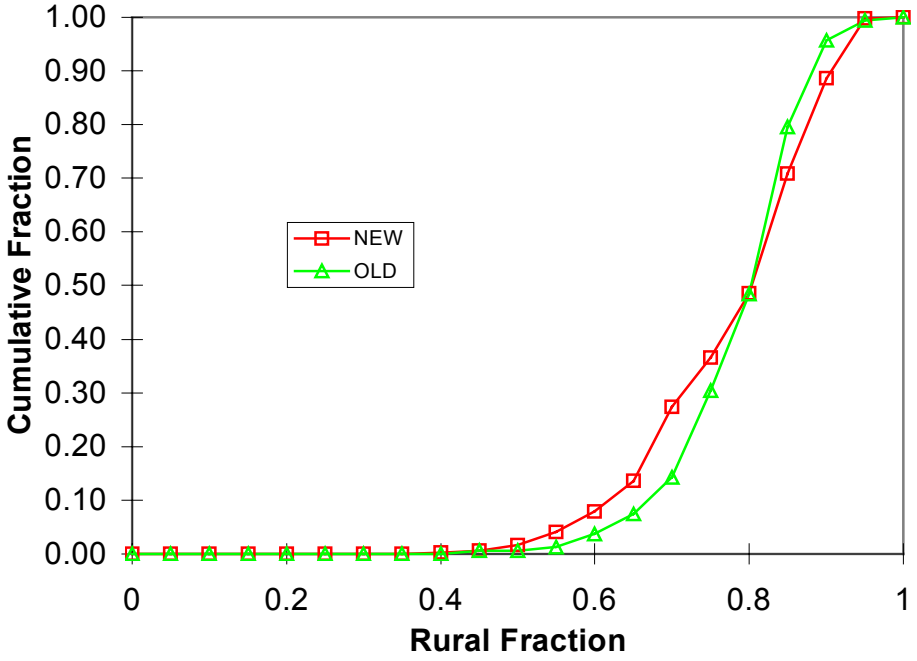

Figure 3.1b Comparison of the cumulative distributions of route *rural fractions* for truck.

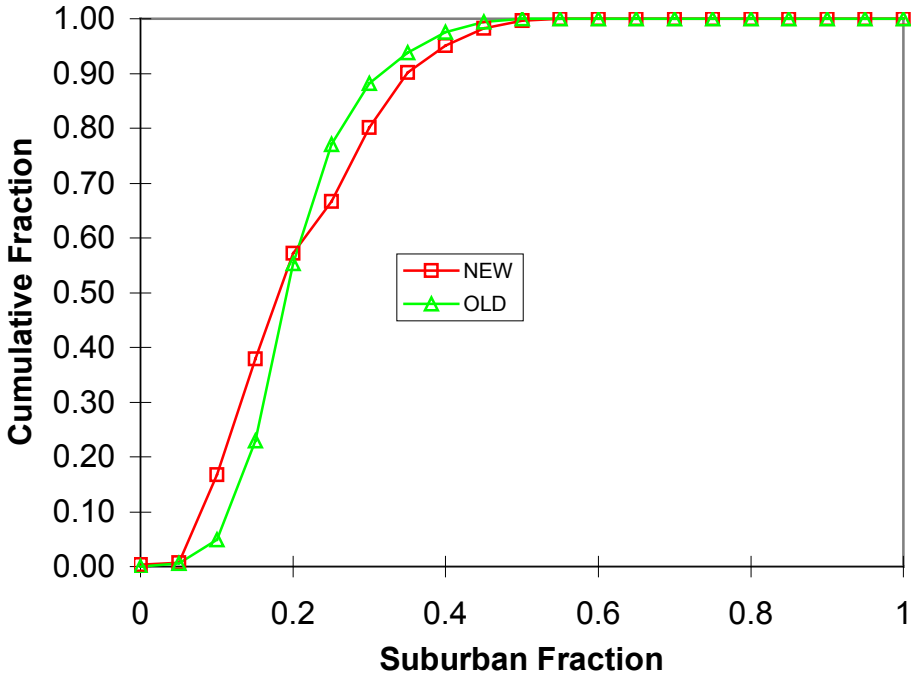

Figure 3.1c Comparison of the cumulative distributions of route *suburban fractions* for truck.

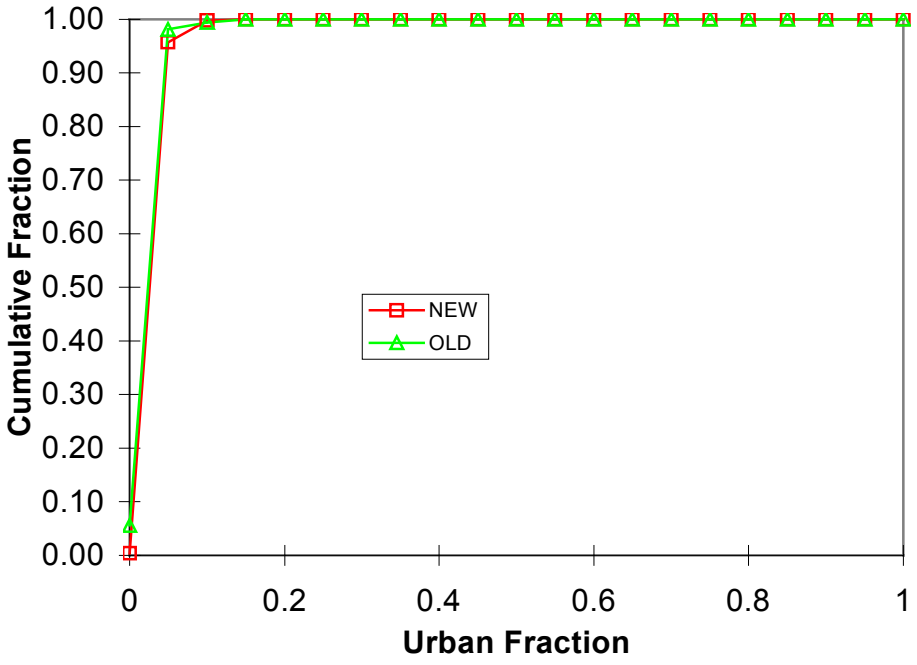

Figure 3.1d Comparison of the cumulative distributions of route *urban fractions* for truck.

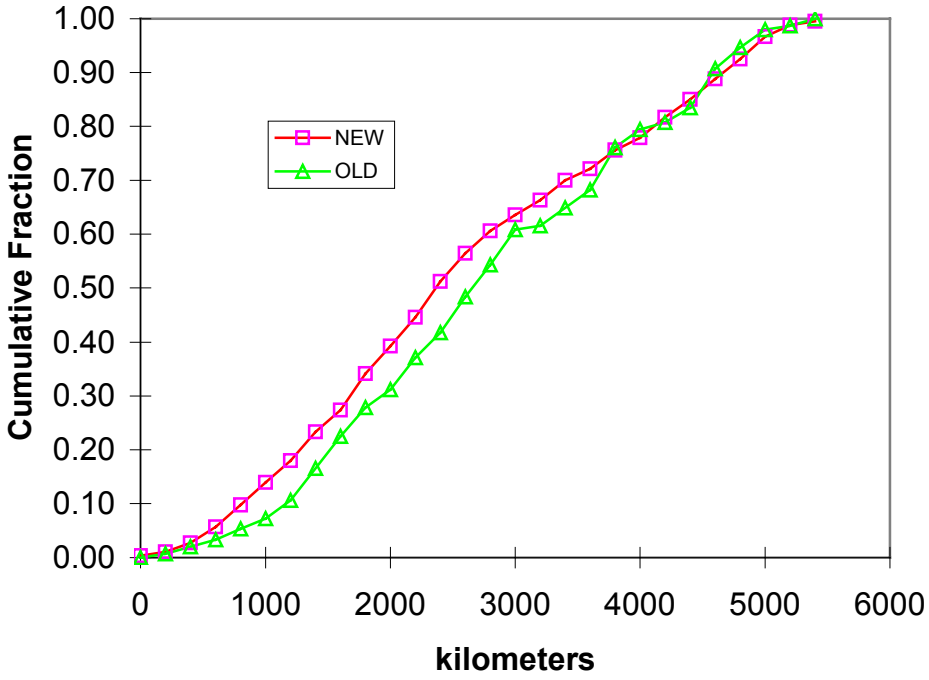

Figure 3.2a Comparison of the cumulative distributions of route *lengths* for rail.

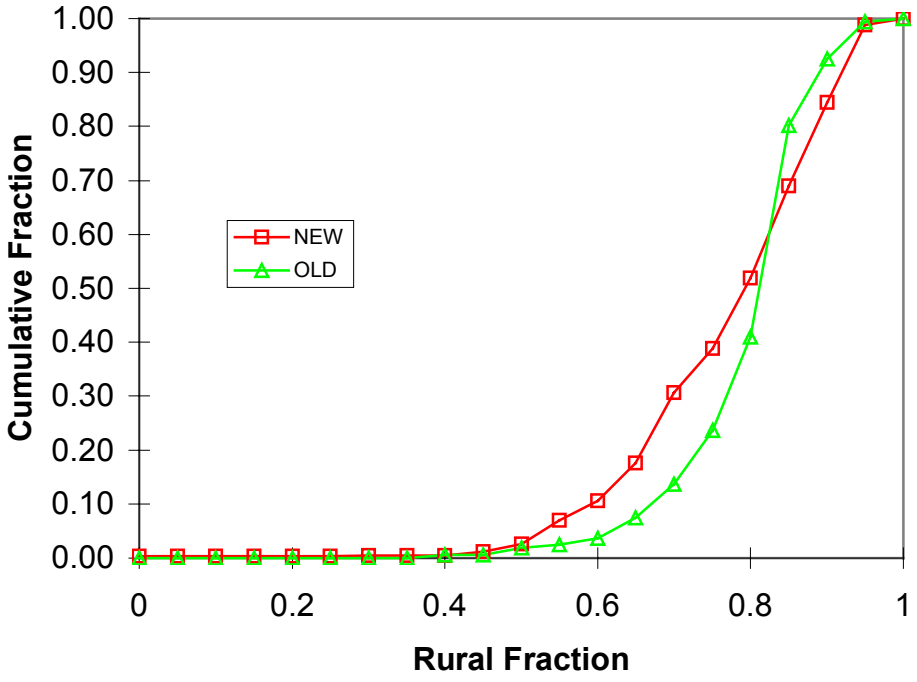

Figure 3.2b Comparison of the cumulative distributions of route *rural fractions* for rail.

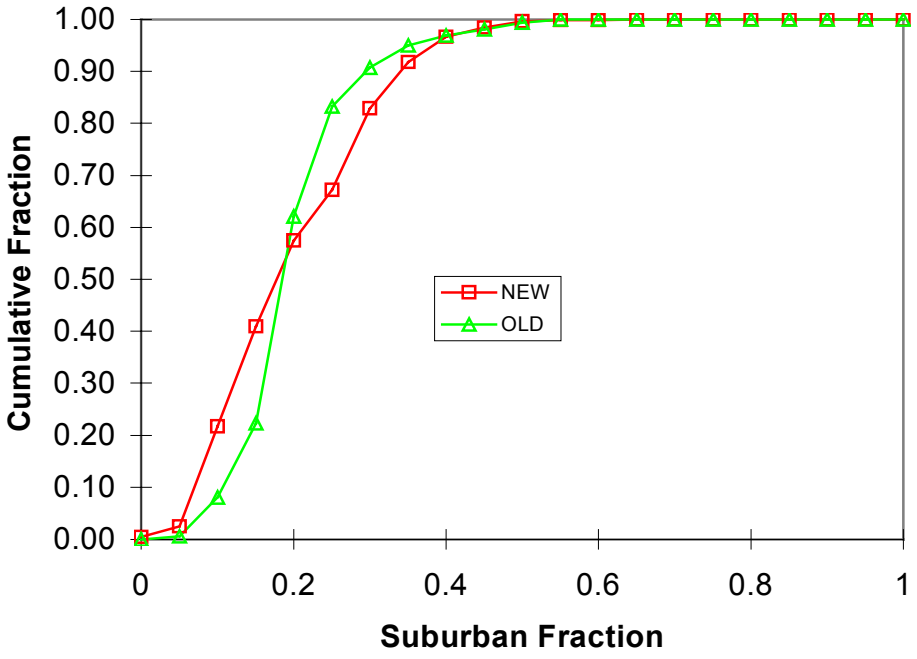

Figure 3.2c Comparison of the cumulative distributions of route *suburban fractions* for rail.

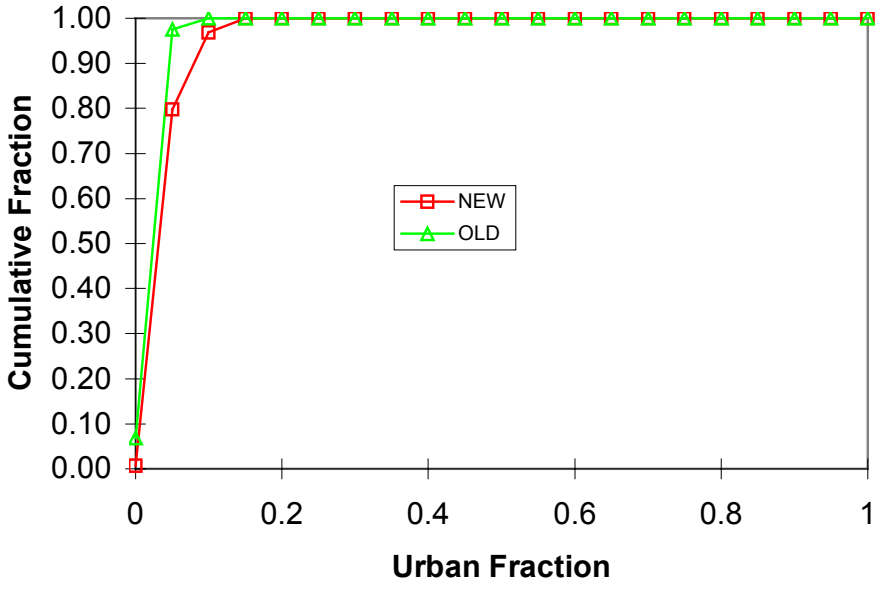

Figure 3.2d Comparison of the cumulative distributions of route *urban fractions* for rail.

3.4.1.2 Route Lengths

The length of any route is a key parameter in determining the risks associated with that route because accident probabilities on the segments of a route are the products of the accident rate (number per vehicle-km) and the length of each segment. In addition, incident-free doses are proportional to route length (e.g., total stop time and driver exposure time for truck shipments) and route-length multiplied by population-density (populations sharing and neighboring the route). Histograms of route lengths derived from the combined route data are presented in Figures 3.3a and 3.3b respectively for truck and rail routes. Integration of these histograms and normalization to a total cumulative probability of 1.0 yielded the final cumulative route-length distributions presented in Figures 3.4a and 3.4b.

3.4.1.3 Rural, Suburban, and Urban Route Fractions

The same data base described in Section 3.4.1.1 provided values for the aggregate fractions of each route that traversed areas with Rural, Suburban, or Urban population densities. Table 3.5 presents the population densities ranges that were used in NUREG-0170 and in this study to define urban, suburban, and rural route segments.

Table 3.5 Definition of Population Density Categories (persons/km^2)

Category	Minimum	Maximum	Mean
Rural	0	66	6
Suburban	67	1670	719
Urban	1670	- - -	3861

Histograms of the Rural, Suburban, and Urban fractions, constructed from the combined data, are shown in Figures 3.5a and 3.5b. The cumulative distribution functions derived from these histograms, are presented in Figures 3.6a and 3.6b.

3.4.1.4 Rural, Suburban, and Urban Population Densities

As part of the route compilation described in Section 3.4.1.2, the distance-weighted average population density values for the rural, suburban, and urban categories were also tabulated in the route characteristics data base. Values for truck routes were sorted and aggregated, then integrated and normalized to create the histograms and cumulative distributions shown in Figures 3.7a through 3.7c; similar processing of the rail route data yielded the plots in Figures 3.8a through 3.8c. Note that the Urban values in Table 3.5 were influenced by the inclusion of city-street route options while the present study is limited to interstate highways and loops that do not traverse such high population-density areas.

3.4.1.5 Application Notes

Each of the cumulative distributions presented in the following figures serves as input to the LHS sampling code. Sampled values of route length, route fractions, and segment population

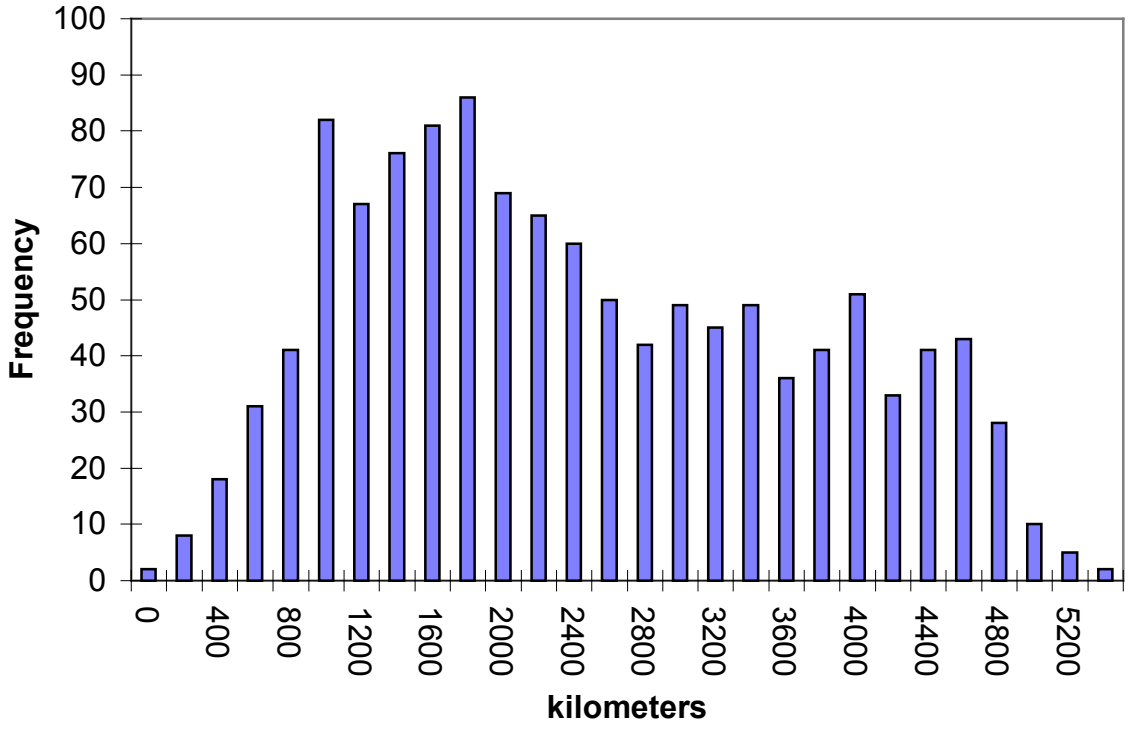

Figure 3.3a Histogram of truck route lengths.

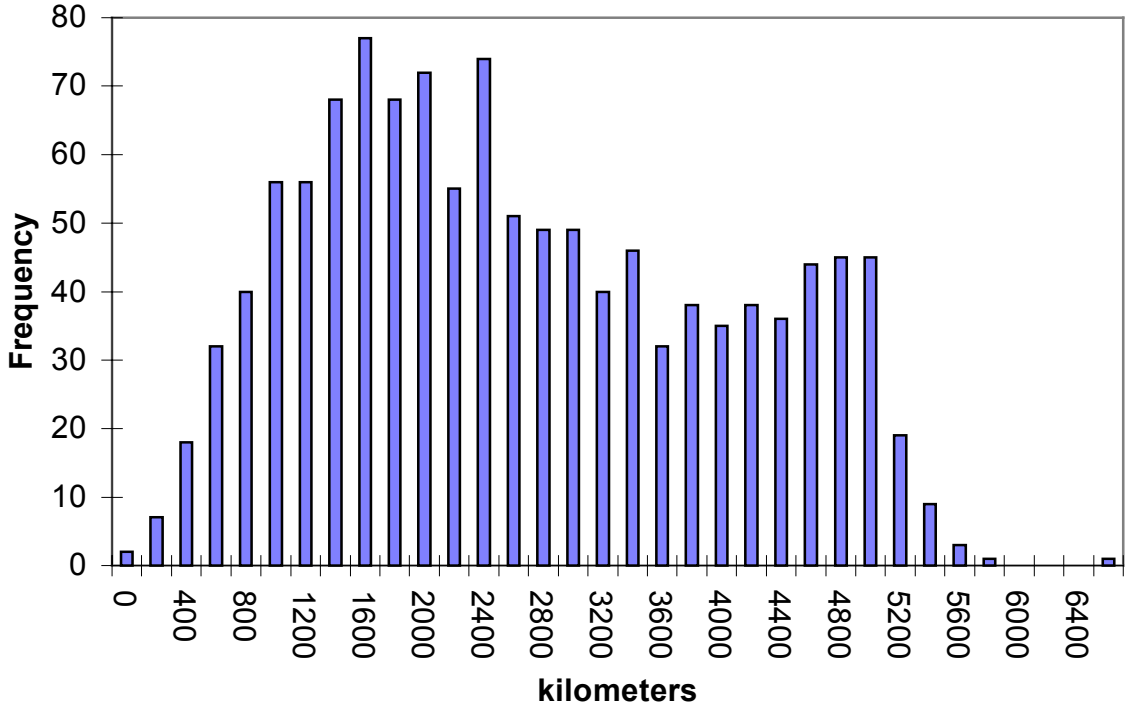

Figure 3.3b Histogram of rail route lengths.

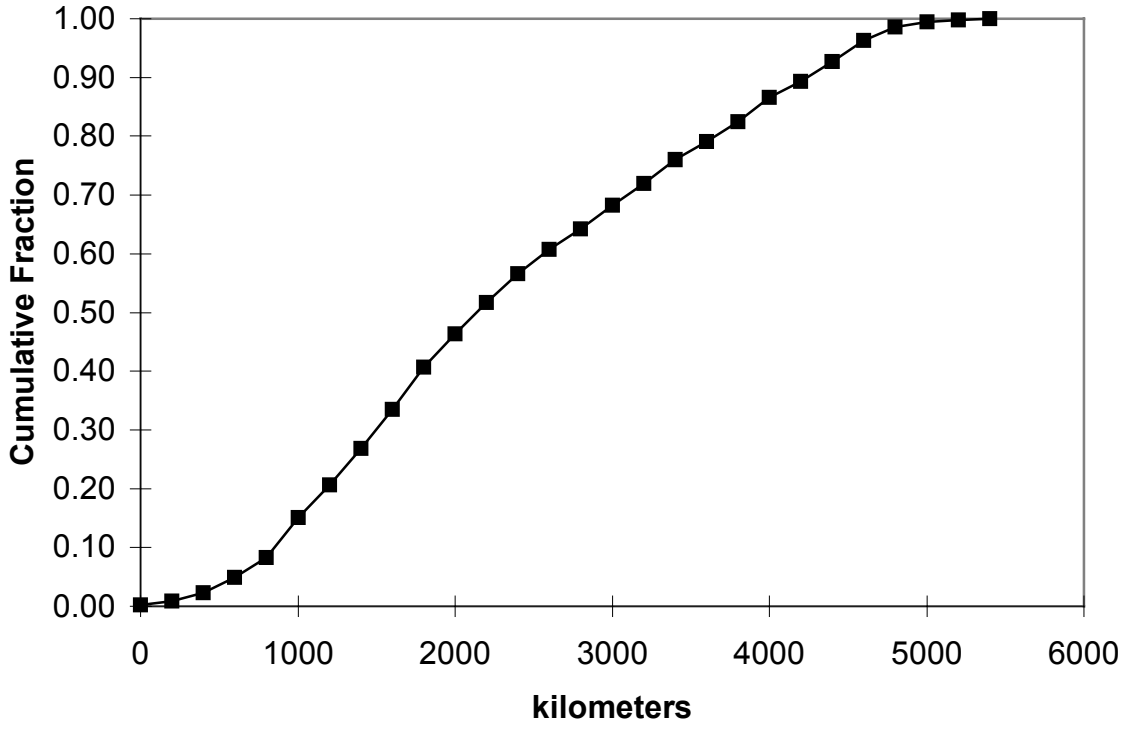

Figure 3.4a Cumulative distribution of truck route lengths.

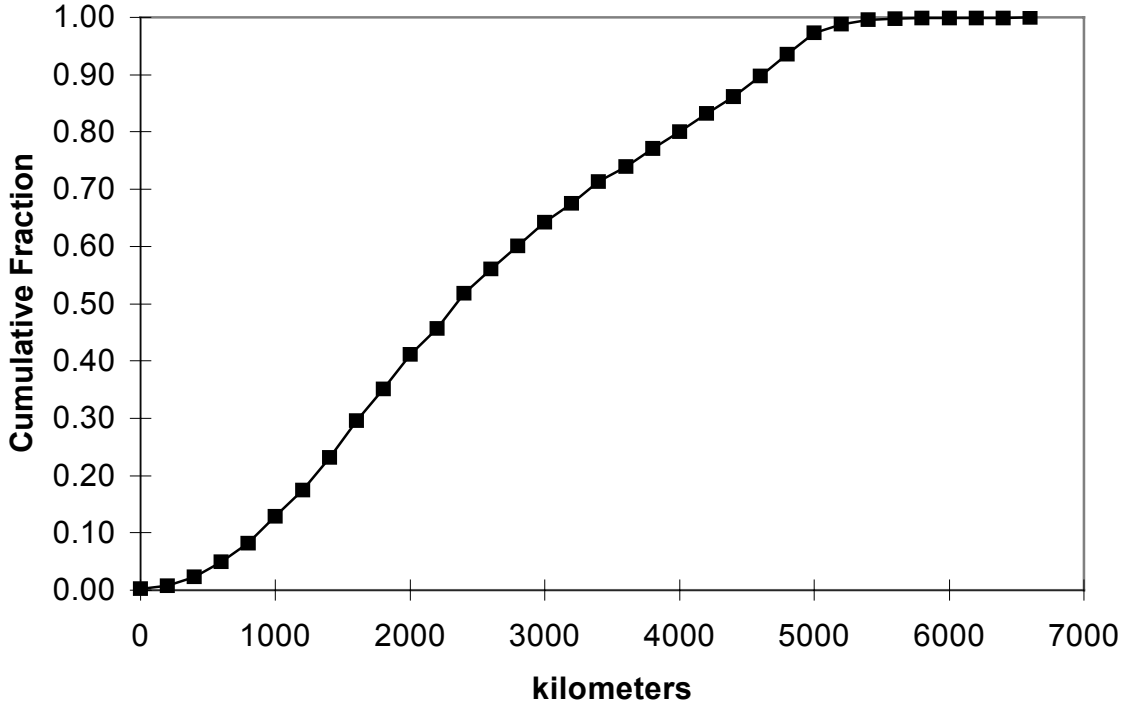

Figure 3.4b Cumulative distribution of rail route lengths.

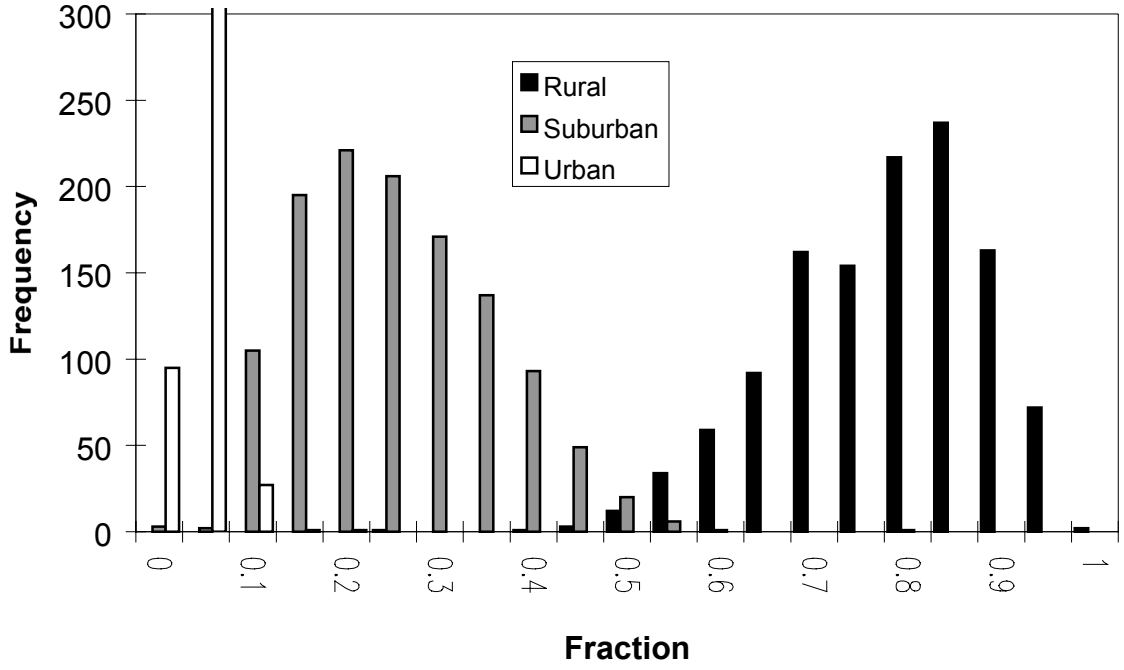

Figure 3.5a Histograms of rural, suburban, and urban length fractions for truck routes.

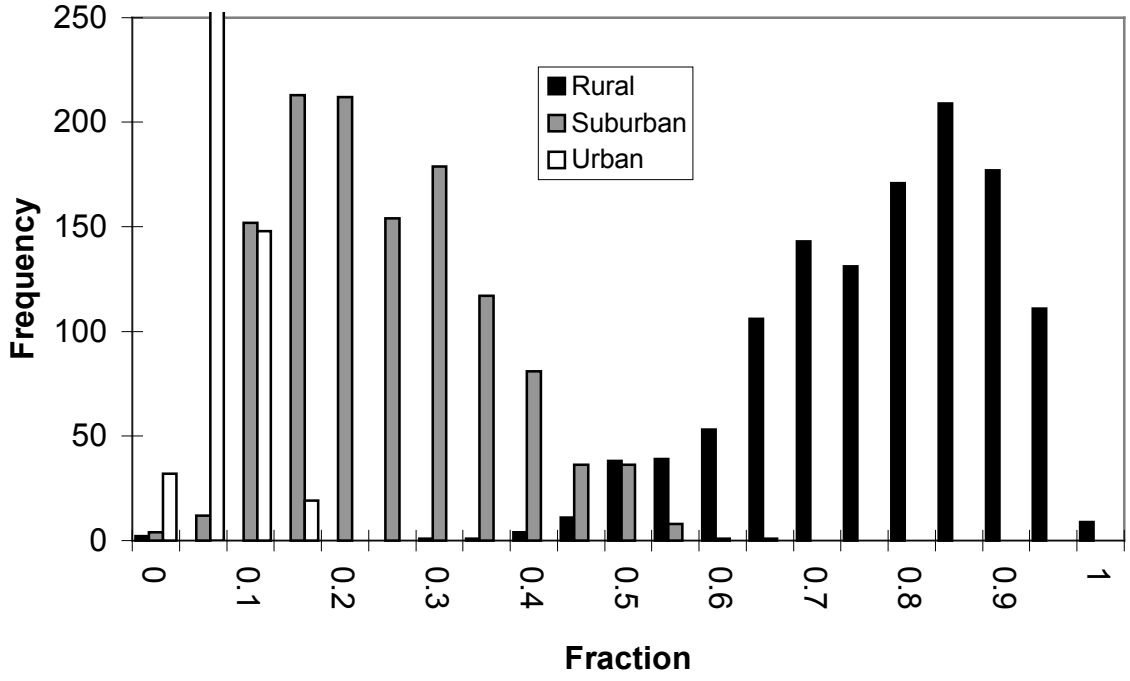

Figure 3.5b Histograms of rural, suburban, and urban length fractions for rail routes.

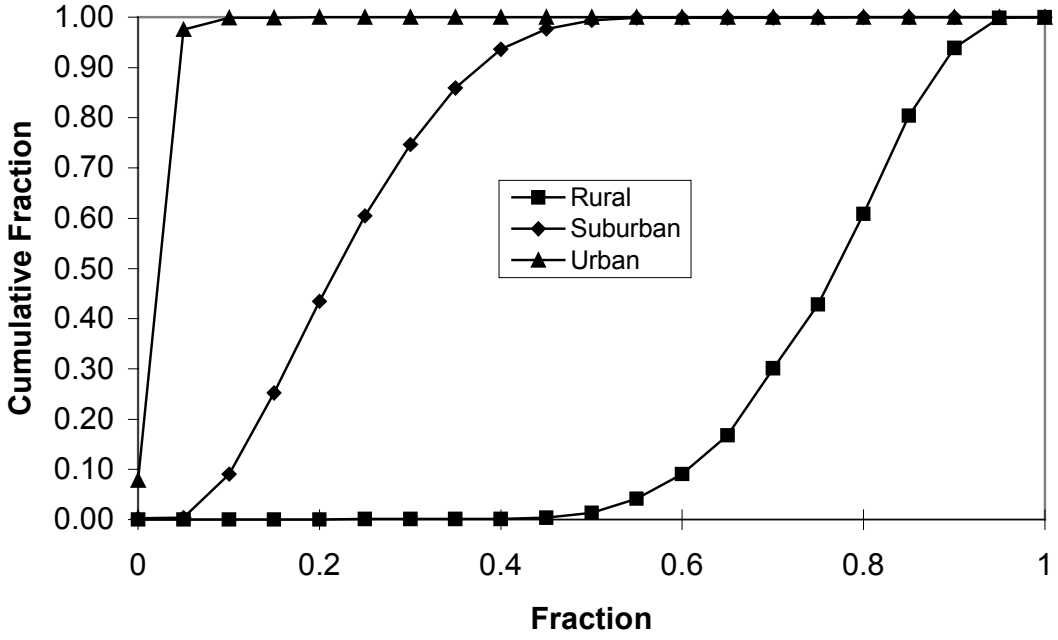

Figure 3.6a Cumulative distributions of rural, suburban, and urban length fractions for truck routes.

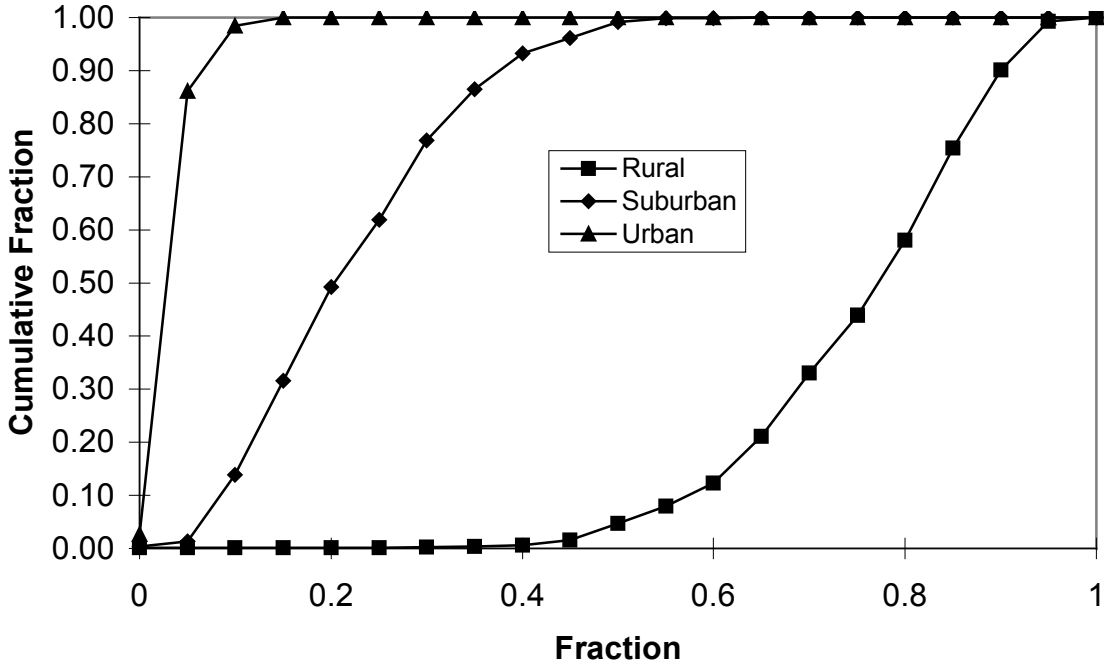

Figure 3.6b Cumulative distributions of rural, suburban, and urban length fractions for rail routes.

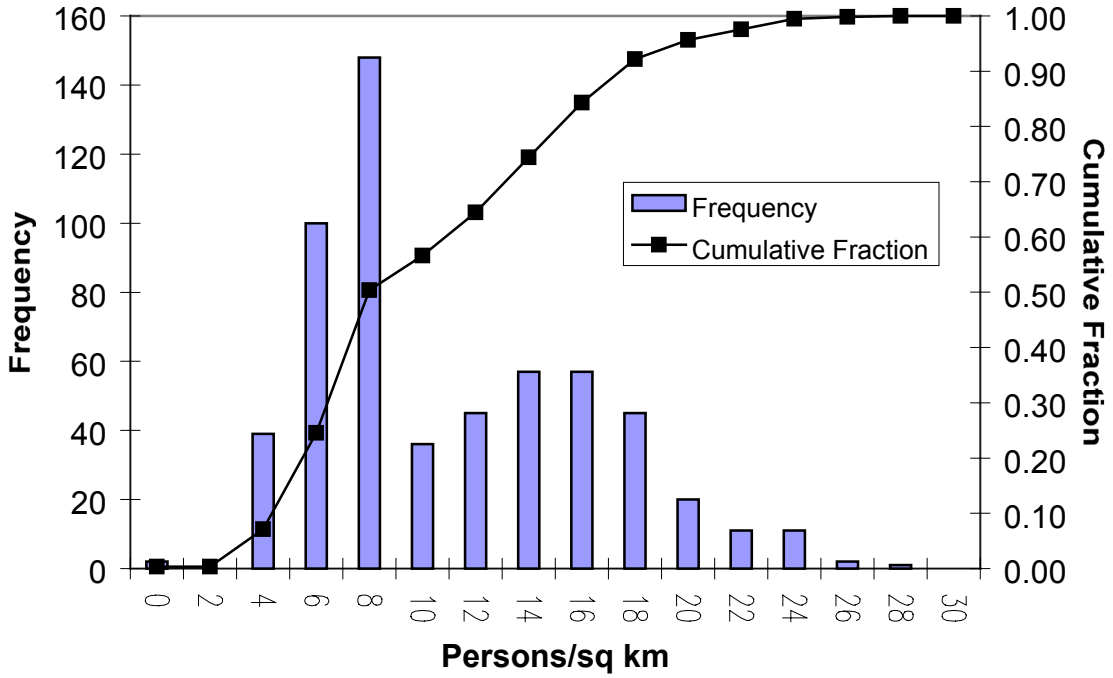

Figure 3.7a Histogram and cumulative distribution for *rural population density* for rural truck route segments.

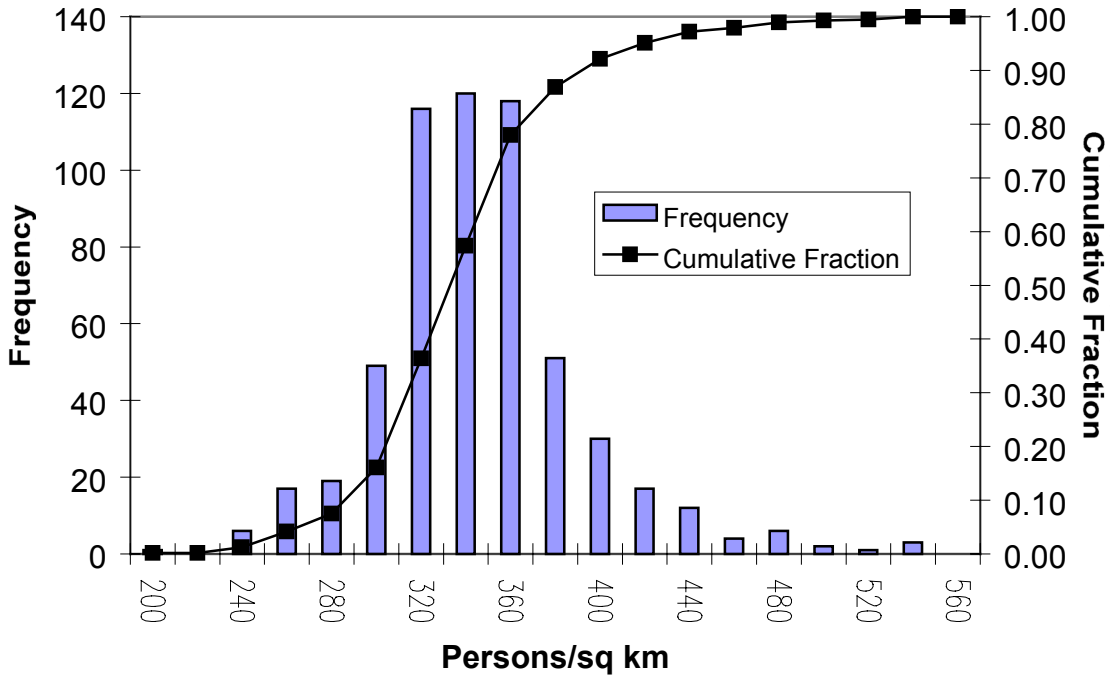

Figure 3.7b Histogram and cumulative distribution for *suburban population density* for suburban truck route segments.

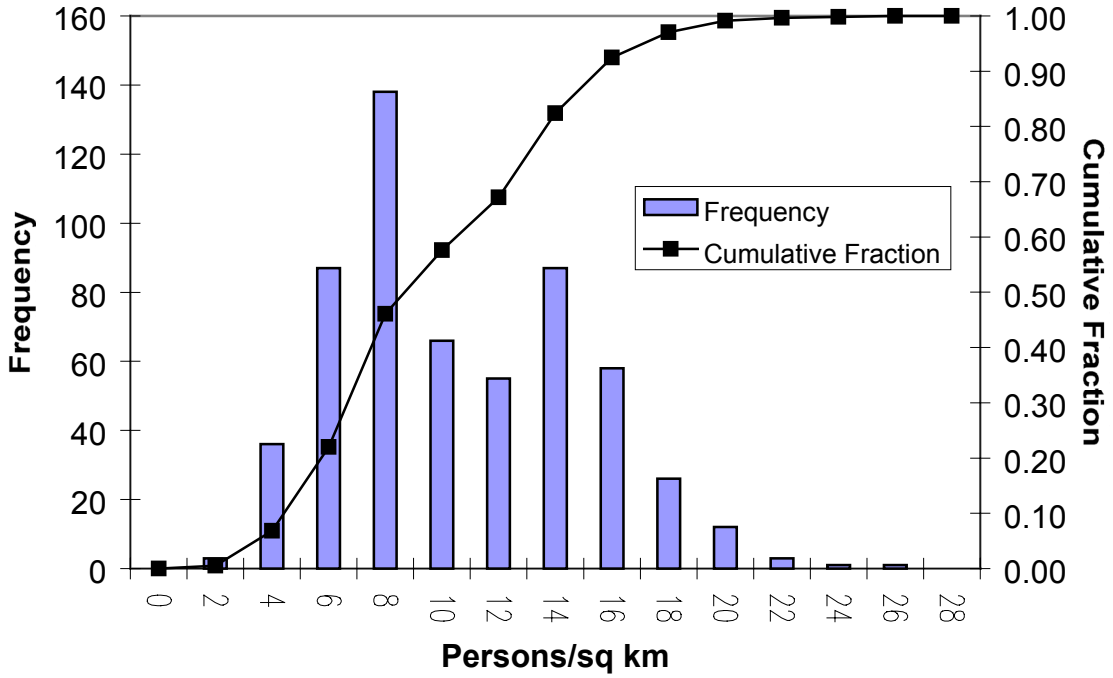

Figure 3.7c Histogram and cumulative distribution for *urban population density* for urban truck route segments.

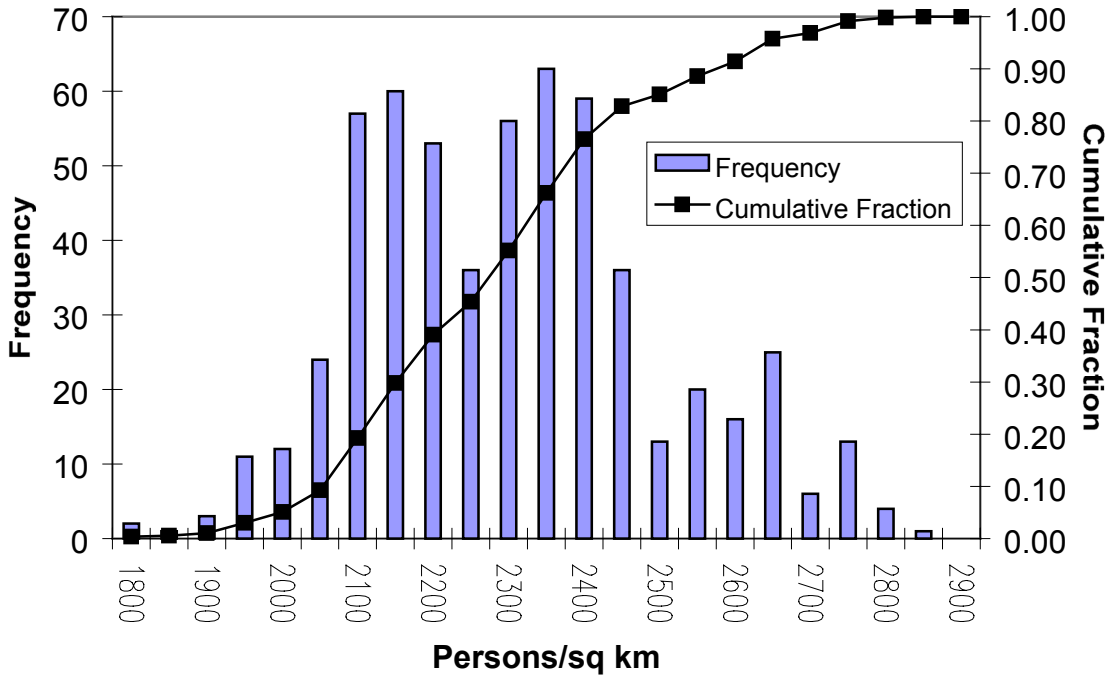

Figure 3.8a Histogram and cumulative distribution for *rural population density* for rural rail route segments.

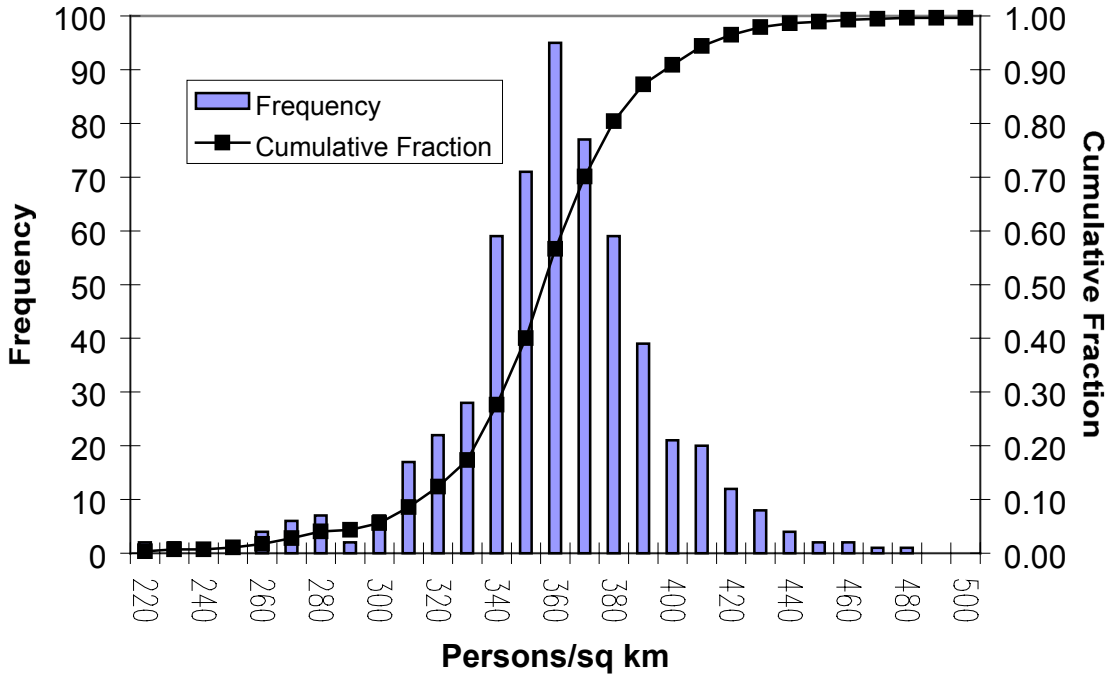

Figure 3.8b Histogram and cumulative distribution for *suburban population density* for suburban rail route segments.

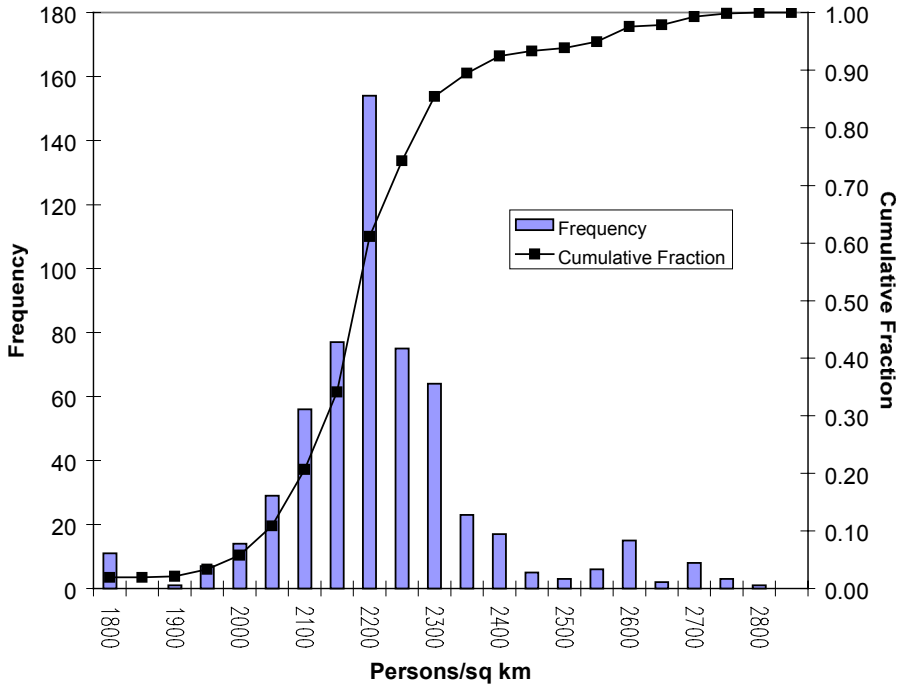

Figure 3.8c Histogram and cumulative distribution for *urban population density* for urban rail route segments.

densities from these distributions provide the necessary route-description inputs for a RADTRAN calculation. The number of sets of sampled values (and the number of RADTRAN calculations) is dependent on the number of individual parameter values to be selected by sampling, and the requirements for statistically meaningful results (at least twice the number of parameters). The size of the sample that is required to develop statistically meaningful results is discussed in Section 8.2.2

3.4.2 Truck and Train Accident Statistics

3.4.2.1 Introduction

Table 3.2 in Section 3.2 indicates that one of the More Important ("Proportional") parameters in calculating accident risks is the LINK Accident Rate. RADTRAN 5 determines the probability of an accident occurring on a particular truck- or train-route link (segment) by computing the product of its length (in kilometers) and the accident rate (number of accidents per vehicle-kilometer) for that link. In general, accident rates vary with highway or rail line classification, e.g., Interstate, U.S. and State highways, or Main and Branch rail lines. The code RADTRAN (version 1 or 5) also distinguishes between Rural, Suburban and Urban links, as defined by the population density bordering the link. For maximum specificity, distinct accident-rate values would be assigned to these distinct portions of a route as well. In reality, such detailed data are not usually available and more generalized accident rates must be used. Regulations of the DOT for truck transport of Highway Route Controlled Quantities of RAM, including spent nuclear fuel specify that Interstate highways (HM-164) be used exclusively, except where not available. Therefore, Interstate highway accident rates are of primary interest for the truck transport portion of this study.

Rail accident data available from the DOT does not identify the character (urban, suburban, or rural) of the region where the accident occurred or the population density of the accident location. However, in DOT compilations of truck accident statistics, Interstate accident rates are reported for accidents occurring in Urban and Rural areas. However, this division is not made on the basis of population density as is done for RADTRAN route segments (0 to 66, 67 to 1670, and greater than 1670 persons/km^2 for Rural, Suburban and Urban areas, respectively). Instead, the DOT division distinguishes between incorporated areas (cities) and unincorporated areas. Since there can be Suburban (or even Rural) population densities (as specified for RADTRAN) within city limits or Suburban population densities outside of city limits, the DOT division of accident statistics does not easily map into the division required by RADTRAN. Past practice has been to use the DOT Urban accident rate for Interstate highway links identified as Urban in RADTRAN and to use the DOT Rural accident rate for Interstate highway links identified as Suburban or Rural in RADTRAN. For the present study, accident rates for the entire set of routes examined, were used to construct cumulative probability distributions from which representative samples of route parameters were selected, by LHS, for use as input for RADTRAN calculations. This approach permitted an approximate separation of the tabulated DOT data into Rural, Suburban and Urban accident rates for Interstate highways, as is described in Section 3.4.2.2.

3.4.2.2 Truck Accident Data

Over the years since NUREG-0170 was published, several studies of truck accident rates were performed by the DOT, the DOE, or their contractors and the results published in formats with variable applicability to the needs of this present study. These studies are described briefly in chronological order in the following paragraphs.

Urban Study. This was an investigation of actual accident experience on city streets in an urban area (New York City) performed to answer criticisms of the single, point-estimate accident rate used in NUREG-0170. The data were gathered in the mid-1970's and the results were published in 1980 [3-18]. The accident rates obtained are not applicable to Interstate highways but are included here to indicate a potential upper limit to be reached by accident-rate distributions employed in the current study.

California Highway Department Study. Highway accident rates for three truck types and several highway types were derived from California collision reports. Data for 1980 and 1981 were extracted from individual accident files by the State of California Department of Transportation in response to a request from SNL. The results were published in a SNL report [3-28].

Modal Study. Lawrence Livermore National Laboratory (LLNL) performed an analysis of spent nuclear fuel truck transport [3-29] in which truck accident rates were derived from three sources of data: DOT Bureau of Motor Carrier Safety (BMCS, now Office of Motor Carriers), American Petroleum Institute (API), and California Department of Transportation. For the Modal Study, LLNL chose to use the API rate data because of the similarity of tanker-trucks to the trucks used to transport spent nuclear fuel casks. However, the API data included light truck accidents, which were atypical and inflated the accident rates. For this study, the BMCS accident rate data are judged to be most appropriate because the data reflects trucks and highways like those that will characterize spent fuel shipments.

SIS Project EIS. The DOE published an Environmental Impact Statement (EIS) on the Special Isotope Separation Project in which a national average accident rate for combination trucks (tractor/trailers) on Interstate highways was derived from DOT data [3-30]. Average accident rates for the specific routes considered in the EIS were also calculated and found to be nearly the same as the national average (48 states).

BMCS Data. Four years (1984 and 1986 through 1988) of accident data derived from reports submitted to the DOT by commercial carriers have been tabulated for Interstate highways inside and outside city limits (Urban and Rural by DOT definition) for each of the 48 contiguous United States. Data for 1986 through 1988 were collected in a study performed by Argonne National Laboratory (ANL Longitudinal Review) for the DOE [3-31]. BMCS data are biased (toward more severe accidents compared to total accident statistics) by the reporting criteria imposed by the DOT, but they apply most specifically to the vehicle and highway types employed in spent nuclear fuel truck shipments.

Truck accident rates and the years from which data were obtained in these various reports are presented in Table 3.6 together with the value quoted in NUREG-0170.

Table 3.6 Truck Accident Rates (Accidents per Million Vehicle-Kilometers)

Source	Period	Urban or Total Rate*	Non-Urban Rate	Comments
NUREG-0170	pre-1975	0.46		
Urban Study (NY City)	pre 1980	7.2 - 91		Depends on time of day
		15		Average
Calif. Hwy. Dept.	1980	0.8	1.1	Truck/Trailers on Freeways
	1981	0.7	1.0	Total Accidents
Modal Study				
BMCS	1960-72	1.6		Reportable Accidents
Am. Petrol. Inst.	1968-81	4.0		Used in the Study
Calif. Hwy. Dept.	1981-83	0.6		Limited Access
		3.1		4-Lane
SIS Project**	1984	0.31		Tractor-Trailers
BMCS**	1984	0.20	0.28	Interstate Highways
ANL Long. Rev.	1986-88	0.36	0.20	Interstate Highways

* Urban rate if distinguished, otherwise Urban and Non-Urban rate
** Average over 48 states

It should be noted that these values are not necessarily based on the same accident definition, truck type, highway type, or sample sizes. However, they give an indication of the range of values that pertain to different types of highways, different demographic areas, and different points in time. The data collection period was of particular concern because nearly all of these data were collected when the national speed limit, which was recently cancelled, was 55 mph.

In April of 1999, an update of the ANL Longitudinal Review was published which analyzes heavy combination truck accident data for 1994 to 1996 [3-32]. Because of changes in the way truck accident data are currently reported, the data in this report are not directly comparable with the data in the earlier ANL study [3-31]. Nevertheless, the average accident rate on Interstate highways for the three-year period for the continental United States is 3.45 accidents per 10 million truck-kilometers which is quite similar to the means of the Rural and Suburban accident-rate distributions (respectively 2.2 and 4.1 accidents per 10 million truck-kilometers) that are derived in the following paragraphs. In addition, the ANL report authors note that the accident rate on Interstate highways increased by 37% in states which increased speed limits in 1995 or 1996. The authors caution that available data do not yet establish whether this is a sustained change or a transient; in any case, it is not a large enough change to invalidate the accident-rate distributions employed in the current analysis.

The most comprehensive and recent of the data sets available at the time accident-rate distributions were developed were the BMCS accident-rate listings for all 48 states which related directly to combination truck accidents on Interstate highways. However, they were not separated into accidents within Rural, Suburban, and Urban portions of the Interstate highway system, as required for RADTRAN input; they were distinguished only according to whether accidents occurred inside incorporated areas ("Urban," referred to as City in the following

discussion) or outside incorporated areas ("Rural," referred to as non-City in the following discussion). A method for separating these sets of accident-rate data into the required population-density groups, based on correlations between non-City or City accident rates with state population densities outside or inside incorporated areas (as determined by the U.S. Bureau of the Census for 1990) for each state, was developed.

For each of the 48 states, the BMCS Interstate-highway city accident rates from 1984 and the city accident rates in the ANL Longitudinal Review (1986-88), were averaged; this was also done for the non-city accident rates. In Figure 3.9a, the non-City average state accident rates that correspond to rural population densities, as defined for RADTRAN calculations (i.e., $\leq$ 67 persons/km^2), are plotted versus the population densities of the state's unincorporated areas (state population minus incorporated population divided by state area minus incorporated area). In Figure 3.9b, the average City accident rates for each state that correspond to suburban or urban population densities, as defined for RADTRAN calculations (i.e., > 67 persons/km^2), are plotted versus the average population densities of incorporated areas (cities with populations $\geq$ 25,000). This plot also contains six non-city accident rate points because they correspond to RADTRAN suburban population densities (densities greater than 67 persons/km^2). This figure also contains three points that correspond to RADTRAN urban population densities (densities greater than 1670 persons/km^2). After dropping the three urban points, histograms of the accident rates in Figures 3.9a and 3.9b were separately computed, summed, and normalized, thereby generating cumulative distributions of accident rates for accidents on Rural Interstate Highways and also on Suburban plus Urban Interstate highways in areas that have population densities that fall within the RADTRAN population density range for rural or suburban regions. These cumulative distributions are presented in Figures 3.10a and 3.10b.

These two cumulative distributions were sampled, using LHS, to provide accident-rate values for the Rural and Suburban fractions of the 200 routes in the LHS sample of More Important parameter values. Because of the lack of data for accidents in Urban areas, the three points in Figure 3.9b that have Urban densities (> 1670 persons/km^2) were averaged to provide a point-estimate accident rate of 5.2 accidents per 10^7 vehicle-kilometer for the relatively small Urban fractions of the 200 representative routes. Although less than the highest accident rate depicted in Figure 3.9b, this rate is considered reasonable for urban regions, since interstate highway speeds within the densely populated urban areas are generally lower than they are in suburban or rural regions, therefore there should be fewer reportable accidents and consequently a lower frequency of reportable accidents.

3.4.2.3 Train Accident Data

The additional sources of rail accident-rate data, that have become available since NUREG-0170 was published, are not as numerous as those for truck accident-rate data. The sets of data that were used for this study are a subset of the sources described in Section 3.4.2.2; these sets of data are listed in Table 3.7.

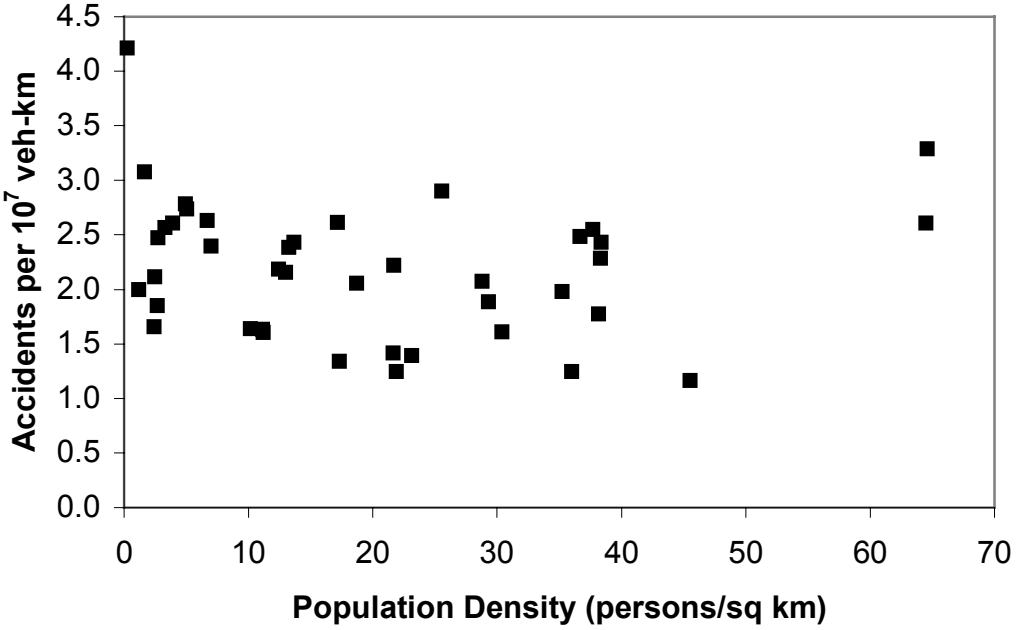

Figure 3.9a Accident rate versus rural population density.

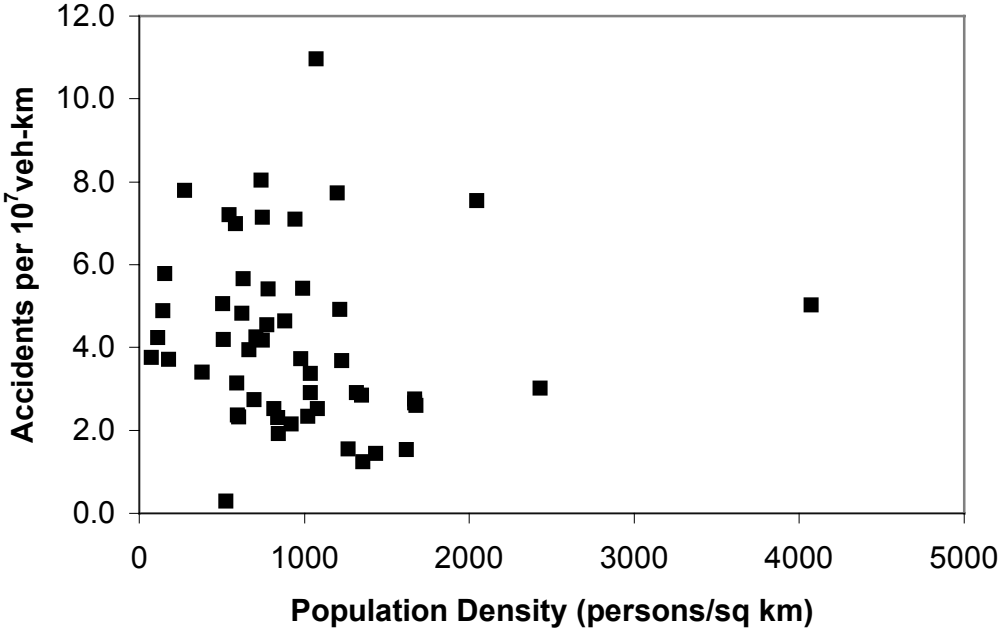

Figure 3.9b Accident rate versus suburban population density.

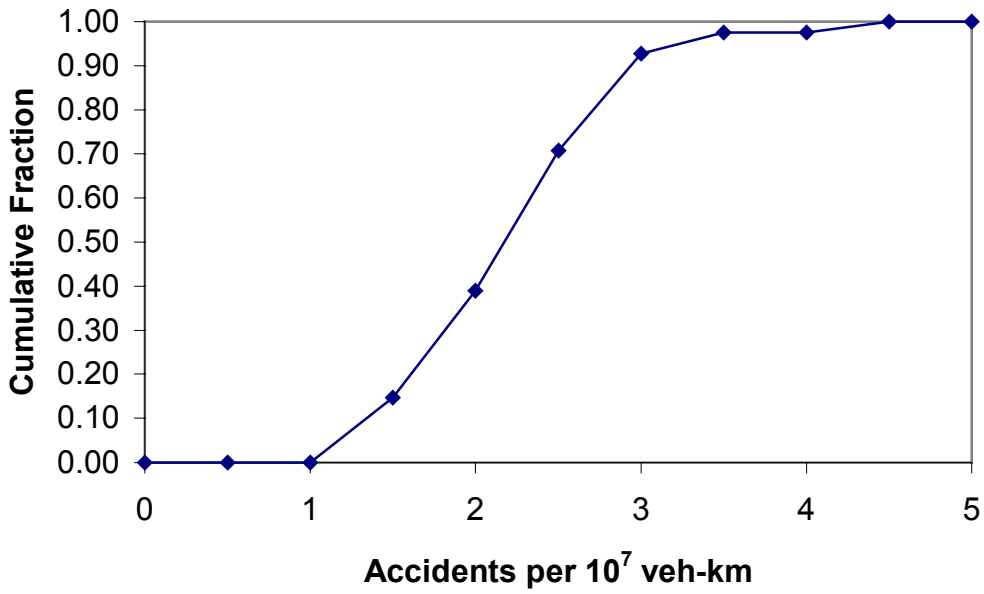

Figure 3.10a Cumulative distribution of rural accident rates.

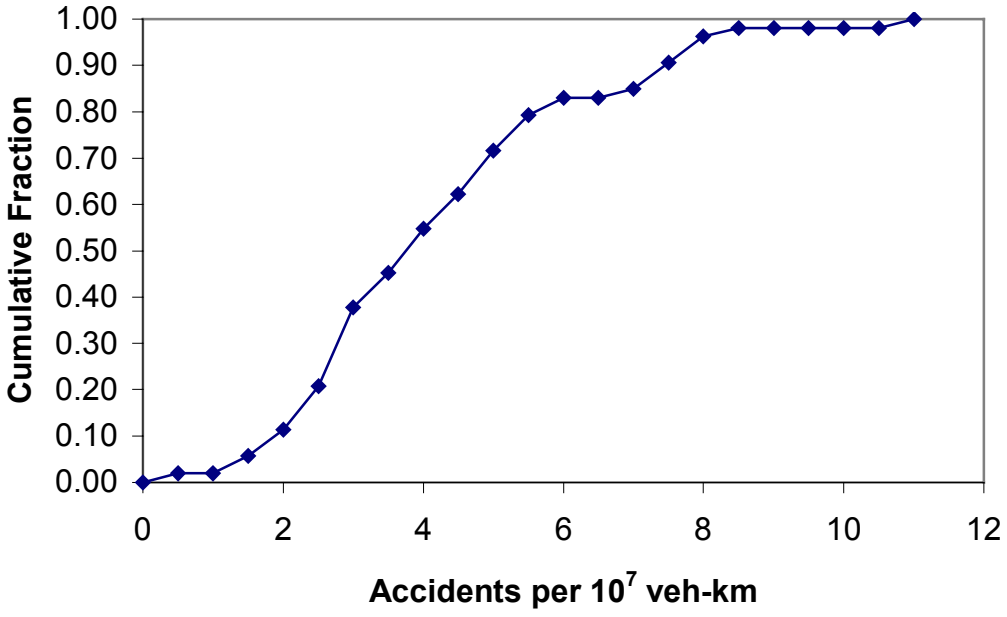

Figure 3.10b Cumulative distribution of suburban and urban accident rates.

Table 3.7 Rail Accident Rates per Million Rail Car km

Source	Date	Urban or Total*	Comments
NUREG-0170	pre-1975	0.9	Per Rail Car km
Modal Study			
Fed. Rail Admin.	1975-82	7.5 [0.11]	Per Train km, All trains & tracks Per Rail Car km @68 cars/train
ANL Long. Rev.**	1985-88	0.06	Per Rail Car km, All tracks
		0.03	Per Rail Car km, Main Line Only

* Urban rate if distinguished, otherwise Urban and Non-Urban rate
** Average over 48 states

Note that the rate from the Modal Study is per *train*-km which must be corrected to car-km for comparison to the other values. Comparing car-miles to train-miles on Class I railroads for 1980 and 1990, as obtained from the DOT Internet Web page, indicates that the approximate number of cars per train is 68. This value leads to a Modal Study accident rate of 0.11E-6 per car-km which lies between the NUREG-0170 and ANL values in Table 3.7.

A histogram and cumulative distribution of data for accidents on main lines by state, as compiled in the ANL study, were computed and the distribution is presented in Figure 3.11. The ANL study did not distinguish accidents on the basis of population densities; therefore, this distribution was sampled, using LHS, to provide accident rates for all portions of the rail routes analyzed.

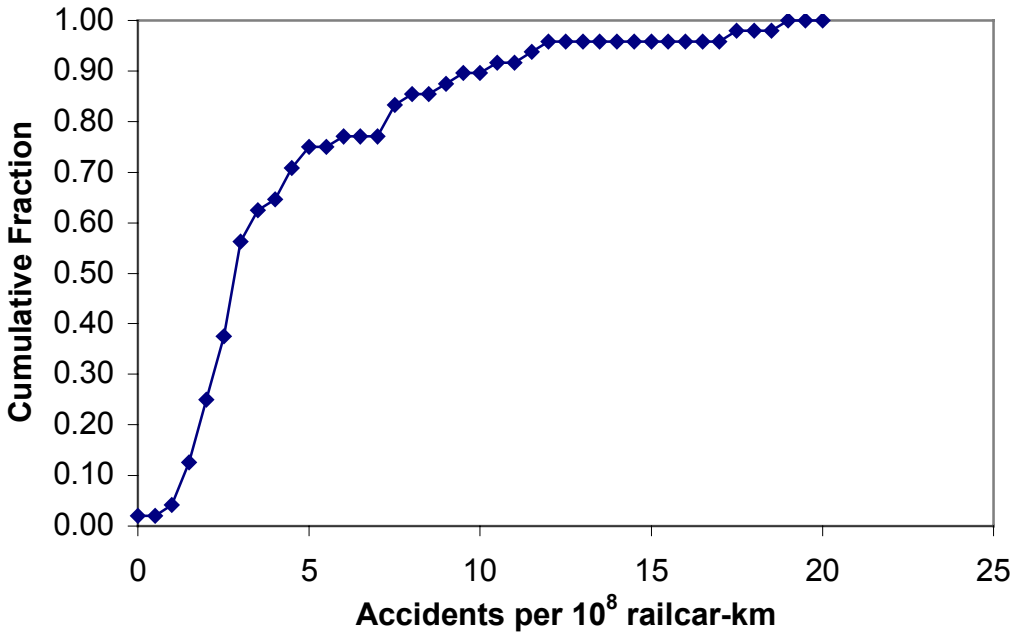

Figure 3.11 Cumulative distribution of rail accident rates (used for all segments: Rural, Suburban, and Urban).

3.4.3 Development of Miscellaneous Distributions

In addition to route parameters (length, population zone fractions, population densities and accident rates), several additional parameters were selected as suitable input for LHS. In this section, the development of distributions for the remaining LHS parameters is described.

3.4.3.1 Truck Stop Time

Fueling, eating, and other stops were characterized in a study of commercial truck stops serving a major truck transport route (Interstate 40) [3-19]. The study provided a tabulation of individual stop times (in minutes) versus number of observed stops suitable for constructing a histogram and a cumulative distribution. The results of the study were adapted to represent the totality of stops made during a typical spent nuclear fuel shipment by scaling up the observed times to values appropriate for the length of the shipment. The parameter employed in previous RADTRAN versions for estimating total stop time (0.011 hours per km of shipment length) and the average distance from the distribution of shipment distances (~1800 km) yielded an average total stop time per truck shipment of: $1800 \times 0.011 = 19.8$ hours. The individual stop times (from the study, in hours) were scaled up to yield a stop time of 20 hours at the peak of the histogram (Number of Observed Stops = 10). Table 3.8 lists the original stop times in minutes (first column), the original stop times in hours (second column), the scaled stop times in hours (third column) and the corresponding stop counts (fourth column). The cumulative distribution (fourth and fifth columns of Table 3.8) is shown in Figure 3.12; this distribution was added to the LHS input file. Note that the value of 0.011 hours of stop time per km of shipment length is descriptive of normal commercial trucking operations and includes time required by regulations for sleep.

Table 3.8 Distribution of Normal Commercial Truck Stop Times

Stop Time (min)	Stop Time (hr)	Scaled Stop Time (hr)	Number of Observed Stops	Cumulative Distribution
0	0	0	0	0
8	0.13	7	3	0.06
11	0.18	10	6	0.17
14	0.23	12	8	0.33
17	0.28	15	9	0.50
20	0.33	17	8	0.65
23	0.38	20	10	0.85
26	0.43	23	2	0.88
29	0.48	25	2	0.92
32	0.53	28	2	0.96
35	0.58	30	1	0.98
50	0.83	43	1	1.00

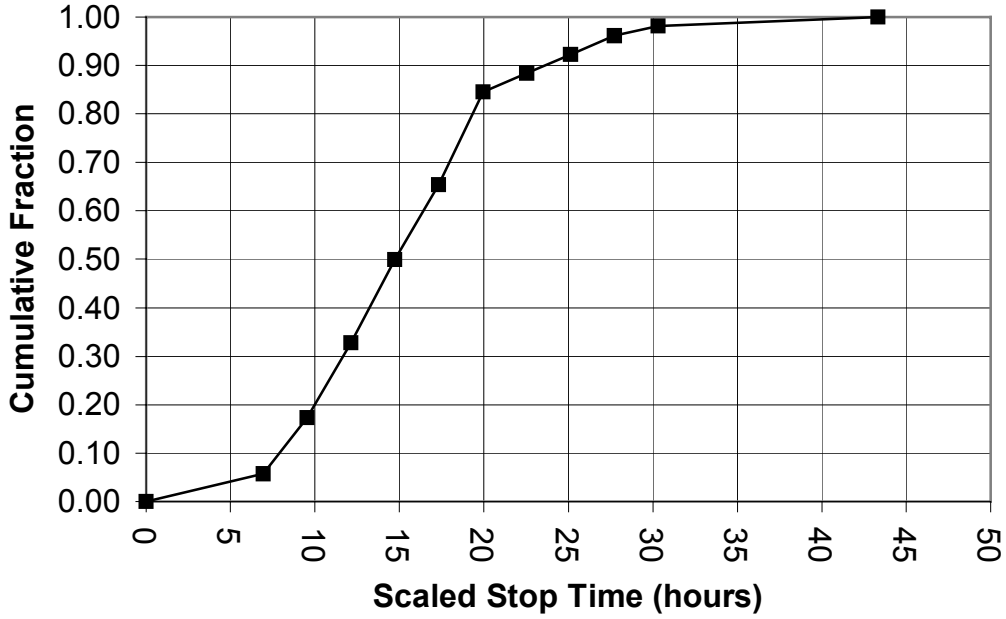

Figure 3.12 Distribution of normal commercial truck stop times.

As is discussed in Section 8.6, industry practice for spent fuel shipments under exclusive use conditions is to use two-man crews and to minimize stop time by not making stops to sleep. As is shown in Section 8.6, when spent fuel shipments are made under these special operating conditions, the incident-free risks calculated using the stop times specified by the distribution in Table 3.8 and Figure 3.12 are found to be conservative by a factor of approximately 28. In Section 8.6, this factor is used to correct by scaling the incident-free doses that are calculated using the stop time distribution presented in Table 3.8 and Figure 3.12.

3.4.3.2 Evacuation Time

The elapsed time between an accident occurrence and completed evacuation of the area around an accident site was set at 24 hours in RADTRAN I. A study of evacuation times [3-33], in which news reports of accidents requiring evacuations (e.g., transportation, refinery, and chemical plant accidents) were followed up by telephone interviews of the authorities involved in handling the accident/evacuation, provided a distribution of the times required to evacuate an accident site and the surrounding area threatened by release of hazardous materials. The data from this study were subsequently supplemented [3-34] by Department of Transportation data describing elapsed time between accidents and arrival of first-responders (Emergency Medical Service personnel) [3-35]. A histogram and cumulative distribution were constructed from the combined elapsed-time data sets. As Figure 3.13 shows, the points of the cumulative distribution are fit with high precision by a log-normal distribution. This log-normal distribution of evacuation times in days was incorporated into the LHS input files for truck and rail shipments.

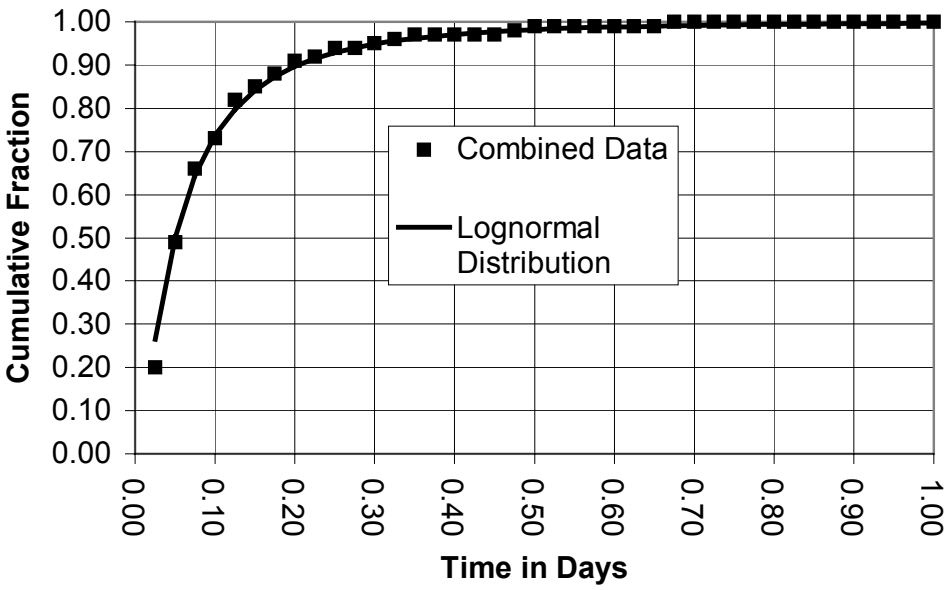

Figure 3.13 Distribution of response team arrival plus evacuation times.

3.4.3.3 Pasquill Stability Category

The relative speed of dispersion of a cloud of aerosols is related to atmospheric stability as indicated by Pasquill Stability categories A through F (in order of increasing stability). Table 3.9 presents the occurrence frequencies of these six atmospheric stability classes as calculated from national average observed stability conditions for the continental United States [3-36] and the cummulative distribution of these frequencies. This discrete cumulative distribution was used to select one of the six Pasquill atmospheric stability categories for use in each of the 200 sets of More Important parameter values selected by LHS sampling.

For risk assessment purposes, the distribution of stability class frequencies of occurrence must be very broadly based because the site of a transportation accident cannot be pre-determined nor can the atmospheric stability at a random location be reliably specified by measurements available from a distant weather station. Regional stability class occurrence statistics could be used but, for these calculations, the additional precision their use might produce was not expected to be worth the effort required to gather and process the data.

Table 3.9 Distribution of Pasquill Categories

Pasquill Category	Occurrence Frequency	Cumulative Distribution
A	0.043	0.043
B	0.190	0.233
C	0.190	0.423
D	0.216	0.639
E	0.241	0.88
F	0.120	1.00

3.4.3.4 Truck and Rail Transportation Index

Values of cask dose rates at one meter from the cask surface (RADTRAN input parameter, TI) have been calculated for truck and rail spent fuel casks by Parks et al. [3-37] for spent fuel with various cooling times. Pairing of these values, with the number of PWR and BWR assemblies in the 1994 spent fuel inventory [3-38] that have cooling times equal to the time that produced the calculated surface dose rate at 1 m from the surface, allowed cumulative distributions of cask surface dose rates to be constructed for PWR and BWR spent fuel for both truck and rail casks. Tables 3.10 and 3.11 present these distributions. Because the upper limits of these distributions were less than the regulatory limit for cask dose rates (10 mrem/hour at 2 m from the cask surface), in order to be conservative, the calculated dose rates at 1 m were scaled so that the upper limits of both distributions equaled 13 mrem/hour at 1 m, which for a cask with a maximum dimension of 5 meters is equivalent to the regulatory cask dose rate limit. Finally, because the difference between the PWR and BWR distributions was insignificant compared to the expected accuracy of the model, a single distribution of TI values was constructed by pooling the truck cask or rail cask PWR and the BWR data. These distributions are presented in the last column of Tables 3.10 and 3.11.

Table 3.10 Distribution of Dose Rate at 1 m (RADTRAN parameter TI) for Truck Casks

Cooling Time (yr)	TI	BWR		PWR		Distribution Used in Calculations
		Assys. of that Age	Cumulative Distribution	Assys. of that Age	Cumulative Distribution	
5	**13.0**	3781	1.000	2824	1.00	**1.00**
10	**6.39**	3832	0.725	2785	0.711	**0.72**
15	**4.57**	2735	0.447	1937	0.427	**0.44**
20	**3.49**	2131	0.248	1662	0.229	**0.24**
25	**2.76**	1290	0.094	575	0.059	**0.08**

Table 3.11 Distribution of Dose Rate at 1 m (RADTRAN parameter TI) for Rail Casks

Cooling Time (yr)	TI	BWR		PWR		Distribution Used in Calculations
		Assys. of that Age	Cumulative Distribution	Assys. of that Age	Cumulative Distribution	
3	**13.0**	1900	1.000	1400	1.000	**1.00**
5	**6.72**	3781	0.879	2824	0.875	**0.87**
10	**3.95**	3832	0.637	2785	0.622	**0.63**
15	**3.03**	2735	0.393	1937	0.373	**0.38**
20	**2.43**	2131	0.218	1662	0.200	**0.21**
25	**1.99**	1290	0.082	575	0.051	**0.08**

3.4.3.5 Highway Traffic Density

Traffic density information is used in calculating On-LINK incident-free doses in RADTRAN 5. Distributions of this parameter (in units of vehicles per hour per lane) for rural and suburban areas were developed from Department of Transportation publications tabulating miles of rural interstate highway together with vehicle-miles per year for each state [3-39] and daily freeway traffic per lane for 377 urbanized areas [3-40], respectively. For the rural distribution, the annual vehicle-miles value for each state was converted to vehicles per hour (dividing by the state's miles of interstate and the number of hours per year). The value of vehicles per hour per lane (as required by RADTRAN) was approximated by assuming that rural interstate highways typically have two lanes in each direction. These values were used to construct the histogram and cumulative distribution shown in Figure 3.14. The data for urbanized areas included population density for each area. In an effort to separate the data into suburban and urban groups, the traffic densities were plotted versus their respective population densities (Figure 3.15). Nearly all of the data points lie in the suburban range (67 to 1670 persons/km^2); the points within the range were used to construct the suburban traffic density histogram and cumulative distribution shown in Figure 3.16. The 200 values of rural and suburban truck traffic density incorporated into the 200 sets of More Important parameter values were selected from these distributions using LHS sampling methods.

Because there were so few points in the urban population density range (> 1670 persons/km^2), the value of the largest traffic density, 930 vehicles per hour per lane, was assumed to be a conservative point-estimate for urban portions of the truck shipment routes.

3.4.3.6 Persons per Vehicle Sharing a Highway Route

Persons per vehicle data are used in RADTRAN 5 to calculate On-LINK incident-free doses. A tabulation of private vehicle occupancy in the United States for 1990 [3-41] derived from the 1990 Census of Population by the Journey-to-Work and Migration Statistics Branch, Population Division, U.S. Bureau of the Census was converted to a discrete cumulative distribution for LHS input (Table 3.12). Because the original tabulation did not distinguish vehicle occupancy according to population density, the same distribution was used in the LHS input for rural, suburban, and urban portions of the truck shipment routes.

Table 3.12 Distribution of Persons per Vehicle on Highway Routes

Persons per Vehicle	Fraction of Vehicles	Cumulative Distribution
1	0.846	0.846
2	0.121	0.967
3	0.02	0.987
4	0.007	0.994
5	0.002	0.996
6	0.001	0.997
>6	0.003	1

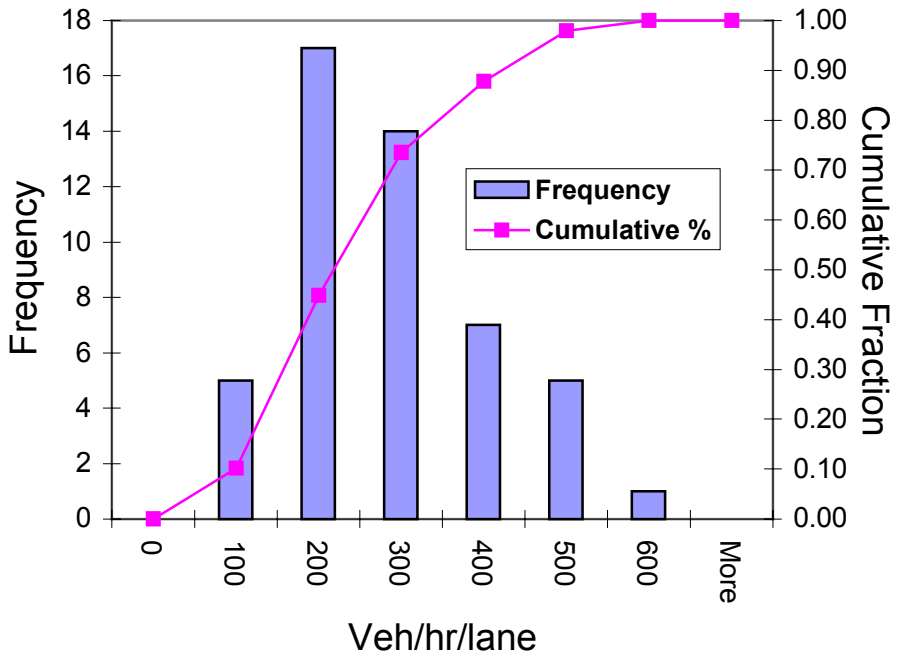

Figure 3.14 Histogram and cumulative distribution of rural interstate traffic density.

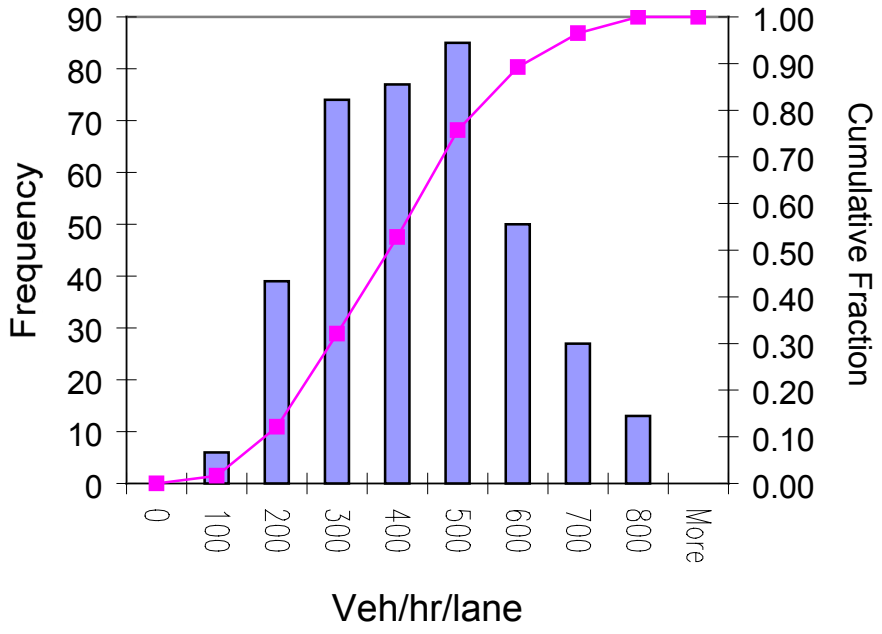

Figure 3.15 Histogram and cumulative distribution of interstate traffic density for urbanized areas

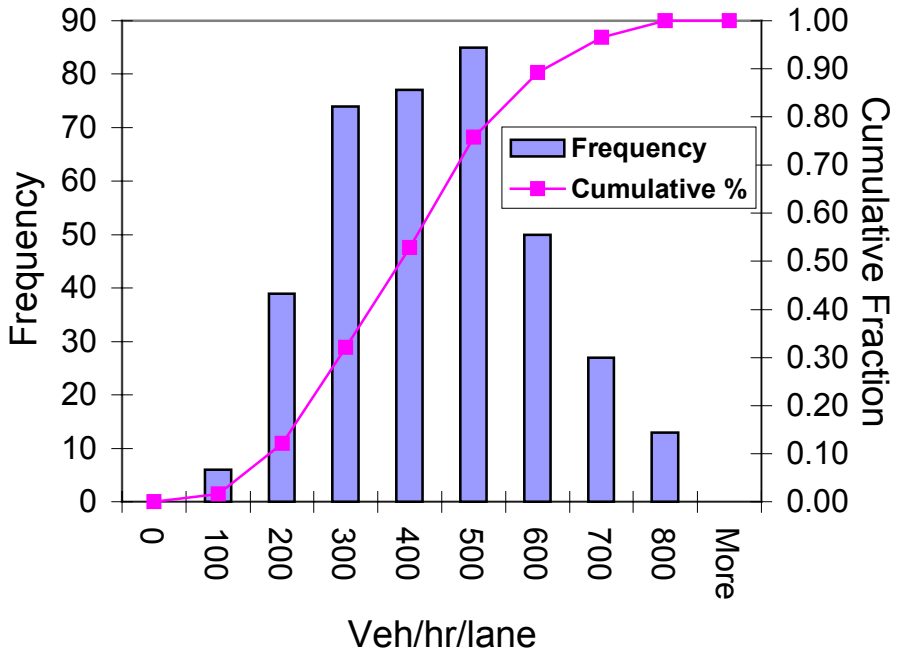

Figure 3.16 Histogram and cumulative distribution of suburban interstate traffic density.

3.5 References

[3-1] K. S. Neuhauser and F. L. Kanipe, "RADTRAN 5, Technical Manual," Sandia National Laboratories, Albuquerque, NM (in preparation, draft available on request).

[3-2] K. S. Neuhauser and F. L. Kanipe, "RADTRAN 5, User Guide," Sandia National Laboratories, Albuquerque, NM (draft available on the RADTRAN web site).

[3-3] G. S. Mills and K. S. Neuhauser, "Sensitivity Analysis for RADTRAN 4 Input Parameters," 88th Annual Meeting of the Air & Waste Management Association, San Antonio, TX, 1995.

[3-4] G. S. Mills, K. S. Neuhauser, and F. L. Kanipe, "Application of Latin Hypercube Sampling to RADTRAN 4 Truck Accident-Risk Sensitivity Analysis," Proceedings of PATRAM '95, Las Vegas, NV, 1995.

[3-5] G. S. Mills, K. S. Neuhauser, and F. L. Kanipe, "RADTRAN 4 Truck Accident Risk Sensitivity Analysis," Proceedings of Waste Management 95, WM Symposia, Tucson, AZ, 1995a.

[3-6] A. G. Croff, "ORIGEN2 - A Revised and Updated Version of the Oak Ridge Isotope Generation and Depletion Code," ORNL-5621, Oak Ridge National Laboratory, Oak Ridge, TN, July 1980.

[3-7] G. D. Wyss and K. H. Jorgensen, "A User's Guide to LHS: Sandia's Latin Hypercube Sampling Software," SAND98-0210, Sandia National Laboratories, Albuquerque, NM, 1998.

[3-8] U.S. Nuclear Regulatory Commission, "Reactor Safety Study," WASH-1400, Washington, DC, 1975.

[3-9] M. L. Abbott and A. S. Rood, "COMIDA: A Radionuclide Food-Chain Model for Acute Fallout Deposition," EGG-GEO-10367, Idaho National Engineering Laboratory, Idaho Falls, ID, 1994.

[3-10] M. M. Madsen, and E. L. Wilmot, "Truck Transportation of Radioactive Materials," Proceedings of the 7th International Conference on the Packaging and Transportation of Radioactive Materials (PATRAM '83), Vol. I, p. 724, New Orleans, LA, 1983.

[3-11] R. M. Ostmeyer, "A Revised Rail-Stop Exposure Model for Incident-Free Transport of Nuclear Waste," SAND85-1722, Sandia National Laboratories, Albuquerque, NM, 1986.

[3-12] K. S. Neuhauser and R. F. Weiner, "Intermodal Transfer of Spent Fuel," Proceedings of the 10th International Conference on the Packaging and Transportation of Radioactive Materials (PATRAM '92), Vol. I, p. 427, Yokohama, Japan, 1992.

[3-13] H. S. Javitz, et al., "Transport of Radioactive Material in the United States: Results of a Survey to Determine the Magnitude and Characteristics of Domestic, Unclassified Shipments of Radioactive Materials," SAND84-7174, Sandia National Laboratories, Albuquerque, NM, 1985.

[3-14] K. F. Eckerman and J. C. Ryman, Federal Guidance Report No. 12, "External Exposure to Radionuclides in Air, Water, and Soil," Oak Ridge National Laboratory, Oak Ridge, TN, 1993.

[3-15] R. J. Engelman, "Effectiveness of Sheltering in Buildings and Vehicles for Plutonium," DOE/EH-0159T, U.S. Department of Energy, Washington, DC, 1990.

[3-16] J. M. Taylor and S. L. Daniel, "RADTRAN II: Revised Computer Code to Analyze Transportation of Radioactive Materials," SAND80-1943, Sandia National Laboratories, Albuquerque, NM, 1982.

[3-17] Waste Isolation Pilot Plant Disposal Phase Final Supplemental Environmental Impact Statement, Volume II Appendices, DOE/EIS-0026-S-2, U.S. Department of Energy, Carlsbad, NM, 1997.

[3-18] N. Finley, et al., "Transportation of Radionuclides in Urban Environs: Draft Environmental Impact Assessment," Volumes 1 and 2, NUREG/CR-4829, Nuclear Regulatory Commission, Washington, DC, 1980.

[3-19] N. R. Griego, J. D. Smith, and K. S. Neuhauser, "Investigation of RADTRAN Stop Model Input Parameters for Truck Stops," Conference Proceedings, Waste Management 96, Tucson, AZ, 1996.

[3-20] County and City Data Book, 1988, U. S. Department of Commerce, Washington DC, 1988.

[3-21] J. D. Smith, K. S. Neuhauser, and F. L. Kanipe, "Expected Residence Time Model," Conference Proceedings, Waste Management '96, Tucson, AZ, 1996.

[3-22] U.S. Environmental Protection Agency, Proposed Guidance on Dose Limits for Persons Exposed to Transuranic Elements in the General Environment, EPA-520/4-77-016, U.S. Environmental Protection Agency, Washington, D.C., 1977.

[3-23] D. Chanin and W. B. Murfin, "Site Restoration: Estimation of Attributable Costs from Plutonium-Dispersal Accidents," SAND96-0957, Sandia National Laboratories, Albuquerque, NM, 1996.

[3-24] International Council on Radiation Protection, "Limits on Intakes of Radionuclides by Workers, Parts 1-3," Annals of the International Council on Radiation Protection, Vol. 2 (3-4), 1979 through Vol. 8 (1-3), 1982), Pergamon Press, Oxford, England, 1979.

[3-25] P. E. Johnson, et al., "HIGHWAY 3.1 – An Enhanced Highway Routing Model: Program Description, Methodology, and Revised User's Manual," ORNL/TM-12124, Oak Ridge National Laboratory, Oak Ridge, TN, 1993.

[3-26] P. E. Johnson, et al., "INTERLINE 5.0 – An Expanded Railroad Routing Model: Program Description, Methodology, and Revised User's Manual," ORNL/TM-12090, Oak Ridge National Laboratory, Oak Ridge, TN, 1993.

[3-27] J. W. Cashwell, et al., "Transportation Impacts of the Commercial Radioactive Waste Management Program," SAND85-2715, Sandia National Laboratories, Albuquerque, NM, April 1986.

[3-28] R. N. Smith and E. L. Wilmot, "Truck Accident and Fatality Rates Calculated from California Highway Accident Statistics for 1980 and 1981," SAND82-7066, Sandia National Laboratories, Albuquerque, NM, 1982.

[3-29] L. E. Fischer, et al., "Shipping Container Response to Severe Highway and Railway Accident Conditions," NUREG/CR-4829 UCID-20733, Lawrence Livermore National Laboratory, Livermore, CA, 1987.

[3-30] U.S. Department of Energy, "Final Environmental Impact Statement on Special Isotope Separation Project," DOE/EIS-0136, U.S. DOE, Washington, DC, 1988.

[3-31] C. Saricks and T. K. Kvitek, "Longitudinal Review of State-Level Accident Statistics for Carriers of Interstate Freight," ANL/ESD/TM-68, Argonne National Laboratory, Argonne, IL, 1994.

[3-32] C. L. Saricks and M. M. Tompkins, "State-Level Accident Rates of Surface Freight Transportation, A Reexamination," ANL/ESD/TM-150, Argonne National Laboratory, Argonne, IL, 1999.

[3-33] G. S. Mills, et al., "Study of Evacuation Times Based on General Accident History," Proceedings of the 11th International PATRAM Conference, Las Vegas, NV, 1995.

[3-34] G. S. Mills, et al., "Study of the Components of Evacuation Times," Proceedings of the 12th International PATRAM Conference, Paris, France, 1998.

[3-35] "1992 Traffic Safety Facts Annual Report," U.S. Department of Transportation, Bureau of Transportation Statistics, BTS-CD-04-01.

[3-36] D. Bruce Turner, "Workbook of Atmospheric Dispersion Estimates," PHS Publ. No. 999-AP-26, U.S. Department of Health, 1969.

[3-37] C. V. Parks, et al., "Parametric Study of Radiation Dose Rates from Rail and Truck Spent Fuel Transport Casks," ORNL/CSD/TM-227, 1985.

[3-38] "Spent Nuclear Fuel Discharges from U.S. Reactors," Energy Information Administration, U.S. Department of Energy, SR/CNEAF/96-01, 1994.

[3-39] Federal Highway Administration, Combination of Tables HM-50 and VM-2 in Section V of "Highway Statistics for 1997" derived from the Highway Performance Monitoring System, U.S. Department of Transportation Web site.

[3-40] Federal Highway Administration, Table HM-72 in Section V of "Highway Statistics for 1997" derived from the Highway Performance Monitoring System, U.S. Department of Transportation Web site.

[3-41] www.census.gov/population/socdemo/journey/usveh90.txt.

Page intentionally left blank

4. SELECTION OF GENERIC CASKS

4.1 Description of Casks

Generic casks were used in this study to relate the behavior of typical examples of a broad packaging type to the risks that might be realized during a spent fuel shipping campaign. Detailed analyses of these casks can be used to demonstrate differences (or similarities) among various construction features for this type of package. Casks for the transportation of power reactor fuel are generally available in three weight classes (legal weight truck, overweight truck, and rail) and with three gamma-shielding materials (steel, lead, and depleted uranium). Casks that are most likely to be used in future shipping campaigns only use four of the nine possible combinations of weight and shielding. These are lead and depleted uranium (DU) shielded truck casks and steel and lead shielded rail casks. A survey of currently licensed and proposed casks was used to develop the generic casks used for this study. Tables 4.1 to 4.4 list the casks that were examined to develop generic designs. Most of the information was obtained from "Shipping and Storage Cask Data for Commercial Spent Nuclear Fuel," by JAI Corporation [4-1]. Other information was obtained from the certificates of compliance for the casks or from safety analysis reports.

Tables 4.1 to 4.4 list the casks used in derivation of the generic casks and provide details about the generic casks. Because of the way the generic casks were developed, they may not meet all of the requirements of 10 CFR 71. Real packages must meet these requirements, and are therefore, likely to be more robust than the generic casks used in this study. For the monolithic steel rail casks, the currently licensed casks use some type of ferritic steel for the cask body and lid. The current regulatory position favors the use of stainless steel or a ferritic steel with very high ductility (requirements are given in NRC Regulatory Guide 7.12 [4-2]). For this reason, and to be consistent with the sandwich wall casks, stainless steel was chosen as the material for the monolithic cask. Figures 4.1 to 4.4 show artist renditions of the generic casks. Other features that are typical of transportation casks but are not included in the generic casks are fill and drain ports, lifting and tiedown trunnions, and personnel barriers. The omission of these features is not believed to significantly effect the behavior of the casks. The personnel barrier absorbs energy during an impact and acts as a thermal shield during a fire event. Therefore, omitting this feature is conservative. For the extra-regulatory impacts considered in this report, impact onto a trunnion is less damaging than impact onto the side of the cask, as the impact area is smaller and the trunnion will act as an impact limiter. Therefore, omitting this feature is also conservative. The fill and drain ports are generally in the very substantial base and lid structure of the cask. These are regions with small deformations, and it is very unlikely that a failure will occur at these points.

Table 4.1 Steel-Lead-Steel Truck Casks

Name	Weight (pounds)	Material	Closure Bolts (no./size)	Wall Thickness (inches)	Outside Diameter (inches)	Cavity Diameter (inches)	Length (inches)	Impact Limiter	Design Heat Rejection (kW)	Seal Material	C of C
NAC-LWT	52,000	stainless	12 1”	0.75,5.75,1.2	44.2	13.375	199.80	honeycomb	2.5	both	71-9225
NAC-1	49,000	stainless	6 1.25”	0.31,6.63,1.25	38	13.5	214	balsa	11.5	elast.	71-9183
NLI-1/2*	49,250	stainless	12 1”	0.5,2.125Pb, 2.75DU,0.875	47.125	13.375	195.25	balsa	10.6	metal	71-9010
TN-8**	79,200	steel	16 1.25”	0.23,5.32,0.79	67.6	~30	217.2	balsa	35.5	elast.	71-9015
TN-9**	79,200	steel	16 1.25”	0.23,5.04,0.79	67.6	~21	226.6	balsa	24.5	elast.	71-9016
TN-FSV	47,000	stainless	12 1”	1.12,3.44,1.5	31.0	18.0	207	wood	0.36	elast.	71-9253
Modal Study	N.A.	stainless	N.A.	0.5,5.25,1.25	27.5	13.5	193	yes	0.8-5.4	N.A.	-
Generic	**50,000**	**stainless**	**12 1”**	**0.5,5.5,1.0**	**27.5**	**13.5**	**205**	**yes**	**2.5**	**elast.**	**-**

* This cask has a steel-lead-DU-steel wall configuration and was therefore not used in the determination of the generic cask.
** These casks are overweight-truck casks and were therefore not used in the determination of the generic cask.

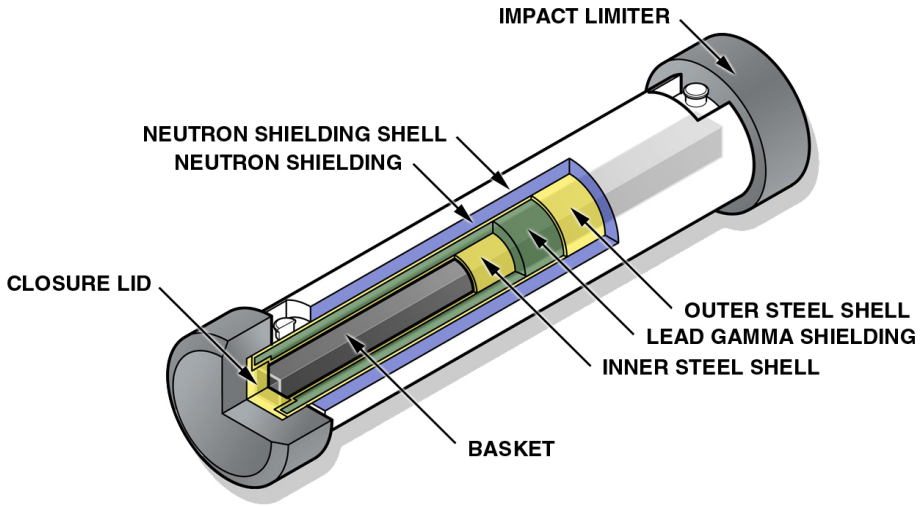

Figure 4.1 Conceptual design of a generic steel-lead-steel truck cask.

Table 4.2 Steel-DU-Steel Truck Casks

Name	Weight (pounds)	Material	Closure Bolts (no./size)	Wall Thickness (inches)	Outside Diameter (inches)	Cavity Diameter (inches)	Length (inches)	Impact Limiter	Design Heat Rejection (kW)	Seal Material	C of C
FSV-1	47,600	stainless	24 1.25”	0.67,3.5,0.91	28.0	17.7	208	yes	4.1	elast.	71-6346
GA-4	53,610	stainless	12 1”	0.375,2.64,1.5	39.75	18.16 sq.	187.75	honeycomb	2.47	elast.	71-9226
GA-9	54,000	stainless	12 1”	0.25,2.45,1.75	39.75	18.16 sq.	198.3	honeycomb	2.12	elast.	-
NLI-1/2*	49,250	stainless	12 1”	0.5,2.125Pb, 2.75DU,0.875	47.125	13.375	195.25	balsa	10.6	metal	71-9010
Generic	**50,000**	**stainless**	**12 1”**	**0.5,3.5,0.9**	**28**	**18**	**200**	**yes**	**2.5**	**elast.**	**-**

* This cask has a steel-lead-DU-steel wall configuration and was therefore not used in the determination of the generic cask.

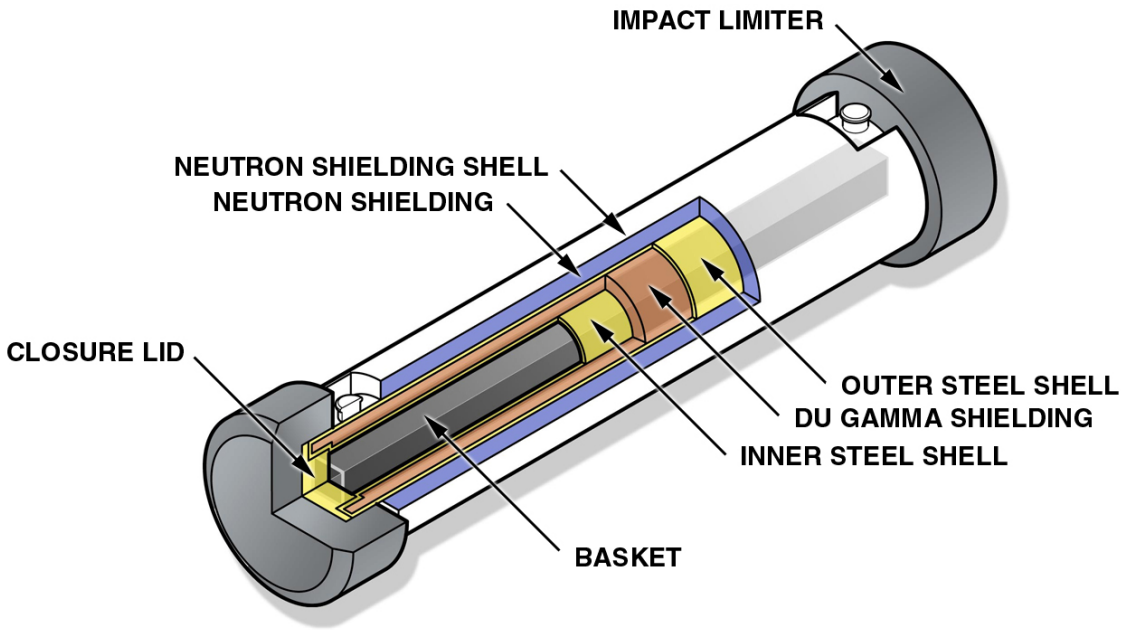

Figure 4.2 Conceptual design of a generic steel-DU-steel truck cask.

Table 4.3 Steel-Lead-Steel Rail Casks

Name	Weight (pounds)	Material	Closure Bolts (no./size)	Wall Thickness (inches)	Outside Diameter (inches)	Cavity Diameter (inches)	Length (inches)	Impact limiter	Design Heat Rejection (kW)	Seal Material	C of C
NAC-STC	250,000	stainless	42 1.5”	1.5,3.7,2.65	87.0	71.0	193	wood	22.3	metal	71-9235
TranStor	244,000	stainless	N.A.	N.A.	87.0	67.0	210.0	honeycomb	26	metal	-
125B	181,500	stainless	32 1.5”	1.0,3.88,2.0	65.5	51.25	207.5	foam	0.7	elast.	71-9200
Excellox-6	194,000	ferritic steel	N.A.	N.A.	83.23	32.8	200.5	yes	N.A.	N.A.	-
NLI-10/24	194,000	stainless	16	.75,6,2	96.0	45.0	204.5	balsa	70	both	71-9023
BR-100	202,000	stainless	32 2.5”	1.0,4.5,1.75	82	58.5	202	wood	15	elast.	-
Modal Study		stainless	N.A.	0.5,5.25,1.5	52	37.5	193	yes	3.4-24	N.A.	-
Generic	**225,000**	**stainless**	**24 1.75”**	**1.0,4.5,2.0**	**80**	**65**	**200**	**yes**	**24**	**elast.**	**-**

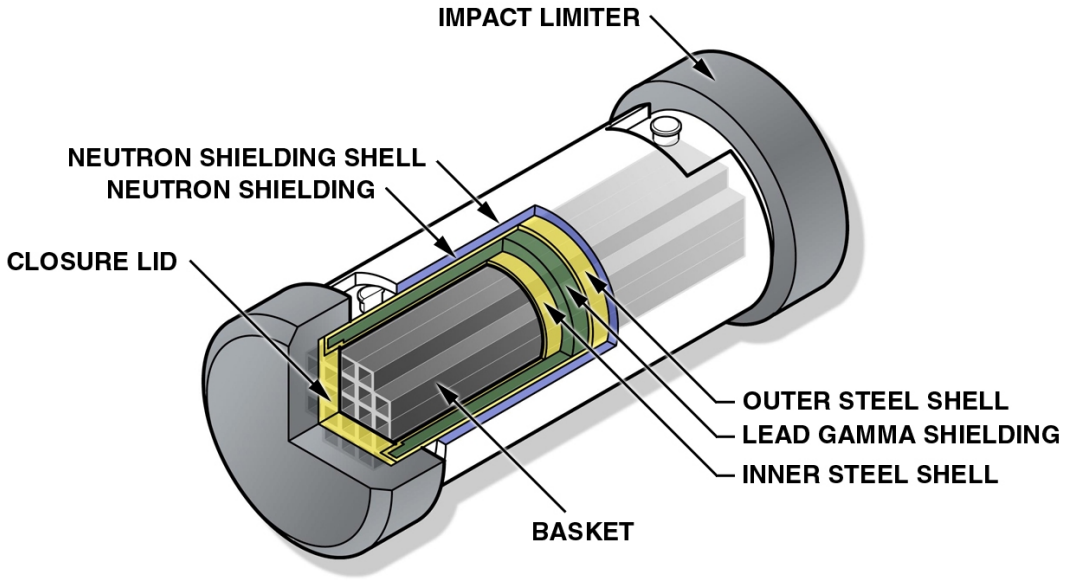

Figure 4.3 Conceptual design of a generic steel-lead-steel rail cask.

Table 4.4 Monolithic Rail Casks

Name	Weight (pounds)	Material	Closure Bolts (no./size)	Wall Thickness (inches)	Outside Diameter (inches)	Cavity Diameter (inches)	Length (inches)	Impact Limiter	Design Heat Rejection (kW)	Seal Material	C of C
TN-24**	224,000	SA-350	N.A.	9.5	92.4	57.25	186.8	none	24	metal	72-1005
REG	225,000	SA-350	48 1.625”	9.25	90.25	71.25	180	redwood	2.7	both	71-9206
BRP	215,000	SA350 LF3	48 1.625”	9.62	83.25	64	190.5	redwood	3.1	both	71-9202
Hi-Star 100	244,000	ferritic steel	N.A.	13.6	95.9	68.75	202.9	?	23.4	N.A.	71-9261*
C-E Dry Cap	224,000	Steel	N.A.	12.7	90.0	64.6	196.9	none	N.A.	N.A.	-
TN-12	144,800	ferritic steel	40 1.65”	15.9	78.74	33.2	210	wood	120	elast.	-
Castor-V/21**	234,000	NCI	N.A.	15.0	93.9	60.1	192.4	none	28	metal	72-1000
Generic	**224,000**	**stainless steel**	**24 1.75”**	**10**	**85**	**65**	**190**	**yes**	**24**	**elast.**	**-**

* Certificate pending

** These casks are only licensed for storage in the U.S. but are used for transportation in other countries.

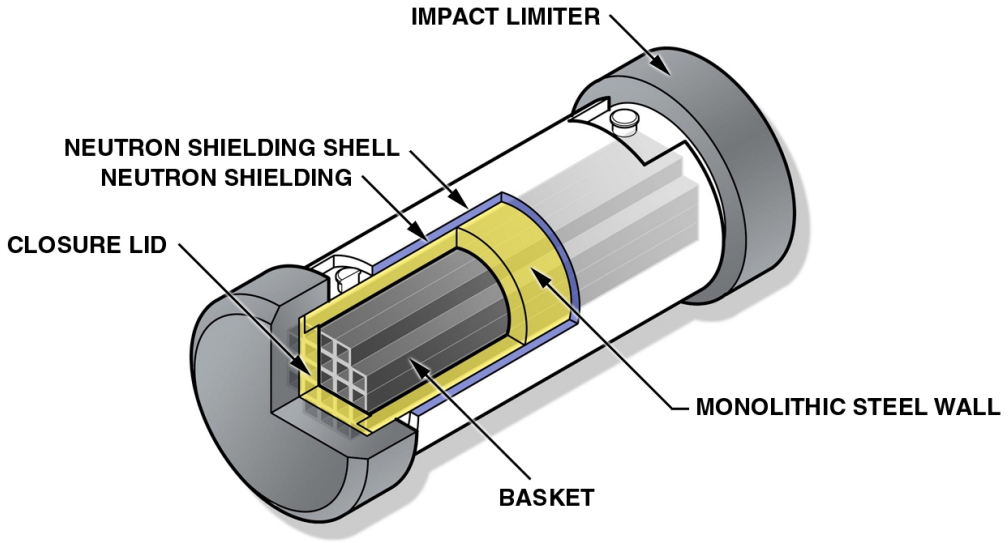

Figure 4.4 Conceptual design of a generic monolithic steel rail cask.

The capacity of the generic casks was assumed to be 24 pressurized water reactor (PWR) or 52 boiling water reactor (BWR) assemblies for the steel-lead-steel and monolithic steel rail casks, 1 PWR or 2 BWR assemblies for the steel-lead-steel truck cask, and 3 PWR or 7 BWR assemblies for the steel-DU-steel truck cask. No attempt was made to specify a generic basket. It may not be physically possible to fit the assumed number of assemblies in the cavity volume of the generic casks. It may also be possible that the generic casks would not be suitable for the assumed number of assemblies for all conceivable fuel types that may be shipped. For example, the surface dose rate or internal temperatures may be too high for short-cooled high-burnup fuel.

The wall thickness listed in the tables does not include neutron shielding, which is generally in the central region of the cask and outside of the containment system of the walls. The neutron shielding does not contribute significantly to the strength of the cask. Therefore, ignoring it will have little effect on the results of the structural modeling discussed in the following chapter. In the structural finite element model, the weight of the neutron shielding and its liner are added to the contents so that the total weight of the package is correct. For the thermal analyses a neutron shield consisting of 4.5 inches of water (considered empty in the analyses) contained by a 0.25-inch steel shell is assumed for all of the casks. Even though most modern casks use a solid neutron-shielding material, the thermal analyses assumed that an empty neutron-shielding layer would provide a more conservative assessment of the heating of the cask for cases where the fire does not follow a severe impact that collapses the neutron shielding tank, thereby eliminating the 4.5 inch air gap.

In other aspects of the cask construction where there is a major difference between older casks and newer casks, the generic casks specifications more closely simulated the newer designs. Many of the older casks are of designs where additional packages cannot be built, so a fleet of these casks will not be used for a major transportation campaign. For all casks to be used in transportation it is assumed there will be an impact limiter. The information available about the impact limiters was not sufficient to develop a generic design, but it will be assumed that the regulatory impact (9-m free drop onto an unyielding target) uses the full amount of energy absorbing capacity of the impact limiter prior to the lock-up region of the force-deflection curve. For all of the structural analyses, the finite element model includes an impact limiter that has been fully crushed in all directions.

All of the generic casks are assumed to have elastomeric o-ring seals inboard of the bolt location. It is possible, using the results of the finite element analysis in the next section, to derive source-terms for casks with metallic seals in addition to the source-terms derived for the casks with elastomeric seals, but this has not been done. The closure on all of the casks is recessed into the cask body, with a face-seal configuration. Figure 4.5 shows the lid of one of the casks and the location of the bolts. This type of closure is the most common configuration used in spent fuel casks, but other configurations are seen. For example, the 125-B cask uses bore seals instead of face seals.

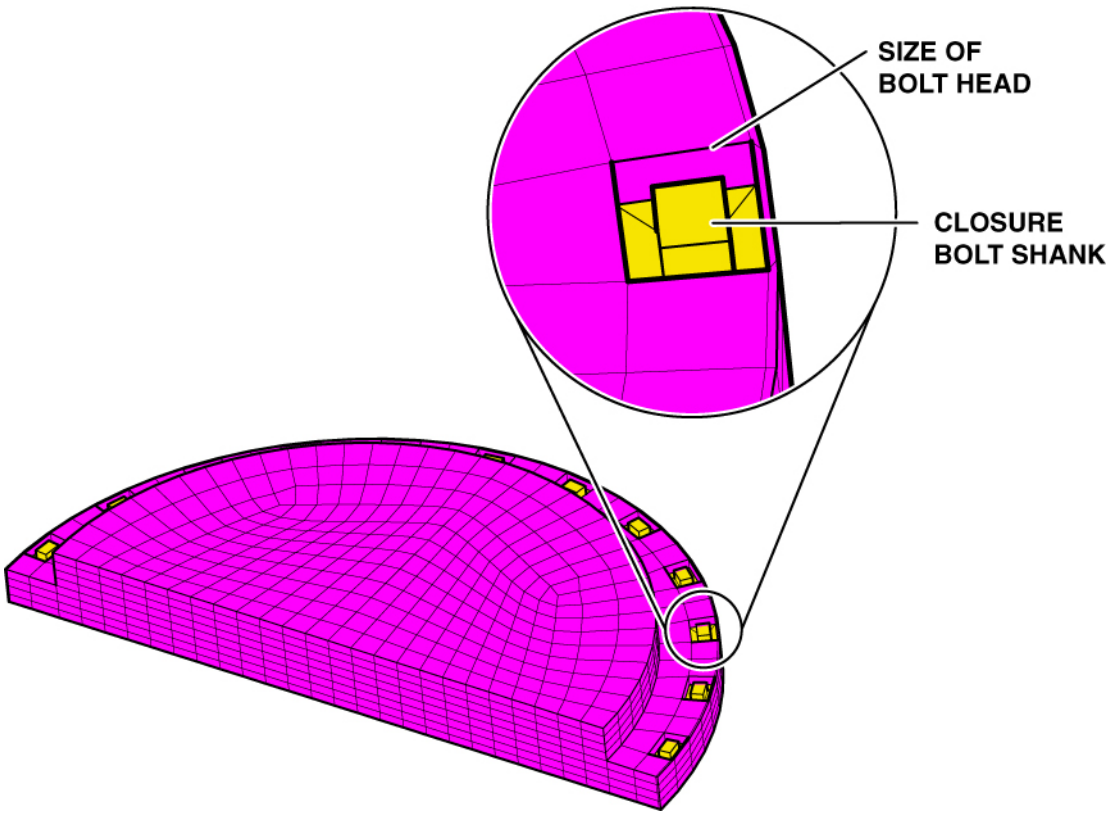

Figure 4.5 Finite element representation of a typical closure lid for structural analysis, showing the locations of the bolts.

4.2 Conservatism in Cask Selection

The specifications of the generic casks for this study were defined with the intent of producing a conservative analysis. That is, a design that is more likely to develop a leak path and lose containment integrity than any of the certified/planned designs listed.

All of the sandwich wall generic casks have shell thicknesses that are less than those of modern designs. Thicker shells result in smaller deformations, lower probabilities of puncture, and reduced lead slump. For the rail casks the number of bolts chosen for the generic design is lower than the number being used for modern designs. Increasing the number of bolts decreases the closure openings, resulting in reduced probabilities for radioactive material release.

Although generic specifications are likely to lead to conservative results, it should not be assumed that designs with similar dimensions could not be implemented in a real cask that could gain certification by the NRC.

4.3 References

[4.1] JAI Corporation, "Shipping and Storage Cask Data for Commercial Spent Nuclear Fuel," JAI-421, Fairfax, VA, July 1996.

[4.2] US Nuclear Regulatory Commission, "Fracture Toughness Criteria of Base Material for Ferritic Steel Shipping Cask Containment Vessels with a Wall Thickness Greater Than 4 inches (0.3m)," Regulatory Guide 7.12, June 1991.

5. STRUCTURAL RESPONSE

5.1 Finite Element Calculations for Impacts onto Rigid Targets

5.1.1 Introduction

To determine the response of the generic casks, finite element calculations for impacts onto rigid targets were conducted. For all of the analyses in this report, the Sandia-developed non-linear transient dynamics finite element program PRONTO-3D [5-1, 5-2, 5-3] was used to determine the damage resulting from each impact. PRONTO is a shock-wave propagation code, especially developed for impact problem types. It uses a time marching explicit integration of the equation of motion to determine the response of the structure. Inputs to the code are geometry (including boundary conditions), material properties, and initial velocities. This type of code updates the position of each node at each time step, which allows for both material and geometric non-linearities. One result of this approach is that strains reported are true strains, rather than engineering strains that are based upon the undeformed geometry. PRONTO has been extensively benchmarked for analyses of cask response [5-4, 5-5]. For each generic cask, calculations were performed for impacts in end-on, CG-over-corner, and side-on orientations. The response of the casks at other orientations is sufficiently similar to (or bounded by) these results to be enveloped by them. For impact angles between end-on and 5 degrees from vertical, the end-on analysis results will be used. For impacts between 5 degrees from vertical to 70 degrees from vertical the CG-over-corner analysis results will be used. For impacts between 70 degrees from vertical to horizontal, the side-on analysis results will be used. All impacts are assumed to be onto a flat, rigid surface with the initial velocity perpendicular to the surface. While it is possible for a cask to impact a surface that is not flat (such as a bridge column) in a side impact orientation (such that the contact occurs between the impact limiters), this type of accident was not considered. An impact of this type only provides loading and, therefore, deformation to the cylindrical portion of the cask away from the closure area. This part of the cask is extremely ductile, and can withstand deformations greater than the cask diameter without causing the cask to release radioactive material.

To shorten the analysis times and avoid calculation of the very large shear strains that occur in the impact limiter, at the start of all of the analyses it was assumed that the impact limiter has already been driven into the lock-up region (the point at which the material stops behaving in a crushable manner). The initial and crushed size of the impact limiters for each cask are given in Table 5.1. Figure 5.1 shows the initial and pre-crushed geometry of an impact limiter. The amount of energy absorbed by the impact limiter prior to lock-up is equivalent to the kinetic energy from the regulatory drop test. Using the pre-crushed impact limiter, analyses with impact velocities of 30, 60, 90, and 120 mph are conducted for each cask and orientation. If the energy required to crush the impact limiters is added to the initial kinetic energy of the cask, these analysis velocities correspond to actual impact velocities of 42, 67, 95, and 124 mph. However, throughout this report the calculations will be identified as 30, 60, 90, and 120 mph impact cases.

Table 5.1 Impact Limiter Geometry (in inches)

Cask	Cask Diameter	Engagement Length	Initial End Thickness	Crushed End Thickness	Initial Side Thickness	Crushed Side Thickness
Steel-Lead-Steel Truck	27.5	12	12	4	12	4
Steel-DU-Steel Truck	28	12	12	4	12	4
Steel-Lead-Steel Rail	80	14	14	4.67	14	4.67
Monolithic Rail	85	14	14	4.67	14	4.67

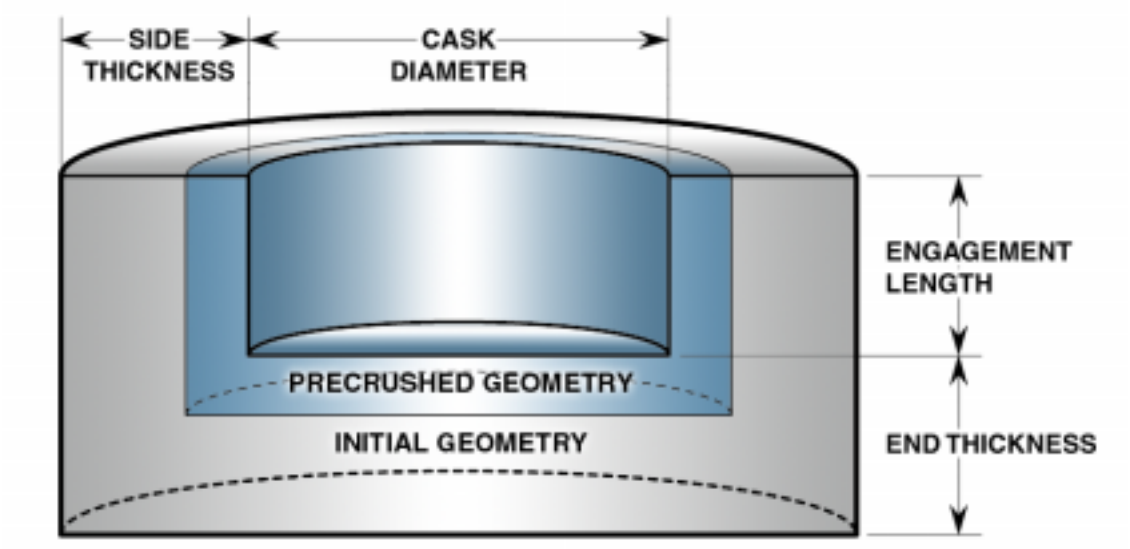

Figure 5.1 Geometry of the initial and pre-crushed impact limiter.

5.1.2 Assumptions for Finite Element Models

While it is possible to create a finite element mesh that accurately models all of the details of the generic cask models, using these models requires too much computation time for the many cases considered in this work. For this reason, simplifying assumptions were made. All of the impacts considered have a plane of symmetry through the long axis of the cask, so it is only necessary to model one-half of the structure. Figure 5.2 shows the finite element model used for the lead shielded rail cask, typical of the models used for all of these analyses.

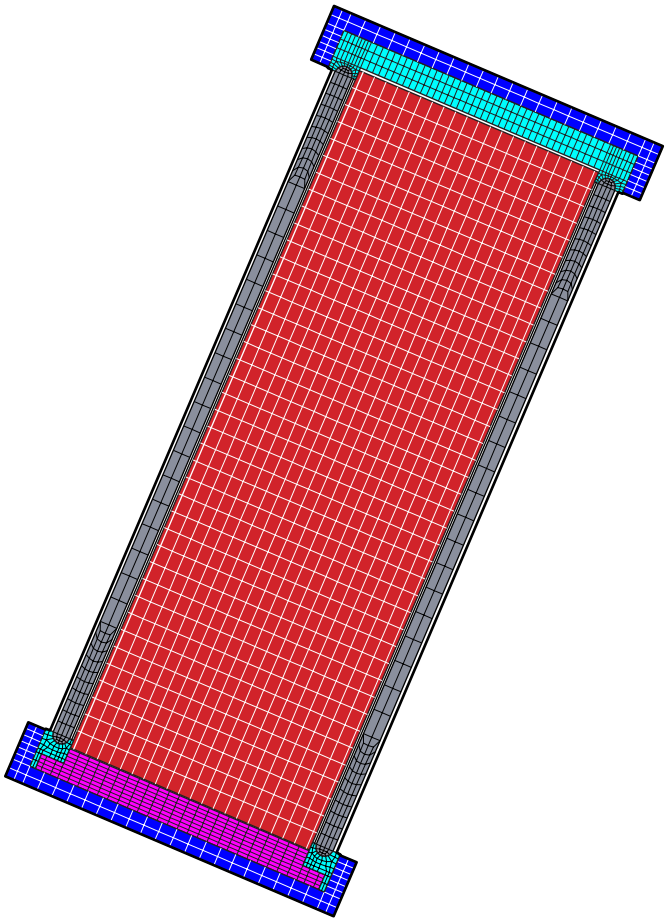

Figure 5.2 Finite element model of the steel-lead-steel rail cask in the CG-over-corner drop orientation.

For all of the sandwich-wall casks the inner and outer steel layers were modeled with zero-thickness shell elements. This type of element accurately captures the bending behavior and axial forces in the shell, but does not incorporate stresses in the direction perpendicular to the shell surface. Where this fact has the greatest influence is in the contact between the various layers. If the geometry of the contents and shielding layer are modeled correctly, it is impossible for a zero-thickness shell element to be contacting both the contents and the shielding. In these finite element models the shell elements are located at the mid-thickness of the wall layer they represent. This leaves a gap between the contents and the shell and between the gamma shielding and the shell. The gap between the contents and the shell is typical of spent fuel casks, but the gap between the gamma shielding and the shells results in having the gamma shielding (and the shells) unsupported for motion in the direction transverse to the shells. This results in larger deflections and strains in the sandwich wall for the model than would occur in reality. For casks with lead gamma shielding the lack of lateral support results in a significant over-prediction of the amount of lead slump. Figure 5.3 shows a detailed view of the end of the steel-lead-steel rail cask.

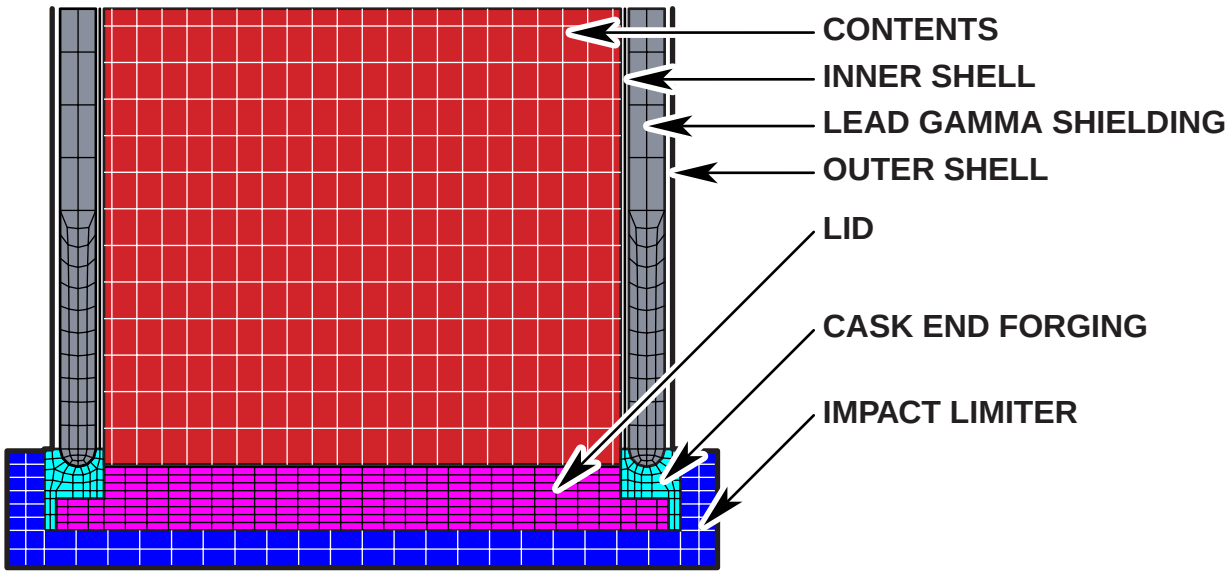

Figure 5.3 Detail of the end of the steel-lead-steel rail cask finite element model.

The behavior of the neutron shielding and its liner has little effect on deformations to the remainder of the cask, but any effect is beneficial. For this reason, these components are not modeled, but rather their mass is lumped with the mass of the contents to achieve the correct package weight. The contents and basket are treated as a homogenous crushable material. The crush strength of this material is chosen from the buckling strength of PWR fuel pins subjected to axial loads. The density of this material is adjusted so that the total weight of the cask is equal to the specified weight from Chapter 4. Modeling of the basket and contents in this manner does not allow direct determination of the behavior of the fuel rods, but provides an assessment of the loads that these components transmit into the structural portions of the cask. Because the only purpose of the contents within the model is to provide loading onto the cask, variations in their material properties has little effect on the analysis results. A description of how fuel behavior is determined from the finite element results is given in Section 5.4.

As indicated earlier, the crushing behavior of the impact limiters is not modeled. They are pre-crushed at the beginning of the analysis. To account for the post-crush behavior of the impact limiters they are treated as a solid with a density equivalent to a typical density for fully crushed aluminum honeycomb. The yield strength of this crushed material is typical for fully crushed 1000-psi aluminum honeycomb. The finite element model assumes that the entire impact limiter has been fully crushed, so the geometry in the model remains axi-symmetric. No attempt is made to model the attachments of the impact limiters; they are held in place only by inertia. If the inertial forces are not sufficient to keep the impact limiter in place during the impact event, then the cask body will impact directly onto the rigid surface. Real casks have impact limiter attachments that are usually designed so the impact limiters stay attached during the regulatory impact tests.

For all of the analyses, the initial velocity vector of the cask is assumed to be perpendicular to the rigid surface. All of the interior contact surfaces in the model (between the contents and the inner shell, the gamma shielding and both shells, the lid and the cask body, and the cask body and the impact limiter) are assumed to be frictionless. The contact between the cask and the rigid

surface is also frictionless. For most aspects of the problem this assumption is conservative, as there is no loss of impact energy because of frictional heating. Including friction at contact surfaces tends to cause the various parts of the modeled structure to behave more like a single piece (decreases separation of the parts of the structure being modeled). Including friction would also decrease the amount of impact energy available to cause structural deformation, as some of the energy would be absorbed by frictional heating. Lack of friction and the direction of the initial velocity guarantee that the displacement, velocity, and acceleration vectors will always be in a direction that is perpendicular to the rigid surface. This will be important when deriving the force-deflection curves for the casks in Section 5.2.2.

The closure of the cask is explicitly modeled. The lid is recessed into the body of the cask and held in place with either 12 (6 in the half-symmetric model) 1-inch diameter bolts for the truck casks or 24 (12 in the half-symmetric model) 1.75-inch diameter bolts for the rail casks. The bolt model cross-section is square with square heads. The area of the square bolt shank is the same as the area of a round bolt. The edges of the heads are rigidly attached to the cask lid, and the bottom of the shank is rigidly attached to the cask body. Figure 5.4 shows the cross-section through the center of a typical bolt and an isometric view of a single bolt. All of the contacts are tied via coincident nodes. The initial preload in the bolts caused by the torque applied to them when the cask is closed is neglected. Neglecting this preload is conservative because the preload must be overcome by loading from the contents before there is any deformation to the bolts. This factor makes a preloaded closure have smaller openings than a closure without preload.

Modeling the bolt in this way forces all of the deformation of the closure to take place in the short section that represents the shank of the bolt. Figure 5.5 shows how this method of modeling the bolt depicts shear deformations and tensile deformations. In a real closure, movement between the lid and the cask body will be accommodated by deformation of the bolt head and seat, sliding in the clearance hole, and stretching over a longer length of the bolt. These differences make the modeled bolts stiffer than the real bolts for tensile deformations, which leads to an over-prediction of bolt strain and an under-prediction of bolt stretch. Because the bolts (in the model and in reality) are much less stiff than the closure, the over-prediction of strain is much more significant than the under-prediction of displacement. The effect on leak area is discussed in section 5.1.4.

The O-ring grooves and O-rings for the seals are not included in the model, but the deformations in the sealing surfaces at the locations of the O-rings are tracked to determine when there is sufficient opening to cause permanent failure of the seal. From tests performed at Sandia on closure movements using 0.25-inch nominal O-rings, it has been determined that elastomeric O-rings can withstand greater than 0.070 inches of opening without losing their ability to contain helium at one atmosphere of differential pressure [5-6]. These O-rings had an initial pre-compression of about 0.075 inches. For the larger O-rings (compared to the Sandia study) typical of spent fuel casks, the larger amount of pre-compression implies there should be no material release for openings up to 0.100 inches.

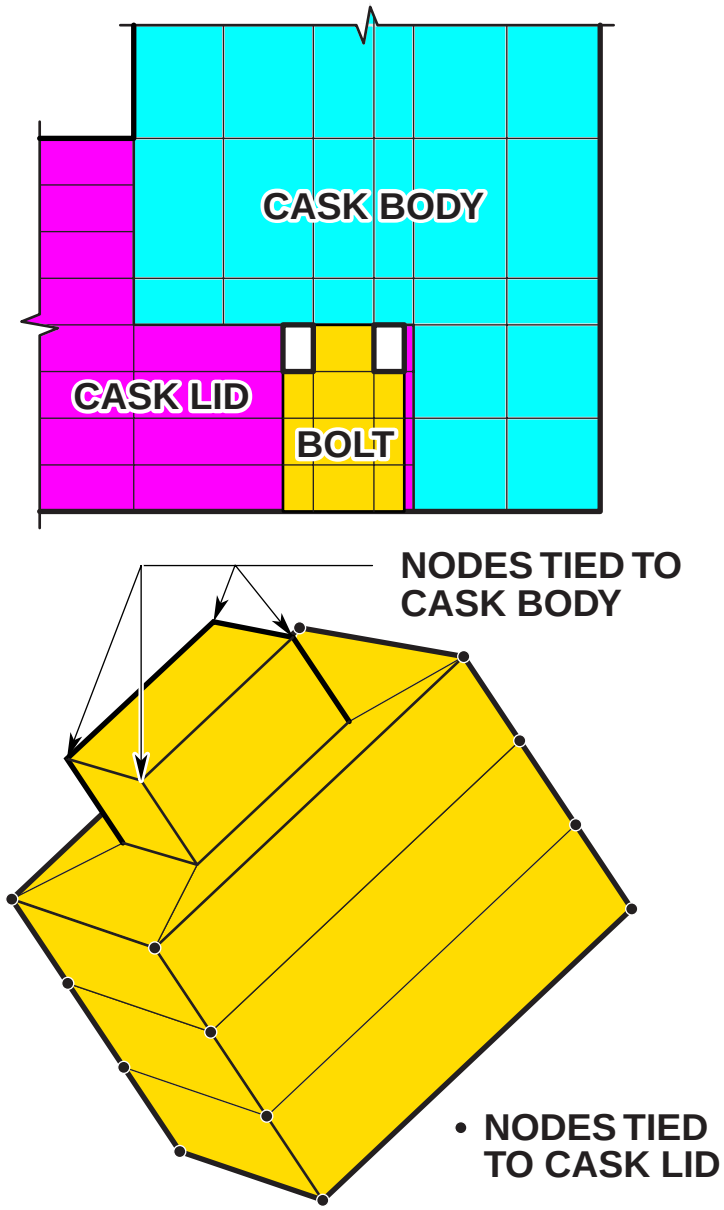

Figure 5.4 Typical model of a bolt used in the finite element analyses.

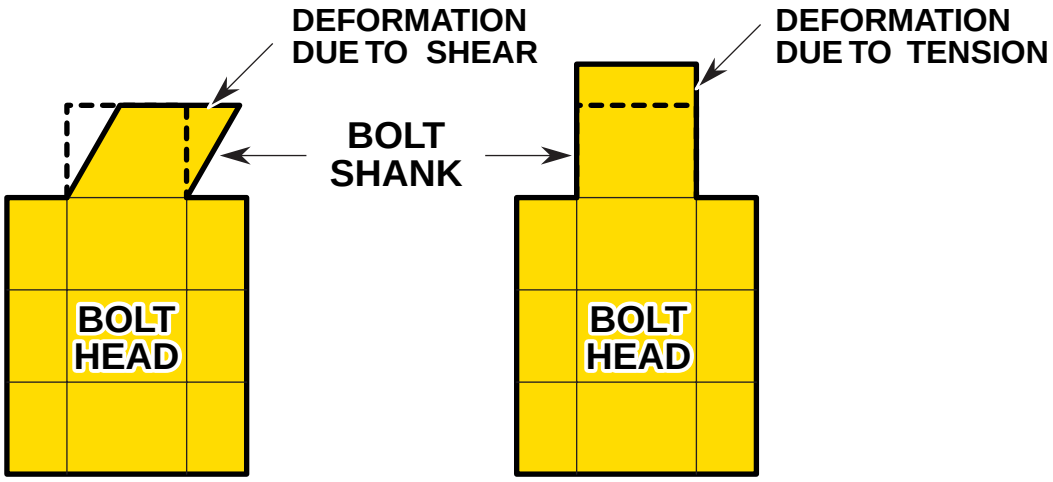

Figure 5.5 Modeling of the deformation in the bolts. The solid lines indicate the bolt position after being deformed and the dashed lines indicate the initial bolt position.

5.1.3 Material Models

The casks and contents modeled in this study consist of six different materials. The lids, ends, and structural portions of the walls are 304L stainless steel. The bolts are a high-strength stainless steel. The impact limiters are crushed aluminum honeycomb. The gamma shielding is either lead, depleted uranium, or stainless steel. The basket and spent fuel are modeled as a homogenized crushable material.

The stainless steel is modeled with a power-law hardening material model. This model treats the material as elastic up to the limit of proportionality and captures the plasticity by the equation:

$$\sigma = \sigma_p + A\langle \varepsilon_p - \varepsilon_L \rangle^n \tag{1}$$

where σ_p is the stress at the limit of proportionality, A is the hardening constant, ε_p is the equivalent plastic strain, ε_L is the Luder's strain (the flat portion of the stress-strain curve immediately after yielding for low-carbon steels), $\langle\ \rangle$ indicates the Heaviside function where the expression enclosed in the brackets is unchanged when positive and equal to zero when negative, and n is the hardening exponent.

For 304L stainless steel the parameters used are σ_p = 28 ksi, A = 192.746 ksi, ε_L = 0, and n = 0.74819. For the elastic part of the curve E = 28,000 ksi and ν = 0.27 [5-7].

The high-strength bolts (SA-540 Grade B23 Class 5 [5-8]) are modeled with a bi-linear elastic-plastic material model. The parameters used are σ_y = 105 ksi, E = 30,000 ksi, ν = 0.3, and E_p = 30 ksi. The crushed aluminum honeycomb impact limiters are modeled using the power-law hardening model with σ_p = 4250 psi, A = 32.7 ksi, ε_L = 0, n = 0.325722, E = 9,900 ksi and ν = 0.33. The lead is modeled using the power-law hardening model with σ_p = 2000 psi,

A = 800 psi, ε_L = 0, n = 0.5, E = 2,000 ksi and ν = 0.27. These are the same material properties that were used in the benchmarking analyses of Ludwigsen and Ammerman [5-4]. The depleted uranium is modeled with a bi-linear elastic-plastic material model with σ_y = 20 ksi, E = 28,000 ksi, ν = 0.3, and E_p = 150 ksi [5-9].

The homogenized basket and spent fuel are modeled with a material model originally developed for low-density polyurethane foams. This model is defined by the initial yield strength of the material (σ_y), initial elastic stiffness (E) and Poisson's ratio (ν), the hardening modulus (A), the solid material volume fraction (ϕ), the initial gas pressure in the material (p_o), and the strength of the solid portions (poly) [5-10]. For these analyses the values for the material properties are σ_y = 1700 psi, A = 1700 psi, poly = 30,000 psi, p_o = 14.7 psi, ϕ = 0.6, E = 1000 ksi, and ν = 0.0.

A summary of the material properties for all of the materials used in the analyses is given in Table 5.2. All of these material models accurately capture the three-dimensional state of stress and strain within finite element analyses.

Table 5.2 Material Properties Used in the Finite Element Analyses

Item	Material Model	E (ksi)	ν	σ_y or σ_p (ksi)	A or E_p (ksi)	n	poly (ksi)	ϕ	p_o (psi)
Stainless Steel	Power-law hardening	28,000	0.27	28	193	0.7482			
Bolts	Elastic-plastic	30,000	0.30	105	30				
Impact Limiters	Power-law hardening	9,900	0.33	4.25	32.7	0.3257			
Lead	Power-law hardening	2,000	0.27	2	0.8	0.5			
Depleted Uranium	Elastic-plastic	28,000	0.3	20	150				
Contents	Crushable	1,000	0.0	1.7	1.7		30	0.6	14.7

5.1.4 Finite Element Results

Using finite element analyses to determine the ability of the casks to maintain containment requires investigation of all of the areas and factors that may result in a loss of containment. For these casks the main factors to consider are maximum tensile plastic strains in the containment boundary, maximum tensile plastic strains in the closure bolts, and deformations in the region of the seals. For the sandwich-wall casks the containment boundary is the inner shell, but the development of a tear in this shell does not necessarily imply a loss of containment if the outer shell remains intact. None of the finite element impact analyses indicated strains above 70 percent in this shell, so no tearing is predicted to take place (the true strain at failure for 304L is

greater than 120 percent). Table 5.3 shows the maximum level of plastic strain observed in the inner shell for the three sandwich wall casks. The strain levels in the other portions of the cask were lower than those in the shells. A strain fringe plot for the 120-mph impact of the steel-lead-steel truck cask is shown in Figure 5.6. EQPS is the equivalent plastic strain, and is the non-directional three-dimensional measure of stretching in the material. Similar figures for all of the analyses are given in Appendix A.

Table 5.3 Maximum Plastic Strain in the Inner Shell of the Sandwich Wall Casks

Cask	Corner Impact Speed	Corner Impact Strain (%)	End Impact Speed	End Impact Strain (%)	Side Impact Speed	Side Impact Strain (%)
Steel-Lead-Steel Truck	30 mph	12	30 mph	3.9	30 mph	n.a.
	60 mph	29	60 mph	12	60 mph	16
	90 mph	33	90 mph	18	90 mph	24
	120 mph	47	120 mph	27	120 mph	27
Steel-DU-Steel Truck	30 mph	11	30 mph	1.8	30 mph	6
	60 mph	27	60 mph	4.8	60 mph	13
	90 mph	43	90 mph	8.3	90 mph	21
	120 mph	55	120 mph	13	120 mph	30
Steel-Lead-Steel Rail	30 mph	21	30 mph	1.9	30 mph	5.9
	60 mph	34	60 mph	5.5	60 mph	11
	90 mph	58	90 mph	13	90 mph	15
	120 mph	70	120 mph	28	120 mph	n.a.

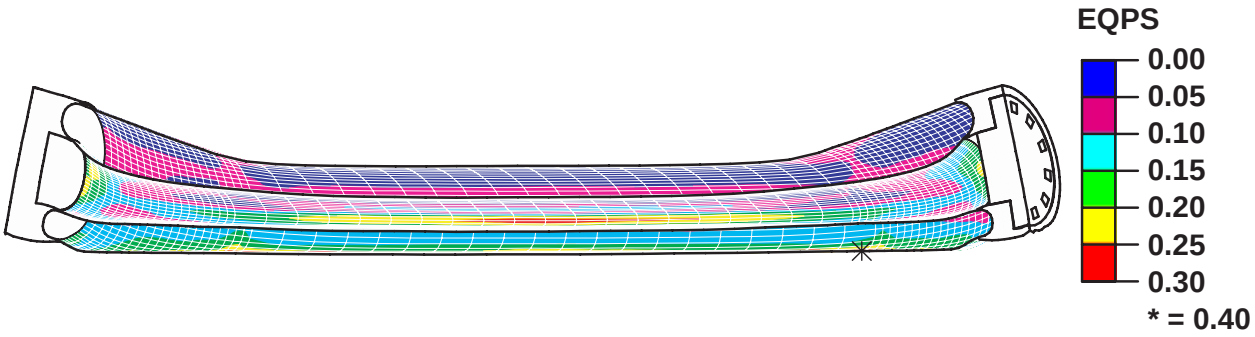

Figure 5.6 Deformed shape and plastic strain fringes for the steel-lead-steel truck cask following a 120-mph impact in the side-on orientation. The maximum plastic strain (indicated by the asterisk) occurs in the outer shell. The maximum strain in the inner shell is 0.27.

For the monolithic rail cask the maximum strain on the interior surface of the cask is less than 60 percent for all analyses. The maximum occurs at the lid-cask interface for the 120-mph side impact case. At this location most of the plasticity is caused by compression, so there is no possibility of material failure. Table 5.4 lists the maximum strains on the inside of the cask for these analyses.

Table 5.4 Maximum Plastic Strains on the Inside of the Monolithic Rail Cask

Corner Impact		End Impact		Side Impact	
Speed	**Strain (%)**	**Speed**	**Strain (%)**	**Speed**	**Strain (%)**
30 mph	< 10	30 mph	< 2	30 mph	< 10
60 mph	< 20	60 mph	< 5	60 mph	< 30
90 mph	< 30	90 mph	< 10	90 mph	< 50
120 mph	< 50	120 mph	< 17	120 mph	< 60

The chance of a closure failure is directly related to the deformations between the cask lid and cask body and tensile or shear failure of the bolts. For the conservative bolt model used in these analyses, the maximum strain in any of the bolts is shown in Table 5.5. Several of these analyses indicate bolt strains that are high enough that failure of the bolt is likely (strains greater than 50 percent). The bolt material has a specified percent elongation greater than 15 percent and a specified percent reduction of area greater than 50 percent [5-8]. This correlates to a true strain at failure of 69 percent. A value of 50 percent is conservatively chosen to indicate bolt failure because the material model used for the bolts has the true stress in the bolts equal to the ultimate tensile stress (an engineering stress) at a strain of 50 percent. Limiting the bolt stress to the ultimate tensile stress also assures that the bolt threads will not fail. Bolt true strains that are higher than 50 percent are shown in **bold** in the table. Several other analyses indicate bolt strains that are high enough that failure of the bolts is possible (true strains higher than 25 percent). These bolt strains are shown in *italics* in the table. Analysis for one of the cases where bolt strains indicate that bolt failure could occur including a failure model for bolts with strains greater than 50 percent shows that even if some of the bolts fail, the remaining bolts will hold the lid in place. Comparison of the closure deformations for this case with those for the same case without the bolt failure model indicates only minor differences (less than 20% for the side impact and only a few percent for the corner impact). This is because the bolt loads are primarily caused by a displacement discontinuity between the cask body and the lid.

Table 5.5 Maximum True Strain in the Closure Bolts

Cask	Corner Impact Speed	Strain (%)	End Impact Speed	Strain (%)	Side Impact Speed	Strain (%)
Steel-Lead-Steel Truck	30 mph	3	30 mph	1	30 mph	n.a
	60 mph	6	60 mph	3	60 mph	2
	90 mph	9	90 mph	5	90 mph	5
	120 mph	11	120 mph	7	120 mph	10
Steel-DU-Steel Truck	30 mph	5	30 mph	0	30 mph	1
	60 mph	9	60 mph	3	60 mph	4
	90 mph	19	90 mph	7	90 mph	10
	120 mph	22	120 mph	9	120 mph	18
Steel-Lead-Steel Rail	30 mph	19	30 mph	6	30 mph	14
	60 mph	*37*	60 mph	3	**60 mph**	**106**
	90 mph	**60**	90 mph	9	**90 mph**	**151**
	120 mph	**102**	120 mph	16	**120 mph**	**n.a.**
Monolithic Rail	30 mph	14	30 mph	4	30 mph	15
	60 mph	*40*	60 mph	14	*60 mph*	*32*
	90 mph	**67**	*90 mph*	*35*	**90 mph**	**104**
	120 mph	**80**	**120 mph**	**58**	**120 mph**	**170**

The amount of deformation between the cask body and the lid at the location of the O-ring seals determines if a leak path from the cask is generated. Because the seal grooves were not explicitly included in the model, the deformation at a location that is near where the O-rings would be located is used. For each model the displacement of two sets (upper point and lower point) of two nodes on the cask lid and one node on the cask body are tracked for all times. Initially these three nodes are co-linear, with the body node lying between the two lid nodes. From the displacement time histories, the amount of seal separation and seal sliding can be determined. The seal separation is defined as the movement of the body node that is normal to the line between the two lid nodes. The sliding is defined as the movement of the body node along the line between the two lid nodes. Figure 5.7 shows these displacements for the 90-mph end impact of the monolithic steel rail cask. Figure 5.8 shows a typical time history for opening displacement. Similar curves for all of the analyses are included in Appendix A. Table 5.6 shows the seal region displacements at the end of the finite element analysis. Because the only location for leakage of radioactive materials is at the closure, and the high degree of variability in closure designs, identical analyses with less stiff bolts were performed for the 60 mph corner and side impacts of the monolithic steel rail cask. To perform these analyses the elastic modulus and strain-hardening modulus of the bolt steel were reduced by a factor of three. These analyses resulted in nearly identical opening displacements as the original analyses. These results support the hypothesis that the cask wall and lid are much stiffer than the closure bolts, and the opening displacements are the result of displacement discontinuities between the cask body and lid, and are not greatly affected by bolt clamping force.

For the end-on impact orientation analyses the displacements at the end of the finite element run had not reached a stable value. For these analyses a range of final displacements is given in the table. This oscillatory response is caused by the lack of friction and material damping within the finite element model. Numerically these oscillations will continue while the cask is rebounding. In reality, the friction and other damping mechanisms will quickly cause these oscillations to stop, and the final displacements will be at about the middle of the range shown in the table.

The many factors affecting closure opening and the way they interact can lead to surprising results. For example, the maximum true strain in the closure bolts for the lead shielded rail cask is higher for the 30-mph impact than it is for the 60-mph impact. In addition, for many of the impacts increasing the impact velocity results in a decrease in closure opening as shown in Table 5.6.

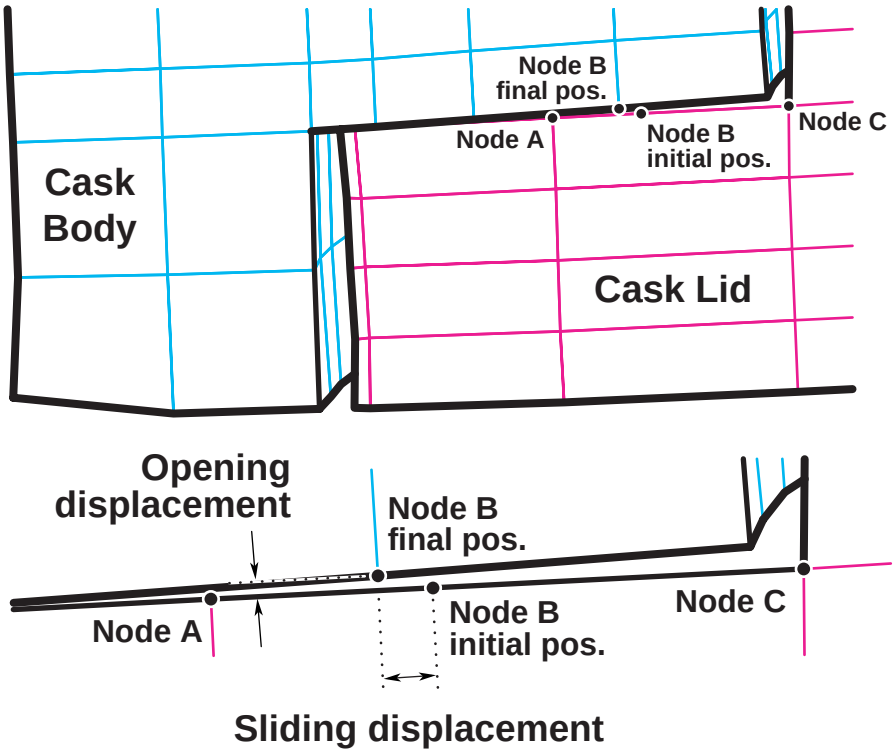

Figure 5.7 Seal region displacements for the 90-mph end impact of the monolithic steel rail cask.

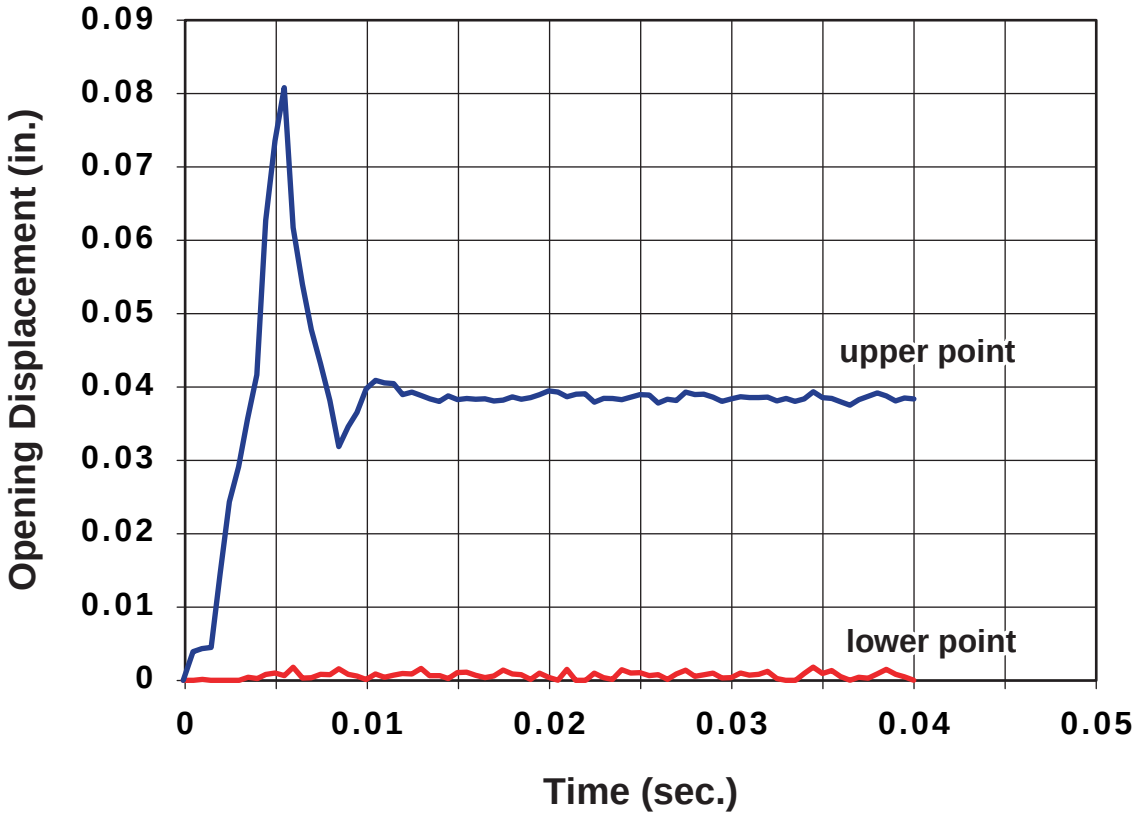

Figure 5.8 Time history for lid opening displacement for the 60 mph side-impact of the monolithic steel rail cask.

Table 5.6 Seal Closure Displacements, in Inches, at the End of the Analysis

Cask	Analysis Velocity	Corner Impact		End Impact		Side Impact	
		Opening	Sliding	Opening	Sliding	Opening	Sliding
Steel-Lead-Steel Truck	30 mph	0.02	0.01	0.000-0.002	0.000-0.002	-	-
	60 mph	0.02	0.03	0.001-0.003	0.001-0.004	0.01	0.02
	90 mph	0.02	0.06	0.000-0.002	0.003-0.005	0.02	0.02
	120 mph	0.04	0.04	0.002	0.02	0.02	0.01
Steel-DU-Steel Truck	30 mph	0.02	0.07	0.005-0.012	0.001-0.005	0.01	0.02
	60 mph	0.08	0.07	0.01-0.02	0.003-0.006	0.01	0.01
	90 mph	0.02	0.10	-	-	0.01	0.02
	120 mph	0.03	0.15	0.013	0.03	0.004	0.02
Steel-Lead-Steel Rail	30 mph	0.01	0.14	0.001-0.022	0.009-0.012	0.01	0.02
	60 mph	0.08	0.32	0.000-0.016	0.01-0.02	0.02	0.01
	90 mph	0.24	0.74	0.004-0.005	0.097-0.101	0.02	0.02
	120 mph	0.51	1.18	0.001-0.018	0.20-0.22	-	-
Monolithic Rail	30 mph	0.04	0.20	0.007-0.053	0.04-0.05	0.01	0.01
	60 mph	0.10	0.36	0.04-0.12	0.09-0.10	0.04	0.01
	90 mph	0.22	0.48	0.03-0.13	0.38-0.39	0.08	0.09
	120 mph	0.44	0.59	0.09-0.16	0.668	0.12	-

To determine the leak area that results from these opening displacements, the influence of the pre-compression of the elastomeric O-ring and the width of the opening must be considered. For cases with maximum openings of less than 0.100 inches, the pre-compression of the O-ring (as much as 0.112 inches for 3/8-inch O-rings and 0.150 inches for 1/2-inch O-rings at 30 percent compression for static face seal configurations [5-11]) will allow it to recover sufficiently to maintain an adequate seal to prevent release of radioactive material. For opening displacements between 0.100 and 0.200 inches, the difference in bolt strains indicates that the opening only occurs at the location of one bolt. The width of the leak path is then equal to the bolt spacing (6.38 inches for the rail casks). However, for part of this width, the actual opening displacement will be less than the O-ring compression; therefore, the area of the resulting hole is calculated by truncating the base (the truncated part has a height of 0.100 inches) of an isosceles triangle with a height of the opening displacement and a width of the bolt spacing. For opening displacements between 0.200 and 0.300 inches, the opening occurs over two bolt spacings, and for opening displacements greater than 0.300 inches, it is assumed the opening occurs over three bolt spacings. For opening displacements greater than 0.300 inches, the resulting leak area is sufficiently large that increasing the width of the opening has little or no effect on the amount of release. Table 5.7 summarizes the leak path calculations for the analyses where the maximum closure opening is greater than 0.100 inches.

Table 5.7 Calculated Rail Cask Closure Hole Sizes

Cask	Velocity (mph)	Orientation	Opening Displacement (inches)	Opening Width (inches)	Leak Path Area (in^2)
Steel-Lead-Steel Rail	90	Corner	0.243	12.76	0.54
	120	Corner	0.512	19.14	3.2
Monolithic Rail	60	Corner	0.103	6.38	0.00028
	90	Corner	0.216	12.76	0.40
	120	Corner	0.439	19.14	2.5
	120	Side	0.123	6.38	0.014

An additional result of impact accidents can be loss of shielding. For the two lead-shielded casks, loss of shielding is a result of the slumping of the lead. For the monolithic steel rail cask there is no loss of shielding, but there may be some radiation streaming through the closure. For the steel-DU-steel truck cask, the model does not include any gaps between forged DU segments, so there is no loss of shielding. Lead slump occurs mostly in the end-on impact orientation, with a lesser amount in the CG-over-corner orientation. In the side-on orientation there is no significant reduction in shielding. The zero-thickness shell elements in the finite element model allow the lead additional space to flow to before contacting the wall. This increases the observed amount of lead slump. Figure 5.9 shows the steel-lead-steel rail cask following a 120-mph end impact.

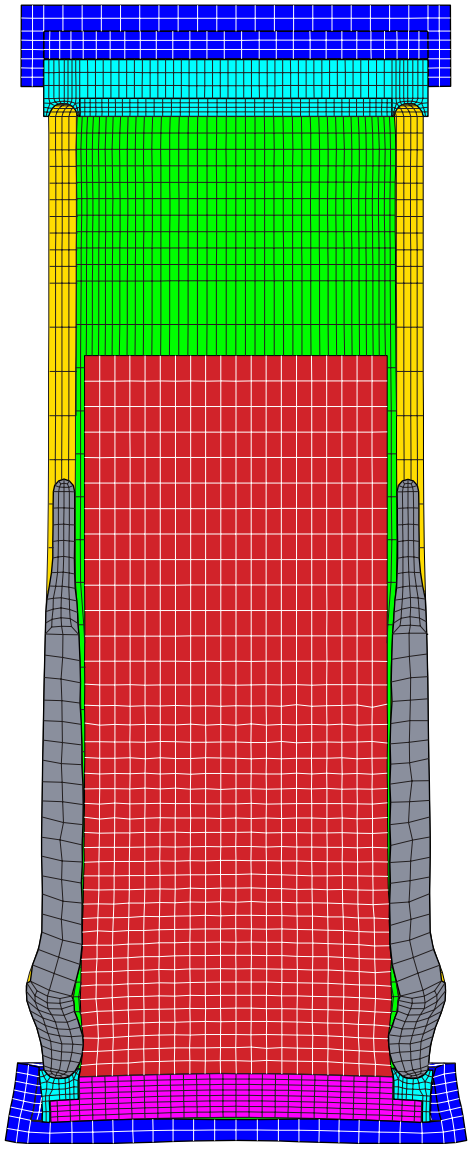

Figure 5.9 Slumping of lead and contents following a 120-mph end-on impact of the steel-lead-steel rail cask.

5.1.5 Benchmarking of Finite Element Calculations

Typical analyses used to certify a cask do not indicate the large levels of strains seen in these analyses. To be confident that analyses of this type are capturing the true response of the package they must be compared to similar analyses that have been demonstrated to be accurate. In the mid 1990s Sandia performed a series of tests and analyses of the Structural Evaluation Test Unit (SETU). End impact tests of 30, 45, and 60 mph were performed. This test unit was roughly a 1/3-scale model of a steel-lead-steel walled rail cask. In this program excellent agreement was obtained between two-dimensional axi-symmetric finite element analyses and end impact tests. In addition, a 7 degrees off-axis impact test at 60 mph was performed and compared to 3-D finite element calculations. Again there was excellent agreement between the analysis and test results. The finite element models used in the SETU program were very similar

to those used here [5-4]. For the 3-D finite element analysis the inner and outer shells were modeled using the same shell elements as this report. However, in the SETU analyses the location of the zero-thickness shell elements was adjacent to the lead because there was no possibility for 2-sided contact on the shells. Appendix B of this report gives a detailed description of the SETU analyses.

5.2 Impacts onto Real Targets

5.2.1 Introduction

The finite element results discussed in the previous section are all for impacts onto a rigid target. For this type of impact, the entire kinetic energy of the impact is absorbed by the cask. For finite element analyses a rigid target is easily implemented by enforcing a no displacement boundary condition at the target surface. In real life, the construction of a rigid target is impossible, but it is possible to construct a target that is sufficiently rigid that increasing its rigidity does not increase the amount of damage to the cask. This is because in real impacts there is a sharing of energy absorption between the cask and the target. If the target is much weaker than the cask, the target will absorb most of the energy. If the target is much stronger than the cask, most of the energy will be absorbed by the cask. In this section the partitioning of the drop energy between the four generic casks and several "real-world" targets will be developed in order to obtain impact speeds onto real surfaces that give the same damage as impacts onto rigid targets. Impacts onto hard desert soil, concrete highways, and hard rock are considered. Impacts onto water surfaces are not explicitly treated, but are discussed. In addition, the probability of puncture of the cask caused by impact against a non-flat surface (or impact by a puncture probe) is developed.

5.2.2 Methodology

The finite element analyses discussed in the preceding sections were all conducted assuming the impact limiter had already been fully crushed. As a result, it is not possible to use these analyses to determine real target impact velocities that equate to the regulatory impact. Impact limiters are typically designed to protect the baskets and spent fuel in a cask from high accelerations. For this reason, most spent-fuel casks have very similar impact limiter designs. Cask behavior for regulatory impacts is primarily a function of impact limiter design, and not cask design. This allows the results from the Modal Study [5-15] steel-lead-steel casks (which included the impact limiters for 30-mph impacts) to be used for the generic casks used in this study to determine equivalent real target impact velocities at rigid target impact velocities of 30 mph. Therefore, for impacts onto real targets that equate to the regulatory impact, the results from the Modal Study are used for all surfaces except hard rock. For the hard rock impacts it is assumed the target absorbs no energy and the equivalent velocity is equal to the rigid target velocity. For impacts at higher velocities, the methodology described below is used.

For each finite element calculation for impact onto a rigid target the total kinetic energy of the finite element model is output at 100 time-steps through the analysis. The total kinetic energy is one half of the sum of the mass associated with each node times the velocity of that node squared. Figure 5.10 shows kinetic energy time-histories for the steel-lead-steel truck cask for

each orientation from the 120-mph impact analyses with pre-crushed impact limiters. From the time-history of kinetic energy, a velocity time history is derived. The rigid-body velocity for each time-step is calculated assuming that all of the kinetic energy of the model is caused by velocity in the direction of the impact. Equation 2 shows this mathematically.

$$V_t = \sqrt{\frac{2KE_t}{\sum m_i}} \tag{2}$$

where v_t is the velocity at time t, KE_t is the kinetic energy at time t, m_I is the mass associated with node I, and the summation is over all of the nodes in the finite element model.

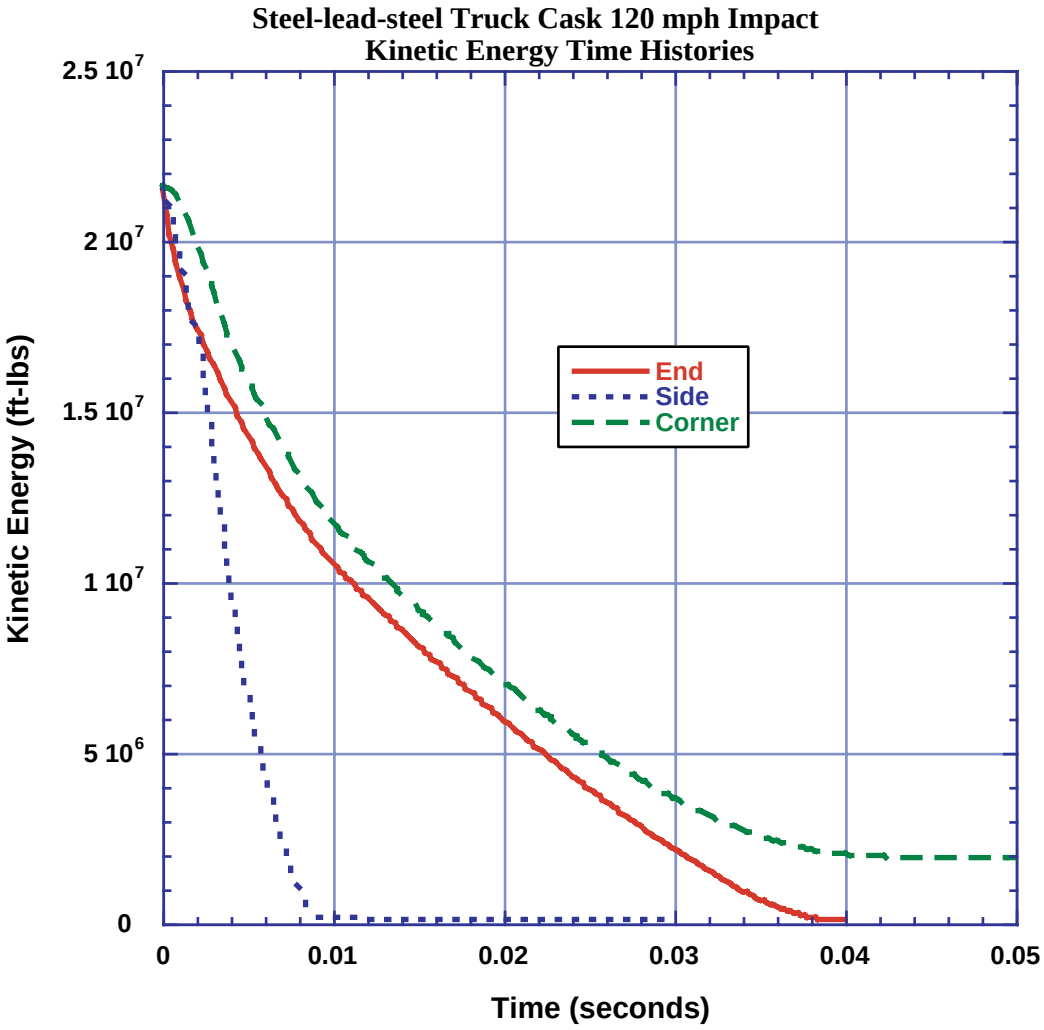

Figure 5.10 Kinetic energy time histories for the steel-lead-steel truck cask from 120-mph impact analyses in the end, side, and corner orientations.

Numerical integration of the velocity time-history gives the displacement of the center-of-gravity of the model. A large portion of this displacement is the result of the center-of-gravity moving down from the geometric center of the cask due to lead and contents slump. Numerical differentiation of the velocity time-history gives rigid-body acceleration. The contact force between the rigid target and the cask at any time is assumed to be equal to the rigid-body acceleration times the mass of the cask. This results in a force time-history. Combination of the force time-history and the displacement time-history results in a force-deflection curve for each cask and impact velocity. Figure 5.11 shows the force deflection curves derived from the kinetic energy time-histories shown in Figure 5.10. Numerical integration of the force-deflection curve results in energy absorbed by the cask. At the end of the analysis the energy absorbed by the cask is equal to the initial kinetic energy.

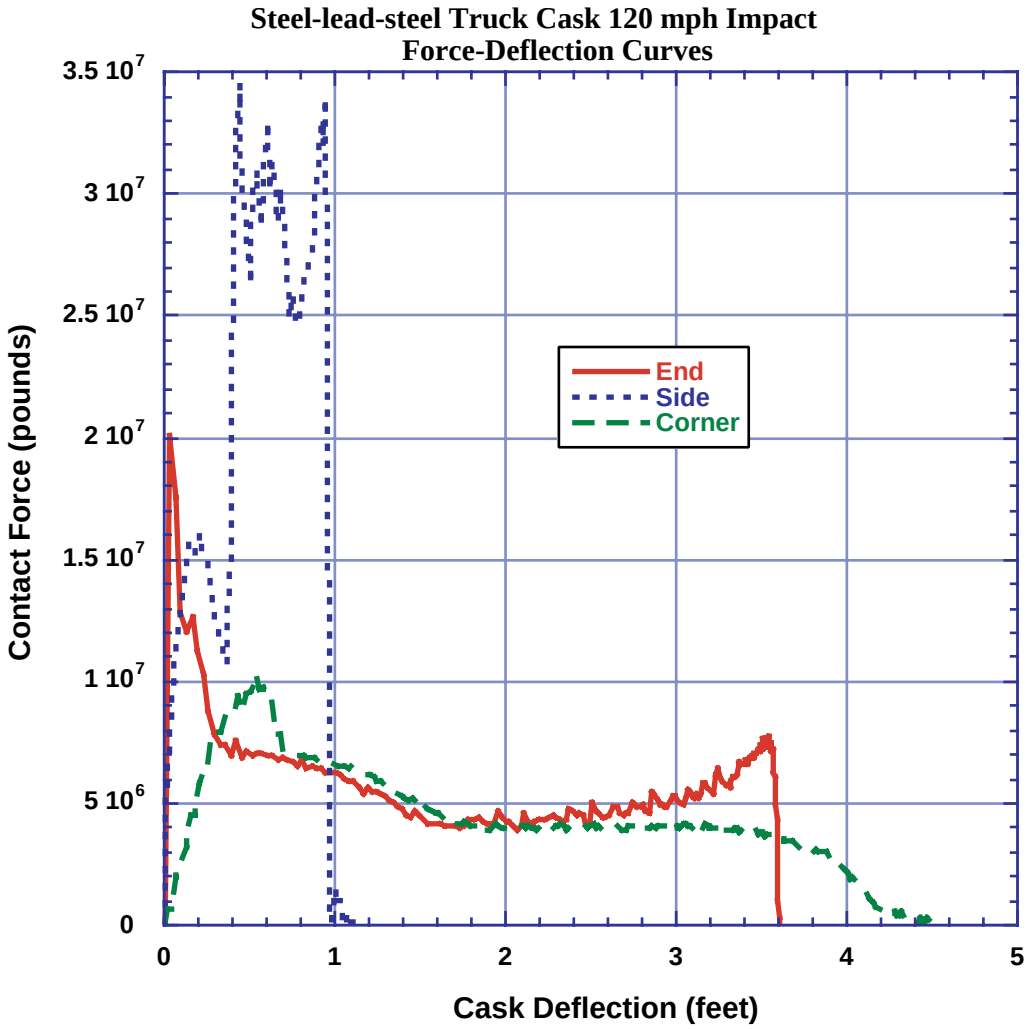

Figure 5.11 Force-deflection curves for the steel-lead-steel truck cask from the 120-mph impact analyses in the end, side, and corner orientations.

For each analysis the peak contact force is determined. Table 5.8 lists these forces. For an impact onto a real target to be as damaging to the cask as the impact onto the rigid target, the target must be able to impart a force equal to this peak force to the cask.

The energy absorbed by the target in developing this force is added to the initial kinetic energy of the cask. This total absorbed energy is used to calculate an equivalent velocity by replacing KE_t in Equation 2 with the total energy.

Table 5.8 Peak Contact Force From Impacts Onto Rigid Targets (Pounds)

Cask	Corner Impact		End Impact		Side Impact	
Steel-Lead-Steel Truck	30 mph	2.3E6	30 mph	9.0E6	30 mph	5.7E6
	60 mph	5.0E6	60 mph	1.3E7	60 mph	1.4E7
	90 mph	7.0E6	90 mph	1.7E7	90 mph	2.2E7
	120 mph	1.0E7	120 mph	2.0E7	120 mph	3.4E7
Steel-DU-Steel Truck	30 mph	6.5E6	30 mph	1.0E7	30 mph	9.0E6
	60 mph	1.1E7	60 mph	1.3E7	60 mph	2.3E7
	90 mph	1.4E7	90 mph	1.5E7	90 mph	3.4E7
	120 mph	1.7E7	120 mph	1.7E7	120 mph	4.9E7
Steel-Lead-Steel Rail	30 mph	1.3E7	30 mph	3.8E7	30 mph	1.8E7
	60 mph	2.3E7	60 mph	6.8E7	60 mph	4.4E7
	90 mph	3.6E7	90 mph	8.3E7	90 mph	6.2E7
	120 mph	n.a.	120 mph	1.1E8	120 mph	n.a.
Monolithic Rail	30 mph	2.1E7	30 mph	3.8E7	30 mph	2.2E7
	60 mph	3.9E7	60 mph	9.5E7	60 mph	5.4E7
	90 mph	5.8E7	90 mph	1.1E8	90 mph	9.5E7
	120 mph	7.5E7	120 mph	1.3E8	120 mph	1.1E8

5.2.3 Soil Targets

The force that hard desert soil imparts onto a cask following an impact was derived from results of impact tests performed by Gonzales [5-13], Waddoups [5-14], and Bonzon and Schamaun [5-15]. The tests by Gonzales and Waddoups used casks that were comparable to the generic casks of this study. The tests by Bonzon and Schamaun were with casks that were less stiff than the generic casks. This large amount of test data was used to develop an empirical soil target force-deflection equation that is a function of impactor area. Figure 5.12 shows the force-deflection curves for impact of the steel-lead-steel truck cask. Corner impacts were assumed to have the same contact area on the soil target as the end impacts, so only two curves are shown. Similar curves were developed for each of the other casks. Comparison of Figure 5.12 with the forces in Table 5.8 show that many of the impacts will result in very large soil penetrations. This is consistent with the results seen in Waddoups' tests, where casks were dropped 2,000 feet from a helicopter. Penetration depths for these impacts were up to 8 feet, and the equivalent rigid target impact velocity was less than 30 mph. Integration of the force-deflection curve up to the peak contact force determines the amount of energy absorbed by the target.

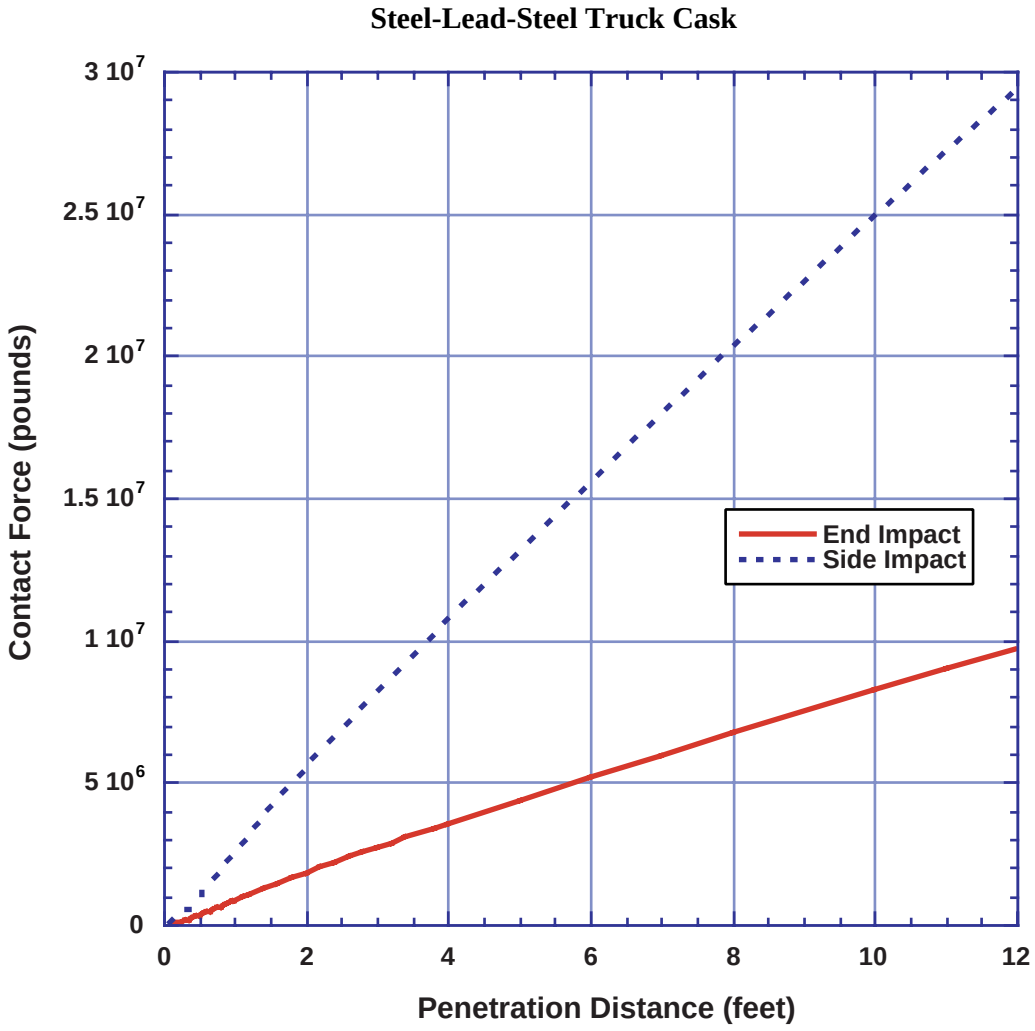

Figure 5.12 Force-deflection curves for impact onto hard desert soil.

5.2.4 Concrete Targets

The force imparted to a cask by impact onto a concrete target is derived from test results by Gonzales [5-13]. In his series of tests, a cask-like test unit was impacted onto two types of concrete targets, one 12 inches thick and one 18 inches thick, at velocities from 30 to 60 mph. All of the impacts were in an end-on orientation. Based upon the results of these tests and engineering mechanics, an empirical relationship between the force and energy absorbed was derived. For impacts onto concrete slab targets there are two mechanisms that produce large forces onto the cask. The first is the generation of a shear plug in the concrete. The force required to produce this shear plug is linearly related to the impact velocity, the diameter of the impacting body, and the thickness of the concrete. Equation 3 gives the empirical equation for the force required to produce the shear plug.

$$F_s = C_s v_e d_i t_c \tag{3}$$

where F_s is the force required to produce the shear plug, C_s is an empirical constant (16.84), v_e is the equivalent impact velocity, d_i is the diameter of the impactor, and t_c is the thickness of the concrete slab.

The energy absorbed in producing this shear plug is linearly related to the cask diameter, the square of the impact velocity, and the fourth root of the slab thickness. Equation 4 gives the empirical equation for the energy required to produce the shear plug.

$$E_s = C_e d_i v_e^{\,2} t_c^{\,0.25} \tag{4}$$

where E_s is the energy required to produce the shear plug and C_e is an empirical constant (0.00676).

After the shear plug is formed, further resistance to penetration is achieved by the behavior of the subgrade and soil beneath the concrete. This material is being penetrated by the cask and the shear plug. Generally, the shear plug forms with 45-degree slopes on the side. Therefore, the diameter of the soil being penetrated is equal to the cask diameter plus twice the slab thickness. The behavior of the subgrade and soil is assumed to be the same as the hard desert soil used for the soil target impacts. Figure 5.13 shows a comparison of the empirical relationship with one of Gonzales' tests. Figure 5.14 shows the force-deflection curve for the steel-lead-steel truck cask impacting a 9-inch thick concrete roadway at 120 mph. For corner and side impacts an equivalent diameter is calculated to fit with the empirical equations. For each case the diameter is calculated by assuming the shear plug forms when the concrete target has been penetrated two inches. The area of the equivalent diameter is equal to the area of the concrete in contact with the cask when the penetration depth is two inches. To calculate the equivalent velocity for concrete targets the force required to generate the shear plug must be compared to the peak contact force for the impact onto the rigid target. The velocity required to produce this force can be calculated from Equation 3. The kinetic energy associated with this velocity is absorbed by a combination of producing the shear plug, penetration of the subgrade and soil beneath the concrete, and deformation of the cask. The energy absorbed in producing the shear plug is calculated by Equation 4, the energy absorbed by the cask is equal to the kinetic energy of the rigid target impact, and the energy absorbed by the subgrade and soil is calculated in a manner similar to that for the soil impact discussed above. If the amount of energy to be absorbed by the soil is sufficiently high, the force in the soil will be higher than the force required to produce the shear plug. In this case, an iterative approach is necessary to derive an equivalent velocity so that the maximum force generated in penetrating the subgrade and soil beneath the concrete is equal to the peak contact force for the rigid target impact.

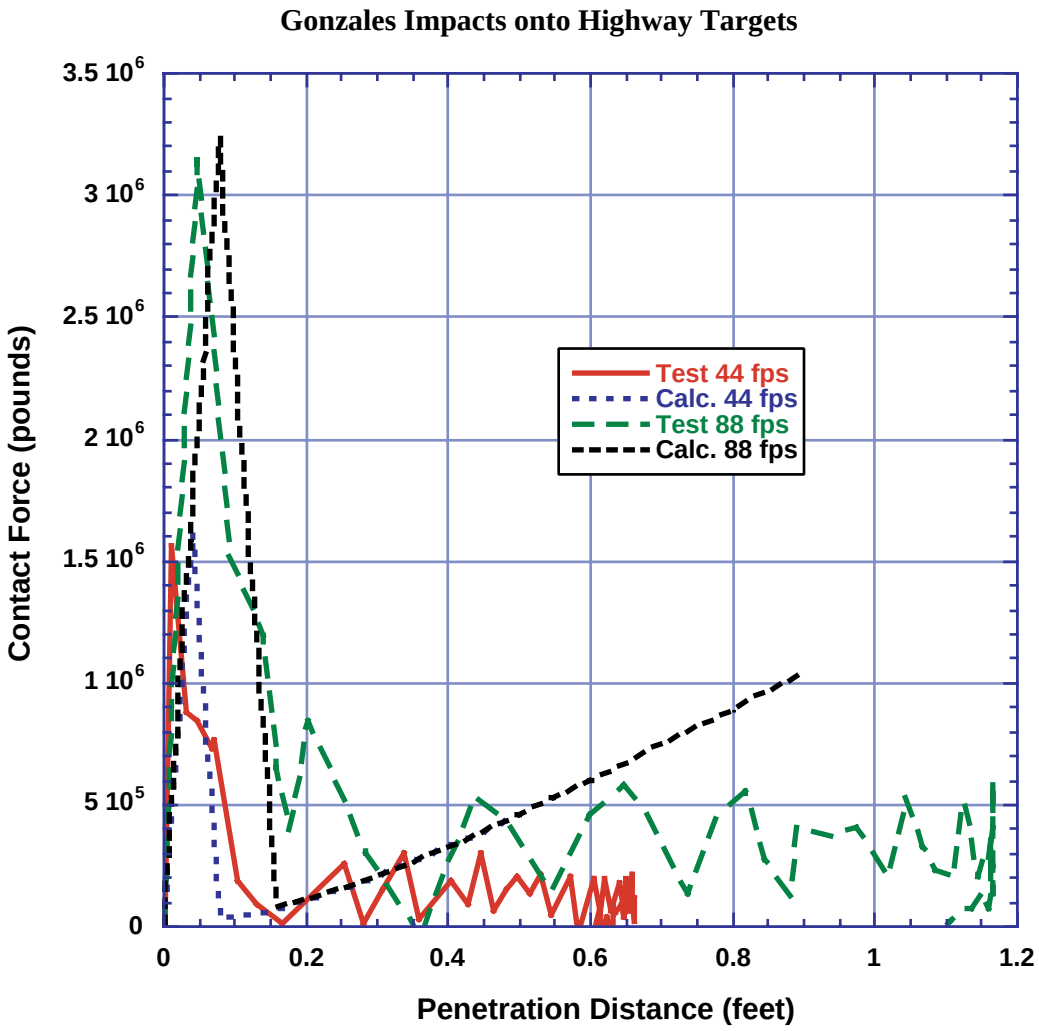

Figure 5.13 Comparison of test force-deflection curves with those derived from the empirical equations.

The only orientation of impacts onto concrete targets where test data is available is for end impacts. In this orientation the contact area between the cask and the concrete does not increase with increasing penetration distance. In order to use the empirical relationships developed for end impacts with other impact orientations, an equivalent diameter must be determined. For both the side and corner impacts, the equivalent diameter was calculated to have an area equal to the area of the cask two inches above the contact point. For side impact orientations, this area is a rectangle. For corner impact orientations this area is a truncated parabola. Table 5.9 gives the equivalent diameters used for each of the casks. For all of the casks, the equivalent diameter for the corner impact is much smaller than the cask diameter. This is especially pronounced for the rail casks. In reality, the failure mode for a concrete target being impacted by a large cask in a corner orientation is probably not generation of a shear plug, but rather a splitting tensile failure and subsequent rotation of the slab to allow perforation by the cask. After penetration of the concrete occurs, the area of the cask plus concrete penetrating the soil is equal to the cask cross-sectional area (the same area used for the soil target impacts).

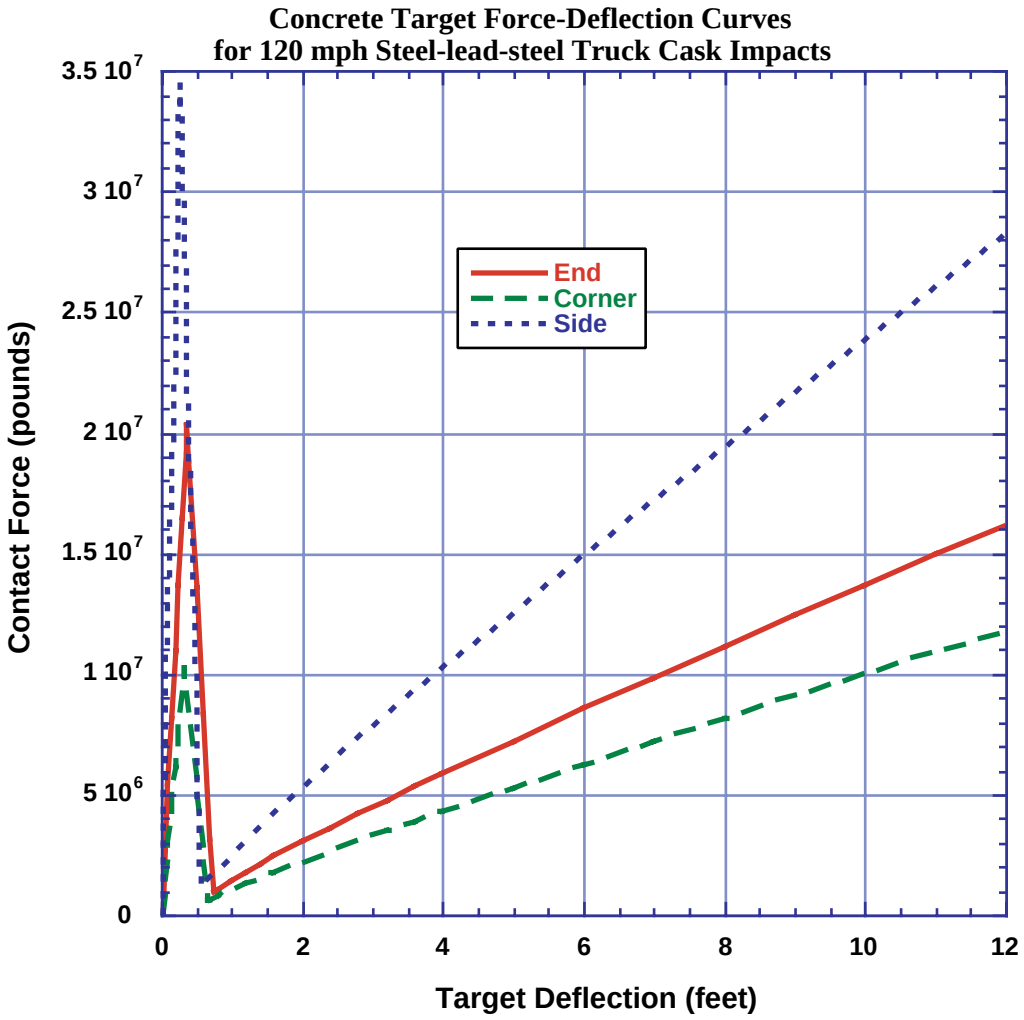

Figure 5.14 Force-deflection curves for concrete target impacts of the steel-lead-steel truck cask at 120 mph.

Table 5.9 Equivalent Diameters for Concrete Impacts

Cask	Orientation	Equivalent Diameter (inches)
Steel-Lead-Steel Truck	Corner	15.3
	End	27.5
	Side	61.1
Steel-DU-Steel Truck	Corner	20.2
	End	28.0
	Side	60.6
Steel-Lead-Steel Rail	Corner	13.6
	End	80.0
	Side	79.8
Monolithic Rail	Corner	13.0
	End	85.0
	Side	79.0

5.2.5 Hard Rock Targets

For impacts onto hard rock targets the target is assumed to be a semi-infinite half plane. The force and energy absorbed by the target is determined by the volumetric behavior of the rock. For hard rock surfaces this behavior is sufficiently stiff that very little energy is absorbed by the target. For this reason these impacts are treated as rigid target impacts.

5.2.6 Example Calculation

In this section, the methodology discussed in Section 5.2.2 will be applied to the steel-lead-steel truck cask using the soil target properties from Section 5.2.3. For the 120 mph impact in the end-on orientation the peak contact force acting on the cask is 20×10^6 pounds (from Figure 5-11 or Table 5-8). For a soil target to generate this amount of force, the cask must penetrate slightly over 12 feet (from Figure 5.12). The energy absorbed by the soil target while it is being penetrated to this distance is equal to the integral under the force-deflection curve up to this penetration distance. For this case, this is equal to 136×10^6 foot-pounds. The kinetic energy of this 50,000 pound cask travelling at 120 mph is 24.1×10^6 foot-pounds. This is the amount of energy absorbed by the cask for impact onto a rigid target. For the impact onto the soil target, the cask will therefore absorb 24.1×10^6 foot-pounds of energy and the soil will absorb 136×10^6 foot-pounds of energy for a total of 160×10^6 foot-pounds of energy. The cask velocity that is associated with this amount of kinetic energy is 309 mph. This velocity is much higher than the 150-mph top velocity in the accident velocity distributions. Note that all of the equivalent velocities determined in this manner neglect the energy absorbed by the impact limiter.

5.2.7 Results for Real Target Calculations

Tables 5.10 to 5.13 summarize the results for impacts onto soil and concrete targets.

Table 5.10 Real target Equivalent Velocities (mph) for the Steel-Lead-Steel Truck Cask

Target/Orientation	Rigid Target Velocity			
	30 mph w/o limiter	60 mph w/o limiter	90 mph w/o limiter	120 mph w/o limiter
Soil				
End	>150	>>150	>>150	>>150
Side	70	>150	>>150	>>150
Corner	61	135	>150	>>150
Concrete Slab				
End	123	>150	>>150	>>150
Side	35	86	135	>150
Corner	56	123	>150	>>150

Table 5.11 Real Target Equivalent Velocities (mph) for the Steel-DU-Steel Truck Cask

Target/Orientation	Rigid Target Velocity			
	30 mph w/o limiter	60 mph w/o limiter	90 mph w/o limiter	120 mph w/o limiter
Soil				
End	>150	>>150	>>150	>>150
Side	99	>>150	>>150	>>150
Corner	128	>150	>>150	>>150
Concrete Slab				
End	134	>150	>150	>150
Side	56	142	>150	>>150
Corner	121	>150	>>150	>>150

Table 5.12 Real Target Equivalent Velocities (mph) for the Steel-Lead-Steel Rail Cask

Target/Orientation	Rigid Target Velocity			
	30 mph w/o limiter	60 mph w/o limiter	90 mph w/o limiter	120 mph w/o limiter
Soil				
End	>>150	>>150	>>150	>>150
Side	72	>150	>>150	>>150
Corner	68	133	>150	>150
Concrete Slab				
End	>150	>>150	>>150	>>150
Side	85	>150	>>150	>>150
Corner	>>150	>>150	>>150	>>150

Table 5.13 Real Target Equivalent Velocities (mph) for the Monolithic Steel Rail Cask

Target/Orientation	Rigid Target Velocity			
	30 mph w/o limiter	60 mph w/o limiter	90 mph w/o limiter	120 mph w/o limiter
Soil				
End	>150	>>150	>>150	>>150
Side	92	>150	>>150	>>150
Corner	111	>150	>>150	>>150
Concrete Slab				
End	>150	>>150	>>150	>>150
Side	104	>>150	>>150	>>150
Corner	>>150	>>150	>>150	>>150

5.2.8 Impacts onto Water

Equivalent velocities for impacts onto water targets for velocities greater than the regulatory impact are assumed to be above the range of possible impact velocities (150 mph). The incompressible nature of water makes perfectly flat impacts quite severe. As the impact velocity increases smaller deviations from the perfectly flat orientation are sufficient to cause the lack of shear strength in water to dominate the response. Because perfectly flat impacts are very improbable, this approach is justified.

5.2.9 Correlation of Results with Modal Study Event Trees

The Modal Study [5-12] event trees specify impact surfaces for each accident type. Because these event trees are used in this study to determine accident probabilities, this section will discuss which of the velocities determined above correlate to the surfaces specified in the event trees. For this study the event tree surface of railbed/roadbed will be treated as soil. The soil impacted in the tests used to calibrate the model was very hard desert soil, typical of Albuquerque, New Mexico. This soil is generally harder than the soil found on railbeds and roadbeds. For impacts onto the event tree surface of clay/silt the equivalent velocities will always be higher than the soil impact velocity derived here, but this velocity will be conservative and is therefore used. For the event tree surface of soft rock/hard rock/concrete the data from the concrete slab analyses will be used. In the Modal Study the equivalent velocities for the event tree surfaces of column and abutments were the same as those for the soft rock/hard soil/concrete surface. This approach will be repeated in this study. The event tree surface of hard rock will be treated as unyielding at all velocities, because the amount of energy absorbed by the rock is only a small portion of the impact energy. For all of the other impact surfaces the 30-mph equivalent velocity is taken directly from the Modal Study.

5.3 Puncture Analyses

Review of data from the Association of American Railroads (AAR) on the puncture of railroad tank cars indicates that cars with a shell thickness greater than or equal to one inch rarely experience puncture failures[1]. Because the steel-lead-steel rail cask in this study has an outer shell thickness of two inches, it is highly unlikely that even the outer shell will be punctured in any rail accident. The containment boundary on the sandwich-wall casks is the inner shell, so puncture failure of the outer wall will not result in any release. The residual energy necessary to puncture the inner shell after the outer shell and shielding layers have been perforated is similar in magnitude to that required to puncture the outer shell, making loss of containment in puncture accidents even more unlikely. Figure 5.15 shows the relationship between tanker shell thickness and fraction of cars involved in puncture-type accidents that were failed because of puncture. Even the truck casks, which have thinner outer shells than rail casks, have a composite wall strength that is significantly greater than the strength of the strongest tank cars. The probability that these casks will be failed because of puncture is extremely low. This

1. Personal communication with D. J. Pasternak and data from RPI-AAR Railroad Tank Car Safety Research and Test Project, June 1998.

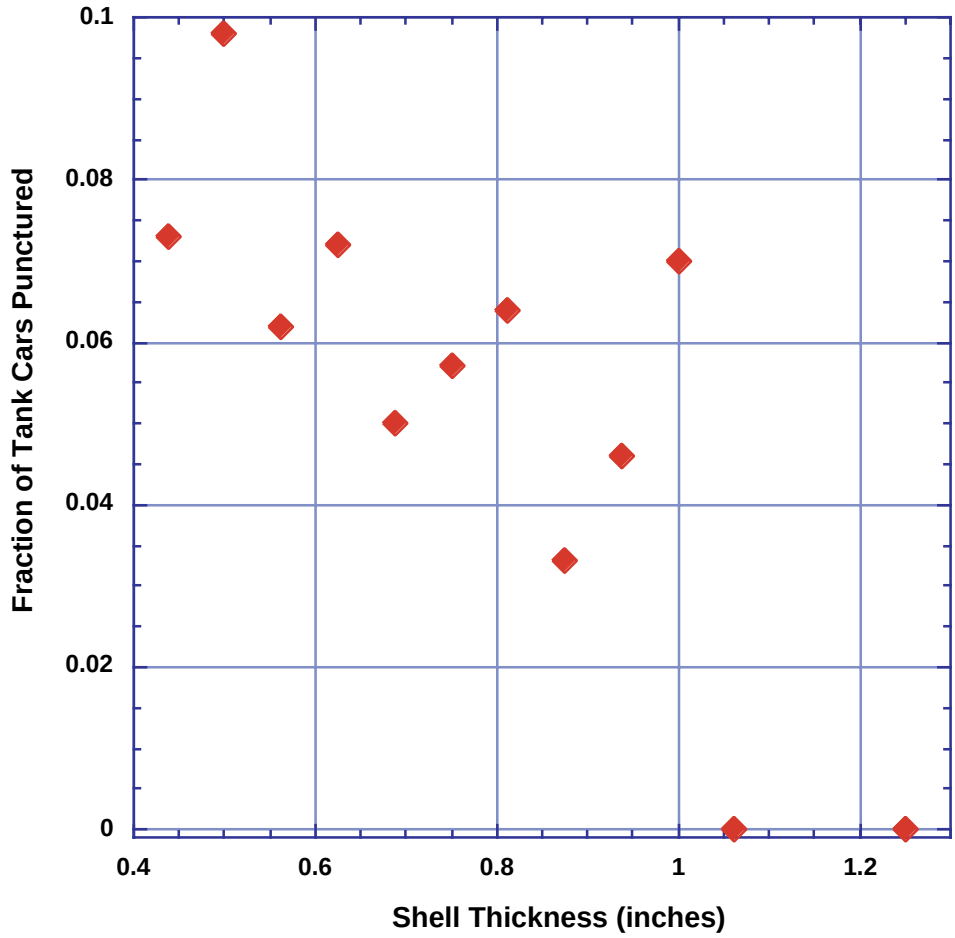

Figure 5.15 Fraction of railroad tank cars involved in puncture-type accidents that failed because of puncture.

is consistent with recent analyses performed by the NRC in response to questions from the AAR. These analyses concluded that it would be impossible for a rail coupler or a regulatory puncture spike to puncture the wall of a rail cask [5-16].

5.4 Failure of Rods

The percentage of fuel pins damaged for each impact is estimated based on the peak rigid-body acceleration. The STACE report [5-17] provides strains in the fuel pin cladding for a 100-G side impact for both PWR and BWR assemblies. In that report, it was shown that side impact provides the most severe loading to the fuel assemblies. During end-on impacts, the fuel assemblies are loaded by axial compressive loads. This type of loading will cause the individual rods to eventually buckle. Because of the limited space for lateral motion that results from this buckling and the very slender nature of the fuel rods, relatively low strains are produced. Therefore, in this report, the maximum strain generated in a fuel rod due to impacts onto a rigid target at any of the four speeds and three impact orientations modeled by the finite element calculations will be estimated using the peak acceleration of the impact to scale the largest strain generated in a fuel rod by a 100-G side impact. The rod will then be said to fail whenever the scaled strain level equals or exceeds the strain failure criterion developed in the next section.

5.4.1 Rod Failure Strain Criterion

As of 1994, the U.S. commercial spent fuel inventory contained about 49 percent low burnup (0 to 30 GWDt/MTU) fuel, about 49 percent intermediate burnup (30 to 45 GWDt/MTU) fuel, about 2 percent intermediate to high burnup (45 to 50 GWDt/MTU) fuel, and only 0.2 percent high burnup (50 to 60 GWDt/MTU) fuel [5-18]. Recent data suggest that, as of 1998, about 25 to 30 percent of PWRs and 15 to 20 percent of BWRs were producing high burnup fuel[1]. Since hardly any high burnup fuel was being produced in 1994, linear extrapolation of this data suggests that by 2010 almost all U.S. commercial reactors will be producing high burnup spent fuel and about half will be producing high burnup fuel in 2002.

In 1994, the 109 power reactors that were operating in the United States generated 1883 MT of spent fuel [5-18] or 17.28 MT per reactor-year. If all of the U.S. commercial power reactors operating in 1999 extend their plant lives to 40 years, then data published in Nuclear News [5-19] allows the amounts of spent fuel that will be generated over the remaining life of these reactors to be calculated. The rate of conversion to high burnup fuel can be captured by assuming that from 1995 through 2001, all operating reactors will generate fuel with burnups of 40-45 GWDt/MTU and from 2002 through the end of their operating lives they will all generate high burnup fuel (fuel with burnups of 55-60 GWDt/MTU). Thus, during the seven year period from 1995 through 2001, 13181 MTU = (7 yrs)(1883 MTU per yr) of 40-45 GWDt/MTU fuel will be produced; and, after 2001, 33600 MTU = (17.28 MT per reactor)(1945 reactor-yrs) of high burnup fuel will be produced where, as Table 5.14 shows, 1945 is the number of years of reactor operation after 2001 that will occur if all of the reactors operating in 1999 extend their plant lives to 40 years.

The strains that cause rod failure are expected to lie somewhere between the uniform plastic elongation (UE) and total plastic elongation (TE) strains that produce rod failure, probably well below the total elongation strains and not much above the uniform elongation strains[2]. For average burnup fuel, the results of Bauer and Lowry [5-20] suggest that, when heated to 200 to 300° C, average burnup spent fuel will fail when UE strain levels reach 4 percent or TE strain levels reach 8 percent. For average burnup fuel, Sanders et al. [5-17] estimate that the probability of rod failure due to an impact that generates a biaxial stress ratio (pressurized fuel under tension) of 0.9 is 50 percent when the rupture strain is 4 percent. For high burnup fuel, the data of Smith et al. [5-21] and Garde et al. [5-22] indicate that at 300° C high burnup fuel will fail when UE stain levels reach 1 percent or TE strain levels reach 3.8 percent. Accordingly, 1 percent and 4 percent strains respectively are assumed to cause the cladding of high (55-60 GWDt/MTU) and high intermediate (40-45 GWDt/MTU) burnup spent fuel rods to fail, which suggests that the rod failure strain criterion will increase 1 percent for each 5 GWDt/MTU increase in burnup.

---

1. Personal communications, J. Finucane, Coal, Nuclear, and Renewable Fuels Division, U.S. Department of Energy, 1999.
2. Personal communication, M. Billone, Argonne National Laboratory, 1999.

Table 5.14 Calculation of Reactor-Years Producing High Burnup Fuel

Reactor	Type	Start Year	Years >2001	Reactor	Type	Start Year	Years >2001	Reactor	Type	Start Year	Years >2001
Calloway	PWR	85	23	Arkansas 1	PWR	74	12	Hope Creek	BWR	86	24
Cook 1	PWR	75	13	Arkansas 2	PWR	80	18	Salem 1	PWR	77	15
Cook 2	PWR	78	16	Grand gulf	BWR	85	23	Salem 2	PWR	81	19
Palo Verde 1	PWR	86	24	River Bend	BWR	86	24	R.E. Ginna	PWR	70	8
Palo Verde 2	PWR	86	24	Waterford 3	BWR	85	23	Virgil C. Summer	PWR	84	22
Palo Verde 3	PWR	88	26	Davis Besse	PWR	78	16	South Texas 1	PWR	88	26
Calvert Cliffs 1	PWR	75	13	Perry 1	BWR	87	25	South Texas 2	PWR	89	27
Calvert Cliffs 2	PWR	77	15	St Lucie 1	PWR	76	14	San Onofre 2	PWR	83	21
Pilgrim	BWR	72	10	St Lucie 2	PWR	83	21	San Onofre 2	PWR	84	22
Brunswick 1	BWR	77	15	Turkey Point 1	PWR	72	10	Farley 1	PWR	77	15
Brunswick 2	BWR	75	13	Turkey Point 2	PWR	73	11	Farley 2	PWR	81	19
Robinson 2	PWR	71	9	Crystal River 3	PWR	77	15	Hatch 1	BWR	75	13
Shearon Harris	PWR	87	25	Oyster Creek	BWR	69	7	Hatch 2	BWR	79	17
Braidwood 1	PWR	88	26	Three Mile Island 1	PWR	74	12	Vogtle 1	PWR	87	25
Braidwood 2	PWR	88	26	Duane Arnold	BWR	75	13	Vogtle 2	PWR	89	27
Bryon 1	PWR	85	23	Clinton	BWR	87	25	Bellefonte1	PWR	95	33
Bryon 2	PWR	87	25	Cooper	BWR	74	12	Bellefonte2	PWR	95	33
Dresden 2	BWR	70	8	FitzPatrick	BWR	75	13	Browns Ferry 1	BWR	74	12
Dresden 3	BWR	71	9	Indian Point 3	PWR	76	14	Browns Ferry 2	BWR	75	13
LaSalle 1	BWR	84	22	Nine Mile Point 1	BWR	69	7	Browns Ferry 3	BWR	77	15
LaSalle 1	BWR	84	22	Nine Mile Point 1	BWR	88	26	Sequoyah 1	PWR	81	19
Quad Cities 1	BWR	73	11	Seabrook	PWR	90	28	Sequoyah 1	PWR	82	20
Quad Cities 2	BWR	73	11	Millstone 2	PWR	75	13	Watts Bar 1	PWR	96	34
Indian Point 2	PWR	74	12	Millstone 3	PWR	86	24	Watts Bar 2	PWR	95	33
Palisades	PWR	71	9	Monticello	BWR	71	9	Comanche Peak 1	PWR	90	28
Fermi 2	BWR	88	26	Prairie Island 1	PWR	73	11	Comanche Peak 2	PWR	93	31
Catawba 1	PWR	85	23	Prairie Island 2	PWR	74	12	Vermont Yankee	BWR	72	10
Catawba 2	PWR	86	24	Fort Calhoun	PWR	73	11	North Anna 1	PWR	78	16
McGuire 1	PWR	81	19	Susquehanna 1	BWR	83	21	North Anna 2	PWR	80	18
McGuire 2	PWR	84	22	Susquehanna 1	BWR	85	23	Surry 1	PWR	72	10
Oconee 1	PWR	73	11	Diablo Canyon 1	PWR	85	23	Surry 2	PWR	73	11
Oconee 2	PWR	74	12	Diablo Canyon 2	PWR	86	24	WPN-2	BWR	84	22
Oconee 3	PWR	74	12	Limerick 1	BWR	86	24	Point Beach 1	PWR	70	8
Beaver Valley 1	PWR	76	14	Limerick 2	BWR	90	28	Point Beach 2	PWR	72	10
Beaver Valley 2	PWR	87	25	Peach Bottom 1	BWR	74	12	Kewaunee	PWR	74	12
				Peach Bottom 2	BWR	74	12	Wolf Creek	PWR	85	23

Reactor-Years at High Burnup 1945

Use of the combination of the extrapolated amounts of intermediate and high burnup fuel with the 1994 data for metric tons of spent fuel by burnup range produces the basis for constructing an average strain failure level as a weighted sum of strain failure levels weighted by the amount of spent fuel in each burnup range. To do this, the cladding strains that produce rod failure are assumed to increase roughly linearly with decreasing fuel burnup. High burnup (55 to 60 GWDt/MTU) spent fuel is assumed to fail at 1 percent strain, intermediate burnup (40 to 45 GWDt/MTU) spent fuel fails at 4 percent strain, and low burnup (0 to 25 GWDt/MTU) spent fuel fails at 8 percent strain. As Table 5.15 shows, weighted summation of these cladding strain levels by burnup range produces an average failure stain level of 3.6 percent. This average is probably somewhat low for three reasons: (a) because it is derived using uniform elongation strains which are expected to underestimate somewhat the strains required to produce rod failure, (b) because not all operating reactors will extend their operating life to 40 years, and (c) because not all operating reactors will convert to a fuel management cycle that produces high burnup fuel. Accordingly, in agreement with the STACE report [5-17] and consistent with failure strains reported by Westinghouse for several burst tests [5-23], an average strain failure criterion of 4 percent seems reasonable for the U.S. commercial power reactor spent fuel inventory even after correcting for the amounts of high-burnup fuel likely to be produced during the remainder of the nuclear fuel cycle in the United States. Finally, a sensitivity calculation described below in Section 8.10.3, shows that, when rod failure fractions are set to 1.0 for all collision scenarios regardless of their severity, mean accident dose risks are increased by only a factor of 2.0. Thus, mean accident doses and dose risks are not particularly sensitive to the average value chosen for the strain criterion for rod failure during collision accidents.

Table 5.15 Calculation of Mass Weighted Sum of Burnup Dependent Rod Strain Failure Levels

GWDT per MTU	MTU	Criterion	
		Range	Weighted
0-25	8437	8	0.88
25-30	6177	7	0.56
30-35	6815	6	0.53
35-40	5149	5	0.34
40-45	2570	4	0.13
45-50	636	3	0.02
50-55	44	2	0.00
55-60	5	1	0.00
AvBU	13181	4	0.69
HBU	33600	1	0.44
Total	76614	Sum	3.60

5.4.2 Estimation of the Fraction of Rods Failed During Impacts

If the cladding strains are scaled by the ratio of peak rigid-body accelerations calculated in Section 5.2.2 to the 100-G acceleration used in the STACE report, the number of pins with cladding strains larger than 4 percent can be determined. These results are used to provide an estimate of fuel pin failure percentages. Table 5.16 gives the peak rigid-body accelerations for each of the analyses. Table 5.17 gives the strains in the fuel rods resulting from a 100-G impact, taken from Figures III-60 and III-64 of the STACE report. Scaling the strains in Table 5.17 by the accelerations in Table 5.16 and counting the number of rods with strains greater than 4 percent results in the fraction of rods failed given in Table 7.18 for each of the analyses.

Table 5.16 Peak Accelerations from Rigid Target Impacts without Impact Limiters, Gs

Cask	Orientation	30 mph	60 mph	90 mph	120 mph
Steel-Lead-Steel Truck	Corner	51.3	111.4	156.0	222.9
	End	200.6	289.8	378.9	445.8
	Side	127.0	312.1	490.4	757.8
Steel-DU-Steel Truck	Corner	132.6	224.3	291.6	346.7
	End	203.9	254.9	297.8	346.7
	Side	183.5	469.1	693.4	999.3
Steel-Lead-Steel Rail	Corner	50.6	94.4	145.9	n.a.
	End	167.3	303.0	371.1	483.6
	Side	73.3	178.8	349.7	n.a.
Monolithic Rail	Corner	93.8	174.2	259.1	335.1
	End	169.8	424.4	513.8	580.8
	Side	98.3	241.3	424.4	491.5

5.5 Conservatism in Calculating Structural Response

In this section the conservatism associated with the various assumptions in the determination of the structural response of the generic casks will be discussed in approximately the same order as the sections of this chapter.

Treating all corner impacts as if they were CG-over-corner forces all of the impact energy to be absorbed on the primary impact end. For corner impacts away from CG-over-corner, some of the initial kinetic energy of the cask will be converted into rotational kinetic energy at the end of the primary impact. This rotational kinetic energy will be absorbed by a secondary impact on the opposite end of the cask. Another conservatism in choosing the impact angles to be analyzed is the assumption that all end and corner impacts occur on the closure end of the cask. The deformations on the end away from the impact are much smaller, so if the impact occurs on the end away from the closure there will only be small deformations in the closure region and no releases for even the 120 mph impacts. In addition, the velocity vectors for all of the accidents are assumed to be perpendicular to the impact surface. In reality, there will be a distribution of angles between the velocity vector and the impact surface, and only the component of the

velocity vector that is perpendicular to the impact surface will cause damage to the cask. If the median of the distribution is at 45 degrees, this results in a 70% reduction, on average, in the component of velocity that produces damage.

Table 5.17 Peak Strains in Fuel Rods Resulting from a 100 G Impact

Fraction of PWR Rods	Peak Strain, %	Fraction of BWR Rods	Peak Strain, %
1/15	3.3	1/7	1.1
2/15	2.9	2/7	1
3/15	2.2	3/7	0.85
4/15	2	4/7	0.83
5/15	1.7	5/7	0.78
6/15	1.5	6/7	0.66
7/15	1.4	7/7	0.62
8/15	1.4		
9/15	1.4		
10/15	1.3		
11/15	1.3		
12/15	1.2		
13/15	1.2		
14/15	1.1		
15/15	1.1		

Treating the impact limiter material as completely locked-up from a 30-mph impact neglects the design margin that cask designers include in their impact limiter designs. For most cask designs the regulatory impact only uses about 50% of the energy absorbing capability of the impact limiter. If the impact limiter can absorb twice as much energy (the energy from a 60-foot free drop) the accident velocities associated with the 30, 60, 90 and 120 mph finite element calculations become 52, 73, 99, and 127 mph respectively instead of the 42, 67, 95, and 124 mph respectively used in this report.

The use of zero-thickness shell elements to represent the structural portions of the sandwich walls for the lead and DU shielded casks results in an overprediction of lead slump and strain in the walls. Because none of the walls had strains that were sufficiently high to indicate tearing of the stainless steel, the overprediction of these strains did not have any consequences. Therefore, the only consequence of the zero-thickness shells is for loss-of-shielding analyses.

Omitting the neutron shielding and any liner that is outside of it ignores the energy that will be absorbed by these components. During regulatory drops (30 mph) this is insignificant, but for higher velocity side impacts it is possible for the neutron shielding and its liner to absorb enough energy to reduce the damage to the remainder of the cask.

The seal leak path areas are only calculated at the location of one of the two o-rings typical in casks (the one that is closest to the interior of the cask). In reality, the o-rings at both locations can provide containment. For most of the analyses, the opening deflection at the location of the second o-ring is about half of the deflection at the inner o-ring.

The use of minimum material properties for the closure bolts results in a reduction of bolt clamping force and an over-estimation of bolt elongation. The specified bolt material (SA-540 Grade B23 Class 5) can have yield strengths more than 50% higher than the values used. Using more realistic values for bolt material parameters would result in smaller openings.

For soil impacts all of the results are based upon soil properties around Albuquerque, NM. This desert location has very hard soils (generally not tillable) compared to most of the rest of the nation. For impacts onto more typical soils even higher velocities would be required to obtain the damage levels from the rigid target finite element analyses. For impacts onto highway surfaces, all of the surfaces are assumed to be concrete. Impacts onto asphalt highway surfaces would be less severe. For impacts onto rock these analyses assumed the rock would absorb none of the impact energy. In reality, if a spent fuel cask were to impact into solid rock there would be some cracking and spalling of the rock surface as a result of the impact. This damage to the rock surface implies that it is absorbing some amount of energy.

Although the puncture data given in this chapter indicate the probability for puncturing a cask with a wall thickness greater than 1 inch is extremely remote, the risk analyses in this report assume the truck casks are punctured in 0.1% of the accidents. Even more conservative is the assumption that the rail casks are punctured in 1% of the rail-coupling impacts and 0.1% of all other impacts.

Scaling the strains in the spent fuel rods calculated for a 100 G impact by the accelerations for more severe impacts significantly overestimates the rod strains. As the geometry of a spent fuel assembly changes in the more severe impacts, the deformations become constrained due to limited space. Once this happens, the strains will no longer increase with increasing load.

5.6 References

[5-1] L. M. Taylor and D. P. Flanagan, "PRONTO 3D, A Three-Dimensional Transient Solid Dynamics Program," SAND87-1912, Sandia National Laboratories, Albuquerque, NM, March 1989.

[5-2] S. W. Attaway, "Update of PRONTO 2D and PRONTO 3D Transient Solid Dynamics Program," SAND90-0102, Sandia National Laboratories, Albuquerque, NM, November 1990.

[5-3] V. L. Bergmann, "Transient Dynamics Analysis of Plates and Shells with PRONTO 3D," SAND91-1182, Sandia National Laboratories, Albuquerque, NM, September 1991.

[5-4] J. S. Ludwigsen and D. J. Ammerman, "Analytical Determination of Package Response to Severe Impacts," Proceedings of PATRAM 95, Las Vegas, NV, December 1995.

[5-5] D. J. Ammerman, "Benchmarking of Finite Element Codes for Radioactive Material Transportation Packages," in Development, Validation, and Application of Inelastic Methods for Structural Analysis and Design, PVP-Vol. 343, ASME, New York, NY, 1996.

[5-6] D. J. Ammerman, “Effect of Closure Movement and O-ring Properties on Leak Rate,” Contract report #239004, Sandia National Laboratories, Albuquerque, NM, September 1993.

[5-7] G. W. Wellman and R. Salzbrenner, “Quasistatic Modeling and Testing of Exclusion Region Barrier Mock-Ups”, SAND92-0024, Sandia National Laboratories, Albuquerque, New Mexico, March 1992.

[5-8] American Society of Mechanical Engineers, “Specification for Alloy-Steel Bolting Materials for Special Applications,” SA-540, ASME, New York, NY, 1998.

[5-9] H. J. Rack and G. A. Knorovsky, "An Assessment of Stress-Strain Data Suitable for Finite-Element Elastic-Plastic Analysis of Shipping Containers," NUREG/CR-0481, SAND77-1872, Sandia National Laboratories, Albuquerque, NM, Sept. 1978.

[5-10] M. K. Nielsen, H. S. Morgan, and R. D. Krieg, “A Phenomenological Constitutive Model for Low Density Polyurethane Foams,” SAND86-2927, Sandia National Laboratories, Albuquerque, NM, April 1987.

[5-11] Parker Seal Group, “Parker O-Ring Handbook,” Parker Hannifin Corporation, Cleveland, OH, 1992, pp. A4-7.

[5-12] L. E. Fisher, et al., “Shipping Container Response to Severe Highway and Railway Accident Conditions,” NUREG/CR-4829, Lawrence Livermore National Laboratory, Livermore, CA, February 1987.

[5-13] A. Gonzales, “Target Effects on Package Response: An Experimental and Analytical Evaluation,” SAND86-2275, Sandia National Laboratories, Albuquerque, NM, May 1987.

[5-14] I. G. Waddoups, “Air Drop Test of Shielded Radioactive Material Containers,” SAND75-0276, Sandia National Laboratories, Albuquerque, NM, September 1975.

[5-15] L. L. Bonzon and J. T. Schaumann, “Container Damage Correlation with Impact Velocity and Target Hardness,” IAEA-SR-10/21, Transport Packaging for Radioactive Materials, IAEA, Vienna, Austria, 1976.

[5-16] S. F. Shankman, Letter to R. E. Fronczak, Association of American Railroads – Responses to AAR’s February 7, 1997 Questions, Nuclear Regulatory Commission, May 23, 1997.

[5-17] T. L. Sanders, et al., “A Method for Determining the Spent-Fuel Contribution to Transport Cask Containment Requirements,” SAND90-2406, Sandia National Laboratories, Albuquerque, NM, November 1992.

[5-18] Spent Nuclear Fuel Discharges from U.S. Reactors, Energy Information Administration, U.S. Department of Energy, SR/CNEAF/96-01, 1994.

[5-19] "World List of Nuclear Power Plants," *Nuclear News*, p. 52, March 1999.

[5-20] A. A. Bauer and L. M. Lowry, *Nuclear Technology* **41**, 359 (1978).

[5-21] G. P. Smith, et al., The Evaluation and Demonstration of Methods for Improved Nuclear Fuel Utilization, DOE.ET/34013-15, Combustion Engineering, Inc., Windsor, CT, 1994.

[5-22] A. M. Garde, et al., "Effects of Hydride Precipitate Localization and Neutron Fluence on the Ductility of Irradiated Zircoloy-4," Zirconium in the Nuclear Industry: 11th International Symp., ASTM STP 1295, American Society for Testing and Materials, 1996, p. 407.

[5-23] M. G. Balfour, et al., "Final Report, EP80-16, Hot Cell Examination of Zion Fuel Cycles 1 Through 4," WCAP-10473, Westinghouse Energy Systems, Pittsburgh PA 15230, April 1985.

This page intentionally left blank.

6. THERMAL ANALYSIS OF THE GENERIC CASKS IN A LONG DURATION FIRE

6.1 Introduction

Thermal analyses were performed on the four generic casks defined in Section 4. The analyses examined two fire environments, a 1000°C extra-regulatory fire environment and an 800°C regulatory fire environment. Both fires were assumed to be fully engulfing and optically dense. The analyses were performed with PATRAN/PThermal, a commercial heat transfer code [6-1], that includes the conduction, convection and radiation heat transfer modes. The casks were modeled as one-dimensional (1-D) axisymmetric cylinders, including a neutron shield. The heat that would be released to the cask interior by the decay of radionuclides in the spent fuel that each cask would be carrying was treated as an internal heat source.

6.2 Generic Casks Modeled

Figures 6.1 through 6.4 present schematic drawings of the four generic casks modeled in these analyses. The two generic truck casks modeled were a steel-lead-steel cask (Figure 6.1) and a steel-DU-steel cask (Figure 6.2), where DU refers to depleted uranium. The rail casks modeled were a steel-lead-steel cask (Figure 6.3) and a monolithic steel cask (Figure 6.4). These casks have dimensions similar to currently available casks, but have not been optimized for their thermal properties for any particular fuel load. Figure 6.5 presents a radial cross section at the center of these generic casks. The dimensions of these four generic casks, including the thicknesses of the four shells labeled A, B, C, and D in Figure 6.5, are given in Table 6.1. The maximum number of fuel assemblies assumed to be shipped in each cask is given in Table 6.2.

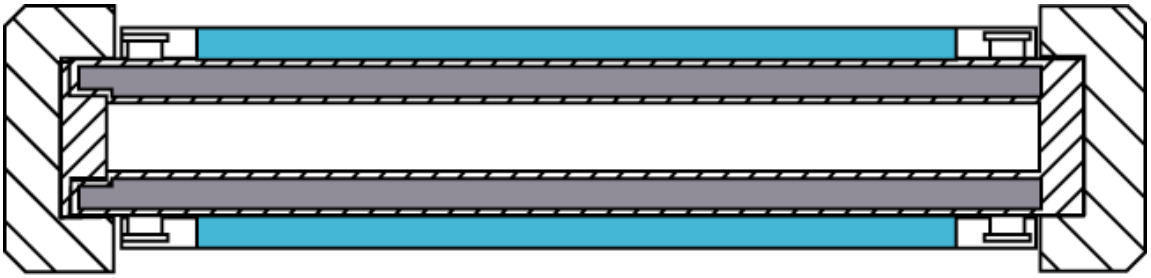

Figure 6.1 A generic, steel-lead-steel truck cask.

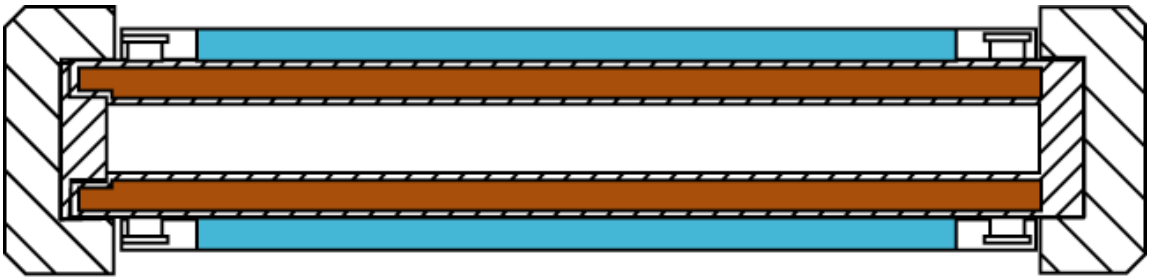

Figure 6.2 A generic, steel-DU-steel truck cask.

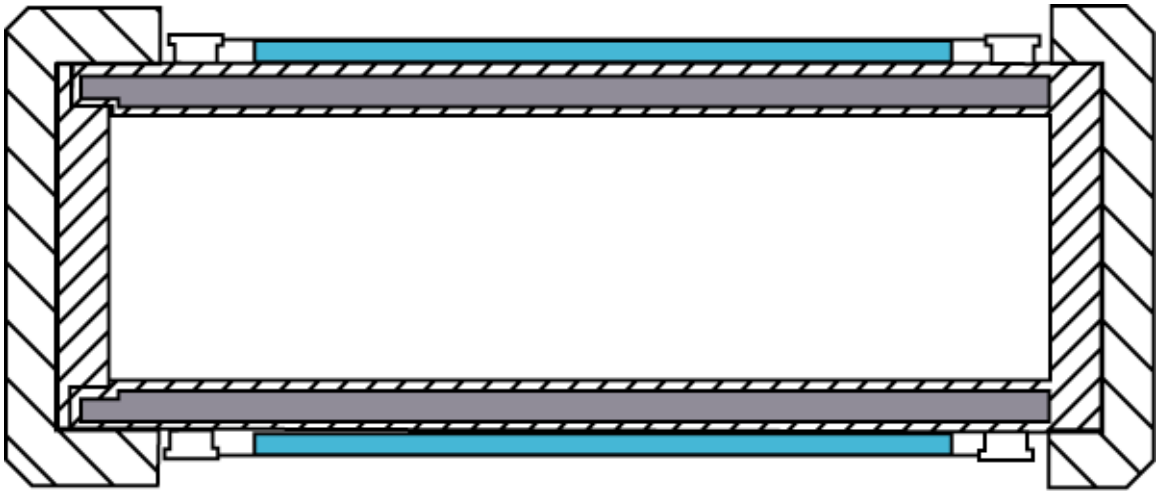

Figure 6.3 A generic, steel-lead-steel rail cask.

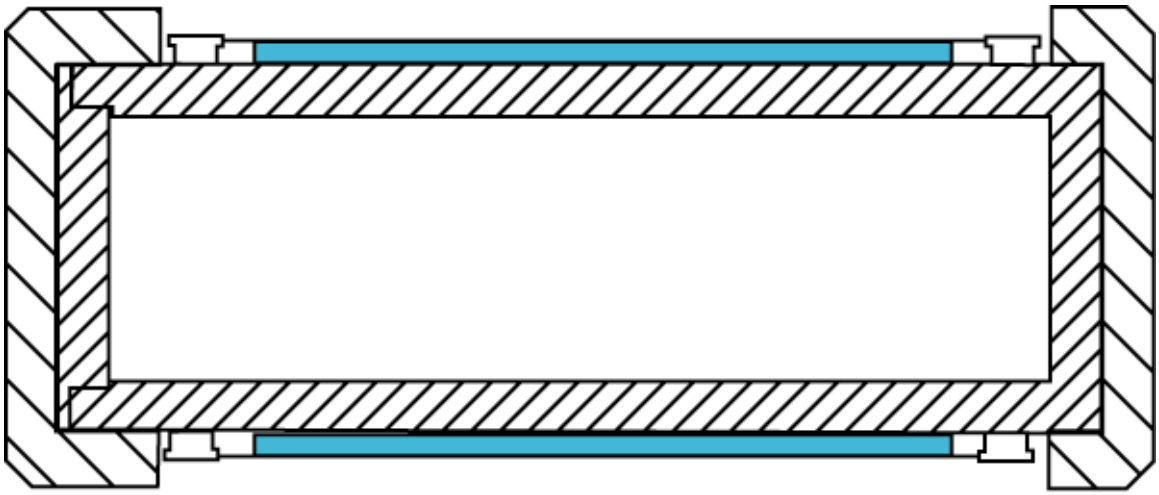

Figure 6.4 A generic, monolithic steel rail cask.

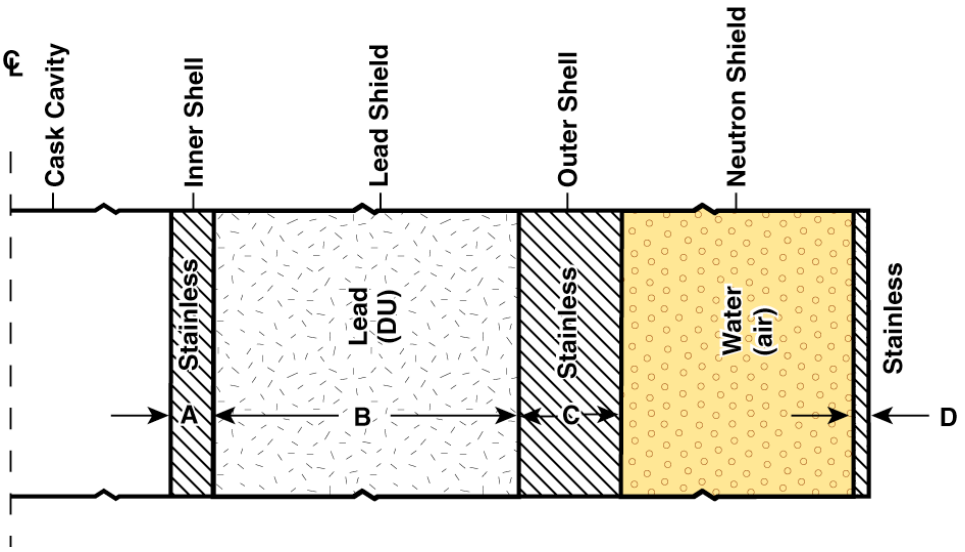

Figure 6.5 Generic wall cross section used in the 1-D axisymmetric, thermal modeling.

Table 6.1 Generic Cask Dimensions (m)

Cask	Wall Thicknesses				Neutron Shield Thickness	Outside Diameter	Cavity Diameter	Cask Length
	A	B	C	D				
Steel-Lead-Steel Truck Cask	0.0127 (0.5”)	0.1397 (5.5”)	0.0254 (1”)	0.006 (0.25”)	0.114 (4.5”)	0.94 (37”)	0.343 (13.5”)	5.207 (205”)
Steel-DU-Steel Truck Cask	0.0127 (0.5”)	0.0889 (3.5”)	0.0229 (0.9”)	0.006 (0.25”)	0.114 (4.5”)	0.953 (37.5”)	0.457 (18”)	5.08 (200”)
Steel-Lead-Steel Rail Cask	0.0254 (1”)	0.1143 (4.5”)	0.0508 (2”)	0.006 (0.25”)	0.114 (4.5”)	2.273 (89.5”)	1.651 (65”)	5.08 (200”)
Monolithic Steel Rail Cask	0.254 (10”)			0.006 (0.25”)	0.114 (4.5”)	2.4 (94.5”)	1.651 (65”)	4.826 (190”)

Table 6.2 Assumed Loading of PWR and BWR Assemblies for the Generic Casks

Cask	Truck Casks		Rail Casks	
	Steel-Lead-Steel	Steel-DU-Steel	Monolithic Steel	Steel-Lead-Steel
PWR	1	3	24	24
BWR	2	7	52	52

6.3 PATRAN/PThermal Model

The thermal effects of a long duration, external fire conditions on the casks were modeled in 1-D with an axisymmetric model (see Figure 6.5). The simulations were done in two steps. First, a steady-state simulation of the cask with its internal heat load from the fuel assemblies was done to obtain initial conditions for the analysis. A transient analysis in the presence of a long duration fire was then completed.

In the first stage, the neutron shield was assumed to be filled with water. Ambient temperature was set at 38°C. The internal heat load in each cask, generated by the decay of radionuclides in the spent fuel as calculated by ORIGEN [6-2], was set to the value presented in Table 6.3. Note that the generic casks are similar to modern casks designed for ten-year-old, moderate-burn-up fuel. This heat load was modeled as a flux onto the internal surface of each cask. Heat deposited in the inner shell of the cask by this heat flux was transferred by conduction in the solid shells of the cask, by conduction and convection in the water in the cask's neutron shield compartment, and by convection [6-3] and radiation in the air surrounding the cask. Thermal radiation was calculated with the gray-body approximation. In all cases, a cask outer surface emittance of 0.8 and a fire emittance of 0.9, consistent with 10 CFR 71 and at the high end of the normal range of surface emittances, were assumed. Thermal radiation across the neutron shield interior, when empty, was calculated using a typical stainless steel surface emittance of 0.5. Conduction and convection in the neutron shield water was modeled with a convection correlation that provided an effective value for conductivity in the water [6-4]. This model provided a steady state temperature profile in the cask characteristic of normal conditions of transport.

Table 6.3 Internal Heat Loads for Each of the Generic Casks for Three-Year-Old High Burnup Spent Fuel

Fuel Type	Assembly Heat Load	Rail Casks		Truck Casks	
		Monolithic Steel	Steel-Lead-Steel	Steel-Lead-Steel	Steel-DU-Steel
PWR	2796 W	67104 W (2289 W/m^2)	67104 W (2190 W/m^2)	2796 W (482 W/m^2)	8388 W (1100 W/m^2)
BWR	902.5 W	46930 W (1600 W/m^2)	46930 W (1532 W/m^2)	1805 W (312 W/m^2)	6318 W (828 W/m^2)

The temperature profile from the steady state calculation was used as a starting point for a transient calculation for the cask in the presence of an engulfing, optically dense, long duration fire. In the transient calculation, the water was replaced with air, the ambient temperature was increased from 38°C to 1000°C over one minute and held at 1000°C for 11 hours. Heat transfer to the outer surface of the cask from the fire was calculated with convection and radiation, through the air in the empty neutron shield compartment with conduction and radiation, and through the cask shells to the interior surface of the cask by conduction. All of the calculations used PWR decay heat loads, because these loads represent a conservative upper limit for the heat flux from spent fuel to the cask's internal surface.

6.4 Thermal Modeling Results

The PATRAN/PThermal analyses of the four generic casks determined the initial internal and external temperatures of the cask shell during normal transport conditions and the temperature response of the casks during a long duration, engulfing, optically dense fire.

6.4.1 Cask Initial Temperature Profiles

The steady state calculations determined the temperature profiles of the casks during the normal conditions of transport. The temperatures of the internal and external cask surfaces calculated for normal transport conditions are given in Table 6.4.

Table 6.4 Internal and External, Steady State, Cask Surface Temperatures

Cask	Internal	External
Steel-Lead-Steel Truck	72°C	69°C
Steel-DU-Steel Truck	113°C	104°C
Monolithic Steel Rail	215°C	193°C
Steel-Lead-Steel Rail	218°C	194°C

These temperatures are calculated for the generic casks that were not optimized for the postulated thermal loading, and therefore do not meet the surface temperature requirements of 10 CFR 71.43g. However, these temperatures do represent a conservative set of baseline cask temperatures for the purposes of this analysis.

6.4.2 Thermal Response to a Long Duration, 1000°C Fire

Figure 6.6 presents the time-dependent temperature change of the interior surface of each of the four generic casks while the cask is exposed to a long-duration, engulfing, optically dense 1000°C fire. Changes in the slopes of these temperature curves occur because of internal phase transitions in carbon steel (at 770°C) and depleted uranium (at 667°C and 775°C) and the melting of lead (at 327.5°C).

The times to reach the following three characteristic temperatures are of interest: 350°C where the rate of thermal degradation of elastomeric seals becomes significant, 750°C where spent fuel rods can fail by burst rupture, and 1000°C where the cask has come into equilibrium with the fire. The choice of the seal degradation and rod-burst temperatures is discussed in detail in Section 7. The times at which the casks reach these temperatures when heated continuously by an engulfing, optically dense, 1000°C fire are given in Table 6.5. Note that, because of thermal lags, some cask temperatures would continue to rise if the fire went out at each of these times.

The times required to reach the indicated temperatures at the inside surface of the inner shell, as shown in Figure 6.6, were used in Section 7.0 to estimate the probability of seal degradation and rod burst during cask exposure to long duration hydrocarbon fueled fires. The temperature of the inner surface of the cask body was used as an indicator of seal and rod response to heating in a fire for several reasons. First, inspection of the results of these calculations indicates that, when

heated by a fire, temperatures in the lead or depleted uranium gamma shield are similar to, though usually 10 to 20°C hotter than, the temperature of the cask's inner surface. Second, although seal location is dependent on cask design, seal well temperatures are also expected to closely track cask inner surface temperatures. Thus, because a somewhat low seal degradation temperature of 350°C was chosen, the uncertainty in the time to reach seal degradation temperature is expected to be conservative, i. e., shorter than actual. Moreover, inspection of the probability distributions for fire duration presented in Tables 7.26 and 7.27 indicate, as is discussed below, that risk estimates will not be very sensitive to this choice. Through similar arguments, fuel rod bundle temperatures are also expected to closely track the temperature of the inside surface of the cask, although for "hot" fuel, the inner-fuel-assembly temperatures could be significantly higher. However, the assumption is made that this temperature should be a reasonable surrogate for average spent fuel rod temperatures.

There are four characteristic fire duration times of interest in a risk analysis: 10 minutes—the duration of a typical automobile fire, 30 minutes—the duration of a regulatory fire, 60 minutes—the typical duration of an experimental pool fire with fuel from one tanker truck, and 400 minutes—the typical duration of an experimental pool fire with fuel from one rail tank car. Table 6.6 presents the temperatures reached by each of the generic casks at these times in a long duration 1000°C fire.

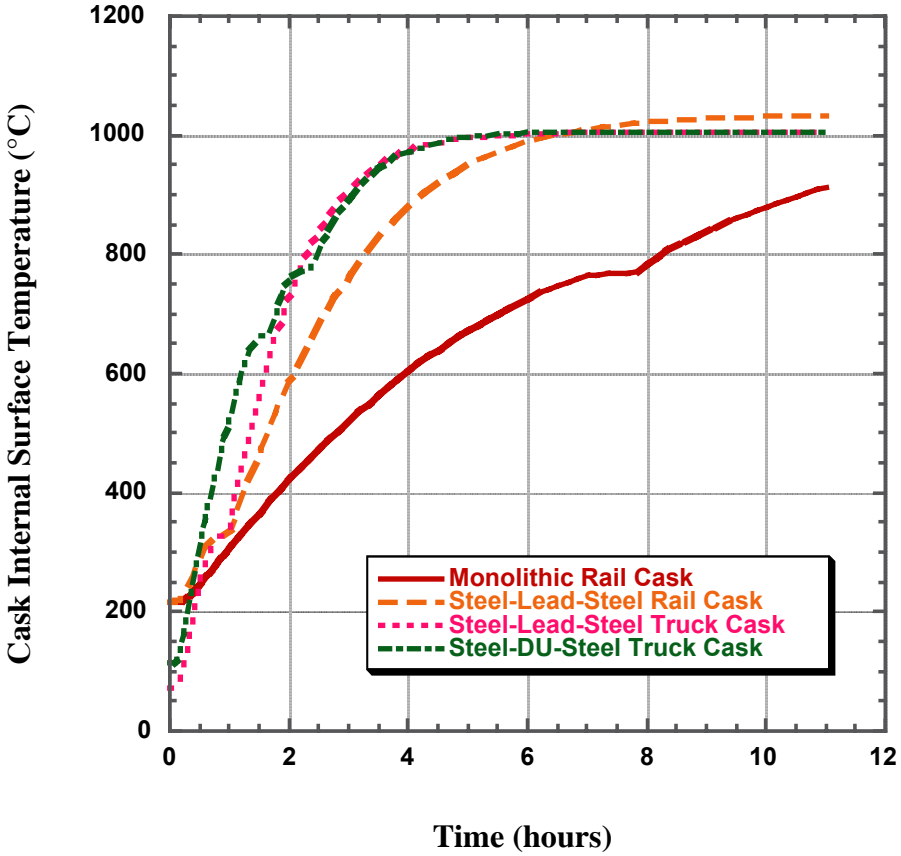

Figure 6.6 Internal surface temperature histories of the generic casks in an 1000°C long duration fire.

Table 6.5 Time (hours) Required for the Generic Cask Internal Surface to get to the Three Characteristic Temperatures in a Long Duration Engulfing, Optically Dense, 1000°C Fire.

Temperature (°C)	Truck Casks		Rail Casks	
	Steel-Lead-Steel	Steel-DU-Steel	Steel-Lead-Steel	Monolithic Steel
350	1.04	0.59	1.06	1.37
750	2.09	1.96	2.91	6.57
1000	5.55	5.32	6.43	>11

Table 6.6 Cask Internal Surface Temperatures (°C) for Four Characteristic Times in a Long Duration, Engulfing, Optically Dense, 1000°C Fire.

Time (minutes)	Truck Casks		Rail Casks	
	Steel-Lead-Steel	Steel-DU-Steel	Steel-Lead-Steel	Monolithic Steel
10	91	139	222	222
30	252	313	275	230
60	337	531	338	300
400	1000	1000	1000	750

6.4.3 Thermal Response to a Long Duration 800°C Fire

The regulatory requirements specify that thermal cask analysis be done with an 800°C fire. The response of the generic casks to an 800°C fire is given here for comparison. Table 6.7 lists the time required for the interior surface of each generic cask to climb to 350°C and 750°C in the 800°C fire and Table 6.8 presents the interior surface temperatures reached in that fire at each of the four characteristic times.

Table 6.7 Time (hours) Required for the Generic Cask Internal Surface to get to the Two Characteristic Temperatures in a Long Duration Engulfing, Optically Dense, 800°C Fire.

Temperature (°C)	Truck Casks		Rail Casks	
	Steel-Lead-Steel	Steel-DU-Steel	Steel-Lead-Steel	Monolithic Steel
350	1.77	1.06	1.69	2.37
750	4.88	5.07	6.32	>11

Table 6.8 Cask Internal Surface Temperatures for Four Characteristic Times in a Long Duration Engulfing, Optically Dense, 800°C Fire.

Time (minutes)	Truck Casks		Rail Casks	
	Steel-Lead-Steel	Steel-DU-Steel	Steel-Lead-Steel	Monolithic Steel
10	79	123	220	216
30	161	211	256	231
60	289	341	314	265
400	793	775	766	562

6.5 Sensitivity Discussion

Three-year high burn-up spent fuel was used for the thermal calculations in contrast with the ten-year average burn-up fuel that will typically be transported in the casks of the design types considered. The conservatism introduced by this assumption is large. For example, thermal loads for a three-year high-burn-up PWR fuel assemblies are on the order of 2.8 kilowatts, while the ten-year average-burn-up fuel assembly produces less than 600 watts of decay heat. With thermal calculations, the three-year high burn-up spent-fuel assumption leads to conservative risk estimates, because more rapid heating means that seal degradation and rod burst temperatures can be reached with fires of shorter duration.

While conservative, the calculations in the report do not include some secondary effects that would need to be considered if the cask designs were to be used for transport of three-year high-burn-up fuel. For example, the use of the cask inner-surface temperature to estimate rod burst-rupture temperature would not be acceptable with three-year spent fuel. This is because the overall temperature increase from the cask inner surface to highest fuel rod temperature could reach several hundred degrees Celsius for multiple three-year assemblies. For the ten-year average burn-up fuel, the temperature increase from the cask inner surface to the center of the fuel assemblies is typically less than 100°C [6-5]. Inspection of the calculations used in this section demonstrated that the use of the three-year high burn-up fuel in the risk calculations adequately compensates for the neglect of the temperature increase between the cask inner surface and the fuel rods for ten-year average burn-up fuel.

In an additional conservatism, the phase change of the neutron shield material at the outside of the cask is also neglected. The neutron shield can be water or a solid hydrogenous material. For this analysis water is assumed. The neutron shield material thermal properties are changed in the calculation instantaneously at the start of the fire from water to air. In the calculations, when the neutron shield is voided instantaneously, the inner surface of the neutron shield rapidly reaches fire temperature within one to two minutes. When the liquid remains, the increase to boiling temperature and the boiling of the water limits the temperature increase of the cask interior to 100°C for several minutes, depending on the amount of water left in the collision-damaged shield. For example, for a full shield on the SDUST cask, the boiling of water would limit the shield-inner-surface temperature to near 100°C for about 20 minutes at the start of a fire. Similar conservative results would be obtained if a solid neutron shield material were to be used.

To estimate the conservatism introduced with the three-year spent fuel assumption, an additional 1000°C long-duration fire calculation was performed for the most rapidly responding cask, the steel-DU-steel truck cask. The time to reach the seal degradation temperature of 350°C, given in Table 6.5 for three-year high burnup fuel, increased from 0.59 hours to 0.86 hours. Similarly, the time to reach the rod burst temperature of 750°C increased from 1.96 to 2.68 hours. This indicates that time-to-temperature increases on the order of 30 to 50 percent are anticipated if ten-year average burn-up fuel is used in calculations rather than three-year high burnup fuel. The effect of this change on overall risk probabilities is much smaller, however, because for the assumed fuel, times-to-failure already fall into the low-probability tail of the fire duration probability distribution curves (see Tables 7.26 and 7.27). Increasing these times simply places the probabilities further out on the tail of these distribution curves.

6.6 Summary

Thermal analysis of the generic casks provided input for risk analysis of characteristic times at which the casks may undergo elastomeric seal failure or rod burst/rupture. This analysis was conservative for the following reasons:

- The casks, although similar in dimension to casks available from manufacturers, were not optimized for their thermal response.
- The analysis assumed that the casks were uniformly engulfed in the fire.
- The fire temperature was assumed to be 1000°C.
- The water in the neutron shield was immediately replaced by air at the onset of the long duration fire to simulate fluid loss as a result of puncture of the neutron shield.

6.7 References

[6-1] PATRAN Thermal User Guide and Model Description Manual (http://www.macsch.com/support/support.html).

[6-2] A. G. Croff, "ORIGEN2: A Versatile Computer Code for Calculating the Nuclide Compositions and Characteristics of Nuclear Materials," *Nuclear Technology* **62**, p. 335 (1983).

[6-3] B. V. Karlekar, and R. M. Desmond, *Engineering Heat Transfer,* West Publishing Co., 1977.

[6-4] G. D. Raithby, and K. G. T. Hollands, "A General Method of Obtaining Approximate Solutions to Laminar and Turbulent Free Convection Problems," A*dvances in Heat Transfer,* Academic Press, NY, 1974.

[6-5] G. W. Thomas and R. W. Carlson, "Evaluation of the Use of Homogeneous Fuel Assemblies in the Thermal Analysis of Spent Fuel Storage Casks," UCRL-ID-134567, Lawrence Livermore National Laboratory, Livermore, CA, July, 1999.

Page intentionally left blank

7. SOURCE TERMS AND SOURCE TERM PROBABILITIES

7.1 Truck and Train Accident Scenarios

7.1.1 Event Trees

To estimate accident source terms, the mechanical and thermal environments that a cask might experience during truck and train accidents must be estimated. Because all of the variations of all of the accidents in the historic record plus all plausible accidents not yet observed constitutes far too many accidents to examine individually, a smaller representative set of accidents is formulated and the frequencies of occurrence of each representative accident are estimated.

Representative sets of accidents can be developed by constructing accident event trees. Event trees for truck and train accidents were developed during the course of the Modal Study [7-1]. Figures 7.1 and 7.2 present these event trees. Inspection of these figures shows that an event tree depicts an accident scenario as a sequence of events and also gives the probability of each event in the sequence. Thus, a path on the event tree constitutes a unique sequence of events and the product of all of the probabilities of the events on a path (branch point probabilities) gives the probability of that accident scenario. For example, in the truck accident event tree shown in Figure 7.1, a truck accident that leads to a collision with a pedestrian is depicted by the uppermost branches of the tree, specifically the branches labeled "Collision," "Non-fixed object," and "Cones, animals, pedestrians." Because the probabilities of these branches are 0.7412, 0.8805, and 0.0521, the chance that this accident scenario occurs (expressed as a percent), given that any truck accident has been initiated, is 3.4002 = 100 [(0.7412)(0.8805)(0.0521)], where 3.4002 is called the path (scenario) probability and gives the fraction of all truck accidents that follow this path. Because the probability of any accident occurring is not included in this product, the resulting fraction is a conditional probability, that is conditional on the occurrence of an accident of any severity and type. Further, because of the way the tree is constructed, each probability on the tree is conditional on the branch point probabilities that precede it and many branch point probabilities are represented by far more significant figures than is warranted by the underlying data because the sum of the branch point probabilities for any single branch of the tree must sum exactly to one.

Because each event tree path (accident scenario) defines a set of accident conditions (mechanical and/or thermal environments), the impact of each scenario on a radioactive material transportation cask can be estimated by hypothetically subjecting the cask to the conditions that characterize the end point of the path. The Modal Study performed such an analysis for each path on their truck and train accident trees. On these trees, paths that seemed capable of failing a Type B spent fuel cask are indicated by placing an asterisk (*) after the path number (path Accident Index). Thus, the Modal Study analyses found, for example, that collisions of a truck with a train might generate mechanical loads large enough to fail a Type B spent fuel cask thereby allowing radioactivity to be released from the cask to the environment. Accordingly, the truck accident scenario, denoted by the Accident Index 5, which has a conditional chance of occurring of 0.7701 percent (conditional on the occurrence of some truck accident), is tagged with an asterisk.

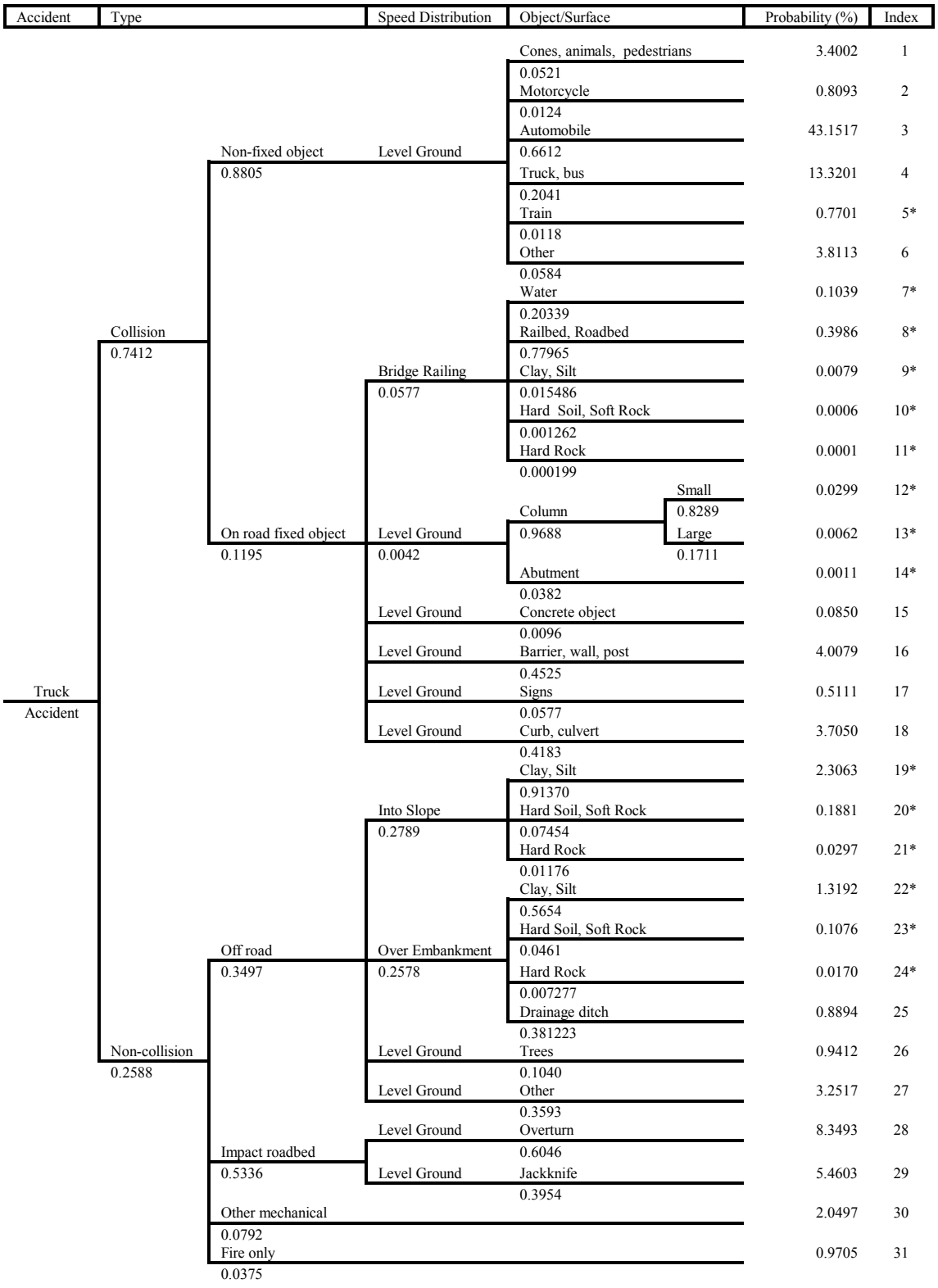

Figure 7.1 Modal Study truck accident event tree.

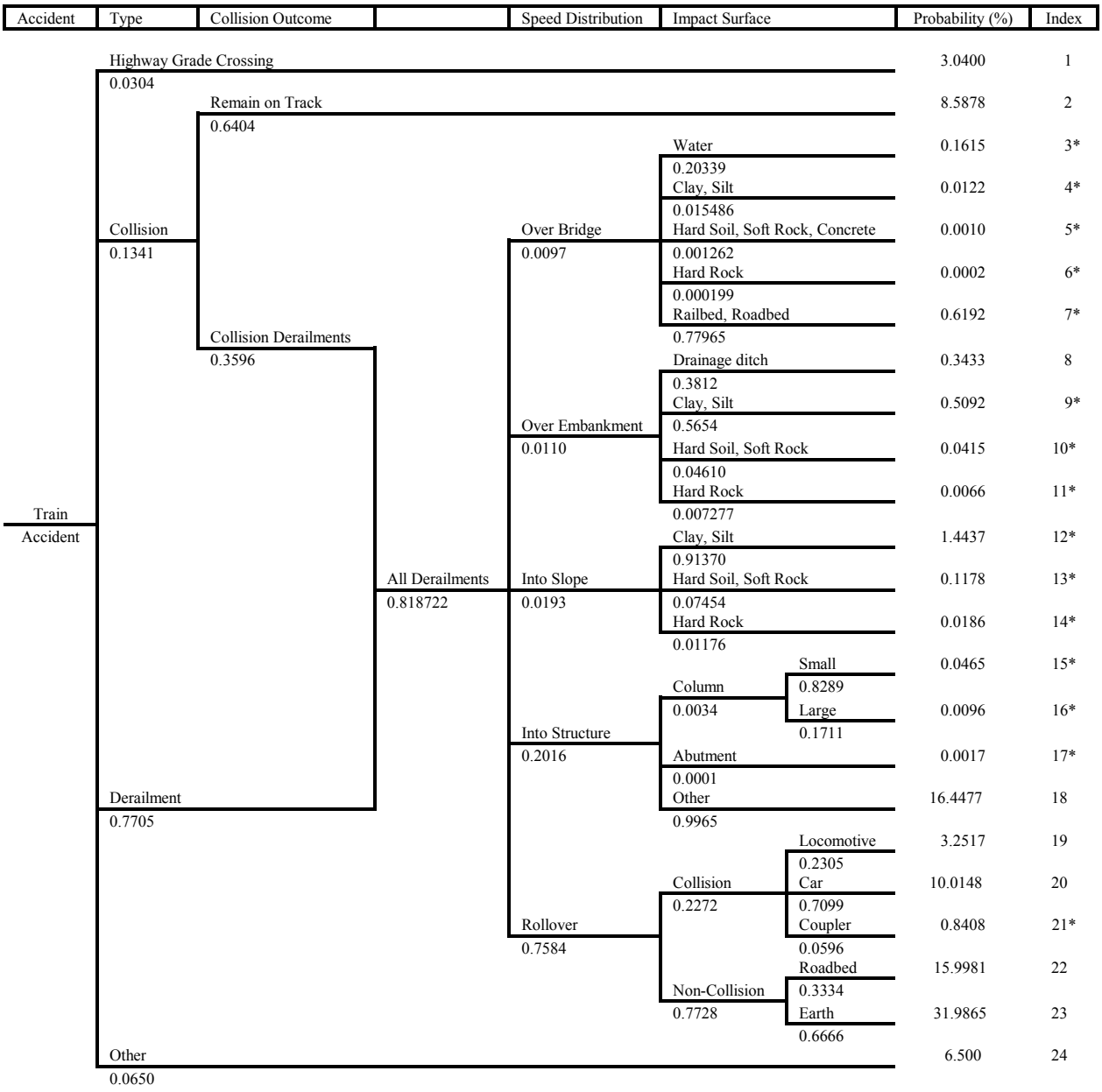

Figure 7.2 Modal Study train accident event tree.

The suitability of an event tree depends on whether it depicts a suitable representative set of accidents and on the whether the data used to estimate the event tree branch point probabilities, and thus the probability of occurrence of each accident scenario, are still current. Inspection of Figures 7.1 and 7.2 shows that early branches on these event trees define accident conditions (e.g., on the truck event tree, a collision with a non-fixed object) while later branches provide information that specifies the accident speed distribution (e.g., the branch labeled "Over Embankment" on the train event tree) and the object (e.g., column or abutment on both trees) or surface (e.g., hard rock, clay/silt on both trees) that is struck. Inspection of these trees suggests that each tree depicts a comprehensive set of credible accidents (i.e., all probable accident scenarios appear to have been included and no unusually severe but credible accident scenarios

appear to have been omitted). Accordingly, the structures of both trees seem appropriate. Therefore, the suitability of these trees for use in this study depends principally on the currency of the branch point probabilities. For each tree, this was investigated by comparing tree branch point probabilities to similar but more recent data.

7.1.2 Route Wayside Surface Characteristics

The occurrence frequencies of route wayside surfaces (clay/silt, hard soil/soft rock, hard rock), presented in the Modal Study were developed by performing visual surveys of two segments of California interstate highways (Interstate 80 from Davis, California, to the Nevada border and Interstate 5 from the San Diego County/Orange County line to the Los Angeles County/Kern County line). Each survey classified visible wayside surfaces as hard rock, untilled soil (which was equated to hard soil/soft rock), and tilled soil (which was equated to clay/silt). After comparing the results of these visual surveys to data available from agricultural soil surveys and geological highway maps, Modal Study analysts chose the following values for wayside route surface frequencies of occurrence: clay/silt, 0.9137; hard soil/soft rock, 0.07454, and hard rock, 0.01176. Moreover, although developed by survey of interstate highway wayside surfaces, because rail wayside surface data was not available, as the "Into Slope" branches on Figures 7.1 and 7.2 show, these surface occurrence frequencies were used for both the truck and the train event trees.

Because the finite element cask impact calculations described in Section 5 showed that only impact at a high speed onto an essentially unyielding surface (e.g., a large monolithic chunk of rock that doesn't fragment easily) was likely to cause the seal of a Type B spent fuel cask to leak, the frequency of occurrence of wayside hard rock becomes an unusually important branch point probability. But for high-speed impacts, shallow layers of soft soil will easily be penetrated without significant expenditure of kinetic energy. Therefore, if only high-speed impacts onto hard rock are likely to cause a spent fuel cask seal to leak, then not only is visible hard rock of concern, but so is hard rock that lies beneath but close to the soil surface.

7.1.2.1 U.S. Geologic Survey Data

The amount of hard rock (expressed as a percent of the route length) traversed by the two segments of I-80 and I-5 surveyed for the Modal Study was reestimated using data developed by the U.S. Geologic Survey (USGS) [7-2]. To do this, a digital (electronic) USGS map of the surface geology of the continental United States was analyzed using a Geographic Information System (GIS). The analysis identified the number of kilometers of each interstate segment that traverse plutonic and intrusive rock formations, the two hardest rock-types depicted on the USGS map. Table 7.1 compares the Modal Study visual estimates of the percentage of each route segment length that is hard rock to the results developed by GIS analysis of the USGS data.

The USGS data in the table suggest that substantially larger portions of the two interstate segments traverse hard rock than was found by the Modal Study visual surveys of these two route segments. However, because the USGS map does not indicate the depth of the soil layers that lie over these hard rock layers, it is not possible to decide whether a cask impacting the overlying soil would penetrate to and be damaged by impacting the underlying hard rock layer.

Table 7.1 Wayside Hard Rock on Modal Study Segments of I-5 and I-80

Route Segment	Hard Rock (%)
Interstate 5	
Modal Study Visual Survey	0.0
GIS Analysis of USGS Data	5.7
Interstate 80	
Modal Study Visual Survey	2.4
GIS Analysis of USGS Data	22.9

7.1.2.2 U.S. Agricultural Department Data

Because the USGS data could not identify overlying soil layers thick enough to absorb most of the cask impact energy before the layer was penetrated, the GIS analysis performed using the USGS data was repeated using a digitized U.S. Agricultural Department map [7-3] that showed the locations of coherent, monolithic rock formations in the continental United States that must be removed by blasting (i.e., hard rock) and rock that can be removed by a backhoe because it fragments relatively easily (i.e., soft rock), and also specified the amount of dirt that lies above each type of rock. In addition, the map showed the locations of surface soil layers of various depths (thicknesses) that contained rocks with average diameters (d_{rock}) larger than some reference diameters (e.g., $d_{rock} \geq 3$ inches, $d_{rock} \geq 10$ inches). Given the information about the character of near-surface soil and rock layers provided by the Agricultural Department map, the following definitions were adopted for hard rock, soft rock, hard soil, and soft soil.

Hard Rock: Rock that must be removed by blasting that lies on average within 24 inches of the route wayside surface (minimum distance to the rock layer ≤ 12 inches; maximum distance to the rock layer ≤ 36 inches).

Soft Rock: Rock that can be removed by a backhoe that lies on average within 24 inches of the route wayside surface (minimum distance to the rock layer ≤ 12 inches; maximum distance to the rock layer ≤ 36 inches).

Hard Soil: Soil that contains ≥ 10 percent rocks with average diameters ≥ 3 inches.

Soft Soil: Everything else.

Four observations about these definitions are in order. First, rock layers that lie more than three feet below the surface are not of concern because penetration by the cask of three feet of surface soil will consume so much of the cask's impact energy that impact onto a rock layer that lies below this soil will be unlikely to cause the cask seal to leak. Second, a layer of soil that contains rocks of a significant size (e.g., diameters ≥ 3 inches) that occupy a significant fraction (e.g., ≥ 10 percent) of the volume of the layer will significantly increase the effective hardness of the layer. Third, the preceding definitions mean that any wayside surface that isn't hard or soft rock will be hard soil if the surface soil layer contains ≥ 10 percent rocks with average diameters

≥ 3 inches; if it does not, it will be soft soil. And fourth, implicit in the definition of hard soil is the assumption that a thin layer of surface soil that contains rocks is unlikely to lie over a thick layer of rock-free soil. Thus, if the surface soil layer is thin, then the wayside surface character will be determined by the near-surface underlying rock layer, and if the surface layer is not thin, then its characteristics will be determined by the characteristics of the rocks that it contains.

The wayside surface characteristics of the two interstate highway segments surveyed for the Modal Study were reanalyzed using GIS techniques to interrogate the digitized U.S. Agricultural Department map. Table 7.2 presents the results (expressed as percentages) obtained for the two California interstate segments and compares them to the results obtained by the visual surveys conducted for the Modal Study. Inspection of Table 7.2 again suggests that the Modal Study visual survey of wayside interstate highway surfaces significantly underestimated the presence of hard rock, soft rock, and hard soil layers that lie close enough to the surface of the ground so that cask penetration to and/or impact onto these layers will determine the extent of cask damage during collision accident scenarios.

Table 7.2 Wayside Surfaces on Modal Study Segments of I-5 and I-80

Route Segment	I-80		I-5	
	Modal Study	US Ag. Data	Modal Study	US Ag. Data
Hard Rock	2.4	17.4	0.0	0.0
Hard Soil/Soft Rock	7.4		7.2	
Soft Rock		13.4		20.3
Hard (rocky) Soil		21.0		0.0
Soft Soil	90.2	48.2	92.9	79.7

7.1.2.3 New Route Wayside Surface Occurrence Frequencies

Because of the importance of impacts onto hard rock and because the visual surveys of interstate wayside surfaces conducted for the Modal Study appeared to significantly underestimate surface or near-surface hard rock layers, new wayside surface occurrence frequencies were developed for the four illustrative real truck and rail routes described in Section 8.3 (Crystal River to Hanford, Maine Yankee to Skull Valley, Maine Yankee to the Savannah River Site, and Kewaunee to the Savannah River Site) by GIS interrogation of the digitized U.S. Agricultural Department map. Table 7.3 presents the results of these GIS analyses.

Finally, in order to be somewhat conservative with respect to the wayside occurrence of hard rock and soft rock/hard soil, the average fractional frequencies of occurrence of hard rock and soft rock/hard soil presented in Table 7.3, rounded up to the next integer, were chosen for use in this study, and the frequency of occurrence of soft soil was calculated by subtraction of the sum of these two occurrence frequencies from 1.0. Table 7.4 presents the frequencies of occurrence obtained by this procedure.

Table 7.3 Wayside Surface Characteristics for Three Illustrative Shipping Routes

Route	Hard Rock	Soft Rock	Hard (Rocky) Soil
Truck			
Crystal River to Hanford	2.1%	4.0%	2.9%
Maine Yankee to Savannah River Site	5.4%	0.0%	6.9%
Kewaunee to Savannah River Site	2.7%	0.0%	0.9%
Rail			
Crystal River to Hanford	2.5%	1.9%	3.9%
Maine Yankee to Savannah River Site	2.8%	0.0%	2.5%
Kewaunee to Savannah River Site	0.3%	0.0%	1.4%

Table 7.4 Fractional Occurrence Frequencies for Route Wayside Surfaces Selected for Use in This Study

Mode	Clay/Silt	Hard Soil/Soft Rock	Hard Rock
Truck	0.91	0.05	0.04
Rail	0.91	0.06	0.03

7.1.3 Truck Accident Data

The Modal Study truck accident event tree was constructed using Bureau of Motor Carrier Safety (BMCS) accident data for the years 1973 through 1983 for all trucks (no accidents were discarded based on truck size) and all types of roads (i.e., city streets, county roads, state highways, interstate highways) [7-4]. The frequency with which various roadside structures (e.g., bridge railings, columns, abutments, barriers, and signs) are struck during collisions was developed from California Department of Transportation reports for the years 1975 through 1983. The sizes of columns and abutments next to highways, a distribution of highway bridge heights and of the surfaces below highway bridges were all developed during the Modal Study by counting these features while conducting the two surveys of segments of Interstate Highways 5 and 80.

Because the Modal Study truck event tree is based on data that is now more than 15 years old, that data was compared to more recent accident data developed by Clauss, et al. [7-5]. The data developed by Clauss, et al. was drawn from two databases, the TIFA (Trucks Involved in Fatal Accidents) file maintained by the University of Michigan Transportation Research Institute, and the GES (General Estimates System) file maintained by the National Highway Traffic Safety Administration. TIFA file entries report data for medium and heavy duty truck accidents that occurred on U.S. highways and caused fatalities. GES file entries report data extracted from

police reports for fatal and non-fatal accidents. Clauss, et al. used TIFA file data for the years 1980 through 1990, and GES file data for the years 1988 through 1990.

Table 7.5 compares the conditional probabilities of occurrence of Modal Study truck accident scenarios to estimates of the probabilities of occurrence of the same type of accident drawn from the study of Clauss, et al. Inspection of Table 7.5 shows that Modal Study conditional accident probabilities are similar to TIFA and GES accident probabilities, usually differing from the TIFA or GES result by about a factor of two. As the Modal Study examined all truck accidents (both fatal and non-fatal) without any restriction on truck size, while the TIFA and GES data excludes small truck accidents, the fact that the probabilities agree to about a factor of two suggests that truck accidents that occurred during the 1980s are not substantially different in character from those that occurred during the late 1970s and early 1980s. Thus, the Modal Study conditional probabilities would seem to still be representative of current truck accidents. Accordingly, it was concluded that the structure of the tree (set of scenarios embedded in the tree) reasonably depicted the variety of possible truck accidents and did not omit important accident branches.

Table 7.5 Conditional Probabilities of Occurrence of Various Truck Accident Scenarios (%)

Scenario/Accident	Modal Study	TIFA (fatal)	GES (all)	GES (fatal)
Collision Scenarios				
Truck + Bus Truck + Tanker	13.32	6.13	6.65	7.90
Car	43.15	68.83	66.05	74.88
Train	0.77	0.57	0.18	0.42
Water Immersion	0.10	0.20		
Hard Object[a]	0.81	2.04	1.94	0.51
Soft Object[b]	4.93	2.59	7.46	0.43
Non-Fixed Object	7.21	9.67	6.57	4.94
Non-Collision Scenarios				
Overturn Rollover	8.35	8.17	4.48	10.03
Fire	0.97	1.80	0.46	0.39

a. For Modal Study, sum of Hard Soil, Soft Rock, Hard Rock, and Columns and Abutments.
b. For Modal Study, sum of Clay, Silt, Railbed, Roadbed, and Drainage Ditch.

Both the Modal Study and the study of Clauss, et al. developed estimates of the probability that a truck collision would initiate a fire. The Modal Study developed estimates of the fractions (expressed as percentages) of various types of truck collisions (e.g., collision with a car) that initiated fires. The study of Clauss, et al. developed estimates of the fractions (expressed as percentages) of all truck accidents that were collisions with trucks, cars, tankers, or other objects that also caused both fires and a fatality. Clauss, et al. also found that 1.7 percent of all fatal truck collisions led to fires. Therefore, multiplication of the results of Clauss, et al. for fatal

collisions with cars, or trucks and tankers, or other objects that initiate fires and cause a fatality by 1.7 percent (e.g., for truck collisions with cars, 37.5 × 0.017 = 0.6) yields a result directly comparable with the results given in the Modal Study. Table 7.6 presents and compares these estimates. Inspection of Table 7.6 shows that the Modal Study results and those of Clauss, et al. differ by factors of two, which suggests that the Modal Study results are most likely still representative.

Table 7.6 Truck Accidents that Initiate Fires (Percentages)

	Clauss, et al.		Modal Study
	Fraction All Fatal Collisions that Initiate Fires that Impact Listed Object (%)	Fraction Accidents of this Type that Initiate Fires (%)	Fraction Accidents of this Type that Initiate Fires (%)
Collision with			
Car	37.5	0.6	0.3
Truck, Tankers	24.0	0.4	0.8
Truck	22.1	0.37	
Tanker	1.9	0.03	
Other Objects	38.6	0.7	1.3
Non-Collisions			
Ran off road			1.1
Overturns			1.2
Other			13.0

Finally, weighted summation of the Modal Study results in Table 7.6 using the probabilities of occurrence of each accident type as given in Figure 7.1 shows that, in agreement with Clauss, et al., 1.8 percent of all of the truck accidents examined by the Modal Study initiate fires, where

$$1.8 = 0.432(0.3) + 0.132(0.8) + 0.177(1.3) + 0.091(1.1) + 0.083(1.2) + 0.085(13.0)$$

Accordingly, as Figure 7.3 shows, the Modal Study truck accident event tree was used in this study with only one modification, replacement of the Modal Study wayside route surface frequencies of occurrence, that were developed by visual surveys of interstate highway segments, by the frequencies developed by GIS analysis of three representative real spent fuel highway transportation routes using U.S. Agricultural Department data.

7.1.4 Train Accident Data

The Modal Study train accidents event tree was constructed using data published in Federal Railroad Administration Accident/Incident Bulletins for the years 1975 through 1982 [7-6]. Because no rail line wayside surface data were available and because rail and highway routes were believed to traverse similar terrain [7-7], the Modal Study used the results of the survey of California Interstates 5 and 80 to specify the branch point probabilities for the train derailment accident branches labeled “Over Bridge,” “Over Embankment,” and “Into Slope,” and also for the occurrence frequencies of the impact surfaces “Water,” “Clay, Silt,” “Hard Soil, Soft Rock, Concrete,” “Hard Rock,” “Railbed, Roadbed,” and “Drainage Ditch.” In addition, although train accident experts stated [7-8] that most train derailments leave the derailed cars upright or tipped

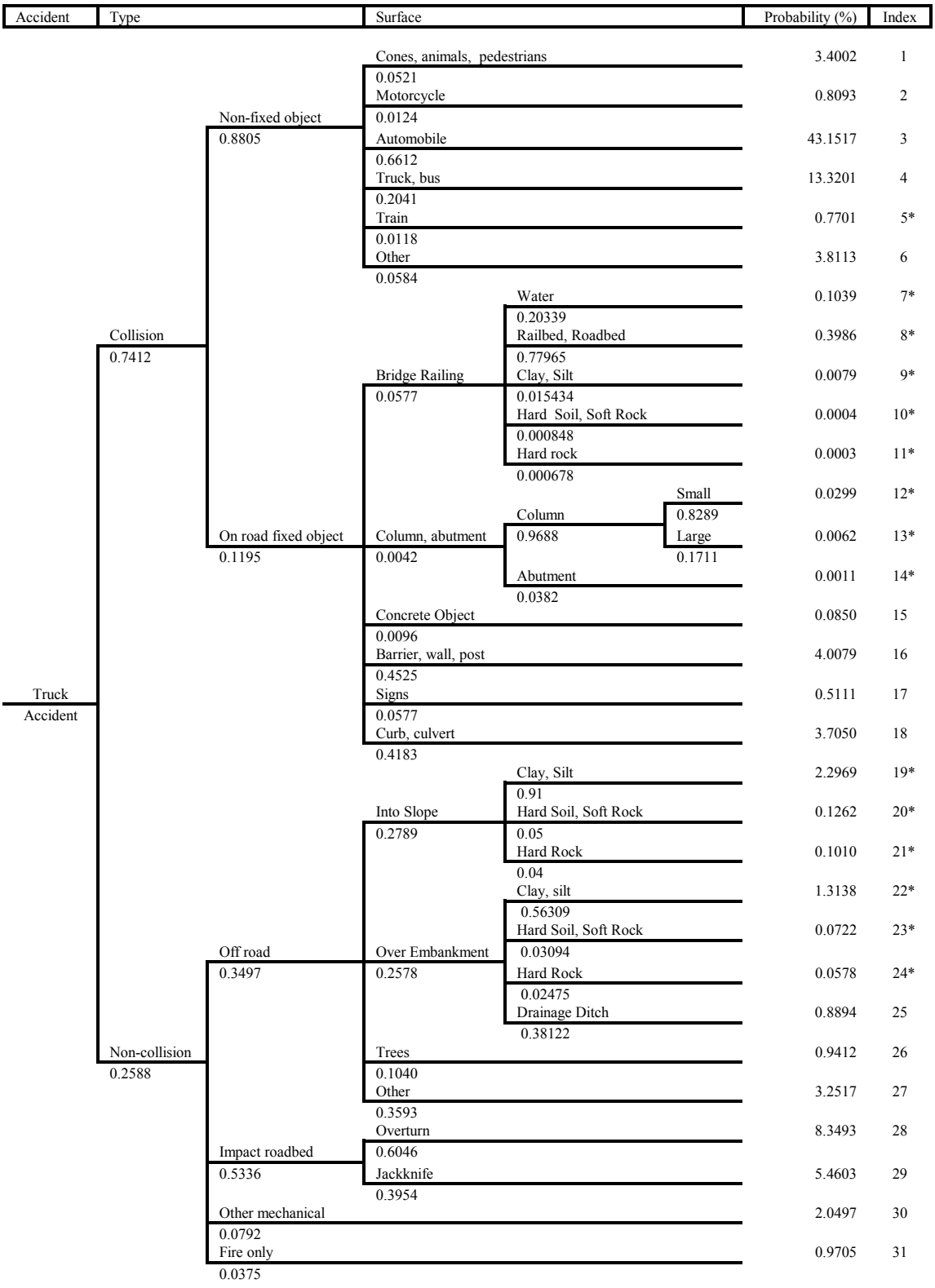

Figure 7.3 Modified Modal Study truck accident event tree.

over but only slightly damaged, the Modal Study train accident event tree does not divide derailment accidents into minor derailments (those where the derailed cars remain upright or simply tip over) and major derailments (those where at least some of the derailed cars are severely damaged). Lastly, the Modal Study train accident event tree does not contain a branch for fire-only accidents (i.e., fires not initiated by collisions or derailments).

Rail accident data for the years 1988 through 1995 were reviewed for this study by Department of Transportation (DOT) Volpe Center staff. Table 7.7 compares the conditional occurrence probabilities developed by the Modal Study for train accidents to those developed by the DOT Volpe Center. Inspection of Table 7.7 shows that train accident scenario probabilities constructed from recent data generally differ from the probabilities constructed during the Modal Study by factors of two or less. Inspection of the Modal Study train accident event tree suggests that the following three derailment paths probably lead only to minor damage: (1) derailments that lead to impacts into structures other than columns or abutments, (2) rollover derailments that do not lead to additional collisions, and (3) rollover derailments where the cars that roll over bump into other cars or locomotives and that the fraction of all derailments that these paths account for is 0.9490, where

$$0.9490 = (0.2016)(0.9965) + (0.7584)(0.2272)(0.2305+0.7095) + (0.7584)(0.7728)$$

Now, because (1) this fraction agrees well with the Volpe Center estimate of 0.9782 for the frequency of occurrence of minor derailments, (2) the paths that contribute to this fraction were all judged in the Modal Study to generate minor accidents, and (3) Table 7.7 shows that recent train accident data are consistent with the data developed by the Modal Study, as Figure 7.4 shows, the Modal Study train accident tree is used with only two modifications. First, the Modal Study wayside route surface frequencies of occurrence, that were developed by visual surveys of Interstate Highway segments, were replaced by the frequencies developed by GIS analysis of

Table 7.7 Conditional Probabilities of Occurrence of Various Train Accident Scenarios (%)

Scenario/Accident	Modal Study	DOT Volpe Center
Grade Crossing	0.0304	0.1298
Collision	0.1341	0.0875
Remain on Track	0.6404	0.4429
Collision Derailment	0.3596	0.5162
Derailment	0.7705	0.6511
Minor Damage		0.9782
Severe Damage		0.0218
Other	0.0650	0.1315
Fire/Explosion		0.0147
Obstruction/Other		0.1168

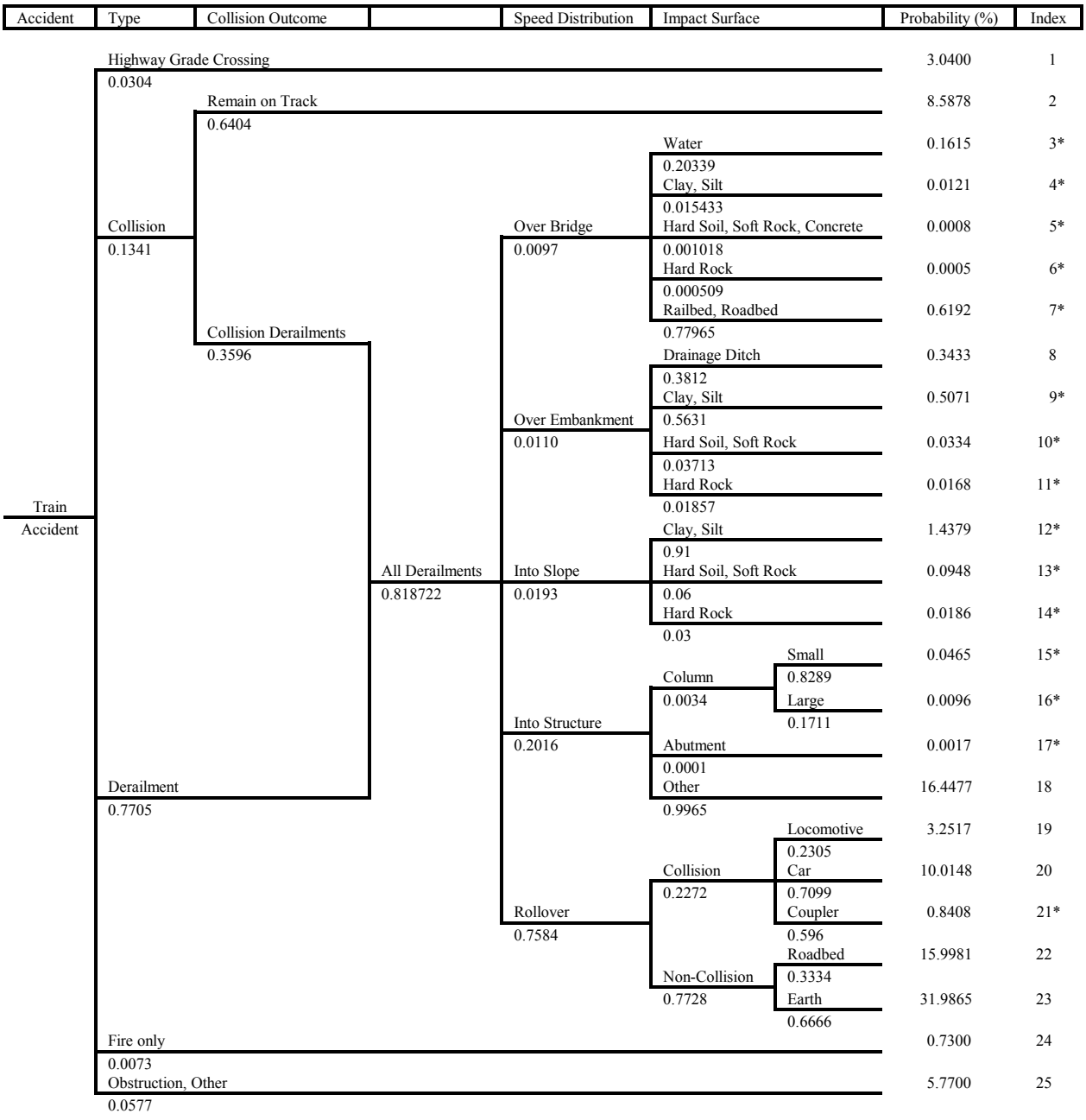

Figure 7.4 Modified Modal Study train accident event tree.

three representative real spent fuel rail transportation routes using U.S. Agricultural Department data; and second, consistent with Volpe Center results, the first-level branch on the Modal Study train event designated "Other" that has an occurrence probability of 0.0650, is split into a "Fire only" branch and an "Obstruction, Other" branch that have respectively the following occurrence probabilities:

Fire only	0.0073 = (0.0650)(0.0147/0.1315)
Obstruction, Other	0.0577 = (0.0650)(0.1168/0.1315)

7.2 Source Term and Source Term Probability Expressions

Type B spent fuel transportation casks are massive, extremely strong structures deliberately designed to withstand large mechanical and/or thermal loads without losing containment integrity. Nevertheless, although unlikely, it is possible that a truck or a train that is carrying a Type B spent fuel cask could be involved in an accident so severe that both the cask and at least some of the spent fuel rods in the cask may fail. Were this to happen, radioactive species would be released from the spent fuel into the cask interior and some of these species could be transported from the cask interior through the cask leak to the environment.

To estimate the risks associated with accidents that might occur during the transport of spent fuel by truck or train, estimates of the magnitude of the radioactive releases that might be caused by severe transportation accidents and of the probability of occurrence of these releases must be developed for three broad classes of transportation accidents: fires without collisions, collisions without fires, and collisions that lead to fires.

7.2.1 RADTRAN Risk Equations

By definition, risk is the product of the magnitude (M) of an undesirable accident consequence and its probability of occurrence (P). Thus, risk = P· M where M is calculated using a transportation consequence code, for example RADTRAN [7-9, 7-10], and is a strong function of the accident source term, the prevailing meteorology at the time of the hypothesized accident, the population that might be exposed to radiation as a result of the accident, and the effectiveness of any actions taken to avoid radiation exposures, for example, evacuation and/or relocation of population, and decontamination, temporary interdiction, and/or condemnation of contaminated property. The meteorological, population, and emergency response input required by the RADTRAN code are discussed in Sections 3.4.3.3, 3.4.1.4, and 3.4.3.2. This section derives expressions for accident source terms and for their probabilities of occurrence. Values for the parameters in these expressions are developed in subsequent sections.

7.2.2 Accident Source Terms

Accident source terms (ST_{jk}) depend on the accident scenario (j) and on the cask (k) involved in the accident. Here they are calculated as the product of the inventory of each radionuclide (i) in the spent fuel being carried in the transportation cask and two release fractions, the fraction of that inventory that is released from each failed rod to the cask interior, and the fraction of the inventory that is released to the cask interior that is transported through the cask leak to the environment. Thus,

$$ST_{jk} = \sum_i ST_{ijk} = \sum_i I_{ik} f_{release,ijk} = f_{rod,jk} \sum_i I_{ik} f_{RCijk} f_{CEijk}$$

where ST_{ijk} is the amount of radionuclide i released from cask k during accident scenario j, I_{ik} is the number of curies of nuclide i in the inventory of cask k, $f_{release,ijk}$ is the fraction of the inventory of radionuclide i in cask k that is released to the environment during accident scenario j, $f_{rod,jk}$ is the fraction of the rods in cask k that fail during accident scenario j, f_{RCijk} is the fraction

of nuclide i that is released during scenario j to the interior of cask k from each failed rod, and f_{CEijk} is the fraction of the amount of each radionuclide released to the cask interior that is transported to the environment through the cask leak.

7.2.3 Cask Inventories

Spent fuel assemblies contain radionuclides that were produced by fissioning of uranium and by activation of assembly hardware and of materials in deposits on assembly surfaces. For this study, the ORIGEN code [7-11, 7-12] was used to calculate inventories for a generic pressurized water reactor (PWR) assembly that contained 289 fuel rods and for a generic boiling water reactor (BWR) assembly that contained 64 rods. As is described below, after dropping radionuclides that do not contribute significantly to radiation doses and adding important radionuclides formed by activation of deposits on assembly surfaces (e.g., Co-60), cask inventories were calculated by multiplying the modified single assembly inventories by the number of assemblies transported in each of the four generic casks defined in Tables 4.1 through 4.4.

7.2.3.1 Fuel Burnup

Because inventory size depends on fuel burnup, which is an ORIGEN input, and the length of the fuel cooling time after fuel discharge from the reactor, which is an ORIGEN output, initially a DOE report [7-13] was consulted to identify average and maximum BWR and PWR fuel burnups, and then, for each burnup, an ORIGEN calculation was performed that depicted the variation of inventory size with fuel cooling time. The DOE report contains data on spent fuel that has been discharged from commercial power reactors located in the United States. Table 7 in that report presents a tabulation by fuel burnup ranges of the number of metric tons of uranium in BWR and PWR spent fuel discharged during the years 1968 through 1994. This table showed that the maximum burnups reported were about 45 to 50 GWDt/MTU (gigawatt-days thermal per metric ton of uranium) for BWR spent fuel and about 55 to 60 GWDt/MTU for PWR spent fuel; and that the most probable burnups were approximately 30 GWDt/MTU for BWR spent fuel and 35 GWDt/MTU for PWR spent fuel. In addition, extrapolation to 1998 of data in Table 5 in that report showed that ten years was the quantity-weighted (weight in MTU) average age of all of the tabulated spent fuel.

7.2.3.2 ORIGEN Calculations

ORIGEN calculations were performed for the most probable and the maximum PWR and BWR fuel burnup levels, where these levels are 30 and 50 GWDt/MTU for BWR spent fuel and 35 and 60 GWDt/MTU for PWR spent fuel. Full descriptions of these calculations are presented in Appendix C. Table 7.8 summarizes the results of these calculations. Table 7.8 shows that—for both BWR and PWR spent fuel and for any fuel cooling time—the total number of curies in high (maximum) burnup spent fuel is less than a factor of two greater than the number in spent fuel having the most probable burnup. The table also shows that, due to decay, the number of curies decreases rapidly during the first three years after discharge and rather slowly after five years of cooling, and also that the number of curies at three years after discharge is approximately a factor of two greater than the number of curies at ten years, which is the quantity-weighted average age

of the fuel. Nevertheless, even though most of the spent fuel that will eventually be shipped is likely to be average burnup fuel that has cooled for about ten years, in order to be conservative, the ORIGEN results for maximum burnup fuel after three years of cooling were chosen for use in this study. This choice means that the total curie content of the inventories used in the RADTRAN risk calculations described in Section 8 are most likely conservative by about a factor of four.

Table 7.8 Summary of ORIGEN Calculations, Total Curies per Assembly for All Radionuclides

Burnup (GWDt/MTU)	Fuel Cooling Time (years)						
	At Discharge	0.5	1.0	3.0	5.0	10.0	30.0
BWR							
Most probable, 30	2.87E+07	5.66E+05	3.38E+05	1.40E+05	9.38E+04	6.60E+04	3.55E+04
Maximum, 50	2.99E+07	7.04E+05	4.52E+05	2.06E+05	1.44E+05	1.03E+05	5.61E+04
PWR							
Most probable, 35	1.30E+08	2.29E+06	1.28E+06	4.60E+05	2.85E+05	1.93E+05	1.04E+05
Maximum, 60	1.07E+08	2.34E+06	1.47E+06	6.34E+05	4.32E+05	3.05E+05	1.68E+05

7.2.3.3 Elimination of Unimportant Radionuclides

An ORIGEN inventory contains approximately 800 radionuclides. This large set of radionuclides was reduced to a much smaller set that contained only radionuclides that together accounted for 99.9 percent of the health hazard posed by the total inventory using radionuclide A_2 values [7-14, 7-15] as a measure of radiation health hazard. The RADSEL code [7-16] was used to perform this reduction. For each radionuclide in the total inventory, RADSEL computes the ratio of the nuclide's number of curies and its A_2 value, sums and normalizes these ratios, sorts the ratios according to magnitude, and then retains the smallest set of radionuclides whose ratios sum to 0.999.

7.2.3.4 Radioactive Gases

Although tritium gas and tritiated water are very active biologically, the quantities per assembly calculated by ORIGEN for three-year cooled PWR (482 Ci) and BWR (168 Ci) fuel are so small compared to the A_2 value for tritium (1080 Ci) that they contribute less than 0.1% to the health hazard of the total inventory. Therefore, tritium was not included in the reduced, maximum burnup, three-year cooled, BWR or the PWR inventories. However, although the relative contribution to total health hazard of Kr-85 is also less than 0.1% for the three-year cooled fuel, because Kr is the most important member of the non-condensible gas chemical element group, it was retained in the reduced BWR and PWR assembly inventories despite its minor contribution to health hazard. Accordingly, the following quantities per assembly of Kr-85 were added back into the reduced BWR and PWR inventories generated by RADSEL: 5.87E3 Ci to the PWR assembly inventory, and 1.74E3 Ci to the BWR assembly inventory.

7.2.3.5 CRUD

During reactor operation, corrosion products formed in the reactor's primary cooling system deposit on fuel assembly surfaces where elements in these deposits are activated by neutron bombardment. The resulting radioactive deposits are called CRUD [7-17]. Due to vibratory loads during incident free transportation, impact loads during collision accidents, and thermal loads during accidents that lead to fires, portions of these radioactive deposits may spall from the rods. Then, if some of these spalled materials become airborne during an accident, their release to the atmosphere could contribute to the radiation exposures caused by the accident. Although CRUD contains a number of radionuclides, only Co-60 would contribute significantly to these radiation exposures. Since the CRUD deposits on typical PWR and BWR spent fuel rods contain respectively 0.2 and 1.0 Ci of Co-60 per rod [7-17] and the generic PWR and BWR assemblies for which ORIGEN inventories were calculated contain respectively 289 and 64 spent fuel rods, the amounts of Co-60 produced by activation of deposits on assembly surfaces is 57.8 Ci for the generic PWR assembly and 64 Ci for the generic BWR assembly.

7.2.3.6 Inventories for Generic PWR and BWR Assemblies

The final generic PWR and BWR assembly inventories were now constructed by adding the amounts per assembly of Kr-85 and of the Co-60 in CRUD to the reduced generic assembly inventories that were generated by eliminating all radionuclides shown by the RADSEL calculation to contribute negligibly to radiation exposures from the full assembly inventories calculated by ORIGEN. Table 7.9 presents these reduced modified generic assembly inventories.

7.2.4 Chemical Element Classes

To simplify the development of accident source terms, fission products are assigned to chemical element classes that have similar physical and chemical properties and therefore are expected to have similar transport characteristics. Each group is called a chemical element class and for convenience each is denoted by one of the elements assigned to the class. After assignment to classes, rod-to-cask and cask-to-environment release fractions are developed for each chemical element class.

Fission products are usually assigned to one of three general chemical element classes: non-condensible gases, condensible gases, and particulates. Each class may be further subdivided if the transport properties of its member elements differ widely. For example, because the volatile forms of cesium and iodine, Cs, CsOH, CsI, I_2, have very different volatilities and chemical properties, Cs and I are usually assigned to different classes of condensible gasses. In addition, elements with unique chemistries are placed in special chemical element classes. For transportation accident analysis, Co and Ru are usually placed in special classes. Co is placed in a special element class because it is the major constituent of the radioactive deposits called CRUD that form on the outside of spent fuel rods during reactor operation. Ru is placed in a special element class because, if exposed to oxygen while at elevated temperatures, involatile RuO_2 can be converted to RuO_3 and RuO_4, which are much more easily vaporized, thereby greatly increasing the rate of release of Ru from fuel pellets.

Table 7.9 Generic High Burnup, Three-Year Cooled, Fuel Assembly Inventories for RADTRAN Calculations (Ci/assembly)

Generic BWR Assembly	
Nuclide	**Amount (Ci)**
Co-60	6.40e+01
Kr-85	1.74e+03
Sr-90	1.59e+04
Y-90	1.59e+04
Ru-106	1.42e+04
Cs-134	2.15e+04
Cs-137	2.59e+04
Ce-144	1.03e+04
Pm-147	8.49e+03
Pu-238	1.67e+03
Pu-239	7.44e+01
Pu-240	1.36e+02
Pu-241	2.91e+04
Am-241	2.05e+02
Am-242M	8.09e+00
Am-243	1.22e+01
Cm-242	1.82e+02
Cm-243	1.42e+01
Cm-244	2.95e+03

Generic PWR Assembly	
Nuclide	**Amount (Ci)**
Co-60	5.78e+01
Kr-85	1.74e+03
Sr-90	5.36e+04
Y-90	5.36e+04
Ru-106	4.43e+04
Cs-134	6.99e+04
Cs-137	7.90e+04
Ce-144	3.87e+04
Pm-147	2.58e+04
Eu-154	8.42e+03
Pu-238	4.81e+03
Pu-239	2.14e+02
Pu-240	4.28e+02
Pu-241	6.52e+04
Am-241	4.36e+02
Am-242M	1.33e+01
Am-243	2.51e+01
Cm-242	3.76e+02
Cm-243	2.88e+01
Cm-244	5.62e+03

For this study, fission products are assigned to five chemical element classes. The five classes and the representative element that denotes each class are:

Representative Element	Description
Xe	Noble (non-condensible) gases
Cs	Condensible gases
Ru	Single element group
Co	Fission products found in CRUD
Part	All other fission products

Condensible gases are not subdivided into a cesium (Cs) and an iodine (I) class because, by the time spent fuel is removed from a reactor's spent fuel pool and released for transport to an interim or a permanent repository, almost all iodine nuclides except I-129 will have decayed away and the remaining I-129 will have reacted with Cs to form CsI. Thus, an iodine chemical element class is not needed. Finally, the class denoted by Part represents all fission products that exist in chemical forms (usually refractory hydroxides and oxides, e.g., Sr which transports as $Sr(OH)_2$, Pu which transports as PuO_2) that transport only as particles.

7.2.5 Release Fractions

This section develops expressions for accident release fractions. Expressions are developed for four broad classes of accidents: collision accidents that do not initiate fires (Collision only), collision accidents that initiate fires and generate mechanical or thermal loads that cause the cask seal to leak (Collision + Fire, 1 leakage path), collision accidents that initiate fires and generate mechanical or thermal loads that cause the cask seal to leak and also lead to failure of the cask shell by puncture or shear (Collision + Fire, 2 leakage paths), and fire accidents that do not involve collisions (Fire only). The first three of these four accident categories correspond to accident categories 4, 5, and 6 in the six-category accident severity scheme that is frequently used when performing RADTRAN calculations [7-18]. The last accident category, fires not initiated by collisions, leads to accidents that have severities that are similar to those of Category 5 accidents, but release fraction expressions that are different than those used to calculate release for accidents initiated by collisions that lead to fires. Because their release fraction expressions are unique, they are here not lumped into Category 5, but are placed in a separate fire-only category. Collisions that lead both to double cask failures and to fires are separated from collisions that lead to fires, but only a single cask failure, because differential thermal heating of a cask with a double failure may cause combustion gases, including some air, to flow through the cask. Flow of gas through the cask could sweep most fission products released to the cask interior out of the cask to the environment, thereby minimizing fission product retention in the cask. Flow of air into the cask could also lead to the oxidation of UO_2 to UO_3 and of RuO_2 to RuO_3 and RuO_4 [7-19]. Because Cs diffuses though UO_3 more easily than through UO_2, oxidation of fuel enhances Cs release rates. Because RuO_3 and RuO_4 are much more volatile than RuO_2, conversion of RuO_2 to RuO_3 and RuO_4 substantially increases release of Ru.

7.2.5.1 Mechanical Failure of Cask Seals and Spent Fuel Rods.

The response of four generic Type B spent fuel casks—two truck casks and two rail casks—and of the spent fuel rods carried in the casks, to high-speed impacts onto yielding real-world surfaces (clay/silt, hard soil/soft rock, hard rock, water, railbed/roadbed) and objects (small columns, large columns, abutments) is discussed in Section 5. Puncture and shear failures of rail tank cars during collision accidents were also analyzed in that section.

The analysis of puncture and failures presented in Section 5.3 suggests that formation of a puncture or shear probe during a collision accident depends only weakly on accident speed. Therefore, probe formation is possible during any collision accident. But a probe, if formed (or already present at the accident site), can puncture a cask only if the probe (a) is sharp enough and so oriented upon impact with the cask that it initiates a puncture or tear in the cask shell (does not glance off of the cask surface) and (b) has a stem that is sufficiently robust so that it does not break before the cask shell is completely penetrated by the probe. Since these two conditions are both improbable, the analysis concluded that failure of a cask by puncture or shear was possible during any collision accident but also was most unlikely.

The finite element calculations described in Section 5 and their extrapolation to real-world yielding surfaces strongly suggest that only extremely high-speed impacts onto slightly yielding surfaces (e.g., hard rock) are likely to cause the seals of Type B steel-lead-steel and steel-DU-

steel spent fuel truck casks to leak. Specifically, the calculations show so little distortion of the cask closures of the generic steel-lead-steel and steel-DU-steel spent fuel truck casks following 120 mph impacts onto an unyielding surface that seal leakage cannot be predicted with certainty even for impacts this severe. Nevertheless, even though not large enough to predict that seal leakage is certain to occur, because distortion of the cask closure is clearly discernable, 120 mph impacts onto an unyielding surface are assumed to cause the seal of truck casks to leak and that leak path is arbitrarily assumed to have a cross-sectional area of 1 mm^2. Thus, if v_{seal} is the speed that produces a seal leak, then by definition v_{seal} = 120 mph for impacts of truck casks onto an unyielding surface at any orientation and $v_{seal} = v_{120}$ for impacts of truck casks at any orientation onto real world yielding surfaces, where v_{120} is the impact speed for the specified impact orientation onto the real yielding surface that causes the same damage to the truck cask and its contents as is caused by a 120 mph impact at the same impact orientation onto an unyielding surface.

For rail casks, the finite element calculations indicate that seal leakage occurs for impacts onto an unyielding surface at some impact orientations at speeds as low as 60 mph. Specifically, for both the steel-lead-steel and the monolithic steel generic rail casks, closure region distortions are sufficiently large for 60 mph impacts onto an unyielding surface in the center of gravity over corner impact orientation to allow seal leakage to be predicted (i.e., the predicted separation of the lid well from the cask lid is larger than the compliance of the O-ring seal, which means that sealing function should be lost). Closure region distortion also appears to be large enough to predict seal leakage for side impacts of the monolithic steel generic rail cask onto an unyielding surface at 60 mph.

The finite element calculations also show that, for some yielding surfaces, many impact accidents, that do not cause the cask seal to leak, will cause slumping of cask contents or inward collapse of the cask shell that is sufficiently severe so that fuel rods would be expected to fail either by buckling or tearing and also that the impact speed that produces failure of some fraction of the rods in the cask will be different for end, corner, and side impacts. Thus, the impact speeds that cause rod to fail or seals to leak depend on both the nature of the impact surface and the cask orientation at the time of impact.

Although failure of some fuel rods is expected for most severe collision accidents, the finite element analyses described in Section 5.1 do not predict the fraction of rods failed. They did, however, provide estimates of the peak rigid body accelerations that the fuel rods would experience as a result of cask impacts onto unyielding surfaces. This allowed results from an analysis of the strains generated in PWR and BWR fuel rods carried in a typical PWR or BWR assembly [7-20] for regulatory impacts to be scaled to match the accelerations produced by impacts onto unyielding surfaces at 60, 90, and 120 mph. Comparison of the scaled rod strains to the rod failure criterion developed for the analysis of regulatory impacts [7-21] then allowed the fraction of the rods in a typical PWR or BWR assembly failed by 30, 60, 90, and 120 mph impacts onto an unyielding surface to be estimated.

Accordingly, for each impact orientation examined in Section 5.1 and each class of real-world yielding surfaces, four speeds were determined, v_{30}, v_{60}, v_{90}, and v_{120}, where v_{30}, v_{60}, v_{90}, and v_{120} are the impact speeds for the stated impact orientation (end, corner, or side) onto the real yielding

surface that inflict damage onto the cask and its contents equivalent to the damage caused by 30, 60, 90, and 120 mph impacts onto an unyielding surface. These four speeds define four speed ranges, $v_{30} \le v < v_{60}$, $v_{60} \le v < v_{90}$, $v_{90} \le v < v_{120}$ and $v_{120} \le v$, where v is the cask impact speed onto the real yielding surface or object at the stated impact orientation.

7.2.5.2 Thermal Failure of Cask Seals and Spent Fuel Rods

During normal transport under ambient conditions, the peak temperature of spent fuel in a Type B spent fuel cask is about 300°C [7-22]. Because the average temperature of free burning hydrocarbon fuel fires is about 1000°C [7-23], elastomeric cask seals and spent fuel rods can both fail if the cask that contains them is heated long enough by a hot fire.

Type B spent fuel casks are usually equipped with elastomer seals (e.g., Viton O-rings). When heated to temperatures above 350°C at rates comparable to the heating rates of engulfing hydrocarbon fuel fires, these seal materials degrade thermally losing about 5 percent of their mass if heated to 380°C, 10 percent if heated to 400°C, and 70 percent if heated to 450°C [7-24]. Elastomeric O-rings lose sealing function, as measured by helium leak detection, if heated to about 400°C, but can be repeatedly cycled from ambient temperatures to temperatures approaching 380°C without loss of sealing function [7-25]. Loss of mass without loss of sealing function upon heating to 380°C occurs because elastomeric O-rings usually contain or are coated with volatile organics (e.g., oils). Thus, the mass loss that occurs first upon heating is due to the vaporization of these volatile organics and not to thermal decomposition of rubber matrix materials, which causes the O-ring to shrink and, when shrinkage is appreciable, sealing function to be lost. Accordingly, heating of elastomeric cask seals to temperatures above 400°C is probably required, if loss of sealing function is to be large enough to allow significant quantities of gasborne aerosols to escape from the cask through the failed seal. Nevertheless, it is here assumed that elastomeric cask seals begin to leak when heated to 350°C and, in order to be consistent with the treatment of seal failures caused by impacts, it is also assumed that the seal leak produced by heating to 350°C has a cross-sectional leak area of about 1 mm^2 (because no credit is taken for vapor and particle deposition during most of the 60 to 80 minutes that is required for an engulfing fire to heat a cask to seal failure temperatures, source term magnitudes and thus accident consequences are relatively insensitive to seal failure temperatures). Finally, the substantial mass loss that is caused by heating to 450°C is assumed to cause O-ring sealing function to be lost around the entire circumference of the cask closure producing a leak area that is determined by the roughness of the surfaces of the cask lid and lid well where they contact each other and the length of the closure circumference.

When heated to elevated temperatures, spent fuel rods fail by burst rupture. During the experiments of Lorenz, et al. [7-26], sections of spent fuel rods that had been heated to 900°C failed by burst rupture when rod pressures reached 275 psig. Wilmot's analysis of release of fission products from spent fuel rods during transportation accidents assumes rod failure by burst rupture occurs at 850°C [7-27]. The critical review of spent fuel transportation accident conditions by Sanders, et al. [7-28] indicates that rod burst rupture is expected to occur at temperatures near 725 to 750°C. And, after correcting for differences in burnup and internal pressure, data in the Cask Designers Guide suggest that spent fuel rods may fail due to creep

rupture occurs at 850°C [7-27]. The critical review of spent fuel transportation accident conditions by Sanders, et al. [7-28] indicates that rod burst rupture is expected to occur at temperatures near 725 to 750°C. And, after correcting for differences in burnup and internal pressure, data in the Cask Designers Guide suggest that spent fuel rods may fail due to creep rupture at temperatures as low as 700°C [7-29]. Because the release of Cs vapors will be greater when rods fail at higher rather than lower temperatures, the temperature at which rods fail by thermal burst rupture is assumed to be 750°C, the middle of this range, rather than 700°C, the bottom of the range.

Let the internal temperature of a Type B spent fuel cask during normal transport under ambient conditions be T_a = 300°C, the temperature where elastomeric spent fuel cask seals begin to leak through a leak path with a cross-sectional area of 1 mm^2 be T_s = 350°C, the temperature where spent fuel rods fail by burst rupture be T_b = 750°C, and the average temperature of hydrocarbon fuel fires be T_f = 1000°C. These four temperatures define three temperature ranges, $T_a \le T_{cask} \le T_s$, $T_s < T_{cask} < T_b$, and $T_b \le T_{cask} \le T_f$, where T_{cask} is the internal temperature of the cask.

7.2.5.3 Collision-Only Scenarios

Collisions that do not initiate fires must be unusually severe if seal leakage is to caused by impact. For impacts onto an unyielding surface at 60 mph by a Type B rail cask and at 120 mph by a Type B truck cask, the finite element cask impact calculations described in Section 5 indicate that, even though slumping of cask internal structures is so great that many of the rods in the cask are likely to fail, distortion of the cask seal region is not great enough to conclude that seal leakage definitely occurs. Despite this, here it is assumed that (a) leakage of the cask's elastomeric seals is produced by all collisions that lead to impact of a Type B spent fuel cask onto a yielding surface at a velocity that subjects the cask to mechanical loads equal to those generated by impacts onto an unyielding surface at 60 mph for rail casks and at 120 mph for truck casks, (b) the leakage area produced by these impacts is about 1 mm^2, and (c) such impacts cause at least some of the rods in the cask to fail.

MELCOR calculations [7-30] indicate that, when cask leak path cross-sectional areas are small (~ 1 mm^2), the mass deposition rate of vapors and particles onto cask interior surfaces is rapid compared to the mass rate of their release from the cask to the environment. Thus, unless cask depressurization is rapid, deposition of vapors and large particles onto cask interior surfaces will be efficient which means that deposition of radioactive materials will also be efficient. Therefore, for collision accidents that do not initiate fires, deposition of particles and vapors onto cask interior surfaces during rod depressurization is assumed to be appreciable whenever cask seal leakage areas are small. Thus, for Collision-Only scenarios (Category 4 accidents), $f_{release}$, the total release fraction for release of fission products from failed rods to the environment, is given by

$$f_{release} = f_{rod,impact} f_{RC} \left(1 - f_{deposition}\right) \left(1 - \frac{p_{atm}}{p_{Imp}}\right) \quad (1)$$

where $f_{rod,impact} = 1.0$ is the fraction of the rods in the cask that are failed by the collision impact, f_{RC} is the fraction of the materials in a spent fuel rod that is released to the cask interior upon rod failure, $f_{deposition}$ is the fraction of those materials that rapidly deposit onto cask interior surfaces upon release from the failed spent fuel rods, p_{atm} is atmospheric pressure, and p_{Imp} is the cask internal pressure after depressurization of the fuel rods that failed as a result of the collision impact. Note that although the values of f_{RC} and $f_{deposition}$ will depend on the physical and chemical properties of the materials (radionuclide species) being released from the failed fuel rods, for simplicity in this and subsequent equations, they are written without attachment of the radionuclide species subscript i (e.g., as f_{RC} rather than f_{RCi}).

7.2.5.4 Collision Plus Fire Scenarios

Consider a collision accident that is severe enough to fail some of the rods in the spent fuel cask, but not the cask seal, and that also initiates a fire that heats the cask to the temperature T_s where the cask seal fails due to thermal degradation causing the cask to depressurize. Now let p_{atm} be atmospheric pressure, p_{Imp} be the cask internal pressure after depressurization of the fuel rods that failed as a result of the collision impact, T_a be the cask internal temperature during normal transport under ambient conditions, V_{cask} be the internal free volume of the cask, $V_{expansion}$ be the volume that the gases initially in the cask plus the gases released to the cask by rod failure would occupy at T_s and atmospheric pressure, and f_{CE} be the fraction of the gasborne radioactive materials that escape from the cask to the environment when the cask seal fails due to thermal degradation. But

$$f_{CE} = 1 - \frac{V_{cask}}{V_{expansion}} \quad \text{and} \quad \frac{p_{Imp} V_{cask}}{T_a} = \frac{p_{atm} V_{expansion}}{T_s} \quad \text{and therefore} \quad \frac{V_{cask}}{V_{expansion}} = \frac{p_{atm} T_a}{p_{Imp} T_s}$$

So, if deposition of particles and vapors is neglected during the time required for the fire to heat the cask from T_a to T_s,

$$f_{CE} = 1 - \frac{V_{cask}}{V_{expansion}} = 1 - \frac{p_{atm} T_a}{p_{Imp} T_s}$$

By extending this approach, a conservative expression can now be developed for release due to failure of some rods by an impact that does not fail the cask seal followed by heating of the cask in a fire first to the temperature T_s where the cask seal begins to leak, then to the temperature T_b where the remaining rods fail by burst rupture, and finally to the temperature of the fire T_f. As before, let p_{Imp} be the cask pressure after rod failure due to impact and p_{atm} be atmospheric pressure. In addition, let f_{imp} be the fraction of the rods failed by impact, f_{bur} be the fraction of rods failed by thermal burst rupture, p_b be the cask pressure after rod failure due to burst rupture, f_{RCimp} be the release fraction for fission products to the cask interior from a rod failed by impact, f_{RCf} be the release fraction for fission products to the cask interior from a rod failed by thermal burst rupture due to a fire, and f_{dep} be the fraction of the materials released from failed rods to the cask interior that deposits rapidly onto cask internal surfaces. Then, the total release fraction f_{rel}

for release of fission products from failed rods to the environment during Category 5 accidents is given by

$$f_{rel} = f_{imp} f_{RCimp} \left(1 - f_{dep}\right) \left\{ \left[1 - \frac{p_{atm}}{p_{imp}} \frac{T_a}{T_s} \right] + \left[\frac{p_{atm}}{p_{imp}} \frac{T_a}{T_s} \right] \left[1 - \frac{T_s}{T_b} \right] + \left[\frac{p_{atm}}{p_{imp}} \frac{T_a}{T_b} \right] \left[1 - \frac{p_{atm}}{p_b} \frac{T_b}{T_f} \right] \right\}$$
$$+ f_{bur} f_{RCf} \left(1 - f_{dep}\right) \left\{ \left[1 - \frac{p_{atm}}{p_b} \frac{T_b}{T_f} \right] \right\} \quad (2)$$

where $f_{bur} = 1 - f_{imp}$, because all rods not failed by impact are assumed to fail when the rod burst rupture temperature is reached, and the expression is conservative because deposition of particles and vapors is assumed to occur only immediately following rod failure and not during the time periods during which the cask is heated by the fire to elevated temperatures.

Inspection of Equation 2 shows that the first term in the equation gives the release fraction for materials released due to rod failure caused by collision impacts and the second term gives the release fraction for materials released due to rod failure caused by thermal burst. In addition, the three parts of the first term respectively reflect the effect on release of (1) cask pressurization due to rod depressurization upon impact failure followed by heating of cask gases to the temperature where seal leakage begins, (2) heating of cask gases from the temperature of seal leakage almost to the temperature of rod burst rupture, and (3) cask pressurization due to burst rupture of the remaining unfailed rods followed by heating of cask gases from the burst rupture temperature to the temperature of the engulfing fire.

Equation 2 also is used to calculate the release fraction for Category 6 accidents, collisions that initiate fires and fail not only the cask seal by impact but also the cask body by puncture or shear. For these accidents, f_{dep} in the last term of the equation is set to zero, because the flow of gases through the cask during these accidents is assumed to transport all materials released to the cask interior from the failed rods through the cask failures to the environment.

Finally, for Category 5 and Category 6 accidents that heat the cask to temperatures $\geq T_b$, all Cs in particles deposited on cask internal surfaces is assumed to volatilize. Volatilization of all Ru in particles deposited on cask internal surfaces is also assumed to occur during all Category 6 accidents since, during these accidents, air is assumed to be flowing through the failed cask which would cause involatile RuO_2 to be oxidized to volatile RuO_4.

7.2.5.5 Fire-only Scenarios

For fires not initiated by collisions (Category Fire-only accidents), when the inner wall of the cask shell reaches a temperature of 350°C = T_s, thermal degradation of the cask's elastomeric seal is assumed to cause the cask seal to begin to leak through a leak path that has a cross-sectional area of 1 mm^2. In addition, whenever the cask shell temperature exceeds 450°C, decomposition of the elastomeric seal is assumed to be so extensive that the effective leak path has a cross-sectional area equal to the product of the closure circumference and the roughness height of the lid and the lid well where they contact inside of the closure. In addition, all of the

rods in the cask are assumed to fail by burst rupture when the cask inner shell temperature reaches 750°C = T_b, and, whenever rod failure occurs, the fire is assumed to burn long enough to heat the cask to T_f = 1000°C, the average temperature T_f of a hydrocarbon fuel fire which is here assumed to be 1000°C. Therefore, for Category Fire-only accidents,

$$f_{rel} = f_{bur} f_{RCf} \left(1 - f_{dep}\right) \left[1 - \frac{p_{atm}}{p_b} \frac{T_b}{T_f}\right] \tag{3}$$

where f_{bur} = 1.0 is the fraction of rods in the cask that fail when the cask internal temperature reaches the rod burst temperature T_b.

7.2.5.6 Expansion Factor Ratios

Now let $f_{e1} = (p_{atm}/p_{imp})(T_a/T_s)$, $f_{e2} = T_s/T_b$, $f_{e3} = (p_{atm}/p_{imp})(T_a/T_b)$, $f_{e4} = (p_{atm}/p_b)(T_b/T_f)$, and $f_{e5} = (p_{atm}/p_{lmp})$. After substitution of these expansion factor symbols, the equations for release caused by collisions that do not initiate fires, by collisions that do initiate fires, and fires not initiated by collisions reduce to:

Accident Category	Term	Part	Failure Mode	Temperature Range
Collisions that do not initiate Fires				
$f_{rel} = f_{imp} f_{RCimp} (1-f_{dep})(1-f_{e5})$	1		Impact	T_a
Collisions that initiate Fires				
$f_{rel} = f_{,imp} f_{RCimp} (1-f_{dep})(1-f_{e1})$	1	1	Impact	$T_a \le T_{cask} \le T_s$
$+ f_{imp} f_{RCimp} (1-f_{dep})(f_{e1})(1-f_{e2})$	1	2		$T_s < T_{cask} < T_b$
$+ f_{imp} f_{RCimp} (1-f_{dep})(f_{e3})(1-f_{e4})$	1	3		$T_b \le T_{cask} \le T_f$
$+ (1-f_{imp}) f_{RCfire} (1\text{-}f_{dep})(1-f_{e4})$	2		Rupture	$T_b \le T_{cask} \le T_f$
Fires without Collisions				
$f_{rel} = (1-f_{imp}) f_{RCfire} (1-f_{dep})(1-f_{e4})$	1		Rupture	$T_b \le T_{cask} \le T_f$

7.2.6 Accident Cases

The four accident categories, the four velocity ranges, and the three temperature ranges defined above allow 18 truck accident cases and 20 train accident cases that lead to release of radionuclides to be defined (because RADTRAN requires that the probabilities of the cases supplied as input sum to one, before being input to RADTRAN, these accident cases are augmented by one case that includes shipments not subject to accidents and shipments that involve accidents that do not lead to a release of radionuclides, i.e., 19 total truck cask and 21 total train cases). For truck accidents, the 18 accident cases consist of one Category 4 case, twelve Category 5 cases, four Category 6 cases, and one Category Fire-only case. Table 7.10

presents the characteristics (cask failure mechanism, impact velocity range, and temperature range) of each truck accident case.

In Table 7.10, the single Category 4 accident case represents collisions that do not initiate fires but are so severe that the impact forces cause the cask seal to leak and all of the rods in the truck cask to fail. The twelve Category 5 accident cases occur in four groups of three accident cases. The first three groups represent collisions that are not severe enough to cause seal leakage but initiate fires that heat the cask to temperatures greater than the temperature where the cask seal begins to leak due to thermal degradation. The fourth group of three Category 5 accident cases represents collisions that both initiate fires and are also so severe that the impact causes the cask seal to leak. Because for these three cases $v_{seal} \geq v_{120}$, the initial impact also fails all of the rods in the cask. Cases 14 through 17, the Category 6 accident cases, are the same as Cases 4, 7, 10, and 13 except that a second failure of the cask by puncture or shear is assumed. Because of the

Table 7.10 Truck Accident Cases

Category	Case	Cask Seal Failure by		Velocity Range				Temperature Range		
		Impact	Fire	v_{30}-v_{60}	v_{60}-v_{90}	v_{90}-v_{120}	$\geq v_{120}$	T_a-T_s	T_a-T_b	T_a-T_f
4	1	X					X			
5	2		X	X				X		
	3		X	X					X	
	4		X	X						X
	5		X		X			X		
	6		X		X				X	
	7		X		X					X
	8		X			X		X		
	9		X			X			X	
	10		X			X				X
	11	X					X	X		
	12	X					X		X	
	13	X					X			X
6	14		X	X						X
	15		X		X					X
	16		X			X				X
	17	X					X			X
Fire Only	18		X							X
No Release	19									

double failure of the cask, it is also assumed first that flow of combustion gases or air through the cask carries out to the environment all fission products released from the rods to the cask interior while the cask is hot, and second that oxidation of fuel and of RuO_2 enhances the releases of Cs and Ru compared to the releases that characterize Case 4, 7, 10, and 13 accidents. Finally, the single case in the Fire Only category represents fires not initiated by collisions that heat the cask to temperatures high enough to fail all of the spent fuel rods by burst rupture and also the cask seal by thermal degradation.

If a term for the deposition of particles and vapors, while a fire is heating the cask to elevated temperatures, were added to Equation 2, then Category 5 accident Cases 8, 9, and 10 would have slightly smaller release fractions than Category 5 accident Cases 11, 12, and 13. Because particle and vapor deposition during periods of cask heating by a fire is neglected, the release fractions

calculated for accident Cases 11, 12, and 13 will be the same as those calculated for accident Cases 8, 9, and 10. Finally, because the rod failure fractions ($f_{rod,impact}$) for the four Category 6 accident cases (Cases 14, 15, 16, and 17) are ordered as follows,

$$f_{rod,impact,Case\ 14} < f_{rod,impact,Case\ 15} < f_{rod,impact,Case\ 16} = f_{rod,impact,Case\ 17}$$

the release fractions for these four accident cases have the following order:

$$f_{release,Case\ 14} > f_{release,Case\ 15} > f_{release,Case\ 16} = f_{release,Case\ 17}$$

Increasing the fraction of rods failed by impact decreases the release fraction for Category 6 accidents because for this accident category, deposition processes are assumed to be effective for materials released to the cask interior when rods are failed by impact but is neglected when rods fail by burst rupture. Deposition is neglected following burst rupture because the combustion gases that are assumed to be flowing through the cask during Category 6 accidents are also assumed to carry all materials released to the cask interior out to the environment without significant depletion by deposition to cask interior surfaces.

For train accidents, because rail cask seals may leak after impacts onto an unyielding surface at some orientations at speeds as low as 60 mph, the train accident matrix consists of 20 accident cases, three Category 4 cases, twelve Category 5 cases, four Category 6 cases, and one Category Fire-only case. Table 7.11 presents the characteristics (cask failure mechanism, impact velocity range, and temperature range) of each train accident case.

Table 7.11 Train Accident Cases

Category	Case	Cask Seal Failure by		Velocity Range				Temperature Range		
		Impact	Fire	v_{30}-v_{60}	v_{60}-v_{90}	v_{90}-v_{120}	≥ v_{120}	T_a-T_s	T_a-T_b	T_a-T_f
4	1	X			X					
	2	X				X				
	3	X					X			
5	4		X	X				X		
	5		X	X					X	
	6		X	X						X
	7	X			X			X		
	8	X			X				X	
	9	X			X					X
	10	X				X		X		
	11	X				X			X	
	12	X				X				X
	13	X					X	X		
	14	X					X		X	
	15	X					X			X
6	16		X	X						X
	17	X			X					X
	18	X				X				X
	19	X					X			X
Fire Only	20		X							X
No Release	21									

7.2.7 Source Term Probabilities

For transportation accidents, the probability P that an accident is so severe that it generates a source term that leads to consequences with magnitude M is expressed as the product of the probability that any accident occurs ($P_{accident}$), the probability that the truck or rail car carrying the cask is involved in the accident ($P_{vehicle}$), and the fraction of all possible accidents ($F_{severity}$) that lead to releases of radioactivity that cause consequences of magnitude M. Therefore,

$$P = P_{accident} P_{vehicle} F_{severity} \quad (4)$$

7.2.7.1 Accident Probabilities

The probability that a truck or train is involved in an accident of any severity while traveling a route of length L is usually expressed as the sum of the chances that an accident occurs on the urban, suburban, and rural portions of the route. Thus,

$$P_{accident} = \sum_{m=1}^{3} L f_m Rate_{accident,m}$$

where m is a link index, which is here used to denote the urban, suburban, and rural portions of the route, $Rate_{accident,m}$ is the accident frequency, without regard to severity, per unit distance traveled on the urban, suburban, and rural portions of the route, and f_m is the fraction of the route length that is urban, suburban, or rural. Values for L, f_m, and $Rate_{accident,m}$ were developed in Sections 3.3.1 and 3.3.2.

7.2.7.2 Vehicle Involvement

Values for $P_{vehicle}$, the probability that the vehicle carrying the spent fuel cask is involved in the accident, are developed in Section 7.4.2 directly from accident data. Thus, $P_{vehicle}$ is not formulated as an algebraic combination of other variables.

7.2.8 Accident Severities

The massive nature and robust construction of Type B spent fuel casks mean that only an extremely severe collision and/or a hot, long-duration fire can cause both the cask and a significant fraction of the spent fuel rods being transported in the cask to fail. The severity of a collision accident depends on accident type, accident speed, cask impact angle, the hardness of the impact surface, the fraction of the accident energy that is consumed damaging structures other than the cask, the size of the cask leak, and the fraction of the rods in the cask that are failed by the impact loads. Because only a hot, long duration fire can heat a spent fuel cask to temperatures that are high enough to cause both the cask seal and spent fuel rods to fail, the severity of fire accidents depends on fuel type (combustion characteristics), the amount of fuel available to be burned, the effects of fuel runoff and of adsorption of fuel by the ground, fuel availability and rate of combustion, the stand-off distance of the fire from the cask, and the size of the cask leak.

7.2.8.1 Severity Fraction Expressions

Let $P_{scenario,j}$ be the probability that an accident follows accident scenario j (the probability of path j on the truck or rail accident event trees depicted in Figures 7.3 and 7.4). For collision accidents, let $P_{puncture/shear}$ be the conditional probability that during the collision the cask shell is failed by puncture or shear and $P_{speed,j}$ be the probability that the cask impact speed v for collision accident scenario j is large enough to cause consequences of magnitude M by itself for collision-only accidents or in conjunction with the effects of any ensuing fires for collision accidents that initiate fires. For accidents that involve fires (collisions that initiate fires and fire-only accidents), let $P_{fire/scenario,j}$ be the probability that accident scenario j initiates a fire and $P_{severe\ fire,k}$ be the probability that the fire raises the temperature of cask k high enough to cause the additional damage (seal leakage due to thermal degradation and rod failure by burst rupture) required to produce consequences of magnitude M.

Given these definitions and assuming that these probabilities are largely independent, for collisions that don't initiate fires (Category 4 accidents),

$$F_{severity,j} = P_{scenario,j}\, P_{speed,j} \tag{5}$$

where $P_{scenario,j}$ is the probability of accident scenario j and $P_{speed,j}$ is the probability that the cask impact speed for accident scenario j is large enough to cause consequences of magnitude M, and all of the probabilities are conditional probabilities that are conditional on the occurrence of an accident and each probability in this and subsequent expressions is also conditional on the probabilities in the expression that precede it.

For Category 5 accidents that involve collisions that initiate fires,

$$F_{severity,j} = P_{scenario,j}\, P_{speed,j}\, P_{fire/scenario,j}\, P_{severe\ fire,k} \tag{6}$$

For Category 6 accidents that involve collisions sufficiently severe to fail the cask shell by puncture or shear and its seal by warping of the seal seat,

$$F_{severity,j} = P_{scenario,j}\, P_{speed,jm}\, P_{fire/scenario,j}\, P_{severe\ fire,k}\, P_{puncture/shear} \tag{7}$$

And for Category Fire-only accidents that don't involve collisions,

$$F_{severity,j} = P_{scenario,j}\, P_{severe\ fire,k} \tag{8}$$

because by definition $P_{fire/scenario,j} = 1.0$ for fire-only accidents.

7.2.8.2 Accident Velocity Probabilities

In Section 7.2.5.1, four ranges for the cask impact speed v were defined, $v_{30} \le v < v_{60}$, $v_{60} \le v < v_{90}$, $v_{90} \le v < v_{120}$, and $v_{120} \le v$, where v_{30}, v_{60}, v_{90}, and v_{120} are the impact speeds for end, corner, or side impact orientations onto real yielding surfaces that cause the same damage to the cask and its contents (spent fuel) as is caused respectively by end, corner, and side impacts at speeds of 30, 60, 90, and 120 mph onto an unyielding surface. Thus, $P_{speed,j}$, the probability that the cask

impact speed v for collision accident scenario j is large enough to cause consequences of magnitude M has four values, one for each speed range. Specifically,

$$P_{speed,j}(v_{30}, v_{60}) = \sum_{m=1}^{3} P_{orientation,m}\left[P_{speed,jm}(v_{60}) - P_{speed,jm}(v_{30})\right]$$

$$P_{speed,j}(v_{60}, v_{90}) = \sum_{m=1}^{3} P_{orientation,m}\left[P_{speed,jm}(v_{90}) - P_{speed,jm}(v_{60})\right]$$

$$P_{speed,j}(v_{90}, v_{120}) = \sum_{m=1}^{3} P_{orientation,m}\left[P_{speed,jm}(v_{120}) - P_{speed,jm}(v_{90})\right]$$

$$P_{speed,j}(\geq v_{120}) = \sum_{m=1}^{3} P_{orientation,m}\left[1.0 - P_{speed,jm}(v_{120})\right]$$

where v_{30}, v_{60}, v_{90}, and v_{120} have different values for each cask/surface combination, $P_{orientation,m}$ is the probability that the cask impact is an end, corner, or side impact and $P_{speed,jm}(v_{30})$, $P_{speed,jm}(v_{60})$, $P_{speed,jm}(v_{90})$, and $P_{speed,jm}(v_{120})$ are respectively the cumulative probabilities for impact orientation m and accident scenario j that the cask impact speed v is $\leq v_{30}$, $\leq v_{60}$, $\leq v_{90}$, and $\leq v_{120}$.

7.2.8.3 Accident Fire Probabilities

In Section 7.2.5.2, the internal temperature of the cask under ambient conditions T_a, the cask seal leakage temperature T_s, the rod burst rupture temperature T_b, and the average temperature of hydrocarbon fueled fires T_f were used to define three temperature ranges: $T_a \leq T_{cask} \leq T_s$, $T_s < T_{cask} < T_b$, and $T_b \leq T_{cask} \leq T_f$. Now, for fire-only accidents or collisions that initiate fires, let $P_{co\text{-}located}$ be the probability that the cask and the fire are co-located (i.e., that the cask is not significantly offset from the fire), $P_{optically\ dense}$ be the probability that the fire diameter is large enough to make the fire optically dense to loss of energy from the cask (i.e., the fire diameter is about 3 m larger than the fire diameter that just engulfs the cask), $P_{flame\ temp}$ be the probability that the flame temperature of the fire is high enough to raise the temperature of the cask internals to a temperature that falls within one of the three temperature ranges, and $P_{duration}$ be the probability that the fire burns long enough so that the cask internals actually reach a temperature in that temperature range. Finally, for collisions that initiate fires, let $P_{fire/scenario,j}$ be the conditional probability that scenario j initiates a fire.

Given these definitions

$$P_{severe\ fire,k} = P_{co\text{-}located}\ P_{optically\ dense}\ P_{flame\ temp}\ P_{duration,k} \qquad (9)$$

where $P_{co\text{-}located}$, $P_{optically\ dense}$, $P_{engulfing}$, $P_{flame\ temp}$, and $P_{duration,k}$ will have different cask-specific values for each of the three temperature ranges, $T_a \leq T_{cask} \leq T_s$, $T_s < T_{cask} < T_b$, and $T_b \leq T_{cask} \leq T_f$.

7.3 Values for Release Fraction Parameters

7.3.1 Fission Product Release from Failed Rods to the Cask Interior

When a spent fuel rod is failed during a transportation accident, depressurization of the rod causes particles (fuel fines) and fission product gases, for example, noble gases and condensible vapors such as Cs atoms, gasborne at the time of rod failure, to be carried into the cask by the flow of He out of the failed rod. Release of fuel fines may be increased if fines on pellet surfaces are entrained into the depressurization flow of rod gases and might be decreased if these fines must flow through and thus be filtered by a bed of larger fines before they reach the location of the rod failure. Release of vapors may be increased if exposure of fuel pellets to the cask atmosphere upon rod failure leads to changes that increase the rate of release of fission product species from the pellets (e.g., oxidation of UO_2 or RuO_2).

7.3.2 Noble Gases

Because spent fuel rods are usually pressurized with He to about 30 atm, when a rod fails, depressurization to 1 atm causes 29/30 of the He in the rod to flow into the cask. Thus, the rod-to-cask release fraction F_{RC} for noble gases is $29/30 = 0.97 \approx 1.0$.

7.3.3 Particles

When first removed from a reactor, spent fuel rods contain particles of UO_2 called fuel fines. If during a transportation accident a spent fuel rod is subjected to large impact forces, fracturing of fuel pellets will generate additional particles of UO_2. If these impact forces or heating of the rod by a fire cause the rod to fail, the rush of rod gases over pellet surfaces during rod depressurization will cause some of the UO_2 particles to be entrained into the depressurization flow of gases which may then transport them to and through the rod failure into the cask interior. Transport of particles through the gap to the rod failure will be inefficient for particles with diameters similar to the gap width. In addition, if the large fuel fines in the gap act as a granular bed, then transport of particles with diameters smaller than the gap width may also be inefficient if these particles are efficiently captured by the bed of larger fuel fines.

Significant transport of particles from failed rods to the cask interior will occur only during rod depressurization. Once rod depressurization has occurred, deposition of particles still gasborne within the failed rod onto cladding and pellet surfaces will be much more rapid than transport by diffusion out of the rod to the cask interior, and entrainment of particles off of fuel pellet and cladding surfaces into diffusive gas flows will not occur as the velocities of diffusive flows are much to small to cause particle entrainment.

Release of particles (fuel fines) from H. B. Robinson one-foot-long spent fuel rod sections upon rod failure due to burst rupture was examined experimentally by Lorenz, et al. [7-26] during high temperature tests. Most of the particles released from the rod were found to be of sizes that deposited very rapidly onto surfaces inside of the furnace tube used to heat the test sections to burst rupture temperatures. Examination of five radioactive particles by scanning electron microscopy indicated that the particles deposited in the furnace tube were large (range of diameters, 140 to 210 μm) while the particles that escaped from the furnace tube had diameters

≤ 10 μm. Lorenz, et al. calculated release fractions for fuel fines (particles of UO_2) for release into the furnace and for escape from the furnace. Table 7.12 summarizes these experimental release fractions and shows that the fraction of respirable particles (particles with diameters ≤ 10 μm) that escaped from H. B. Robinson spent fuel rod test sections during the burst rupture tests of Lorenz, et al. was about $3.1 \times 10^{-6} = (2.4 \times 10^{-4})(0.013)$.

Table 7.12 Experimental Release Fractions for Fuel Fines

Test	Fraction UO_2 Released from the Test Section to the Furnace Tube	Fraction of UO_2 Mass Released to the Furnace Tube that Escapes from Furnace Tube
HBU-7	1.6×10^{-4}	~ 0.02
HBU-8	4.1×10^{-4}	< 0.01
HBU-9	1.8×10^{-4}	~ 0.01
HBU-10	2.2×10^{-4}	~ 0.02
Average	2.4×10^{-4}	~ 0.013

Release of particles (fuel fines) from one-foot-long sections of Turkey Point spent fuel rods upon rod failure due to burst rupture was examined experimentally by Burian, et al. [7-31, 7-32] during high temperature tests. In a typical test, the fraction of UO_2 mass released upon rod rupture was 4.2×10^{-5} and about 90 percent of this particle mass deposited onto surfaces inside of the furnace used to heat the test sections to burst rupture temperatures. The particles that constituted the remaining 10 percent of the particle mass escaped from the furnace and were collected on the stages of a bank of downstream impactors. These particles had aerodynamic diameters of 4 μm or less. Thus, the fraction of respirable particles that escaped from Turkey Point spent fuel rod test sections during the burst rupture tests of Burian, et al. was about $4.2 \times 10^{-6} = (4.2 \times 10^{-5})(0.1)$, which is quite similar to the results obtained by Lorenz, et al. and suggests the use of this value to estimate release from the one-foot portion of a real spent fuel rod that contains the rod rupture.

During collision accidents, the impact forces should lead to the production of additional fuel fines due to fracturing of fuel pellets. In 1994, DOE published a Handbook of airborne release fractions for nuclear materials [7-33]. The handbook presents the following relationship between the fraction $F_{respirable}$ of a brittle material that is converted to respirable particles upon impact onto a hard surface.

$$F_{respirable} = A\rho gh$$

where $A = 2 \times 10^{-11}$ cm^3/g cm^2sec^{-2} is an empirical constant determined by impact tests on glass and ceramic specimens, ρ is the material (specimen) density, g is the acceleration due to gravity, and h is the fall-height. But $mgh = 0.5m(v_{impact})^2$ where v_{impact} is the impact velocity of the specimen onto the hard surface. So $F_{respirable} = 0.5A\rho(v_{impact})^2$. Therefore, because fuel pellet densities are about 10 g/cm^3, for 30, 60, 90, and 120 mph pellet impacts onto cladding surfaces,

one might expect the following fractions of the pellet mass to be converted to respirable particles, 1.8×10^{-4} at 30 mph, 7.2×10^{-4} at 60 mph, 1.6×10^{-3} at 90 mph, and 2.9×10^{-3}, at 120 mph.

The distribution of particle sizes produced by impact fracturing of depleted UO_2 pellets has been determined experimentally [7-34]. Figure 7.5 presents the experimental cumulative distribution of particle sizes. The figure shows that almost 99.99 percent of the particles produced by impact fracturing of depleted UO_2 pellets have diameters ≥ 10 μm. This data suggests that, during impact accidents, pellet fracturing would be expected to generate a bed of particles with diameters ≥ 10 μm that fills the pellet cladding gap in the spent fuel rod and any internal crack network in the fuel pellets.

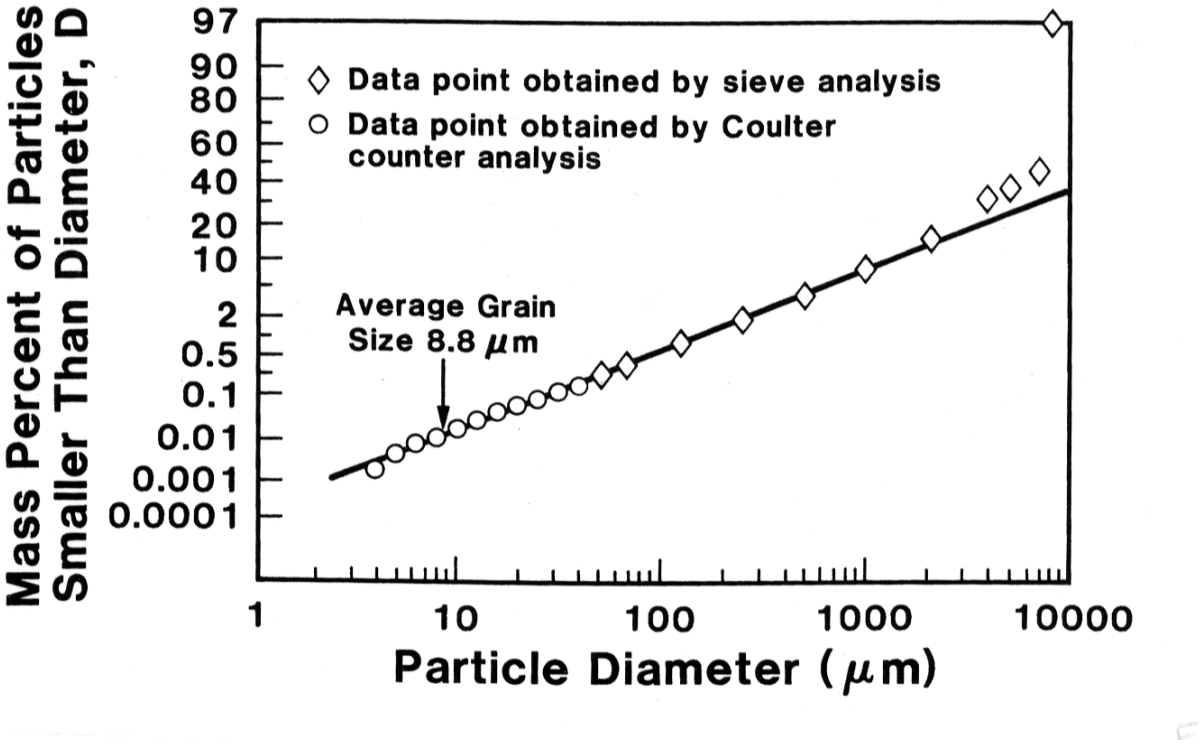

Figure 7.5 Fracture particle size distribution for depleted UO_2.

Capture of particles by a granular bed has been examined by Otani, et al. [7-35] who find that interception is the dominant removal mechanism for particles that are somewhat smaller than the average diameter of the bed particles. For such particles, Otani, et al. state that the single particle interception removal efficiency η_R is

$$\eta_R = 16R^{2-[\mathrm{Re}/(\mathrm{Re}^{1/3}+1)^3]}$$

and the total bed removal efficiency E is

$$\eta = -\frac{2}{3}\left[\frac{1-\alpha}{\alpha}\right]\frac{d_g}{L}\ln(1-E)$$

where $R = d_p/d_g$, d_p is the diameter of the particles entrained in the gases flowing through the granular bed, d_g is the diameter of the particles that comprise the granular bed; $Re = \rho_f d_g u_i/\mu$ is the Reynolds number of the gas flowing through the bed (He for spent fuel rods); $u_i = u_s/\alpha$; ρ_f, u_i, u_s, and μ are the density, interstitial velocity, superficial velocity, and dynamic viscosity of the gas flowing through the bed; α is the particle volumetric packing density, and L is the bed length.

Now, if η is equated to η_R (i.e., all removal mechanisms other than interception are neglected), then for a fixed value of E, for example 0.99, L increases as η_R decreases. Thus, use of larger values for d_g and Re will generate larger values for L. Accordingly, since the experiments of Lorenz, et al. show that the largest particles that escaped from the spent fuel rod sections upon burst rupture had diameters of about 200 μm, let d_g = 200 μm. A CONTAIN calculation described below indicates that $u_s = 6 \times 10^2$ cm s^{-1} for He flow through a one-foot section of a spent fuel rod that has a 20 μm gap and is pressurized to 18.6 atm. Because u_s should be increased by higher pressures and decreased by longer flow lengths, this value is reasonable for a full length rod pressurized to 30 atm. Thus, $u_i = 1.2 \times 10^3$ cm s^{-1}. Because a bed of 200 μm particles formed in the 20 μm pellet cladding gap must look something like a single layer of spheres, $\alpha = (4/3)\pi r^3/(2r)^3 = 0.5$. For He at 750 C, the likely burst rupture temperature for spent fuel rods pressurized to 30 atm, Re = 77 and thus $\eta_R = 16R^{1.47}$. For He at 350°C, the approximate temperature of spent fuel rods during normal transport and thus the rod depressurization temperature when failure is caused by collision impact rather than burst rupture, Re = 311 and $\eta_R = 16R^{1.34}$.

Now, let the bed efficiency E = 0.99, whereupon $L = 6.14 \times 10^{-2}/\eta_R$. Table 7.13 presents, for several particle diameters d_p of interest, values of η_R and L for a single layer bed of 200 μm particles with He Reynolds numbers of Re = 77 or 311. The table shows that this bed will remove particles with diameters ≥ 1 μm with an efficiency of 0.99. Thus, respirable fines with diameters of 1 to 10 μm should also be removed with similar efficiencies from the depressurization flow of He through the gap of a full length spent fuel rod that occurs when the rod fails due to impact loads or thermal burst rupture.

Table 7.13 Granular Bed Lengths that Provide 99 Percent Filtering Efficiencies

d_p(μm)	Re = 77		Re = 310	
	η_R	L(cm)	η_R	L(cm)
30	1.00	0.06	1.00	0.06
10	0.20	0.31	0.29	0.21
1	6.6×10^{-3}	9.3	1.3×10^{-2}	4.7
0.1	8.4×10^{-5}	728	6.0×10^{-4}	102

Table 7.13 indicates that beds with lengths of 0.06, 0.31, and 9.26 cm would be expected to provide 99 percent filtering efficiency respectively for particles with diameters ≥ 30, ≥ 10, and ≥ 1 μm. Thus, it seems reasonable to conclude that only about one percent of the respirable fuel fines in a spent fuel rod will be able to be transported by depressurization gas flows through a rod gap filled with fuel fines with diameters of order 50 to 200 μm.

Based on the preceding discussion, a rod not subject to impact (no particle production by fracturing of UO_2) might be expected to generate during depressurization a plug (bed) of fuel fines in the rod gap that would cause fines not in the one-foot section of the rod that contains the rod rupture to be filtered while the fines in the one-foot section would escape with negligible diminution due to filtering. Therefore, a reasonable estimate for F_{RC}, the rod to cask release fraction for respirable fuel fines (particulates), for a rod not subjected to impact (no particle production by fracturing of UO_2) is

$$F_{RC} = \left(4.2 \times 10^{-6}\right)\left[\frac{1}{12} + \frac{11}{12}(0.01)\right] = 3.9 \times 10^{-7}$$

and because an 0.3 cm long bed of 200 μ particles will capture 99 percent of the respirable fuel fines that enter the bed, reasonable estimates for rods subject to impact fracturing are

$$F_{RC} = \left(4.2 \times 10^{-6} + 2.9 \times 10^{-3}\right)\left[\frac{0.25}{144} + \frac{143.75}{144}(0.01)\right] = 3.4 \times 10^{-5} \quad \text{for 120 mph impacts,}$$

$$F_{RC} = \left(4.2 \times 10^{-6} + 1.6 \times 10^{-3}\right)\left[\frac{0.25}{144} + \frac{143.75}{144}(0.01)\right] = 1.9 \times 10^{-5} \quad \text{for 90 mph impacts,}$$

$$F_{RC} = \left(4.2 \times 10^{-6} + 7.2 \times 10^{-4}\right)\left[\frac{0.25}{144} + \frac{143.75}{144}(0.01)\right] = 8.5 \times 10^{-6} \quad \text{for 60 mph impacts,}$$

$$F_{RC} = \left(4.2 \times 10^{-6} + 1.8 \times 10^{-4}\right)\left[\frac{0.25}{144} + \frac{143.75}{144}(0.01)\right] = 2.2 \times 10^{-6} \quad \text{for 30 mph impacts,}$$

where the first term in the brackets in these expressions represents particle release from the 0.25 inch (0.25 inch = 2 x 0.3 cm) portion of the rod that contains the rupture and the second term represents particle release from the other 143.75 inches of the rod, 0.01 represents the fraction of respirable fines that will pass through a plug or a bed of larger fuel fines, the release fraction value of 4.2 x 10^{-6} reflects the experimental release fractions for respirable fuel fines measured for the one-foot-long experimental test sections of Lorenz, et al. [7-26] and Burian, et al. [7-31], and 2.9 x 10^{-3}, 1.6 x 10^{-3}, 7.2 x 10^{-4}, and 1.8 x 10^{-4} are estimates of the fractions of UO_2 mass in fuel pellets converted to respirable fuel fines by impact fracturing as a result of 120, 90, 60, and 30 mph impacts. Finally, given the precision of this analysis, use of values of 4 x 10^{-7} and 3 x 10^{-5} respectively for F_{RC} for release of particles during non-impact and impact accidents seems appropriate.

7.3.4 Cesium

The amount of a condensible vapor (e.g., Cs atoms) carried from a failed rod to the cask interior should be determined by the free volume of the rod (the sum of the rod plenum volumes, the cladding gap volume, and the volume of the internal network of cracks in the fuel pellets contained in the rod) and by the partial pressure of the condensible vapor at the rod temperature at the time of rod failure. If rod depressurization leads to the adiabatic expansion of rod gases, significant cooling of those gases and of the cladding and pellet surfaces that they contact could take place. If this happens and if the condensible vapors in the rod helium encounter a cooled surface before they are carried out of the rod into the cask, significant condensation onto fuel pellet and rod internal cladding surfaces may take place which would significantly decrease the amounts of condensible vapors released to the cask. Thus, one might expect release fractions for condensible vapors to reflect the partial pressure of the vapor at either the burst rupture temperature of the rod or the temperature of pellet and/or cladding surfaces that have been substantially cooled by adiabatic expansion of gases during rod depressurization.

After a failed rod has depressurized, if the cask and rods are heated by a fire to elevated temperatures, fission products volatile at fire temperatures may vaporize from pellet surfaces and then diffuse out of the rod into the cask interior. Thus, condensible vapors could be released both by transport in rod depressurization gas flows and, after rod depressurization, by diffusion from the rod free volume through the rod failure into the cask.

7.3.4.1 Cs Release Fractions for Burst Rupture and Diffusion

Lorenz, et al. examined release of Cs from heated sections of simulated [7-36] and real [7-26] spent fuel rods by diffusion and during depressurization following rod failure due to burst rupture. By fitting their experimental results, Lorenz, et al. developed empirical models for the release of volatile fission products due to burst rupture of pressurized spent fuel rods and diffusion subsequent to burst rupture [7-37, 7-38]. For burst rupture, the following model applies,

$$F_{burst} = \frac{M_{burst}}{M_{inventory}} = \alpha V_{burst} M_{inventory}^{-0.2} \left(\frac{F_{gap}}{A_{clad}} \right)^{0.8} \exp\left[-\left(C \diagup T \right) \right] \qquad (10)$$

where M_{burst} is the mass (g) of the volatile fission product released due to rupture of the fuel rod while pressurized, $M_{inventory}$ is the mass (g) of the total inventory of the fission product in the rod, V_{burst} is the volume (cm^3) of rod gases released from the rod due to rod rupture calculated at 0°C and system pressure (0.3 MPa in the experiments of Lorenz, et al.), F_{gap} is the fraction of the total inventory of the fission product that was in the fuel-clad gap at the time the rod ruptured, A_{clad} is the area (cm^2) of the clad with which the fission products in the fuel-clad gap are associated (the surface area of the active length of the fuel rod), T is the temperature (K) of the gap gases at the time of rod rupture, and α and C are adjustable constants determined experimentally for each fission product.

For release by diffusion after rod failure, the following model applies,

$$F_{diffusion} = \frac{M_{diffusion}}{M_{inventory}} = F_{gap}\left\{1 - \exp[-R_o t / F_{gap} M_{inventory}]\right\} \tag{11}$$

$$R_o = \delta (W/P)\left(F_{gap} M_{inventory} / A_{clad}\right)^{0.8} \exp[-(\gamma/T)]$$

where R_0 is the initial rate of diffusive release (g/hr), T is the diffusion temperature (K), t is the time at the diffusion temperature (hr), W is the width of the fuel-cladding gap (μm), P is the system pressure (MPa), and δ and γ are adjustable constants determined experimentally for each fission product.

Table 7.14 presents the values determined experimentally for Cs by Lorenz, et al. for the adjustable constants in Equations 10 and 11.

Table 7.14 Parameter Values for Lorenz Release Expressions for Cs

Parameter	Cesium
α $(g/cm^3)(g/cm^2)^{-0.8}$	3.49
C K^{-1}	7420
δ $(g\ MPa/\mu m\ hr)(g/cm^2)^{-0.8}$	1.90×10^3
γ K^{-1}	1.98×10^4

7.3.4.2 Relative Importance of Cs Release by Burst Rupture and Diffusion

Table 7.15 presents release fractions for Cs from spent fuel for several temperatures of interest for release due to burst rupture and for 24 hours of release by diffusion. These release fractions were calculated by Sanders et al. [7-39] using Equations 10 and 11 and the values of the adjustable constants presented in Table 7.14.

Table shows (1) that, relative to burst release, release by diffusion is not significant at or below 600°C and (2) that, during a long duration (24 hours) engulfing hydrocarbon fuel fire, diffusion increases total release by a factor of about three over release by burst rupture:

$$\text{(burst rupture + diffusion)/(burst rupture)} = (5.7 \times 10^{-4} + 9.8 \times 10^{-4})/(5.7 \times 10^{-4}) = 2.7$$

The thermal analyses presented in Section 6 showed that it takes about six hours for an engulfing hydrocarbon fire to heat a spent fuel cask to the average temperature of the fire (1000°C) and the fire statistics presented in Section 7.4.4.1 show that hydrocarbon fires with durations of 6 hours or more are quite rare. Therefore, only a highly improbable fire will be able to heat a cask to average hydrocarbon fire temperatures for more than a few hours. Now, because the exponent in Equation 11 is small, diffusive release for 2 hours at 1000°C will be about 1/12 of the diffusive

release produced by 24 hours at 1000°C. Therefore, the diffusive release fraction for a 6-hour fire during which the cask is at 1000°C for 2 hours will be about 0.8×10^{-4} or about 1/7 of the burst rupture release fraction. So for almost all fires, diffusive release will not be important compared to burst release. Consequently, release of Cs by diffusion is neglected.

Table 7.15 Comparison of Cs Release Fractions for Rod Burst Rupture and Diffusive Release

Temperature		Release Fraction	
Value (C)	Condition	Burst Rupture	Diffusion (for 24 hours)
300	Normal Transport	4.6×10^{-7}	1.3×10^{-11}
530	Regulatory Maximum	1.9×10^{-5}	1.7×10^{-7}
600		3.9×10^{-5}	1.1×10^{-6}
800	Regulatory Fire	1.9×10^{-4}	6.4×10^{-5}
1000	Hydrocarbon Fuel Fire	5.7×10^{-4}	9.8×10^{-4}

7.3.4.3 Rod Cooling During Burst Rupture

The influence of adiabatic expansion of rod gases during rod depressurization on the temperature of those gases was examined by performing CONTAIN code [7-40] calculations that modeled the temperatures of the rod gases during depressurization upon burst rupture of the HBU-7 spent fuel test section examined by Lorenz, et al. [7-41]. The analysis focused on the thermal-hydraulic conditions of the helium fill gas in the test section during the blowdown from the initial test section pressure, after rod failure caused by induction heating.

7.3.4.3.1 HBU-7 Test Section Model

The six-cell model used to represent the HBU-7 rod test section during these calculations is depicted in Figure 7.6. Table 7.16 presents the identities, volumes, and initial conditions of these six cells just prior to rod failure. As Figure 7.6 and Table 7.16 show, the helium reservoir attached to the 30.48-cm-long HBU-7 test segment was modeled by one cell, the rod test segment by four cells, and the bulge formed in the test segment cladding just prior to segment failure by one cell. Upon failure of the bulge by burst rupture, gases in the test section were vented through the failure to the environment, which was thus in effect a seventh cell. Three of the six cells described in Figure 7.6 and Table 7.16, Cells 3, 4, and 5, represent those sections of the rod test section that were directly heated by induction during the burst rupture experiment. Because they were not directly heated, the temperatures in Cells 1, 2, and 6 were much lower than the temperatures in Cells 3, 4, and 5. The volumes assigned in Table 7.16 to the cells include an estimate of the effects of clad swelling, as described in Reference 1. The volumes are several times larger than the volumes implied by the hydraulic diameter, $D_H = 43.2$ μm, of the annular gap in the rod test segment, a value that was deduced from the steady-state rod blowdown measurements [7-42].

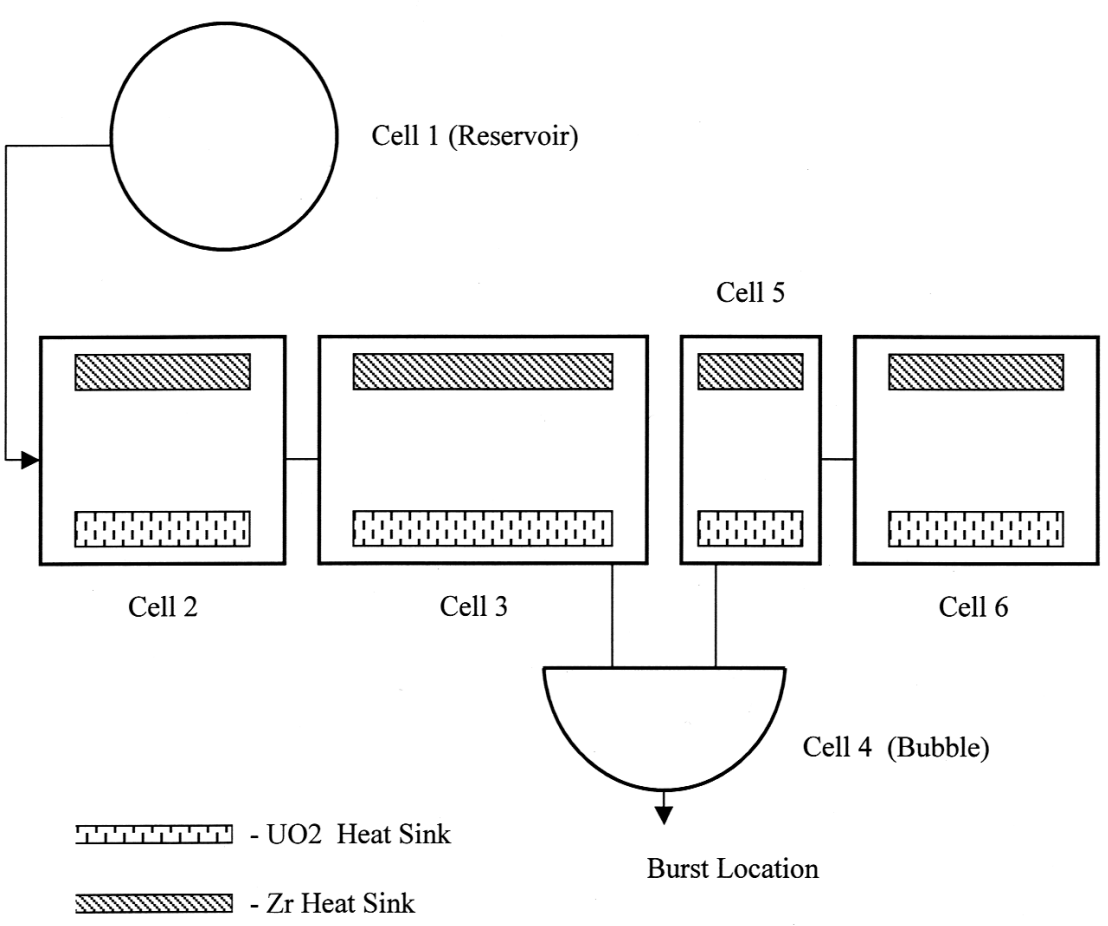

Figure 7.6 Schematic of the CONTAIN Model for the HBU-7 rod blowdown test.

Table 7.16 Initial Conditions and Volumes for the CONTAIN Model Cells

		Test Section Cells				
Cell Name	**Reservoir**	**Left End**	**Left Middle**	**Bulge**	**Right Middle**	**Right End**
Cell No.	1	2	3	4	5	6
Rod Length in Cell (cm)	0	8	12	2*	4	6.48
Initial Pressure (bars)	18.66	18.66	18.66	18.66	18.66	18.66
Initial Temperature (K)	303	742	1181	1181	1181	742
Cell Volume (cm^3)	4.33	0.44	0.45	1.9	0.15	0.36

*Heat sinks were not modeled in the bulge.

As indicated in Figure 7.16, Zr and UO_2 heat sinks were modeled in Cells 2, 3, 5, and 6. Each of the Zr and UO_2 sinks in a cell were assumed to have an effective heat transfer area πDL, where D is the fuel pellet diameter (0.932 cm), and L is the length of the rod section represented by the cell. These heat sinks are expected to be important during the blowdown of the test segment,

because they tend to offset the cooling effects caused by gas expansion. Note that the heat transfer areas of the UO_2 heat sinks were calculated assuming that the gas in the rod test section is confined to the rod's annular gap. Because this assumption neglects the surface area of any internal crack network in the fuel pellets, the UO_2 heat sink areas are minimums.

The time constant t_h for heating of gas within the annular gap can be estimated by

$$t_h = \frac{C_p \rho D_H^2}{4 Nu\, k}$$

where C_p is the specific heat of the gas, ρ is the gas density, k is the gas conductivity, and Nu is the heat transfer Nusselt number. Here, Nu is taken to be Nu = 8.32, the Nusselt number appropriate for fully developed laminar flow in an annular gap [7-43]. This value corresponds to the case with equal heat flux from the inner and outer walls into the gap. As discussed below, an order of magnitude result, not a precise value, is of interest here. For this Nusselt number, the above equation gives very small values for the time constant, e.g., $t_h = 5.5 \times 10^{-7}$ s at 1180°K. This value for t_h implies nearly instantaneous equilibration between the heat sinks and the gas passing through the annular gap. However, it also indicates that the timesteps required for stability in the CONTAIN calculation would be much less than the code was designed for. Therefore in the CONTAIN results discussed below, Nu was taken to be 1,000 times smaller (Nu = 0.00832), a value that allows reasonable calculation times but still demonstrates the isothermal nature of the blowdown at late time.

Along with the heating time constant, the time constant t_m for equilibration of volatile fission product concentrations in the gap is also needed. From the heat and mass transfer analogy [7-44], this time constant is given by

$$t_m = \frac{D_H^2}{4 Nu\, D_f}$$

where D_f is the diffusivity of the fission product in helium. One can estimate this time constant from kinetic theory. For I_2, for example, at 1180°K and a total pressure of 20 atm, one obtains $t_m = 2.9 \times 10^{-6}$ s, which is also a very short time.

In the CONTAIN calculation, flow between cells was assumed to be governed by a combination of laminar and turbulent losses of the form

$$\Delta P = K \upsilon W + C_{FC} \frac{W^2}{\rho A^2}$$

where ν is the gas kinematic viscosity, K is the laminar loss coefficient (m^{-3}), W is the mass flow rate, C_{FC} is the CONTAIN turbulent loss coefficient, and A is the flow area. To determine K, the effective hydraulic diameter D_H for the annular gap was used. From the standard expression for

laminar flow, this corresponds to a coefficient K equal to 4.07×10^{16} L, where L is in meters. In the CONTAIN model, the laminar loss along the rod was allocated to the flow junctions so that one-half of the laminar loss within a cell was assigned to each junction involving that cell. The flow junction characteristics are summarized in Table 7.17.

Table 7.17 Flow Junction Characteristics in the CONTAIN Model

Junction	Cells 1-2	Cells 2-3	Cells 3-4	Cells 4-5	Cells 5-6	Cells 4-7
Flow Area (cm^2)	0.0198	0.00632	0.00632	0.00632	0.00632	0.02
K (m^{-3})	1.63×10^{15}	4.07×10^{15}	2.44×10^{15}	8.14×10^{14}	2.13×10^{15}	0
C_{FC}	1.35	0	0	0	0	1.35

7.3.4.3.2 CONTAIN Calculation Results

Figures 7.7 and 7.8 present the CONTAIN predictions for the HBU-7 rod burst rupture test. Figure 7.7 gives the pressures in the cells along the principal blowdown path, starting with Cell 1 (the reservoir) and ending with the bulge region (Cell 4) where the rod failure occurred. This figure indicates that the bulge region depressurizes on a very short time scale. The reservoir, on the other hand, blows down on a much longer time scale. There is reasonable agreement between the measured depressurization rate and the CONTAIN prediction. Note that somewhat higher experimental depressurization rate may be the result of clad swelling effects, which would lead to a larger D_H than was deduced from the steady-state experiments. Figure 7.8 indicates that gas initially in the bulge cools rapidly due to adiabatic expansions. However, as gas from the rest of the system refills the bulge, there is a rapid temperature rise, and after the initial transient, the blowdown is essentially isothermal. The gas velocity in the flow junction between Cells 3 and 4, based on the gap flow area from the steady-state experiments, is also shown in Figure 7.8. The indicated velocities are consistent with an isothermal process, given the time constant for gas equilibration in the annular gap as discussed above.

Since the temperature behavior shown in Figure 7.8 corresponds to a Nusselt number that is three orders of magnitude smaller than it should be, there is ample margin to accommodate factors such as clad swelling that were ignored in this analysis. The discrepancy between the measured and calculated depressurization rates indicates that clad swelling could have been important. Because the laminar loss coefficient (which depends on D_H to the third power) is somewhat more sensitive to D_H than the time constant for equilibration (which depends on D_H squared), one can conclude that the effect on gap heat transfer would be at most comparable to that in the depressurization rate. The clad swelling would therefore not be large enough to change the essentially isothermal nature of the blowdown at late time.

These results suggest that the work done expanding the gases in the plenum region of the rod causes the gases in the plenum region to cool significantly. However, during transport of plenum gases through the gap region of the rod to the burst rupture location, heat transfer from cladding and fuel pellets to the gases flowing through the gap region heats these gases back to the temperatures near to the rod burst rupture temperature. Therefore, since the characteristic time

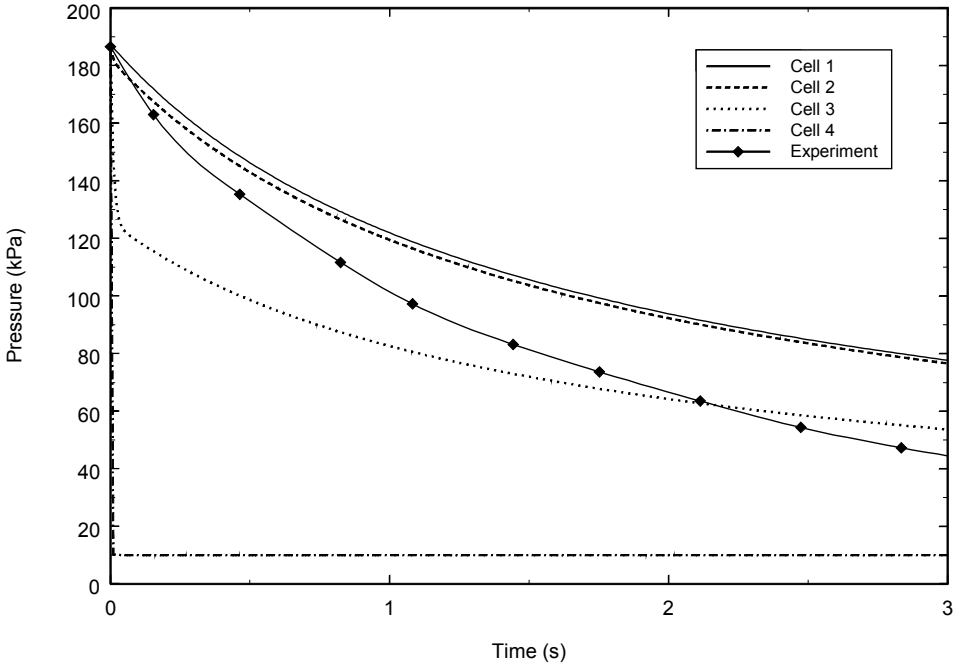

Figure 7.7 CONTAIN predictions for the pressures in the HBU-7 experiment.

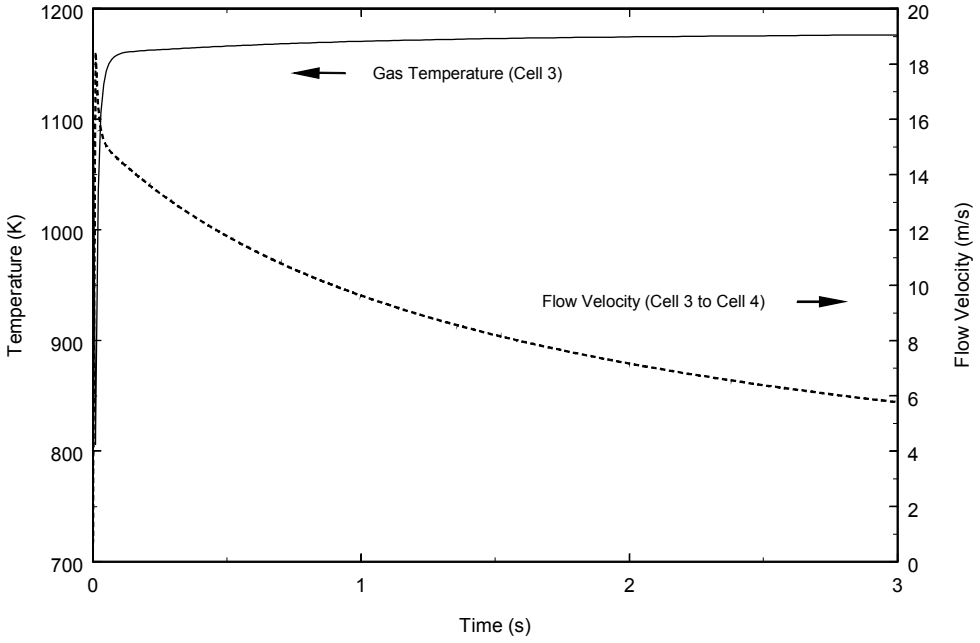

Figure 7.8 CONTAIN predictions for the temperature in Cell 3 and the flow velocity from Cell 3 to Cell 4.

for heat transfer to these gases during flow through the gap region is significantly shorter than the time required to flow through the gap region, when these gases reach the burst rupture location, they will again be saturated with Cs vapor species at the burst rupture temperature of the rod.

7.3.4.4 Burst Rupture Release Expressions for Vapors that Contain Cs

Release of a vapors that contain Cs from a failed spent fuel rod, when depressurization does not lead to significant cooling of the gases escaping from the rupture, should be determined by the vapor pressure of the Cs containing vapor at the temperature (T_b) of the rod at the time burst rupture occurs. For this case, the mass of elemental Cs released (M_R) is given by combining an experimental or theoretical expression for the vapor pressure of the Cs species (Log P = –a/T+b) with the ideal gas equation (PV = nRT) to obtain the following expression:

$$M_R = n_R MW = MW \frac{PV}{RT_b} = MW \frac{V_{rod}}{RT_b} 10^{-a/T_b + b} \tag{12}$$

where n_R is the moles of Cs vapors released, MW is the molecular weight of Cs (133 g mole^{-1}), P is the saturation vapor pressure of the Cs vapor at the rod burst rupture temperature T_b, V_{rod} is the free volume of the spent fuel rod, and R is the gas constant.

7.3.4.4.1 Cs Vapor Species

Condensible Cs vapors likely to exist in the free volume of a spent fuel rod (or rod section) at burst rupture temperatures were identified using the VICTORIA equilibrium thermodynamics code [7-45], which models chemical equilibrium between 288 chemical species. Of these 288 species, 27 were active during these VICTORIA calculations.

The initial molar abundances for active species were taken from the output of the ORIGEN calculation described in Section 7.2.3.2. In addition, all of the calculations assumed that:

- The spent fuel rod (or rod section) is moisture free.

  This assumption is consistent with manufacturing specifications which limit moisture in fuel pellets to 1 ppm by mass and moisture in rod gases to 115 ppm by volume[1].

- All cesium and iodine had migrated to the surfaces of the fuel pellets.

  This is a conservative assumption, because only a few percent of the cesium and iodine in a fuel pellet would be present on or would migrate to the surface of the pellet under transportation accident conditions. Moreover, the calculation of equilibrium is insensitive to the abundances of species on fuel surfaces as long as there are sufficient amounts of the equilibrating species to establish an equilibrium between species that exist in both the condensed and vapor phases.

1. Personal Communication, J. Clauss, 1998.

- All iodine is initially present as cesium iodide (CsI).
- Excess cesium not initially present as CsI is initially present as Cs_2UO_4.
- CsI and Cs_2UO_4 form an ideal solution.
- The gas phase (free volume of the rod) is initially pure helium.

Figure 7.9 shows the variation with temperature of the concentrations of Cs vapor species predicted by the VICTORIA code to exist in the rod free volume. The figure shows that the important cesium species are predicted to be Cs_2I_2, CsI, Cs, and Cs_2O. The figure also shows that at 750°C (1023°K), the likely burst rupture temperature of intact spent fuel rods, CsI(g) is the dominant Cs vapor.

Finally, to test the importance of the assumptions that the rod was dry and that Cs not initially present CsI is present as Cs_2UO_4, calculations were performed with $Cs_2U_2O_7$ as the initial dominant cesium species and with about 0.01 mole-percent steam in the gas phase. The net effect of these changes was to reduce the vapor pressures of Cs species.

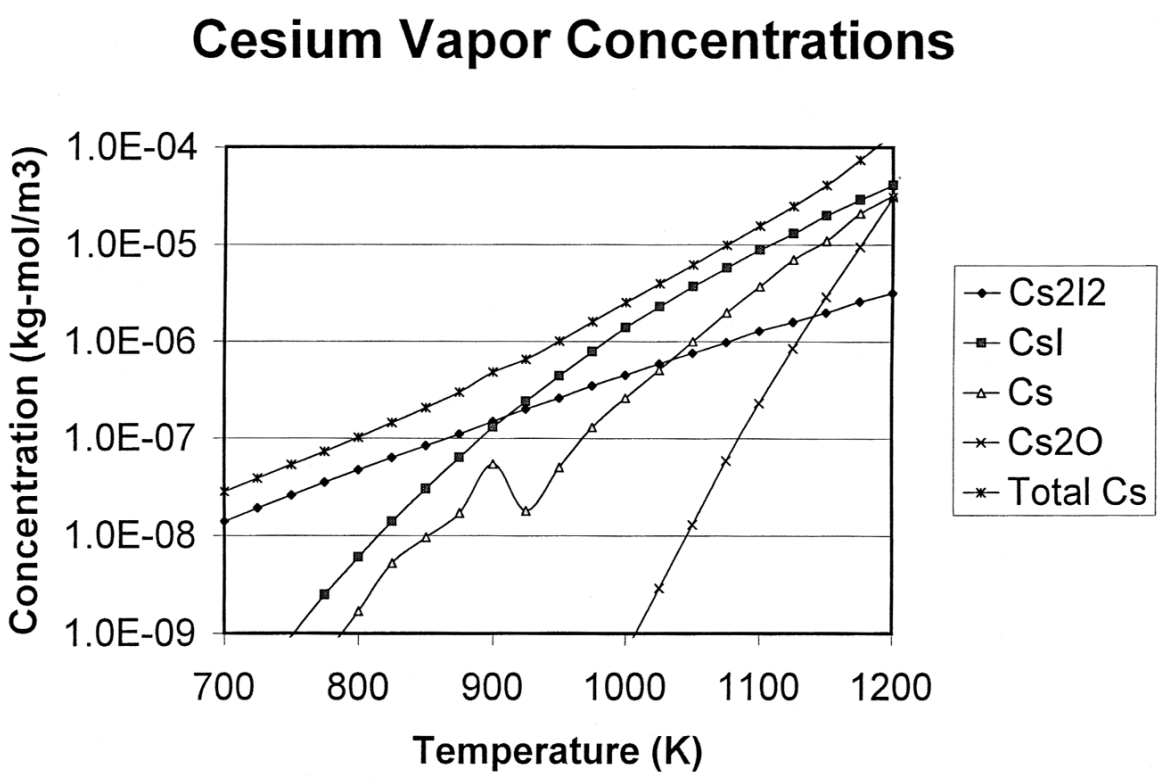

Figure 7.9 Variation with temperature of the concentrations of Cs vapor species predicted by the VICTORIA code.

7.3.4.4.2 Exponential Terms in Release Expressions

Because

$$F_{gap} M_{inventory} = M_{gap}$$

where M_{gap} is the mass of a radionuclide, for example Cs, on surfaces in the gap of the spent fuel rod or rod test section, Equation 10 can be rearranged to yield

$$M_{burst} = \alpha V_{burst} \left(\frac{M_{gap}}{A_{clad}} \right)^{0.8} \exp\left[-\left(C \diagup T \right) \right] \tag{13}$$

The experiments of Lorenz, et al. yielded a value of 7240 K^{-1} for C. Now, if the exponential term in this equation expresses the dependence of Cs vapors on temperature, then one might expect that C/2.303 = 7240/2.303 = 3144 K^{-1} to be similar in magnitude to the value of a for CsI(g) in Equation 12. But for CsI(g), a = 7960 K^{-1}. Thus, the value of C determined by Lorenz, et al. does not seem to be consistent with release of Cs principally as CsI(g). However, as the following derivation shows, the Lorenz value of C is quite consistent with the release of vapor forms of Cs that are comprised principally of CsI(g), provided release of Cs in particles is also considered.

As was stated above, Cs should be released both as a constituent of Cs containing vapors and also as a constituent of fuel fines blown out of the failed rod or rod section upon burst rupture. If Equation 13 is equated to the sum of a vapor release term and a particle release term, then the following equation results

$$\alpha V_{burst} \left(\frac{M_{gap}}{A_{clad}} \right)^{0.8} \exp\left[-\left(C \diagup T_b \right) \right] = MW \frac{V_{rod}}{RT_b} 10^{-a/T_b + b} + M_{inventory} F_{particles} \tag{14}$$

where $F_{particles}$ is the fraction of the mass of the fuel pellets in the rod or rod section that is released as fuel fines. But for the 900°C burst rupture tests conducted by Lorenz, et al. using sections of spent fuel rods, α = 3.49, V_{burst} = 97 cm^3, $V_{rod} = V_{test\ section}$ = 2.5 cm^3, M_{gap}/A_{clad} = 12.4 x 10^{-6} g, T_b = 1173°K, $M_{inventory}$ = 0.456 g Cs, and $F_{particles}$ = 2.4 x 10^{-4}; and for Cs, MW = 133 g, and, when P is expressed in MPa, R = 8.2 cm^3 MPa K^{-1} $mole^{-1}$, a = 7960 K^{-1}, and b = 4.18. Substitution of these values into Equation 14 followed by solving for C now yields a value of 6250 K^{-1} for C, which agrees quite well with the value determined experimentally by Lorenz, et al., which suggests that Cs release at temperatures like those examined by Lorenz, et al. (700 to 900°C) can be treated as the sum of a term for release of vapors that contain Cs, principally CsI(g), and a term for release of fuel fines that contain Cs atoms. Accordingly, division of the right hand side of Equation 14 by $M_{inventory}$ yields a phenomenologically reasonable expression for the rod-to-cask release fraction for Cs that is consistent with the experimental results of Lorenz, et al. Therefore, for Cs

$$F_{RC} = \frac{MW}{M_{inventory}} \frac{V_{rod}}{RT_b} 10^{-a/T_b + b} + F_{particles} \quad (15)$$

A maximum value for F_{RC} for Cs can be calculated by substituting values of a and b for CsI(g) into this expression and using the values for $F_{particles}$ calculated above for impact and non-impact events. Accordingly, because MW_{Cs} = 133 g mole^{-1}, V_{rod} = 30 cm^3, $M_{Cs,rod}$ = 8.0 g, T_b = 1023°K, $F_{particles} = 4 \times 10^{-7}$ and 3×10^{-5} respectively, for non-impact and impact events, and for CsI(g) a = 7960 K^{-1} and b = 4.18 when P is in MPa, $F_{RC} = 1.5 \times 10^{-5} + 4 \times 10^{-7} = 1.5 \times 10^{-5}$ for fire-only events and $1.5 \times 10^{-5} + 3 \times 10^{-5} = 4.5 \times 10^{-5}$ for impact events that initiate fires. As a check, if the CONTAIN result for the molar concentration of Cs in Cs vapors (e.g., CsI, Cs, Cs_2O, and Cs_2I_2) in the free volume of a PWR fuel rod at T = 1025°K is used to calculate F_{RC}, then for non-impact and impact events, respectively, $F_{RC} = 1.3 \times 10^{-5}$ and 4.3×10^{-5}. Therefore, to be slightly conservative, use of $F_{RC} = 2 \times 10^{-5}$ for fire-only events and 5×10^{-5} for impact events that initiate hot, engulfing, optically dense, long-duration fires seems appropriate. Finally, to ensure that these release fractions for cesium vapors are somewhat conservative, for fire scenarios that heat the cask to rod burst rupture temperatures, no credit is taken for deposition of cesium vapors onto cool cask surfaces (say at the ends of the cask), and for collision scenarios that initiate fires, revaporization of cesium from particles that deposited onto cask interior surfaces following release to the cask due to impact failure of rods is modeled whenever cask internal temperatures equal or exceed rod burst rupture temperatures.

7.3.5 Release Following Fuel Oxidation

Lorenz, et al. found [7-46] that the diffusive release of Cs, I, and Ru at 700°C was increased respectively by factors of 54.6, 22.4, and 2.02×10^4 during tests that lasted 5 hours, when the experimental atmosphere was dry air (test HBU-6) rather than steam (test HBU-1). Increased release of Cs and I was attributed to the substantial increase in UO_2 surface area that accompanies the oxidation of UO_2 to UO_{2+x} when UO_2 is exposed to air while at elevated temperatures. Increased release of Ru was attributed to the oxidation of non-volatile asymmetric RuO_2 to volatile symmetric RuO_4.

Assume that release of Cs and Ru from the test segment is complete (release fraction = 1.0) for that region of the test segment that is subject to extensive fuel oxidation. Let $F_{diffusion}$ be the release fraction per hour for Cs or Ru caused by diffusive release in a steam atmosphere, $F_{oxidized}$ be the release fraction per hour for Cs or Ru caused by extensive oxidation of a portion of the test segment, and $R_{air/steam}$ be the ratio of the total release fraction from the test segment per hour in air to that in steam. Then,

$$\frac{F_{oxidized} + F_{diffusion}}{F_{diffusion}} = \frac{F_{oxidized}}{F_{diffusion}} + 1 = R_{air/steam} \quad (16)$$

The diffusive release fractions for Cs and Ru in steam were found by Lorenz, et al. [7-47] to have the following experimental values for test HBU-1: 2.62×10^{-7} for Cs and 3.6×10^{-10} for Ru. Substitution of values for $F_{diffusion}$ and $R_{air/steam}$ into Equation 16 allows the following values to be calculated for $F_{oxidized}$: 1.40×10^{-5} for Cs and 7.27×10^{-6} for Ru. Now, given the precision of the

experimental data, these two values are essentially the same, which suggests that the enhanced release of Cs and Ru does occur from the same volume, the volume of the fuel which is extensively oxidized as a result of the exposure to air while at elevated temperatures, and that release of volatile species from this small volume of fuel that becomes extensively oxidized is essentially complete. Now, because $F_{oxidized}$ is referenced to the total volume of the test segment (V_T) rather than to the portion of the test segment that is extensively oxidized due to exposure to air while at elevated temperatures ($V_{oxidized}$),

$$F_{oxidized} V_T = 1.0 V_{oxidized} \tag{17}$$

Because the test segment has a length of 12 inches and the fuel pellets that occupy that length have a diameter of 9.32 mm, the total volume of the test segment (V_T) is 2.08×10^4 mm^3. Therefore, use of the larger value for $F_{oxidized}$, the value for Cs, yields $V_{oxidized} = 0.29$ mm^3. Now, assume that the enhanced release of Cs and Ru occurs from a disc of oxidized fuel that lies just under the hole predrilled in the cladding of the test segment used in test HBU-6, the test that measured diffusive release in air at 700°C through a predrilled hole with a diameter of 1.6 mm. Thus, if the diameter of the disc is $2d_{oxidized} + d_{hole}$, then

$$V_{oxidized} = \pi \left[\left(2d_{oxidized} + d_{hole} \right) / 2 \right]^2 d_{oxidized} \tag{18}$$

whereupon substitution of 1.6 mm for d_{hole} and 0.29 mm^3 for $V_{oxidized}$ gives $d_{oxidized} = 0.11$ mm and $d_{oxidized} + d_{hole} = d_{disc} = 1.71$ mm. Since the rate of weight gain by UO_2 powder, when oxidized by exposure to low partial pressures of oxygen ($p_{O_2} = 1$ mm) at 500 or 1000°C, is 0.3 mg min^{-1} [7-48], oxidation of the amount of UO_2 in a disc of sintered UO_2 powder having a diameter of 1.61 mm and thickness of 0.11 mm should occur in less than a minute, provided that diffusion of oxygen into the surface layer of a sintered UO_2 pellet isn't extremely slow. Accordingly, oxidation of a disc of sintered UO_2 with dimensions similar to those considered here, and also of all of the Ru in that disc, seems quite reasonable if the disc is exposed to oxygen for several hours while at elevated temperatures (500 to 1000°C).

Fuel pellet surfaces can be exposed to an oxidizing agent (oxygen or carbon dioxide) while at elevated temperatures only during accidents that involve fires. For Category 5 and Fire-only accidents, air can enter the cask through the single cask leakage path only after the fire dies out and cask cooling causes air to flow into the cask. Because cooling will cause any fission product vapors (e.g., CsI or RuO_4) to condense onto cask interior surfaces before they can diffuse out of the cask to the atmosphere, oxidation of fuel during accidents that fall into either of these fire accident categories is not of concern. However, fuel oxidation during Category 6 accidents is of concern because these accidents by definition lead to double failures of the cask. Because of the double failure, differential heating of the cask could induce a buoyant flow of gases through the cask. While the fire is burning, the gases flowing through the cask would be combustion gases, which should contain little molecular oxygen. After the fire dies out, the gas flow would be air. Because fuel cladding is a getter and UO_2 is more easily oxidized the RuO_2, oxidation of Ru and RuO_2 to RuO_4 will not be significant until all of the cladding and all of the UO_2 near the burst rupture hole in the cladding has been oxidized. Nevertheless, because hydrocarbon fuel fires with durations of several hours may occur, if the collision that initiates these fires also causes a

double failure of the cask, then any sizeable buoyancy driven flow of combustion gases or air through the cask would be expected to significantly oxidize exposed spent fuel surfaces, which would substantially increase the release of fission products from these oxidized fuel regions. Finally, if combustion gases or air is flowing through the cask, any fission products released to the cask interior would be transported to the environment by the gases that are flowing through the cask with little deposition onto cask interior surfaces.

By definition, Category 6 accidents fail all of the rods in the cask. The finite element cask impact calculations described in Section 5.1.4 show (see Figure 5.6) that severe impacts onto hard surfaces cause substantial slumping of the materials carried in the cask, that is, slumping of the fuel baskets and the rods they contain. Severe slumping means that most of the rods in the cask will be subjected to significant bending. Rod failure mechanisms due to rod bending have been discussed by Sanders, et al., who identified three failure modes, transverse tearing, longitudinal tearing, and rod breakage [7-49]. Assume that tearing of clad produces a crack with a width (w_{crack}) of 1 mm and a length equal to half the circumference of the rod. Then, since typical PWR and BWR rods have inside diameters respectively of about 0.9 and 1.2 cm [7-50], typical cladding tears will expose about 15 mm^2 of pellet surface area to the cask atmosphere, where 15 $mm^2 = \pi d_{pellet} w_{crack}/2 = \pi(10\ mm)(1\ mm)/2$. By comparison, a full rod break will expose at least the ends of two fuel pellets to the cask atmosphere (more if pellets spill from the broken rod) and thus at least 160 $mm^2 = 2\pi(d_{pellet}/2)^2$ of pellet surface area. So, rod breakage will expose much more pellet surface area to the cask atmosphere than will be exposed by a single cladding tear.

In typical spent fuel baskets, the PWR and BWR rods carried in the baskets are supported by six or seven spacers. Thus, the rods will have seven or eight regions between spacers that might undergo bending during a severe accident. Since all of the unsupported portions of a single rod will not undergo the same amount of bending and different rods will be bent in different ways, most rods will fail by cracking or tearing, usually at a single location, some rods may fail by cracking or tearing at more than one location, and a few rods may experience full circumferential breaks. Here, it is assumed that the average set of failures per rod exposes an amount of pellet surface equal to three times the cross-sectional area of a fuel pellet, which is equivalent to assuming that each rod suffers three full rod breaks. But Equation 17 shows that $F_{oxidized} = V_{oxidized}/V_T$. So if rod failure exposes on average an amount of pellet surface equal to six pellet ends, then $V_{oxidized} = 6\pi(d_{pellet}/2)^2 d_{oxidized}$ and $V_T = \pi(d_{pellet}/2)^2 L_{active}$, where L_{active} is the total length of the all of the pellets in the fuel rod (the active length of the rod), typical values of L_{active} for PWRs and BWRs are 3.6 and 3.0 m, respectively [7-50], and $d_{oxidized} = 0.11(2/5) = 0.044$ mm when fuel oxidation occurs over a two-hour rather than a five-hour time period. Therefore, a maximum value for $F_{oxidized}$ for a full spent fuel rod subject to multiple breaks and exposed to air for about two hours is

$$F_{oxidized} = \frac{V_{oxidized}}{V_T} = \frac{6\pi(d_{pellet}/2)^2 d_{oxidized}}{\pi(d_{pellet}/2)^2 L_{active}} = \frac{6 d_{oxidized}}{L_{active}} = \frac{6(0.044\,mm)}{3\times10^3\,mm} = 8.8\times10^{-5}$$

and, given the approximate nature of this analysis, rounding up to the next order of magnitude is appropriate. Therefore, $F_{oxidized} = 10^{-4}$ and thus for Category 6 accidents $F_{RC,6} = F_{RC,5} + F_{oxidized}$

which means that for Cs $F_{RC,6} = 5 \times 10^{-5} + 10^{-4} = 1.5 \times 10^{-4}$, and for particles $F_{RC,6} = 3 \times 10^{-5} + 10^{-4} = 1.3 \times 10^{-4}$.

7.3.6 CRUD

The formation of radioactive deposits called CRUD on the surfaces of spent fuel rods and the release to the cask interior by spallation of these materials during transportation in a spent fuel cask has been critically reviewed by Sandoval, et al. [7-17]. Sandoval, et al. state that "CRUD is a mixture of reactor primary cooling system corrosion products that have deposited on fuel rod surfaces," that the "deposits contain neutron-activated nuclides," and that during transport in a spent fuel cask portions of the deposits "may spall from the rods, become airborne in the cask cavity, and be released to the environment should a leak develop in the cask…." During routine (accident free) transportation of spent fuel, CRUD spallation from rod surfaces is principally caused by vibration of the rods. However, should an accident occur during the course of the trip, the mechanical loads experienced by the rods during the accident might cause large fractions of the CRUD on the rods to spall from the rod surfaces forming flakes and particles, some of which would become gasborne in the cask interior. To develop an expression for $ST_{CRUD,i}$, the contribution of radionuclide i in CRUD to a transportation accident source term, let $I_{CRUD,i}$ be the inventory of radionuclide i in all of the CRUD on all of the spent fuel rods in the spent fuel transportation cask, $F_{CRUD,RCi}$ be the fraction of the CRUD on an average rod that spalls from the rod surface during an accident to form particles that become gasborne in the cask interior, and F_{CEi} be the fraction of the gasborne CRUD particles that is transported from the cask interior to the environment through the cask leak. Then, $ST_{CRUD,i} = I_{CRUD,i}F_{CRUD,RCi}F_{CEi}$.

Sandoval, et al. measured surface concentrations of radionuclides in CRUD on rod surfaces upon discharge from the reactor [7-51]. They found that the following radionuclides accounted for most of the radioactivity at the time of fuel discharge: ^{58}Co, ^{60}Co, ^{54}Mn, ^{51}Cr, ^{59}Fe, ^{95}Zr, ^{125}Sb and ^{65}Zn. However, because all of these radionuclides except ^{60}Co decay rapidly, after storage for 5 years, ^{60}Co accounts for 92 percent of the radioactivity in CRUD on PWR rods and 98 percent on BWR rods. The measurements also showed that maximum ^{60}Co activity densities at discharge ranged from 2 to 140 μCi/cm^2 on rods from U.S. PWRs and from 11 to 595 μCi/cm^2 on rods from U.S. BWRs. Now given that PWR and BWR spent fuel rods have total surfaces areas of approximately 1200 and 1600 cm^2, respectively [7-50], maximum ^{60}Co CRUD inventories per rod are respectively about 2×10^5 μCi = (1200 cm^2)(140 μCi/cm^2) for PWRs and 1×10^6 μCi = (1600 cm^2)(595 μCi/cm^2) for BWRs. Finally, multiplication of these maximum ^{60}Co inventories per rod by the number of rods per cask will yield maximum values for ^{60}Co for $I_{CRUD,i}$.

Scanning Electron Microscopic examination of CRUD shows [7-52] that CRUD deposits are not solid films but instead consist of agglomerates comprised of irregularly shaped particles with diameters that range from approximately 0.1 to 10 μm. The agglomerates have a log-normal size distribution that has a number geometric mean diameter of 3.0 μm and a geometric standard deviation of 1.87. The CRUD layer has a density of 1.1 g cm^{-3} and a void fraction of 0.8. Thus, the density of the CRUD particles is about 5.5 g cm^{-3}, which means that the aerodynamic equivalent Geometric Mass Median Diameter of the particles is about 22.8 μm and the fraction of the mass of the CRUD layer that is in particles with sizes ≤ 10 μm is about 0.094.

Spallation of CRUD from spent fuel rods was reviewed by Sandoval, et al. [7-53]. That review found data for CRUD spallation (a) from rods exposed to flowing gases (air, nitrogen, argon) for long periods of time at ambient or moderately elevated temperatures (230°C), (b) from rods heated to elevated temperatures (300 to 450°C) for short time periods (0.5 to 2.0 hours), but no data for spallation of CRUD from rods subjected to impact loads. Heating of PWR and BWR rods to 230°C for 0.5 hours caused at least 5 to 6 percent of the CRUD on the rods to be removed by spallation and possibly 8 percent when experimental uncertainties are considered. Heating to 300°C for 0.5 hours, then to 400°C for 1.0 hour, and finally to 450°C for 2.0 hours was estimated to cause 12 to 15 percent of the CRUD on the rods to be removed by spallation.

The following equation gives the fraction $F_{respirable}$ of a brittle material that is converted to respirable particles upon impact onto a hard surface,

$$F_{respirable} = A\rho gh$$

where $A = 2 \times 10^{-11}$ $cm^3/g\ cm^2sec^{-2}$ is an empirical constant determined by impact tests on glass and ceramic specimens, ρ is the material (specimen) density, g is the acceleration due to gravity, and h is the fall-height [7-33]. But $mgh = 0.5m(v_{impact})^2$ where v_{impact} is the impact velocity of the specimen onto the hard surface. So $F_{respirable} = 0.5A\rho(v_{impact})^2$. Therefore, because the density of CRUD is 5.5 g/cm^3, if CRUD behaved like a brittle solid, it would have a spallation fraction for respirable particles of about 1.6×10^{-3} for a 120 mph impact onto a hard surface. Because CRUD spallation fractions when subjected to thermal loads are so much larger than this value, it seems likely that CRUD spallation fractions during collisions will also be much larger than 10^{-3}, probably similar to the values found for spallation due to thermal loads, and thus of order 10^{-1}. Therefore, since citation and key-word searches identified no additional CRUD spallation data other than that presented by Sandoval, et al., the following values were used for $F_{CRUD,RC}$, the CRUD spallation fraction: for fires not initiated by collisions, $F_{CRUD,RC} = 0.15$; for collisions that don't initiate fires, $F_{CRUD,RC} = 0.1$; and for collisions that lead to fires, $F_{CRUD,RC,impact} = 0.1$ and $F_{CRUD,RC,fire} = 0.05$.

7.3.7 Impact Failure of Spent Fuel Rods

In Section 5.4, estimates of the fraction of rods failed by end, corner, and side impacts onto an unyielding surface at four speeds, 30, 60, 90, and 120 mph, were developed for each of the four generic casks being examined by this study when each cask is carrying PWR or BWR fuel assemblies. Table 7.18 presents these fractions (expressed as percents), the average result for each impact orientation, and a weighted summation of these average results using as weights the expected frequencies of end (0.056), corner (0.722), and side (0.222) impacts that are defined below in Section 7.4.3.2.

Inspection of Table 7.18 shows that failure of all of the rods in a PWR assembly is predicted for 60 mph corner impacts onto an unyielding surface by steel-DU-steel truck casks and 60 mph end impacts onto an unyielding surface by monolithic steel rail casks. For BWR assemblies, failure of all of the rods is not predicted at 60 mph for any cask or impact orientation but is predicted for corner impacts at 90 mph onto an unyielding surface by steel-DU-steel truck casks. Nevertheless, because the finite element calculations show that slumping of cask internal

structures (i.e., the fuel assemblies being carried in the cask) is substantial for 90 mph impacts onto an unyielding surface, failure of all of the rods in PWR or BWR assemblies is assumed for any impact onto an unyielding surface by any cask at any orientation whenever the impact speed is ≥ 90 mph, and thus failure of all rods is also assumed for any impact onto a real yielding surface at a speed that is equivalent to a 90 mph impact onto an unyielding surface (i.e., for impacts onto any real yielding surface, $f_{rod,impact} = 1.0$ whenever $v_{cask} \geq v_{90}$ where v_{90} is the impact speed onto the real surface that is equivalent to a 90 mph impact onto an unyielding surface). For the speed ranges, v_{30} to v_{60} and v_{60} to v_{90}, $f_{rod,impact}$ is assumed to equal the midpoint value of the range of values given in Table 7.18. Thus, for PWR assemblies, $f_{rod,impact} = 0.25$ when $v_{30} \leq v_{cask} < v_{60}$, 0.59 when $v_{60} \leq v_{cask} < v_{90}$, and 1.0 when $v_{90} \leq v_{cask} < v_{120}$ or whenever $v_{cask} \geq v_{120}$. And for BWR assemblies, $f_{rod,impact} = 0.03$ when $v_{30} \leq v_{cask} < v_{60}$, 0.20 when $v_{60} \leq v_{cask} < v_{90}$, and 1.0 when $v_{90} \leq v_{cask} < v_{120}$ or whenever $v_{cask} \geq v_{120}$.

Table 7.18 PWR and BWR Rod Failure Fractions (percent) for Four Generic Casks

a. PWR Fuel Assembly

Cask	Impact Orientation	Impact Speed (mph)			
		30	60	90	120
Steel-Lead-Steel Truck	end	27	60	100	100
	corner	7	73	100	100
	side	0	0	13	27
Steel-DU-Steel Truck	end	27	33	60	87
	corner	13	100	100	100
	side	7	27	60	87
Steel-Lead-Steel Rail	end	13	60	100	100
	corner	0	13	33	100
	side	0	0	13	87
Monolithic Steel Rail	end	13	100	100	100
	corner	0	33	100	100
	side	0	13	33	73
All	end	20.0	63.3	90.0	96.8
	corner	5.0	54.8	83.3	100.0
	side	1.8	10.0	29.8	68.5
All	All	5.1	45.3	71.8	92.8

Table 7.18 PWR and BWR Rod Failure Fractions (percent) for Four Generic Casks (continued)

b. BWR Fuel Assembly

Cask	Impact Orientation	Impact Speed (mph)			
		30	60	90	120
Steel-Lead-Steel Truck	end	0	0	14	29
	corner	0	0	57	100
	side	0	0	0	0
Steel-DU-Steel Truck	end	0	0	0	0
	corner	0	29	100	100
	side	0	0	0	0
Steel-Lead-Steel Rail	end	0	0	14	43
	corner	0	0	0	43
	side	0	0	0	0
Monolithic Steel Rail	end	0	29	57	71
	corner	0	0	29	57
	side	0	0	0	0
All	end	0	7.3	21.3	35.8
	corner	0	7.3	46.5	75.0
	side	0	0.0	0.0	0.0
All	All	0	5.6	34.8	56.2

7.3.8 Fission Product Transport from the Cask Interior to the Environment

Transport of aerosols and fission product vapors, released to the interior of a Type B TN-125 cask, from the cask interior to the environment was modeled by Shaffer using the MELCOR code [7-30]. Figures 7.10 and 7.11 present results from this study for a collision scenario that does not initiate a fire.

Figure 7.10 compares the size distribution of the particles sourced into the cask from the spent fuel rods upon failure due to impact to the distribution of the particles that escape from the cask. The figure shows that for leak paths with cross-sectional areas of 4 and 100 mm^2, deposition processes largely deplete the source distribution of particles with diameters larger than 10 μm.

Figure 7.11 displays the dependence of cask-to-environment release fractions (F_{CE}) on the cross-sectional area of the seal leakage path that was calculated for a TN-125 cask, when the cask is pressurized to 5 atm by the failure of all of the rods in the cask during a high-speed collision and then depressurizes to atmospheric pressure (p_{atm}) at a rate determined by the seal leak area. Figure 7.11 shows that cask-to-environment release fractions (F_{CE}) increase as cask leak areas increase. This is to be expected since, after pressurization due to the failure of the fuel rods, cask depressurization times decrease as cask leak areas increase. Thus, a large leak area means a short depressurization time, little time for fission product deposition to cask interior surfaces, and

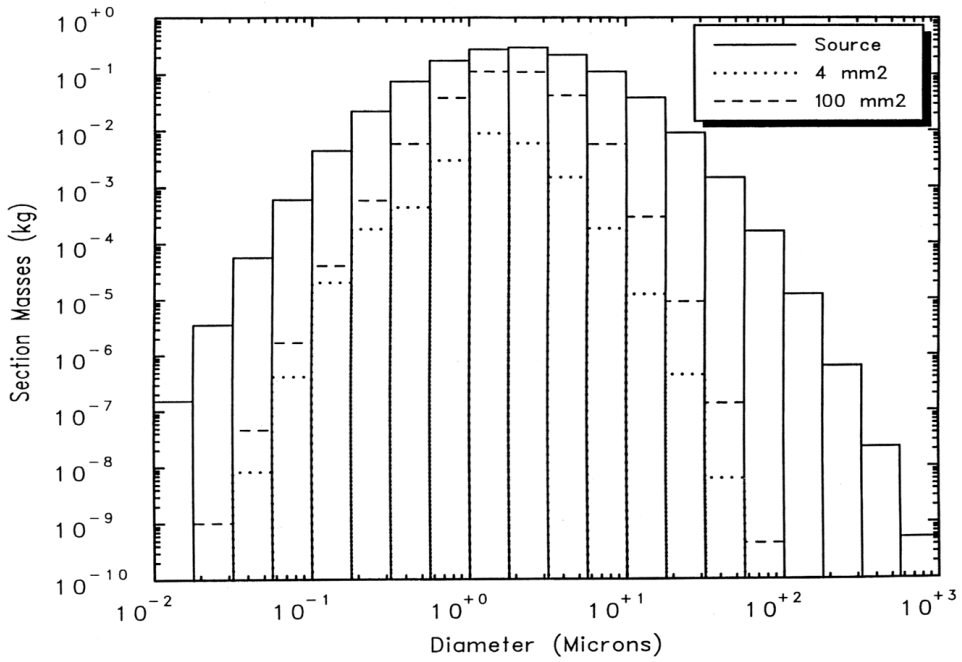

Figure 7.10 Size distributions of the particles sourced into the TN-12 cask from failed spent fuel rods, and of the particles that escaped from the cask through 4 and 100 mm^2 cask failures.

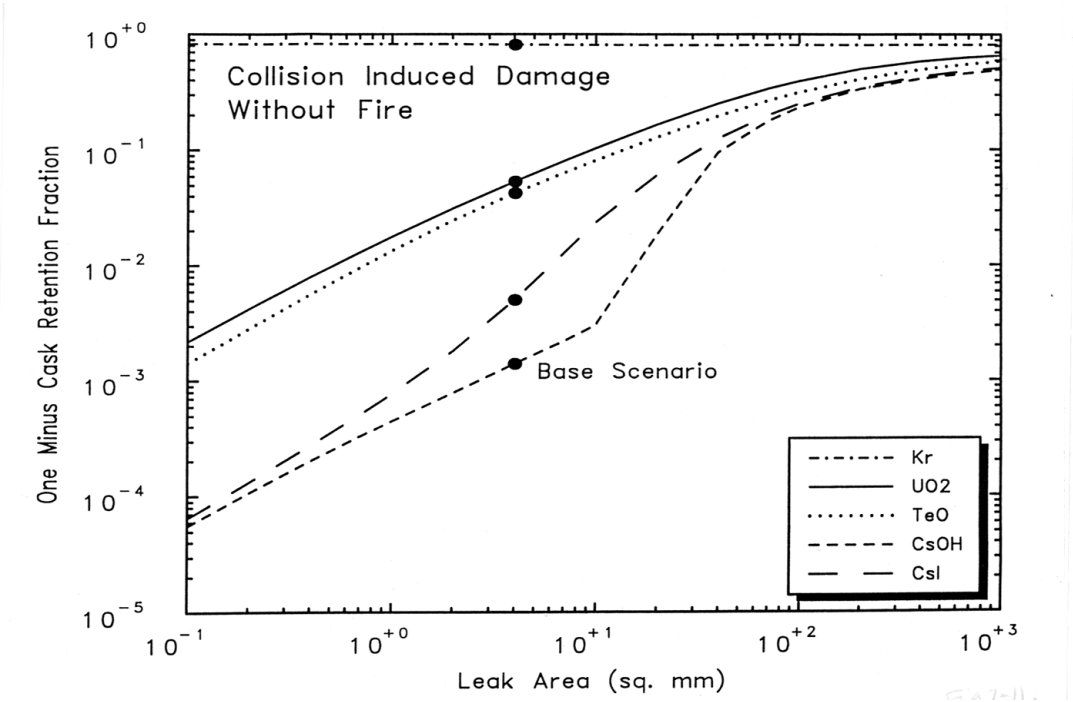

Figure 7.11 Dependence of Cask-to-Environment Release Fractions (1.0 – Retention Fraction) on the Size of the Cask Failure (leak area).

consequently large cask-to-environment release fractions. In Figure 7.11, the curve for TeO closely tracks the curve for fuel fines (i.e., UO_2), while the curves for CsI and CsOH, which exist partly as vapors at cask internal temperatures, diverge from the UO_2 curve as hole sizes decrease. The TeO curve tracks the UO_2 curve because TeO is released and transports as a constituent of particles. The CsI and CsOH curves diverge from the UO_2 curve as hole sizes decrease because, when hole sizes are small and there is significant time for deposition to occur, deposition onto cool interior cask surfaces of the small fraction of CsI and CsOH that is initially released as vapors is significantly more efficient than is deposition of CsI and CsOH that is released as a constituent of particles.

As was stated in Sections 7.2.5.1 and 7.2.5.2, leakage of elastomeric truck and train cask seals due to heating by fires to 350ºC and of elastomeric rail and truck cask seals due to cask impacts onto yielding surfaces at speeds equivalent respectively to 60 and 120 mph impacts onto an unyielding surface are assumed to produce 1 mm^2 leak areas. In Section 7.2.5.2, it was concluded that, when heated above 450ºC, elastomeric seals will fail catastrophically causing seal leak areas to be set by the space between the contacting surfaces of the cask lid and the cask lid well. In Section 5.1.4, the closure region distortions in rail casks produced by impacts onto an unyielding surface at speeds of 60, 90, and 120 mph were used to estimate the seal leak areas that these impacts would cause. Table 7.19 presents the estimates of rail cask seal leak areas developed by this analysis, the values selected for use in developing release fractions, and the values of the cask-to-environment release fractions for particles and CsI(g) that Figure 7.11 shows correspond to these leak areas.

Table 7.19 Seal Leak Areas and Values of F_{CE} for Rail Casks

Cask Impact		Leak Area (mm^2)			F_{CE}	
		Calculated Values		Analysis Values		
Speed	Orientation	Steel-Lead-Steel Cask	Monolithic Steel Cask	All Rail Casks	Particles	CsI(g)
60	Corner		0.18	1[a,b]	0.02	0.0008
90	Corner	346	256	300[c]	0.6	0.4
120	Corner	2046	1616	1800[d]	0.8	0.8
120	Side		9	10	0.2	0.06

a. Rounded to 1 mm^2 so as to be consistent with treatment of truck cask leak areas.
b. The oblong nature of seal leak cross sections and the log-normal character of particle size distributions means that leaks with areas significantly smaller than 1 mm^2 need not be considered. For example, an 0.1 mm^2 leak that is one bolt spacing (35 to 60 mm) long is only 1.5 to 3 μm wide and thus will not transmit significant quantities (by mass) of respirable particles (particles with diameters ≤ 10 μm).
c. Average of steel-lead-steel and monolithic steel rail cask results.
d. Scaled by a factor of six, the average of the ratios of calculated 120 and 90 mph results.

Let $f_{deposition}$ be the fraction of the particles or vapors, released to the interior of a RAM transport cask upon rod failure, that deposit onto cask interior surfaces before they can escape from the cask to the environment. This fraction is related to F_{CE} by the following equation:

$$F_{CE} = (1 - f_{deposition})(1 - p_{atm}/p_{Imp})$$

Since p_{atm} =1.0 and p_{Imp} = 5.0 for the TN-125 cask calculation, values for $f_{deposition}$ can be calculated for the rail cask leak areas presented in Table 7.19 by substitution of the values for F_{CE} that correspond to these leak areas. Then weighted summation of the resulting orientation-dependent leak areas using as weights the expected frequencies of end (0.056), corner (0.722), and side (0.222) impacts that are defined below in Section 7.4.3.2 yields the values for $f_{deposition}$ for the indicated speed ranges listed in Table 7.20.

Table 7.20 Values of $f_{deposition}$ for Rail Casks

Speed Range (mph)	$f_{deposition}$	
	Particles	CsI(g)
60 to 90	0.98	0.999
90 to 120	0.45	0.64
≥ 120	0.2	0.26

Finally, because elastomeric cask seal leakage caused by heating by a fire to 350ºC and elastomeric truck cask seal leakage caused by cask impacts at 120 mph and any orientation onto an unyielding surface are assumed to produce 1 mm^2 seal leak areas, for these seal leak, $f_{deposition}$ equals 0.98 for particles and 0.999 for CsI(g). However, no credit is taken for deposition of Cs vapor species during scenarios that involve fires that heat the cask to temperatures ≥ 750ºC. Thus, whenever release of Cs as a vapor (e.g., CsI) is significant, deposition of that vapor species onto cool cask interior surfaces is neglected (e.g., $f_{deposition,CsI} = 0.0$). Thus, Cs vapor deposition is treated when rod failure is caused by impact but not when it is caused by burst rupture.

7.3.9 Expansion Factor Values

Transport of radioactive species from the cask to the environment during depressurization of the cask or due to heating of cask gases by a fire was discussed in Sections 7.2.5.4 and 7.2.5.5. In Section 7.2.5.6, expansion factor expressions were derived that allowed the fraction of the cask gases that escape from the cask to the environment during cask depressurization or heating by a fire to be calculated. Table 7.21 presents the values of the parameters that enter each expansion factor and the value of the expansion factor produced by these parameter values. Values of p_{Imp} and p_b, which are respectively the pressure of the cask after some fraction of the rods in the cask are failed by impact and by burst rupture, are calculated using the following equations:

$$p_{Imp} = 1.0\,\text{atm} + 4.0\,\text{atm}\,(F_{rod,impact}) \quad \text{and} \quad p_b = 1.0\,\text{atm} + 4.0\,\text{atm}\,(1.0 - F_{rod,impact})$$

where 1.0 atm is the internal pressure of the cask during normal transport and 4.0 atm is the pressure rise produced by the failure of all of the rods in the cask. Thus, for example, p_{imp} = 3.36 atm = 1.0 + 4.0(0.59), when 59 percent of the rods in the cask fail upon impact and p_b = 4.20 atm = 1.0 + 4.0(1.0 − 0.20), when the 80 percent of the rods not failed by collision impact are later failed by burst rupture due to heating by an ensuing fire.

Table 7.21 Expansion Factor Values

Expansion Factor	$F_{rod,impact}$		Temperatures (K)				Pressures (atm)			Value
	PWR	BWR	T_a	T_s	T_b	T_f	p_{atm}	p_{Imp}	p_b	
$f_{e1} = (p_{atm}/p_{Imp})(T_a/T_s)$	1.00	1.00	573	623			1.0	5.00		0.184
	0.59		573	623			1.0	3.36		0.274
	0.25		573	623			1.0	2.00		0.460
		0.20	573	623			1.0	1.80		0.511
		0.03	573	623			1.0	1.12		0.821
$f_{e2} = (T_s/T_b)$		all		623	1023					0.609
$f_{e3} = (p_{atm}/p_{imp})(T_a/T_b)$	1.00	1.00	573		1023		1.0	5.00		0.112
	0.59		573		1023		1.0	3.36		0.167
	0.25		573		1023		1.0	2.00		0.280
		0.20	573		1023		1.0	1.80		0.311
		0.03	573		1023		1.0	1.12		0.500
$f_{e4} = (p_{atm}/p_b)(T_b/T_f)$	1.00	1.00			1023	1273	1.0		1.0	0.804
	0.59				1023	1273	1.0		2.64	0.304
	0.25				1023	1273	1.0		4.00	0.201
		0.20			1023	1273	1.0		4.20	0.191
		0.03			1023	1273	1.0		4.88	0.165
	0.0	0.0			1023	1273	1.0		5.00	0.161
$f_{e5} = (p_{atm}/p_{imp})$	1.00	1.00					1.0	5.00		0.200
	0.59						1.0	3.36		0.298
	0.25						1.0	2.00		0.500
		0.20					1.0	1.80		0.556
		0.03					1.0	1.12		0.893

7.4 Values for Severity Fraction Parameters

7.4.1 Introduction

Severity fraction expressions were formulated in Section 7.2.8. In this section, values are developed first for the parameters that enter those expressions and then for the severity fractions themselves by substitution of the parameter values into the individual severity fraction expressions.

7.4.2 Cask Involvement

When a spent fuel cask is transported by truck, the truck is always a tractor semi-trailer. Trucks that haul more than one trailer are never used. Therefore, for truck accidents, $P_{cask} = 1.0$, because the vehicle that is carrying the cask, the tractor semi-trailer, is always involved in the accident.

Train accident data for 1972 were reviewed by Clarke, et al. [7-54] who found that freight trains typically contain about 66 cars, that on average 10 cars are involved in side or raking collisions, and that the number of cars involved in derailment accidents is speed dependent. For derailment accidents, Clarke, et al. determined the average number of cars derailed during derailment accidents that had derailment speeds that fell into the following four speed ranges: 0 to 10, 10 to 30, 30 to 60, and 60 to 80 mph. Now because the Modal Study [7-55] developed a cumulative distribution of derailment accident speeds, the chance that a derailment accident occurs at a speed

that falls within each of these four speed ranges can be calculated. Table 7.22 presents, for each derailment accident speed range, the probability of occurrence of derailment accidents with derailment speeds that fall in each speed range and the average number of cars derailed during those accidents.

Table 7.22 Probability of Occurrence and Average Number of Cars Derailed for Train Derailment Accidents by Accident Speed Range

Speed Range (mph)	0 to 10	10 to 30	30 to 60	30 to 60
Probability of Occurrence	0.402	0.4079	0.1829	0.0050
Average Number of Cars Derailed	5	6	11	17

If the derailment data of Clarke, et al. is weighted using the cumulative speed distribution data for derailment accidents presented in the Modal Study [7-55], the following weighted summation results:

$$N_{cars/derailment} = \sum_i W_i N_i = 5(0.402) + 6(0.4079) + 11(0.1829) + 17(0.0050) = 6.6$$

where the four speed ranges are respectively 0 to 10, 10 to 30, 30 to 60, and 60 to 80 mph. Thus, about six or seven cars will derail during a typical derailment accident. But derailment accidents that occur at speeds < 30 mph will fail neither the cask seal nor any of the spent fuel rods being carried in the cask. So if these accidents are ignored, construction of a weighted sum for the speed ranges 30 to 60 and 60 to 80 mph shows that the average number of cars involved in derailment accidents of concern is

$$N_{cars/derailment} = \sum_i W_i N_i = 11(0.9734) + 17(0.0266) = 11.2$$

Therefore, because the average number of cars involved in side and raking collisions is usually about ten and the average number of cars involved in derailment accidents that occur with speeds ≥ 30 mph is about 11, 0.17 = 11/66 is a reasonable estimate for P_{cask} for train accidents.

7.4.3 Values for Collision Conditional Probabilities

Truck and train accident scenarios were discussed in Section 7.1. That section presented event trees that depicted possible accident scenarios, where a specific scenario is a unique path on the tree. Inspection of the truck and rail event trees depicted in Figures 7.3 and 7.4 shows that each tree lists the conditional probabilities of occurrence of each scenario (path) on the tree, identifies the scenarios that may lead to cask failure (the paths marked with an asterisk), and for collision scenarios specifies an associated accident speed distribution and an impact surface. Accordingly, the value of the conditional probability of truck or train accident scenario j, $P_{scenario,j}$ is read from the appropriate event tree.

7.4.3.1 Accident Velocity Probabilities

For collision accidents, $P_{speed,j}(v_{30},v_{60})$, $P_{speed,j}(v_{60},v_{90})$, $P_{speed,j}(v_{90},v_{120})$, and $P_{speed,j}(\geq v_{120})$ are calculated using the following equations:

$$P_{speed,j}(v_{30},v_{60}) = \sum_{m=1}^{3} P_{orientation,m}\left[P_{speed,jm}(v_{60}) - P_{speed,jm}(v_{30})\right]$$

$$P_{speed,j}(v_{60},v_{90}) = \sum_{m=1}^{3} P_{orientation,m}\left[P_{speed,jm}(v_{90}) - P_{speed,jm}(v_{60})\right]$$

$$P_{speed,j}(v_{90},v_{120}) = \sum_{m=1}^{3} P_{orientation,m}\left[P_{speed,jm}(v_{120}) - P_{speed,jm}(v_{90})\right]$$

$$P_{speed,j}(\geq v_{120}) = \sum_{m=1}^{3} P_{orientation,m}\left[1.0 - P_{speed,jm}(v_{120})\right]$$

where v_{30}, v_{60}, v_{90}, and v_{120} are the impact speeds for end, corner, or side impact orientations onto real yielding surfaces that would cause the same damage to the cask and its contents (spent fuel) as is predicted respectively for end, corner, and side impacts at speeds of 30, 60, 90, and 120 mph onto an unyielding surface; v_{30}, v_{60}, v_{90}, and v_{120} have different values for each cask/surface combination; $P_{orientation,m}$ is the probability that the cask impact is an end, corner, or side impact; and $P_{speed,jm}(v_{30})$, $P_{speed,jm}(v_{60})$, $P_{speed,jm}(v_{90})$, and $P_{speed,jm}(v_{120})$ are respectively the cumulative probabilities for impact orientation m and accident scenario j that the cask impact speed v is $\leq v_{30}$, $\leq v_{60}$, $\leq v_{90}$, and $\leq v_{120}$.

In Section 5.1, cask-specific values for the impact velocities, v_{30}, v_{60}, v_{90}, and v_{120}, were determined by finite element analyses for impacts onto an unyielding surface for each of the four generic casks being examined by this study. In Section 5.2, these unyielding surface impact velocities were extrapolated to yielding surfaces by partitioning the impact energy between the cask and the yielding surface. Table 7.23 presents the cask specific real surface impact velocities determined by those analyses.

7.4.3.2 Cask Impact Orientation Probabilities

The finite element cask impact calculations described in Section 5 examined three cask impact orientations, side, corner, and end, where the cask impact orientation is specified by the angle between the cask axis and the plane of the impact surface. By definition, side impacts have impact angles between 0 and 20 degrees, corner impacts have impact angles between 20 and 85 degrees, and end impacts have angles between 85 and 90 degrees. Thus, for example, a cask must strike an impact surface nearly end-on for the impact orientation to be classed as an end impact. Now, although the probability of occurrence of each of these impact orientations is

Table 7.23 Impact Speeds (mph) onto Real Yielding Surfaces that are Equivalent to 30, 60, 90, and 120 mph Impacts onto an Unyielding Surface

a. Type B Steel-Lead-Steel Spent Fuel Truck Cask

Impact Surface	Impact Orientation	Impact Speed			
		v_{30}	v_{60}	v_{90}	v_{120}
Hard Rock	End	30	60	90	120
	Corner	30	60	90	120
	Side	30	60	90	120
Soft Rock/Hard Soil/Concrete (slab, column, abutment)	End	38*	177	232	273
	Corner	35*	123	172	245
	Side	32*	86	135	209
Clay/Silt	End	84*	>277	>367	>448
	Corner	58*	>135	>195	>279
	Side	32*	>170	>273	>426
Railbed/Roadbed	End	38*	277	367	448
	Corner	35*	135	195	279
	Side	32*	170	273	426
Water	End	78*	∞	∞	∞
	Corner	150*	∞	∞	∞
	Side	42*	∞	∞	∞

* From the Modal Study, driven by impact limiter response, rather than cask response.

b. Type B Steel-DU-Steel Spent Fuel Truck Cask

Impact Surface	Impact Orientation	Impact Speed			
		v_{30}	v_{60}	v_{90}	v_{120}
Hard Rock	End	30	60	90	120
	Corner	30	60	90	120
	Side	30	60	90	120
Soft Rock/Hard Soil/Concrete (slab, column, abutment)	End	38*	167	196	228
	Corner	35*	204	266	316
	Side	32*	142	210	303
Clay/Silt	End	84*	>253	>303	>360
	Corner	58*	>223	>298	>360
	Side	32*	>263	>394	>575
Railbed/Roadbed	End	38*	253	303	360
	Corner	35*	223	298	360
	Side	32*	263	394	575
Water	End	78*	∞	∞	∞
	Corner	150*	∞	∞	∞
	Side	42*	∞	∞	∞

* From the Modal Study, driven by impact limiter response, rather than cask response.

Table 7.23 Impact Speeds (mph) onto Real Yielding Surfaces that are Equivalent to 30, 60, 90, and 120 mph Impacts onto an Unyielding Surface (continued)

c. Type B Monolithic Spent Fuel Rail Cask

Impact Surface	Impact Orientation	Impact Speed			
		v_{30}	v_{60}	v_{90}	v_{120}
Hard Rock	End	30	60	90	120
	Corner	30	60	90	120
	Side	30	60	90	120
Soft Rock/Hard Soil/Concrete (slab, column, abutment)	End	38*	419	507	573
	Corner	35*	1129	1679	2171
	Side	32*	256	451	522
Clay/Silt	End	84*	>521	>632	>750
	Corner	58*	>218	>321	>418
	Side	32*	>230	>394	>505
Railbed/Roadbed	End	38*	521	632	750
	Corner	35*	218	321	418
	Side	32*	230	394	505
Water	End	78*	∞	∞	∞
	Corner	150*	∞	∞	∞
	Side	42*	∞	∞	∞

* From the Modal Study, driven by impact limiter response, rather than cask response.

Table 7.23 Impact Speeds (mph) onto Real Yielding Surfaces that are Equivalent to 30, 60, 90, and 120 mph Impacts onto an Unyielding Surface (continued)

d. Type B Steel-lead-steel Spent Fuel Rail Cask

Impact Surface	Impact Orientation	Impact Speed			
		v_{30}	v_{60}	v_{90}	v_{120}
Hard Rock	End	30	60	90	120
	Corner	30	60	90	120
	Side	30	60	90	120
Soft Rock/Hard Soil/Concrete (slab, column, abutment)	End	38*	319	391	509
	Corner	35*	640	990	>990
	Side	32*	207	289	>289
Clay/Silt	End	84*	>386	>480	>635
	Corner	58*	>133	>208	>223
	Side	32*	>180	>256	>262
Railbed/Roadbed	End	38*	386	480	635
	Corner	35*	133	208	>223
	Side	32*	180	256	>262
Water	End	78*	∞	∞	∞
	Corner	150*	∞	∞	∞
	Side	42*	∞	∞	∞

* From the Modal Study, driven by impact limiter response, rather than cask response.

likely to depend on accident scenario, because such scenario dependencies cannot be easily estimated, it is assumed that impacts at any angle are equally probable. Therefore, the probabilities of side, corner, and end impacts (values of $P_{orientation,m}$) are P_{side} = 20/90 = 0.222, P_{corner} = 65/90 = 0.722 and P_{end} = 5/90 = 0.056.

7.4.3.3 Modal Study Accident Velocity Distributions

The Modal Study developed eight cumulative velocity distributions for truck and train accidents, four truck accident and four train accident distributions. These distributions are presented in Tables 7.24 and 7.25. Values of $P_{speed,jm}$ were calculated by linear interpolation using the data presented in these tables.

The cumulative velocity distributions presented in Tables 7.24 and 7.25 are of three types: (1) a velocity distribution for accidents that occur on level ground, which means that the velocity at accident initiation of the cask and the truck or train is assumed to be the cask impact velocity, (2) a velocity distribution for accidents where the cask and the truck or train plunge off of a bridge and fall to the ground below and thus have an impact velocity that depends on the height of the bridge, and (3) a velocity distribution for accidents where the cask and the truck or train plunge down an embankment and then strike an object or a surface. As stated in the Modal Study, the velocity distributions for truck accidents on level ground (velocity distribution v1) reflect a reduction in velocity due to braking, the velocity distribution for train accidents that occur on level ground (velocity distribution Tv1) take no credit for braking, and the velocity distributions for accidents where the cask and the truck or train plunge down an embankment were developed by constructing the vector sum of the level ground and bridge height velocity distributions [7-56].

7.4.3.4 Puncture/Shear Probability

Collision accidents may generate sharp objects that could fail a cask by puncture or shearing of the cask shell. Puncture and shear failure data for rail tank cars was reviewed in Section 5.3. The review developed an estimate for the probability that a probe capable of causing puncture or shear failures of a Type B spent fuel cask will be both formed during a collision accident, will strike the cask in an orientation that might allow it to cause a cask failure, and will not break before it causes the failure. The review concluded that a sharp probe capable of failing a cask by puncture or shear might be formed during any collision accident, that probe formation would be possible at any accident speed, and that formation was most unlikely at any speed. Accordingly, although there are no data on the frequency of formation of very sharp very robust puncture/shear probes during truck or train accidents, because spent fuel casks have two 1 inch steel shells and only about 4 tank car puncture accidents in 100 lead to puncture of tank cars with 1 inch shells, it is assumed that $P_{puncture/shear} = 0.001 = (0.04)^2$ for all truck accidents and also for all train accidents except train pileup accidents during which the cask is struck by a train car coupler. For train pileup accidents, where the cask is struck by a coupler and therefore puncture or shear is more likely to occur, it is assumed that $P_{puncture/shear} = 0.01$.

Table 7.24 Truck Accident Velocity Distributions

v1 Initial Truck Velocity Adjusted for Braking		v2 Impact Velocity Based on Bridge Heights		v3 Vector Sum of First and Second Distributions		v4 Train Grade Crossing Accident Velocities	
Velocity (mph)	Cumulative Probability[a]	Velocity (mph)	Cumulative Probability[a]	Velocity (mph)	Cumulative Probability[a]	Velocity (mph)	Cumulative Probability[a]
0.0	0.0	0.0	0.0	0.0	0.0	0.0	0.0
2.0	0.03834	7.74	0.00621	5.0	0.0	2.0	0.06014
6.0	0.12916	10.94	0.01550	10.0	0.00141	6.0	0.17906
10.0	0.23508	15.48	0.04754	15.0	0.00821	10.0	0.29398
14.0	0.34886	18.95	0.1051	20.0	0.03387	14.0	0.40255
18.0	0.46237	21.89	0.1952	25.0	0.11129	18.0	0.50280
22.0	0.56877	24.47	0.3178	30.0	0.28292	22.0	0.59331
26.0	0.66345	26.81	0.4629	35.0	0.51279	26.0	0.67319
30.0	0.74353	28.95	0.6124	40.0	0.70110	30.0	0.74210
34.0	0.80877	30.95	0.7464	45.0	0.81951	34.0	0.80022
38.0	0.86020	32.83	0.8508	50.0	0.89168	38.0	0.84814
42.0	0.89961	34.61	0.9217	55.0	0.93543	42.0	0.88676
46.0	0.92881	36.29	0.9635	60.0	0.96178	46.0	0.91718
50.0	0.95009	37.91	0.9849	65.0	0.97751	50.0	0.94062
54.0	0.96547	39.46	0.9945	70.0	0.98680	54.0	0.95826
58.0	0.97634	41.67	0.9991	75.0	0.99227	58.0	0.97125
62.0	0.98383	43.08	0.9998	80.0	0.99547	62.0	0.98060
66.0	0.98908	44.45	0.9999	85.0	0.99766	66.0	0.98717
70.0	0.99261	56.86	1.0	90.0	0.99901	70.0	0.99169
74.0	0.99503			95.0	0.99961	74.0	0.99473
78.0	0.99670			100.0	0.99985	78.0	0.99672
82.0	0.99825			105.0	0.99995	82.0	0.99800
86.0	0.99910			110.0	0.99998	86.0	0.99881
90.0	0.99956			115.0	0.99999	90.0	0.99930
94.0	0.99979			150.0	1.0	94.0	0.99960
98.0	0.99990					98.0	0.99977
102.0	0.99995					102.0	0.99987
106.0	0.99998					106.0	0.99993
110.0	0.99999					110.0	0.99996
150.0	1.0					114.0	0.99998
						118.0	0.99999
						150.0	1.0

a. Probability that the accident or impact velocity is less than or equal to the listed velocity.

Table 7.25 Train Accident Velocity Distributions

Tv1 Collision Accident Train Velocities without Braking		Tv2 Derailment Accident Train Velocities without Braking		Tv3 Impact Velocity Based on Bridge Heights		Tv4 Vector Sum of Second and Third Distributions	
Velocity (mph)	Cumulative Probability[a]	Velocity (mph)	Cumulative Probability[a]	Velocity (mph)	Cumulative Probability[a]	Velocity (mph)	Cumulative Probability[a]
0.0	0.0	0.0	0.0	0.0	0.0	0.0	0.0
2.0	0.09385	2.0	0.07543	7.74	0.00621	5.0	0.0
6.0	0.26286	6.0	0.22036	10.94	0.01550	10.0	0.00232
10.0	0.40788	10.0	0.35480	15.48	0.04754	15.0	0.01244
14.0	0.53042	14.0	0.47634	18.95	0.1051	20.0	0.04814
18.0	0.63240	18.0	0.58341	21.89	0.1952	25.0	0.14919
22.0	0.71598	22.0	0.67534	24.47	0.3178	30.0	0.35837
26.0	0.78345	26.0	0.75225	26.81	0.4629	35.0	0.60624
30.0	0.83709	30.0	0.81495	28.95	0.6124	40.0	0.77834
34.0	0.87908	34.0	0.86477	30.95	0.7464	45.0	0.87230
38.0	0.91147	38.0	0.90385	32.83	0.8508	50.0	0.92649
42.0	0.93606	42.0	0.93246	34.61	0.9217	55.0	0.95855
46.0	0.95446	46.0	0.95386	36.29	0.9635	60.0	0.97727
50.0	0.96801	50.0	0.96920	37.91	0.9849	65.0	0.98792
54.0	0.97784	54.0	0.97991	39.46	0.9945	70.0	0.99379
58.0	0.98486	58.0	0.98720	41.67	0.9991	75.0	0.99692
62.0	0.98980	62.0	0.99204	43.08	0.9998	80.0	0.99852
66.0	0.99323	66.0	0.99516	44.45	0.9999	85.0	0.99932
70.0	0.99557	70.0	0.99713	56.86	1.0	90.0	0.99970
74.0	0.99714	74.0	0.99834			95.0	0.99987
78.0	0.99818	78.0	0.99906			100.0	0.99995
82.0	0.99886	82.0	0.99948			105.0	0.99998
86.0	0.99929	86.0	0.99972			110.0	0.99999
90.0	0.99957	90.0	0.99985			150.0	1.0
94.0	0.99974	94.0	0.99992				
98.0	0.99985	98.0	0.99996				
102.0	0.99991	102.0	0.99998				
106.0	0.99995	106.0	0.99999				
110.0	0.99997	150.0	1.0				
114.0	0.99998						
118.0	0.99999						
150.0	1.0						

a. Probability that the accident or impact velocity is less than or equal to the listed velocity.

7.4.4 Values for Fire Probabilities

For fires that are initiated by collisions, the probability that a fire of concern occurs is the product of the conditional probability that the collision scenario j initiates a fire, $P_{fire/scenario,j}$, and the fraction of these fires, $P_{severe\ fire,k}$, that are severe enough to cause the cask seal to leak and/or the spent fuel rods being transported in the cask k to fail. Of course, if the accident in question is a fire not initiated by a collision (a fire-only accident), then $P_{fire/scenario,j} = 1.0$.

Because of the large mass of Type B spent fuel transportation casks, only a hot, co-located, fully engulfing, optically dense, long-duration fire can heat one of these casks to temperatures where spent fuel rods being transported in the cask will fail by burst rupture. Therefore, the fraction of all fires that can cause thermal burst rupture of spent fuel rods (heat a cask to temperatures in the temperature range $T_b \leq T_{cask} \leq T_f$) is given by

$$P_{severe\ fire,k} = P_{co\text{-}located}\ P_{optically\ dense}\ P_{flame\ temp}\ P_{duration,k} \quad (9)$$

where $P_{co\text{-}located}$ is the probability that the cask and the fire are co-located (i.e., that the cask is not significantly offset from the fire), $P_{optically\ dense}$ is the probability that the fire diameter is large enough to make the fire optically dense to loss of energy from the cask to the atmosphere (i.e., the fire diameter is about 3 m larger than the fire diameter that just engulfs the cask), $P_{flame\ temp}$ is the probability that the average temperature of the fire is high enough to heat the cask to a temperature $\geq T_b$, the temperature at which intact spent fuel rods fail by thermal burst rupture, $P_{duration,k}$ is the probability that the fire will burn long enough to heat generic cask k to that temperature, T_{cask} is the temperature of the cask internals, and T_f is the average flame temperature of a hydrocarbon fuel fire.

It is important to note that the four probabilities that enter the preceding expression for $P_{severe\ fire,k}$ should usually be largely independent. For example, large truck fires can occur only if more than one vehicle is involved in the accident and train fires always involve more that one rail car as the car carrying the spent fuel cask carries no fuel. So fire size and fire location should not be correlated for large fires. Similarly, fuel character and thus fire temperature should not depend on fire location or fire size or fire duration (smoldering smoky fires are probably optically dense but are not likely to be large enough or hot enough to be of concern). And although fire duration might be expected to be inversely proportional to fire size, runoff or soaking of fuel into the ground will cause the seeming correlation to be greatly weakened. So, although some of these four probabilities may be weakly correlated, for this analysis they are treated as though they are uncorrelated.

Although only an unusually severe long-duration fire can heat the internals of a spent fuel cask to rod burst rupture temperatures, less severe fires should be easily able to heat a spent fuel cask to lower temperatures. To capture the lessened fire severity needed to heat a cask to lower temperatures, some of the probabilities in the preceding formula can be relaxed by assuming that all fires meet the requirement represented by that probability. For example, because elastomeric cask seals begin to leak at about 350ºC, a temperature only 50 to 100ºC above normal cask internal temperatures, it would seem that most fires that burn hot enough and long enough to heat a spent fuel cask to 350ºC would be able to do so even if they were somewhat offset (not co-

located) and weren't optically dense (smoldering fires, very small collocated fires, and large offset fires located far from the cask are exceptions to this statement). Accordingly, the fraction of all fires that can heat a spent fuel cask to a temperature in the temperature range $T_a \le T_{cask} \le T_s$, where T_a is the cask internal temperature under ambient (normal transport) conditions and T_s is the cask seal leakage temperature, is here taken to be

$$P_{severe\ fire,k} = P_{co\text{-}located}\, P_{optically\ dense}\, P_{flame\ temp}\, P_{duration,k} = P_{flame\ temp}\, P_{duration,k}$$

since for this temperature range it is assumed that $P_{co\text{-}located} = P_{optically\ dense} = 1.0$.

Similarly, any moderately large fire not well-separated from the cask that burns hot enough and long enough should be able to heat the cask to a temperature greater than the temperature that cause the cask seal to leak but not to the temperature where rods fail by burst rupture, that is, to some temperature in the temperature range $T_s<T_{cask}<T_b$. Thus, the fraction of all fires that can heat a spent fuel cask to a temperature in the temperature range $T_s<T_{cask}<T_b$ is taken to be

$$P_{severe\ fire,k} = P_{co\text{-}located}\, P_{optically\ dense}\, P_{flame\ temp}\, P_{duration,k} = P_{co\text{-}located}\, P_{flame\ temp}\, P_{duration,k}$$

or

$$P_{severe\ fire,k} = P_{co\text{-}located}\, P_{optically\ dense}\, P_{flame\ temp}\, P_{duration,k} = P_{optically\ dense}\, P_{flame\ temp}\, P_{duration,k}$$

since, for a fire to heat a cask to temperature in this temperature range, the fire must either be fairly large (i.e., $P_{optically\ dense} = 1.0$) but not colocated (i.e., $P_{co\text{-}located} < 1.0$) or it must be co-located (i.e., $P_{co\text{-}located} = 1.0$) but not optically dense ($P_{optically\ dense} < 1.0$).

Finally, the conditional probability, $P_{duration,k}$, that the fire burns long enough so that generic cask k is heated to a temperature that falls within one of the three temperature ranges, $T_a \le T_{cask} \le T_s$, $T_s < T_{cask} < T_b$, and $T_b \le T_{cask} \le T_f$, is calculated using the following expressions:

$$P_{duration,k}(T_a \le T_{cask} \le T_s) = P_{duration,k}(t_{k,T_s})$$
$$P_{duration,k}(T_s < T_{cask} < T_b) = P_{duration,k}(t_{k,T_b}) - P_{duration,k}(t_{k,T_s})$$
$$P_{duration,k}(T_b \le T_{cask} \le T_f) = 1.0 - P_{duration,k}(t_{k,T_b})$$

where for example t_{k,T_s} is the time that it takes an optically dense, co-located, hydrocarbon fueled fire to heat generic cask k to its seal leakage temperature T_s given that the normal internal temperature of the cask is T_a, and $P_{duration,k}(t_{k,T_s})$ and $P_{duration,k}(t_{k,T_b})$ are respectively the cumulative probabilities that the fire duration is $\le t_{k,T_s}$ and $\le t_{k,T_b}$.

Cask-specific values for the heating times, t_{k,T_s}, t_{k,T_b}, and t_{k,T_f}, were determined by 1-D thermal calculations for each of the four generic casks being examined by this study. Those calculations were described in Section 6. Table 7.26 presents the cask specific heating times determined by those calculations.

Table 7.26 Durations (hr) of Co-Located, Fully Engulfing, Optically Dense, Hydrocarbon Fuel Fires that Raise the Temperature of Each Generic Cask to T_s, T_b, and T_f

Cask	Temperature (°C)		
	T_s = 350	T_b = 750	T_f = 1000
Steel-Lead-Steel Truck	1.04	2.09	5.55
Steel-DU-Steel Truck	0.59	1.96	5.32
Steel-Lead-Steel Rail	1.06	2.91	6.43
Monolithic Steel Rail	1.37	6.57	11

7.4.4.1 Modal Study Fire Duration Distributions

The Modal Study developed eight cumulative fire duration distributions for truck and train fires, five truck fire distributions and three train fire distributions. Tables 7.27 and 7.28 present these cumulative fire duration distributions. Values of $P_{duration,k}(t_{k,T_s})$, $P_{duration,k}(t_{k,T_b})$, and $P_{duration,k}(t_{k,T_f})$ were determined by linear interpolation using the data in these tables.

7.4.4.2 Optically Dense Fire Size

The four generic casks being examined by this study all have lengths of about 5 m (200 inches). Therefore, if engulfed by a fire, the fire must have a diameter of about 8 m (26.7 ft) if it is to be optically dense with respect to the engulfed cask (large enough so that the cask doesn't lose heat by radiation through the fire plume to the atmosphere) [7-57,7-58].

7.4.4.3 Truck Collision Fire Statistics

Cumulative distributions of fire temperatures, diameters, stand-off distances, and durations for fires initiated by collisions of trucks with other vehicles, with trains, or with fixed and non-fixed objects have been developed by Clauss, et al. [7-5]. Clauss, et al. find that

- essentially all fires have average fire temperatures greater than 650ºC, which agrees well with the results of Lopez, et al. who found [7-59] that essentially all fires have average flame temperatures greater than 725ºC,
- only one fire in two reaches average fire temperatures of 1000ºC,
- no more than one fire in two is an engulfing fire,
- 80 percent of all fires not caused by train collisions have diameters < 25 ft,
- all fires caused by train collisions have diameters > 25 ft,
- fires with diameters ≥ 25 ft initiated by truck collisions with other trucks, with cars, and with fixed or non-fixed objects all have fire durations < 60 minutes (i.e., there is not enough fuel available to support fires of longer durations),

- 85 percent of all fires initiated by truck collisions with tankers have durations longer than 60 minutes, and

- only 25 percent of all fires initiated by the collision of a train with a truck have durations longer than 60 minutes (this is because most train fires are so large, i.e., have such large diameters, that they do not burn very long).

Table 7.27 Truck Accident Fire Durations

Duration (hr)	Non-Collision Accidents	Off-Road Accidents and Collisions with Fixed Objects	Truck/Truck Collisions	Truck/Car Collisions	Train Grade Crossing Accidents
0.	0.	0.	0.	0.	0.
0.083	0.3311	0.0321	0.0035	0.0131	0.00238
0.167	0.6596	0.2821	0.0451	0.1653	0.07222
0.250	0.8551	0.5860	0.1572	0.4179	0.16427
0.333	0.9625	0.7754	0.3488	0.6516	0.31099
0.417	0.9801	0.8769	0.5001	0.7878	0.43757
0.500	0.9897	0.9358	0.6034	0.8725	0.54957
0.583	0.9944	0.9643	0.6771	0.9161	0.64690
0.667	0.9970	0.9800	0.7322	0.9456	0.73075
0.750	0.9985	0.9902	0.7750	0.9662	0.80265
0.833	0.9992	0.9949	0.7960	0.9761	0.86416
0.917	0.9996	0.9973	0.8123	0.9838	0.87612
1.0	0.9998	0.9989	0.8257	0.9898	0.88589
1.083	0.99991	0.9995	0.8367	0.9936	
1.167	0.99996	0.9998	0.8459	0.9964	0.89828
1.250	0.99999	0.99995	0.8535	0.9984	
1.333	1.0	0.99998	0.8596	0.9993	0.90934
1.417		0.99999	0.8652	0.9997	
1.500		1.0	0.8696	0.9999	0.91874
1.583			0.8737	0.99996	
1.667			0.8779	0.99997	0.92730
1.750			0.8812	0.99999	
1.833			0.8847	1.0	0.93452
1.917			0.8882		
2.0			0.8917		0.94126
3.0			0.9287		0.96792
4.0			0.9503		0.98247
5.0			0.9641		0.99056
6.0			0.9773		0.99643
7.0			0.9905		1.0
8.0			1.0		

Table 7.28 Train Accident Fire Durations

Duration (hr)	Collision Accidents	Derailment Accidents	Fire-Only Accidents
0.083	0.00238	0.01009	0.00943
0.167	0.07222	0.09213	0.09180
0.250	0.16427	0.17603	0.17574
0.330	0.31099	0.29164	0.29183
0.417	0.43757	0.39717	0.39789
0.500	0.54957	0.49517	0.49648
0.583	0.64690	0.58120	0.58291
0.667	0.73075	0.65917	0.66075
0.750	0.80265	0.72958	0.73139
0.833	0.86416	0.79154	0.79373
0.917	0.87612	0.80544	0.80765
1.0	0.88589	0.81870	0.82036
1.167	0.89828	0.83308	0.83454
1.333	0.90934	0.84752	0.91874
1.500	0.91874	0.86071	0.86292
1.667	0.92730	0.87388	0.87564
1.833	0.93452	0.88537	0.88704
2.0	0.94126	0.89665	0.89792
3.0	0.96792	0.94290	0.94342
4.0	0.98247	0.96790	0.96821
5.0	0.99056	0.98166	0.98239
6.0	0.99643	0.98868	0.98941
7.0	1.0	0.99380	0.99403
8.0		0.99702	0.99754
9.0		0.99910	0.99928
10.0		0.99978	0.99985
11.0		1.0	1.0

Now because only hydrocarbon fuel (or liquid chemical) fires will have average fire temperatures ≥ 1000ºC, while essentially all fires will have average fire temperatures > 650ºC, for trucks, $P_{\text{flame temp}}(T_a \le T_{\text{cask}} \le T_b) = 1.0$ and $P_{\text{flame temp}}(T_b \le T_{\text{cask}} \le T_f) = 0.5$. Since only fully engulfing fires with diameters > 25 ft will be optically dense and all truck/train accident fires have diameters > 25 ft, $P_{\text{optically dense/train}} = 1.0$. Because 80 percent of all other truck accidents lead to fires with diameters < 25 ft, $P_{\text{optically dense/not train}} = 0.2$. Because one truck fire in two is an engulfing fire, $P_{\text{co-located}} = 0.5$. Substitution of these values into Equation 9 yields the following expressions for the probability of fires sufficiently severe to heat a truck spent fuel cask to a temperature in the indicated temperature range.

$$P_{severe\ fire,k}(T_b \le T_{cask} \le T_f) = P_{optically\ dense}\ P_{co\text{-}located}\ P_{flame\ temp}(T_b \le T_{cask} \le T_f)\ P_{duration,k}(T_b \le T_{cask} \le T_f)$$

$$= (0.2)(0.5)(0.5)\ P_{duration,k} = 0.05\ P_{duration,k}(T_b \le T_{cask} \le T_f)$$
for truck accidents that don't involve trains

$$= (1.0)(0.5)(0.5)\ P_{duration,k} = 0.25\ P_{duration,k}(T_b \le T_{cask} \le T_f)$$
for train collisions with trucks

$$P_{severe\ fire,k}(T_s \le T_{cask} \le T_b) = P_{optically\ dense}\ P_{co\text{-}located}\ P_{flame\ temp}(T_s \le T_{cask} \le T_b)\ P_{duration,k}(T_s \le T_{cask} \le T_b)$$

$$= (0.2)(1.0)(1.0)\ P_{duration,k} = 0.2\ P_{duration,k}(T_s \le T_{cask} \le T_b)$$
for truck accidents that don't involve trains

$$= (1.0)(1.0)(1.0)\ P_{duration,k} = P_{duration,k}(T_s \le T_{cask} \le T_b)$$
for train collisions with trucks at grade crossings

since, for fires in this temperature range, it is assumed that $P_{co\text{-}located} = 1.0$.

$$P_{severe\ fire,k}(T_a \le T_{cask} \le T_s) = P_{optically\ dense}\ P_{co\text{-}located}\ P_{flame\ temp}(T_a \le T_{cask} \le T_s)\ P_{duration,k}(T_a \le T_{cask} \le T_s)$$

$$= (1.0)(1.0)(1.0)\ P_{duration,k} = P_{duration,k}(T_a \le T_{cask} \le T_s)$$
for all truck accidents

since, for fires in this temperature range, it is assumed that $P_{optically\ dense} = P_{co\text{-}located} = 1.0$.

Finally, Clauss et al. developed cumulative distributions of fire diameters for truck collisions with cars, trucks, trains, and off-road objects. In addition, for each of these classes of collisions, they also developed cumulative distributions of fire duration for fires of different sizes (ranges of fire diameters). Now, if P_{di} is the probability that a truck collision with another truck leads to a fire with a diameter d that lies in the diameter range d_i to d_{i+1}, and P_i is the probability that fires in this size range have durations ≤ 1 hour, then the chance P_T that a truck collision will produce a fire of any size that has a duration ≤ 1 hour is

$$P_T = \sum_i P_{di} P_i$$

Table 7.29 compares the values of cumulative fire duration probabilities for fires of any size with durations ≤ 1.0 hour for various truck collisions developed using this summation and the data of Clauss, et al. to the values developed by the Modal Study.

Table 7.29 Comparison of Modal Study Cumulative Fire Durations for Various Truck Accidents to Those Developed by Weighted Summation of Data from Clauss, et al. [7-5]

Collision	With Car	With Truck	With Train	Off-Road
Clauss, et al.	0.99	0.80	0.94	0.995
Modal Study	0.9898	0.8257	0.8859	0.9989

Inspection of the table suggests that the results of Clauss, et al. are quite consistent with those presented in the Modal Study. Accordingly, use of values of $P_{\text{optically dense}}$, $P_{\text{co-located}}$, and $P_{\text{flame temp}}$ developed from the data of Clauss, et al. with Modal Study fire duration data and truck accident event tree probabilities seems appropriate.

7.4.4.4 Train Collision Fire Statistics

Because a modern study of train collision fire statistics was not identified, estimates of $P_{\text{optically dense}}$, $P_{\text{co-located}}$, and $P_{\text{flame temp}}$ for fires initiated by train collisions had to be developed by considering other data. The results of Clauss, et al. show that fires initiated by the collision of a train with a truck almost always have diameters ≥ 25 ft and that half of these fires have diameters ≥ 30 ft. Because these collisions are unlikely to lead to train derailments, the fires they initiate may involve the fuel that powers the diesel engine that was hauling the train but are not likely to involve liquid chemicals in tank cars further back in the train's consist (the set of cars that make up the train). Accordingly, because train accidents that lead to derailments that also initiate fires frequently involve more than one car in the consist, the cumulative probability distribution of the sizes of fires initiated by train derailments should lie higher than the distribution found for fires initiated by train collisions with trucks. Therefore, because (a) fires with diameters ≥ 25 ft will be optically dense to a cask that is engulfed by the fire, (b) fires initiated by train derailments are likely to be larger than fires initiated by the collision of a train with a truck, and (c) essentially all fires initiated by train collisions with a truck have diameters ≥ 25 ft, for all train fires it is assumed that $P_{\text{optically dense}} = 1.0$.

Data on truck and train cargoes, specifically commodity flow statistics, has been compiled by the Department of Transportation for the year 1993. Table 7.30 presents the ton-miles and ton-mile fractions of highly combustible cargoes (commodities) that were transported over long distances by trucks and by trains during 1993.

Table 7.30 Truck and Train Commodity Flow Statistics for 1993

Highly Combustible Cargo	Train			Truck		
	Ton-miles (millions)	Fraction		Ton-miles (millions)	Fraction	
		w Coal	w/o Coal		w Coal	w/o Coal
Coal	3.93×10^{5}	0.417		7.24×10^{3}	0.012	
Petroleum	na	na	na	na	na	na
Chemicals	1.13×10^{5}	0.120	0.205	5.73×10^{4}	0.091	0.092
Petroleum Products	4.76×10^{4}	0.050	0.087	3.00×10^{4}	0.048	0.048
Rubber, Plastics	1.11×10^{3}	0.001	0.002	1.94×10^{4}	0.031	0.031
Lumber, Wood Products	3.04×10^{4}	0.032	0.055	2.29×10^{4}	0.036	0.037
Pulp, Paper	3.77×10^{4}	0.040	0.069	4.74×10^{4}	0.075	0.076
All Highly Combustible – w Coal	6.23×10^{5}	0.661		4.28×10^{5}	0.680	
All Highly Combustible – w/o Coal	2.30×10^{5}		0.418	4.21×10^{5}		0.677
All – w Coal	9.43×10^{5}			6.29×10^{5}		
All – w/o Coal	5.50×10^{5}			6.22×10^{5}		

Table 7.30 shows that, when coal is excluded from consideration, the number of ton-miles of highly combustible cargoes transported by truck is about twice that transported by train, and that the relative amounts of the types of combustibles carried by the two transport modes are quite similar, differing principally in that trains carry more chemicals and petroleum products than trucks while trucks carry more rubber and plastics than trains. Because, when shipped by train, most coal is hauled in unit trains, and because little petroleum is transported by train (long distance transport of gaseous and liquid hydrocarbons is almost always done by pipeline), while petroleum fuels (diesel, gasoline) are almost always transported from tank farms to gasoline stations by truck, it is clear that large quantities of petroleum are transported by truck but little by train. Therefore, derailments of regular trains which haul little coal or petroleum should be less likely to initiate fires fueled by highly combustible fuels than are fires initiated by truck collisions. Accordingly, the chance that a train derailment will initiate a fire that has an average temperature ≥ 1000°C should be smaller than the chance that a fire initiated by truck collision initiates such a fire. But $P_{\text{flame temp}}(T_b \le T_{\text{cask}} \le T_f) = 0.5$ for fires initiated by truck collisions. Therefore, for fires initiated by train derailments, use of $P_{\text{flame temp}}(T_b \le T_{\text{cask}} \le T_f) = 0.5$ should be conservative.

The discussion presented in Section 7.4.2 above suggests that side and raking collisions and train derailments typically involve about ten rail cars. Inspection of Table 7.30 shows that about 42 percent of all cargo in regular trains (not unit trains such as coal trains) is highly combustible. So a typical train accident will involve four cars that are carrying highly combustible cargo. Now, given that the train accident has led to a fire and that the car carrying the spent fuel cask is one of the cars involved in the accident, an upper bound on the chance that the ensuing fire engulfs the cask can be calculated as the ratio of the 50 percentile fire area to the minimum area occupied by the ten cars. Thus,

$$P_{\text{engulfing}} = \frac{\pi(r_{\text{fire}})^2}{10(w_{\text{car}}\, l_{\text{car}})} = \frac{\pi(15\,\text{ft})^2}{10(10\text{ft x }21\text{ft})} = 0.3$$

where 10 ft and 21 ft are the width and length of a typical flat bed rail car.

Substitution of the values developed for $P_{\text{optically dense}}$, $P_{\text{flame temp}}$, and $P_{\text{co-located}}$ for train fires into Equation 9 yields the following expressions for the probability of train fires sufficiently severe to heat a rail spent fuel cask to a temperature in the indicated temperature range.

$$\begin{aligned} P_{\text{severe fire,k}}(T_b \le T_{\text{cask}} \le T_f) &= P_{\text{optically dense}}\, P_{\text{co-located}}\, P_{\text{flame temp}}(T_b \le T_{\text{cask}} \le T_f)\, P_{\text{duration,k}}(T_b \le T_{\text{cask}} \le T_f) \\ &= (1.0)(0.3)(0.5)\, P_{\text{duration,k}} = 0.15\, P_{\text{duration,k}}(T_b \le T_{\text{cask}} \le T_f) \end{aligned}$$

$$\begin{aligned} P_{\text{severe fire,k}}(T_s \le T_{\text{cask}} \le T_b) &= P_{\text{optically dense}}\, P_{\text{co-located}}\, P_{\text{flame temp}}(T_s \le T_{\text{cask}} \le T_b)\, P_{\text{duration,k}}(T_s \le T_{\text{cask}} \le T_b) \\ &= (1.0)(0.3)(1.0)\, P_{\text{duration,k}} = 0.2\, P_{\text{duration,k}}(T_s \le T_{\text{cask}} \le T_b) \end{aligned}$$

since, for fires in this temperature range, it is assumed that $P_{\text{flame temp}} = 1.0$.

$$\begin{aligned} P_{\text{severe fire,k}}(T_a \le T_{\text{cask}} \le T_s) &= P_{\text{optically dense}}\, P_{\text{co-located}}\, P_{\text{flame temp}}(T_a \le T_{\text{cask}} \le T_s)\, P_{\text{duration,k}}(T_a \le T_{\text{cask}} \le T_s) \\ &= (1.0)(1.0)(1.0)\, P_{\text{duration,k}} = P_{\text{duration,k}}(T_a \le T_{\text{cask}} \le T_s) \end{aligned}$$

since, for fires in this temperature range, it is assumed that $P_{\text{flame temp}} = P_{\text{co-located}} = 1.0$.

7.5 Values for Release Fractions and Severity Fractions

7.5.1 Introduction

Severity fraction values can now be calculated by substituting the severity fraction parameter values developed in Section 7.4 into the severity fraction expressions developed in Section 7.2. When this is done, four sets of severity fractions are obtained, one for each of the four generic casks, the steel-lead-steel and steel-DU-steel truck casks, and the steel-lead-steel and monolithic steel rail casks, for which specifications were developed in Section 4.

Similarly, release fraction values can now be calculated by substituting the release fraction parameter values developed in Section 7.3 into the release fraction expressions developed in Section 7.2. When this is done, because low to moderate impact loads are estimated to fail more PWR rods than BWR rods, two sets of release fractions are obtained for each generic cask, one for PWR spent fuel and another for BWR spent fuel. Thus, eight sets of release fractions are constructed, four sets of PWR release fractions (one set for each generic cask) and four sets of BWR release fractions (again one set for each generic cask).

7.5.2 Calculational Method

Release fractions and severity fractions were calculated using spreadsheets. Copies of these spreadsheets are presented in the Appendix D. Calculation of release fraction values was done using a single spreadsheet. Four linked spreadsheets were used to calculate the severity fraction values for each generic cask.

The first of the four severity fraction spreadsheets is the truck or train accident event tree that gives constructs values for individual accident scenarios, $P_{scenario,j}$ values. The second severity fraction spreadsheet calculates values for $P_{speed,j}$ (v_{30},v_{60}), $P_{speed,j}$ (v_{60},v_{90}), $P_{speed,j}$ (v_{90},v_{120}), and $P_{speed,j}$ $(\geq v_{120})$, where v_{30}, v_{60}, v_{90}, and v_{120} are the cask impact speeds for accident scenario and accident surface j that are equivalent to 30, 60, 90, and 120 mph impacts onto an unyielding surface, and for example $P_{speed,j}$ (v_{30},v_{60}) is the chance that the cask impact velocity onto that surface falls within the speed range (v_{30},v_{60}). These speed range probabilities are calculated by linear interpolation using the appropriate Modal Study cumulative accident velocity distribution and the real-surface values of v_{30}, v_{60}, v_{90}, and v_{120} developed from the finite element cask impact results for unyielding surfaces described in Section 5.1 by partitioning of the impact energy between the cask and the real yielding surface as described in Section 5.2.

The third severity fraction spreadsheet calculate values for $P_{duration,k}$ (T_a,T_s), $P_{duration,k}$ (T_s,T_b), and $P_{duration,k}$ (T_b,T_f), where T_a, T_s, and T_f are respectively the normal internal temperature of the spent fuel cask, the temperature at which cask elastomeric seals begin to leak due to thermal loads, and the average temperature of a hydrocarbon fuel fire, and for example $P_{duration,k}$ (T_a,T_s) is the chance that the fire initiated by the accident burns long enough to raise the temperature of cask k into the temperature range (T_a,T_s). As was done for cask impact velocities, these fire duration probabilities are calculated by linear interpolation using the appropriate Modal Study cumulative accident fire duration distribution and the values of T_a, T_s, and T_f that were developed in Section 6 for each of the four generic casks. Finally, the fourth severity fraction spreadsheet calculates

individual severity fraction values for each combination of one of the 31 truck accident scenarios with one of the 18 truck accident cases, or one of the 25 train accident scenarios with one of the 20 rail accident cases, and then sums the results for each accident case over all of the accident scenarios that contribute to that accident case thereby producing a set of 18 truck accident severity fractions for each generic truck cask or 20 train accident severity fractions for each generic rail cask.

7.5.3 Source Term Severity Fraction and Release Fraction Values

Finally, Table 7.31 presents the severity fraction and release fraction values developed by the process outlined in the preceding section.

7.6 Conservatisms

Some of the source term models developed in this section use treatments of phenomena or parameter values that are significantly conservative. The more significant of these conservatisms are:

- the use of high burnup, three year cooled cask inventories rather than average burnup, ten year cooled cask inventories that would better represent the average characteristics of the spent fuel generated to date;
- the assumption that during collision accidents all of the pellets in a fuel rod fracture and the calculation of the degree of fracturing assuming that the pellets are subjected to forces equal to those generated by a 120 mph impact onto an unyielding surface;
- the assumption that the particle size distribution produced by spallation of CRUD from rod surfaces due to mechanical or thermal loads is identical to the size distribution of the agglomerated crystalites that comprise the CRUD deposits on the rod surfaces;
- the treatment of particle and vapor deposition onto cask interior surfaces only during the short time period that immediately follows rod failure (e.g., during collisions accidents that lead to fires, particle and vapor deposition is neglected during the long time periods between the failure of some of the rods due to impact and the failure of the rest of the rods due to burst rupture, and the neglect of vapor deposition onto cooler cask interior surfaces following rod failure by burst rupture); and
- the neglect of plugging of small seal leak paths (leaks with cross sectional areas of order 1 mm^2) which are likely to be cracks that are much longer (at least one bolt spacing) than they are wide (< 30 μm) and thus easily subject to plugging by larger particles entrained in the cask's blowdown gas flow.

Table 7.31 Source Term Severity Fractions and Release Fractions

Steel-DU-Steel Truck Cask						
Number of PWR Fuel Assemblies: 3						
Case	Severity Fraction	PWR Release Fractions				
		Kr	Cs	Ru	Particulates	CRUD
1	1.53E-08	8.0E-01	2.4E-08	6.0E-07	6.0E-07	2.0E-03
2	5.88E-05	1.4E-01	4.1E-09	1.0E-07	1.0E-07	1.4E-03
3	1.81E-06	1.8E-01	5.4E-09	1.3E-07	1.3E-07	1.8E-03
4	7.49E-08	8.4E-01	3.6E-05	3.8E-06	3.8E-06	3.2E-03
5	4.65E-07	4.3E-01	1.3E-08	3.2E-07	3.2E-07	1.8E-03
6	3.31E-09	4.9E-01	1.5E-08	3.7E-07	3.7E-07	2.1E-03
7	0.00E+00	8.5E-01	2.7E-05	2.1E-06	2.1E-06	3.1E-03
8	1.13E-08	8.2E-01	2.4E-08	6.1E-07	6.1E-07	2.0E-03
9	8.03E-11	8.9E-01	2.7E-08	6.7E-07	6.7E-07	2.2E-03
10	0.00E+00	9.1E-01	5.9E-06	6.8E-07	6.8E-07	2.5E-03
11	1.44E-10	8.2E-01	2.4E-08	6.1E-07	6.1E-07	2.0E-03
12	1.02E-12	8.9E-01	2.7E-08	6.7E-07	6.7E-07	2.2E-03
13	0.00E+00	9.1E-01	5.9E-06	6.8E-07	6.8E-07	2.5E-03
14	7.49E-11	8.4E-01	9.6E-05	8.4E-05	1.8E-05	6.4E-03
15	0.00E+00	8.5E-01	5.5E-05	5.0E-05	9.0E-06	5.9E-03
16	0.00E+00	9.1E-01	5.9E-06	6.4E-06	6.8E-07	3.3E-03
17	0.00E+00	9.1E-01	5.9E-06	6.4E-06	6.8E-07	3.3E-03
18	5.86E-06	8.4E-01	1.7E-05	6.7E-08	6.7E-08	2.5E-03
19	0.99993	0.0	0.0	0.0	0.0	0.0
	1.00000					

Steel-DU-Steel Truck Cask						
Number of BWR Fuel Assemblies: 7						
Case	Severity Fraction	BWR Release Fractions				
		Kr	Cs	Ru	Particulates	CRUD
1	1.53E-08	8.0E-01	2.4E-08	6.0E-07	6.0E-07	2.0E-03
2	5.88E-05	5.4E-03	1.6E-10	4.0E-09	4.0E-09	4.5E-04
3	1.81E-06	1.5E-02	4.5E-10	1.1E-08	1.1E-08	1.3E-03
4	7.49E-08	8.4E-01	4.1E-05	4.9E-06	4.9E-06	3.1E-03
5	4.65E-07	9.8E-02	2.9E-09	7.3E-08	7.3E-08	1.2E-03
6	3.31E-09	1.4E-01	4.1E-09	1.0E-07	1.0E-07	1.7E-03
7	0.00E+00	8.4E-01	3.7E-05	4.0E-06	4.0E-06	3.2E-03
8	1.13E-08	8.2E-01	2.4E-08	6.1E-07	6.1E-07	2.0E-03
9	8.03E-11	8.9E-01	2.7E-08	6.7E-07	6.7E-07	2.2E-03
10	0.00E+00	9.1E-01	5.9E-06	6.8E-07	6.8E-07	2.5E-03
11	1.44E-10	8.2E-01	2.4E-08	6.1E-07	6.1E-07	2.0E-03
12	1.02E-12	8.9E-01	2.7E-08	6.7E-07	6.7E-07	2.2E-03
13	0.00E+00	9.1E-01	5.9E-06	6.8E-07	6.8E-07	2.5E-03
14	7.49E-11	8.4E-01	1.2E-04	1.1E-04	2.4E-05	6.5E-03
15	0.00E+00	8.4E-01	1.0E-04	8.9E-05	2.0E-05	6.4E-03
16	0.00E+00	9.1E-01	5.9E-06	6.4E-06	6.8E-07	3.3E-03
17	0.00E+00	9.1E-01	5.9E-06	6.4E-06	6.8E-07	3.3E-03
18	5.86E-06	8.4E-01	1.7E-05	6.7E-08	6.7E-08	2.5E-03
19	0.99993	0.0	0.0	0.0	0.0	0.0
	1.00000					

Aerosolized Fraction = 1.0
Respirable Fraction = 1.0

Table 7.31 Source Term Severity Fractions and Release Fractions (continued)

Steel-Lead-Steel Truck Cask						
Number of PWR Fuel Assemblies: 1						
Case	Severity Fraction	PWR Release Fractions				
		Kr	Cs	Ru	Particulates	CRUD
1	1.53E-08	8.0E-01	2.4E-08	6.0E-07	6.0E-07	2.0E-03
2	6.19E-05	1.4E-01	4.1E-09	1.0E-07	1.0E-07	1.4E-03
3	2.81E-07	1.8E-01	5.4E-09	1.3E-07	1.3E-07	1.8E-03
4	6.99E-08	8.4E-01	3.6E-05	3.8E-06	3.8E-06	3.2E-03
5	4.89E-07	4.3E-01	1.3E-08	3.2E-07	3.2E-07	1.8E-03
6	9.22E-11	4.9E-01	1.5E-08	3.7E-07	3.7E-07	2.1E-03
7	3.30E-12	8.5E-01	2.7E-05	2.1E-06	2.1E-06	3.1E-03
8	1.17E-08	8.2E-01	2.4E-08	6.1E-07	6.1E-07	2.0E-03
9	1.90E-12	8.9E-01	2.7E-08	6.7E-07	6.7E-07	2.2E-03
10	0.00E+00	9.1E-01	5.9E-06	6.8E-07	6.8E-07	2.5E-03
11	1.49E-10	8.2E-01	2.4E-08	6.1E-07	6.1E-07	2.0E-03
12	2.41E-14	8.9E-01	2.7E-08	6.7E-07	6.7E-07	2.2E-03
13	0.00E+00	9.1E-01	5.9E-06	6.8E-07	6.8E-07	2.5E-03
14	6.99E-11	8.4E-01	9.6E-05	8.4E-05	1.8E-05	6.4E-03
15	3.30E-15	8.5E-01	5.5E-05	5.0E-05	9.0E-06	5.9E-03
16	0.00E+00	9.1E-01	5.9E-06	6.4E-06	6.8E-07	3.3E-03
17	0.00E+00	9.1E-01	5.9E-06	6.4E-06	6.8E-07	3.3E-03
18	5.59E-06	8.4E-01	1.7E-05	6.7E-08	6.7E-08	2.5E-03
19	0.99993	0.0	0.0	0.0	0.0	0.0
	1.00000					

Steel-Lead-Steel Truck Cask						
Number of BWR Fuel Assemblies: 2						
Case	Severity Fraction	BWR Release Fractions				
		Kr	Cs	Ru	Particulates	CRUD
1	1.53E-08	8.0E-01	2.4E-08	6.0E-07	6.0E-07	2.0E-03
2	6.19E-05	5.4E-03	1.6E-10	4.0E-09	4.0E-09	4.5E-04
3	2.81E-07	1.5E-02	4.5E-10	1.1E-08	1.1E-08	1.3E-03
4	6.99E-08	8.4E-01	4.1E-05	4.9E-06	4.9E-06	3.1E-03
5	4.89E-07	9.8E-02	2.9E-09	7.3E-08	7.3E-08	1.2E-03
6	9.22E-11	1.4E-01	4.1E-09	1.0E-07	1.0E-07	1.7E-03
7	3.30E-12	8.4E-01	3.7E-05	4.0E-06	4.0E-06	3.2E-03
8	1.17E-08	8.2E-01	2.4E-08	6.1E-07	6.1E-07	2.0E-03
9	1.90E-12	8.9E-01	2.7E-08	6.7E-07	6.7E-07	2.2E-03
10	0.00E+00	9.1E-01	5.9E-06	6.8E-07	6.8E-07	2.5E-03
11	1.49E-10	8.2E-01	2.4E-08	6.1E-07	6.1E-07	2.0E-03
12	2.41E-14	8.9E-01	2.7E-08	6.7E-07	6.7E-07	2.2E-03
13	0.00E+00	9.1E-01	5.9E-06	6.8E-07	6.8E-07	2.5E-03
14	6.99E-11	8.4E-01	1.2E-04	1.1E-04	2.4E-05	6.5E-03
15	3.30E-15	8.4E-01	1.0E-04	8.9E-05	2.0E-05	6.4E-03
16	0.00E+00	9.1E-01	5.9E-06	6.4E-06	6.8E-07	3.3E-03
17	0.00E+00	9.1E-01	5.9E-06	6.4E-06	6.8E-07	3.3E-03
18	5.59E-06	8.4E-01	1.7E-05	6.7E-08	6.7E-08	2.5E-03
19	0.99993	0.0	0.0	0.0	0.0	0.0
	1.00000					

Aerosolized Fraction = 1.0

Respirable Fraction = 1.0

Table 7.31 Source Term Severity Fractions and Release Fractions (continued)

Monolithic Rail Cask						
Number of PWR Fuel Assemblies: 24						
Case	Severity Fraction	PWR Release Fractions				
		Kr	Cs	Ru	Particulates	CRUD
1	4.49E-09	4.1E-01	1.2E-08	2.5E-07	2.5E-07	1.4E-03
2	1.17E-07	8.0E-01	8.6E-06	1.3E-05	1.3E-05	4.4E-02
3	4.49E-09	8.0E-01	1.8E-05	1.9E-05	1.9E-05	6.4E-02
4	3.05E-05	1.4E-01	4.1E-09	1.0E-07	1.0E-07	1.4E-03
5	1.01E-06	1.8E-01	5.4E-09	1.3E-07	1.3E-07	1.8E-03
6	1.51E-08	8.4E-01	3.6E-05	1.4E-05	1.4E-05	5.4E-03
7	7.31E-08	4.3E-01	1.3E-08	2.6E-07	2.6E-07	1.5E-03
8	2.43E-09	4.9E-01	1.5E-08	2.9E-07	2.9E-07	1.7E-03
9	3.61E-11	8.5E-01	2.7E-05	6.8E-06	6.8E-06	4.5E-03
10	9.93E-10	8.2E-01	8.8E-06	1.3E-05	1.3E-05	4.5E-02
11	3.30E-11	8.9E-01	9.6E-06	1.5E-05	1.5E-05	4.9E-02
12	4.91E-13	9.1E-01	1.4E-05	1.5E-05	1.5E-05	5.1E-02
13	3.82E-11	8.2E-01	1.8E-05	2.0E-05	2.0E-05	6.5E-02
14	1.27E-12	8.9E-01	2.0E-05	2.1E-05	2.1E-05	7.1E-02
15	1.88E-14	9.1E-01	2.2E-05	2.2E-05	2.2E-05	7.4E-02
16	5.69E-11	8.4E-01	9.6E-05	8.4E-05	1.8E-05	6.4E-03
17	3.61E-14	8.5E-01	5.5E-05	5.0E-05	8.9E-06	5.4E-03
18	4.91E-16	9.1E-01	1.4E-05	1.8E-05	1.5E-05	5.1E-02
19	1.88E-17	9.1E-01	2.2E-05	2.3E-05	2.2E-05	7.4E-02
20	6.32E-06	8.4E-01	1.7E-05	2.5E-07	2.5E-07	9.4E-03
21	0.99996	0.0	0.0	0.0	0.0	0.0
	1.00000					

Monolithic Rail Cask						
Number of BWR Fuel Assemblies: 52						
Case	Severity Fraction	BWR Release Fractions				
		Kr	Cs	Ru	Particulates	CRUD
1	4.49E-09	8.9E-02	2.7E-09	5.3E-08	5.3E-08	8.9E-04
2	1.17E-07	8.0E-01	8.6E-06	1.3E-05	1.3E-05	4.4E-02
3	4.49E-09	8.0E-01	1.8E-05	1.9E-05	1.9E-05	6.4E-02
4	3.05E-05	5.4E-03	1.6E-10	4.0E-09	4.0E-09	4.5E-04
5	1.01E-06	1.5E-02	4.5E-10	1.1E-08	1.1E-08	1.3E-03
6	1.51E-08	8.4E-01	4.1E-05	1.8E-05	1.8E-05	5.4E-03
7	7.31E-08	9.8E-02	2.9E-09	5.9E-08	5.9E-08	9.8E-04
8	2.43E-09	1.4E-01	4.1E-09	8.3E-08	8.3E-08	1.4E-03
9	3.61E-11	8.4E-01	3.7E-05	1.5E-05	1.5E-05	4.9E-03
10	9.93E-10	8.2E-01	8.8E-06	1.3E-05	1.3E-05	4.5E-02
11	3.30E-11	8.9E-01	9.6E-06	1.5E-05	1.5E-05	4.9E-02
12	4.91E-13	9.1E-01	1.4E-05	1.5E-05	1.5E-05	5.1E-02
13	3.82E-11	8.2E-01	1.8E-05	2.0E-05	2.0E-05	6.5E-02
14	1.27E-12	8.9E-01	2.0E-05	2.1E-05	2.1E-05	7.1E-02
15	1.88E-14	9.1E-01	2.2E-05	2.2E-05	2.2E-05	7.4E-02
16	5.69E-11	8.4E-01	1.2E-04	1.1E-04	2.4E-05	6.5E-03
17	3.61E-14	8.4E-01	1.0E-04	8.9E-05	2.0E-05	5.9E-03
18	4.91E-16	9.1E-01	1.4E-05	1.8E-05	1.5E-05	5.1E-02
19	1.88E-17	9.1E-01	2.2E-05	2.3E-05	2.2E-05	7.4E-02
20	6.32E-06	8.4E-01	1.7E-05	2.5E-07	2.5E-07	9.4E-03
19	0.99996	0.0	0.0	0.0	0.0	0.0
21	1.00000					

Aerosolized Fraction = 1.0
Respirable Fraction = 1.0

Table 7.31 Source Term Severity Fractions and Release Fractions (continued)

Steel-Lead-Steel Rail Cask						
Number of PWR Fuel Assemblies: 24						
Case	Severity Fraction	PWR Release Fractions				
		Kr	Cs	Ru	Particulates	CRUD
1	8.20E-06	4.1E-01	1.2E-08	2.5E-07	2.5E-07	1.4E-03
2	5.68E-07	8.0E-01	8.6E-06	1.3E-05	1.3E-05	4.4E-02
3	4.49E-09	8.0E-01	1.8E-05	1.9E-05	1.9E-05	6.4E-02
4	2.96E-05	1.4E-01	4.1E-09	1.0E-07	1.0E-07	1.4E-03
5	8.24E-07	1.8E-01	5.4E-09	1.3E-07	1.3E-07	1.8E-03
6	1.10E-07	8.4E-01	3.6E-05	1.4E-05	1.4E-05	5.4E-03
7	6.76E-08	4.3E-01	1.3E-08	2.6E-07	2.6E-07	1.5E-03
8	1.88E-09	4.9E-01	1.5E-08	2.9E-07	2.9E-07	1.7E-03
9	2.51E-10	8.5E-01	2.7E-05	6.8E-06	6.8E-06	4.5E-03
10	4.68E-09	8.2E-01	8.8E-06	1.3E-05	1.3E-05	4.5E-02
11	1.31E-10	8.9E-01	9.6E-06	1.5E-05	1.5E-05	4.9E-02
12	1.74E-11	9.1E-01	1.4E-05	1.5E-05	1.5E-05	5.1E-02
13	3.70E-11	8.2E-01	1.8E-05	2.0E-05	2.0E-05	6.5E-02
14	1.03E-12	8.9E-01	2.0E-05	2.1E-05	2.1E-05	7.1E-02
15	1.37E-13	9.1E-01	2.2E-05	2.2E-05	2.2E-05	7.4E-02
16	4.15E-10	8.4E-01	9.6E-05	8.4E-05	1.8E-05	6.4E-03
17	2.51E-13	8.5E-01	5.5E-05	5.0E-05	8.9E-06	5.4E-03
18	1.74E-14	9.1E-01	1.4E-05	1.8E-05	1.5E-05	5.1E-02
19	1.37E-16	9.1E-01	2.2E-05	2.3E-05	2.2E-05	7.4E-02
20	4.91E-05	8.4E-01	1.7E-05	2.5E-07	2.5E-07	9.4E-03
21	0.99991	0.0	0.0	0.0	0.0	0.0
	1.00000					

Steel-Lead-Steel Rail Cask						
Number of BWR Fuel Assemblies: 52						
Case	Severity Fraction	BWR Release Fractions				
		Kr	Cs	Ru	Particulates	CRUD
1	8.20E-06	8.9E-02	2.7E-09	5.3E-08	5.3E-08	8.9E-04
2	5.68E-07	8.0E-01	8.6E-06	1.3E-05	1.3E-05	4.4E-02
3	4.49E-09	8.0E-01	1.8E-05	1.9E-05	1.9E-05	6.4E-02
4	2.96E-05	5.4E-03	1.6E-10	4.0E-09	4.0E-09	4.5E-04
5	8.24E-07	1.5E-02	4.5E-10	1.1E-08	1.1E-08	1.3E-03
6	1.10E-07	8.4E-01	4.1E-05	1.8E-05	1.8E-05	5.4E-03
7	6.76E-08	9.8E-02	2.9E-09	5.9E-08	5.9E-08	9.8E-04
8	1.88E-09	1.4E-01	4.1E-09	8.3E-08	8.3E-08	1.4E-03
9	2.51E-10	8.4E-01	3.7E-05	1.5E-05	1.5E-05	4.9E-03
10	4.68E-09	8.2E-01	8.8E-06	1.3E-05	1.3E-05	4.5E-02
11	1.31E-10	8.9E-01	9.6E-06	1.5E-05	1.5E-05	4.9E-02
12	1.74E-11	9.1E-01	1.4E-05	1.5E-05	1.5E-05	5.1E-02
13	3.70E-11	8.2E-01	1.8E-05	2.0E-05	2.0E-05	6.5E-02
14	1.03E-12	8.9E-01	2.0E-05	2.1E-05	2.1E-05	7.1E-02
15	1.37E-13	9.1E-01	2.2E-05	2.2E-05	2.2E-05	7.4E-02
16	4.15E-10	8.4E-01	1.2E-04	1.1E-04	2.4E-05	6.5E-03
17	2.51E-13	8.4E-01	1.0E-04	8.9E-05	2.0E-05	5.9E-03
18	1.74E-14	9.1E-01	1.4E-05	1.8E-05	1.5E-05	5.1E-02
19	1.37E-16	9.1E-01	2.2E-05	2.3E-05	2.2E-05	7.4E-02
20	4.91E-05	8.4E-01	1.7E-05	2.5E-07	2.5E-07	9.4E-03
21	0.99991	0.0	0.0	0.0	0.0	0.0
	1.00000					

Aerosolized Fraction = 1.0
Respirable Fraction = 1.0

7.7 References

[7-1] L. E. Fischer, et al., "Shipping Container Response to Severe Highway and Railway Accident Conditions," NUREG/CR-4829, Lawrence Livermore National Laboratory, Livermore, CA, February 1987.

[7-2] ARC/INFO Coverages and Arc View Project, K. C. Bayer Digital Map of the U.S., purchased from Geologic Data Systems, Inc., 1600 Emerson St., Denver, CO 80218.

[7-3] State Soil Graphics (STATSGO) Data Base, available on the Internet at ftp.ftw.nrcs.usda.gov/pub/statsgo.

[7-4] Accidents of Motor Carriers of Property (for the years 1973 through 1983), Bureau of Motor Carrier Safety, Federal Highway Administration, U.S. Department of Transportation, Washington, DC, 1975-1984.

[7-5] D. B. Clauss, et al., "A Statistical Description of the Types and Severities of Accidents Involving Tractor Semi-Trailers," SAND93-2580, Sandia National Laboratories, Albuquerque, NM, June 1994.

[7-6] Accident/Incident Bulletins Nos. 145 through 151, Office of Safety, Federal Railroad Administration, U.S. Department of Transportation, Washington, DC, 1977-1983.

[7-7] Ref. [7-1], p. 2-30.

[7-8] Comments by meeting attendees at the Rail Accident Event Tree Meeting held at the American Association of Railroads Offices in Washington, DC, November 3, 1997.

[7-9] K. S. Neuhauser and F. L. Kanipe, "RADTRAN 4, Volume II, Technical Manual," SAND89-2370, Sandia National Laboratories, Albuquerque, NM, May 1994.

[7-10] K. S. Neuhauser and F. L. Kanipe, "RADTRAN 4, Volume III, User Guide," SAND89-2370, Sandia National Laboratories, Albuquerque, NM, January 1992.

[7-11] A. G. Croff, "ORIGEN2 - A Revised and Updated Version of the Oak Ridge Isotope Generation and Depletion Code," ORNL-5621, Oak Ridge National Laboratory, Oak Ridge, TN, July 1980.

[7-12] ORIGEN2 Isotope Generation and Depletion Code, CCC-371, Oak Ridge National Laboratory, Oak Ridge, TN, 1991.

[7-13] Spent Nuclear Fuel Discharges from U.S. Reactors, Energy Information Administration, U.S. Department of Energy, SR/CNEAF/96-01, 1994.

[7-14] *International Atomic Energy Agency, Safety Series No. 7, IAEA Safety Guides, Explanatory Material for the IAEA Regulations for the Safe Transport of Radioactive Material* (1985 Edition), 2nd Edition, Vienna, 1987.

[7-15] Code of Federal Regulations, Volume 49, Part 173.435 (49 CFR 173.435).

[7-16] RADSEL, unpublished Sandia code, available upon request.

[7-17] R. P. Sandoval, et al., "Estimate of CRUD Contribution to Shipping Cask Containment Requirements," SAND88-1358, Sandia National Laboratories, Albuquerque, NM, January 1991.

[7-18] "Environmental Assessment of Urgent-Relief Acceptance of Foreign Research Reactor Spent Nuclear Fuel," DOE/EA-0912, U.S. Department of Energy, Washington, DC, April 1994, Table E-7, p. E-12.

[7-19] D. A. Powers, et al., "A Review of the Technical Issues of Air Ingression During Severe Reactor Accidents," NUREG/CR-6218, Sandia National Laboratories, Albuquerque, NM, September 1994.

[7-20] T. L. Sanders, et al., "A Method for Determining the Spent-Fuel Contribution to Transport Cask Containment Requirements, Appendix III, Spent Fuel Response to Transport Environments," SAND90-2406, Sandia National Laboratories, Albuquerque, NM, November 1992.

[7-21] Ref. [7-20], p. III-48.

[7-22] Ref. [7-20], p. II-138.

[7-23] J. J. Gregory, et al., Thermal Measurements in Large Pool Fires, *J. Heat Transfer* **111**, 446 (1989).

[7-24] P. J. Nigrey, "Prediction of Packaging Seal Life Using Thermoanalytical Techniques," Proceedings of the 12th International Conference on the Packaging and Transportation of Radioactive Materials (PATRAM '98), IAEA, Vol. 4, p. 1730, 1998.

[7-25] H.-P. Weise, et al., "Untersuchung der Sicherheitreserven von Dichtsytemen für Umschliessungen zum Transport und zur Lagerung Radioaktiver Stoffe," Research Project BMU/St. Sch. 1081, Final Report, 1992.

[7-26] R. A. Lorenz, et al., "Fission Product Release from Highly Irradiated LWR Fuel," NUREG/CR-0722, Oak Ridge National Laboratory, Oak Ridge, TN, February 1980, pp. 48-80.

[7-27] E. L. Wilmot, "Transportation Accident Scenarios for Commercial Spent Fuel," SAND80-2124, Sandia National Laboratories, Albuquerque, NM, February 1981.

[7-28] Ref. [7-20], p. II-149.

[7-29] L. B. Shappert, et al., "Cask Designers Guide," ORNL-NSIC-68, Oak Ridge National Laboratory, Oak Ridge TN, February 1970, p. 156.

[7-30] J. L. Sprung, et al., "Data and Methods for the Assessment of the Risks Associated with the Maritime Transport of Radioactive Materials: Results of the SeaRAM Program, Vol. 2, Appendix IV, Cask-to-Environment Release Fractions," SAND97-2222, Sandia National Laboratories, Albuquerque, NM, August 1997.

[7-31] R. J. Burian, et al., "Response of Spent LWR Fuel to Extreme Environments," SAND85-7213, Sandia National Laboratories, Albuquerque, NM, August 1985 (unpublished contractor report prepared by Battelle Columbus Laboratories; available on request).

[7-32] R. P. Sandoval, R. J. Burian, et al., "Response of Spent LWR Fuel to Extreme Environments," Proceedings of International Symposium on the Packaging and Transportation of Radioactive Materials (PATRAM '86), IAEA, Vol. 2, p. 695, 1987.

[7-33] Airborne Release Fractions/Rates and Respirable Fractions for Nonreactor Nuclear Facilities, DOE-HDBK-3010-94, U.S. Department of Energy, Washington, DC, Vol. 1, p. 5-23.

[7-34] Ref. [7-20], p. IV-13.

[7-35] Y. Otani, *Aerosol Science Technol.* **10**, 463 (1989).

[7-36] R. A. Lorenz, "Fission Product Release from Simulated LWR Fuel," NUREG/CR-0274, Oak Ridge National Laboratory, Oak Ridge, TN, October 1978.

[7-37] R. A. Lorenz, et al., "Fission Product Source Terms for the Light Water Reactor Loss-of-Coolant Accident, *Nuclear. Technology*. **46**, 404 (1979).

[7-38] R. A. Lorenz, et al., "Fission Product Source Terms for the Light Water Reactor Loss-of-Coolant Accident," NUREG/CR-1288, Oak Ridge National Laboratory, Oak Ridge, TN, July 1980.

[7-39] Ref. [7-20], p. IV-5.

[7-40] K. K. Murata, et al., "Code Manual for CONTAIN 2.0: A Computer Code for Nuclear Reactor Containment Analysis," NUREG/CR-6533, SAND97-1735, Sandia National Laboratories, Albuquerque, NM, December 1977.

[7-41] Ref. [7-26], p. 48.

[7-42] Ref. [7-26], p. 128.

[7-43] F. P. Incropera and D. P. DeWitt, *Fundamentals of Heat and Mass Transfer,* John Wiley & Sons, New York, 1985.

[7-44] R. B. Bird, W. E. Stewart, and E. N. Lightfoot, *Transport Phenomena,* John Wiley & Sons, New York, 1960.

[7-45] N. E. Bixler, "VICTORIA 2.0: A Mechanistic Model for Radionuclide Behavior in a Nuclear Reactor Coolant System Under Severe Accident Conditions," NUREG/CR-6131, Sandia National Laboratories, Albuquerque, NM, 1998.

[7-46] Ref. [7-26], p. 104.

[7-47] Ref. [7-26], pp. 18-22.

[7-48] S. R. Dharwadkar and M. D. Karkhanavala, *Indian J. Chem,* **13**, 685 (1975).

[7-49] Ref. [7-20], p. III-51.

[7-50] Ref. [7-20], Table I-3, p. I-10.

[7-51] Ref. [7-20], Table I-17, p. I-51.

[7-52] Ref. [7-20], Figures I-10 through I-12, p. I-36.

[7-53] Ref. [7-20], p. I-30.

[7-54] R. K. Clarke, et al., "Severities of Transportation Accidents, Vol. IV, Train," SLA-74-0001, Sandia National Laboratories, Albuquerque, NM, July 1976, pp. 15-17.

[7-55] Ref. [7-1], Table 5.2, p. 5-10.

[7-56] Ref. [7-1], Table 5.1, p. 5-8 and Table 5.2, p. 5-10.

[7-57] 10CFR71.73

[7-58] L. A. Gritzo, et al., "Transient Measurements of Radiative Properties, Soot Volume Fraction and Soot Temperature in a Large Pool Fire," *Combust. Sci. and Tech*. 139, 113 (1998).

[7-59] A. R. Lopez, et al., "Risk Assessment Compatible Fire Models (RACFMs)," SAND97-1562, Sandia National Laboratories, Albuquerque, NM, July 1998.

8. RADTRAN CALCULATIONS

8.1 Calculations Performed

Seven sets of RADTRAN calculations and three RADTRAN sensitivity calculations are described in this section. Each calculation develops estimates of the radiological consequences and risks that are associated with the shipment of a single generic Type B cask that contains power reactor spent fuel. Two types of consequences and risks are estimated—those that are associated with the occurrence of accidents during the shipment and those associated with shipments that take place without the occurrence of accidents.

The seven sets of RADTRAN calculations examine four cask designs, two shipment modes, two sets of routes, and three sets of accident source terms. The four generic cask designs examined are steel-lead-steel truck and rail casks, a steel-DU-steel truck cask, and a monolithic steel rail cask. The two shipment modes are truck and rail. The two sets of routes are (a) 200 representative routes selected by Latin Hypercube Sampling (LHS) of route parameter distributions and (b) four illustrative real routes plus the NUREG-0170 shipment route (Illus). The three sets of accident source terms are the NUREG-0170 [8-1] source terms, the Modal Study source terms [8-2], and the new source terms developed by this study.

Table 8.1 lists the seven sets of RADTRAN calculations that were performed and the defining characteristics of each individual calculation. Table 8.1 shows that

- the **first set** of calculations examines the risks associated with shipping PWR and BWR spent fuel by truck (T) in steel-lead-steel (SLS T) and steel-DU-steel (SDUS T) casks;
- the **second set** examines the risks of performing these shipments by rail (R) in steel-lead-steel (SLS R) and monolithic steel (Mono R) casks;
- the **third set** examines the risks of shipping PWR spent fuel by truck in a steel-lead-steel cask over the following five illustrative (Illus) shipment routes: Crystal River Nuclear Plant in Florida to Hanford, Washington (C/H), Maine Yankee Nuclear Plant in Maine to Skull Valley, Utah (M/SV), Maine Yankee Nuclear Plant to the Savannah River Site in South Carolina (M/SR), Kewaunee Nuclear Plant in Wisconsin to the Savannah River Site (K/SR), and the representative truck route examined by NUREG-0170 [8-1];
- the **fourth set** repeats these PWR spent fuel shipment calculations for rail shipments in a monolithic steel cask;
- the **fifth set** examines the influence on spent fuel truck accident risks of the inventory, source term, and exposure pathway models that were used in NUREG-0170;
- the **sixth set** calculates spent fuel truck accident shipment risks using Modal Study and NUREG-0170 Model I (Mod I) and Model II (Mod II) source terms; and
- the **seventh set** repeats the sixth set for spent fuel rail shipments.

The three sensitivity calculations examine the dependence of accident risks on rod failure fractions, the risks associated with heavy haul truck transport of spent fuel, and the risks posed by Loss of Shielding (LOS) accidents during spent fuel transport. These sensitivity calculations are described in Sections 8.10.3, 8.11 and 8.12 respectively.

Table 8.1 Characteristics of Sets of RADTRAN Calculations

Set	Calc.	Routes		Inventory[a]			Severity and Release Fractions														Exp. Paths		Section where calculation discussed
		LHS	Illus	This Study		0170	This Study								NUREG-0170				Modal Study		All	Inhal	
							SLS T		SDUS T		SLS R		Mono R		Mod 1		Mod 2						
				PWR	BWR		PWR	BWR	PWR	BWR	PWR	BWR	PWR	BWR	T	R	T	R	T	R			
1	1	X		X			X														X		Sect. 8.6
	2	X			X			X													X		
	3	X		X					X												X		
	4	X			X					X											X		
2	5	X		X							X										X		Sect. 8.7
	6	X			X							X									X		
	7	X		X									X								X		
	8	X			X									X							X		
3	9		C/H	X			X														X		Sect. 8.10.1
	10		M/SV	X			X														X		
	11		M/SR	X			X														X		
	12		K/SR	X			X														X		
	13		0170	X			X														X		
4	14		C/H	X									X								X		Sect. 8.10.2
	15		M/SV	X									X								X		
	16		M/SR	X									X								X		
	17		K/SR	X									X								X		
	18		0170	X									X								X		
5	19	X		X											X						X		Sect. 8.13
	20	X		X													X				X		
	21	X				X											X				X		
	22	X				X											X					X	
6	23	X				X									X							X	Sect. 8.14
	24	X		X															X		X		
7	25	X				X										X						X	
	26	X				X												X				X	
	27	X		X																X	X		

Table 8.1 also shows that (a) calculations, that do not examine a single specific real route, examine the representative set of 200 truck or rail routes constructed by LHS sampling of route parameter distributions and (b) four of the five calculations, that use the NUREG-0170 inventory, model only radiation exposures occur via inhalation pathways (Inhal).

8.2 The RADTRAN 5 Computational Scheme

The core computation embedded in the RADTRAN 5 code estimates the risks associated with the shipment of a single radioactive material along a single route. Given a radioactive material, package specifications, route data, prevailing weather conditions, an accident source term, and emergency response actions (i.e., population evacuation and decontamination and/or condemnation of contaminated property), RADTRAN 5 calculates the population dose that would result if the specified accident occurs (the accident dose) and if the accident does not occur (the incident-free dose). RADTRAN's computational scheme allows this core calculation to be repeated by looping over additional route segments, weather conditions, and accident source terms. The number of cases that can be examined using this internal loop structure is limited. Therefore, when a very large number of cases needs to be examined, the examination is accomplished using code's Latin Hypercube Sampling computational shell [8-3], which allows large sets of parameter values, selected by sampling from distributions, to be sequentially provided to RADTRAN 5 as separate input files.

8.2.1 Latin Hypercube Sampling

LHS is a structured Monte Carlo sampling method that produces results comparable to those obtained with random Monte Carlo sampling methods using samples that are much smaller than those required by the random sampling methods. Although originally developed to support uncertainty and sensitivity studies, Latin Hypercube Sampling was used in this study to generate representative sets of values for a number of RADTRAN 5 input parameters, for example, route parameters, that can take on a wide range of values in the real world.

8.2.2 Size of the LHS Sample

The size of the LHS sample that provides adequate coverage of the sampled distributions was determined by comparing results calculated (a) with samples of different sizes and (b) with samples of the same size selected using different random seed values. Table 8.2 compares the accident population dose risks (maximum value, minimum value, and the mean value and its standard deviation) obtained for a particular spent fuel shipment calculation using 100, 200, 300, 400, and 500 sets of RADTRAN 5 input selected by LHS sampling. Table 8.2 shows that mean result and its standard deviation are quite stable for samples of size 200 or larger (for example, the mean and standard deviation for the samples of size 200 and 500 are nearly identical), and that increasing sample size beyond 200 principally affects the values of the largest (maximum) and smallest (minimum) observations in the sample. The adequacy of a sample of size 200 was further examined by varying the value of the random seed used to generate the LHS sample. Table 8.3 shows that for samples of size 200, changing the value of the random seed principally affects the values of the maximum and minimum observations in the sample and has little effect on the value of the mean or its standard deviation. Thus, the results presented in these two tables indicate that an LHS sample of size 200 (a sample that contains 200 sets of RADTRAN 5 input

values for the parameters sampled) will develop a representative set of values for each sampled parameter (e.g., for the parameters that define the truck and rail routes used in the calculations that examine representative rather than illustrative routes), and consequently reasonable estimates of the mean values for calculated results.

Table 8.2 RADTRAN 5/LHS Accident-Risk Results versus Number of Observations

Observations	100	200	300	400	500
Mean	2.73E-7	2.87E-7	2.90E-7	2.82E-7	2.86E-7
Standard Deviation	2.45E-7	2.83E-7	3.06E-7	2.94E-7	2.85E-7
Maximum	1.13E-6	1.79E-6	1.70E-6	2.34E-6	2.00E-6
Minimum	5.3E-9	1.68E-9	3.42E-9	2.70E-9	1.14E-9

Table 8.3 RADTRAN 5/LHS Accident-Risk Results for 200 Observations versus "Seed"

Random Seed	#1	#2	#3	#4	#5
Mean	2.87E-7	2.96E-7	2.80E-7	2.85E-7	2.78E-7
Standard Deviation	2.83E-7	3.20E-7	2.89E-7	3.13E-7	2.70E-7
Maximum	1.79E-6	1.64E-6	1.71E-6	1.92E-6	1.38E-6
Minimum	1.68E-9	4.17E-9	4.40E-9	8.88E-11	4.47E-9

8.3 Input Parameters and Results Calculated

All of the RADTRAN 5 calculations performed for this study examined spent fuel transported in a Type B cask. All of the routes examined had three aggregate segments, one urban, one suburban, and one rural. Thus, all of the RADTRAN 5 calculations used the following input:

- the cask's spent fuel inventory (three-year cooled, high-burnup PWR and BWR inventories with respective burnups of 60 and 50 gigawatt-days per metric ton of uranium) or the NUREG-0170 inventory that specifies the curie amounts released to the atmosphere during spent fuel transportation accidents of the three radionuclides (Kr-85, I-131, and Cs-137) used to represent all radionuclides contained in the cask inventory;

- 200 representative routes, 1 illustrative route, or the NUREG-0170 route, each having three segments;

- traffic densities and speeds, average vehicle occupancy, accident rates, population densities, and lengths for each of the three aggregate route segments;

- the number of times the spent fuel transport vehicle (the truck or train) stops (e.g., rest stops or stops for inspections), while traversing each segment, the duration of each stop, and the number of people that might be exposed to radiation as a result of the stop;

- the dose rate 1 m from the surface of the spent fuel cask (the package dose rate);

- the weather conditions that prevail while the segment is traversed (the Pasquill-Gifford atmospheric stability class that characterizes the prevailing weather conditions at the time of any hypothetical accident);

- the 19 sets of truck accident release fractions or the 21 sets of train accident release fractions developed for this study, the 8 sets of NUREG-0170 Model I or Model II release fractions, or the 20 sets of Modal Study release fractions;

- the fraction of all possible accidents estimated to cause each set of release fractions (the severity fraction of this type of accident);

- an evacuation time (time after the occurrence of an accident when evacuation of possibly exposed population is completed); and

- values for all of the other RADTRAN 5 input parameters (the parameters that have values that do not depend on the nature of the radioactive material being shipped, the shipment route, the accident source term, prevailing weather, or emergency response actions).

Given this input, each RADTRAN 5 calculation performed for this study calculated

- the incident-free doses incurred by various population groups (e.g., inspectors, persons living along the route, persons traveling in other vehicles on the route) while the spent fuel shipment traveled along each aggregate route segment and the sum of these doses for each population group and for all population groups together (i.e., the total incident-free dose); and

- the accident doses that would result if, during the course of the shipment, the spent fuel truck or train were to be involved in an accident that causes some of the rods in the cask to fail, the cask containment to be compromised, and consequently some radioactive material to be released to the environment.

8.4 Number of Cases Examined

For each route modeled, the number of cases, N_{cases}, examined (core calculations performed) by each RADTRAN 5 calculation is given by $N_{cases} = N_{segments}N_{release\ fraction\ sets}$, where $N_{segments} = 3$ and $N_{release\ fraction\ sets} = 8$ when NUREG-0170 source terms are used; $N_{release\ fraction\ sets} = 20$ when Modal Study source terms are used; and as Table 7.31 shows, $N_{release\ fraction\ sets} = 19$ for truck transport and 21 for rail transport when the new source terms developed by this study are used.

The number of sets of new release fractions examined can be less than the total number of sets of release fractions developed in Section 7, because, as Table 7.31 shows, some of the sets of accident release fractions developed in Section 7 have associated severity fraction values of zero,

which means that the accident conditions that lead to the specified set of release fractions are estimated to have zero probability of occurrence (i.e., are estimated to be unattainable during credible accidents). For example, when the steel-DU-steel truck cask is carrying PWR spent fuel, 6 of its 19 sets of release fractions have severity fraction values of zero. Thus, for each route modeled, all of the RADTRAN 5 calculations that used this set of severity fractions and release fractions examined 39 cases where $39 = N_{cases} = N_{segments}N_{release\ fraction\ sets} = 3 \times 13$.

In summary, for each route modeled, the number of cases examined (core calculations performed) by each RADTRAN 5 calculation were as follows: $24 = 3 \times 8$ for calculations that used NUREG-0170 source terms; $60 = 3 \times 20$ for calculations that used Modal Study source terms; and $39 = 3 \times 13$, $45 = 3 \times 15$, and $63 = 3 \times 21$ for calculations that used respectively the steel-DU-steel truck cask source terms, the steel-lead-steel truck cask source terms, and the steel-lead-steel and monolithic steel rail cask source terms developed for this study.

8.5 Complementary Cumulative Distribution Functions

The results calculated for the sets of 24, 60, 39, 45, or 63 cases are displayed as Complementary Cumulative Distribution Functions (CCDFs), which are plots of the probability of occurrence of an accident population dose of a given size or larger (i.e., the probability associated with each consequence value is the sum of the probabilities of that and all larger consequence values). In addition, the area under any of these CCDFs is the expected (mean) population dose risk in person-rem for the set of accidents represented by that curve.

Because 200 different sets of input were examined during each RADTRAN 5 calculation, each of these calculations generated 200-accident dose CCDFs. Figure 8.1 displays the 200 CCDFs that were calculated for the steel-lead-steel cask when that cask was transporting one PWR spent fuel assembly. Because of the density of the CCDF curves plotted in this figure, this plot depicts poorly the information that is embedded in the set of 200 CCDFs that are plotted on the figure.

To better depict the spread of possible consequences and their probabilities of occurrence, four compound CCDFs are constructed. These four compound CCDFs are the expected (mean) result, and the 5^{th}, 50^{th} (median), and 95^{th} percentile results, where for any specific single consequence value the corresponding 5^{th} and 95^{th} percentile probabilities are the probabilities of the CCDFs that lie 10 up from the bottom and 10 down from the top of the set of 200 CCDFs, the corresponding median percentile probability is the average of the probability values for CCDF 100 and CCDF 101, and the expected (mean) result is the average of all of the CCDF probability values that correspond to the specified consequence value.

8.6 Results for the Generic Steel-Lead-Steel and Steel-DU-Steel Truck Casks

The four compound CCDFs that correspond to Figure 8.1 are plotted in Figure 8.2. Specifically, Figure 8.2 presents the expected (mean) CCDF and the CCDFs that represent the 5^{th}, 50^{th} (median), and 95^{th} percentile values of the set of 200 CCDFs that were calculated using the PWR source terms developed for the generic steel-lead-steel truck cask and the representative LHS input sample of size 200. Each element in this LHS sample specified values for all route related

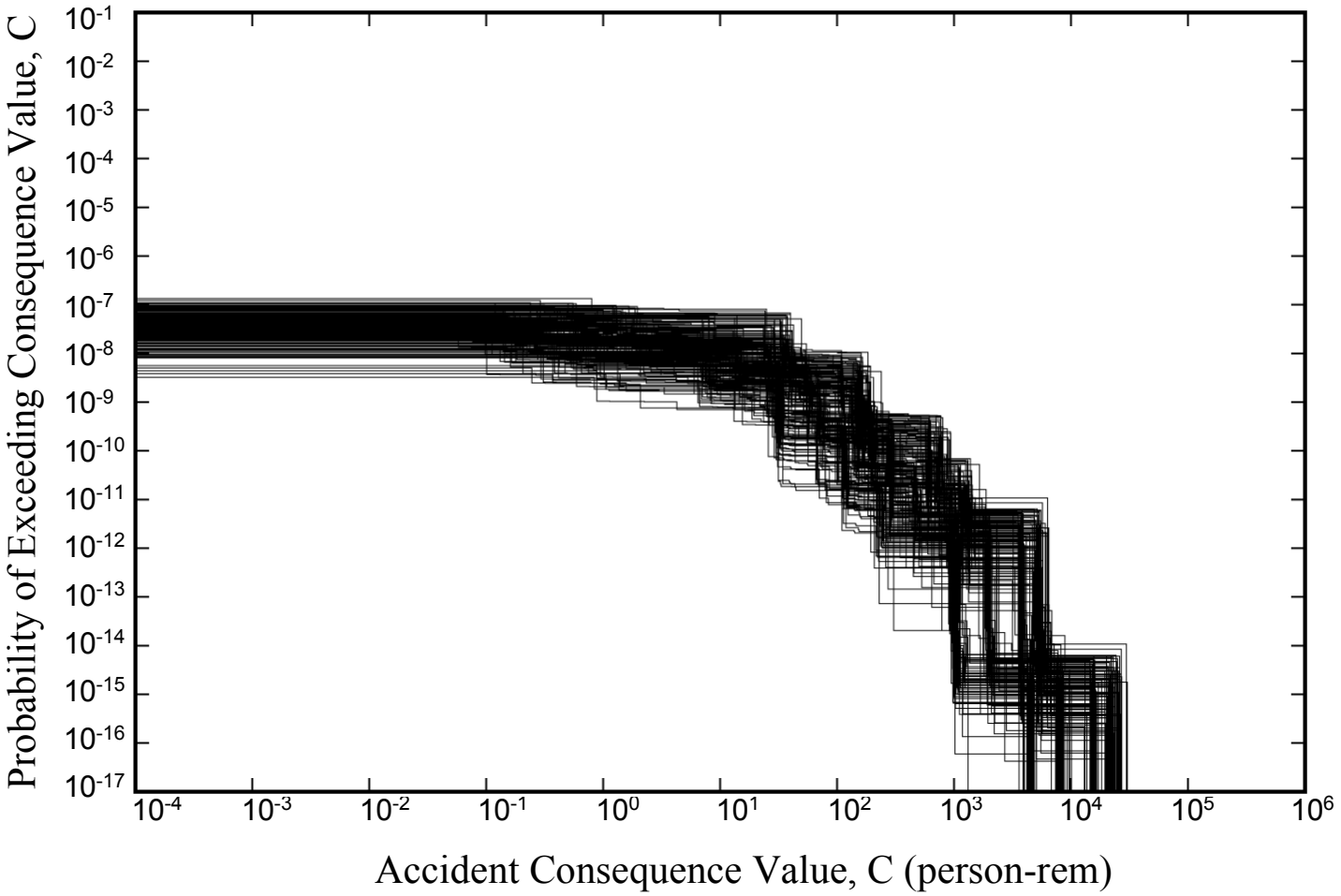

Figure 8.1 Two hundred truck accident population dose risk CCDFs, one CCDF for each representative truck route. Each RADTRAN 5 calculation examined all 19 representative truck accident source terms and assumed transport of PWR spent fuel in the generic steel-lead-steel truck cask.

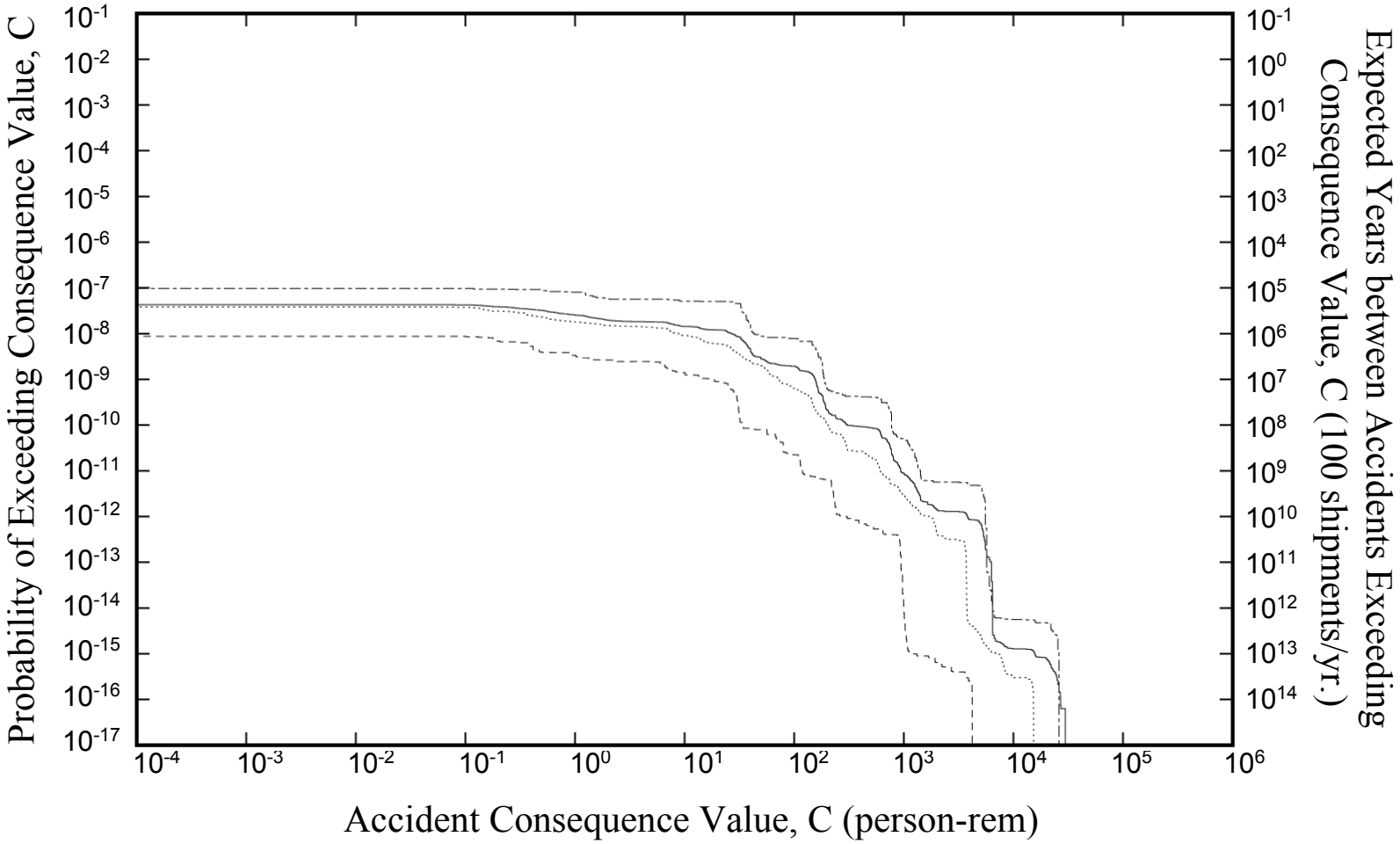

Figure 8.2 Truck accident population dose risk CCDFs for transport of PWR spent fuel in the generic steel-lead-steel truck cask over the 200 representative truck routes. Each underlying RADTRAN 5 calculation generated results for all of the 19 representative truck accident source terms.

Mean (————) CCDF, and 95th (- - - - - - - -), 50th (· · · · · · · · · ·), and 5th (- - - - - - - - - -) quantiles

parameters (e.g., segment length, segment population and segment vehicle densities, and average segment vehicle occupancy and speed), a type of prevailing weather (Pasquill-Gifford stability category), a package dose rate, a set of STOP parameter values, and the time after accident initiation when any evacuation of downwind population is completed. Because the LHS sample contained 200 sets of input data, the compound CCDF for the expected (mean) population dose is based on (derived from) $200 \times 45 = 9000$ cases (core calculations) that each examine one route segment, one prevailing weather, and one value for all of the other sampled parameters. Because the 15 source terms examined by this calculation are not specified in the LHS sample, the effect of the range of source term sizes on accident population dose is depicted by the curvature of each of the four compound CCDFs while the effects of the parameters that are varied within the LHS sample are depicted by the range (spread) of the four compound CCDFs at any single value of accident population dose.

The CCDF in Figure 8.2 and all subsequent CCDFs contain a second y-axis scale that was not present in the CCDF in Figure 8.1. That scale gives an estimate of the expected time between accidents that have consequences that exceed the corresponding x-axis value (consequences > C). Thus, an accident that has an expected time between accidents of 100 years would be expected on average to occur about once every 100 years, although there is a slight chance that two of these accidents could occur within a few years of each other. For example, inspection of the figure shows that an accident that produces a population dose that exceeds 1 rem is expected to occur about once every million years .

The values on the left-hand y-axis, the probability axis, are converted to those on the right-hand y-axis, the expected time between accidents axis, by taking the reciprocal of the product of the probability axis value and an estimate of the number spent fuel shipments likely to occur each year, i.e., years per accident = $[(\text{accidents per shipment})(\text{shipments per year})]^{-1}$. The following qualitative arguments allow an order-of-magnitude estimate of the number of spent fuel shipments per year to be developed.

An interim or permanent storage facility can probably receive at most a few casks per day or perhaps several hundred per year. The U.S. DOE has estimated [8-4] that during the first decade of spent fuel shipments, about 900 MTU will be shipped per year, which is equivalent to about 80 rail shipments per year. If 900 MTU are shipped per year by truck, about 1000 shipments per year would be needed; however, because rail is the preferred shipment mode, many fewer truck shipments are likely to be made per year. The entire spent fuel inventory can be shipped by rail over thirty years at a rate of about 200 shipments per year. Forty rail casks making a round-trip by regular freight once every two weeks can handle about 200 shipments per year. Therefore, because it is easy to scale (e.g., at 200 rather than 100 shipments per year, all of the right-hand y-axis values would be halved), an order-of-magnitude value of 100 shipments per year was used to convert the probability axis values to the values on the expected time between accidents axis.

Figures 8.3 through 8.5 respectively present sets of compound CCDFs for the generic steel-lead-steel truck cask carrying BWR spent fuel, for the generic steel-DU-steel truck cask carrying PWR spent fuel, and for the generic steel-DU-steel truck cask carrying BWR spent fuel, that are

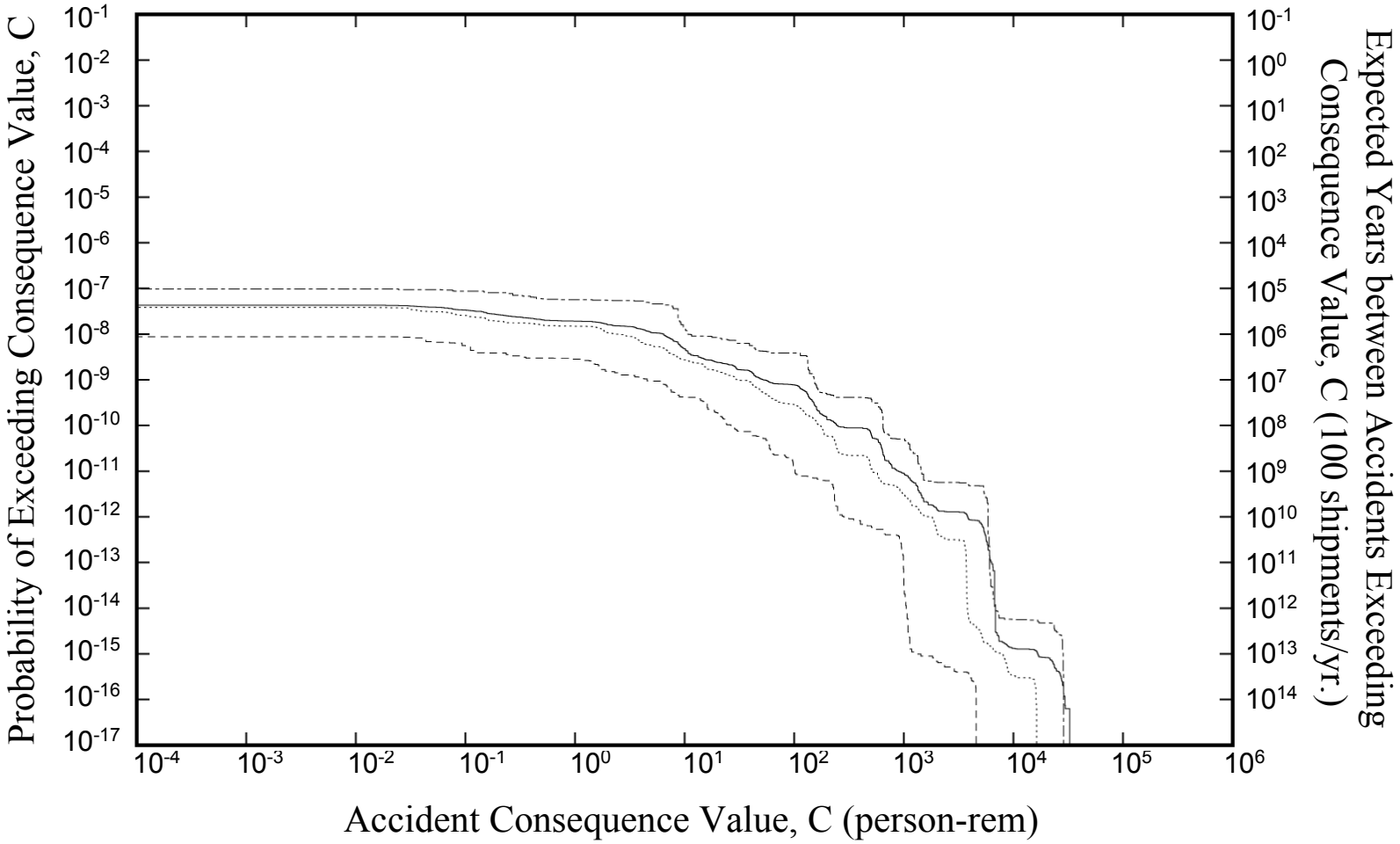

Figure 8.3 Truck accident population dose risk CCDFs for transport of BWR spent fuel in the generic steel-lead-steel truck cask over the 200 representative truck routes. Each underlying RADTRAN 5 calculation generated results for all of the 19 representative truck accident source terms.

Mean (————) CCDF, and 95th (- - - - - - - -), 50th (· · · · · · · · · ·), and 5th (- - - - - - - - - -) quantiles

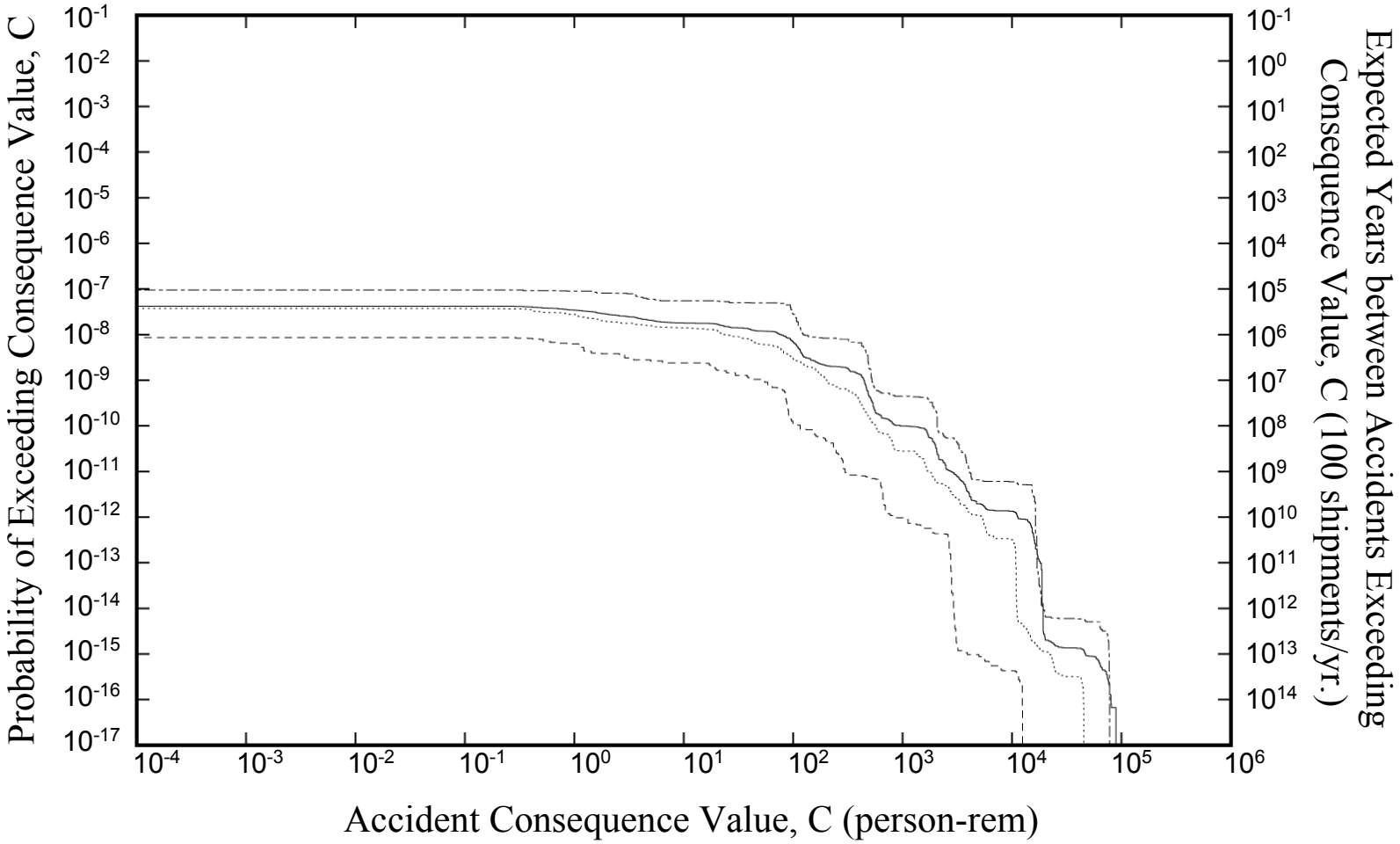

Figure 8.4 Truck accident population dose risk CCDFs for transport of PWR spent fuel in the generic steel-DU-steel truck cask over the 200 representative truck routes. Each underlying RADTRAN 5 calculation generated results for all of the 19 representative truck accident source terms.

Mean (————) CCDF, and 95th (- - - - - - -), 50th (· · · · · · · · · ·), and 5th (- - - - - - - - - -) quantiles

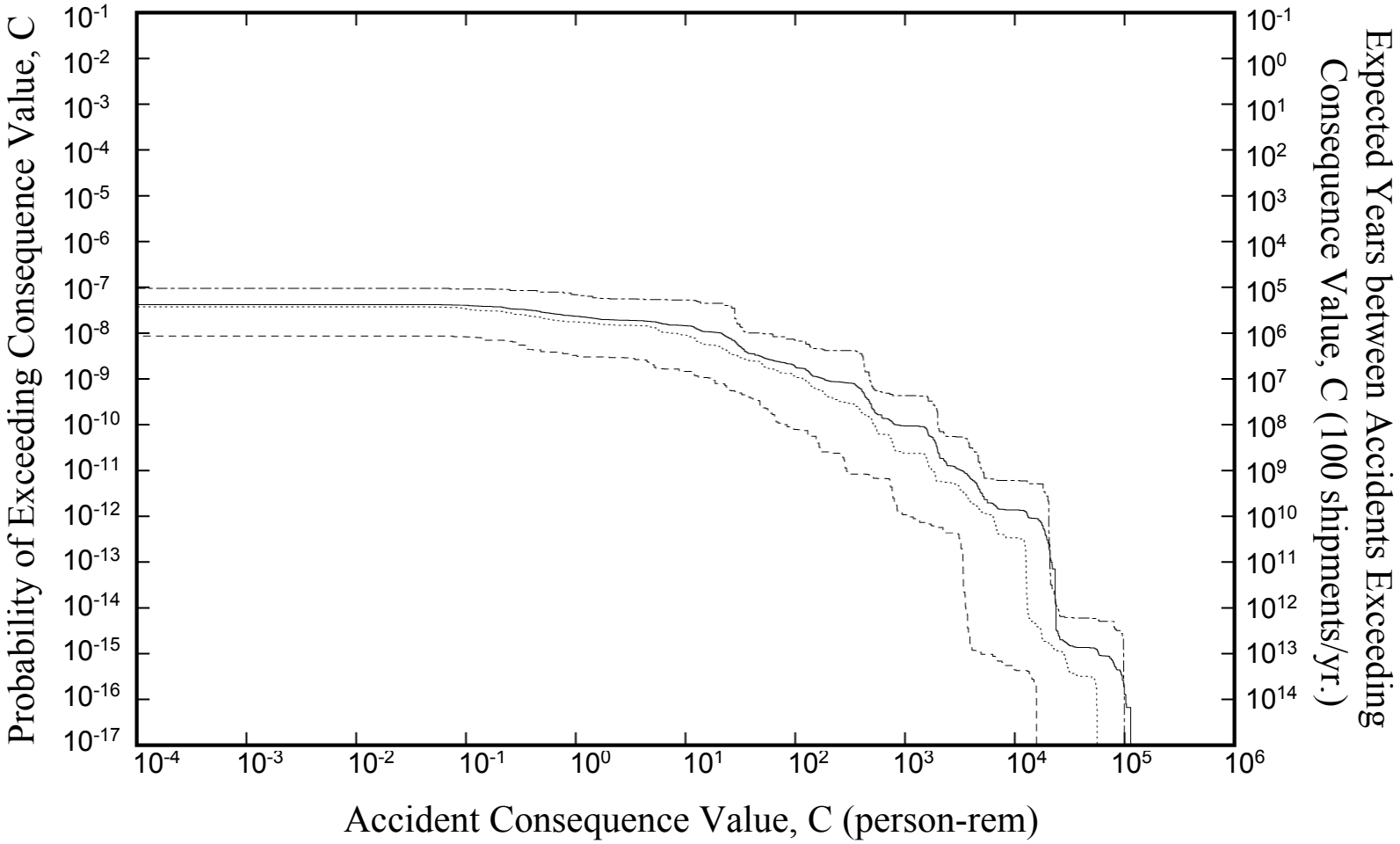

Figure 8.5 Truck accident population dose risk CCDFs for transport of BWR spent fuel in the generic steel-DU-steel truck cask over the 200 representative truck routes. Each underlying RADTRAN 5 calculation generated results for all of the 19 representative truck accident source terms.

Mean (————) CCDF, and 95th (- - - - - - - -), 50th (· · · · · · · · · ·), and 5th (- - - - - - - - - -) quantiles

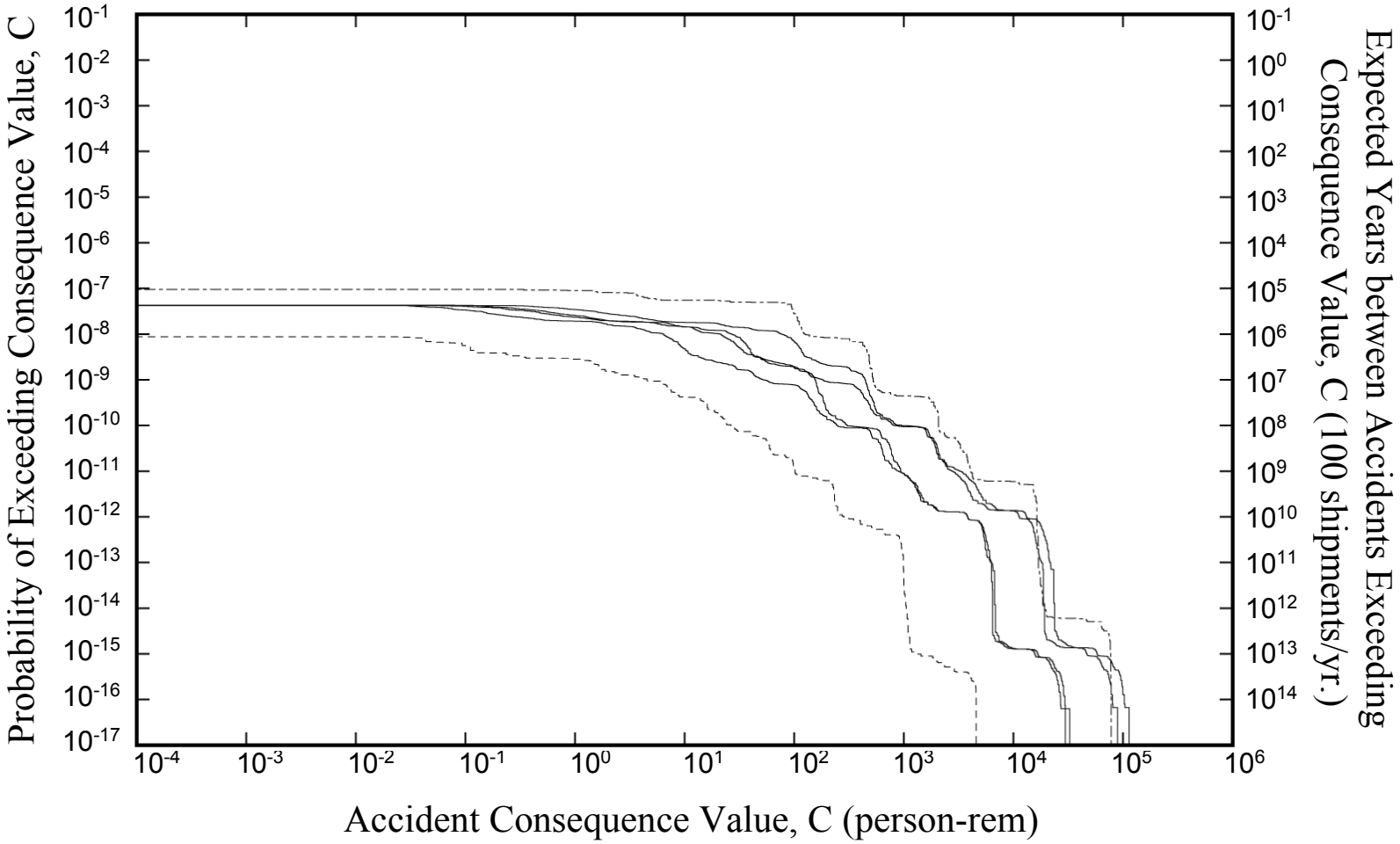

Figure 8.6 Comparison of truck accident population dose risk CCDFs for transport of PWR or BWR spent fuel in generic steel-lead-steel or steel-DU-steel truck casks over the 200 representative truck routes. Each underlying RADTRAN 5 calculation generated results for all of the 19 representative truck accident source terms.

Four Mean CCDFs (———), and Highest 95th (----------) and Lowest 5th (·····) quantiles

exactly analogous to those presented in Figure 8.2. The expected (mean) CCDFs from Figures 8.2 through 8.5 and the highest 95th percentile and lowest 5th percentile CCDF in these four figures are plotted together in Figure 8.6. Thus, this figure depicts the likely range of truck accident population doses for accidents that are severe enough to cause a Type B spent fuel cask to lose containment and to fail some of the rods in the cask.

The area under the expected (mean) CCDF in Figures 8.2 through 8.5 is the expected value of truck accident population dose for the entire set of RADTRAN 5 spent fuel truck transport calculations performed for each generic truck cask and type of spent fuel. Table 8.4 presents these expected truck accident population doses and compares them to the expected (average) values of three incident-free population doses (stop, other, and total incident-free dose) that were developed by the same set of calculations. Because all incident-free doses have a probability of occurrence of one (i.e., if the spent fuel shipment is completed without an accident occurring, the estimated incident-free doses presented in Table 8.4 will be incurred), the value of any incident-free population dose is also the value of the corresponding incident-free population dose-risk, and the average of all of the values of any specific incident-free population dose is the expected (mean) value of that incident-free dose.

In Table 8.4, two values for Stop Dose are presented for each metric. The first value, the "Sleep" value, was calculated assuming that the one-person truck crew makes stops for inspections, to eat, to refuel, and to sleep. Because of these stops, on average the truck stops for 0.011 hour for each kilometer traveled [8-5], where this value was developed by surveying the types of stops and stop times made by typical commercial tractor semi-trailer trucks [8-5]. The second stop dose value, the "No Sleep" value, was calculated by dividing the first value, the "Sleep" value, by 28. This was done after phone calls to shippers of Hazardous materials [8-6] indicated that trucks transporting spent fuel casks have two-person crews, do not make sleep stops, and thus have a stop time per kilometer of travel much smaller than 0.011 hours per kilometer.

The phone calls [8-6] to shippers of Hazardous Material developed the following picture of the types of stops and stop times made by trucks transporting spent fuel casks. First, the 2-person crews of these trucks alternate driving on 4-hour shifts. During each 12-hour period, one driver drives for eight hours and sleeps for four hours and the other driver drives for four hours, sleeps for four hours, and rides as an escort for four hours. During the second 12-hour period in each day, this pattern is reversed. Two types of stops are made, food/refueling stops and inspection stops. Inspection stops are made every 100 miles or every two hours, whichever comes first. Since average truck speeds on interstate highways are greater than 50 mph, an inspection stop is made once every 100 miles, preferably at a truck stop, sometimes on a freeway exit ramp, or, if necessary, on the freeway shoulder. Regulations stipulate that the first inspection stop should be made after 25 miles of travel so that the cask tiedowns can be checked. Additional inspection stops are then made after each additional 100 miles of travel. After each 800 miles of travel, a stop is made for refueling and to eat or buy food. These stops may last as long as an hour, but typically take only 30 minutes. Because the inspections are "walk-around" inspections, they take at most 15 minutes and usually about 10 minutes. Thus, industry practice for spent fuel shipments under exclusive use conditions is to use two-man crews and to minimize stop time by not making stops to sleep.

Table 8.4 Incident-Free and Accident Population Dose Risks for Truck Transport

Metric	Population Dose Risks (person-rem)					
	Incident-Free					Accident
	Stops[a]		Other[b]	Total		
	Sleep[c]	No Sleep[d,e]		Sleep[c]	No Sleep[d]	
PWR Spent Fuel; Steel-Lead-Steel Cask; 1 Assembly						
Mean =	0.427	0.0153	0.0288	0.456	0.0441	8.00E-07
Standard Deviation =	0.296	0.0106	0.0238	0.297	0.0261	8.53E-07
Maximum =	1.840	0.0657	0.1340	1.974	0.1997	4.38E-06
Minimum =	0.017	0.0006	0.0024	0.019	0.0030	4.06E-08
PWR Spent Fuel; Steel-DU-Steel Cask; 3 Assemblies						
Mean =	0.427	0.0153	0.0288	0.456	0.0441	2.29E-06
Standard Deviation =	0.296	0.0106	0.0238	0.297	0.0261	2.44E-06
Maximum =	1.840	0.0657	0.1340	1.974	0.1997	1.24E-05
Minimum =	0.017	0.0006	0.0024	0.019	0.0030	1.14E-07
BWR Spent Fuel; Steel-Lead-Steel Cask; 2 Assemblies						
Mean =	0.427	0.0153	0.0288	0.456	0.0441	3.30E-07
Standard Deviation =	0.296	0.0106	0.0238	0.297	0.0261	3.61E-07
Maximum =	1.840	0.0657	0.1340	1.974	0.1997	1.99E-06
Minimum =	0.017	0.0006	0.0024	0.019	0.0030	1.68E-08
BWR Spent Fuel; Steel-DU-Steel Cask; 7 Assemblies						
Mean =	0.427	0.0153	0.0288	0.456	0.0441	1.08E-06
Standard Deviation =	0.296	0.0106	0.0238	0.297	0.0261	1.20E-06
Maximum =	1.840	0.0657	0.1340	1.974	0.1997	6.51E-06
Minimum =	0.017	0.0006	0.0024	0.019	0.0030	5.22E-08

a. Exposures at rest, food, and refueling stops.
b. Sum of on-link, off-link, and crew doses.
c. Sleep means that the truck makes a rest stop of 8 hours once every 24 hours so the crew can sleep.
d. No Sleep means that the truck doesn't make any rest stops to allow the crew to sleep.
e. The No Sleep stop dose is obtained by dividing the Sleep stop dose by 28.

The pattern of spent fuel shipment stops described above suggests that seven 10 minute inspection stops and one 30 minute food/refueling stop will be made during each 1280 kilometer = 800 mile portion of a truck spent fuel shipment. Thus, the total stop time for each 1280 kilometers of travel when no stops to sleep are made will be 1.67 hrs = [7(10 minutes) +1(30 minutes)]/60 minutes hr^{-1}.

The effect on stop doses of eliminating sleep stops is now developed for two spent fuel shipment routes. The first route, Crystal River to Hanford, is one of the four illustrative real routes examined below in Section 8.10, while the second route has route parameter values that are set to

the means of the distributions of route parameter values that were used to construct the LHS sample of size 200. The lengths and urban, suburban, and rural length fractions and population densities of these two routes are given below in Table 8.7.

The stop model implemented in RADTRAN 5, the version of RADTRAN used in this study, calculates stop doses to people in two radial intervals centered on the stopped truck that is transporting the spent fuel cask, 1 to 10 m and 10 to 800 m. The population density of the first interval is assumed to be 30,000 people per square kilometer (0.03 people per square meter). The population density of the second interval is set equal to the average population density of the suburban portions of the route. No shielding is assumed for persons in the first interval. Because of intervening trucks and buildings, a shielding factor of 0.2 is assumed for persons in the second interval.

When stops to sleep are assumed to occur, the total stop time for the Crystal River-to-Hanford route, which has a length of 4818.5 km, is 53 hours = (4818.5 km)(0.011 hr km-1). Using this total stop time, RADTRAN predicts that the aggregate stop dose received by persons in these two intervals aggregated over all stops will be 0.128 person-rem to persons exposed in the first interval, the area immediately adjacent to the spent fuel truck, and 5.4×10^{-4} person-rem to other persons at the truck stop and residents of the area that immediately neighbors the truck stop.

An estimate of the stop doses that would result for the Crystal River-to-Hanford route if the route is traveled without making stops to sleep can be developed by scaling these two stop doses using scale factors that reflect (a) the smaller stop times incurred when stops to sleep are not made, (b) changes in the densities of the exposed populations, and (c) changes in the shielding factors that apply to each exposed population group. To do this let

D_1 = the dose to persons exposed in the first radial interval = 0.128 person-rem
D_2 = be the dose to persons exposed in the second radial interval = 5.4×10^{-4} person-rem
$f_{shielding}$ = the shielding factor assumed for persons in the second radial interval = 0.2
$t_{rest,sleep}$ = the stop time at rest stops when sleep stops are made = 53 hrs
$t_{rest,no\ sleep}$ = the stop time at rest stops when sleep stops are made = 1.9 hrs = 0.5 hrs (4818.5 km/1280 km)
$t_{inspections}$ = the time spent at inspection stops = 4.4 hrs = (70 min/60 min per hr)(4818.5 km/1280 km)
ρ_{rest} = the population density of the first radial interval = 3×10^4 persons/km^2
ρ_{urban} = the population density of urban portions of the Crystal River-top-Hanford route = 2190 persons/km^2
$\rho_{suburban}$ = the population density of suburban portions of the Crystal River-top-Hanford route = 331 persons/km^2
ρ_{rural} = the population density of rural portions of the Crystal River-top-Hanford route = 7.5 persons/km^2
f_{urban} = the urban length fraction of the Crystal River-top-Hanford route = 0.01
$f_{suburban}$ = the suburban length fraction of the Crystal River-top-Hanford route = 0.15
f_{rural} = the rural length fraction of the Crystal River-top-Hanford route = 0.84

Given these definitions, the population dose for transit of the Crystal River-to-Hanford route if no sleep stops are made is

$$Dose_{no\ sleep} = (D_1 + D_2)\left(\frac{t_{rest,no\ sleep}}{t_{rest,sleep}}\right) + \left(D_1\left[\frac{\rho_{suburban}}{\rho_{rest}}\right] + D_2\left[\frac{1}{f_{shielding}}\right]\right)\left(\frac{t_{inspections}}{t_{rest,sleep}}\right)F_{population}$$

where

$$F_{population} = f_{urban}\left(\frac{\rho_{urban}}{\rho_{suburban}}\right) + f_{suburban}\left(\frac{\rho_{suburban}}{\rho_{suburban}}\right) + f_{rural}\left(\frac{\rho_{rural}}{\rho_{suburban}}\right)$$

In the first equation, the factor ($t_{rest,no\ sleep}/t_{rest,sleep}$) corrects $D_1 + D_2$, the rest stop dose for travel with sleep stops, for the decrease in time spent at rest stops when travel takes place without sleep stops; the factor ($\rho_{suburban}/\rho_{rest}$) adjusts D_1, the dose in the first radial interval, to the dose that would be received if the first radial interval had a suburban population density; the factor ($1/f_{shielding}$) corrects D_2, the dose received in the second radial interval, which is assumed to have a suburban population density, to the dose that would be received by the population of this interval if their shielding factor had a value of 1.0, the value used in RADTRAN for persons who are outdoors; and the factor $(t_{inspections}/t_{rest,sleep})F_{population} = (t_{inspections}/t_{rest,sleep})\Sigma f_i\rho_i/\rho_{suburban}$, where i = urban, suburban, or rural, scales this adjusted rest stop dose for travel with sleep stops for the fraction of time spent at inspection stops in urban, suburban, and rural areas and also for the ratio of the population density of each of these regions to that of the suburban region, which is the reference population density for the adjusted rest stop dose.

Finally, substitution of the values for the parameters that enter these two equations into the equations yields $Dose_{no\ sleep} = 4.69x10^{-3}$ person-rem (note that this value is essentially unchanged if the first radial interval at inspection stops is assumed to be devoid of population, which would likely be true for inspection stops conducted on freeway offramps or shoulders). Accordingly,

$$Dose_{sleep}/Dose_{no\ sleep} = (0.128 \text{ person-rem} + 5.4x10^{-4} \text{ person-rem})/4.69x10^{-3} \text{ person-rem} = 27.4$$

A nearly identical scale factor can be derived using the mean values of the distributions of route lengths and urban, suburban, and rural length fractions and population densities, that were sampled to produce the LHS sample of size 200. Thus, for an 800 mile = 1280 km portion of this route,

$$\frac{Dose_{sleep}}{Dose_{no\ sleep}} = \frac{(person-hours)_{sleep}}{(person-hours)_{no\ sleep}} = \frac{\rho_{rest}(1280\text{ km})(0.011\text{ hr km}^{-1})}{t_{inspection\ stop}\sum_i N_i\rho_i + t_{rest\ stop}\rho_{rest}}$$

where $t_{inspection\ stop} = 0.17$ hr = 10 min/60 min, $t_{rest\ stop} = 0.5$ hr = 30 mi/60 min, as before i = urban, suburban, or rural, N_i = the number of inspection stops in each portion of the route, and, given the fractions of the route length that are urban, suburban, and rural, $N_{urban} = 0$, $N_{suburban} = 2$, and $N_{rural} = 5$. Substitution of parameter values into this equation now yields

$$Dose_{sleep}/Dose_{no\ sleep} = 4.36x10^5 \text{ person-hrs}/1.51x10^4 \text{ person-hrs} = 28.9$$

Since the average of this value and the value for the Crystal River-to-Hanford route is 28.2, stop doses for travel without sleep stops was estimated by dividing the stop dose calculated by RADTRAN for travel with sleep stops by 28.

Table 8.4 shows that all four truck spent fuel transport calculations yield the same set of incident-free population doses. Each calculation yields the same set of incident-free doses because the incident-free portion of these calculations each used the same set of 200 routes and 200 cask dose rate values. Table 8.4 also shows (a) that incident-free population dose incurred at stops exceeds all other incident-free population doses by a factor of 15 if sleep stops are assumed to be taken, (b) that other incident-free doses exceed stop dose by about a factor of 2 if transport is assumed to occur without sleep stops, and (c) that for any combination of a cask and a type of spent fuel (e.g., the steel-lead-steel cask carrying PWR spent fuel) the expected value of the total incident-free population dose risk exceeds the expected value of the accident population dose risk by at least a factor of $2x10^4 = 0.0441/2.29x10^{-6}$, if no stops for sleep are taken, or as much as $1.4x10^6 = 0.456/3.3x10^{-7}$, were sleep stops to be taken. Thus, for any truck shipment, incident-free dose risks greatly exceed accident dose risks.

Division of the dose risk values presented in Table 8.4 by the number of assemblies that produced those dose risks shows that, on a per assembly basis, the expected accident population doses for PWR and BWR spent fuel are respectively about 7.8E-7 and 1.6E-7 person-rem. Thus, the expected accident population dose per assembly for truck transport of PWR spent fuel is about 5 times greater than that for BWR spent fuel, which was to be expected because the rod failure fractions for PWR spent fuel during accidents are about twice those of BWR spent fuel and the curie amounts of those radionuclides that drive population dose in three-year cooled, high-burnup PWR assemblies are about three times greater than those for three-year cooled, high-burnup BWR assemblies.

8.7 Results for the Generic Steel-Lead-Steel and Monolithic Steel Rail Casks

Figures 8.7 through 8.11 and Table 8.5 present for the generic steel-lead-steel and monolithic steel rail casks the same set of results that were developed for the generic truck casks. Figures 8.7 through 8.10 present the CCDFs of expected, 95^{th}, median, and 5^{th} percentile values of accident population dose that were calculated for each generic rail cask using first a PWR and then a BWR cask inventory. Figure 8.11 plots the four expected value CCDFs and compares them to the highest lying 95^{th} and the lowest lying 5^{th} percentile CCDF found in Figures 8.7, 8.8, 8.9, or 8.10. Thus, this figure depicts the likely range of rail accident population doses for accidents that are sufficiently severe to fail a Type B spent fuel rail cask and at least some of the rods in the cask.

Table 8.5 compares the expected values of incident-free population doses to the expected value of the corresponding accident population dose. Table 8.5 shows that, as was true for truck transport, each of the four spent fuel rail transport calculations yields the same set of incident-free doses (again because each calculation uses the same set of routes and cask dose rate values) and that the value of total incident-free rail transport population dose risk again greatly exceeds (by factors of approximately 10^3 to 10^4) the four values of rail transport accident population dose risk. However, in contrast to the result obtained for truck transport, other rail incident-free doses are larger than rail incident-free stop doses (by a factor of 3.6) because in general rail stops expose fewer people to radiation than truck stops, e.g., there are more people at truck rest stops and they are closer to the spent fuel cask and less shielded than at rail classification yards.

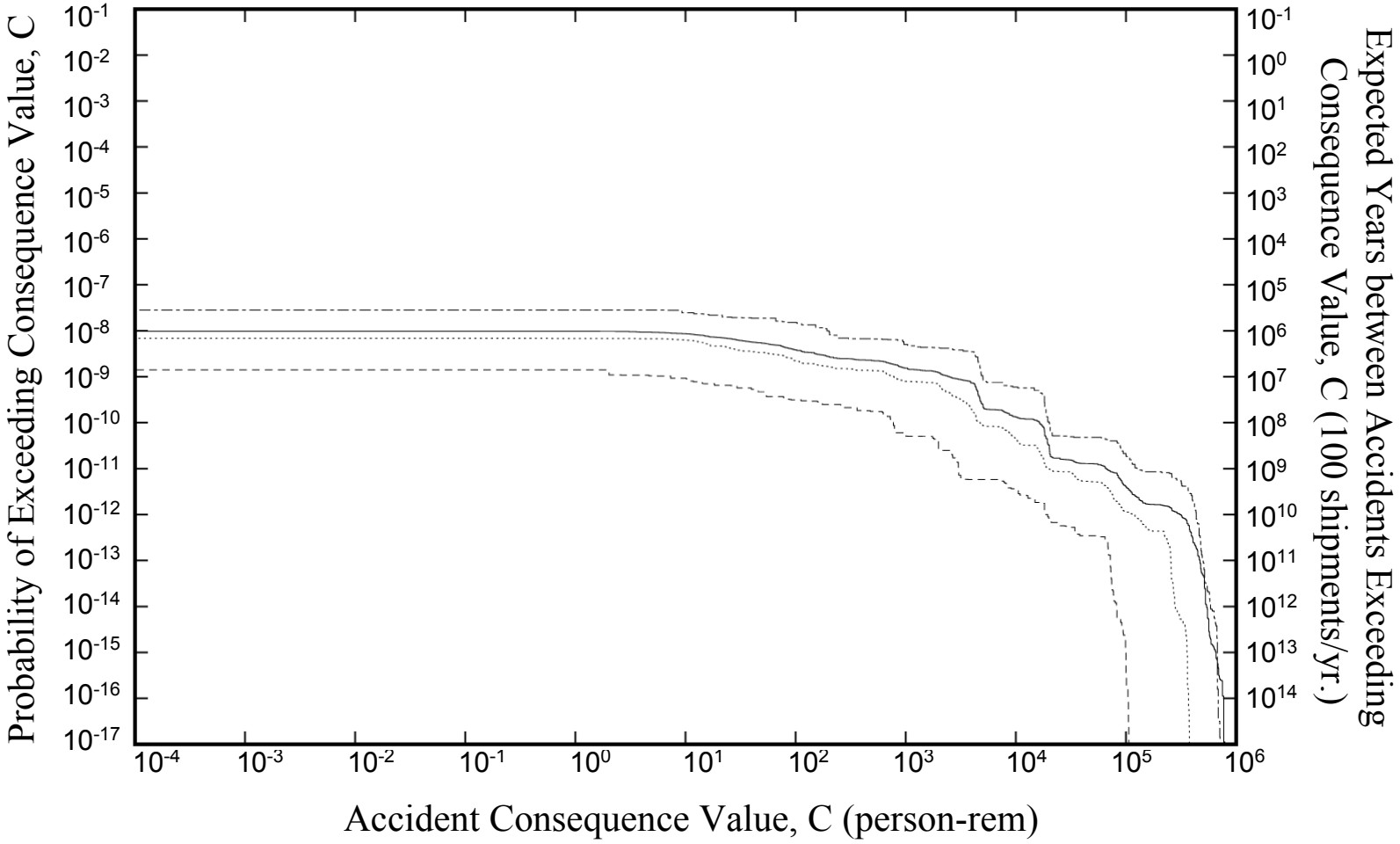

Figure 8.7 Rail accident population dose risk CCDFs for transport of PWR spent fuel in the generic steel-lead-steel rail cask over the 200 representative rail routes. Each underlying RADTRAN 5 calculation generated results for all of the 21 representative rail accident source terms.

Mean (————) CCDF, and 95th (- - - - - - - -), 50th (· · · · · · · · · ·), and 5th (- - - - - - - - - -) quantiles

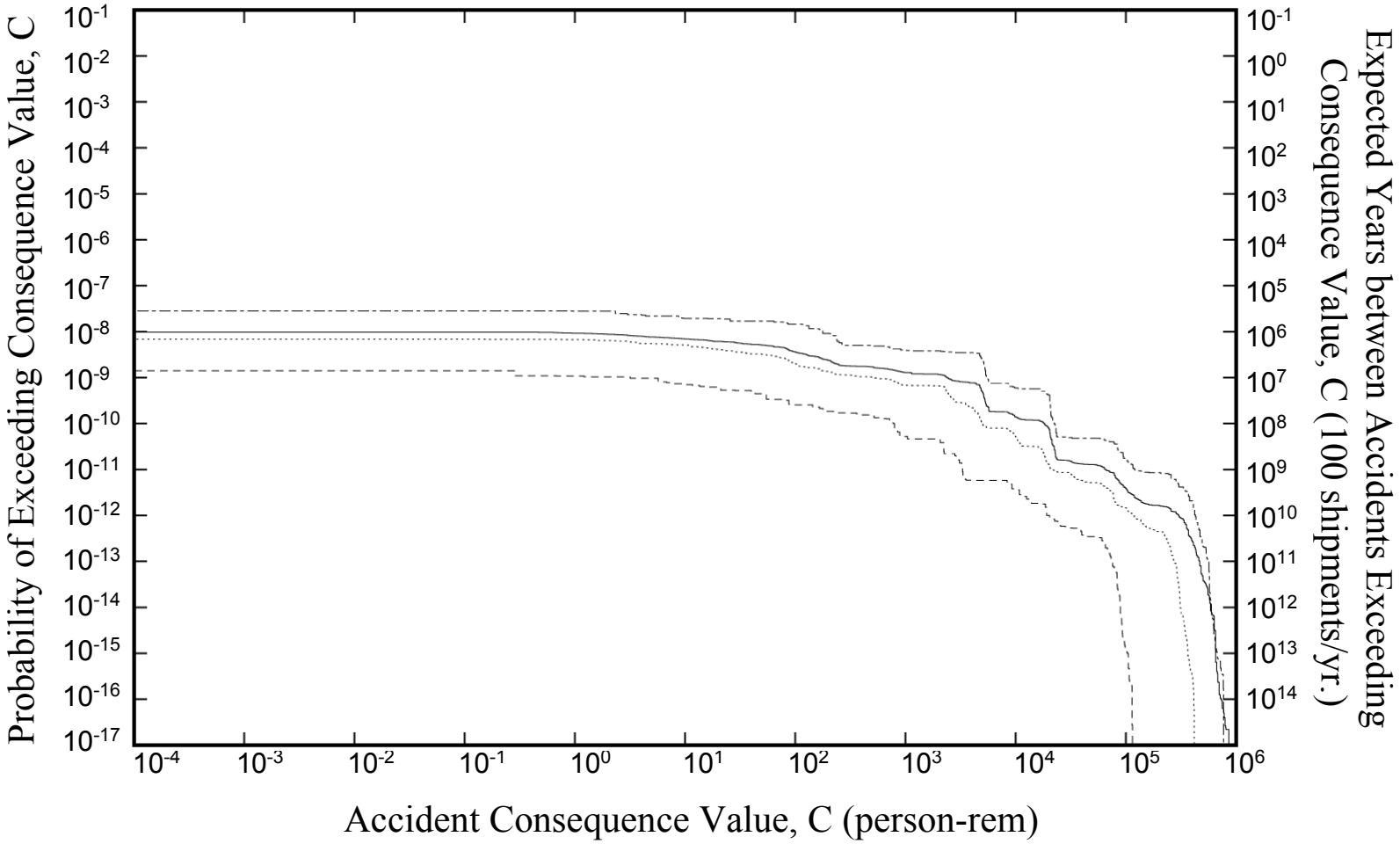

Figure 8.8 Rail accident population dose risk CCDFs for transport of BWR spent fuel in the generic steel-lead-steel rail cask over the 200 representative rail routes. Each underlying RADTRAN 5 calculation generated results for all of the 21 representative rail accident source terms.

Mean (————) CCDF, and 95th (- - - - - - - -), 50th (· · · · · · · · · ·), and 5th (- - - - - - - - - -) quantiles

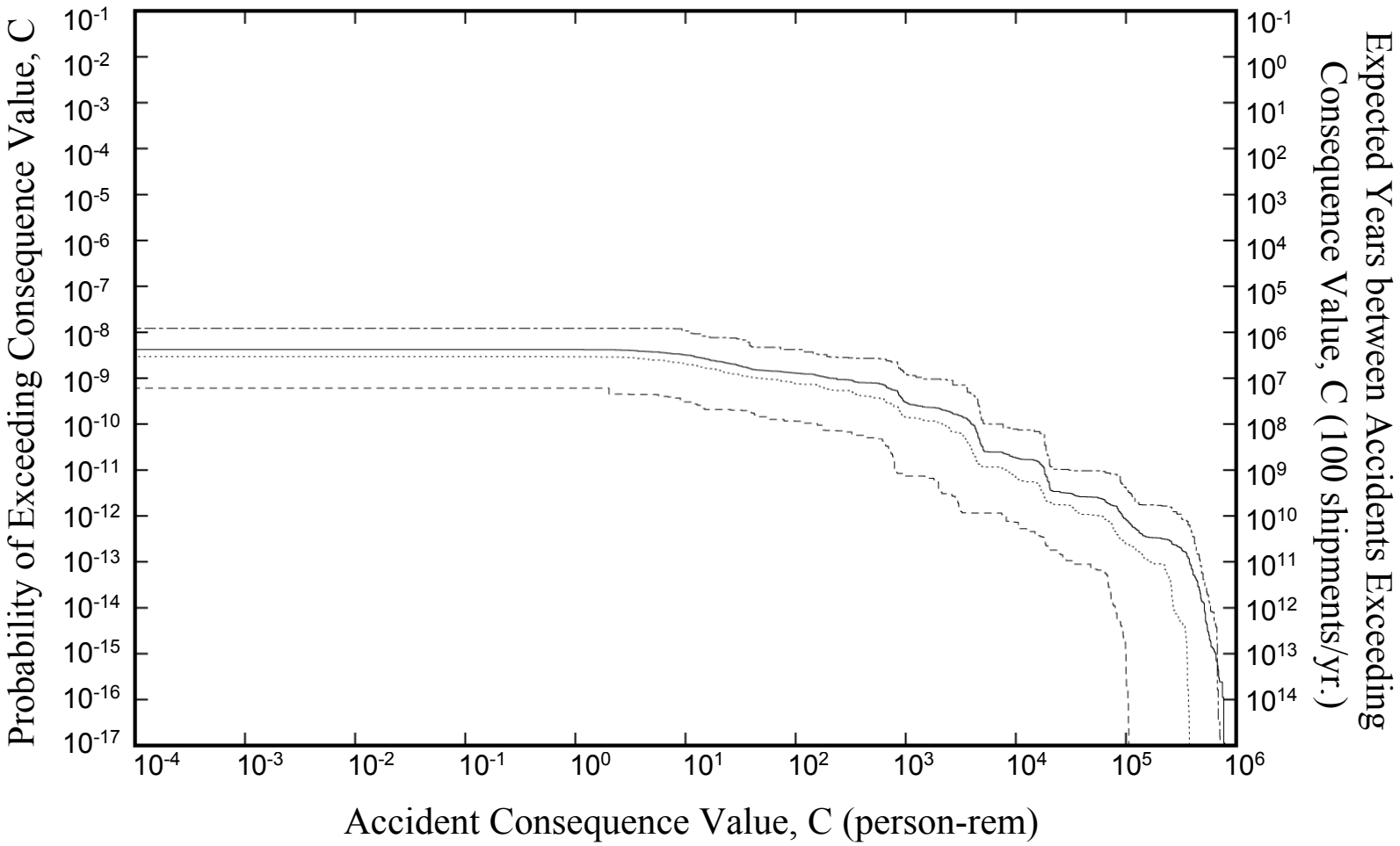

Figure 8.9 Rail accident population dose risk CCDFs for transport of PWR spent fuel in the generic monolithic steel rail cask over the 200 representative rail routes. Each underlying RADTRAN 5 calculation generated results for all of the 21 representative rail accident source terms.

Mean (————) CCDF, and 95th (- - - - - - - -), 50th (· · · · · · · · · ·), and 5th (- - - - - - - - - -) quantiles

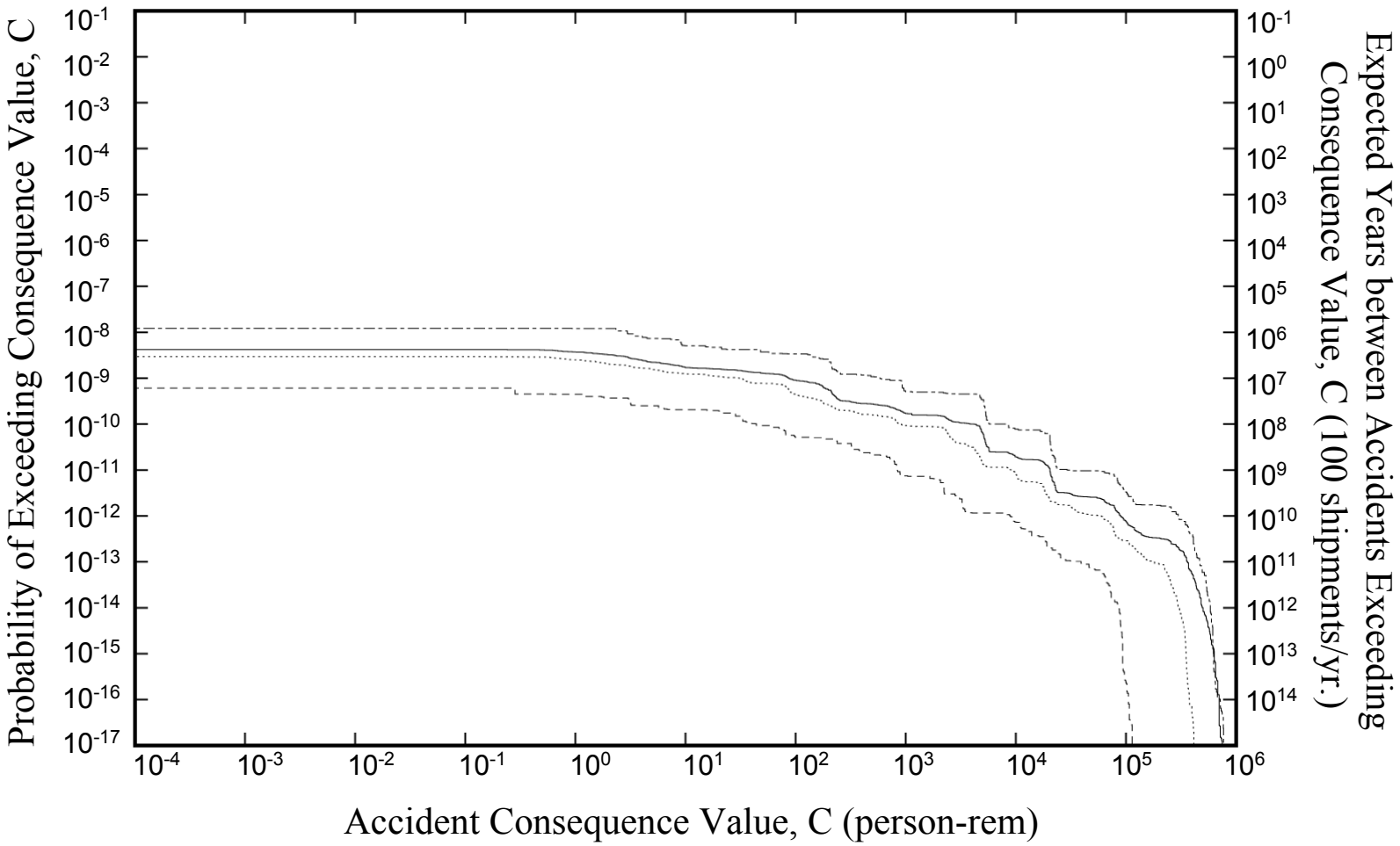

Figure 8.10 Rail accident population dose risk CCDFs for transport of BWR spent fuel in the generic monolithic steel rail cask over the 200 representative rail routes. Each underlying RADTRAN 5 calculation generated results for all of the 21 representative rail accident source terms.

Mean (———) CCDF, and 95th (- - - - - -), 50th (· · · · · · · · · ·), and 5th (- - - - - - - - - -) quantiles

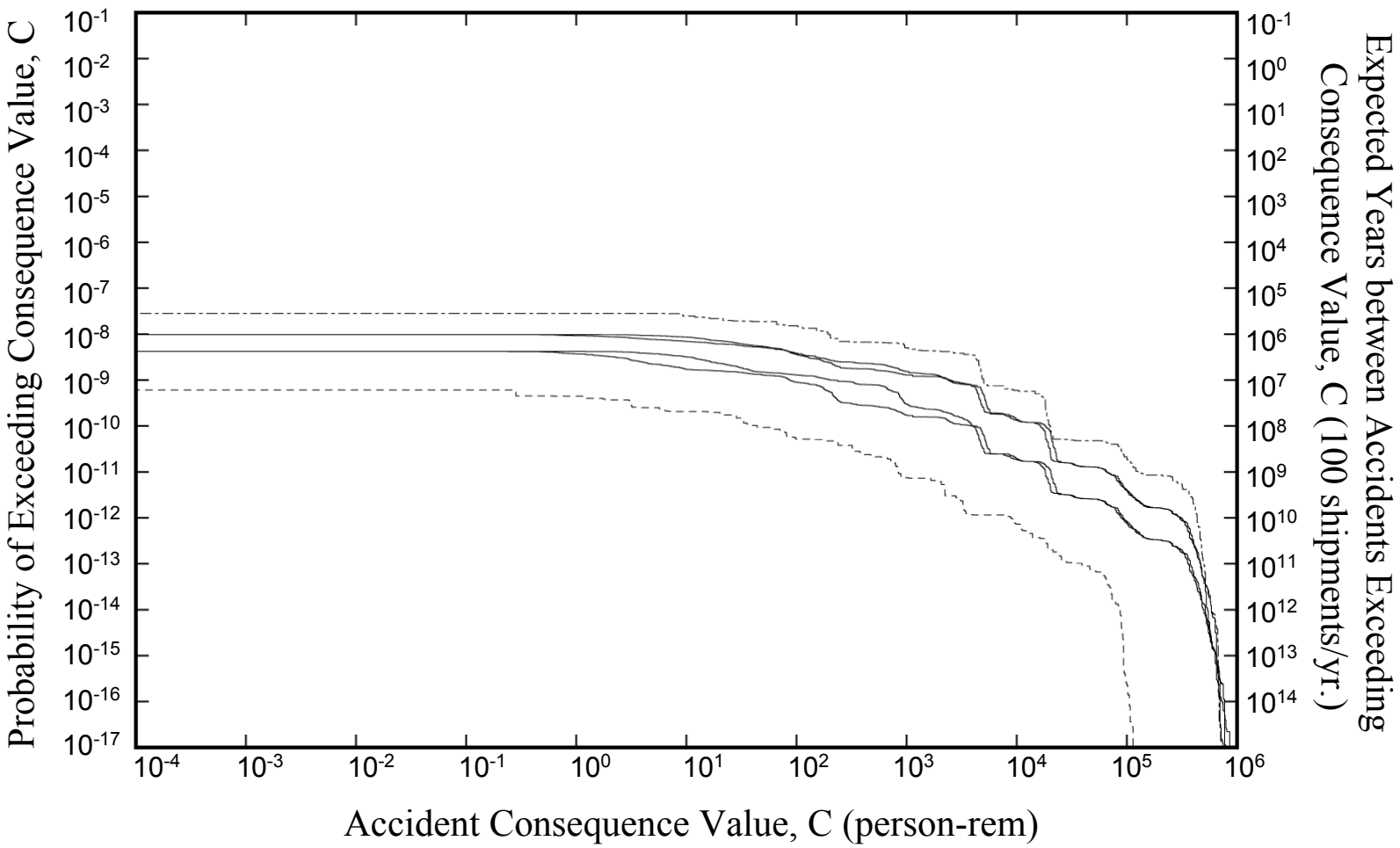

Figure 8.11 Comparison of rail accident population dose risk CCDFs for transport of PWR or BWR spent fuel in generic steel-lead-steel or monolithic steel rail casks over the 200 representative rail routes. Each underlying RADTRAN 5 calculation generated results for all of the 21 representative rail accident source terms.

Four Mean CCDFs (———), and Highest 95th (·-·-·-·-·) and Lowest 5th (----------) quantiles

Table 8.5 Incident-Free Population Dose Risks for Rail Transport

Metric	Population Dose Risks (person-rem)			
	Incident-Free			Accident
	Stops[a]	Other[b]	Total	
PWR Spent Fuel; Steel-Lead-Steel Cask; 24 Assembly				
Mean =	4.37E-03	1.59E-02	2.03E-02	9.43E-06
Standard Deviation =	2.58E-03	1.38E-02	1.40E-02	1.18E-05
Maximum =	1.29E-02	8.26E-02	9.55E-02	6.32E-05
Minimum =	1.73E-03	3.57E-04	2.08E-03	3.39E-08
PWR Spent Fuel; Monolithic Steel Cask; 24 Assemblies				
Mean =	4.37E-03	1.59E-02	2.03E-02	1.99E-06
Standard Deviation =	2.58E-03	1.38E-02	1.40E-02	2.47E-06
Maximum =	1.29E-02	8.26E-02	9.55E-02	1.35E-05
Minimum =	1.73E-03	3.57E-04	2.08E-03	8.08E-09
BWR Spent Fuel; Steel-Lead-Steel Cask; 52 Assemblies				
Mean =	4.37E-03	1.59E-02	2.03E-02	9.23E-06
Standard Deviation =	2.58E-03	1.38E-02	1.40E-02	1.18E-05
Maximum =	1.29E-02	8.26E-02	9.55E-02	6.19E-05
Minimum =	1.73E-03	3.57E-04	2.08E-03	2.97E-08
BWR Spent Fuel; Monolithic Cask; 52 Assemblies				
Mean =	4.37E-03	1.59E-02	2.03E-02	1.46E-06
Standard Deviation =	2.58E-03	1.38E-02	1.40E-02	1.86E-06
Maximum =	1.29E-02	8.26E-02	9.55E-02	9.94E-06
Minimum =	1.73E-03	3.57E-04	2.08E-03	4.87E-09

a. Exposures at rest and refueling stops.
b. Sum of on-link, off-link, and crew doses.

Table 8.5 also shows that when shipped in the same cask, the expected accident population dose risk per assembly for shipping PWR spent fuel exceeds that for BWR spent fuel by factors of about 2 to 3. This ratio is smaller than what might have been expected given that rod failure fractions for PWR spent fuel during accidents are about twice those of BWR spent fuel and the curie amounts of those radionuclides that drive population dose in three-year cooled, high-burnup PWR assemblies are about three times greater than those for three-year cooled, high-burnup BWR assemblies.

8.8 Comparison of Truck and Rail Transport Mean Risks

Comparison of the incident-free doses (incident-free risks and incident-free doses are the same because the probability of occurrence of the incident-free dose is unity) presented in Tables 8.4 and 8.5 shows that, for shipment of a single truck or train spent fuel cask, truck stop doses exceed train stop doses by a factor of 100, if trucks make sleep stops, and by a factor of 35, if

truck sleep stops are not taken; other truck doses exceed other train doses by only a factor of two; and total truck incident-free doses exceed total train incident-free doses by a factor of 22.5, if truck sleep stops are made, and by a factor of 2, if trucks do not make sleep stops. Other truck and other train doses are similar because truck and train spent fuel casks, when undamaged, have similar surface dose rates, so people who reside by the route or are traveling on the route, when the cask passes by, receive similar radiation exposures. Even though rail casks carry many more fuel assemblies than are carried by truck casks, truck and train cask surface dose rates are similar because in rail casks, inner assemblies are shielded by outer assemblies and because cask surface dose rates are limited by regulation. However, because typical truck casks carry either 1 or 3 PWR assemblies or 2 or 7 BWR assemblies, while typical rail casks carry 24 PWR or 52 BWR assemblies, it will take at least 8 = 24/3 and possibly 24 = 24/1 times as many truck shipments as train shipments to transport any given quantity of PWR spent fuel, and at least 7.4 = 52/7 and possibly 26 = 52/2 times as many truck shipments as train shipment to transport a given quantity of BWR spent fuel. Therefore, on a campaign basis, truck incident-free doses might be expected to exceed rail incident-free doses by factors of about 180 = 8 × 22.5 to 585 = 26 × 22.5. Although this factor seems large, it is really of no concern, since all individual incident-free doses will be within regulatory limits and also small when compared to normal yearly background radiation doses.

Because truck casks carry fewer assemblies than rail casks, should a truck cask and a rail cask both be involved in accidents that inflict the same damage on both casks (i.e., both accidents fail the same fraction of the rods in each cask and both fail each cask in the same way, e.g., seal failures of the same size), the overall impact from a train accident would be expected to be larger because the radioactive release from the rail cask would be larger than that from the truck cask. Comparison of Tables 8.4 and 8.5 shows that, depending on the casks used, mean train accident dose risks are either about the same as or about ten times greater than mean truck accident dose risks. Because, for any shipment campaign, transport by truck will require 8 to 26 more shipments than transport by rail on a campaign basis, truck accident dose risks will exceed train accident dose risks by factors of at least 8 = 8 × 1 and possibly as much as 260 = 26 × 10.

8.9 Comparison of NUREG-0170 Incident-Free Doses to Those of This Study

NUREG-0170 [8-1] developed estimates of incident-free doses for eight population groups: passengers, crew, attendants (e.g., flight attendants), handlers, population that resides along the route (off-link population), persons traveling on the route (on-link population), persons exposed at stops, and persons exposed at en route storage locations. For transport by truck or freight train, there are no passenger or attendant doses. Storage doses and handler doses were not examined during this study. Storage doses were not examined because direct shipment from the reactor to the temporary or permanent storage site without storage at any intermediate location was assumed. Handler doses were not examined because the doses incurred by workers loading the spent fuel cask at the reactor site and unloading the spent fuel cask at the temporary or permanent storage site are treated by most recent National Environmental Policy Act analyses as facility doses, not transportation doses. Therefore, incident-free doses were limited to those doses incurred while en route.

Table 8.6 compares the NUREG-0170 expected incident-free truck and rail doses presented in Table 1.2 to the expected incident-free doses presented in Tables 8.4 and 8.5 that were developed by this study. Because the NUREG-0170 doses were developed for all of the spent fuel shipments expected to occur in 1975 or 1985, doses for single shipments are calculated by dividing the 1975 or 1985 doses by the number of spent fuel shipments that NUREG-0170 [8-1] estimated would occur during these years.

Table 8.6 Comparison of NUREG-0170 Incident-Free Doses to the Incident-Free Doses Developed by this Study

Mode	Truck			Rail		
Study	**NUREG-0170**		**This Study**	**NUREG-0170**		**This Study**
Year	1975	1985		1975	1985	
Number of Shipments	254	1530	2489[a]	17	652	100.5[a]
	Expected Dose (person-rem)					
Multiple Shipments						
Handlers + Storage	52.06	313.6	Not Calc.	7.227	277.4	Not Calc.
Stops	4.82	29.0	38	0.089	3.440	0.442
Other[b]	36.92	222.4	72	0.464	17.16	1.598
Stops + Other	41.74	251.4	110	0.553	20.60	2.040
Single Shipment						
Handlers + Storage	0.205	0.205	Not Calc.	0.425	0.425	Not Calc.
Stops	0.0190	0.0190	0.0153[c]	0.0052	0.0053	0.0044
Other[b]	0.145	0.145	0.0288	0.02729	0.02632	0.0159
Stops + Other	0.164	0.164	0.0441	0.0325	0.0316	0.0203

a. Average number of shipments per year required to ship the full 1994 spent fuel inventory over 30 years in steel-lead-steel truck and rail casks.
b. Sum of crew, on-link, and off-link doses.
c. Result for truck shipments that proceed without taking sleep stops.

Table 8.6 shows that for truck transport the single shipment incident-free other doses (i.e., crew, on-link, and off-link doses) calculated for NUREG-0170 are about 5 times larger than those calculated for this study, that the single shipment incident-free stop doses calculated for NUREG-0170 are about 25 percent larger than those calculated for this study, and thus the single shipment total incident-free doses calculated for NUREG-0170 are about 3.7 times those calculated for this study. NUREG-0170 other doses exceed those calculated by this study by a factor of five because the average population density over the entire NUREG-0170 truck route exceeds the average population density of the set of 200 truck routes examined by this study by about a factor of 2.5 and the NUREG-0170 spent fuel cask surface dose rate is about twice the mean of the surface dose rate distribution used in this study.

The fact that NUREG-0170 truck stop doses exceed those developed by this study by 25 percent can be qualitatively explained as follows. Truck stop doses, D_{stop}, are proportional to the product of the cask surface dose rate, the population density at the truck stop, ρ_{pop}, the exposure time of that population, Δt, and the following slowly varying function of radial distance, f(r), that expresses the variation of radiation intensity with distance over the annular area of interest:

$$f(r) = \int_a^b 2\pi r \frac{e^{-\mu r} B(r)}{r^2} dr$$

where μ is the absorption coefficient for radiation by air and B(r) is the Berger buildup factor in air. When stops are made at locations that have different population densities, for example, urban, suburban, and rural rest stops, D_{stop} is proportional to the product of the cask dose rate, f(r), and $\Sigma(\Delta t \rho_{pop})_i$, where Δt and ρ_{pop} are the exposure time and the population density that characterize each stop made on the route.

The NUREG-0170 value for f(r) differs from the value used in this study because different integration limits are used for the function. For NUREG-0170, f(r) is evaluated from 3 to 800 meters and that annulus is assumed to have a population density that is the same as the population density of the urban, suburban, or rural region in which the stop is made. For this study, stop doses are evaluated over two concentric annuli with inner and outer radii of 1 and 10 meters and 10 and 800 meters. Because the population density of the inner annulus is taken to be 0.03 persons per square meter ($3x10^4$ persons per square kilometer) while the population density of the outer annulus is assumed to be that of a suburban route segment, the dose accumulated in the inner annulus dominates the stop dose. Therefore, the integration limits for f(r) for the calculations performed for this study are effectively 1 and 10 meters.

Since the values of TI, f(r), and $\Sigma(\Delta t \rho_{pop})_i$ are respectively 9.5, 27.3, and $1.1x10^4$ where

$$1.1x10^4 = (\Delta t \rho_{pop})_{urban\ stops} + (\Delta t \rho_{pop})_{suburban\ stops} + (\Delta t \rho_{pop})_{rural\ stops}$$

$$= (2\ hr)(3861\ km^{-2}) + (5\ hr)(719\ km^{-2}) + (1\ hr)(6.0\ km^{-2})$$

when NUREG-0170 data is used, and 4.5, 14.2, and $3x10^4$ where

$$3x10^4 = \Delta t\, \rho_{1\text{-}10\ m} = (1\ hr)(3x10^4\ km^{-2})$$

when data from this study is used, the ratio of NUREG-0170 truck stop doses to those estimated by this study should be approximately $1.49 = [(9.5)(1.1x10^4)(27.3)/[(4.5)(3x10^4)(14.2)]$, which is in reasonable agreement with the actual ratio of 1.25.

Table 8.6 also shows that the NUREG-0170 single shipment incident-free stop and other doses for transport by rail are larger than the corresponding doses calculated by this study by factors of 1.2 = 0.0052/0.0044 and 1.7 = 0.0263/0.0159, and therefore, NUREG-0170 total rail incident-free doses exceed those calculated for this study by about a factor of 1.6 = 0.0316/0.0203. The fact that the NUREG-0170 other incident-free rail doses exceed by a factor of 1.7 those calculated for this study is explained as follows. Other incident-free population dose is proportional the product of the cask dose rate and $\Sigma(\Delta t\, \rho_{pop})_i$ where $\Delta t = Lf_i/v_i$, L is the route length, f_i is the fraction of the length that is urban, suburban, or rural, and v_i is the train speed in these regions. Substitution of the values of these parameters used for the NUREG-0170 calculations and the means of the distributions of values used for the calculations performed for this study yields, in good agreement with the actual result, an estimate of 1.8 for this dose ratio, where

$$1.8 = \frac{D_{\text{other incident-free, NUREG-0170}}}{D_{\text{other incident-free, this study}}}$$

$$= \frac{\left[(TI)(L)\sum_i \frac{f_i}{v_i}\rho_i\right]_{NUREG-0170}}{\left[(TI)(L)\sum_i \frac{f_i}{v_i}\rho_i\right]_{\text{this study}}} = \frac{9.5(1210)\left[\frac{0.9}{64}(6)+\frac{0.05}{40}(719)+\frac{0.05}{24}(3861)\right]}{4.5(2560)\left[\frac{0.75}{64}(9.6)+\frac{0.22}{40}(356)+\frac{0.03}{24}(2280)\right]}$$

8.10 Illustrative Real Routes

All of the results presented in Sections 8.6 and 8.7 were calculated using 200 sets of RADTRAN 5 input (an LHS sample of size 200) that contains data for 200 different representative truck or rail routes, none of which exactly matches any real truck or rail route located in the continental United States. In this section, results for four illustrative real truck or rail routes and also for the NUREG-0170 representative truck or rail route are compared to the results developed using the 200 representative truck or rail routes embedded in the LHS samples that provided the input for the calculations described in Sections 8.6 and 8.7. All of the truck calculations examined transport of spent high-burnup PWR fuel in the generic steel-lead-steel truck cask, and all of the rail calculations examined transport of spent high-burnup PWR fuel in the generic monolithic steel rail cask.

Table 8.7 presents route parameter values for the four illustrative real truck and rail routes and also for the NUREG-0170 representative truck and rail routes that were examined by this set of RADTRAN 5 calculations. Also presented in the table are the mean values of the distributions of route parameters that were sampled in order to construct the 200 representative routes that were examined by the calculations described in Sections 8.6 and 8.7.

The four illustrative routes were chosen for the following reasons. The truck and rail routes from the Crystal River nuclear plant to Hanford are about the longest routes possible in the continental United States. Because they traverse the Boston-Washington urban corridor, the routes from the Maine Yankee nuclear plant to the Savannah River Site have urban length fractions and population densities that are about as high as is possible in the continental United States. The routes from the Maine Yankee nuclear plant to Skull Valley represent long routes to the Yucca Mountain area that traverse the urban Midwest. Finally, as Table 8.7 shows, the routes from the Kewaunee nuclear plant to the Savannah River Site have route parameter values (especially the urban parameter values) similar to the means of the route parameter distributions used to construct the 200 representative truck and rail routes contained in the LHS sample of size 200.

Table 8.7 NUREG-0170 and Illustrative Real Truck and Rail Routes

Origin	Destination	Length (km)	Fraction of Total Length			Population Density[a]			Stop Time[b]
			Rural	Suburban	Urban	Rural	Suburban	Urban	
Truck Routes									
Crystal River, FL	Hanford Site, WA	4818.5	0.84	0.15	0.01	7.5	331	2190	53.0
Maine Yankee, ME	Skull Valley, UT	4228.7	0.74	0.24	0.02	9.2	296	2286	46.5
Maine Yankee, ME	Savannah River Site, SC	1917.5	0.52	0.43	0.05	18.3	282	2565	21.0
Kewaunee, WI	Savannah River Site, SC	1765.0	0.63	0.32	0.05	16.3	358	2452	19.4
NUREG-0170		2530.0	0.90	0.05	0.05	6.0	719	3861	8.0
Route Parameter Distribution Mean Values		2550.0	0.76	0.23	0.01	10.1	336	2195	28.0
Rail Routes									
Crystal River, FL	Hanford Site, WA	5178.6	0.83	0.15	0.02	7.9	360	2063	231
Maine Yankee, ME	Skull Valley, UT	4488.7	0.75	0.22	0.03	8.9	337	2429	208
Maine Yankee, ME	Savannah River Site, SC	2252.7	0.52	0.38	0.10	14.3	325	2738	134
Kewaunee, WI	Savannah River Site, SC	1917.2	0.64	0.32	0.04	14.1	351	2268	122
NUREG-0170		1210.0	0.90	0.05	0.05	6.0	719	3861	24
Route Parameter Distribution Mean Values		2560.0	0.75	0.22	0.03	9.6	356	2280	144

a. People per square kilometer.
b. Sum of all stop durations (hours) for the entire shipment. For truck shipments, includes stop time for sleep stops.

8.10.1 Steel-Lead-Steel Truck Cask Results for Illustrative Routes

Figures 8.12 through 8.17 present the accident population dose risk and Table 8.8 presents the incident-free population dose risk results of the RADTRAN 5 calculations that examined spent fuel transport in the generic steel-lead-steel truck cask over the four illustrative truck routes and the NUREG-0170 truck route. Figures 8.12 through 8.15 present the results obtained for the four illustrative real truck routes, and Figure 8.16 presents the results obtained for the NUREG-0170 truck route. Each of these figures presents CCDFs of the expected, 95th, median, and 5th percentile values of accident population dose risks that were calculated for the generic steel-lead-steel truck cask carrying spent PWR high-burnup fuel along the indicated illustrative real truck route or along the NUREG-0170 representative truck route. In Figure 8.17, the mean (expected) CCDFs from each of these calculations are plotted together and compared to the 5th and 95th percentile CCDFs depicted in Figure 8.6. Thus, Figure 8.17 compares the expected accident population dose risks for the illustrative truck and NUREG-0170 truck route calculations to the range of the accident population dose risks developed using the 200 representative truck routes that were constructed by LHS sampling from truck route parameter distributions. Comparison of Figure 8.17 to Figures 8.12 through 8.16 shows (a) that the CCDFs for the four illustrative truck routes are quite similar, (b) that they all lie below the CCDF of 95th percentile values for the LHS calculations that examined the 200 representative truck routes, and (c) that the CCDF for the NUREG-0170 truck route calculation lies below the four illustrative truck route CCDFs when accident population dose risks are below 100 person-rem but then crosses these CCDFs and

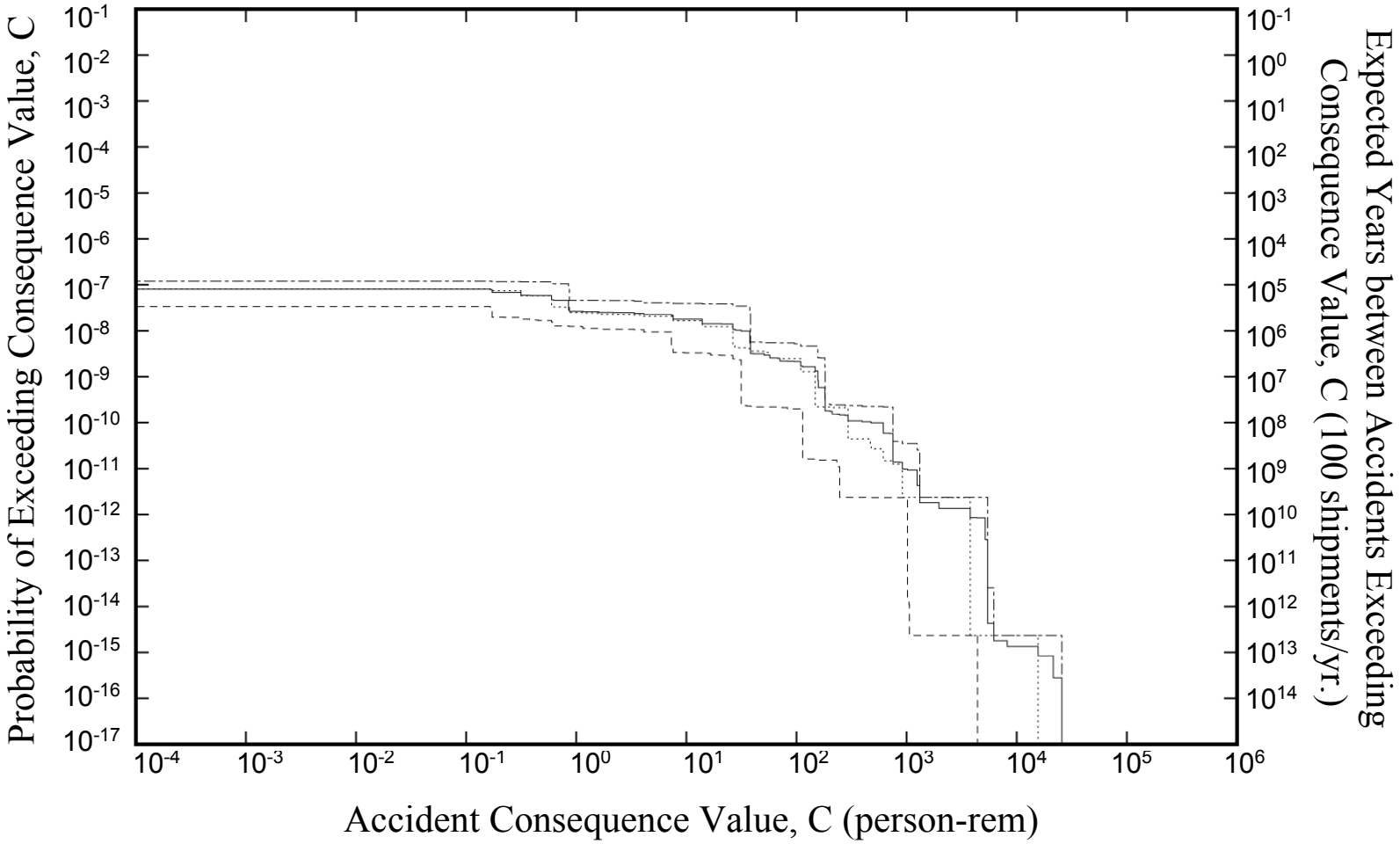

Figure 8.12 Truck accident population dose risk CCDFs for transport of PWR spent fuel in the generic steel-lead-steel truck cask over the Crystal River to Hanford illustrative truck route. Each underlying RADTRAN 5 calculation generated results for all of the 19 representative truck accident source terms.

Mean (————) CCDF, and 95th (- - - - - - - -), 50th (· · · · · · · · · ·), and 5th (- - - - - - - - - -) quantiles

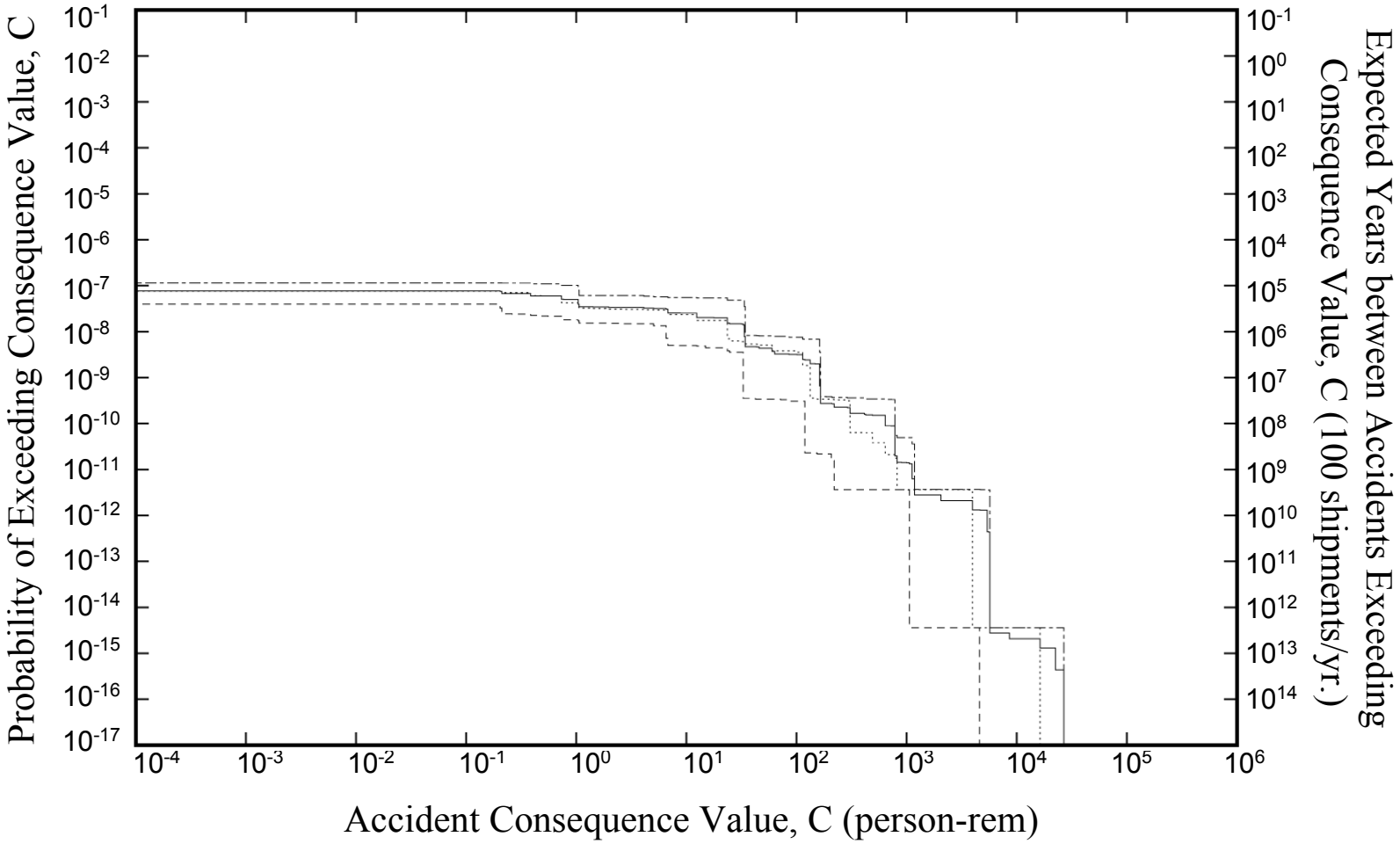

Figure 8.13 Truck accident population dose risk CCDFs for transport of PWR spent fuel in the generic steel-lead-steel truck cask over the Maine Yankee to Skull Valley illustrative truck route. Each underlying RADTRAN 5 calculation generated results for all of the 19 representative truck accident source terms.

Mean (———) CCDF, and 95th (- - - - - -), 50th (· · · · · · · · · ·), and 5th (- - - - - - - - - -) quantiles

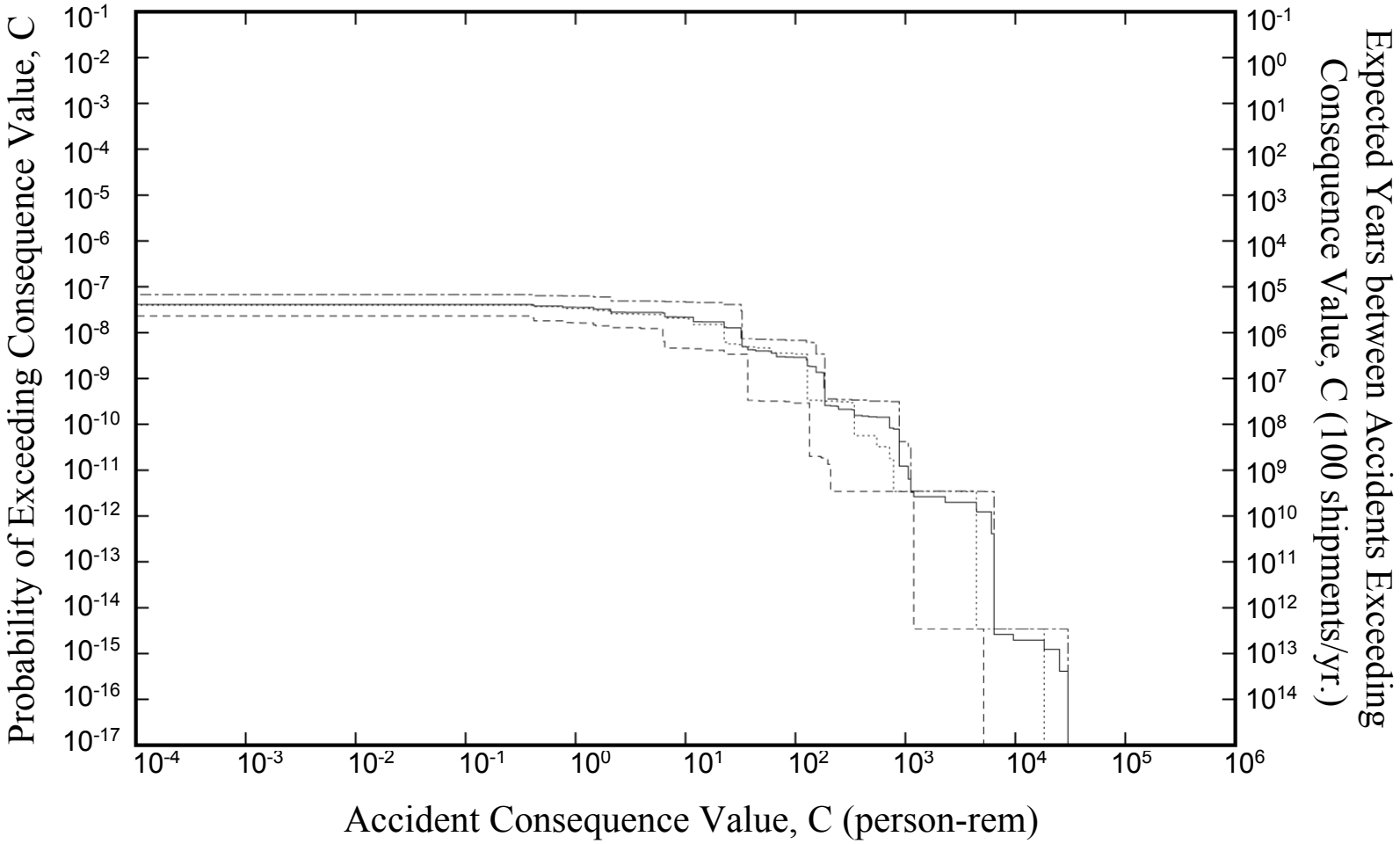

Figure 8.14 Truck accident population dose risk CCDFs for transport of PWR spent fuel in the generic steel-lead-steel truck cask over the Maine Yankee to Savannah River Site illustrative truck route. Each underlying RADTRAN 5 calculation generated results for all of the 19 representative truck accident source terms.

Mean (———) CCDF, and 95th (- - - - - -), 50th (· · · · · · · · · ·), and 5th (- - - - - - - - - -) quantiles

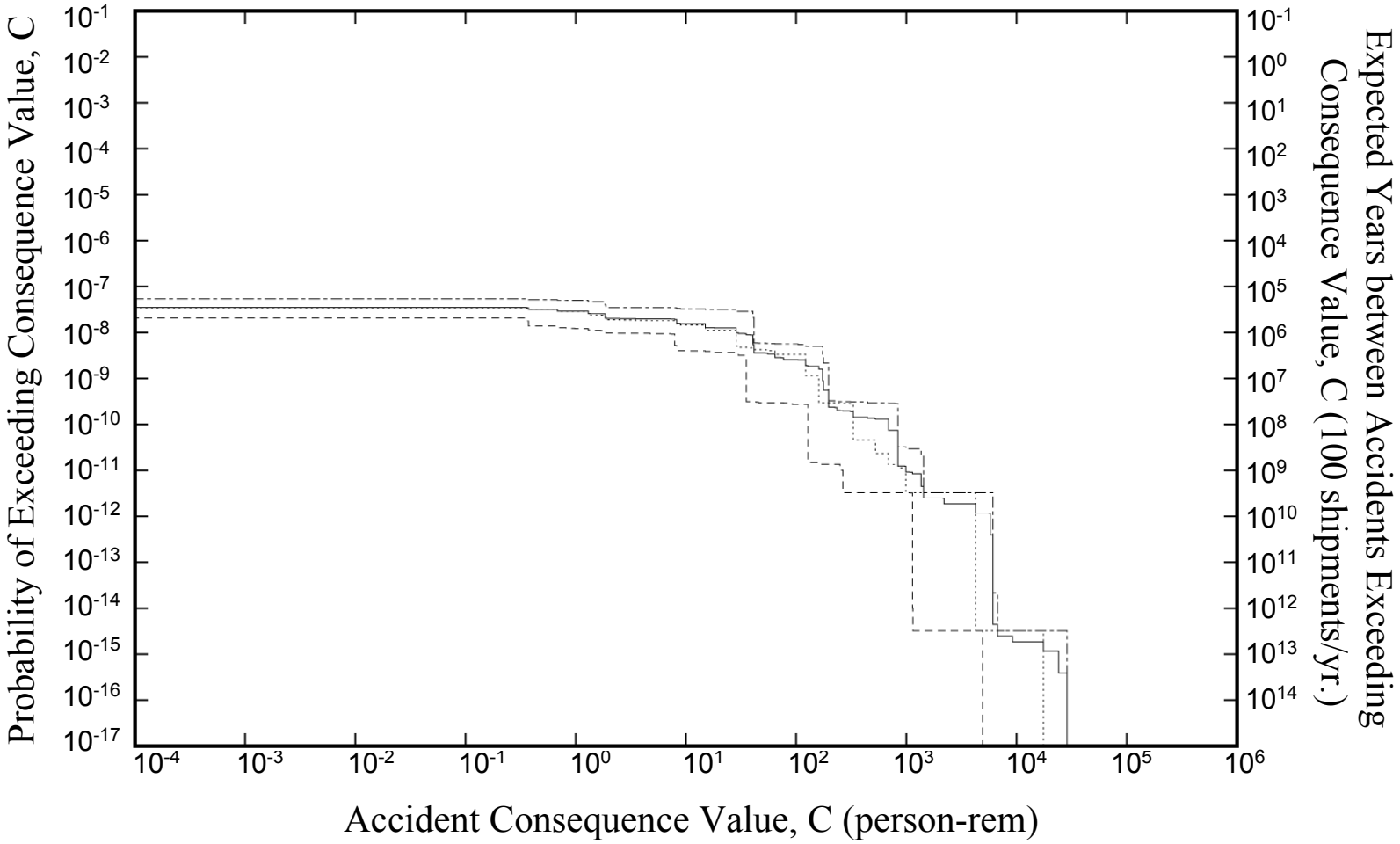

Figure 8.15 Truck accident population dose risk CCDFs for transport of PWR spent fuel in the generic steel-lead-steel truck cask over the Kewaunee to Savannah River Site illustrative truck route. Each underlying RADTRAN 5 calculation generated results for all of the 19 representative truck accident source terms.

Mean (————) CCDF, and 95th (- - - - - -), 50th (· · · · · · · · · ·), and 5th (- - - - - - - - - -) quantiles

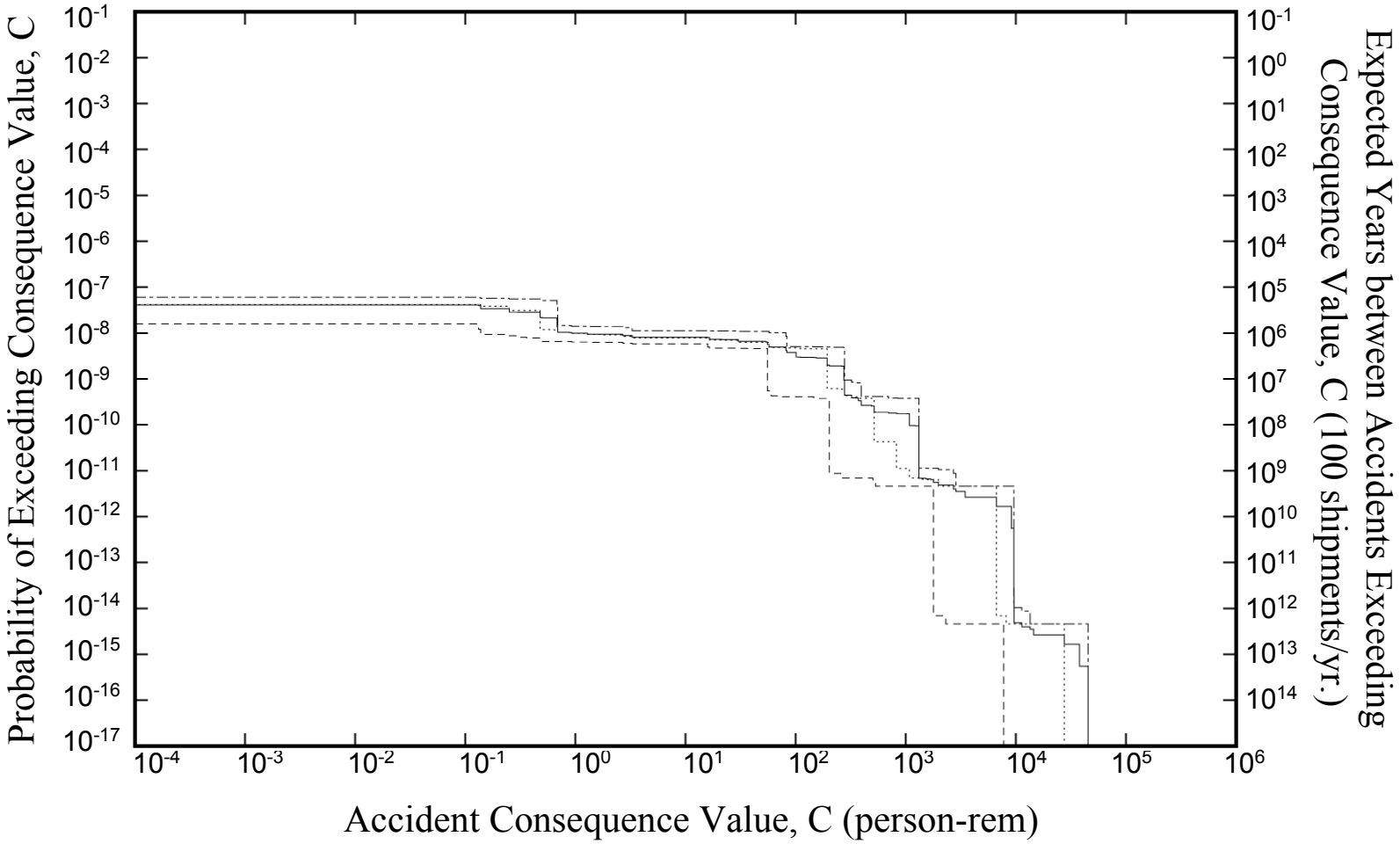

Figure 8.16 Truck accident population dose risk CCDFs for transport of PWR spent fuel in the generic steel-lead-steel truck cask over the NUREG-0170 representative truck route. Each underlying RADTRAN 5 calculation generated results for all of the 19 representative truck accident source terms.

Mean (————) CCDF, and 95th (- - - - - - -), 50th (· · · · · · · · · ·), and 5th (- - - - - - - - - -) quantiles

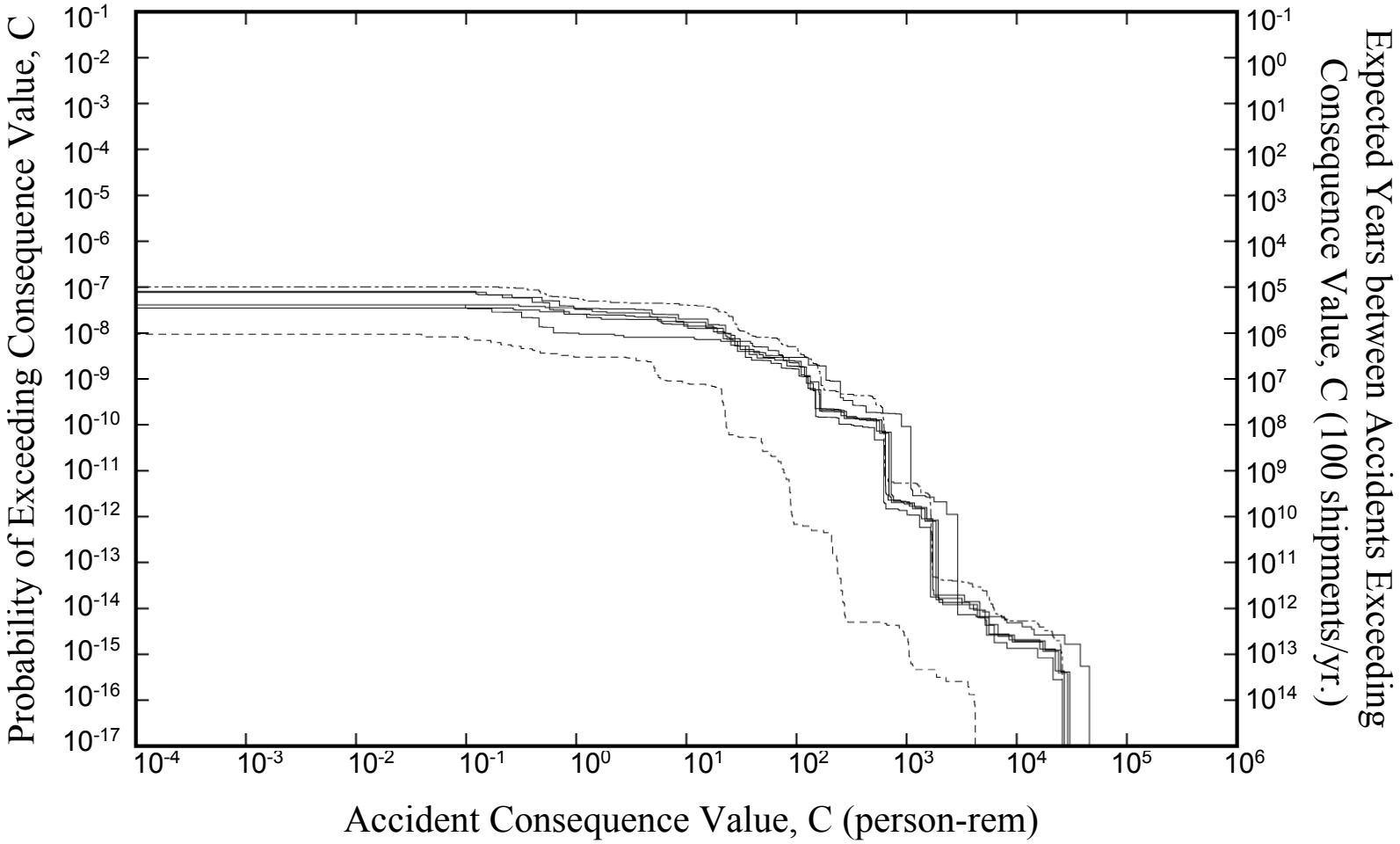

Figure 8.17 Comparison of truck accident population dose risk CCDFs for transport of PWR spent fuel in the generic steel-lead-steel cask over four illustrative truck routes and the NUREG-0170 representative truck route. Each underlying RADTRAN 5 calculation generated results for all of the 19 representative truck accident source terms.

Five Mean CCDFs (———), and Highest 95th (----------) and Lowest 5th (·····) quantiles

Table 8.8 Incident-Free Population Dose Risks for Truck Transport of PWR Spent Fuel in a Generic Steel-Lead-Steel Truck Cask over Illustrative Routes

Metric	Population Dose Risks (person-rem)					
	Incident-Free					Accident
	Stops[a]		Other[b]	Total		
	Sleep[c]	No Sleep[d,e]		Sleep[c]	No Sleep[d]	
Crystal River Nuclear Plant to Hanford Site						
Mean =	1.470	0.0525	0.0581	1.530	0.111	9.53E-07
Standard Deviation =	0.722	0.0258	0.0281	0.722	0.038	5.92E-07
Maine Yankee Nuclear Plant to Skull Valley						
Mean =	1.300	0.0464	0.0524	1.350	0.099	1.29E-06
Standard Deviation =	0.637	0.0228	0.0252	0.637	0.034	7.81E-07
Maine Yankee Nuclear Plant to Savannah River Site						
Mean =	0.585	0.0209	0.0252	0.610	0.046	1.14E-06
Standard Deviation =	0.288	0.0103	0.0122	0.288	0.016	6.73E-07
Kewaunee Nuclear Plant to Savannah River Site						
Mean =	0.541	0.0193	0.0231	0.564	0.042	1.01E-06
Standard Deviation =	0.257	0.0092	0.0112	0.257	0.011	5.93E-07
NUREG-0170 Truck Route						
Mean =	0.779	0.0321	0.0304	0.810	0.063	1.28E-06
Standard Deviation =	0.383	0.0137	0.0147	0.383	0.020	6.68E-07

a. Exposures at rest, food, and refueling stops.
b. Sum of on-link, off-link, and crew doses.
c. Sleep means that the truck makes a rest stop of 8 hours once every 24 hours so the crew can sleep.
d. No Sleep means that the truck doesn't make any rest stops to allow the crew to sleep.
e. The No Sleep stop dose is obtained by dividing the Sleep stop dose by 28.

thereafter lies near to or above the 95th percentile CCDF. Thus, Figure 8.17 shows that the four illustrative truck routes yield accident population dose risks that lie toward the top of the range of accident population dose risks obtained using the LHS sample that contained 200 representative truck routes and, for accident population dose risks that exceed 100 person-rem, below the CCDF obtained using the NUREG-0170 truck route. The NUREG-0170 truck route CCDF lies generally higher than the illustrative truck routes CCDFs because, as Table 8.7 shows, the NUREG-0170 truck route has suburban and urban population densities that are substantially larger than those that characterize the illustrative truck routes.

Finally, Table 8.8 presents the mean (expected) incident-free population doses calculated by RADTRAN 5 for transport of PWR spent fuel in the generic steel-lead-steel cask along the illustrative routes. Table 8.8 shows that, as was true for the LHS calculations that examined truck transport of spent fuel using the representative set of 200 truck routes for specific real truck routes, total incident-free population dose risks again exceed accident population dose risks by factors of at least $3x10^{4} = 0.042/1.29x10^{-6}$, if no sleep stops are made, to as much as

$2x10^6 = 1.530/9.53x10^{-7}$, if sleep stops are made; and that population doses incurred when the truck stops, for example to refuel, are quite similar, when no sleep stops are taken, and exceed all other incident-free population doses (e.g., on-link and off-link doses) by factors of about 25, if sleep stops are taken. Comparison of the results in Table 8.8 to those in Table 8.4 shows that all of the incident-free doses for illustrative truck routes, both those calculated with sleep stops and those calculated without sleep stops, fall within the range (defined by the maximum and minimum values calculated) of results obtained for incident-free doses using the LHS sample that contains 200 representative truck routes.

8.10.2 Monolithic Steel Rail Cask Results for Illustrative Routes

Figures 8.18 through 8.23 present the accident population dose risks and Table 8.9 presents the incident-free population dose risks for the RADTRAN 5 calculations that examined spent fuel transport in the generic monolithic steel rail cask over the four illustrative rail routes and the NUREG-0170 rail route. Figures 8.18 through 8.21 present the results obtained for the four illustrative real rail routes, and Figure 8.22 presents the results obtained for the NUREG-0170 rail route. Each of these figures presents CCDFs of the expected, 95th, median, and 5th percentile values of accident population doses that were calculated for the generic monolithic Steel rail cask carrying spent PWR high-burnup fuel along the indicated illustrative real rail route or for the NUREG-0170 representative rail route. In Figure 8.23, the mean (expected) CCDFs from each of these calculations are plotted and compared to the 5th and 95th percentile CCDFs depicted in Figure 8.11. Thus, Figure 8.23 compares the expected accident population dose results of the illustrative rail and NUREG-0170 rail route calculations to the range of the accident population doses results developed using the 200 representative rail routes that were constructed by LHS sampling from rail route parameter distributions. Figure 8.23 shows that (a) the CCDFs for the four illustrative rail routes are quite similar, (b) they all lie below the CCDF of 95th percentile values for the LHS calculation that examined the 200 representative rail routes, and (c) the CCDF for the NUREG-0170 rail route calculation lies below the illustrative route CCDFs until accident population doses exceed 1000 person-rem and then lies among them until the highest accident population doses are reached, whereupon it crosses all of the illustrative route CCDFs and even crosses the 95th percentile CCDF. Thus, Figure 8.23 shows that the four illustrative rail routes yield accident population doses that lie toward the top of the range of accident population doses obtained using the LHS sample that contained 200 representative rail routes and at all but the very highest population doses above the CCDF of mean population doses obtained using the NUREG-0170 rail route. The NUREG-0170 rail route lies generally lower than the illustrative rail route CCDFs because it is only half as long and because its suburban route fraction is 4 to 6 times smaller than those of the illustrative rail routes.

Finally, Table 8.9 presents the mean (expected) incident-free population doses calculated by RADTRAN 5 for transport of PWR high-burnup spent fuel in the monolithic steel rail cask along the illustrative rail routes. Table 8.9 shows that, as was true for the LHS calculations that examined truck transport of spent fuel using the representative set of 200 rail routes for specific real rail routes, incident-free population dose risks exceed accident population dose risks by factors of about 10^4, and other incident-free population doses (e.g., on- link and off-link doses) are larger than the population doses incurred when the train stops, for example in a classification yard, by factors of 2 to 3. Comparison of the results in Table 8.9 to those in Table 8.5 shows that

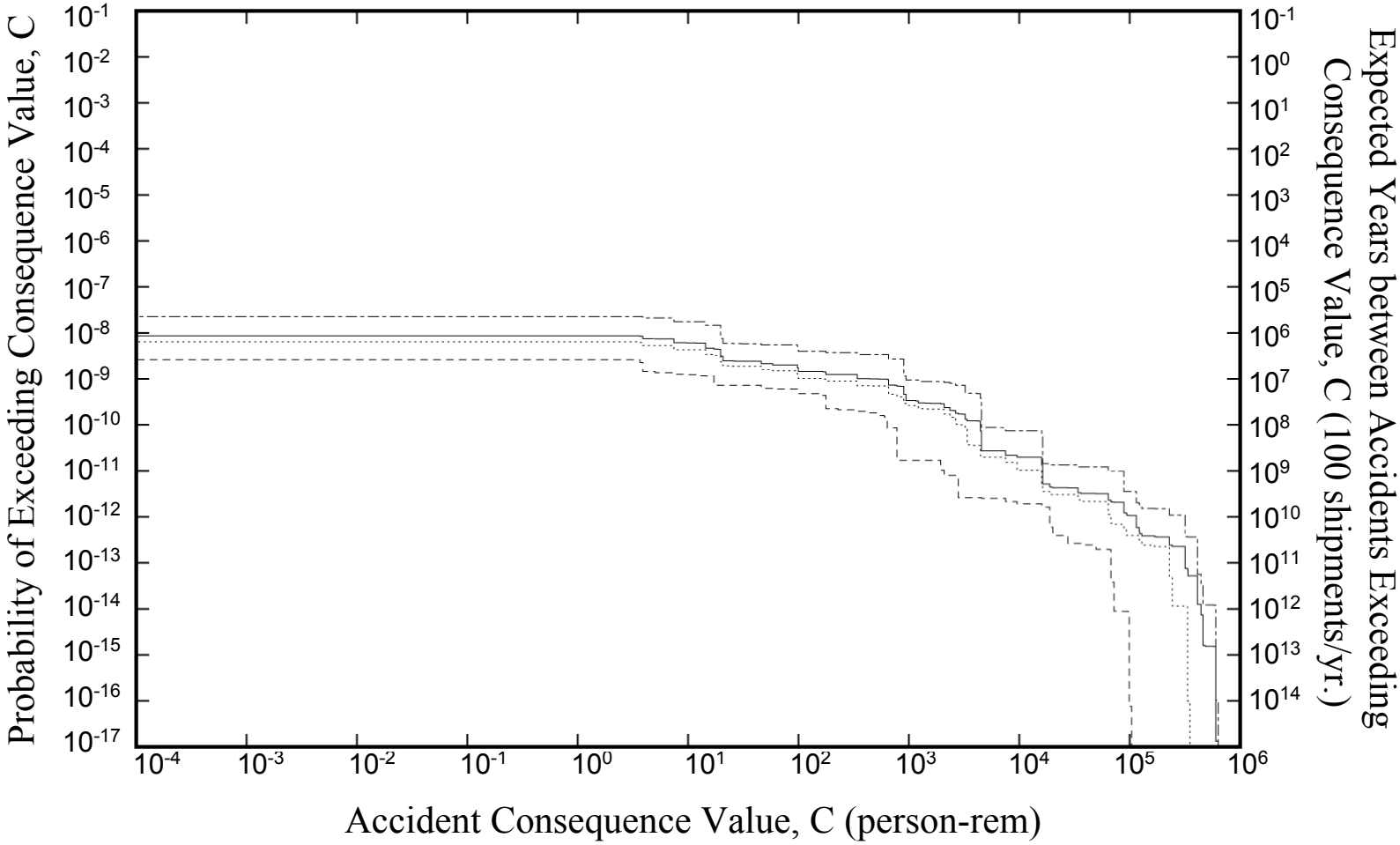

Figure 8.18 Rail accident population dose risk CCDFs for transport of PWR spent fuel in the generic monolithic steel rail cask over the Crystal River to Hanford illustrative rail route. Each underlying RADTRAN 5 calculation generated results for all of the 21 representative rail accident source terms.

Mean (———) CCDF, and 95th (- - - - - -), 50th (· · · · · · · · · ·), and 5th (- - - - - - - - - -) quantiles

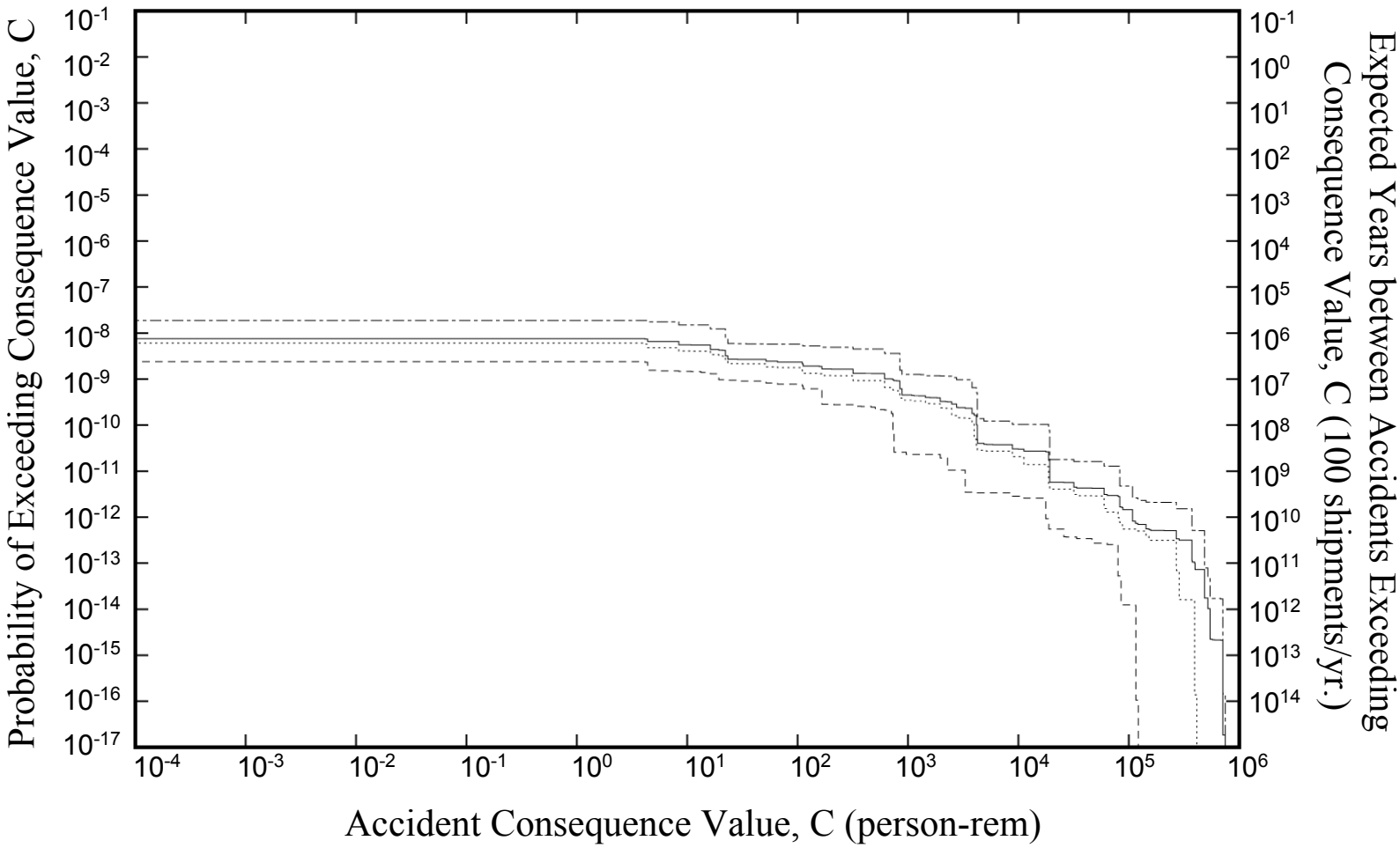

Figure 8.19 Rail accident population dose risk CCDFs for transport of PWR spent fuel in the generic monolithic steel rail cask over the Maine Yankee to Skull Valley illustrative rail route. Each underlying RADTRAN 5 calculation generated results for all of the 21 representative rail accident source terms.

Mean (————) CCDF, and 95th (- - - - - -), 50th (·····), and 5th (- - - - - -) quantiles

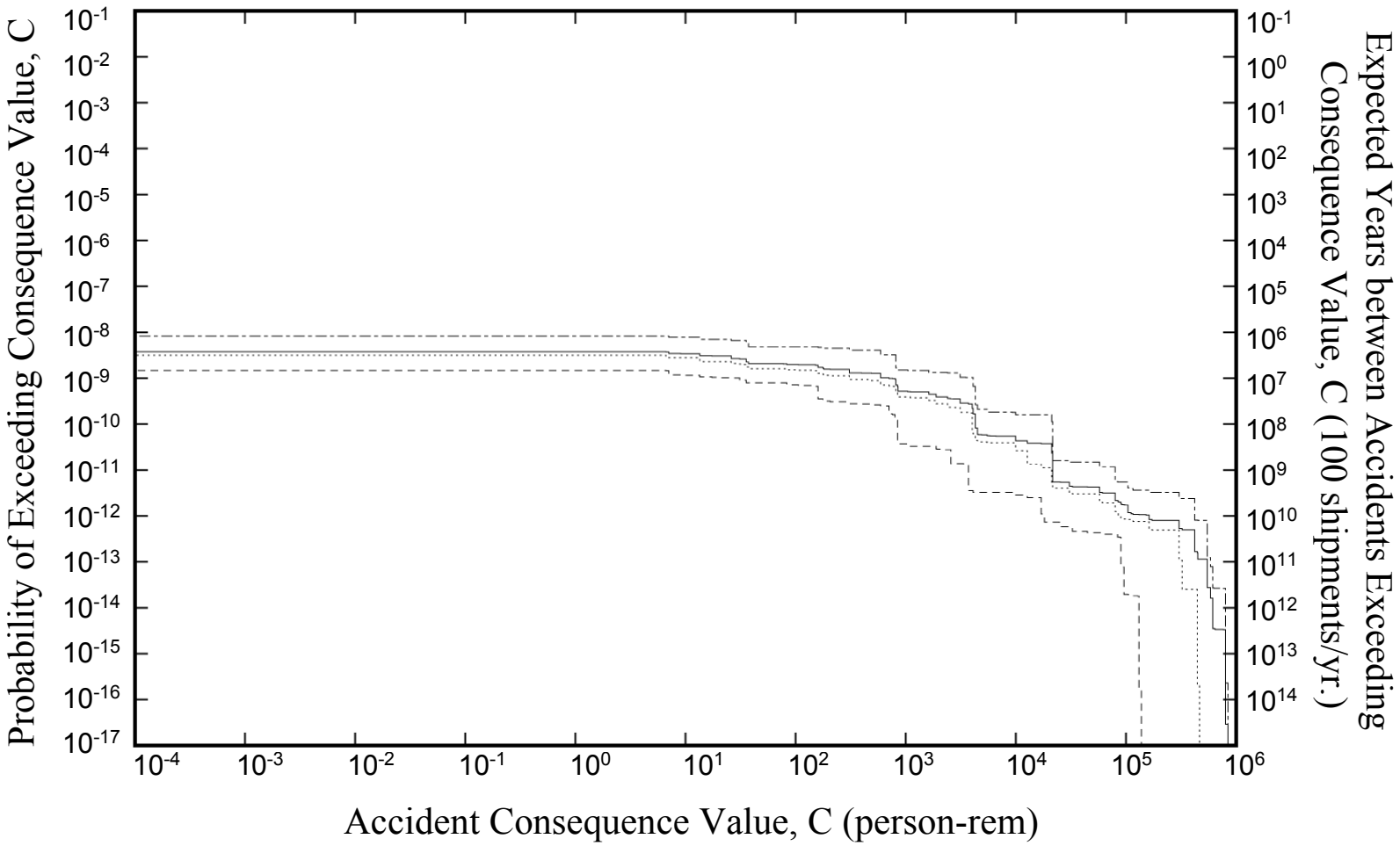

Figure 8.20 Rail accident population dose risk CCDFs for transport of PWR spent fuel in the generic monolithic steel rail cask over the Maine Yankee to Savannah River Site illustrative rail route. Each underlying RADTRAN 5 calculation generated results for all of the 21 representative rail accident source terms.

Mean (———) CCDF, and 95th (- - - - - -), 50th (·····), and 5th (- - - - - -) quantiles

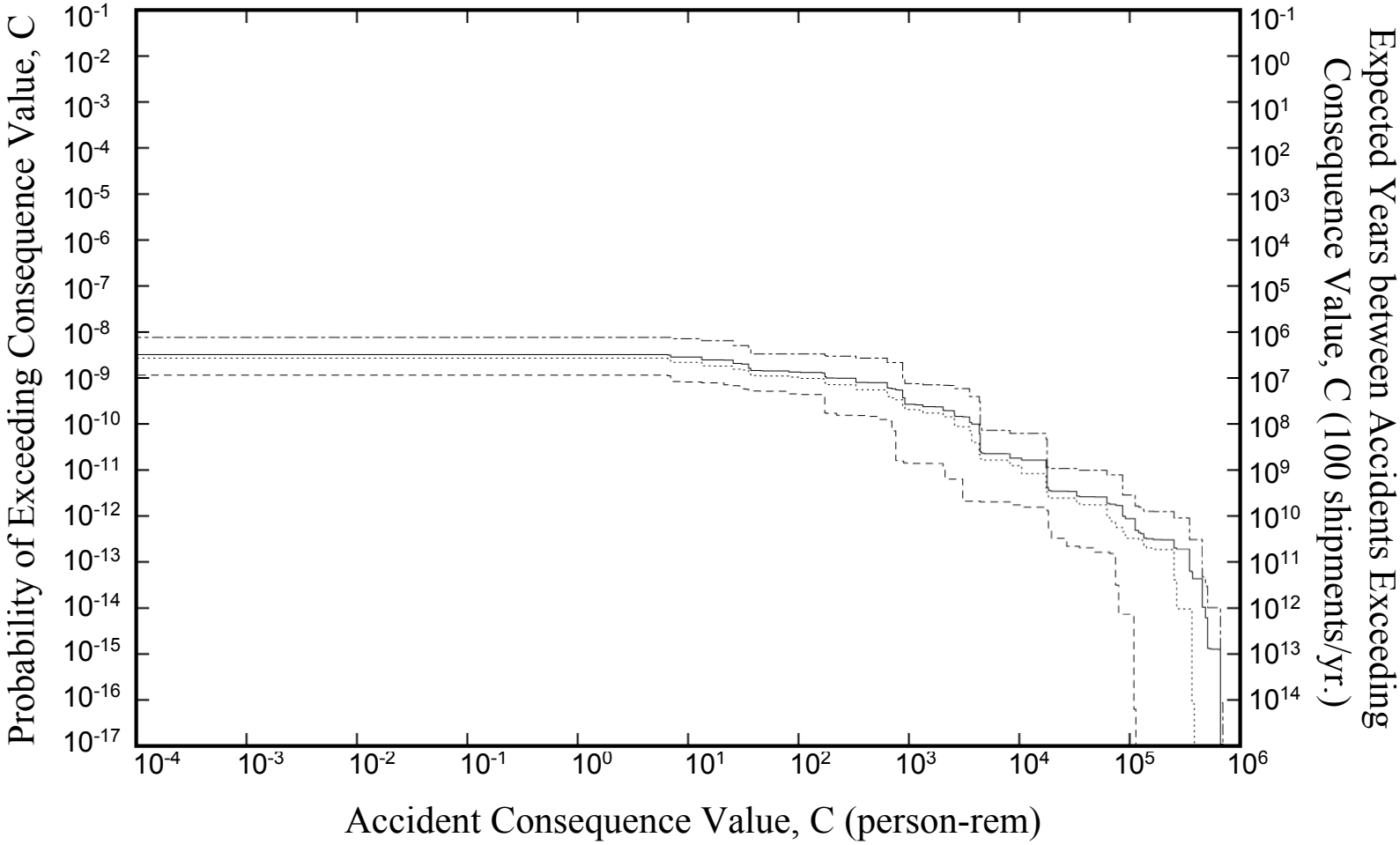

Figure 8.21 Rail accident population dose risk CCDFs for transport of PWR spent fuel in the generic monolithic steel rail cask over the Kewaunee to Savannah River Site illustrative rail route. Each underlying RADTRAN 5 calculation generated results for all of the 21 representative rail accident source terms.

Mean (————) CCDF, and 95th (- - - - - - - -), 50th (· · · · · · · · · ·), and 5th (- - - - - - - - - -) quantiles

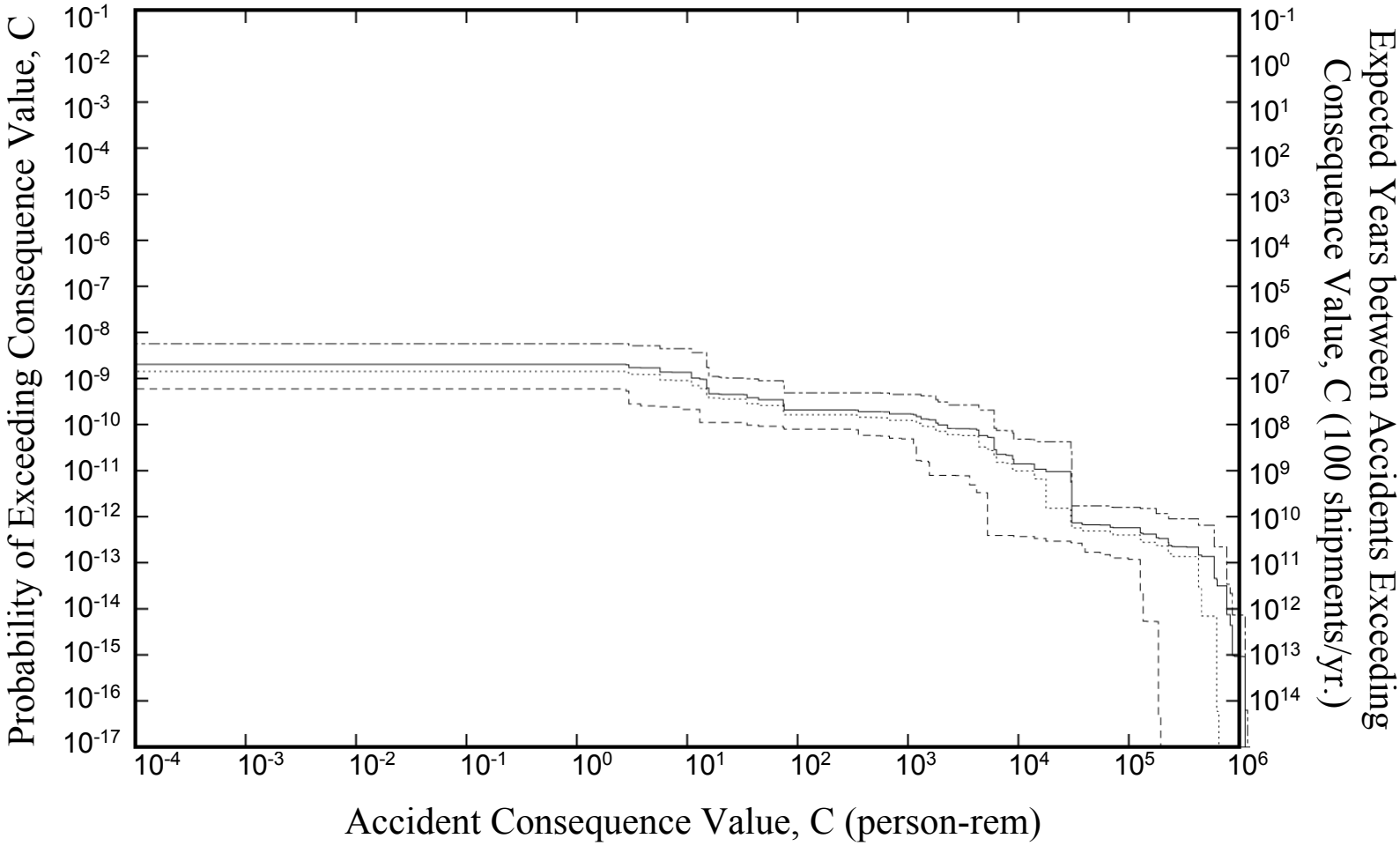

Figure 8.22 Rail accident population dose risk CCDFs for transport of PWR spent fuel in the generic monolithic steel rail cask over the NUREG-0170 representative rail route. Each underlying RADTRAN 5 calculation generated results for all of the 21 representative rail accident source terms.

Mean (———) CCDF, and 95th (- - - - - -), 50th (· · · · · · · · · ·), and 5th (- - - - - - - - - -) quantiles

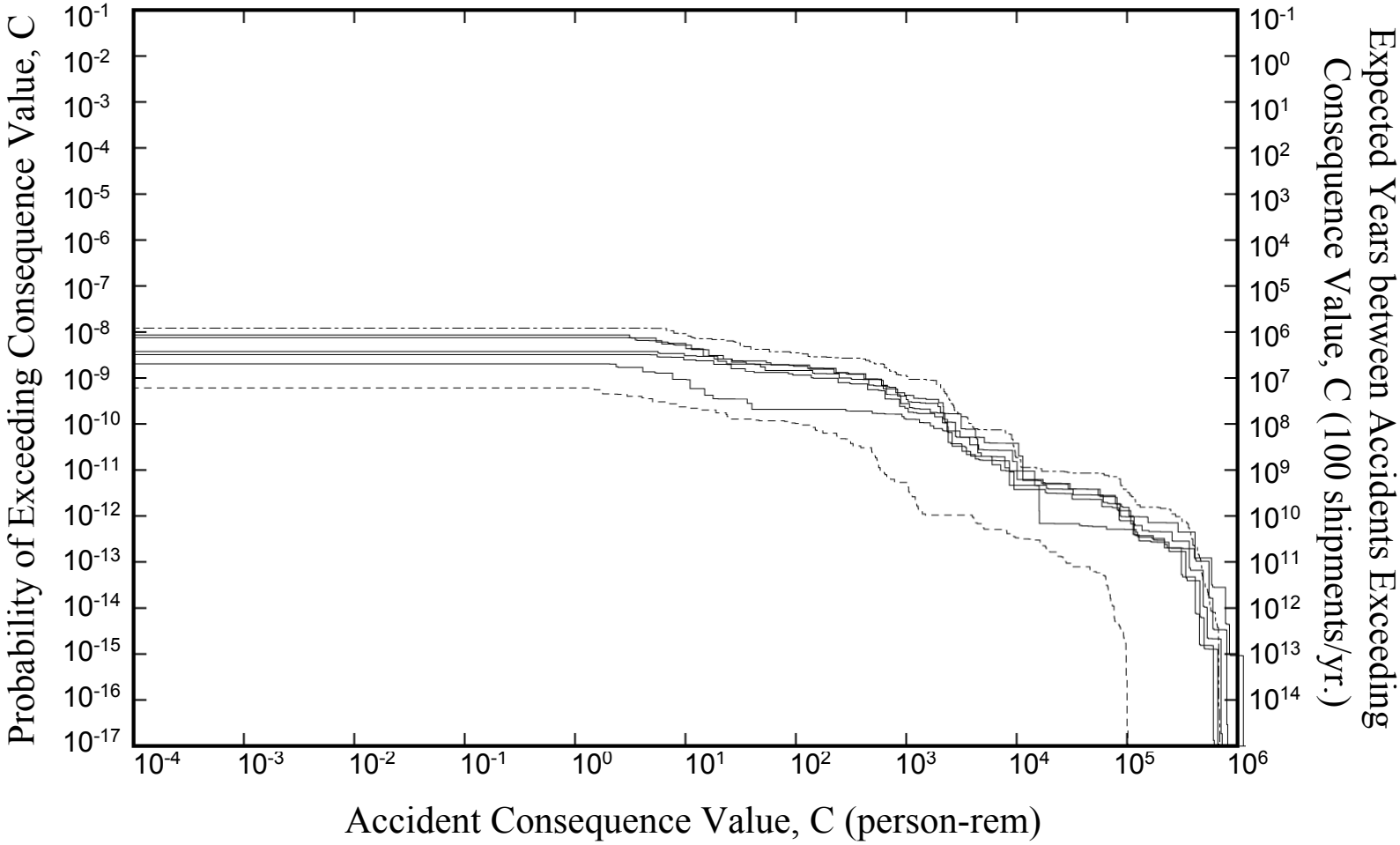

Figure 8.23 Comparison of rail accident population dose risk CCDFs for transport of PWR spent fuel in the generic monolithic steel cask over four illustrative rail routes and the NUREG-0170 representative rail route. Each underlying RADTRAN 5 calculation generated results for all of the 21 representative rail accident source terms.

Five Mean CCDFs (———), and Highest 95th (----------) and Lowest 5th (----------) quantiles

Table 8.9 Incident-Free Population Dose Risks for Rail Transport of PWR Spent Fuel in a Generic Monolithic Steel Rail Cask over Illustrative Routes

Metric	Population Dose Risks (person-rem)			
	Incident-Free			Accident
	Stops[a]	Other[b]	Total	
Crystal River Nuclear Plant to Hanford Site				
Mean =	9.70E-03	2.89E-02	3.86E-02	2.44E-06
Standard Deviation =	5.71E-03	1.71E-02	1.80E-02	2.08E-06
Maine Yankee Nuclear Plant to Skull Valley				
Mean =	1.19E-02	2.75E-02	3.69E-02	3.25E-06
Standard Deviation =	7.00E-03	1.62E-02	1.77E-02	2.77E-06
Maine Yankee Nuclear Plant to Savannah River Site				
Mean =	1.02E-02	1.66E-02	2.70E-02	3.79E-06
Standard Deviation =	6.05E-03	9.84E-03	1.15E-02	3.27E-06
Kewaunee Nuclear Plant to Savannah River Site				
Mean =	7.61E-03	1.33E-02	2.09E-02	1.95E-06
Standard Deviation =	4.50E-03	7.87E-03	9.06E-03	1.68E-06
NUREG-0170 Rail Route				
Mean =	2.05E-03	6.46E-03	8.51E-03	1.11E-06
Standard Deviation =	1.21E-03	3.82E-03	4.01E-03	1.03E-06

a. Exposures at rest and refueling stops.
b. Sum of on-link, off-link, and crew doses.

the mean incident-free dose risks for illustrative rail routes fall largely within the range (defined by the maximum and minimum values calculated) of results obtained for mean incident-free dose risks using the LHS sample that contains 200 representative rail routes.

8.10.3 Rod Strain Failure Criterion Sensitivity Calculation

Because of radiation-induced hardening and hydride formation, the impact strains that cause spent fuel rods to fail during collision accidents decrease significantly as fuel burnup increases. In Section 5.4.1, a 4 percent average strain failure criterion for rod failure due to impact was developed by constructing a weighted summation of strain failure criteria by fuel burnup ranges using the fractional amounts of fuel in each burnup range as the weighting factors. The weighted summation assumed that high burnup spent fuel rods fail when subjected to 1 percent strains and that high average burnup fuel fails when subjected to 4 percent strains. The rod failure fractions presented in Table 7.18 were then developed by comparing the rod strains developed in Section 5.4.2 to this 4 percent strain criterion.

In order to examine the effect of the rod strain failure criterion on accident risks, one of the illustrative route calculations, the Crystal River to Hanford rail calculation that assumed spent fuel transport in a monolithic steel rail cask, was repeated assuming that all of the rods in the cask would fail during any collision accident, rather than some failing during collision accidents with speeds between 30 and 60 mph, more failing at speeds between 60 and 90 mph, and all failing when accident speeds exceed 90 mph. Because high burnup fuel rods will fail whever subjected to strains greater than 1 percent, besides examining the sensitivity of the accident risk analyses to rod failure strain criterion, this calculation also develops a result for high burnup fuel rods which are expected to fail during all collisions that exceed regulatory conditions (a 30 mph impact onto an unyielding surface).

Table 8.9 shows that, when a 4 percent average rod strain failure criterion was assumed, the mean accident risk for the Crystal River to Hanford rail route for a monolithic steel rail cask was calculated to be 2.44E-6 person-rem. When this calculation was repeated assuming rod failure fractions of 1.0 for all accident speed ranges, the calculated mean accident risk was found to be 4.69E-6 person-rem. Thus, even if all of the rods in a spent fuel cask were assumed to fail during any collision accident with a speed greater than 30 mph, accident risk estimates would increase by only a factor of two.

Accident risks increase by only a factor of two for two reasons. First, as the tables in Appendix D show, 10 of the 20 rail accident cases that lead to radioactive releases already have rod failure fractions for collision accidents that have values of 1.0, and 2 of the 10 that have failure fractions for collisions that are less than 1.0 lead to fires that fail all remaining unfailed rods. Second, although failing more rods increases the release of particulates (fuel fines), it decreases the release of Cs vapors because, once generated by heating by a fire, these vapors can now escape from failed rods only by diffusion, which is a very inefficient transport process. Thus, failing all of the rods on impact decreases the total release of Cs (Cs release in particulates increases but not enough to compensate for the virtual elimination of Cs release in vapors). Therefore, accident source terms increase much less than might be expected given the strong dependence of rod failure on rod strain levels. Finally, the fact that accident risks are increased by only a factor of two, when rod failure fractions are set to 1.0, shows that the approximate nature of the analysis used in Section 5.4.1 to develop the 4 percent average rod failure strain criterion was entirely justified.

8.11 Rail Routes with Heavy-Haul Segments and Intermodal Transfers

Transport of spent fuel by rail in a rail cask will require special heavy-haul truck transport over short route segments when either the nuclear power plant (e.g., the Maine Yankee and Kewaunee nuclear plants) or the storage site (e.g., the proposed Skull Valley interim storage site) are not serviced directly by a rail spur. Because the need for heavy-haul truck transport to or from rail route termini was neglected in all of the rail route calculations described in Sections 8.7 and 8.10.2, the magnitude of the incident-free dose risks (including handler dose risks incurred during intermodal transfers) and accident population dose risks that might result during heavy-haul truck transport to or from railheads was investigated for three real heavy-haul route segments:

1. the Maine Yankee nuclear plant to the railhead at Pejepscot Mills, Maine;
2. the Kewaunee nuclear plant to the railhead at Kewaunee, Wisconsin; and
3. the railhead at Timpie, Utah, to the proposed Skull Valley, Utah, interim storage site.

This section describes these calculations and compares the population dose risks calculated for these heavy haul segments to the population dose risks calculated for the specific real rail route that each heavy-haul segment would service.

For each heavy-haul route segment, route parameters for three aggregate segment links (urban, suburban, and rural link distances; population densities; and accident rates) were developed. Segment lengths and population densities were calculated for the non-interstate road segments from 1990 census data using the ArcView GIS software system. Rural and suburban accident rates were set to the means of the accident rate distributions developed in Section 3.4.2.3, and the value used for the urban accident rate was the value used in the LHS truck route calculations. Table 8.10 presents these route parameter values.

Table 8.10 Route Parameters for Heavy-haul Truck Transport Segments

Aggregate Link	Length (km)	Population Density (persons per km^2)	Accident Rate (accidents per km)
Maine Yankee Nuclear Plant to the Railhead at Pejepscot Mills			
Rural	15	31.6	2.2E-7
Suburban	21	318	4.1E-7
Urban	4.0	2570	5.2E-7
Kewaunee Nuclear Plant to the Railhead at Kewaunee			
Rural	17	38.5	2.2E-7
Suburban	1.0	90.8	4.1E-7
Urban	0.0	NA	NA
Railhead at Timpie to the Proposed Skull Valley Interim Storage Site			
Rural	46	0.21	2.2E-7
Suburban	0.0	NA	NA
Urban	0.0	NA	NA

Next, the set of PWR truck accident severity fractions and release fractions in Table 7.31 was modified by eliminating accidents (setting severity fractions to zero) that can not occur given the characteristics of heavy-haul transport (movement under escort at low speeds). Specifically, severity fractions were set to zero for all of the accident categories that describe accidents that occur with speeds greater than 60 mph (Accident Categories 1, 5 through 13, and 15 through 17). In addition, because the formation of a robust puncture probe during very-low-speed accidents is extremely improbable, the severity fraction for Accident Category 14 was also set to zero. Thus, rail cask failure during heavy-haul transport was assumed to be possible only for the three low-speed collision accident categories (Categories 2 through 4) that initiate fires and also for the fire-only accident category (Category 18). Then, because heavy-haul transport speeds are almost always < 30 mph (the calculation assumed 25 mph), the severity fractions for the remaining four

accident categories were each decreased by a factor of ten. Finally, given this input data, RADTRAN 5 was used to calculate the population dose risks associated with heavy-haul truck transport over each of the three heavy-haul routes defined in Table 8.10. The results of these calculations are presented in Table 8.11.

Table 8.11 shows that, for these three heavy-haul route segments, other incident-free dose risks are about 10^3 to 10^6 times larger than the incident-free stop doses, and about 10^4 to 10^7 times larger than the accident dose risks. Comparison of these dose risks to the same dose risks listed in Tables 8.5 and 8.9 for transport over rail routes indicates that incident-free and accident dose risks for heavy haul transport to or from railheads will be negligible when compared to the population dose risks associated with transport over the rail portion of any route that requires both transport by heavy-haul truck and by train. Finally, comparison of the intermodal transfer handler population dose risks in this table to the total incident-free dose risks presented in Tables 8.5 and 8.9 shows that adding intermodal transfers to any rail route will significantly increase total population dose risks because the handlers must work close to the cask for significant periods of time while attaching lifting hardware, inspecting the cask, and performing other transfer operations.

Table 8.11 Heavy-Haul Incident-Free and Accident Population Dose Risks

Metric	Population Dose Risks (person-rem)				
	Incident-Free				
	Stops[a,b]	Other[c]	Total	Accident	Handling[d]
Maine Yankee Nuclear Plant to the Railhead at Pejepscot Mills					
Mean =	3.8E-07	5.1E-04	5.1E-04	8.0E-08	1.4E-02
Standard Deviation =	2.2E-07	3.0E-04	3.0E-04	4.4E-08	8.5E-03
Kewaunee Nuclear Plant to the Railhead at Kewaunee					
Mean =	2.1E-07	1.7E-04	1.7E-04	2.2E-09	1.4E-02
Standard Deviation =	1.2E-07	1.1E-04	1.1E-04	1.4E-09	8.5E-03
Railhead at Timpie to the Proposed Skull Valley Interim Storage Site					
Mean =	4.5E-10	4.2E-04	4.2E-04	2.6E-11	1.4E-02
Standard Deviation =	2.6E-10	2.7E-04	2.7E-04	1.8E-11	8.5E-03

a. Intermodal transfer stop dose to members of the public.
b. Short segment lengths mean no stops are made for inspections or to refuel, eat, or sleep.
c. Sum of on-link, off-link, and crew doses.
d. Intermodal transfer dose risk to cask handlers.

8.12 Loss of Shielding Accidents

The loss of shielding (LOS) accident model uses the entire radionuclide content of the material to determine source strength because it was built for less robust (Type A) packages (e.g., radiopharmaceutical shipments) that could lose all or part of their shielding in serious accidents. With spent-fuel casks, however, loss of shielding is expected to be localized to a small fraction of the total surface area of the cask.

Although the STOP subroutine is generally used to evaluate incident-free doses at stops, it is also suited to spent fuel cask LOS scenarios because the subroutine requires only dose rate, source dimension, and exposure duration as input values. These are used to construct a point source of the appropriate source strength to estimate radiation exposure fields, as is used for the RADTRAN incident-free exposure model. Population may be modeled as being uniformly distributed around the source in one or more annular areas with user-defined radii and population densities. Exposure duration is taken to be the time that passes before emergency responders establish an exclusion area around the accident site. In the absence of specific information for this variable, 25 minutes in urban areas and 40 minutes in rural and suburban areas were the values used.

To use the RADTRAN STOP model to assess LOS consequences for accidents involving casks, three factors must be calculated for each accident severity category:

- Severity fraction for each LOS accident case.
- Dose rate (dose rate at 1 m from surface of cask after the LOS accident has occurred).
- Maximum dimension and geometry of the unshielded area.

8.12.1 Severity Fractions, Dose Rates, and Cask LOS Areas

Severity fractions for ten LOS accident cases are developed by combining the train accident cases presented in Table 7.11 into 6 groups as follows: Cases 4, 5, and 6 which have accident speeds from 30 to 60 mph, Cases 1, 7, 8, and 9 which have accident speeds from 60 to 90 mph, Cases 2, 10, 11, 12, and 13 which have accident speeds from 90 to 120 mph, Cases 3, 13, 14, 15, and 16 which have speeds > 120 mph, Case 20 which is all fire only accidents that produce lead slump by melting, and Cases 16, 17, 18, and 19 which are collision accidents during which the cask shell is punctured, which also lead to large fires and thus to the loss of melted lead out the shell puncture. Severity fractions for these ten LOS accident cases are developed by summing the severity fractions for the accident cases which contribute to each LOS case and multiplying by the chance that the accident is an end or a corner impact (the finite element calculations do not show LOS for side impact accidents).

The maximum exposed length of a spent-fuel assembly (at least for end drops where lead slumps and separates from one end of the cask) is determined from the finite element analyses of cask shielding damage for each scenario. This exposed length is then expressed as a fraction of the length of a full PWR assembly (200 inches).

The LOS fraction is then used to calculate a Source-Strength Multiplier, which is the number by which the maximum dose rate at 1 m from an unshielded fuel assembly must be multiplied to yield the maximum dose rate 1 m from the cask on the centerline of the field of view of the shielding damage. Because lead slump often occurs at the ends of the cask where the fittings are and where the lowest burnup fuel is located, neglect of this consideration increases the conservatism of the source strength estimates.

To calculate the Source-Strength Multiplier of a steel-lead-steel train cask, the following approach was used. As is shown in Figure, 8-24, the dose rate at 1 m in the center of the zone of shielding damage was modeled as the integrated sum of dose rate contributions from the fuel surface extending in an arc from 0 degrees to approximately 60 degrees multiplied by 2 to account for symmetry. The fuel surface was modeled as being a section of a cylinder with a diameter equal to 1.65 m (the same as the cask ID) and a width equal to the maximum exposed length.

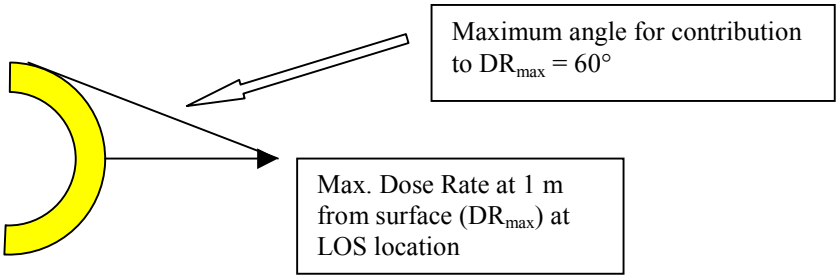

Figure 8.24 Representation of spent fuel surface for dose rate calculation for LOS scenarios.

Table 8.12 presents the severity fractions, LOS fractions, and source strength multipliers used in the LOS accident calculations. The following comments qualify the development of the values of these parameters:

1. For LOS Cases 1 through 8, impact forces are modeled as causing lead slump, and the maximum length of exposed fuel for each of these cases was taken from the appropriate finite element analysis.

2. For LOS Cases 9 and 10, the accident leads to a fire. Case 10 involves lead melt combined with puncture that allows some of the lead to flow out of the cavity between the inner and outer cask shells. Because the location of the puncture with respect to the ground surface cannot be predicted, on the average it is assumed to allow approximately one-half of the lead to flow out. Thus, a value of 0.5 for fractional exposure was assigned to this accident case.

3. In all cases, the approximately 3 inches of steel that comprise the inner and outer shell are modeled as remaining in place, and the shielding they continue to provide is accounted for in this model.

4. The Source-Strength Multiplier is calculated by expressing the result from the integration (Step 1) as a fraction of the dose rate from a single fully exposed assembly and multiplying by the total number of assemblies exposed.

5. This value is then entered as a modifier (shielding factor) into the RADTRAN STOP model, and the package dose rate is replaced by the dose rate for the fully exposed fuel. The product of these two variables yields dose rate in area of LOS.

Table 8.12 Values of Severity Fractions, LOS Fractions, and Source-Strength Multipliers for Ten LOS Accident Cases

LOS Case	Accident Type	Accident Conditions	Train Accident Cases	Sum Case Probabilities	Severity Fraction	LOS Fraction	Source-Strength Multiplier
1	Collision	end	4,5,6	3.049E-05	1.707E-06	0.052	0.215
2	Collision	end	1,7,8,9	8.273E-06	4.633E-07	0.158	0.637
3	Collision	end	2,10,11,12	5.730E-07	3.209E-08	0.264	1.017
4	Collision	end	3,13,14,15	4.524E-09	2.534E-10	0.368	1.336
5	Collision	corner	4,5,6	3.049E-05	2.201E-05	0.033	0.137
6	Collision	corner	1,7,8,9	8.273E-06	5.973E-06	0.096	0.394
7	Collision	corner	2,10,11,12	5.730E-07	4.137E-07	0.158	0.637
8	Collision	corner	3,13,14,15	4.524E-09	3.266E-09	0.255	0.986
9	Fire Only	T > 350°	20	4.905E-05	4.905E-05	0.029	0.120
10	Fire	T > 350°C & puncture	16,17,18,19	4.150E-10	1.660E-09	0.500	1.668
11	No LOS				9.999E-01	0.000	

8.12.2 Maximum Dimension of LOS Area

The maximum LOS area is obtained in a relatively conservative manner by using the product of LOS fraction and fuel assembly length as one dimension of a rectangle. The second dimension is set equal to the ID of the cask. The diagonal of this rectangle is entered into RADTRAN as the maximum characteristic dimension, which is used internally to calculate a shape factor (k_0) for a point source.

8.12.3 Final Calculation

The dose rate and dimension values entered as described above allow the user to calculate population dose for persons, who remain at specified distances from the LOS accident location for specified lengths of time, by treating the results of the LOS event as a point source. For real LOS accidents, cask orientation combined with shielding by the undamaged portions of the cask shell and also by nearby buildings would mean that radiation exposures would be limited in extent by the view factor to the spent fuel through the damaged portions of the cask shell that now provide no shielding. However, because the exact geometry of an accident cannot be predicted in advance, a point-source model and a uniformly distributed surrounding exposed population was used. Accordingly the estimates of the LOS accident dose risks should be somewhat conservative.

8.12.4 An Example of an LOS Calculation

As an example of an LOS risk estimate, a steel-lead-steel rail cask containing PWR fuel assemblies was considered. For an approximate surface dose rate of 50,000 rem/hr for five-year cooled spent fuel, the dose rate at 1 m from the surface of one face at mid-length of the assembly was calculated by modeling the assembly as a line source 5 m long. The resulting value, 3500 rem/hour, was then attenuated by 3 inches of steel using an approximate photon spectrum

derived from the isotopic inventory for PWR spent fuel before subtracting insignificant isotopes relative to their A_2 values [8-7]. Since the source of the surface dose rate quoted above did not specify neutron and gamma fractions, the attenuation due to 3 inches of steel treats the radiation as 100% gamma; this yields a conservative result for radiation outside the cask. The radionuclides that account for 97 percent of the resulting dose rate are Co-60, Cs-134, Cs-137, and Eu-154, as may be expected from the their photon energies. The result, 20 rem/hr, representing the dose rate from a single PWR fuel assembly in a steel-lead-steel rail cask without the lead shielding, was then multiplied by the appropriate Source-Strength Multiplier in Table 8.12 to provide the required RADTRAN 5 input. The source dimension used in modeling the cask as a point source in RADTRAN 5 was taken to be the diagonal of the rectangular exposed area (viewed at right angles to the cask axis) for each case in Table 8.12. These two sets of parameters were used to define ten "VEHICLEs" in RADTRAN 5, one for each of the ten cases in Table 8.12.

The RADTRAN 5 stop model was used to define three LOS accident locations, i.e. rural, suburban, and urban. Population densities for these three stop definitions were assumed to equal the means of the respective population density distributions for each region (i.e., 10.1, 336, and 2195 persons per square kilometer, respectively). The area occupied by these populations was an annulus with a 10 m inner radius and an 800 m (1/2 mile) outer radius; the latter yields a dose rate well below 10 mrem/hour in each case. The standard shielding factors (1.0, 0.87 and 0.018) and emergency response times (0.67, 0.67, and 0.42) for rural, suburban, and urban areas, respectively, were applied to the three stop definitions. Table 8.13 presents route-portion lengths, mean rail accident rates, the severity fractions given in Table 8.13, the consequences calculated by RADTRAN 5, and the risks (probability times consequence) for each of the ten cases defined. The total LOS risk of 9.1E-11 person-rem may be compared with the PWR steel-lead-steel rail cask results given in Table 8.5 to see that this risk is much smaller than the dispersion accident value. In addition, the sum of the two risks (representing an accident in which there is loss of shielding and dispersion of cask contents) is well within the variability of the dispersion value alone.

8.13 Population Dose Risks for Shipment of the Entire 1994 Spent Fuel Inventory

The incident-free and accident population dose risks reported in the previous sections were calculated for single shipments of one Type B spent fuel cask by truck or by train. In this section, the results of those calculations are used to estimate the population dose risks that would be associated with the shipment of the entire 1994 inventory of commercial BWR and PWR spent fuel [8-2]. Table 8.14 presents the total numbers of BWR and PWR assemblies in the 1994 spent fuel inventory, the number of truck or rail shipments required to ship all of the BWR or all of the PWR assemblies in each of the four generic casks examined by this study, and the incident-free and accident population dose risks associated with the shipment of all of the BWR assemblies, all of the PWR assemblies, and their sums (i.e., the population dose risks for shipping the entire 1994 inventory). The population dose risks for transport by rail presented in this table do not include any doses to handlers that might be incurred during intermodal transfers (e.g., from heavy haul truck to rail car).

Table 8.13 Results of Loss of Shielding Risk Calculation

Case	Pop. Zone	Length (km)	Acc. Rate (per km)	Sev. Frac.	Probability	Consequence (dose, rem)	Dose Risk
1	Rural	1777	4.40E-08	1.71E-06	1.34E-10	0.0021	2.81E-13
	Suburban	541	4.40E-08	1.71E-06	4.07E-11	0.06	2.44E-12
	Urban	35	4.40E-08	1.71E-06	2.63E-12	0.0051	1.34E-14
2	Rural	1777	4.40E-08	4.63E-07	3.62E-11	0.0071	2.57E-13
	Suburban	541	4.40E-08	4.63E-07	1.10E-11	0.206	2.27E-12
	Urban	35	4.40E-08	4.63E-07	7.13E-13	0.0175	1.25E-14
3	Rural	1777	4.40E-08	3.21E-08	2.51E-12	0.0133	3.34E-14
	Suburban	541	4.40E-08	3.21E-08	7.64E-13	0.385	2.94E-13
	Urban	35	4.40E-08	3.21E-08	4.94E-14	0.0326	1.61E-15
4	Rural	1777	4.40E-08	2.53E-10	1.98E-14	0.0221	4.37E-16
	Suburban	541	4.40E-08	2.53E-10	6.02E-15	0.639	3.85E-15
	Urban	35	4.40E-08	2.53E-10	3.90E-16	0.0541	2.11E-17
5	Rural	1777	4.40E-08	2.20E-05	1.72E-09	0.0013	2.24E-12
	Suburban	541	4.40E-08	2.20E-05	5.24E-10	0.0373	1.95E-11
	Urban	35	4.40E-08	2.20E-05	3.39E-11	0.0032	1.08E-13
6	Rural	1777	4.40E-08	5.97E-06	4.67E-10	0.004	1.87E-12
	Suburban	541	4.40E-08	5.97E-06	1.42E-10	0.115	1.63E-11
	Urban	35	4.40E-08	5.97E-06	9.19E-12	0.0097	8.92E-14
7	Rural	1777	4.40E-08	4.14E-07	3.24E-11	0.0071	2.30E-13
	Suburban	541	4.40E-08	4.14E-07	9.85E-12	0.206	2.03E-12
	Urban	35	4.40E-08	4.14E-07	6.38E-13	0.0175	1.12E-14
8	Rural	1777	4.40E-08	3.27E-09	2.56E-13	0.013	3.32E-15
	Suburban	541	4.40E-08	3.27E-09	7.78E-14	0.377	2.93E-14
	Urban	35	4.40E-08	3.27E-09	5.04E-15	0.032	1.61E-16
9	Rural	1777	4.40E-08	4.91E-05	3.84E-09	0.0011	4.22E-12
	Suburban	541	4.40E-08	4.91E-05	1.17E-09	0.0331	3.86E-11
	Urban	35	4.40E-08	4.91E-05	7.55E-11	0.0028	2.12E-13
10	Rural	1777	4.40E-08	1.66E-09	1.30E-13	0.035	4.54E-15
	Suburban	541	4.40E-08	1.66E-09	3.95E-14	1.01	3.99E-14
	Urban	35	4.40E-08	1.66E-09	2.56E-15	0.0858	2.19E-16
Total							9.12E-11

Table 8.14 shows that, for shipment of the entire 1994 spent fuel inventory, accident dose risks are negligible when compared to incident-free dose risks, and that the magnitude of these risks changes significantly depending on the mode of shipment (truck or rail) and the type of cask

Table 8.14 Incident-Free and Accident Population Dose Risks for Shipment of the Entire 1994 Spent Fuel Inventory (person-rem)

Spent Fuel Type	Rail Shipments		Truck Shipments	
	Monolithic Steel Cask	Steel-Lead-Steel Cask	Steel-Lead-Steel Cask	Steel-DU-Steel Cask
	Assemblies in Total 1994 Inventory			
BWR	60144			
PWR	44598			
	Assemblies per Cask			
BWR	52	52	2	7
PWR	24	24	1	3
	Required Number of Shipments			
BWR	1157	1157	30072	8592
PWR	1858	1858	44598	14866
Total	**3015**	**3015**	**74670**	**23458**
	Incident-Free Stop Dose Risks[a,b,c]			
BWR	5.1	5.1	460	130
PWR	8.1	8.1	680	230
Total	**13.2**	**13.2**	**1140**	**360**
	Other Incident-Free Population Dose Risks[a,b]			
BWR	18.4	18.4	870	250
PWR	29.5	29.5	1280	430
Total	**47.9**	**47.9**	**2150**	**680**
	Total Incident-Free Population Dose Risks[a,b]			
BWR	24	24	1330	380
PWR	37	37	1960	660
Total	**61**	**61**	**3290**	**1040**
	Accident Population Dose Risks[a]			
BWR	0.0017	0.011	0.010	0.0093
PWR	0.0037	0.018	0.036	0.034
Total	**0.0054**	**0.028**	**0.046**	**0.043**

a. Values have been rounded to two significant figures.
b. Because the probability of occurrence of incident-free doses is 1.0, incident-free doses and incident-free dose risks have the same values.
c. Truck stop dose risks assume shipment without stops to sleep.

used for the shipments. The dependence of incident-free doses on shipment mode and cask type means that the incident-free doses for each year in the full spent fuel shipment campaign could vary significantly depending on the mix of assemblies shipped and the mode and cask used for each shipment made during a given year. For example, if the shipments take place over 20 years, the ratio of PWR to BWR assemblies shipped each year is the same as the ratio in the total inventory, all shipments are by rail in monolithic steel and/or steel-lead-steel rail casks, and handler doses during any intermodal transfers are neglected, then the total incident-free population dose per year would be about 1.3 person-rem. Conversely, if the shipments take place over 20 years, the ratio of PWR to BWR assemblies shipped each year is the same as the ratio in the total inventory, and all shipments are by truck in steel-lead-steel truck casks (the smaller capacity truck cask), then the total incident-free population dose per year would be about 130 person-rem, which is 100 times larger than the incident-free population dose for rail shipments.

8.14 Individual Dose Estimates

Besides the population dose estimates that are the basis of the CCDF's described above, RADTRAN estimates dose within areas downwind of the accident site. Individuals who might be within these areas at various distances from the accident site are counted as having received the dose predicted for that area. These doses are directly dependent on the magnitude of the source term for the specific representative accident being considered and assume that the individual remains outdoors directly in the path of the passing radioactive plume for the entire period of the accident/release event. Under these unlikely conditions and the very unlikely sequence of events that yield a source term at all, there is a potential for persons close to the accident location to receive a relatively large radiation dose. These accident conditions are associated with the population doses at the extreme right edge of the CCDF's in the preceding figures.

As an example of the doses that might be received from accidents involving spent fuel shipments, results from the RADTRAN calculations for rail shipment from Maine Yankee to Skull Valley, one of the illustrative routes discussed earlier, will examined in greater detail. For this discussion, a rail shipment was used because it presented the largest possible source term (because of the large number of spent fuel assemblies a rail cask contains). Generally speaking, the dose that could be received by a person decreases rapidly with distance from the point of release and the highest doses are received at the points closest to the accident. Similarly dose decreases with lateral distance from the maximum dose point (centerline) at any distance, i.e., as the distance from the center of a radioactive plume increases the inhalation/immersion dose decreases. As a result, the areas in which the highest doses could be received have a relatively small area. In addition, locations very close to the site of the accident are unlikely to be occupied by people for any length of time after an accident because of evacuation and crowd control measures by first responders. Thus, the shortest distance at which individuals might be expected to receive doses should be beyond 100 to 200 meters (330 to 660 feet) from the accident site.

In the distance range given, doses that could be received by individuals standing outdoors and directly under the passing radioactive plume for the entire time of passage range from 3 to 500 rem (50 yr CEDE) for the extremely unlikely collision/fire events (on the order of 1×10^{-10} per shipment) estimated to result in a significant release of material from a cask. The doses

associated with these extremely unlikely events are relatively high but not so large that any early fatality is predicted (as is true for all RADTRAN calculations completed for this report) nor would an early fatality from radiation actually be expected to result. The largest of these doses, if received, could pose a significant, though not life threatening, health hazard to anyone so exposed, but there are many conservative factors in the RADTRAN calculations that come into play to make the likelihood of experiencing such doses very small, given that the representative accident producing the dose could even occur (which in itself is a very implausible event).

The principal RADTRAN conservatisms that make it unlikely that these large doses would ever be realized are as follow:

- RADTRAN uses a ground level plume formulation, i.e., the highest concentration point of the plume containing the release material moves along the ground from the release point to the farthest point of the calculation. However, in 17 of the 20 representative accidents that produce high population doses, the source term is the result (in part) of a significant fire event. These fires are hot, fully engulfing, and of duration exceeding 1 hour. In reality, a fire of sufficient duration and temperature to cause a release would cause the released plume to be lofted to an altitude in which the centroid is hundreds of meters off the ground surface. In such situations, zero or extremely low doses will be realized inside of distance that are 10 or more times the lofted height. Beyond that distance the calculated maximum doses will approach those predicted by RADTRAN , but certainly are below 5 rem. The remaining three doses also result from release plumes that are likely to be lofted, though not by the presence of a major fire, though it is likely that there will be fires present near accidents with these collision/impact magnitudes. Lofting for these plumes is a result of the fact that the major component of the gas pressurizing the cask is helium which has a density one seventh that of air. Thus, the plumes from these accidents (even in the absence of a fire) will also be lofted and the resultant dose will be lower than predicted.

- RADTRAN assumes that no measures will be taken by emergency response personnel to limit the progression of the accident. In urban and suburban and most rural areas where people could be exposed, emergency response actions will limit the chain of events that produce many of the source terms and thus act to preclude such releases. In remote areas where there are few people, it is unlikely that there will be any one within the relatively small area of high dose to receive it. Even more unlikely is that individuals would remain close to the scene of an accident and stay outside directly in the passage of a radioactive plume (that looks like a fire cloud/smoke) for the entire passage of the plume.

Thus, in spite of the predicted high doses realized for the high severity accident cases, it is deemed unlikely that the predicted doses would ever be realized in an accident situation. More importantly, it is assumed in this analysis that such accidents can occur, but, in fact, the combination of circumstances needed to release material from a modern spent fuel cask are so improbable as to be impossible.

8.15 Effect of NUREG-0170 Source Term and Exposure Pathway Models on Dose Risk

The treatments of spent fuel accident source terms and exposure pathways used in RADTRAN 5 differ markedly from those used in RADTRAN 1. This section describes these treatments and the effects they have on predictions of population dose risks in three steps. First, the inventories, accident source term equations, and exposure pathways models used in NUREG-0170 are contrasted with those used in this study. Second, results of RADTRAN 4 and RADTRAN 5 calculations are compared to RADTRAN 1 results in order to show that these codes can be made to mimic RADTRAN 1 results. Finally, a series of RADTRAN 5 calculations are performed that depict the effect of the NUREG-0170 source term and exposure pathway treatments on predictions of population dose risks.

8.15.1 Source Term and Exposure Pathway Models in RADTRAN 1 and RADTRAN 5

Both RADTRAN 1 and RADTRAN 5 calculate spent fuel accident source terms (ST_i) as the product of an inventory ($I_{inventory,i}$) of radionuclide I and the fraction ($f_{release,i}$) of that inventory that could be released to the atmnosphere should the spent fuel cask fail during a severe accident. Thus, $ST_i = I_{inventory,i} f_{release,i}$.

In Section 1.2, it was stated that, as it was used in NUREG-0170, $I_{inventory,i}$ is not a cask inventory. Instead, it is the number of curies of radionuclide i estimated to be released from the spent fuel cask to the atmosphere should the cask fail during a severe accident. Thus, for the RADTRAN 1 calculations performed for NUREG-0170, $I_{inventory} = ST_{severe\ accident,i}$, where values for $ST_{severe\ accident,i}$ were developed largely on the basis of conservative engineering judgment and $ST_{severe\ accident,i}$ is the source term for a severe spent fuel accident. Accordingly, as used for NUREG-0170, $f_{release,i}$ is the fraction of the severe accident source term that is released during accidents of lessor severity.

For this study, the number of curies of radionuclide i that is released from a Type B spent fuel cask should the cask and some of the rods in the cask both fail during an accident is calculated as the product of five numbers: the number of assemblies in the cask ($N_{assemblies}$), the inventory of radionuclide i in a single fuel assembly (I_i), the fraction of the number of rods in an assembly that fail (f_{rods}), the fraction of the inventory of radionuclide i in a single rod that escapes to the cask interior upon rod failure ($f_{rod\text{-}to\text{-}cask,i}$), and the fraction of the amount of radionuclide i that reaches the cask interior that escapes from the cask interior through the cask leak to the environment ($f_{cask\text{-}to\text{-}environment,i}$). Thus, for this study, the source term for radionuclide i (ST_i) is calculated as

$$ST_i = N_{assemblies} I_i f_{rods} f_{rod\text{-}to\text{-}cask,i} f_{cask\text{-}to\text{-}environment,i}$$

where $I_{inventory,i} = N_{assemblies} I_i$ and $f_{release,i} = f_{rods} f_{rod\text{-}to\text{-}cask,i} f_{cask\text{-}to\text{-}environment,i}$.

Table 7.9 shows that the single assembly BWR and PWR inventories used in this study contain 19 and 20 radionuclides, respectively. In marked contrast to Table 7.9, Table 1.4 shows that the truck and rail cask accident "inventories" used with RADTRAN 1 for the NUREG-0170 spent fuel calculations contain only three radionuclides, Kr-85, I-131, and Cs-137. Here "inventories"

is in quotes to emphasize the fact that the NUREG-0170 meaning for this term is different from the common meaning. That is, in NUREG-0170 [8-1], "inventory" means the amount of each radionuclide released to the environment upon package failure and not the amount of each radionuclide that is contained (carried) in the package, here the Type B spent fuel cask. Table 7.9 shows that the BWR and PWR inventories developed for this study do not contain I-131. They do not contain I-131 because the RADSEL code calculation described in Section 7.2.3.3 showed that iodine radionuclides in three-year cooled, high-burnup spent fuel do not contribute significantly to radiation health hazards at the level of one-tenth of one percent.

Table 7.31 shows that the source term analysis performed for this study developed 19 source terms for a steel-lead-steel Type B spent fuel truck cask, one of which, Case 19, represents the fraction of all truck accidents that do not lead to a release of radioactivity from the cask because either the cask containment is not compromised or because none of the rods in the cask fail. The table also shows that for a steel-lead-steel Type B spent fuel rail cask, 21 source terms were developed, one of which represents accidents that do not lead to any release of radioactivity. As described in Section 1.2, the source term scheme used in NUREG-0170 [8-1] had eight categories and two release models, Models I and II. Categories I and II represented accidents that respectively do not result in releases from Type A and Type B packages. Categories III through VIII represented accidents that are severe enough to cause radionuclides to be released from a Type B package. Both release models assumed that all materials released from the cask were respirable, that is they were either gases, vapors, or respirable aerosols. Thus, all solid materials released from the cask were assumed to be aerosols with sizes (aerodynamic mass median diameters) $\leq 10\ \mu$. Model I assumed that 100 percent of the NUREG-0170 truck and rail accident "inventories" of Kr-85, I-131, and Cs-137 was released by any accident that fell into Categories III through VIII. Model II tempered this conservative assumption by decreasing the fraction of the NUREG-0170 accident "inventories" released for Categories III and IV accidents from 100 percent to 1 and 10 percent respectively.

RADTRAN 5 models radiation exposures caused by transportation accidents that are delivered via four pathways: direct exposure to the passing radioactive airborne plume (cloudshine), exposures caused by inhalation of radioactive materials in the passing airborne plume (direct inhalation), exposures to radioactivity deposited onto the ground from the passing airborne plume (groundshine), and exposures caused by inhalation of radioactive materials that are resuspended from contaminated ground into the air (resuspension inhalation). In marked contrast to this, RADTRAN 1 only modeled inhalation exposures (both direct inhalation and resuspension inhalation).

Two sets of calculations were performed to examine the impact on estimates of accident consequences calculated with RADTRAN 1 and RADTRAN 5 of these differing treatments of accident source terms and exposure pathways. The first set of calculations compared the mean accident population doses and the mean number of latent cancer fatalities that are obtained when the NUREG-0170 spent fuel transport accident calculation is run using RADTRAN 1, RADTRAN 4, and RADTRAN 5. The second set of calculations examined the impact of various combinations of these treatments on RADTRAN 5 steel-lead-steel truck cask accident CCDFs.

8.15.2 Comparison of Results Calculated with RADTRAN Versions 1, 4, and 5

When this study was initiated, RADTRAN 1, the first version of the RADTRAN code that was developed to support the performance of NUREG-0170 [8-1], existed only as a listing on microfiche appended to the Sandia National Laboratories report that describes RADTRAN 1 [8-8]. Thus, for this study, in order to compare RADTRAN 1 results to results obtained with later versions of the RADTRAN code, RADTRAN 1 had again to be made operational. Reference [8-9] describes the resurrection and verification of RADTRAN 1.

Ideally, RADTRAN 1 results would be compared directly to results obtained using RADTRAN 5, the version of the RADTRAN code used to support this study. This was not done for the following reasons. RADTRAN 1 is able to examine only one radionuclide at a time. Accordingly, three RADTRAN 1 calculations must be performed to develop results for the three radionuclides (Kr-85, I-131, and Cs-137) in the NUREG-0170 spent fuel accident "inventory." RADTRAN 4 and RADTRAN 5 can examine many radionuclides during a single calculation. However, while RADTRAN 4 can output the accident population dose attributable to each radionuclide examined, RADTRAN 5 outputs only the total population dose and not the doses attributable to the individual radionuclides in its package inventory. Further, differences in code input mean that essentially identical input can be developed for RADTRAN 1 and RADTRAN 4 or for RADTRAN 4 and RADTRAN 5, but not for RADTRAN 1 and RADTRAN 5. Because RADTRAN 4 and RADTRAN 5 yield essentially identical results for the NUREG-0170 spent fuel calculation (i.e., total truck and train accident population doses respectively of 2.12E+02 versus 2.13E+02 person-rem), RADTRAN 4 results are an excellent surrogate for RADTRAN 5 results. Therefore, because identical input could be developed for RADTRAN 1 and RADTRAN 4 and because RADTRAN 4 generates population dose results for each radionuclide examined, the calculations that compared accident doses compared RADTRAN 1 results to those obtained with RADTRAN 4.

Replication of RADTRAN 1 input data in the formats required by RADTRAN 4 and RADTRAN 5 was not simple for all input parameters. For example, in RADTRAN 4, the fraction of land occupied by buildings is 0.52, fixed values are used for the fractions of the population that are outdoors and in buildings, and doses for people in buildings are calculated by multiplying the dose for people outdoors by a building dose factor (BDF) which accounts for the lower doses that are received by people in buildings because of particle filtering during air infiltration into buildings. Because RADTRAN 1 does not model the particle filtration during air infiltration into buildings, in order to force RADTRAN 4 to mimic RADTRAN 1, the value of BDF used in the RADTRAN 4 calculations was chosen so $0.52 \times \text{BDF} = 1.0$, which made RADTRAN 4 doses for people in buildings the same as the doses received by people outside of the buildings. For RADTRAN 5, because the fraction of land occupied by buildings and the BDF are both input parameters, RADTRAN 5 could be made to mimic RADTRAN 1 by setting both of these parameters equal to 1.0. RADTRAN 4 and RADTRAN 5 but not RADTRAN 1 calculate pedestrian doses in urban areas. Therefore, for the RADTRAN 4 and RADTRAN 5 calculations, this dose was forced to zero by setting the value of RPD, the ratio of pedestrian density to region population density, to zero. Finally, the value of the inhalation dose conversion factor currently used for RADTRAN 4 and RADTRAN 5 calculations, which is somewhat larger than the value used in RADTRAN 1, was reset to the RADTRAN 1 value.

Table 8.15 presents the mean accident population dose risks predicted by RADTRAN 1 and RADTRAN 4 for the NUREG-0170 truck and rail calculations when each code was run using the same truck or rail route and the same truck or rail accident source terms (i.e., the NUREG-0170 truck or rail route, the NUREG-0170 truck or rail accident "inventory" specified in Table 1.4, and the NUREG-0170 Model II severity and release fractions specified in Table 1.3). Two sets of RADTRAN 4 results are presented. The first set models only inhalation exposures (both the dose from inhalation of radioactive materials directly from the passing plume and the dose caused by inhalation of radioactive materials that are resuspended from the ground), while the second set models not only direct and resuspension inhalation exposures but also exposures from cloudshine and groundshine. Thus, the first set of results is directly comparable to the results generated by RADTRAN 1 while the second set reflects the more complete treatment of exposure pathways as currently modeled in both RADTRAN 4 and RADTRAN 5.

Table 8.15 Mean Accident Population Dose Risks Calculated by RADTRAN 1 and RADTRAN 4 (person-rem)

Radionuclide	Code (Exposure Pathways)		
	RADTRAN 1 (only inhalation and resuspension)	RADTRAN 4 (only inhalation and resuspension)	RADTRAN 4 (all pathways)
NUREG-0170 Truck Route and Truck Accident Model II Source Terms			
Kr-85	1.05E-04	1.83E-04	4.20E-01
I-131	2.68E-03	2.66E-03	2.69E-03
Cs-137	1.32E+00	4.34E+00	1.79E+02
NUREG-0170 Rail Route and Rail Accident Model II Source Terms			
Kr-85	2.32E-05	3.73E-05	8.52E-02
I-131	5.76E-04	5.29E-04	5.33E-04
Cs-137	2.89E-01	8.78E-01	3.20E+01

Table 8.15 shows that

- that the doses caused by the quantities of Kr-85 and I-131 in the NUREG-0170 truck and train accident "inventories" contribute negligibly to the total accident population doses (sum of the doses caused by each radionuclide), which are essentially equal to the dose caused by Cs-137;

- that the RADTRAN 4 total inhalation truck and rail accident population doses are respectively 3.3 and 3.0 times larger than the corresponding RADTRAN 1 doses; and

- that the truck and rail accident population doses calculated by RADTRAN 4, when all exposure pathways are modeled, are respectively about 41 and 36 times larger than the doses calculated when only the direct inhalation and resuspension inhalation pathways are modeled.

Differences between the RADTRAN 1 and RADTRAN 4 inhalation dose models explain the second result. Specifically, in the RADTRAN 1 and RADTRAN 4 equations for D_{inh}, the total inhalation dose (sum of the direct and resuspension inhalation pathway doses) are formed into a ratio and common parameters that have the same value are cancelled, the following expression results

$$\frac{D_{inh}(\text{RADTRAN 4})}{D_{inh}(\text{RADTRAN1})} = \frac{\text{IF x BR}}{2.223\text{E}-2} \times \frac{\text{RESUSP(RADTRAN 4)}}{\text{RESUSP(RADTRAN1)}} = 3.3$$

This expression equals 3.3 because in RADTRAN 4, the time-integrated atmospheric dilution factor, IF = 66.2 Ci s/m^2 for Cs-137, the breathing rate, BR = 3.3E-4 m^3/s, and the resuspension factor, RESUSP = 5.41, while in RADTRAN 1 the constant 2.223E-2 represents the product of a time integrated atmospheric dilution factor and a breathing rate, and RESUSP = 1.62. Thus, the fact that RADTRAN 4 truck and rail accident population doses are respectively 3.3 and 3.0 times larger that the same doses calculated with RADTRAN 1 is almost entirely caused by the differences in the parameter values used in the nearly identical RADTRAN 1 and RADTRAN 4 inhalation dose models.

RADTRAN 1, RADTRAN 4, and RADTRAN 5 all estimate the radiation induced latent cancer fatalities (LCFs) that may occur among a population exposed to radiation due to the transport of a radioactive material, for example spent fuel. Because RADTRAN 1 and RADTRAN 4 use different models to calculate LCF values, comparison of the LCF predictions of these two versions of RADTRAN is not straightforward. However, because both RADTRAN 1 and RADTRAN 5 calculate LCFs from population dose using a simple multiplicative cancer fatality risk factor, the cancer fatality models in these two versions of RADTRAN can be made the same by setting the value of this factor in RADTRAN 5 to 2.220E-05 LCFs/person-rem, the hardwired value that is used in RADTRAN 1 to calculate cancer fatalities caused by inhalation dose to the lungs, or to 1.216E-4 LCFs/person-rem, the value used to calculate cancer fatalities from the dose delivered to the whole body by all exposure pathways.

Table 8.16 presents the predictions of LCF risks for the NUREG-0170 standard spent fuel shipment model for the year 1975 (i.e., 17 rail shipments of length 1,210 km and 254 truck shipments of length 2,530 km) obtained using RADTRAN 1, RADTRAN 4, and RADTRAN 5, the NUREG-0170 truck and rail accident "inventories," and the NUREG-0170 Model II Severity

Table 8.16 RADTRAN 1, RADTRAN 4, and RADTRAN 5 Estimates of the Mean Latent Cancer Fatality Risks Associated with Shipment of Spent Fuel According to the NUREG-0170 Standard Shipment Model for 1975

Code Version (pathways modeled)	Mean Latent Cancer Fatality Risk
RADTRAN 1 (only direct and resuspension inhalation)	3.57E-05
RADTRAN 4 (only direct and resuspension inhalation)	1.15E-04
RADTRAN 5 (only direct and resuspension inhalation)	1.16E-04
RADTRAN 4 (all pathways)	2.50E-02
RADTRAN 5 (all pathways)	2.54E-02

and Release Fractions. Table 8.16 shows that the RADTRAN 5 and RADTRAN 1 LCF predictions differ by a factor of 3.3 when RADTRAN 5 is made to model only the direct and resuspension inhalation pathways, while the RADTRAN 5 result when all exposure pathways are modeled is 700 times larger than the result obtained using RADTRAN 1, which models only inhalation pathways.

Because RADTRAN 4 inhalation doses exceed those predicted by RADTRAN 1 by factors of approximately 3.3, the mean latent cancer fatality prediction of RADTRAN 4 also exceeds that of RADTRAN 1 by about 3.3. Because the dosimetric models in RADTRAN 4 and 5 are essentially identical, and their cancer risk models are equivalent, RADTRAN 4 and RADTRAN 5 yield essentially identical predictions of latent cancer fatalities when these fatalities are based only on inhalation dose and also when they are based on dose delivered by all exposure pathways.

The preceding results demonstrate that RADTRAN 4 and RADTRAN 5 yield nearly identical latent cancer fatality predictions when both run the same problem. Therefore, because RADTRAN 4 inhalation doses exceed those predicted by RADTRAN 1 by a factor that is almost entirely explicable in terms of differences in a few inhalation dose parameter values, the fact that RADTRAN 4 and RADTRAN 5 yield identical results for the same problem means that RADTRAN 5 is a reasonable surrogate for RADTRAN 1. Accordingly, RADTRAN 5 was used to examine the impact that the various components of the NUREG-0170 treatments of source terms and exposure pathways have on population dose CCDFs.

8.15.3 Effect of Treatments on RADTRAN 5 Accident Population Dose CCDFs

Because the accident source terms developed for NUREG-0170 [8-1] are very different from those developed for this study and because RADTRAN 1 models only inhalation exposures while RADTRAN 5 models cloudshine and groundshine exposures in addition to inhalation exposures, five RADTRAN 5 truck transport calculations were performed to illustrate the effect of these different treatments on accident population dose risk. Except for source terms, the input data used in these five calculations (the LHS sample and the values for all other parameters except source term parameters) was identical. Thus, each calculation used the same set of 200 representative routes and route characteristics, and each used the same set of values for all other input parameters except severity fractions and release fractions. Table 8.17 lists for each calculation the source term used, the exposure pathways modeled, and the resulting Mean Accident Population Dose Risk.

Figure 8.25 presents the five Accident Population Dose Risk CCDFs developed by these calculations. Figure 8.25 shows that the five Accident Population Dose Risk CCDFs are ordered as follows:

Calc. 19 CCDF > Calc. 20 CCDF > Calc. 21 CCDF > Calc. 22 CCDF > Calc. 1 CCDF

where > means “lies above.” Calculation 1 in Tables 8.1 and 8.17 is the RADTRAN 5 calculation that examined the risks associated with the transport of a single PWR assembly in the generic steel-lead-steel truck cask and used as input (a) the LHS sample of size 200 that

Table 8.17 Mean Accident Population Dose Risks (person-rem) for Five RADTRAN 5 Calculations that Used Different Source Terms and Exposure Pathways

Calculation Number from Table 8.1	Inventory		Severity and Release Fractions			Exposure Pathways		Mean Accident Population Dose Risk
	PWR[a]	0170[b]	0170[c]		SLS-T[d]	All	Inhalation Only	
			Model I	Model II				
19	X		X			X		1.2E+4
20	X			X		X		7.0E+2
21		X		X		X		2.2E-2
22		X		X			X	7.7E-4
1	X				X	X		8.0E-7

a. See Table 7.9.
b. See Table 1.4.
c. See Table 1.3 in this report and Table 5-8 in Reference [8-1].
d. See Table 7.31.

contained the set of 200 representative truck routes and (b) the set of 19 new steel-lead-steel truck cask source terms developed by this study. Calculation 22 in these tables is the RADTRAN 5 calculation that best replicates, when 200 representative routes are examined, the NUREG-0170 accident population dose risk results for the shipment of a single spent fuel truck cask. Although the CCDFs for these two calculations cross at a population dose of about 2E+3 person-rem, Table 8.17 shows that the mean accident population dose risk for Calculation 22, the calculation that used the NUREG-0170 truck accident source term and modeled only inhalation exposures, is 1000 times larger than the mean accident population dose risk predicted by Calculation 1, the steel-lead-steel truck transport calculation that used the 19 truck accident source terms developed for this study and modeled all exposure pathways. Comparison of the mean accident population dose risk results for Calculations 22 and 21, 21 and 20, and 20 and 19 then shows, respectively, that modeling cloudshine and groundshine increases mean accident population dose risks by about a factor of 30; using the PWR cask inventory instead of the NUREG-0170 truck accident "inventory," which represents the radioactivity released to the environment by the most severe accidents examined by NUREG-0170 [8-1], greatly increases mean accident population dose risks by a factor of about 30,000; and finally, replacing the NUREG-0170 Model II severity and release fractions by the Model I severity and release fractions pushes the knee of the CCDF up a bit and further increases mean accident population doses by a factor of about 20. Mean accident population dose risks increase by a factor of 30,000 when the NUREG-0170 accident "inventory" is replaced by the PWR truck cask inventory, because the NUREG-0170 Models I and II treat all solid materials released as 100 percent aerosolized and 100 percent respirable. Thus, use of a real cask inventory with these assumptions means that all of the actinides in spent fuel contribute to inhalation doses, which greatly increases direct inhalation doses and very greatly increases long-term resuspension inhalation doses.

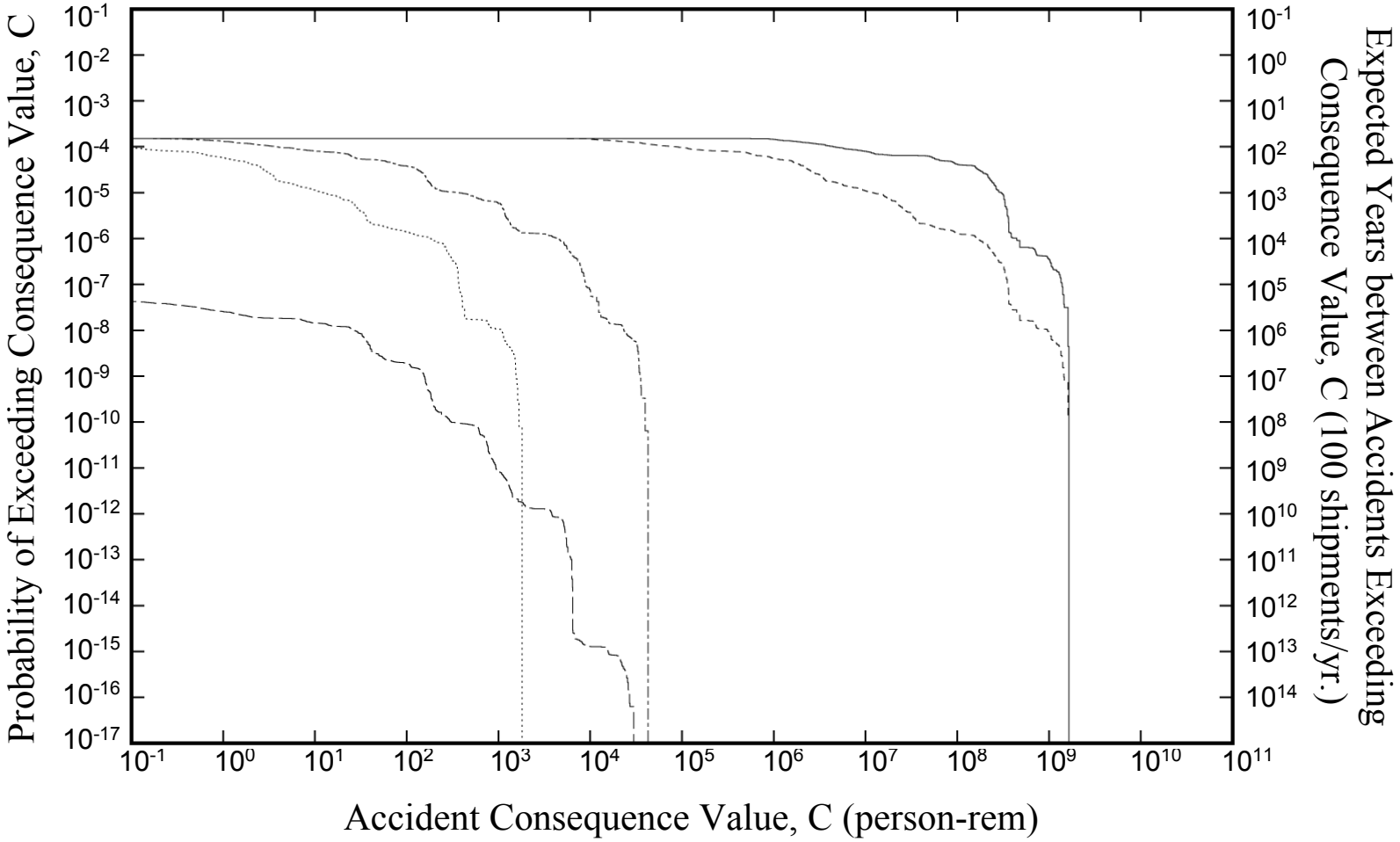

Figure 8.25 Mean truck accident population dose risk CCDFs for calculations that examined the impact on dose risks of NUREG-0170 source terms and exposure pathway models. Each RADTRAN 5 calculation assumed transport in a steel-lead-steel truck cask over each of the 200 representative truck routes and each calculation generated results for all of the 19 representative truck accident source terms.

——— **PWR inventory, NUREG-0170 Model I release fractions, all exposure pathways**

---------- **PWR inventory, NUREG-0170 Model II release fractions, all exposure pathways**

-·-·-·- **NUREG-0170 accident release inventory, NUREG-0170 Model II release fractions, all exposure pathways**

····· **NUREG-0170 accident release inventory, NUREG-0170 Model II release fractions, only inhalation pathways**

– – – PWR inventory, 19 truck accident source terms, all exposure pathways

8.16 Population Dose Risk CCDFs from NUREG-0170, the Modal Study, and this Study

Because the spent fuel risk assessment methodology developed by the Modal Study [8-2] was the basis for all of the analyses conducted by this study, it is of interest to compare accident population dose risk CCDFs and mean accident population doses calculated by RADTRAN 5 using NUREG-0170 Model I and Model II source terms, Modal Study source terms, and the source terms developed by this study. Each of these calculations examined transport of PWR spent fuel in a steel-lead-steel spent fuel cask and used the LHS sample of size 200 that contained the representative set of 200 truck or rail routes. Except for inhalation dose and source term parameters, each calculation used the same set of parameter values for all parameters that had fixed values. Thus, the calculations differed only in the sets of source terms used and in their treatments of exposure pathways (the NUREG-0170 calculations modeled only inhalation dose while the Modal Study calculation and the calculation that used the source terms developed for this study modeled all exposure pathways). Accordingly, these calculations compare the NUREG-0170 result to the Modal Study result and to the result developed by this study.

The NUREG-0170 Model I and Model II source terms were presented in Table 1.5. Table 8.18 presents the Modal Study truck and rail accident source terms developed for generic steel-lead-steel casks. The source terms developed by this study for generic steel-lead-steel casks were presented in Table 7.31.

Figures 8.26 and 8.27 present respectively the truck and rail accident population dose risk CCDFs generated by these calculations. Each figure presents four CCDFs: the NUREG-0170 Model I CCDF, the NUREG-0170 Model II CCDF, the Modal Study CCDF, and the CCDF developed by this study. In each figure, the highest lying CCDF is the NUREG-0170 Model I CCDF, the next highest is the NUREG-0170 Model II CCDF, the next is the Modal Study CCDF, and the lowest lying CCDF is the CCDF developed by this study. The impact of the differences in the source term models used to generate these CCDFs can best be understood by comparing the probability and consequence axis intercepts of these CCDFs and the mean population dose risk associated with each CCDF (the area under each CCDF). The values of the CCDF intercepts and the areas under each CCDF (the mean accident population dose risk) are presented in Table 8.19.

8.16.1 CCDF Probability Axis Intercepts

The probability axis intercepts of the CCDFs in Table 8.19 can each be viewed as the product of an average accident probability per shipment (averaged over the 200 representative truck or rail routes examined) and one minus the chance that the shipment occurs without an accident severe enough to cause the spent fuel cask to fail and release radioactivity to the atmosphere. Tables 1.5, 8.18, and 7.31 show that the chance that an accident will not be severe enough to fail a spent fuel cask was estimated by NUREG-0170 [8-1], the Modal Study [8-2], and this study to be 0.91, 0.994316, and 0.99993, respectively, for truck accidents, and 0.80, 0.993962, and 0.99996, respectively, for rail accidents. But all of the truck calculations used the same set of truck route data and all of the train calculations used the same set of rail route data. So the average accident probability per truck shipment was the same for all truck calculations and the average accident probability per rail shipment was the same for all train shipments. Therefore, ratios of

Table 8.18 Modal Study Truck and Rail Accident Source Terms

Bin	F(rod) (Fig. 8-3)[a]	Release Fractions (Table 8.3[a])					Source Term Fractions = F(rod) × Release Fractions					Severity Fraction	
		Kr	Cs	Ru	Particulates	CRUD	Kr	Cs	Ru	Particulates	CRUD	Truck (Fig. 7-10)[a]	Rail (Fig. 7-11)[a]
1,1	0.03	0.0	0.0	0.0	0.0	0.0	0.0	0.0	0.0	0.0	0.0	0.994316	0.993962
2,1	0.03	2.0E-01	2.0E-04	2.0E-05	2.0E-06	2.0E-06	6.0E-03	6.0E-07	6.0E-08	6.0E-08	6.0E-07	3.8192E-03	2.7204E-03
3,1	0.03	2.0E-01	2.0E-04	2.0E-05	2.0E-06	2.0E-06	6.0E-03	6.0E-07	6.0E-08	6.0E-08	6.0E-07	1.7984E-03	5.5450E-04
1,2	0.1	1.3E-01	1.0E-06	6.7E-06	2.0E-06	2.0E-06	1.3E-02	1.0E-07	6.7E-07	2.0E-07	2.0E-07	1.6870E-05	1.2275E-03
2,2	0.1	1.3E-01	1.0E-06	6.7E-06	2.0E-06	2.0E-06	1.3E-02	1.0E-07	6.7E-07	2.0E-07	2.0E-07	2.3300E-07	5.0110E-07
3,2	0.1	1.3E-01	1.0E-06	6.7E-06	2.0E-06	2.0E-06	1.3E-02	1.0E-07	6.7E-07	2.0E-07	2.0E-07	1.5740E-07	1.0210E-07
1,3	1.0	3.3E-01	2.0E-04	2.7E-05	2.0E-06	2.0E-06	3.3E-01	2.0E-04	2.7E-05	2.0E-06	2.0E-06	2.3620E-05	7.9511E-04
2,3	1.0	3.3E-01	2.0E-04	2.7E-05	2.0E-06	2.0E-06	3.3E-01	2.0E-04	2.7E-05	2.0E-06	2.0E-06	3.0080E-07	3.2550E-07
3,3	1.0	3.3E-01	2.0E-04	2.7E-05	2.0E-06	2.0E-06	3.3E-01	2.0E-04	2.7E-05	2.0E-06	2.0E-06	2.0340E-07	6.6340E-08
1,4	1.0	3.9E-01	2.0E-04	4.8E-05	2.0E-06	2.0E-06	3.9E-01	2.0E-04	4.8E-05	2.0E-06	2.0E-06	1.5250E-05	6.1400E-04
2,4	1.0	3.9E-01	2.0E-04	4.8E-05	2.0E-06	2.0E-06	3.9E-01	2.0E-04	4.8E-05	2.0E-06	2.0E-06	1.5920E-07	2.5310E-07
3,4	1.0	3.9E-01	2.0E-04	4.8E-05	2.0E-06	2.0E-06	3.9E-01	2.0E-04	4.8E-05	2.0E-06	2.0E-06	1.0760E-07	5.1620E-08
4,1	1.0	6.3E-01	2.0E-03	4.8E-04	2.0E-05	2.0E-05	6.3E-01	2.0E-03	4.8E-04	2.0E-05	2.0E-05	1.5320E-07	1.7860E-09
4,2	1.0	6.3E-01	2.0E-03	4.8E-04	2.0E-05	2.0E-05	6.3E-01	2.0E-03	4.8E-04	2.0E-05	2.0E-05	3.9260E-14	3.2900E-13
4,3	1.0	6.3E-01	2.0E-03	4.8E-04	2.0E-05	2.0E-05	6.3E-01	2.0E-03	4.8E-04	2.0E-05	2.0E-05	1.4950E-14	2.1370E-13
4,4	1.0	6.3E-01	2.0E-03	4.8E-04	2.0E-05	2.0E-05	6.3E-01	2.0E-03	4.8E-04	2.0E-05	2.0E-05	7.6810E-16	1.6440E-13
1,5	1.0	6.3E-01	2.0E-03	4.8E-04	2.0E-05	2.0E-05	6.3E-01	2.0E-03	4.8E-04	2.0E-05	2.0E-05	9.5700E-06	1.2490E-04
2,5	1.0	6.3E-01	2.0E-03	4.8E-04	2.0E-05	2.0E-05	6.3E-01	2.0E-03	4.8E-04	2.0E-05	2.0E-05	7.2010E-08	1.0750E-08
3,5	1.0	6.3E-01	2.0E-03	4.8E-04	2.0E-05	2.0E-05	6.3E-01	2.0E-03	4.8E-04	2.0E-05	2.0E-05	4.8370E-08	5.2960E-08
4,5	1.0	6.3E-01	2.0E-03	4.8E-04	2.0E-05	2.0E-05	6.3E-01	2.0E-03	4.8E-04	2.0E-05	2.0E-05	1.0000E-16	3.4500E-14

a. Cited figures and tables are in the Modal Study, Reference [8-2].

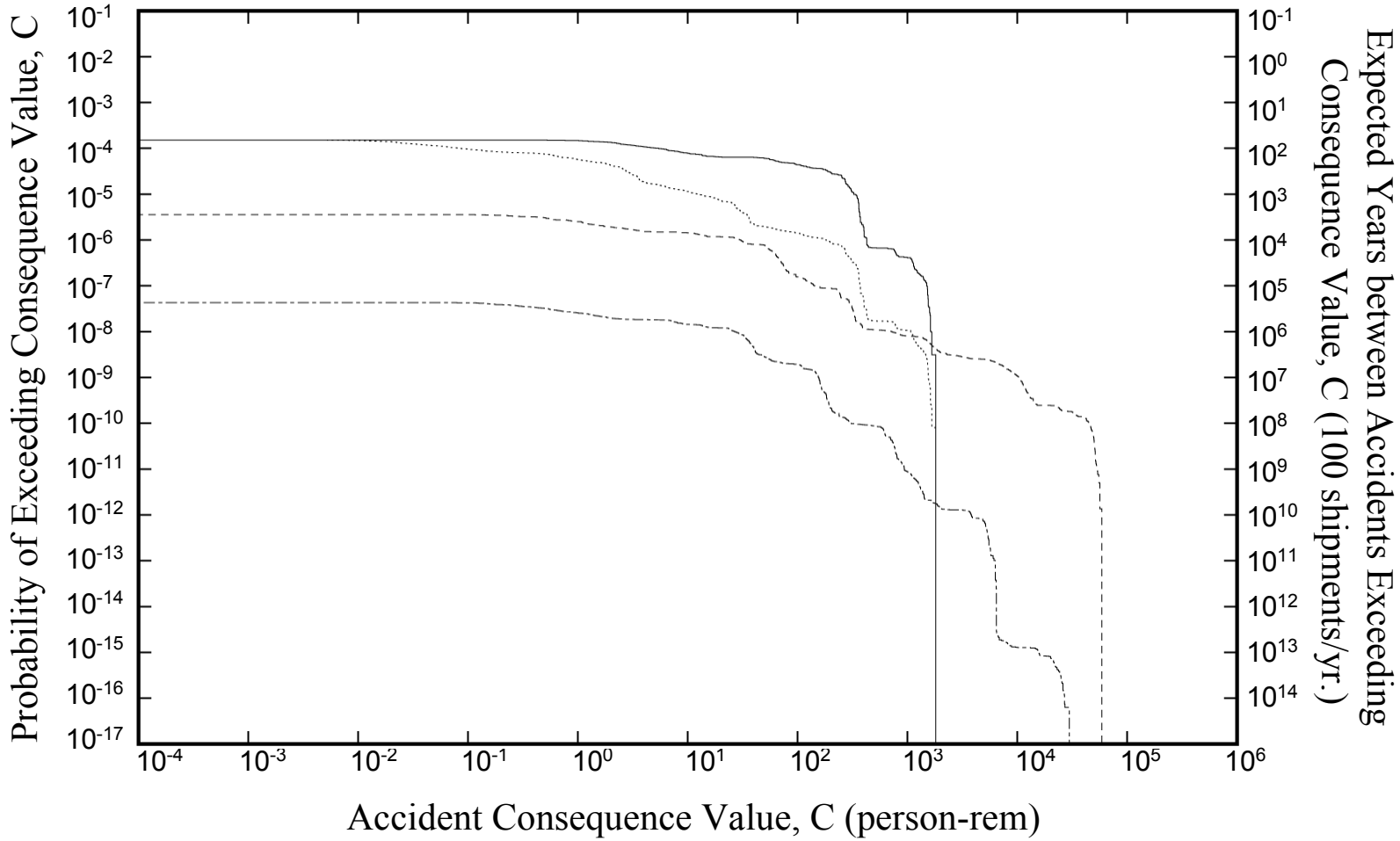

Figure 8.26 Mean truck accident population dose risk CCDFs for calculations that compared the source terms developed by NUREG-0170, the Modal Study, and this study. Each RADTRAN 5 calculation assumed transport in a steel-lead-steel truck cask over each of the 200 representative truck routes and each calculation generated results for all of the 19 representative truck accident source terms.

——— **NUREG-0170 accident release inventory, NUREG-0170 Model I release fractions, only inhalation pathways**

····· **NUREG-0170 accident release inventory, NUREG-0170 Model II release fractions, only inhalation pathways**

---------- **PWR inventory, 20 Modal Study source terms, all exposure pathways**

-·-·-·-·- **PWR inventory, 19 truck accident source terms developed for this study, all exposure pathways**

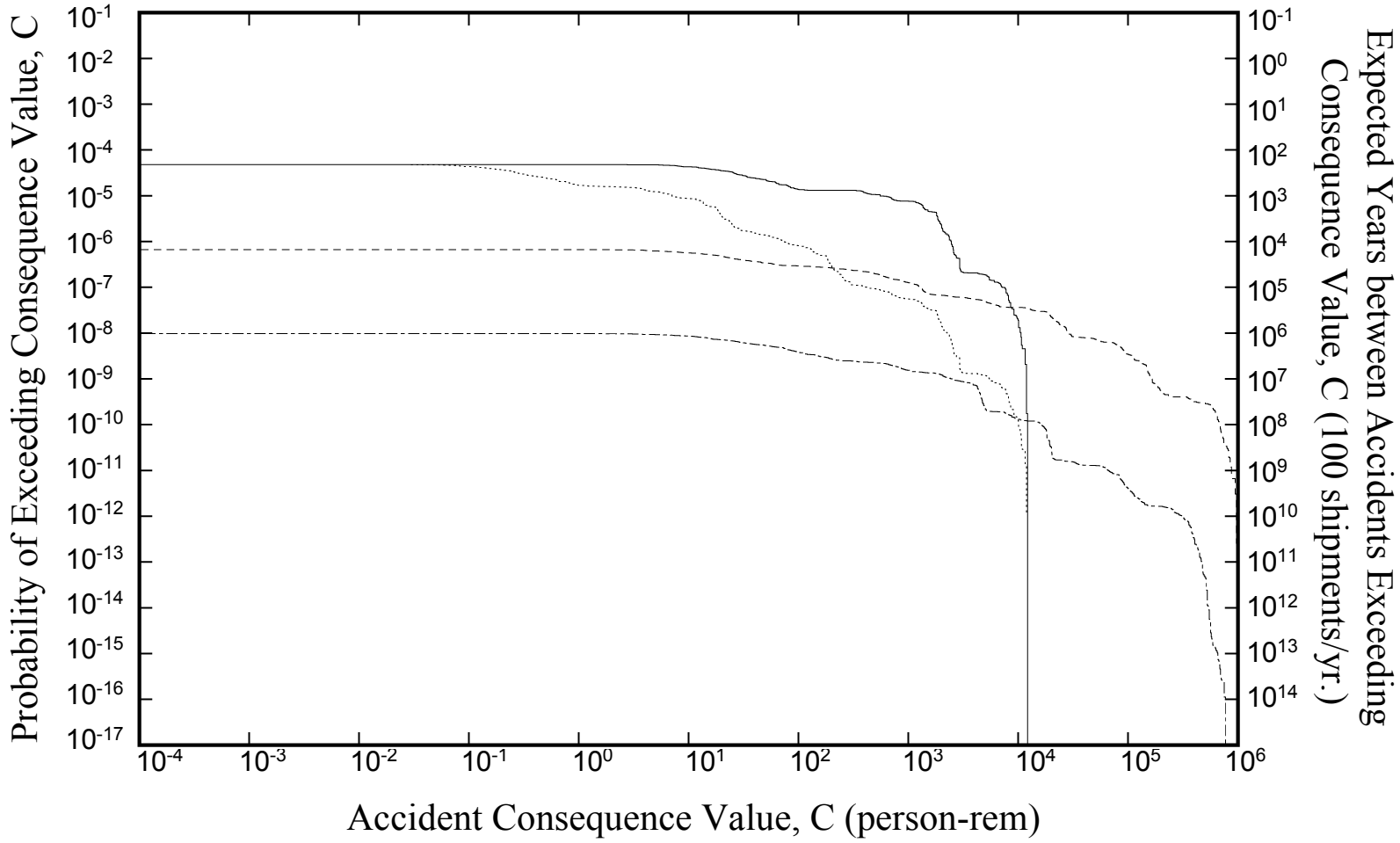

Figure 8.27 Mean rail accident population dose risk CCDFs for calculations that compared the source terms developed by NUREG-0170, the Modal Study, and this study. Each RADTRAN 5 calculation assumed transport in a steel-lead-steel rail cask over each of the 200 representative rail routes and each calculation generated results for all of the 21 representative rail accident source terms.

——— **NUREG-0170 accident release inventory, NUREG-0170 Model I release fractions, only inhalation pathways**

····· **NUREG-0170 accident release inventory, NUREG-0170 Model II release fractions, only inhalation pathways**

---------- **PWR inventory, 20 Modal Study source terms, all exposure pathways**

-·-·-·-·- **PWR inventory, 19 truck accident source terms developed for this study, all exposure pathways**

Table 8.19 Comparison of NUREG-0170 Model I and Model II and Modal Study Probability and Consequence Axis CCDF Intercepts to Those Developed by this Study

	Truck Accident CCDFs	Train Accident CCDFs
Probability Axis Intercepts		
NUREG-0170 Model I	1.5E-4	4.8E-4
NUREG-0170 Model II	1.5E-4	4.8E-4
Modal Study	3.6E-6	6.8E-7
This Study	4.4E-8	9.4E-9
Consequence Axis Intercepts		
NUREG-0170 Model I	1.8E+3	1.2E+4
NUREG-0170 Model II	1.8E+3	1.2E+4
Modal Study	6.0E+4	1.0E+6
This Study	3.0E+4	7.7E+5
Mean Accident Population Dose Risk		
NUREG-0170 Model I	1.3E-2	1.9E-2
NUREG-0170 Model II	7.7E-4	4.9E-4
Modal Study	1.3E-4	1.9E-3
This Study	8.0E-7	9.4E-6

probability intercepts ought to qualitatively equal ratios of the differences from one of the chance that the shipment takes place without a severe accident occurring. As the ratios in Table 8.20 show, within a factor of about two, this prediction holds true.

Table 8.20 Ratios of Probability Axis Intercepts

	Truck		Rail	
	Ratio Probability Intercepts	Ratio Values of $1- f_{\text{not severe accident}}$	Ratio Probability Intercepts	Ratio Values of $1- f_{\text{not severe accident}}$
NUREG-0170/Modal Study	42	16	71	33
Modal Study/This Study	82	81	70	151

This simple analysis shows that the values of the probability axis intercepts on the truck or train accident population dose risk CCDFs are primarily determined by the substantially different estimates developed by each study of the chance that an accident will not be severe enough to cause radionuclides to be released from a spent fuel cask.

The estimates of the fraction of all accidents that lead to radionuclide release from a spent fuel cask differ greatly because whenever cask failure was examined in greater detail, first by the Modal Study [8-2] and then by this study, the chance of encountering impact or thermal loads able to fail a spent fuel cask was found to decrease substantially. For example, the eight-category accident scheme used in the NUREG-0170 analyses derives its severity fraction values

from analyses performed by Clarke, et al. [8-10], who estimated the fraction of all truck and train accidents that were "minor, moderate, severe, extra severe, or extreme." For NUREG-0170, the probabilities of the accidents assigned to each of these five severity categories were reapportioned into two categories that did not lead to cask failure and six that did (the NUREG-0170 Categories I through VIII). When this was done, some of the accidents that fell into the "minor" accident category of Clarke, et al. were judged to be able to cause cask failure, and the "extra severe" and "extreme" categories were split into three categories that became NUREG-0170 Categories VI, VII, and VIII. Inspection of the boundaries between the "minor" and "moderate" truck and rail accident categories of Clarke, et al. shows that some "minor" accidents might involve fires with durations less than 10 minutes, punctures with impact speeds of only a few miles per hour, and crush loadings less than 20,000 pounds. Because some "minor" accidents were apportioned into NUREG-0170 accident Category III, these conditions for the boundary between "minor" and "moderate" accidents show that NUREG-0170 [8-1] made very conservative assumptions about the accident conditions that might produce cask failure. Because of these conservative assumptions, NUREG-0170 found that 9 percent of all truck accidents and 20 percent of all rail accidents were severe enough to fail a spent fuel cask.

The finite element and thermal analyses of cask response to impact and thermal loads performed by the Modal Study [8-2] allowed the NUREG-0170 estimates of the chance of failure of spent fuel truck and rail casks to be lowered respectively by factors of 16 and 33 to 0.57 and 0.60 percent. Moreover, when the Modal Study methodology was extended by this study to allow examination of the response of the cask closure to mechanical and thermal loads, the chance that a severe accident would fail a truck or a rail cask was estimated to be even smaller, specifically, 0.007 percent for truck casks and 0.004 percent for rail casks.

8.16.2 CCDF Consequence Axis Intercepts

Consequence axis intercept values give the largest accident population dose calculated during any of the many trials (cases) examined by a single RADTRAN run. In the absence of decontamination or interdiction of contaminated property, the largest population dose calculated would be expected to be approximately proportional to the size of the radioactive release. However, because the RADTRAN code interdicts ground that (a) is contaminated above an input contamination criterion and (b) cannot be decontaminated to levels less than or equal to the criterion, the maximum population dose calculated (i.e., the consequence axis intercept) may not be caused by the largest set of release fractions examined during the calculation. Despite the complications introduced by decontamination and interdiction, the relative values of the consequence axis intercepts presented in Table 8.17 are instructive.

As Table 8.17 shows, the maximum values of the accident population doses listed in Table 8.17 and depicted in Figures 8.25 and 8.26 are ordered as follows: Modal Study value > value from this study > NUREG-0170 value. As the table shows, the maximum accident population doses calculated by the Modal Study [8-2] and by this study for truck accidents and also for rail accidents differ only slightly (by a factor of two or less). This was to be expected because both accident population dose calculations used the same cask inventory, both assumed failure of all of the rods in the cask for the most severe accidents, both used rod-to-cask release fractions based on the experimental results of Lorenz, and both assumed no deposition onto cask surfaces of materials released to the cask interior from failed spent fuel rods (the Modal Study assumed

$f_{cask\text{-}to\text{-}environment}$ = 1.0 for all accidents; this study assumed $f_{cask\text{-}to\text{-}environment}$ = 1.0 for the most severe accidents, i.e., for all Category 6 accidents, which by definition involve a double cask failure).

Although NUREG-0170 source terms contain only Kr-85, I-131, and Cs-137, NUREG-0170 accident population doses are essentially caused exclusively by the Cs-137 in the source term. Therefore, one would expect the ratio of the maximum NUREG-0170 rail accident population dose and the maximum NUREG-0170 truck accident population dose (the NUREG-0170 consequence axis intercepts listed in Table 8.17) to about equal the ratio of Cs-137 in the NUREG-0170 source terms. The NUREG-0170 Cs-ratio (rail/truck) is 6.4 = 1280 Ci/200 Ci and the NUREG-0170 population dose ratio is 15. So again, the predicted and observed results agree to about a factor of two. However, because interdiction would be expected to perturb the dose caused by the larger release more than that caused by the smaller release, the ratio of the train accident maximum population dose to the truck accident population dose might have been expected to be less than rather than, as is observed, greater than 6.4.

Because the NUREG-0170 accident population doses are entirely caused by Cs-137 and because the maximum amount of Cs-137 that can be released by these source terms is fixed at 200 Ci for truck accidents and 1280 Ci for rail accidents, maximum NUREG-0170 accident population doses are in effect capped. In contrast to this, because the Modal Study source terms and the source terms developed for this study are both calculated as the product of a PWR cask inventory that contains 19 radionuclides, a rod failure fraction, and a set of rod-to-cask and cask-to-environment release fractions, the source term constructs developed by the Modal Study [8-2] and by this study allow larger releases (larger source terms) to occur than are allowed to occur by the NUREG-0170 source term construct. Accordingly, the fact that both the Modal Study calculation and the calculation of this study both predict maximum accident population doses that are larger than those predicted by the NUREG-0170 calculation was to be expected.

Comparison of the expected (mean) accident population dose risks and dose risk CCDFs obtained using NUREG-0170 Model I and Model II source terms shows that, although both calculations yield CCDFs that have identical probability and consequence axis intercepts, the Model I expected accident population dose risk is about 17 times greater for truck accidents and about 39 times greater for rail accidents than the Model II dose risk. This clearly shows that dose risk is determined by the area under the CCDF in the region where the CCDF bends over and then plunges toward the consequence axis.

Each of these calculations examined transport of PWR spent fuel assemblies in steel-lead-steel spent fuel casks and each used the same PWR assembly inventory. For truck and rail transport, the cask was assumed to carry, respectively, 1 and 24 assemblies. Therefore, because the release fractions for the largest truck and train accident source terms of this study and the Modal Study are very similar, the ratio of the maximum accident population doses predicted using these source terms (the consequence axis intercepts of the CCDFs generated by these calculations) should be approximately equal 24, the ratio of the number of assemblies carried by a rail cask to the number carried by a truck cask. In fact, as Table 8.17 shows, the ratio of these maximum doses for the Modal Study is 17 = 1E6/6E4, and the ratio for this study is 26 = 7.7E5/3.0E4.

Lastly, Table 8.17 shows that the expected accident population dose risks stand in the following order and have the following relative magnitudes when normalized to the NUREG-0170 Model I result:

Truck Accidents: NUREG-0170 Model I (1.0) > NUREG-0170 Model II (0.06) > Modal Study (0.01) > This Study (0.00006)

Rail Accidents: NUREG-0170 Model I (1.0) > Modal Study (0.1) > NUREG-0170 Model II (0.03) > This Study (0.0005)

Thus, the detailed analysis of the mechanical and thermal response of the cask shell performed by the Modal Study [8-2] shows that spent fuel cask failure is significantly less probable and spent fuel source terms substantially smaller than was estimated by NUREG-0170. In addition, the analysis of closure behavior performed by this study by extending the Modal Study methodology suggests that the probability of spent fuel cask failure and the magnitudes of spent fuel accident source terms are both much smaller than the estimates developed by the Modal Study.

8.17 References

[8-1] "Final Environmental Statement on the Transportation of Radioactive Material by Air and Other Modes," NUREG-0170, U.S. Nuclear Regulatory Commission, December 1977.

[8-2] L. E. Fischer, et al., "Shipping Container Response to Severe Highway and Railway Accident Conditions," NUREG/CR-4829, Lawrence Livermore National Laboratory, Livermore, CA, February 1987.

[8-3] G. S. Mills et al., "Application of Latin Hypercube Sampling to RADTRAN 4 Truck Accident-Risk Sensitivity Analysis," Proceedings of the 11th International Conference on the Packaging and Transportation of Radioactive Materials (PATRAM '95), IAEA, Vol. 4, p. 705, 1995.

[8-4] "Acceptance Priority Ranking and Annual Capacity Report," DOE/RW-0457, U.S. Department of Energy, Washington DC 20585, March 1995.

[8-5] N. R. Griego, J. D. Smith, and K. S. Neuhauser, "Investigation of RADTRAN Stop Model Input Parameters for Truck Stops," Conference Proceedings, Waste Management 96, Tucson, AZ, 1996.

[8-6] Personal Communications, B. Jody (Davis Transport, November 23, 1999); R. Ledford (TriState, November 24, 1999); and Blake Williams (NAC, November 30, 1999).

[8-7] Regulations for the Safe Transport of Radioactive Material, Safety Standard Series No. ST-1/Requirements, 1996, International Atomic Energy Agency (IAEA), Vienna, Austria (reproduced in Code of Federal Regulations, Volume 10, Part 71, Appendix A).

[8-8] J. M. Taylor and S. L. Daniel, "RADTRAN: A Computer Code to Analyze Transportation of Radioactive Material," SAND76-0243, Sandia National Laboratories, Albuquerque, NM, 1977.

[8-9] P. C. Reardon, "RADTRAN 1 Release 1: Retrieval and Verification from Archive," SAND99-1149, Sandia National Laboratories, Albuquerque, NM, to be published, copy available on request.

[8-10] R. K. Clarke, et al., "Severities of Transportation Accidents, Volume III – Motor Carriers and Volume IV – Train," SLA-74-0001, Sandia National Laboratories, Albuquerque, NM, 1976.

9. SUMMARY AND CONCLUSIONS

Risk assessment is inherently an attempt to anticipate the impact of future events. Because the events that might take place sometime in the future are infinite, no risk analysis can examine all of the possible sequences of events that might characterize the activity of interest, here the transport of spent fuel. Risk analysts address this problem by constructing representative sets of data for each important characteristic of the activity of interest. Then, by estimating the outcomes for all possible combinations of the representative sets of data, a set of outcomes (here the radiological consequences associated with the transport of spent fuel) is developed that is expected to adequately explore the range and variability of the space that contains the infinity of possible outcomes.

Cask design, route characteristics (e.g., accident rates and on-route and wayside population densities), package external dose rates, prevailing weather, accident source terms, and evacuation times are the principal characteristics of spent fuel shipments that affect the radiological consequences associated with spent fuel shipments. For this study, three representative sets of data were developed. The first set developed generic design data for four representative casks, steel-lead-steel truck and rail casks, a steel-DU-steel truck cask, and a monolithic steel rail cask. The second set contained 200 sets of representative truck or rail route data. Associated with each representative set of route data was one possible set of prevailing weather conditions, an external package dose rate, and an evacuation time. The values of these parameters were selected by structured Monte Carlo (Latin Hypercube) sampling from distributions of these parameter values that were derived from actual routes that might be used in spent fuel shipping campaigns. The third set contained 19 representative truck or 21 representative train accident source terms developed by analysis of the

- response of spent fuel casks, including the cask closure, and of the spent fuel rods being transported in the cask to the mechanical and thermal environments that the cask might experience during collision and fire accidents;

- size of the cask leak and the numbers of spent fuel rods that might fail due to these mechanical and thermal environments; and

- amounts of radioactive materials that would escape from the failed rods to the cask interior and then be released through the cask leak path to the environment before being deposited onto cask interior surfaces.

Cask response to mechanical (collision) loads was estimated from the results of finite element calculations. These calculations examined the impact of each of the four generic casks onto an unyielding surface at three impact orientations. The impact speed onto a yielding surface that would cause the same cask damage as was predicted for the impact onto the unyielding surface was then estimated by partitioning the available impact energy between the cask and the yielding surface. Cask response to thermal loads, specifically the times required to heat the cask seal to seal decomposition temperatures and spent fuel rods to burst rupture temperatures, were estimated by performing one-dimensional thermal analyses of the cask shell that took account of

the cask neutron shield compartment and the decay heat load produced by the spent fuel being carried in the cask.

These impact and thermal results were used to estimate the dependence of cask leak areas on collision speed and on the heating times required for an engulfing hydrocarbon fuel fire to heat the cask to temperatures where elastomeric seals are seriously degraded or rods burst rupture. Leak areas were used to estimate cask depressurization times following pressurization due to failure of spent fuel rods. The depressurization time estimates then allowed cask-to-environment release fractions to be estimated from the results of another study that examined transport of noble gases, condensible vapors, and aerosols from a TN-12 cask through leak paths with various cross-sectional areas to the environment. The results of that study show that, when cask leak areas are small, cask depressurization is slow. Thus, considerable time is available during which particles and condensible vapors can deposit onto cask interior surfaces. Conversely, when cask leak areas are large, the rapid flow of gases out of the cask carries most materials released from failed rods out to the environment before they can deposit onto cask interior surfaces. Total release fraction values were calculated by combining the values estimated for cask-to-environment release fractions with rod-to-cask release fraction values based on the experimental results of Lorenz.

The fraction of all accidents that might produce a given source term was estimated using the Modal Study truck and rail accident event trees, accident speed distributions, and accident fire duration distributions. Because only impact onto hard rock at high speed appears to be able to cause a spent fuel cask to leak, the Modal Study event trees were updated to reflect the frequencies of occurrence of hard rock along three long interregional transportation routes as determined by GIS analyses.

Given this input data, the radiological consequences associated with the shipment of spent fuel were then estimated by performing RADTRAN calculations. Two types of radiological consequences were examined: (1) consequences attributable to the population exposures that result from the external dose rate of the undamaged package (incident-free consequences), and (2) consequences caused by accidents that lead to the release of radioactive materials from the damaged cask (accident consequences). Consequences were calculated for PWR and BWR spent fuel shipped in each generic cask via each of the 200 routes in the representative sets of input data, for four illustrative real truck and real rail routes, and for the NUREG-0170 truck and rail routes. All of these calculations used the representative sets of 19 truck and 21 rail accident source terms developed by this study.

The results obtained for the four generic casks using the 200 representative routes and the representative truck and rail accident source terms showed that accident dose risks are negligible when compared to incident-free dose risks, that truck transport stop doses exceed all other truck incident-free doses, and that all other rail incident free doses are comparable in magnitude to rail stop doses. These calculations also showed that for each transport mode the results obtained for the illustrative routes and the NUREG-0170 route fall within the range of results generated by the representative sets of 200 truck or rail routes.

The dependence of accident consequences on accident source terms was examined further by comparing the results of calculations that differed only in the source terms used. Four sets of truck and four sets of rail accident source terms were examined: the NUREG-0170 Model I and Model II source terms, the Modal Study sets of 20 truck and 20 rail accident source terms, and the sets of 19 truck and 21 rail accident source terms developed by this study. Comparison of the mean (expected) accident population dose risks produced by these calculations indicates that, for truck accidents, the NUREG-0170 Model I risks are about 17 times larger than NUREG-0170 Model II risks, which are about 6 times larger than the risks estimated using Modal Study truck accident source terms, which in turn are about 160 times larger than the risks estimated using the truck accident source terms developed by this study. For rail transport, NUREG-0170 Model I accident population dose risks are about 10 times larger than the rail accident risks estimated using Modal study rail accident source terms, which are about 4 times larger than the risks estimated using NUREG-0170 Model II source terms, which are about 50 times larger than the risks estimated using the rail accident source terms developed by this study.

The relative ordering of these accident results is entirely consistent with the assumptions made by each study regarding the probability of radionuclide release during transportation accidents and the magnitude of the source terms generated by accidents of differing severities. Because NUREG-0170 assumed that spent fuel casks might fail when subjected to the loads that characterize minor accidents, the fraction of all truck and train accidents estimated to lead to cask failure is very large and extremely conservative. Similarly, because the NUREG-0170 Model I assumed that all cask failures allowed the entire NUREG-0170 accident inventory (the maximum amount of radioactivity that could be released during an accident) to be released, NUREG-0170 Model I mean accident population doses for truck and rail accidents are quite large. The Modal Study estimated cask leakage from the response of the cask shell to mechanical and thermal loads. As a result, both source term probabilities and source term magnitudes decrease and the accident population dose risks calculated using these source terms are one or two orders of magnitude below those calculated using NUREG-0170 source terms. In this study, source term probabilities and magnitudes were estimated by examining the response of cask closures and spent fuel rods to impact loads, and the burst rupture of spent fuel rods due to heating by fires. Based on this more detailed analysis, cask leakage is found to be even less likely than the estimates of the Modal Study, and retention of particles and condensible vapors by deposition onto cask interior surfaces is found to be substantial. Accordingly, both source term probabilities and magnitudes decrease further, and consequently accident population dose risks are reduced further by factors of 10 to 100.

This summary and the detailed analyses described in Sections 2.0 through 9.0 lead to the following conclusions:

- The single cask truck shipment expected incident-free population doses developed by this study are about one-quarter of those in NUREG-0170.
- The single cask rail shipment expected incident-free population doses developed by this study are about two-thirds of those in NUREG-0170.

- The use of very conservative cask failure criteria in NUREG-0170 caused its estimates of the fraction of all accidents that release radioactive materials to be much too large and thus very conservative.
- The NUREG-0170 estimate of the largest source term that might be released from a failed spent fuel cask during an unusually severe transportation accident is significantly lower than the largest source terms calculated using Modal Study release fractions or the release fractions developed by this study. However, the risks associated with these source terms are lower than the risk of the largest NUREG-0170 source term because these source terms are so very improbable.
- The source terms developed by the Modal Study and by this study, which reflect the complexities of rod failure and cask response to transportation accident impact and thermal loads, yield estimates of expected (mean) spent fuel transportation accident population doses that are orders of magnitude smaller than those developed by the NUREG-0170 study.

Consequently, the results of this study show that the NUREG-0170 estimates of spent fuel transportation incident-free doses are somewhat conservative and the NUREG-0170 estimates of accident population dose risks are very conservative. Since the NUREG-0170 dose and risk estimates were not large enough to require regulatory action, the fact that the incident-free doses estimated by this study are significantly smaller than the NUREG-0170 estimates and the accident dose risks estimated by this study are orders of magnitude smaller than those estimated by NUREG-0170 confirms that spent fuel transportation regulations adequately protect public health and safety.